Proceedings

THIRD INTERNATIONAL SYMPOSIUM ON ICE PROBLEMS

Proceedings

THIRD INTERNATIONAL SYMPOSIUM ON ICE PROBLEMS

18-21 August 1975
Hanover, New Hampshire

Guenther E. Frankenstein, Editor
USA CRREL

November 1975

International Association of Hydraulic Research
Committee on Ice Problems

PREFACE

This symposium on ice problems was sponsored by the U.S. Army Cold Regions Research and Engineering Laboratory and was held on the campus of Dartmouth College. The organizing committee, headed by Mr. G. Frankenstein of CRREL, was made up of members of CRREL and Dartmouth.

The chairman of the organizing committee would like to thank Mr. S. DenHartog of CRREL and Mr. R. MacMillen of Dartmouth for their tremendous assistance.

Requests for copies of the proceedings should be addressed to Mr. Frankenstein at CRREL, Box 282, Hanover, New Hampshire, U.S.A.

CONTENTS

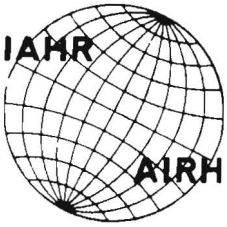

International Association of Hydraulic Research (IAHR)
Committee on Ice Problems
International Symposium on Ice Problems
18-21 August 1975
Hanover, New Hampshire

Welcoming Address

Colonel Robert L. Crosby
Commander and Director
USACRREL

On behalf of the Cold Regions Research and Engineering Laboratory and the United States Army Corps of Engineers, it is my pleasure to welcome each of you as participants in the International Association of Hydraulics Research Symposium on Ice Problems. I believe it is appropriate to note that future developments in the northern latitudes in general and petroleum developments in the Arctic Basin in particular, have serious implications with regard to ice problems of many different types. It is satisfying to know that this group, individually and collectively, is seeking to expand our understanding of the fundamental properties of ice and of icing phenomena.

I am sure that this Symposium will provide the opportunity for a mutually beneficial exchange of information among the participants. I hope that you will enjoy your brief stay in Hanover and will find your visit to CRREL to be interesting.

International Association of Hydraulic Research (IAHR)
Committee on Ice Problems
International Symposium on Ice Problems
18-21 August 1975
Hanover, New Hampshire

Address of the Chairman

O. Starosolszky

Colonel Crosby, Mr. Vice-president!
Distinguished Participants!
Ladies and Gentlemen!

I feel myself very much honoured for having been elected chairman of the Committee on Ice Problems of the International Association for Hydraulic Research.

My first duty is to express on behalf of our Committee sincere gratitude to the hosts, to the U. S. Army Cold Regions Research and Engineering Laboratory for inviting us to this wonderful campus and for the facilities.

Our Committee represents the Section for Ice Problems of our Association and has its purpose to foster a bond between those concerned with ice problems in general and in connection with hydraulic structures.

Our task is in particular - according to the by-laws - to encourage

- exchange of information and dissemination of results from applied research,
- discussion among engineers and scientists on research progress, and
- collaboration of research organizations in pursuing relevant research.

International cooperation is based on fact that ice, just as water, does not respect political borders and its properties and basic behaviour are identical all over the Globe. There is no American and no European ice, only plain ice!

Our Committee was established at the Montreal Congress of 1959. Successful ventures such as seminars during IAHR Congresses and independent Symposia demonstrated the common interests of ice experts. There can be no doubt that these ventures have contributed significantly to the dissemination of scientific knowledge concerning ice.

There is, I believe, no need to draw your attention to the ever-growing economic importance of new fields and new resources for improving the conditions of human life. Nevertheless, I should be permitted to underline the importance of our activity when considering the further future of mankind.

The growing demands of mankind for power and food must be met by stepping up their production. For promoting human welfare new resources must be explored and developed and the hazards jeopardizing such uses must be eliminated or the chances of their occurrence must be reduced to a minimum.

Ice covers a considerable part of our Globe permanently or periodically. This ice cover may develop over land, seas, lakes and rivers, and hinder on the one hand the exploitation of resources, and endanger on the other hand human activities and sometimes even human life. Our goal may be either to promote the exploitation of natural resources by improving the methods thereof under ice conditions or to take measures of protection against ice.

These are global problems which can be solved more effectively by international efforts.

International cooperation has in this field long traditions referring here to the exploration of the Antarctic and Arctic Regions.

The interest of the different nations varies in intensity, in that Northern countries, such as Canada, the United States and the USSR have first-order interest, while others are interested because of their hard winters, or because of the glaciers in their mountains.

Our interest in the solution of ice problems cannot be confined to the countries located under northern climates, mainly on the Northern Hemisphere, and utilizing the results directly. All countries of the Globe must be interested when dealing with problems affecting the future of Mankind.

It should be recognized, however, that the countries faced with ice problems directly, and located in the Northern Hemisphere, will carry the main burden of ice research.

Our Committee has the privilege and duty to promote this internationa; cooperation and to mobilize the efforts for the benefit of development.

Ladies and Gentlemen!

I have the pleasure of announcing to you, that a resolution was adopted at our Committee Meeting yesterday to organize task force groups on voluntary basis. The main objective of these task force groups is to compile state of art reports, to survey the situation

- in river ice hydraulics,
- in river thermodynamics,
- in the mechanical properties of ice,
- in interactions between hydraulic structures and ice,
- in ice control, and
- in sea ice hydraulics.

These are the subjects which can be elaborated by your contributions.

I invite you to participate in these efforts. The volunteers willing to cooperate should kindly contact the members of our Committee, especially Dr. Ashton, Secretary of the Committee.

Your contribution is essential to the successful completion of our work from which the whole engineering community is expected to benefit.

We already have one Task Force Group, headed by Dr. Schwarz, and their work will be reported on just after my address.

We believe this way of conveying cooperation will serve general interests.

This Symposium is in accordance with the views mentioned before.

The extended navigation season on inland waterways makes it possible to utilize low-cost shipping, which consumes small amounts of energy. Ice jam control is a special form of protecting the human environment against disasters. The effects of sea on marine structures is a crucial question in the expansion of the human life - sphere to the oceans and in the exploitation of their natural resources. In other words, our recent Symposium is an important contribution to the improvement of human welfare.

In this concept I wish the participants much success in their contributions during the Symposium!

THIRD INTERNATIONAL SYMPOSIUM ON
ICE PROBLEMS
Hanover, New Hampshire, USA

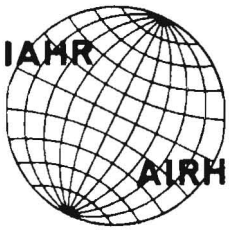

PROLONGATION OF INLAND NAVIGATION TERMS IN THE USSR

Balanin, V. V. Rector of Water Transport Institute Leningrad USSR

Climatic conditions in different regions of the Soviet Union, that is of sizable extent both on latitude and the meridian, differ considerably. At the same time it is to be noted that a large part of its territory lies beyond the Polar circle, while still greater extent, though located southward, is in the zone of severe climatic conditions. All this sets waterways of these regions ice-bound for a long time and hence unserviceable for navigation, unless any special measures are adopted. More detailed description of ice regime on different rivers is given in the paper (1). Taking into account the importance of inland water transport in the operation of the whole transport system in the country (in separate regions, in Siberia for example, it is the main kind of transport), the significance of the problem to prolong the terms of navigation in the USSR is obvious enough.

The problem to prolong the navigation terms, like most other large-scale national-economic problems has a striking engineering and economic nature. The solution of this problem calls for finding out series of technical means as well as their optimum combination with specific economic conditions (freight turnover, distance of transportation, prolongation of navigation terms), that would guarantee minimum expenditures for transportation of goods as well as its high economic efficiency as compared to other kinds of transport that might be used under present specific conditions.

Summarizing the stored experience to prolong the terms of navigation in our country, the following principal trends and stages for prolonging the navigation period may be pointed out:

(a) Complete usage of the whole period of physical navigation, that is operation of transport fleet during the whole period of navigation and distribution of ships into creeks during autumn ice-drift and at the beginning of freezing.

(b) Determination and usage of exact and guaranteed terms of annual start and completion of transport fleet operation irrespectively of ice conditions of each year, that would essentially improve the operation of water transport and its exploitation by users.

(c) Prolongation of the navigation period on some sections of the waterways above the mentioned guaranteed terms up to all-the-year-round navigation, that is caused by special needs of national economy and high economic efficiency.

Prolongation of navigation period is carried out principally according to the above-mentioned procedure, though sometimes there happen some deviations: for instance, conducting expedition voyages in spring on water storages and tributaries to deliver cargo during the high flood period along them.

Characteristics of the navigable channel present principal subject that has a great influence on the economic indices of transportation.

Three principal types of channels may be mentioned:

(a) The channel that is packed with broken ice.

(b) The channel that is regularly cleaned from ice.

(c) The channel in which ice formation is prevented by using some or other technical appliances.

The advantage of the first type channel is that it practically brings no essential changes in the thermal regime of the reservoirs, as heat irradiation through the broken ice layer is nearly the same as that of the compact ice. Such channels in the reservoirs with small flow velocities (in lakes in particular), where current velocities are negligible is firmly kept up. If the navigation is rather intensive and the climatic conditions are not very severe, the broken ice has no time to freeze together. This is also prevented by agitation of the water in the reservoirs called forth by the propellers of passing through the channel ships that results in raising deep warm water to the surface. A striking example of such a channel are navigable routes on Lake Maloren in Sweden. A channel like that is expected to be created in the USSR on the Dnieprodzerzhinsky water reservoir. An essential disadvantage of such channels is a great resistance exposed to passing ships and hence sharp speed reduction of the ship's speed down to about 50% as compared to that of the open water. The more severe are the climatic conditions of the region, the less intensive is the navigation on the given channel section, that is the

more active is freezing up of the broken ice, the more intensive is the above-mentioned reduction of the ship's speed within the channel.

Particularly unfavourable conditions for navigation are created on the channels which are created in the streams with more or less considerable velocities of the flow that causes transposition of the broken ice in one direction as well as its hummocking and as a result of subsequent ship passages the thickness of the ice cover increases sharply. After several ship passages at substantial intervals there arises a necessity either to make a new channel if it is possible, or to stop the navigation.

In different countries (USSR, USA and some others) with the object of eliminating the principal drawback peculiar to the channels filled with broken ice and causing great resistance to the fleet movement there has been suggested a number of devices providing either breaking of the ice and its removal from the navigable channel or only removal of preliminary broken ice.

Leaving out of consideration the design of these separate devices, it is to be pointed out here, that all of them provide disposition of broken and picked up from the channel ice either on the ice cover surface at the edge of the navigable channel, or under the ice cover at the above-mentioned edge. It is absolutely evident that to prolong navigation for a long period at negative temperatures of ambient air one-time clearing the channel from ice is insufficient. To maintain the channel free from ice regular operations of ice-clearing aggregate are absolutely necessary; the aggregate is usually used when the thickness of the ice-cover increases to such an extent that essentially causes resistance to the fleet movement. It is not difficult to determine the volume of the picked up ice from the channel per month. Suppose the channel is 40 m width (that is a minimum width to provide two-line movement of modern ships along the main waterway) at the temperature of ambient air $-20^{\circ}C$. This volume will make about 60 m^3 per 1 linear meter of the channel.

To place this picked up ice on both sides of the ice-cover surface, it is necessary to make spoil heaps up to 5-6 m height and about 10 m width in their footing. It is evident that such ice-spoil-heaps on the ice-cover surface will cause its straining and crushing. As an after-effect, the navigable channel will be refilled with ice. To place such a large quantity of ice under the ice-cover is still less probable. It is to be noted here, that the volume of the picked up ice from the navigable channel depends upon the frequency of its clearing. The more frequent is the clearing, the larger is the volume of the picked up ice from the channel; the less is the ice-cover thickness at constant air temperature, the more intensive is ice formation. It is to be pointed out that the maintenance of such de-iced channels will undoubtedly influence and change, somehow, the thermal regime of the reservoir or water-flow. In the water flows with considerable flow velocities sludge formation is very likely to take place that will hamper the navigation.

All stated above proves that to maintain channels open and de-iced is expedient only in spring when average day temperatures are above or a little below 0°C. That is, once cleared from thick ice-cover channel would not entirely or almost entirely get ice-bound and therefore no repeated clearing would be required.

The third type of the channel, within which ice-cover formation is prevented, may operate only in case the water (the temperature of which is higher than that of freezing) is supplied to the surface of the navigable channel. Nowadays there are objective favourable conditions for creating such de-iced navigable channels. These favourable conditions are stipulated by sharp increase of the specific capacity of some aggregates of thermal and atomic power-stations, that reach about 1.200 thousand kwt while their summary capacity is about 6.0 million kwt.

To ensure normal operation conditions for such thermal giants, dozens and hundreds of cubic meters per second of cold water are required. The former methods for cooling water by means of tower-coolers in the ponds, nowadays proves to be not economic.

The most rational solution of this problem is the extensive use of powerful water storages created while constructing hydropower stations. However, it is to be noted here that disorderly large warm water discharge into the water storages may result in their thermal pollution that negatively affects the flora and fauna of the water storage as well as on fishery that widely uses the above-mentioned water storages. These powerful water storages are also used as the main waterways. The water storages on the Volga, Kama, Dnieper and some other rivers may offer a good example of it. That is why, it is here, that heavy freight traffic may be envisaged. This freight traffic volume should justify all the expenses for creating de-iced navigable channels in winter to maintain all-the-year-round navigation.

All these problems may be solved provided the disorderly warm water discharge is substituted by definite discharge into the fixed limited canals, warm deep waters of the powerful water storages being used as well. The cascade of hydroengineering complexes is typical for our main rivers. From the point of view we are interested in there may be defined three peculiar zones (Fig. 1) in a water storage of the cascade. The first zone is arranged immediately down the stream of the upper hydroengineering complex and has a lane, caused by the warm water discharge from the upper water storage. The extent of such lanes differs considerably depending on the operation schedule of the hydro-power station as well as on the temperature of ambient air. However, it is to be noted that the limited dimensions of the lane are also conditioned by heat dissipation occurring here due to the turbelent exchange of the discharged warm water stream and the water of the reservoir, because the width of the flowbed downstream of the hydroengineering complex is usually much larger than the stream width discharged from the hydro-power station.

In this connection, it is possible to secure considerable increase of the lane length, provided the potentialities of mass-exchange along its lateral surfaces are limited. This may be achieved by means of screens manufactured of synthetic film mounted on the floats as it is shown in Figure 2. The installation of such screens will also provide the possibility to play the discharged warm water stream on the desired direction, that is on the navigable channel.

Downstream the stable lane limits, where intensive sludge formation usually takes place, it is necessary to provide the discharge of warm cooling water of the thermal or atomic power-stations, as it is shown schematically in Figure 3. To prevent this warm water from suction by the water-intake section of the cooling system, between the water-intake and water-discharge of the system, a separate section of the channel equipped with intensively operating pneumatic installations is introduced. It is evident that ships will have no troubles when overcoming this channel section. To direct the discharged warm water after its cooling to the water receivers of the next thermal or atomic power-station without any waste of heat and any heat pollution of the reservoir, it is to be transported along the canal, the cross-section of which is determined both by navigation needs and by the conditions of transporting the discharged water. This canal may be also formed by synthetic films lowered to the bottom of the reservoir where the depths are close to the required navigable depth (Fig. 4a), or having besides the lateral surfaces the bottom where the water depth is too big (Fig. 4b). To aboid considerable transverse load on side walls of the canal that are not designed for such loads, it is necessary to create a water slope in the canal nearly equal to that of the water storage of given cross-section. This is achieved by conformable changes of the canal cross-section along its length as the water slope along the water storage is gradually reduced. Let us assume, that the water depth in the canal is maintained nearly constant, while the cross-section of the canal is rectangular, then using the following equation from the Chezy formula for the width, where the factor of Chezy is determined according to the Manning formula $C = 1.49/n\ R^{1/6}$ hydraulic radius being equal to the depth.

$$b = \frac{n\ Q}{1.49\ h^{5/3}\ J^{1/2}}$$

where b - the unknown quantity of the canal width
Q - the discharge
n - Manning factor of the flow bed roughness
h - the depth
J - the slope

The canal of the cross section mentioned, that is of variable width, runs lengthways the water storage, all along of which several thermal

or atomic power-stations are dispositioned. These stations are dispositioned at such distances that ensure cooling of the discharged warm water up to the designed temperature. During warm season of the year the extent of the canals may be correspondingly increased by introducing additional canal lines.

On the third section of the water storage, where water slopes are extremely small, and the flow direction towards hydro-power station often deflects from that of the navigation channel, and the creation of the canal of necessary width may be complicated here, it is expedient to use the heat of deep waters which have here the greatest temperature.

To avoid waste of heat while lifting water from the depth to the surface, it is expedient to limit the region of ascending flow by means of the synthetic films placed in the way shown in Figure 5. This will sharply reduce heat losses in the jet because of the turbulent exchange.

All the described above offers an opportunity to approximate finally to the problem of all-the-year-round navigation on the main waterways with heavy freight turnover when in definite places of the water storages thermal and atomic power-stations are constructed.

As it was previously stated, prolongation of the navigation terms is a complex problem, which is to be solved in stages and in the first stages of this work, a complex plan for rather a long-term perspective is to be worked out. Such an approach gives the possibility to arrange the work in such a way that the works of the first stages would gradually make an integral part of the subsequent stages of the whole problem.

At present, the principle technical means, that practically may be used to prolong the terms of navigation are different modifications of ice-breakers that were discussed in the paper (1) as well as the attachments to ice-breakers and pushers, variety of which is also given in the paper. This favours to solve the problem of the first stage according to the above-described classification along the full length of the waterway of the single deep-water system of the European part and partially on the Siberian rivers in our country and proceed to solving the problems of the second stage. In some cases under most favourable conditions it is possible to realize all-the-year-round navigation with high frequency of shipping as well as expeditional voyages to the tributaries during spring till breaking up of the large water storage. All this is carried out on navigable channels either filled with broken ice or while clearing the channel from the broken ice when no repeated passages of corresponding arrangements, such as pushers with attachments, are required. Intensively used nowadays expansion of the net of thermal and atomic power-stations if they are placed with due regard for demands of all branches of national economy interested, water transport including, will give the possibility to complete the second stage of prolonging the navigation

terms according to the previously mentioned classification and if the solution is economically substantiated proceed in full scale to the third stage. Naturally, in the latter case it is necessary to have in view the creation of navigable channels where ice formation would be practically eliminated.

References:

1. V. P. Aleksandrov, V. V. Balanin, G. F. Onipchenko, V. P. Tronin, "Inland navigation and maintenance of hydro-technical structures under negative air temperatures in the presence of ice." This volume.

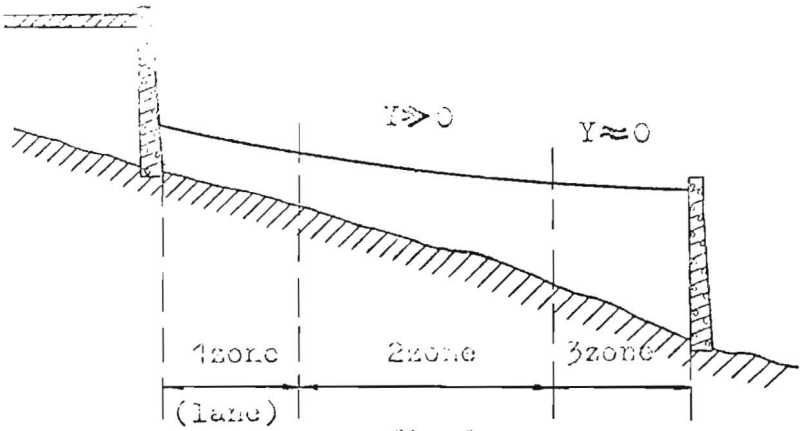

Fig.1

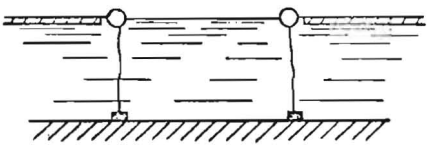

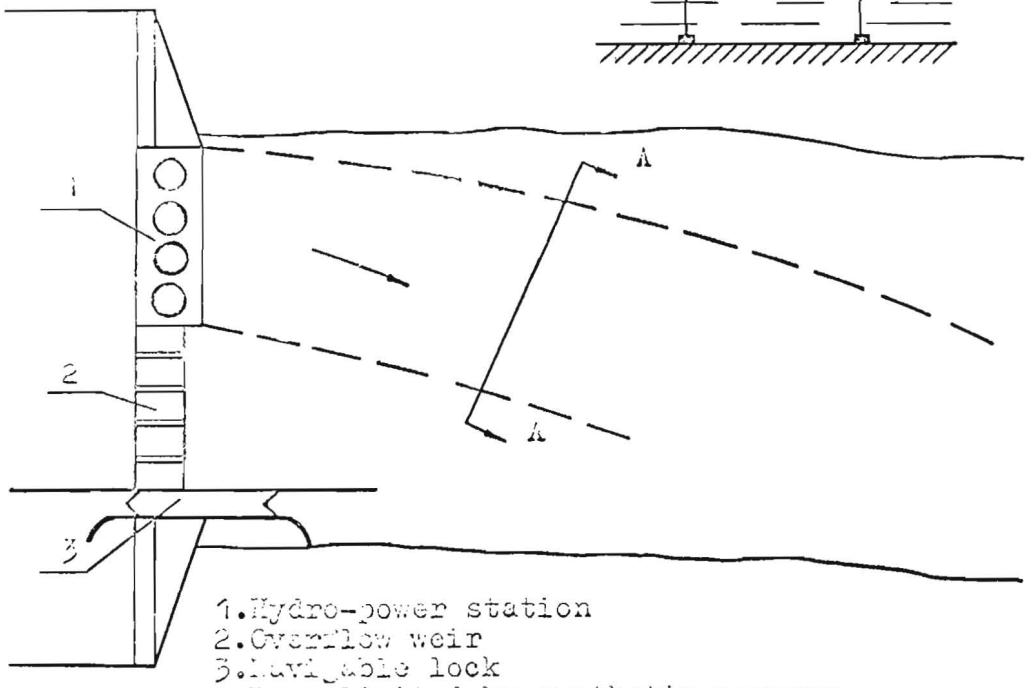

1.Hydro-power station
2.Overflow weir
3.Navigable lock
4.Lane limited by synthetic screens

Fig. 2

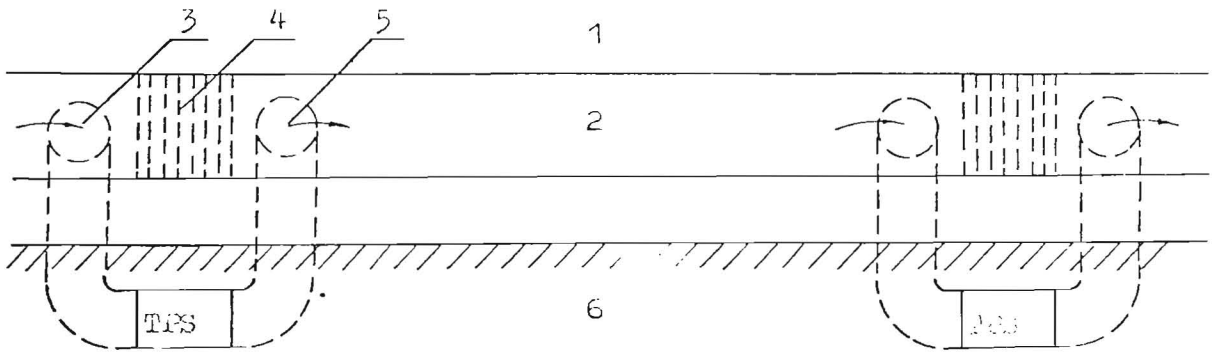

1. Water storage
2. Water cooling canal used for navigation
3. Cold water intake
4. Separate section of the channel, equipped with pneumatic installation
5. Discharge of warm water, that is to be cooled
6. Water storage bank

Fig. 3

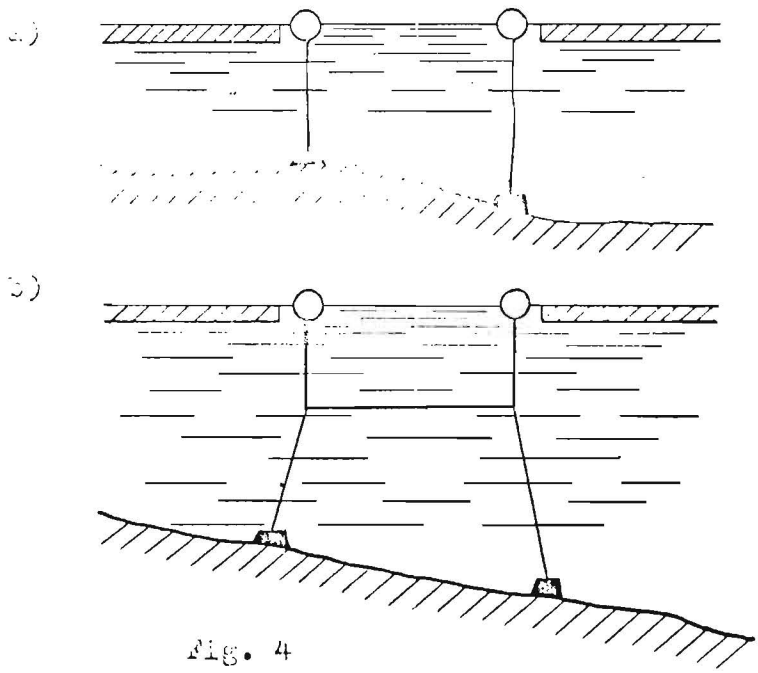

Fig. 4

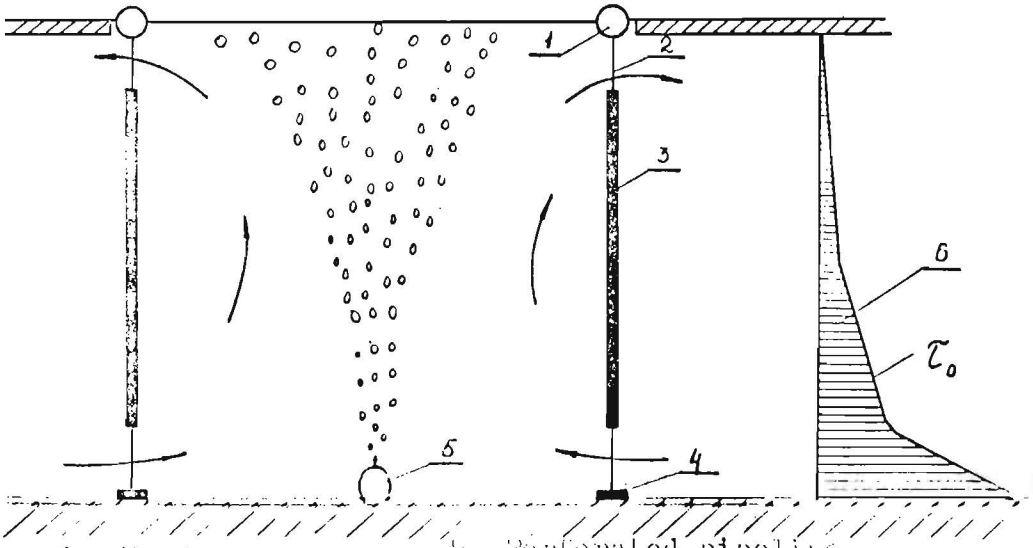

1. Float
2. Cable
3. Film
4. Load
5. Perforated pipeline
6. Graph of temperature distribution all over the depth of the reservoir

Fig. 5

THIRD INTERNATIONAL SYMPOSIUM ON
ICE PROBLEMS
Hanover, New Hampshire, USA

ICE PROBLEMS IN LOCKS AND CANALS ON THE ST. LAWRENCE RIVER

W. E. Webb, Eng.
Chief, Civil Engineering

W. F. Blair, Eng.
Chief, Operational
Systems Analysis

The St. Lawrence Seaway Authority — Canada

Since the days of the early explorers, ice conditions have governed the length of the navigation season on the St. Lawrence River. Today we have year-round navigation on the St. Lawrence as far upstream as Montreal. Above this point, however, navigation is still closed during the winter months due to ice conditions. The present navigation season above Montreal is approximately April 1 to December 15 although some difficulty is still experienced in attaining these dates.

The St. Lawrence River generally flows in a northeasterly direction from its source in Lake Ontario near Kingston to the Gulf (see Figure 1). Ice problems occur first in the furthest downstream and most northerly canalized section, the South Shore Canal near Montreal.

This paper briefly describes the major problems related to operating locks and canals under the conditions encountered during the opening and closing periods and the improvements which have been carried out to minimize the effects of cold weather.

Icing problems can be divided into two categories:

those related to ice formed through direct contact of equipment and structures with water; and those related to interference from floating ice in canals and at locks. Ice formation on lock walls may result either from direct contact with water or by floating ice freezing to the chilled wall surfaces.

The formation of ice on lock equipment and structures is particularly troublesome at mitre gates where it forms on the steel gates and on the timber bumpers in the recesses. This prevents the gates from opening fully. Ice forms as well on other lock equipment such as gate machinery, ship arrestors and sector gates and must be removed or prevented from forming to allow normal operation. Heavy snowfalls can interfere with the operation of bridges and generally make access along the lock coping difficult.

Floating ice tends to obstruct the movement of vessels in the lock approaches, particularly in the lock itself. Floating ice also adheres to the lock walls near the waterline (often being crushed against the walls by vessels) frequently building up a sufficient thickness to impede or prevent the entry and exit of maximum beam vessels. Floating ice can interfere with the operation of mitre gates and must be cleared before they can be fully opened or closed.

The cold weather operation of mechanical and hydraulic machinery for lock equipment and bridges introduces rather difficult maintenance procedures but these problems are similar to those encountered in many other operations.

Starting in 1965 the Authority undertook a program of studies that resulted in excess of $3,000,000. of improvements to provide means of combatting ice and ice formation in the South Shore Canal (see Figure 2), and the Beauharnois locks with respect to compressed air systems, so that despite the extreme downstream location, navigation could continue at least until similar problems arose at the next critical area, the Beauharnois Navigation/Power Canal.

These improvements consisted of:

A. ENLARGEMENT OF COTE STE. CATHERINE REGULATING WORKS AND CONSTRUCTION OF ICE DIVERSION WORKS AT ST. LAMBERT LOCK

One of the major problems facing the Seaway was the early freeze-up of the South Shore Canal which was a direct

result of the small flow in the canal and relatively shallow water in the adjacent areas. It was therefore decided that the capacity of the regulating works at Cote Ste. Catherine should be increased from 100 m^3/s to 300 m^3/s to:

a) minimize cooling throughout the length of the 29 Km canal and thus retard the formation of ice

b) concentrate the flow down the navigation channel to permit ice cover to form first in the shallow water areas along the original shoreline and thus minimize the heat loss

c) permit utilization of the higher flows to divert floating ice through the by-pass at St. Lambert

d) utilize the higher outflows at the lower end, i.e. Montreal Harbour, to significantly reduce the formations of frazil ice which tends to accumulate at the entrance to the canal during the winter and spring

The modifications to the regulating works were successfully completed at Cote Ste. Catherine in 1968, however, upon operation it was determined that under high flow conditions, adverse cross-currents were introduced into the navigation channel in the vicinity of the lower approach wall which influenced vessel movement. Model studies were subsequently conducted to determine the most suitable means of improving these conditions so outgoing vessels could safely pass ships moored at the lower approach wall. The model tests indicated that the strategic placement of two deflector walls in the diversion channel would redirect the flow so that it would enter the navigation channel at a less severe angle. Even with these modifications, actual field trials have shown that it is not possible to fully utilize the maximum discharge of 300 m^3/s without adversely affecting ships in the area. Maximum discharge possible with ships in the area is 170 m^3/s, although some 300 m^3/s is discharged during other periods.

A complementary project to the enlargement of the regulating works at Cote Ste. Catherine was the construction of an ice diversion channel immediately above the St. Lambert Lock. This channel permits the diversion of ice from the channel to alleviate congestion of floating ice above the lock at the closing of the navigation season, and evacuation of all floating ice between Cote Ste. Catherine and St. Lambert Lock prior to the

opening of the navigation season in the spring. The cost for these two projects was $2,000,000.

B. ICE FLUSHING SYSTEMS

One of the principal problems with winter navigation is the accumulation of floating ice within the lock chambers and the buildup of ice on lock walls which reduces the area available for ships and impedes the entry of ships into the locks. The floating ice accumulates in the lock as a result of downbound vessels (and to a lesser extent upbound vessels) pushing large quantities of ice ahead of them into the lock. Since the locks in Eastern Region were designed with their ports located in the central portion of the lock, flow from the ports could not be effectively utilized to evacuate the ice from the dead water zone of approximately 80 m. between the breast wall and the first port. Prototype tests to overcome this problem were carried out at Cote Ste. Catherine Lock utilizing the sector gates to produce various flows through the lock. These tests indicated a flow requirement of 100 m^3/s. An ice flushing culvert was then installed in the breast wall of Cote Ste. Catherine Lock to permit the introduction of water to produce a surface current capable of flushing accumulated ice out of the lock). (See Photos #1 and #2 and Diagram #1).

A similar installation was subsequently made at St. Lambert Lock, however, because of the varying head on this lock and since there are no sector gates, model tests were carried out to obtain the most suitable design. The two ice flushing systems now in operation permit the evacuation of ice from within the lock chambers within 10 to 15 minutes. The installation at Cote Ste. Catherine Lock is very effective while the St. Lambert installation is somewhat slower due to the submergence of the breast wall and flushing culvert. Details of the Cote Ste. Catherine flushing system are shown on Plates 14 and 15. The cost of the ice flushing culverts was $550,000.

C. INSTALLATION OF COMPRESSED AIR SYSTEMS

To combat floating ice which interferes with the operation of the mitre gates by lodging in the gate recesses and thus prevents the gates from fully opening, compressed air systems were installed at St. Lambert, Cote Ste. Catherine and Beauharnois Locks. Air jets have been installed in the gate recesses and on the mitre gates so large quantities of compressed air can be introduced as required to create

sufficient surface currents to move ice away from the gates and gate recess areas. Initial systems employed small portable compressors with local controls and were used for prototype testing. The present installations consist of permanent electrically-driven compressors of 30 m^3/min. with a remotely controlled distribution system that permits the lock operator to direct the air to any gate or pair of gates as required. The normal condition is to direct 22 m^3/min. to the gates to be operated and 8 m^3/min. to the gates at the other end of the lock. Details of the installation are shown on Diagram #2 and Photo #3. The cost for these installations was some $120,000. per lock.

D. INSULATION OF LOWER MITRE GATES

During freezing conditions we normally keep our locks full as much as possible when they are idle so as much of the structure is submerged as possible. However, one side of the lower gates is then exposed to below freezing ambient temperatures while the other side is in contact with water which results in formation of ice on the upstream side of the gates. This accumulation often prevents the gate from fully opening. To minimize the ice formation on the gate, a polyurethane type of insulation was applied to the gate skin with electric heating cables placed along the girders which come in contact with the recess bumpers at the lower gates at St. Lambert and Cote Ste. Catherine Locks. This has significantly reduced the icing problem, although the original installations (electric heating cable) proved to be unreliable with high maintenance costs, and it is now planned to replace these with hydronic heating systems.

The difficulty experienced with ice on the timber gate recess bumpers has also been overcome by replacing the timbers with steel I-beams and attaching electric heating cable to the beams. The I-beams have also been faced with neoprene pads to protect paint on the mitre gates. The cost of this was $100,000./pair of gates. Further details on gate heating are shown on Diagram #3 and Photo #4.

Upon completion of the improvements, weather conditions during the opening and the closing periods were less severe than the average and the improvements could not be fully evaluated for several years. However, they were tested during the 1972 and 1973 closing periods and it was found that they operated satisfactorily under the relatively severe conditions encountered. However,

it must be clearly understood that conditions vary from year to year and as the season is extended more difficult conditions will be encountered which will necessitate further modifications and additional features.

While advances have been made in most areas, little has been accomplished to reduce the problems associated with the build-up of ice on lock walls. Here floating ice that is pushed into the locks by vessels adheres to the walls and in some cases the accumulation builds up to as much as 0.6 meters and is sufficient to impede the entrance of vessels. Various experimental wall coatings have been tested as well as mechanical scarifying. Heating of the lock walls is being evaluated. To date this problem remains to be solved on a long-term basis and scarifying with a small back-hoe has been adopted for the short term. See Photo #5.

Studies are continuing to improve the efficiency and effectiveness of the improvements as well as to investigate means of not only "firming up" but "extending" the season. These studies include the evaluation of:

- air bubbling to prevent ice formation in canalized sections

- the use of flow developers to move floating ice

- ice sluices to evacuate floating ice

- ice booms to prevent the entrance or movement of floating ice

- various means to prevent an ice build-up on lock walls

A series of separate studies of ice problems in the Beauharnois Canal has also been undertaken jointly by the Seaway and Hydro-Quebec and will be the subject of a separate presentation.

The use of hovercraft for icebreaking in shallow water is also being investigated in conjunction with the Ministry of Transport so that ice can be evacuated earlier from areas where conventional icebreakers cannot operate. This will permit earlier placement of lighted navigation aids.

In any case it is the intention of the Seaway to continue to extend the length of the navigation season on a gradual basis and as capacity is required.

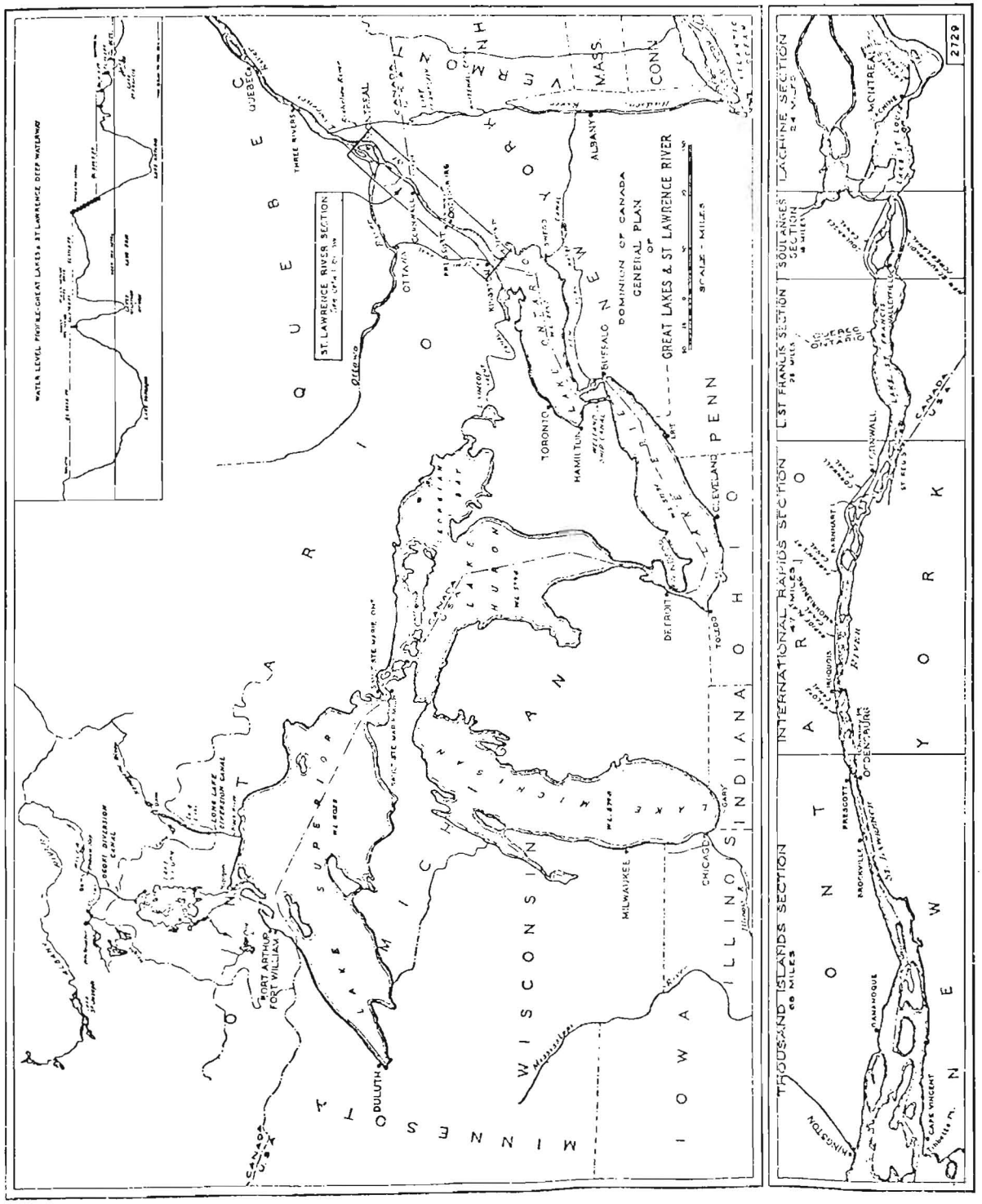
WATER LEVEL PROFILE-GREAT LAKES & ST LAWRENCE DEEP WATERWAY
ST. LAWRENCE RIVER SECTION
DOMINION OF CANADA
GENERAL PLAN
OF
GREAT LAKES & ST LAWRENCE RIVER
SCALE - MILES
THOUSAND ISLANDS SECTION
INTERNATIONAL RAPIDS SECTION
LST FRANCIS SECTION
SOULANGES SECTION
LACHINE SECTION
2729

FIGURE 1

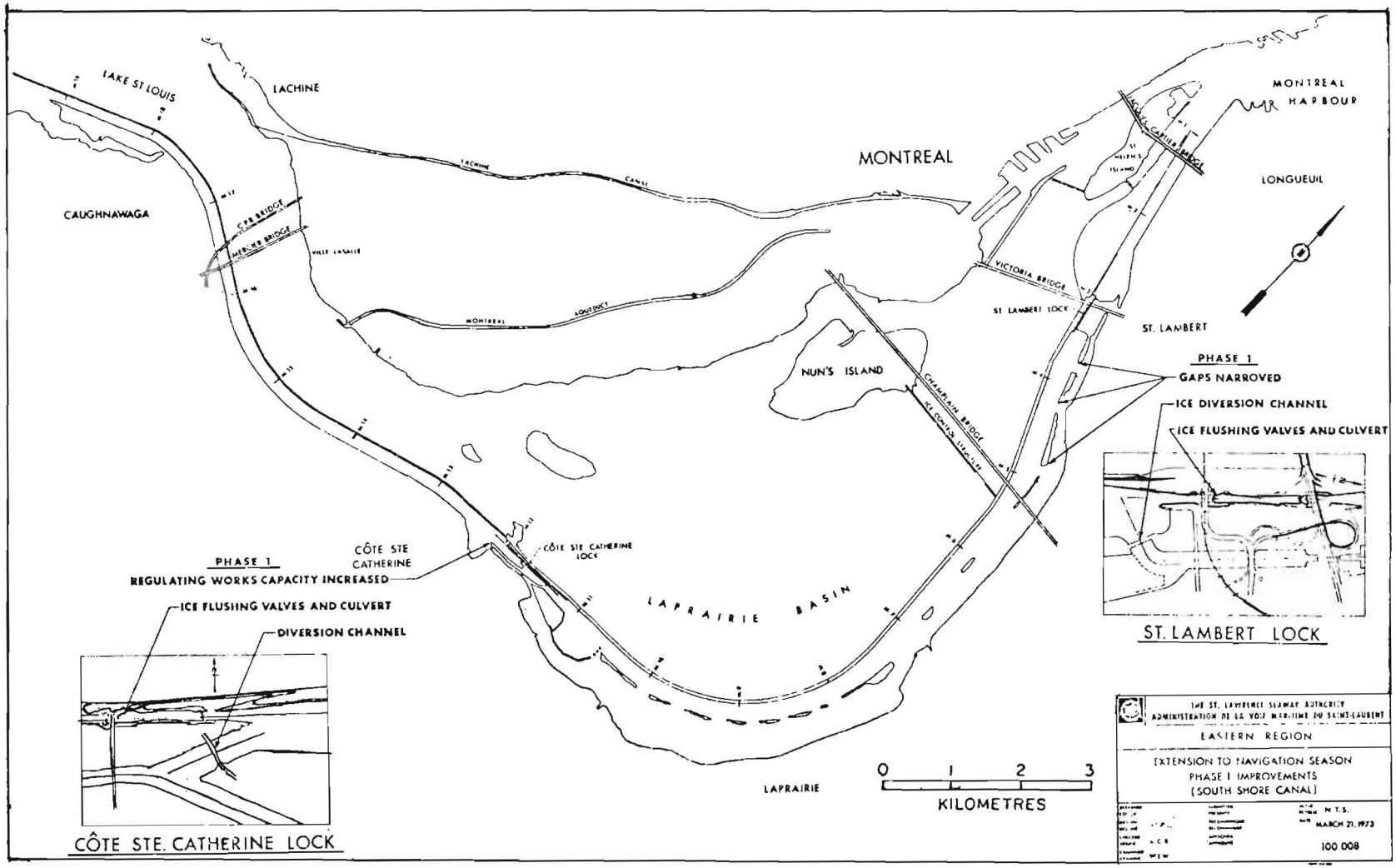
LAKE ST LOUIS
LACHINE
LACHINE CANAL
MONTREAL
MONTREAL HARBOUR
LONGUEUIL
CAUGHNAWAGA
CPR BRIDGE
MERCIER BRIDGE
VILLE LASALLE
MONTREAL AQUEDUCT
VICTORIA BRIDGE
ST LAMBERT LOCK
ST. LAMBERT
NUN'S ISLAND
CHAMPLAIN BRIDGE
PHASE 1
GAPS NARROWED
ICE DIVERSION CHANNEL
ICE FLUSHING VALVES AND CULVERT
ST. LAMBERT LOCK
CÔTE STE CATHERINE
CÔTE STE CATHERINE LOCK
PHASE 1
REGULATING WORKS CAPACITY INCREASED
ICE FLUSHING VALVES AND CULVERT
DIVERSION CHANNEL
LAPRAIRIE BASIN
LAPRAIRIE
0 1 2 3
KILOMETRES
CÔTE STE. CATHERINE LOCK
THE ST. LAWRENCE SEAWAY AUTHORITY
ADMINISTRATION DE LA VOIE MARITIME DU SAINT-LAURENT
EASTERN REGION
EXTENSION TO NAVIGATION SEASON
PHASE I IMPROVEMENTS
(SOUTH SHORE CANAL)
N.T.S.
MARCH 21, 1973
100 008

Figure 2.

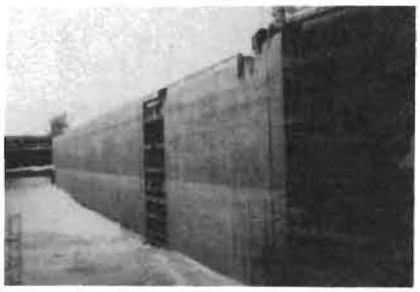

PHOTO #1

ICE
FLUSHING
SHOWING PORTS
IN BREAST WALL
(Lock Dewatered)

PHOTO #2

ICE
FLUSHING
CURRENT UTILIZED
TO MOVE ICE
FROM LOCKS

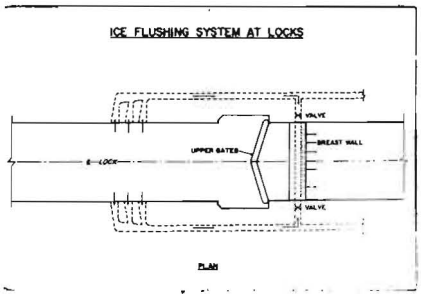

DIAGRAM #1

DESIGN
FOR
ICE
FLUSHING

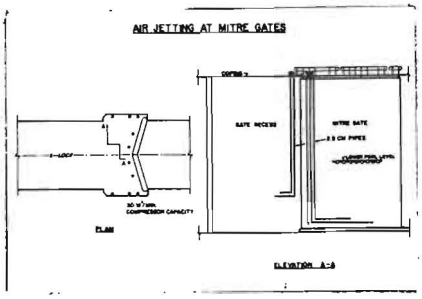

DIAGRAM #2

DESIGN
AIR JETS
COMPRESSED
AIR SYSTEM

PHOTO #3

AIR JETS
IN OPERATION

NOTE ICE BEING MOVED
FROM GATE AREA

MITRE GATE HEATING AND INSULATION

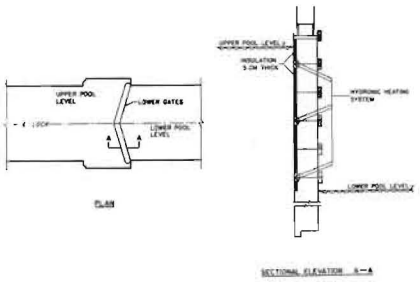

DIAGRAM #3

GATE HEATING

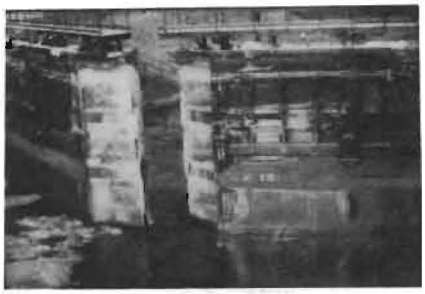

PHOTO #4

GATE HEATING

NOTE CLEAR AREA
ON MITRE GATE

PHOTO #5

BACK-HOE
CLEARING ICE
FROM LOCK WALLS

PRESENT METHOD

THIRD INTERNATIONAL SYMPOSIUM ON
ICE PROBLEMS
Hanover, New Hampshire, USA

ACCUMULATION OF FRAZIL ICE IN AN INTAKE RESERVOIR

EINAR TESAKER
SECTION HEAD

RIVER AND HARBOUR
LABORATORY

TRONDHEIM
NORWAY

SYNOPSIS. This paper reports from a field study of frazil ice accumulation under a solid ice cover. Maximum flow velocities vary in the range 40 - 60 cm/s, with Froude numbers in the range 0.08-0.14 for apparently stable flow sections. The results have been compared with earlier findings about the critical velocity for progress of an ice front against a current.

The intake dam of Gamlebrofoss power plant in Kongsberg Norway, forms a 500 m long and 130 m wide intake pond with a maximum depth of 7.5 m. The total volume is 250 000 m^3. The design flow is 110 m^3/s, which is more than normal winter flow. The gates are therefore rarely used in winter, while automatic level control keeps the pond level almost constant by adjusting the power production. The pond is therefore ice covered earlier than the nearest 800 m upstream river. Parts of this upstream reach are shallow rapids that usually do not freeze at all most winters. Large quantities of frazil are therefore produced and transported to the intake pond, where it is deposited under the ice cover.

Fig. 1 shows a map of the area. The pond is seen from the old bridge on fig. 2, with the intake dam in the background. Fig. 3 shows the upstream edge of the ice cover on the pond, and the rapids below the bridge. Fig. 4 gives a view upstream from the bridge. Fig. 2-4 are taken in January 1971.

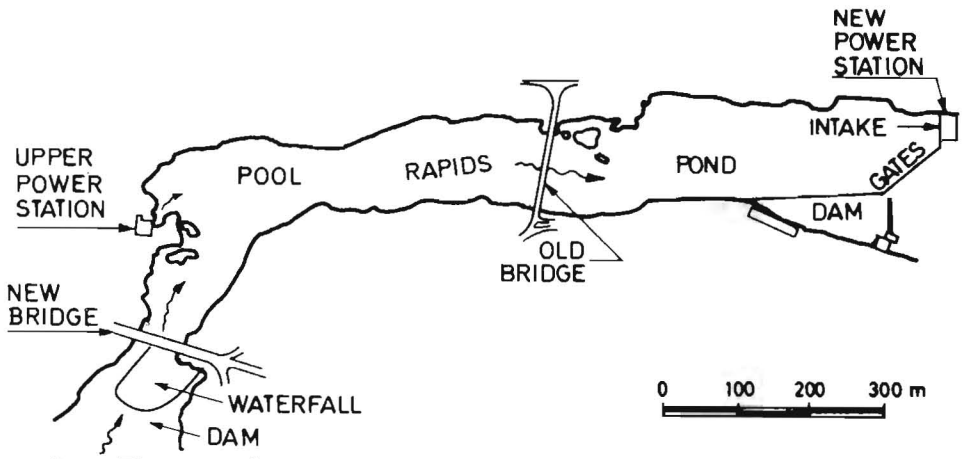

Fig. 1. The study area.

Regular mapping of the ice cover was carried out from Febr. 1971 to April 1972 (Tesaker and Billington [1]). Fig. 5 shows the characteristic progress of the ice cover as it occurred during the season 1971/72. The open areas on fig. 5 are rarely or never frozen, and can be seen also on fig. 2-4, taken the preceeding season.

Surveys of the accumulation pattern of frazil under the ice cover were made in 1971 and 1972. Observations of solid and frazil ice thickness were made through numerous boreholes twice each year. The velocities in a typical cross section were measured once each year.

The thickness was measured by means of a round plate mounted on a rod. The boundary between accumulated ice and free water was well defined and easy to determine within an accuracy of 5 cm.

The velocities were measured by an "Ott" flow meter with propeller diameter 50 mm.

Fig. 6 shows a typical accumulation pattern during an accretion period. The contours show the frazil ice thickness exclusive of the solid ice. Maximum thickness is 420 cm and total volume about 28 000 m^3. The shape of the ice delta has a striking similarity with sand deposited from a river entering a reservoir.

Fig. 7 shows two cross sections, and the velocity distribution in the upper one. The maximum velocity is 60 cm/s, but 30-40 cm/s is typical for most vertical sections.

One month later (March -71) about 80 per cent of the frazil from January had been eroded or melted away, and the maximum thickness of the frazil deposit was 165 cm. Fig. 8.

Fig. 2. The intake pond seen from the old bridge

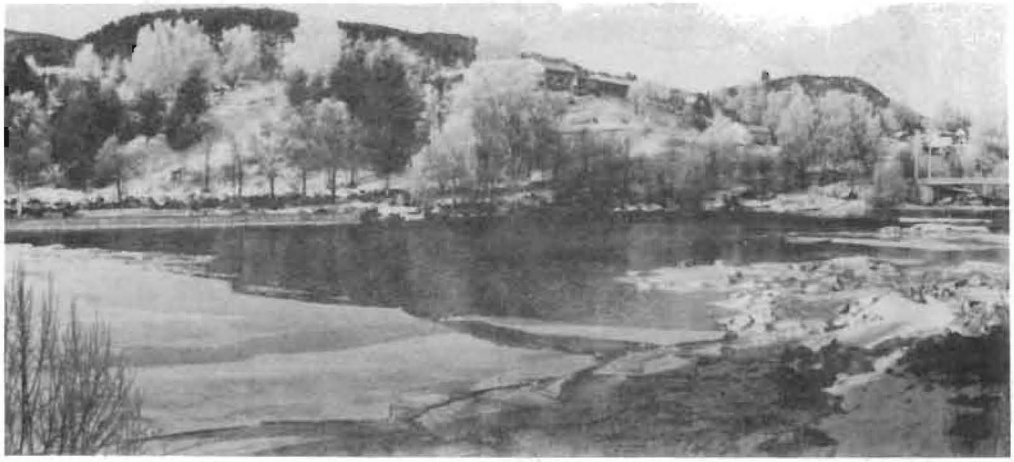

Fig. 3. The upstream edge of the ice cover

Fig. 4. View upstream from the old bridge

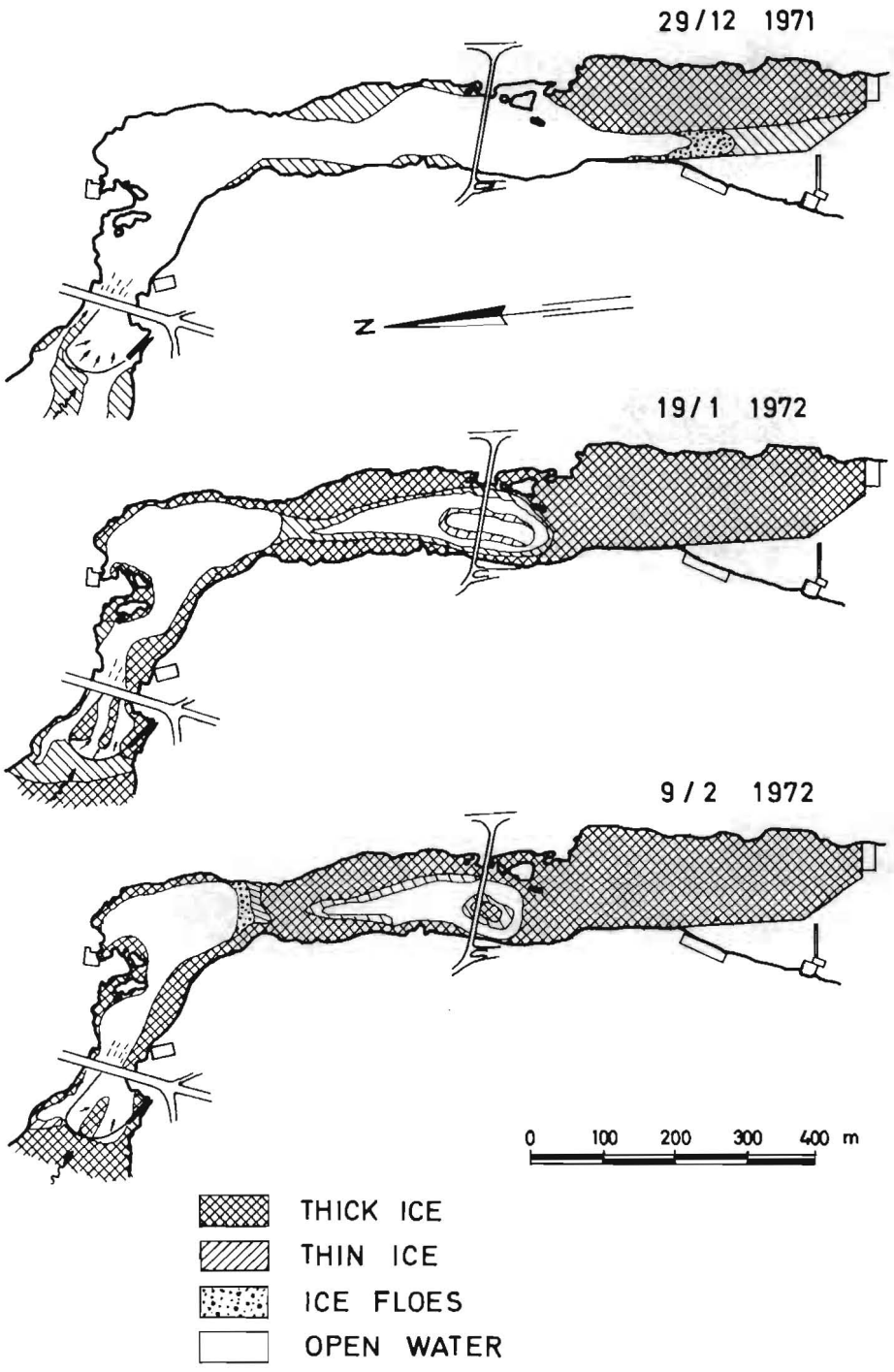

Fig. 5. Typical development of ice cover.

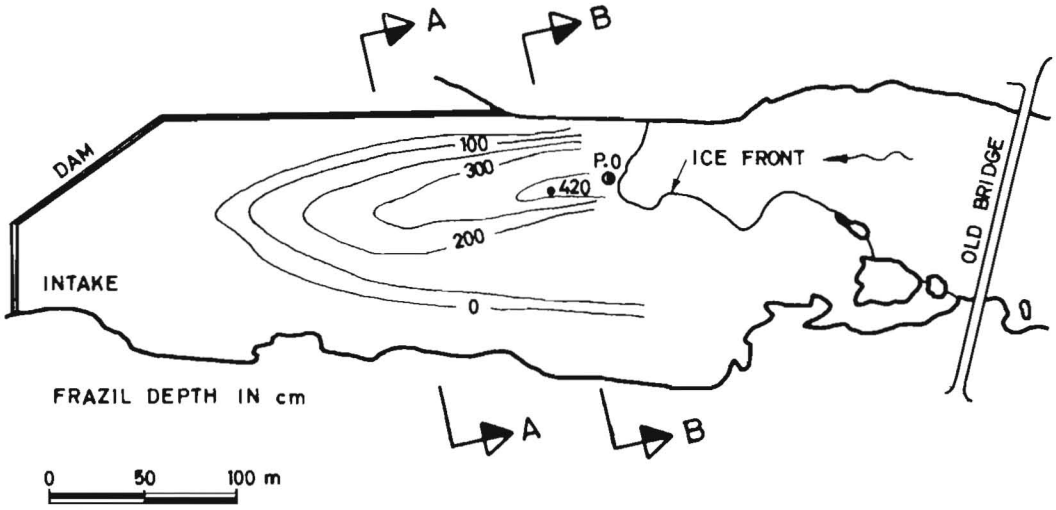

Fig. 6. Frazil ice deposit 4. Febr. 1971

SECTION A - A

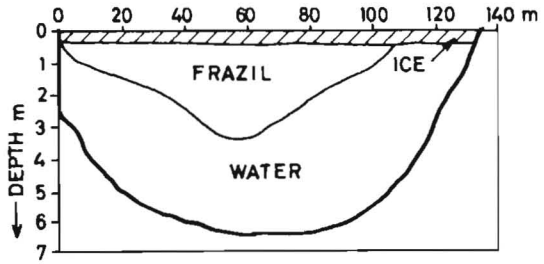

SECTION B - B

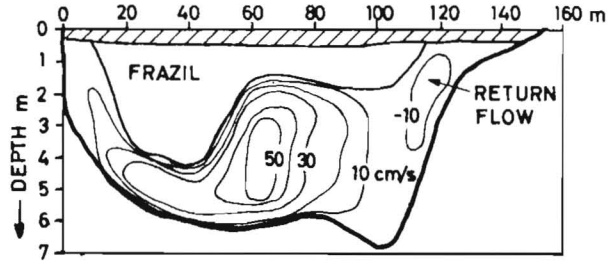

Fig. 7. Cross sections and velocities 4. Febr. 1971

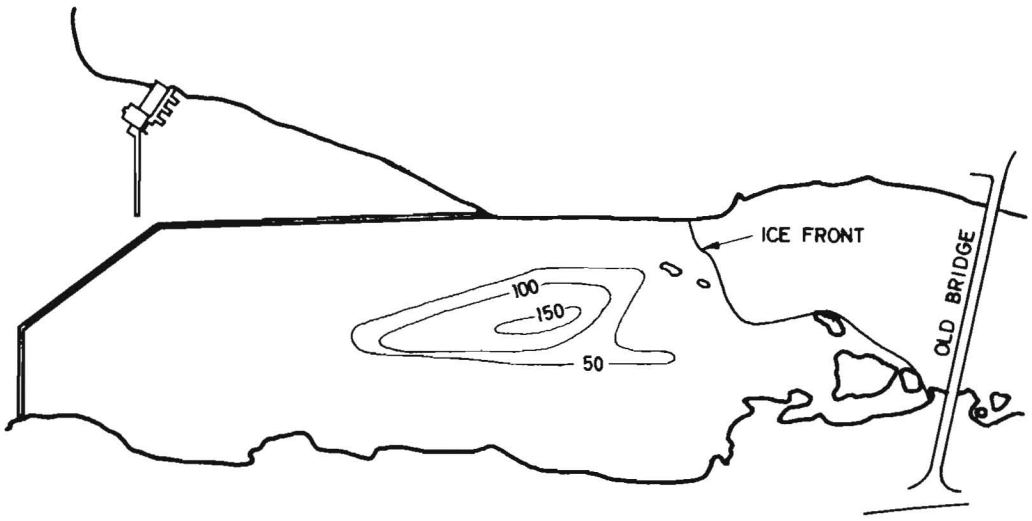

Fig. 8. Frazil ice remains 4th March 1971

Similar accumulations, but larger volumes (43-41 000 m^3) were found in January and February 1972. Fig. 9-11. Only 1-2 m ice free water depth was left under large parts of the frazil pack. The flow section was reduced by up to 60 per cent of the normal icefree area. The frazil volume filled up to 20 per cent of the reservoir. Maximum velocities were 40-50 cm/s.

The two seasons show very similar accumulation patterns. A slightly more east-west-turned axis in the last season is likely to be the result of an accidental opening of one of the gates a few days before the measurements Febr. 4th -71.

In the accumulation phase, when freshly formed frazil is being carried under the ice cover, a stable interface will establish where equal amounts of frazil are deposited and eroded simultaneously. When no frazil is being supplied, the erosion will continue and increase the flow section, until the critical velocity for erosion is reached.

If the latter occurs during a mild weather period, melting of some of the ice pack may add to the erosion. Both processes will occur mostly at the upstream part of the ice deposit, such that its "top" appears to move downstream. This is clearly the trend in both seasons' observations.

The two winter seasons had temperatures slightly above average. Much larger quantities of frazil will be accumulated in extremely cold winters. This may cause intake troubles or at least significant head loss at the power

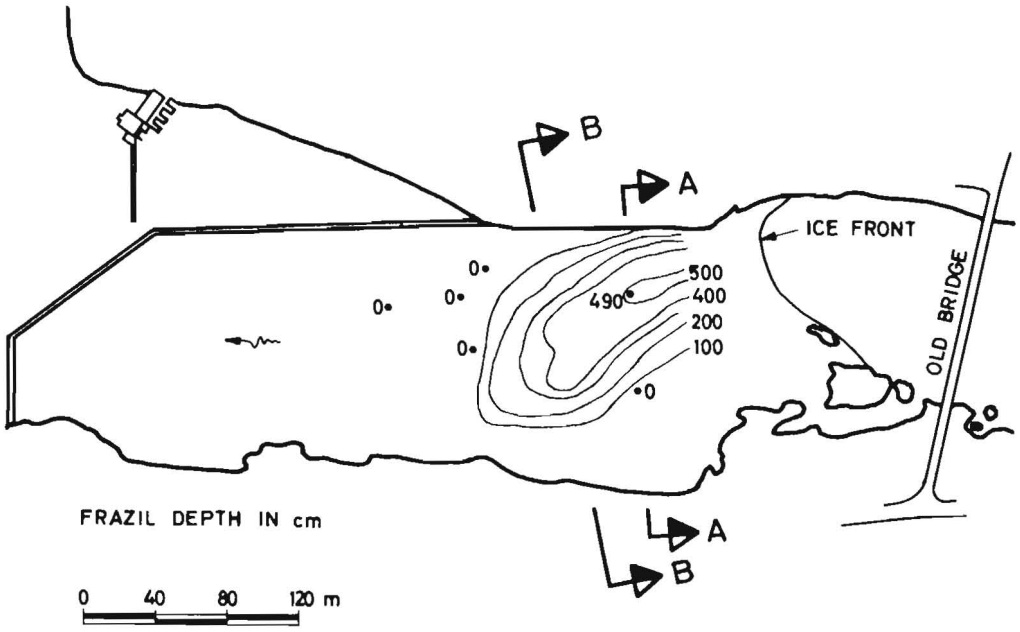

Fig. 9. Frazil ice deposit 13. Jan. 1972

SECTION B-B

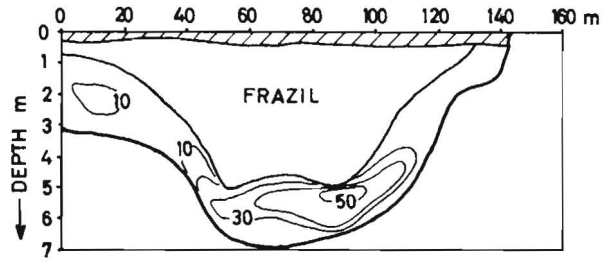

SECTION A-A

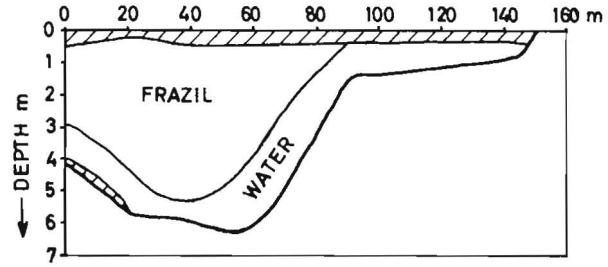

Fig. 10. Cross sections and velocities 13. Jan. 1972.

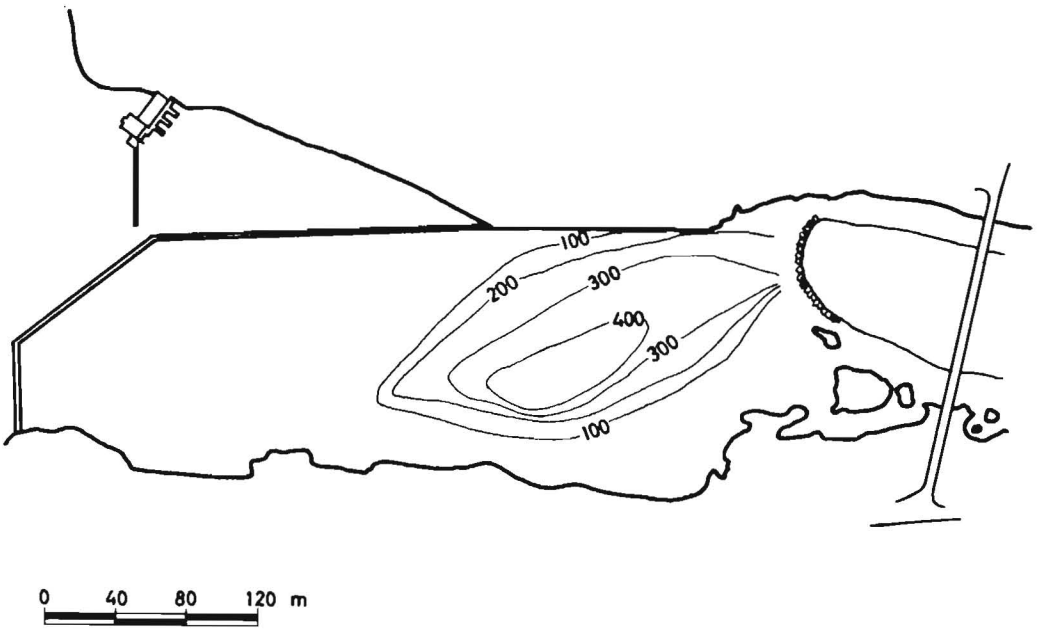

Fig. 11. Frazil ice deposit 7th Febr. 1972

plant. It is therefore important to study the erosion and roughness under the frazil pack.

Shear stresses (τ_o) have been calculated by assuming logaritmic velocity distributions. Critical erosion conditions can then be calculated by means of Shields' formula

$$D_c = \tau_o/(C \cdot g\ (\rho_w - \rho_{ice}))$$

where D_c = critical particle diameter, ρ_w and ρ_{ice} = densities of water and ice, C = constant (0.03 - 0.06). Assuming solid ice particles (ρ_{ice} = 920 kg/m^3), D_c = 2.5 - 7.5 cm were found. It is more likely that the frazil appear in aggregate lumps, however. Assuming ρ_{ice} = 980 kg/m^3 for the lumps gives D_c = 10 - 30 cm, which seems reasonable.

Froude numbers $F = V/\sqrt{g \cdot d}$ are given in table 1 for all the recorded velocity profiles (V = max. velocity, d = free flow depth beneath the ice pack). It is seen that V = 40 - 60 cm/s in sections where an approximate limit of deposition has been reached. F = 0.08 - 0.14 for the same profiles.

It is intersting to compare these values with known limit conditions for progress of an ice front facing open flow. A conventional rule used for Norwegian rivers has been V_c = 60 cm/s (V_c = critical velocity) measured upstream of

Table 1.

Year	Dist.from bank (m)	Max.vel. V(m/s)	Flow depth d(m)	Froude number	Comments
1971	6	0.09	2.9	0.017	Shear zone
	25	0.42	1.8	0.100	
	40	0.37	1.9	0.086	
	60	0.60	4.6	0.090	
	80	0.30	4.2	0.047	
	100	0		-	Shear zone
	113	-0.12	3.0	0.022	Eddy
	P0	0.44	3.2	0.079	
1972	13	0.11	2.3	0.023	
	32	-		-	Shear zone
	52	0.37	1.5	0.097	
	71	0.45	1.2	0.13	
	88	0.53	1.5	0.14	
	106	0.45	2.6	0.09	

Marking P0 represents a single borehole, about 1 m from the edge of the ice front, see fig. 6.

the front. Flatjord [2]found that V_c varied with the temperature, 60 cm/s being the value for 0.02°C. Sinotin [3] found $V_c = \sqrt{0.035\ gL}$ for ice floes, where L is the length of the floes. L = 1.0 m gives V_c = 0.6 m/s.

Kivisild [4] reports F_c = 0.08 as limit, using values of V and d in front of the ice.

Uzuner and Kennedy [5] found a relation between F_c, the ice thickness t, and d in front of the ice, which can be written:

$F_c = 0.08$ for $t/d \approx 0.05$ and $t/l = 0.6$

$F_c = 0.14$ for $t/d \approx 0.2$

See also Carstens [6].

The results in [2], [4] and [5] vary much as should be expected with such simplified systems of parameters.

A closer study of the observations at Kongsberg shows that the largest F-values occur for the smaller depths, in agreement with Uzuner and Kennedy's results. It is therefore a remarkable agreement between the ice front criteria and the stability of the frazil pack boundary despite obvious differences in flow patterns.

The shear stress is more directly related to the motion

or deposition of particles than V or F, and should be preferred as criterion when data are available. For practical purposes, however, there is a need for simple criteria involving a minimum of data.

The shear stress depends both on the maximum velocity and the flow depth. F relates both in a manner that seems appropriate for practical use when the vertical flow profile is typical for a conduit flow, i.e. with logaritmic distribution towards both boundaries. If the velocity profile differs from the typical due to large depths, irregular topography etc., the F_c-criterion is invalid. In such cases the V_c or τ_c-criteria have to be used.

A particular case is when the water depth is so large that the influence of the bottom friction is negligible. The ice will then build up with an upstream slope determined by the friction angle and the shear stress similar to sand dune formation in rivers. This is of practical importance for the operation of ice skimmer walls. The skimmer wall will collect ice along its upstream side until it is filled to capacity. If the supply of ice exceeds the volume determined by the upstream slope and the wall depth, the skimmer will only be a temporary restriction to the passage of ice.

This effect has been observed both in model and prototype for the diversion structure of Burfell power plant, Iceland. One of the favourable results of this model study with respect to cost was that the depth of the skimmer wall could be reduced without significant influence on the ice problems. The only important requirement was to keep the ice moving parallel to the upstream side of the wall in order to avoid permanent accumulation. (Tesaker [7]).

In a recent personal communication with T. LAVENDER it was pointed out that it would be more logical to use the densimetric Froude numbers $F' = V/\sqrt{g \cdot d \cdot (\rho_w - \rho_{ice}/\rho_w}$ instead of F as stability criterion because the submerged weight of the particles is important for their stability. If $\rho_{ice} = 920$ kg/m^3 (solid ice) F = 0.08-0.14 of Table 1 will correspond to F' = 0.28-0.49. Assuming ice lumps with $\rho_{ice} = 980$ kg/m^3, as is more realistic, F = 0.14 will actually correspond to F' = 1.0, which is a well known value for critical Froude numbers in other connections. The apparent variation in F_c-values may be due to different composition of the ice lumps from one case to another, or to a combination of this effect and the depth factor mentioned above.

To come closer towards a general stability criterion for ice deposits requires more knowledge on actual values of ρ_{ice} for the frazil lumps.

REFERENCES:

1. Tesaker and Billington: VHL (River and Harbour Laboratory), Trondheim, Rep. STF60 A74054, 1974.

2. Flatjord: Norw. Water and Electricity Board, Hydr. Dept. Medd. 7, 1964.

3. Sinotin: IAHR Ice Symp., Leningrad 1972.

4. Kivisild: IAHR, 8, Congr., Montreal 1959, Vol. III.

5. Uzuner and Kennedy: IAHR Ice Symp., Leningrad 1972.

6. Carstens, T: Inv. lecture, IAHR Ice Symp., Reykjavik 1970.

7. Tesaker: VHL, Unpublished Rep. 600115, 1966.

International Association of Hydraulic Research (IAHR)
Committee on Ice Problems
International Symposium on Ice Problems
18-21 August 1975
Hanover, New Hampshire

COMMENTS

Paper Title: Accumulation of Frazil Ice in an Intake Reservoir

Author: E. Tesaker

Your name: Kartha, V. C. Tel. (204) 474-3542

Address: Manitoba Hydro, 820 Taylor Ave.,
Winnipeg R3C 2P4, CANADA

Comment:

Your paper described the ice-regime of a river including rapid flow sections and a waterfall. Since the Froude numbers downstream of the waterfall were below the critical value (as you have concluded) suggested by other investigators, would you comment on the nature of hanging dam formation, if any, in the vicinity of the waterfall?

Did the ice jam progress over the waterfall or did it terminate at the foot of the waterfall? In other words, was the ice cover upstream and downstream of the waterfall continuous with little or no slope variation?

Author's Reply:

The waterfall shown on figures in the final paper is 12.5 meters high and always interrupts the ice level. There is a small overflow dam on top of the waterfall. The river has moderate slope several kilometers upstream of the dam and is usually being ice covered early in the season. A hanging ice dam sometimes develops in the pool between the waterfall and the rapids depending on temperature conditions. It is moderate in size and has not been studied in detail. The rapids under the old bridge has not been ice covered since the new plant was constructed but it may occur under strong winters. The waterfalls will in case be the only significant cooling area and frazil ice production will be small.

International Association of Hydraulic Research (IAHR)
Committee on Ice Problems
International Symposium on Ice Problems
18-21 August 1975
Hanover, New Hampshire

COMMENTS

Paper Title: Accumulation of Frazil Ice in an Intake Reservoir

Author: E. Tesaker

Your name: S. T. Lavender

Address: Acres Consulting Services Ltd.
5259 Dorchester Road, P. O. Box 1001
Niagara Falls, Ontario L2E 6W1

Comment:

From surveys of the accumulation of frazil ice under an ice cover, Tesaker has obtained the interesting result that the limit of frazil deposition is apparently reached when the Froude number in the central part of the flow under the deposition reaches a value of 0.08 to 0.14.

In order to test the possible universality of the result, the data from similar surveys on the Madawaska River near Ottawa have been similarly analyzed. Although the Madawaska surveys did not have the advantage of constant water levels and also had large daily variations in discharge due to upstream hydro-electric power operations, a similar result was obtained; that is, Froude numbers in the range of 0.06 to 0.16.

The lower value obtained may simply indicate that the equilibrium profile had not yet been obtained. The higher value was obtained for an ice survey period in which discharges were somewhat above the daily average. Using the corresponding daily mean discharge reduced the higher Froude number to within the range of Tesaker's values. This seems reasonable if one thinks in terms of a "dominant" discharge defining the limit of frazil deposition. That is, brief daily periods of discharge at moderately different discharges would not be expected to alter the deposit profile appreciably because of the lack of time to attain a new profile for the case of lower discharges and because of higher "static" resistance to movement of already deposited frazil being able to withstand the higher discharges.

It would be interesting to have more data from other sites to further test the value of this Froude criterion.

At first glance, the relevance of the Froude number is not immediately evident. However, its relevance can be rationalized if one considers:

(i) the Froude number (ratio of inertia to gravity forces) is roughly equivalent to a densimetric Froude number (ratio of inertia to buoyant forces) for nearly constant values of density difference between the frazil and water

(ii) the shear forces acting to resist the continual movement of a mobile frazil particle are no doubt related to the buoyant forces acting to hold the particle against the underside of the ice cover.

Thus, the Froude number is a measure of the ratio of inertia forces acting on the frazil to the forces acting to resist movement of the frazil. At the limit of deposition, these forces would be in equilibrium.

THIRD INTERNATIONAL SYMPOSIUM ON
ICE PROBLEMS
Hanover, New Hampshire, USA

ICE CONTROL STUDY
LAKE ST. FRANCIS – BEAUHARNOIS CANAL
QUEBEC – CANADA

Messrs	F. Boulanger, Eng.	LaSalle Hydraulic Laboratory	Montreal, Que.
	E. Dumalo, Eng.	The St. Lawrence Seaway Authority	Montreal, Que.
	D. Le Van, Eng.	Hydro-Quebec	Montreal, Que.
	L. Racicot, Chief	Hydro-Quebec	Montreal, Que.

Canada

1. INTRODUCTION

The capability of the easternmost section of the St. Lawrence Seaway, the South Shore Canal located between Montreal and Lake St. Louis, to serve vessels under severe weather conditions had been improved with the completion of a 3 million dollar construction program by the St. Lawrence Seaway Authority. These modifications were carried out over a period of six years beginning in 1965.

The duration of the navigation season has varied from 229 to 272 days since the opening of the Seaway in 1959. Dates for closing ranged from December 3rd to December 23rd, and those for opening ranged from March 26th to April 25th. The opening date of April 25th occurred in 1959, and was exceptional.

Presently, a major concern of winter navigation and power generation is the movement of vessels through the channels which are shared with Power Authorities and where floating ice booms are used to promote the formation of a stable ice cover, maintain water levels, and ensure regulated flows to the powerhouse.

The Beauharnois Power Canal was built in 1932, with a design to allow for a future navigation channel 600 feet (183 m) in width. It links Lake St. Francis to Lake St. Louis and divides the flow with the St. Lawrence River, which flows are controlled by the Coteau Regulating Works. The canal is 15 miles (25 km) long, 3 300 feet (1 006 m) wide and 34 feet (10.0m) deep and supplies the Beauharnois powerhouse owned by Hydro-Quebec. A channel has been dredged along the north side of the power canal for navigation and is an integral part of the Seaway system. The St. Lawrence Seaway Authority has two locks juxtaposed to the powerhouse which is located some 25 miles (40 km) west of Montreal (see figure 1). The Beauharnois powerhouse has a low head and is also in the run-of-river category. The powerhouse operations are subject to an adopted plan promulgated by the International Joint Commission for the regulation of the St. Lawrence

River and Lake Ontario, and administered by the St. Lawrence River Control Board.

The canal is therefore shared by power and navigation authorities each having separate interests. However, they cooperate and work together with an aim to operate the canal in the most effective and profitable way. Sharing of this canal has generally presented few problems except for the periods corresponding to the opening and closing of navigation viz; December and March.

Working in close collaboration with the St. Lawrence Seaway Authority, Hydro-Quebec has managed to optimize winter production as a result of experience gained during the last 15 years. Discreet interpretation of water temperatures, frazil and ice formation, has significantly contributed to the optimization of power generation. By reason of this optimization, winter production can now reach 1 400 MW as compared to 1 500 MW in the summer. However, such results depend largely on care taken with the control of ice at the beginning of winter.

The main control of ice formation in the canal is made principally through a series of ice booms set at different strategic locations in conjunction with manipulations of flow. At the outset, these booms are installed from the south bank of the canal to the southern edge of the navigation channel. When the last ship has passed, the booms are extended across the navigation channel to the north shore. Then, when hydrometeorological conditions are favourable, the ice cover formation is on its way. The formation of the ice cover is accelerated by inducing ice floes from Lake St. Francis. Simultaneously, a reduction in flow is necessary for the formation of a stable and smooth ice cover. A complete ice cover in the power canal will preclude further heat transfer thereby eliminating frazil and ice generation, and attendant ice jams. This operation usually takes one week.

A second aspect deals with break-up conditions and potential ice jams. A reduction of flow at that time in the power canal results in an increase of discharge in the St. Lawrence River with a possible risk of flooding the river banks.

2. OBJECTIVES OF STUDY

A joint team from the St. Lawrence Seaway Authority and Hydro-Quebec had been set up to explore the areas of mutual concern relating to the combined use by navigation and power of the Beauharnois canal during the critical periods in the spring and early winter seasons.

Some improvements to existing booms have already been introduced and it has been concluded that another boom is required at the entrance to the power canal. The LaSalle Hydraulic Laboratory was commissioned to undertake a hydraulic model study for the proposed boom. The objectives are:

- to retain ice from Lake St. Francis until required for the formation of an ice cover in the power canal;
- to allow passage of vessels until the end of the navigation season;
- to control ice movement during spring break-up.

One of the main criteria was to permit a vessel to pass through the boom system via an opening which would allow ice to arch over the opening, thereby precluding the use of complex closure mechanisms.

Realization of the foregoing objectives would help in firming-up the closing date of the navigation season, and it is anticipated that an earlier opening of the season may also be achieved in this area. Furthermore, such a control would be benefical to power generation.

3. TESTS AND RESULTS FROM THE HYDRAULIC MODEL STUDY

The studies described herein were performed on a hydraulic model reproducing an area of 2.5 miles (4km) by 3 miles (5.0km) of the lower end of Lake St. Francis as well as a reach of about 2.5 miles (4km) of the Beauharnois Canal to the Valleyfield Bridge. The model was constructed with a distortion ratio of 4, having a horizontal scale of 1/600 and a vertical scale of 1/150. The overall dimensions of the model were 50 feet by 25 feet (16 m x 8 m).

For all flow conditions simulated on the model, the water level of Lake St. Francis was maintained at 152.3 feet IGLD, and calibration was done at a simulated flow of 250 000 cfs (7 080m^3/s). Current patterns and velocities on the model corresponded quite well with the actual surveys.

Preliminary investigations were first carried out in order to detect the general behaviour of an ice boom at the entrance of the canal. The basic criteria retained for the location of that ice boom were as follows:

- the boom should permit an unrestricted passage of vessels;
- the boom should permit a rapid ingress of ice floes when it is desirable to form an ice cover in the canal;
- the boom should not affect power generation by an increase of head loss in the canal during winter operations;
- the overall length of the boom system should be kept to a minimum while still fulfilling the foregoing criteria.

To allow passage of vessels an opening was located in the boom system on the centerline of the navigation channel. To evaluate the efficiency of the ice boom with respect to its capability of retaining ice without interrupting the passage of vessels, a correlation was established for the time elapsed between the passage of a vessel and the re-formation of a natural ice arch at the opening. For a given flow and a given ice block dimension, a relationship was also established for various gaps in the boom and the time interval corresponding to a closure of these gaps by natural arching.

Ice was simulated by square pieces of thin polyethylene sheet plastic of a specific gravity identical to ice. Cohesion is not reproduced with this material and corresponds therefore only to ice conditions where cohesion could be neglected, like during warmer periods or in the springtime. However, ice floes simulated were relatively large (35ft x 35ft x 3ft or 11 m x 11 m x 1 m and 20 ft x 20 ft x 1.5 ft or 6 m x 6 m x 0.5 m) which corresponded to large pieces of ice and also to the agglomeration of smaller ice blocks which at times culminate in ice floes.

Proposed Boom Layout

After testing several boom configurations, a satisfactory layout which complies best with the aforementioned requirements was found. The proposed boom arrangement, which is located about 1/2 mile (0.8km) from the entrance of the canal, runs southward from Grosse Pointe Island across the navigation channel towards the southern bank of Lake St. Francis, as shown on figure 2 and photograph. 1. A maximum flow of 265 000 cfs (7 500 m^3/s) was first used to establish the layout and was decreased to 160 000 cfs (4 530 m^3/s) to simulate flow conditions during the period of ice cover formation. The corresponding velocities were 2.0 fps (0.6 m/s) and 1.5 fps (0.5 m/s) respectively.

With regards to an opening in the boom for ship passage, the model tests indicated that the time required for the natural arching of ice floes varied with the opening width. Numerous other tests concerning arching across the navigation opening were carried out introducing other parameters such as ice coming solely from a ship's track in a solid lake cover (see photograph. 2), wind, and the size of ice floes. None of these tests precluded the possible need for constricting the navigation opening during part of the cold weather navigation period. Results of these tests can be summarized as follows:

- In the case of a fragmented ice cover formed by 35ft x 35ft (11 m x 11 m) floes, natural arching of a 200 foot (60m) opening occurred in 30 minutes (see figure 3), whereas at 250 feet (76 m) it took 60 minutes, in the absence of wind and under flow conditions of 265 000 cfs (7 500 m^3/s);
- For the same conditions, the time required for arching over a 300 foot (92 m) opening was in the order of 4 hours;
- In the case of a narrow strip of fragmented ice cover representing a ship passage, arching of 35ft x 35ft (11 m x 11 m) ice floes occurred within an hour for a 350 foot (107 m) gap (see figure 3);
- When 20ft x 20ft (6.1m x 6.1m) ice floes are simulated, natural arching occurs within an hour for a 200 foot (61m) gap in the case of a fragmented ice cover. An hour is also required for arching a 300 foot (92 m) gap in the case of a narrow strip representing a ship passage;
- Except for large boom openings, flow variations did not significantly affect the time required for natural ice arching.

These findings underline a possible need for constricting the navigation opening in the boom during part of the cold weather period of navigation. The basic requirement for a navigation opening through the boom is 500 feet (152 m) which opening should be maintained, ice conditions permitting.

Wind effects on the ice boom layout were also investigated and an evaluation of the ice ingress through the gap was also made in order to estimate the progression of the ice cover in the canal. It was found that:

- The prevailing wind (in the direction of the canal entrance) generally hindered natural arching at the boom opening;
- In the absence of natural ice arching, the ice ingress rate through a 250 foot (76 m) navigation opening in the boom, under flow conditions of 265 000 cfs (7 500 m^3/s) and 160 000 cfs (4 530 m^3/s) corresponded to a progression of the ice cover in the canal of about 1/2 mile (0.8km) and 1/4 mile (0.4km) per day, respectively (see figure 4).

Opening for Throttling of Ice

A second aspect o. the problem deals with the admittance of large volumes of ice when the time has come to form an ice cover in the canal. In this regard, a separate opening in the boom layout for the throttling of ice was contemplated (see figure 2 and photograph. 3). Results of tests for various opening widths, and wind effects are shown on figure 5. The tests were carried out at a flow of 160 000 cfs (4 530 m^3/s)with ice floe dimensions of 35ft x 35ft x 3ft (11 m x 11 m x 1 m). The effect of a northeast wid in slowing ice ingress via the opening is quite pronounced. Openings used on the model were 500ft (152 m), 750ft (229 m) and 1 000ft (305 m) wide; and the ice passing in this range of openings was equivalent to about 1 to 3 miles (1.6km to 4.8 km)of cover per day in the absence of wind. The arrangement shown on figure 2, was deemed to be the best of several with respect to ice volume, wind, and current.

Ice at Edge of Ship Track

The build-up of hanging dams at the sides of a ship track in an ice field is of vital concern to power generation in terms of potential head losses. A cursory examination of this action was undertaken using a model of one of the largest lakers in a 125 feet (38 m) wide channel. An ice field some 1.5 feet (0.5 m) thick, extending 1 200 feet (366 m) each side of the 125 ft channel was simulated for a flow of 160 000 cfs (4 530 m^3/s). Polyethylene blocks equivalent to a 6ft x 6ft x 1.5ft (1.8m x 1.8m x 0.5m) ice size were used. The model indicated that the tendency for ice to build up at the edges of the track decreased with an increasing number of passages. After a certain number of passages, the ice build-up at the edges prevented anymore ice to leave the ship track. Build-ups of 5 foot (1.5m) depth extending some 75 feet (23 m) were observed. These results are at best a guide only; inasmuch as that surveys by Hydro-Quebec indicated 8 foot (2.5m) thicknesses extending 30 feet (9.0 m) which build-ups were attributable to downbound ships in Lake St. Francis.

Ice Thrust on Boom

Forces on the proposed boom due to wind and ice were measured on the model for flow conditions of 265 000 cfs and under a westerly wind of 30 mph (48km/hr). Ice blocks equivalent to 6ft x 6ft x 1.5ft (1.8m x 1.8m x 0.5m) were used. Wind from the lake played a significant role; for example, at 30 mph the loading on the boom was increased by 50%. Extrapolations were made from the model test results for a 70 mph (113km/hr) wind, and the loading thereby indicated was in the order of 1 100 pounds per lineal foot (1 490 N/m. The model test results and supplementary theoretical calculations indicate that the wind loadings on a boom in Lake St. Francis are greater than the loadings on some of the booms in the canal proper.

4. CONCLUSIONS

The optimum total length of the proposed ice boom would be between 7 000 and 8 000 feet (2 150 m and 2 450 m), with provisions for a navigable opening varying in width from 250 to 500 feet (76 m to 152 m), and for a separate ice throttling section varying in width from 500 to 1 000 feet (152 m to 305 m). The operational details concerning the closing and opening (if required) of the navigable opening, have yet to be determined for compatibility with power generation and navigation requirements.

There are tangible benefits for Hydro-Québec and the St. Lawrence Seaway Authority which can be attributed to the proposed boom. The finite value of such benefits has not been calculated at this time, which value is being assessed right now by both parties. The estimated cost of the proposed construction is $2 000 000., using 1975 dollars.

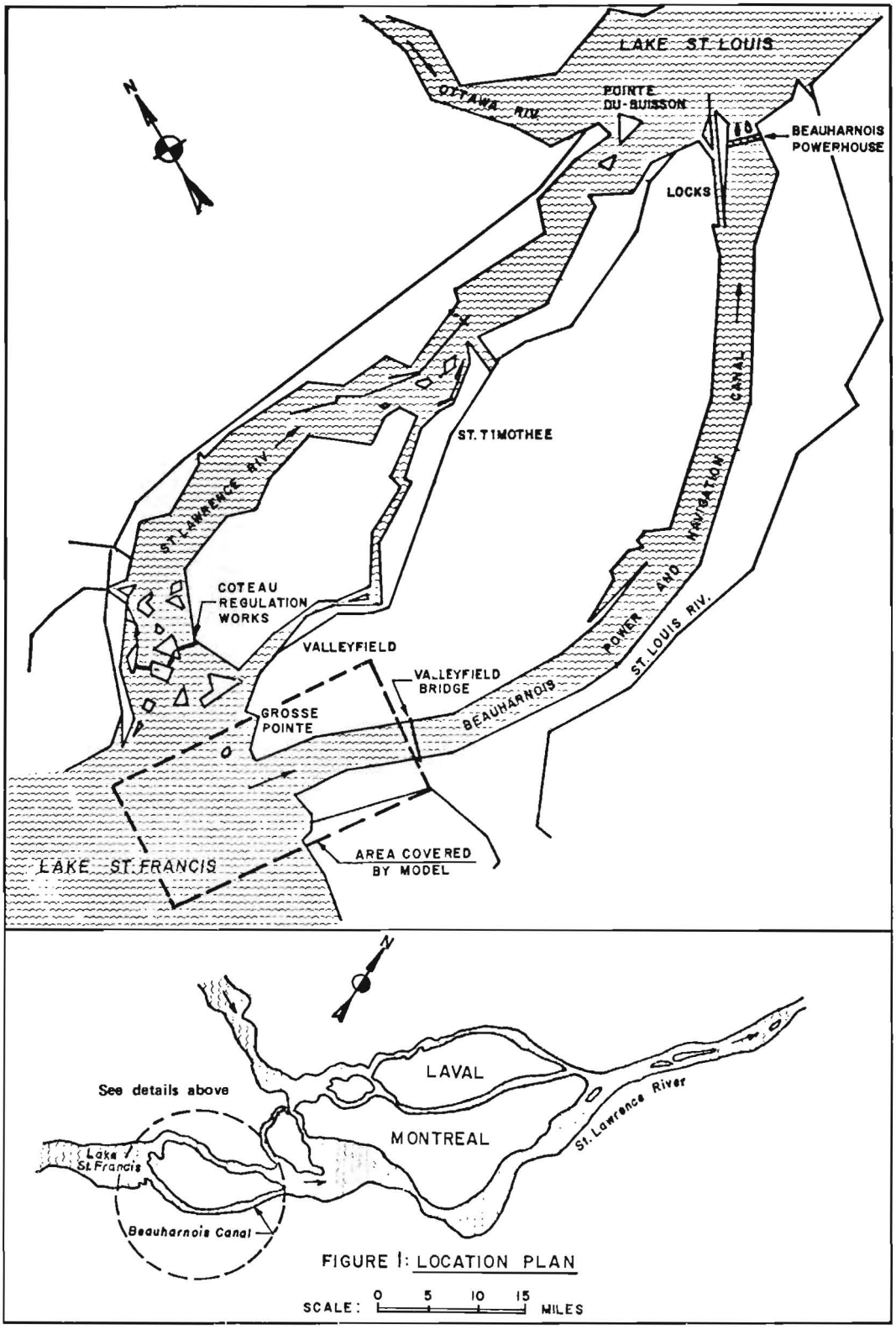

FIGURE 1: LOCATION PLAN

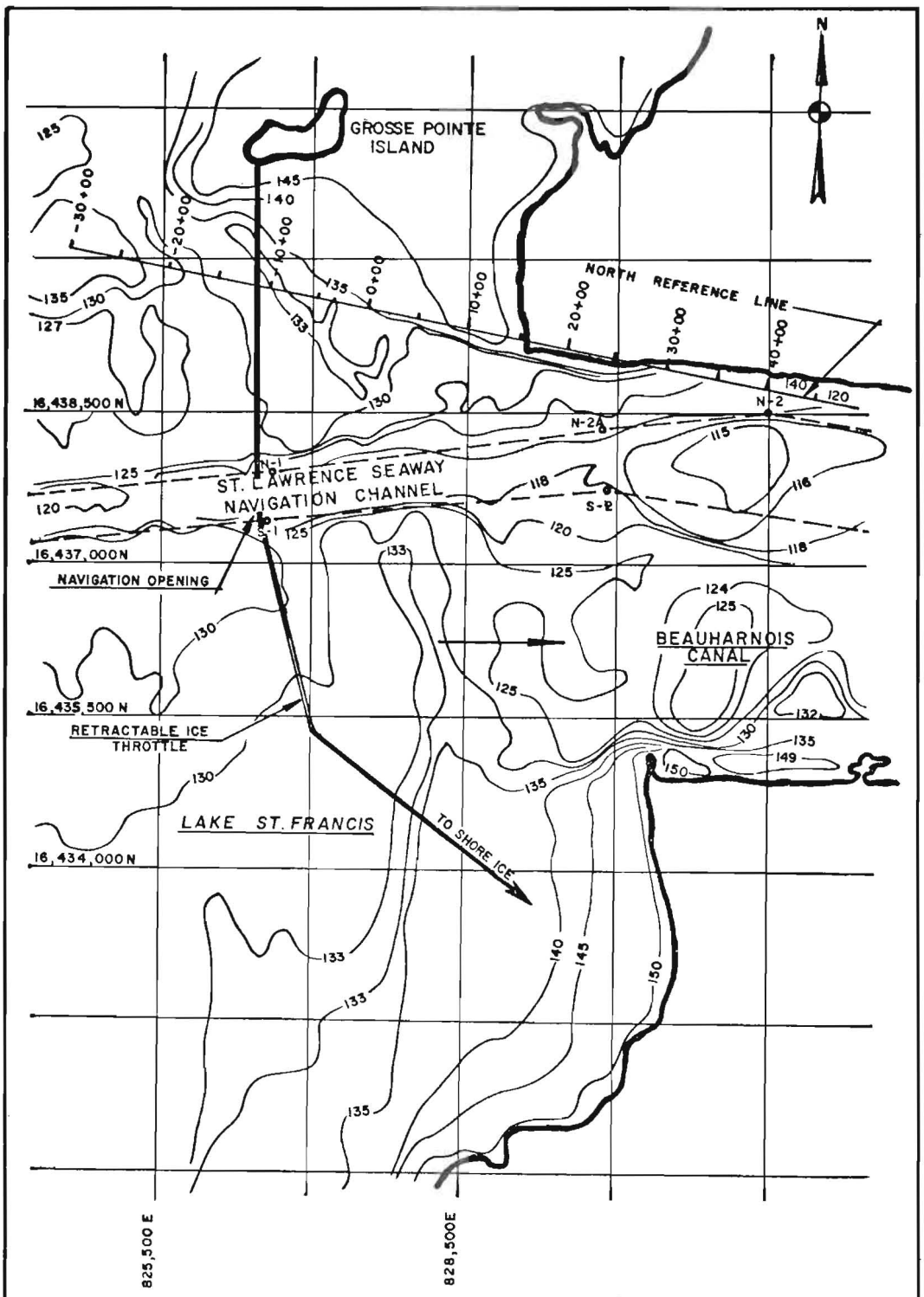

FIGURE 2: PROPOSED BOOM LAYOUT

SCALE: 1"=1500' — CONTOUR LINES IN FEET I.G.L.D.

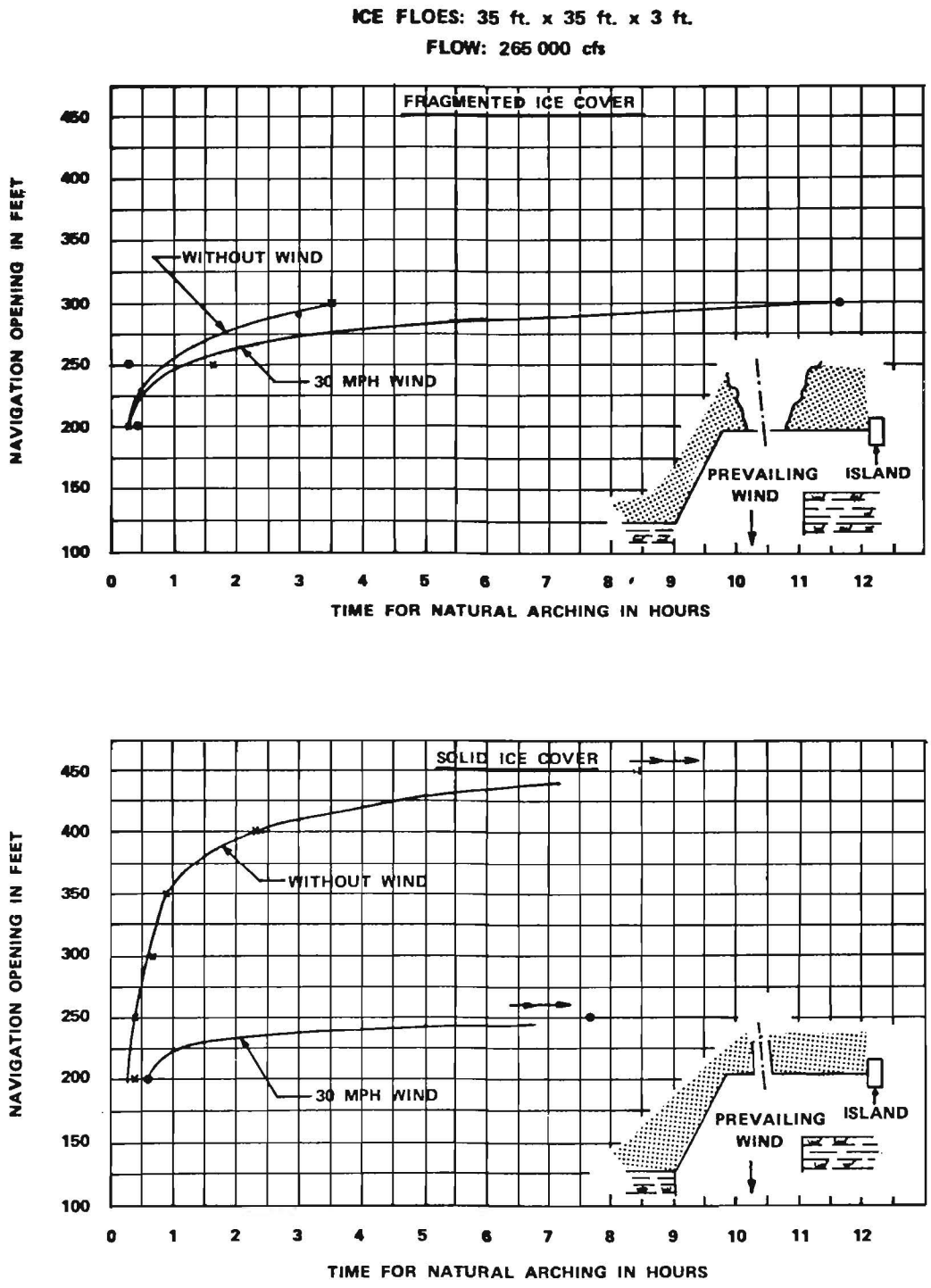

FIGURE 3
ICE ARCHING CURVES

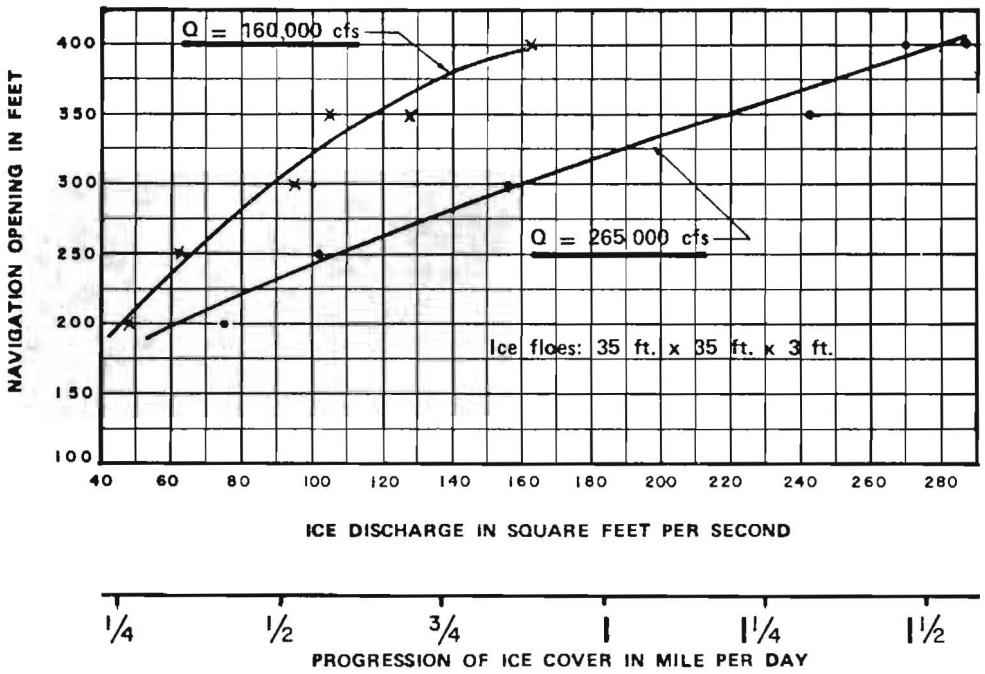

FIGURE 4 – ICE INGRESS VIA NAVIGATION OPENING

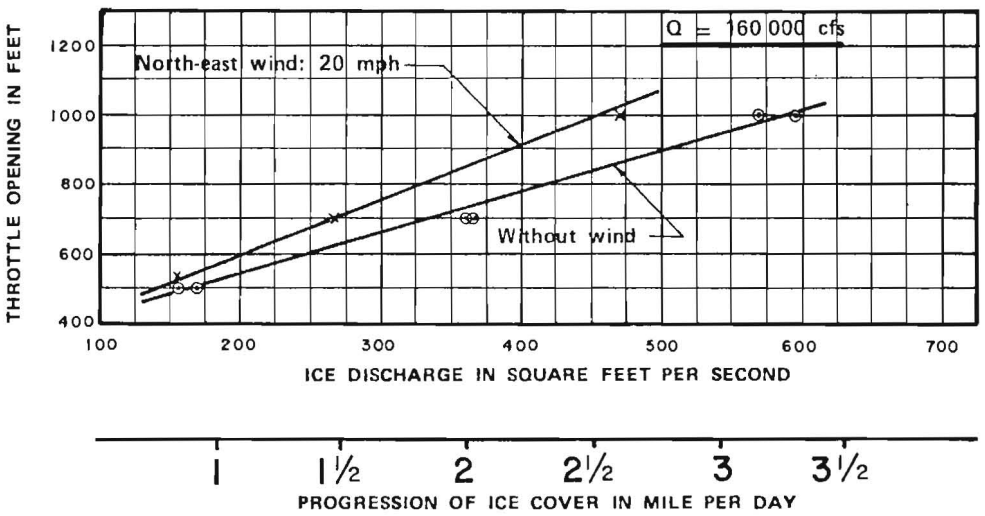

FIGURE 5 – ICE INGRESS VIA THROTTLE

PHOTOGRAPH 1

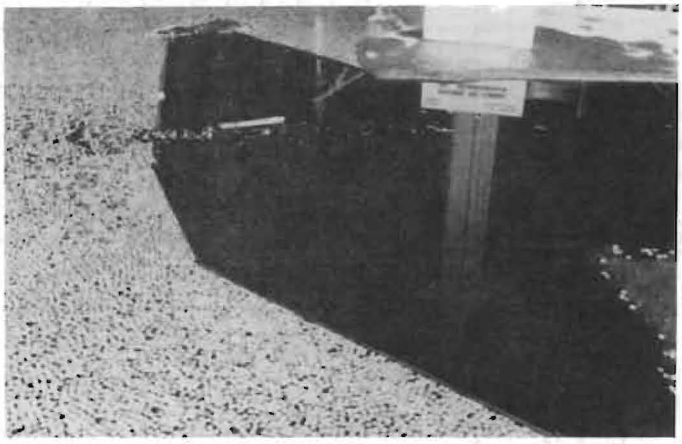

- Fragmented Ice Cover
- Navigation Opening

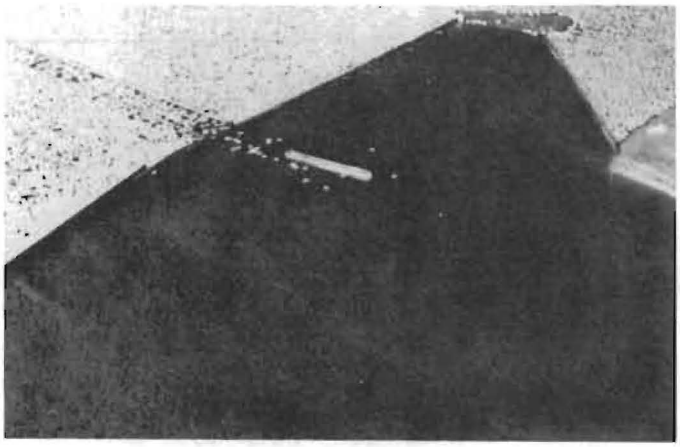

PHOTOGRAPH

- Solid Ice Cover
- Navigation Opening

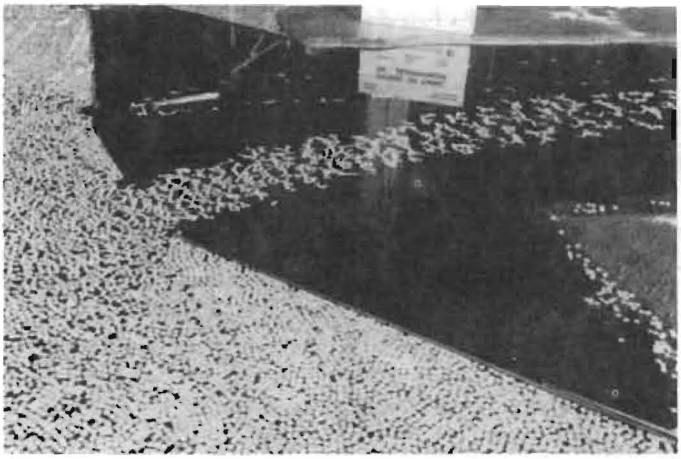

PHOTOGRAPH 3

- Fragmented Ice Cover
- Ice Throttle

THIRD INTERNATIONAL SYMPOSIUM ON
ICE PROBLEMS
Hanover, New Hampshire, USA

SIMULATION OF LOCK OPERATIONS DURING WINTER ICE MONTHS

James J. Peter, Engineer — ARCTEC, Incorporated — Columbia, Md. USA

Thomas V. Kotras, Senior Engineer — ARCTEC, Incorporated — Columbia, Md. USA

ABSTRACT

In any waterway system equipped with locks, the flow of traffic (ships per day) is constrained by the maximum service time of the least efficient lock. During winter, the service time of locks designed for temperate operations increases due to subfreezing temperatures and the presence of ice, thereby reducing the capacity of the system. If this service time increases to the point that the lock capacity is less than the demand for the use of the lock (ship arrival rate) a queue will form at the lock and grow indefinitely as long as the demand exceeds the capacity. In order to investigate the effects of winter conditions and ice on lock operations, a model was developed as part of the SPAN* Study to simulate their operations during both normal conditions and winter months. A description of the model is presented in this paper along with an example of the effect of required ice lockages on lock capacity.

BACKGROUND

In any waterway system equipped with locks, one of the important measures of performance is the system capacity (ships per day). This capacity is controlled by the slowest processing element which is generally the least efficient lock. The maximum number of ship lockages (N) that can be accomplished in a 24-hour day is given by:

$$N(\text{ships/day}) = t_d/t_\ell = (1440 - t_s - t_d)/t_\ell \qquad (1)$$

*"System Plan for All-Year Navigation"

where t_a = time available for locking each day (minutes)

1440 = minutes in a single day

t_s = average slack time per day (minutes)

t_d = average delay time per day (minutes)

t_ℓ = average time required to process one ship (minutes)

The maximum theoretical system capacity is achieved when the lock operates 24 hours per day with no slack or delay time and alternates between locking upbound and downbound ships. During winter, the processing time of locks designed for temperate operations increases due to sub-freezing temperatures and the presence of ice, thereby reducing the system capacity. If the required processing time increases to the point that the capacity is less than the demand (ship arrival rate) a queue will form at the lock and grow indefinitely as long as the demand exceeds the capacity.

As part of the engineering studies undertaken to investigate the economic feasibility of year-round navigation in the St. Lawrence Seaway, a model was developed to simulate the movement of ships through the Seaway [1]*. Included in that simulation was a computer lock model developed specifically to simulate lock operations during both normal and winter conditions for the seven locks in the Seaway. A diagram of a typical lock is shown in Figure 1 along with typical lock particulars.

LOCK MODEL DESCRIPTION

Overview

A conceptual block diagram of the lock model is shown in Figure 2. The model is comprised of two parts. The first part determines the ship transit time through the lock during normal conditions, while the second part determines time delays which result in increased transit times due to winter weather conditions and the presence of ice.

The data and understanding necessary to accurately model the decisions of real persons controlling the locks and ship traffic were obtained by direct contact with traffic controllers, lock operators, and the managers of the St. Lawrence Seaway Development Corporation (SLSDC) and the St. Lawrence Seaway Authority (SLSA). As a result of those discussions, the following rules and assumptions concerning Seaway lock operations were made:

1. Ships are processed so as to maximize the locks' utilization.
2. If queues exist on both sides of a lock, the lock will alternate between processing an upbound and a downbound ship.
3. Ships are processed from a queue on a first-come, first-serve basis.
4. A lock will turn back to lock through consecutive upbound (downbound) ships to maximize the locks' utilization.

---

* Numbers in brackets denote References listed at end of paper.

FIGURE 1

LOCK DIAGRAM AND PARTICULARS

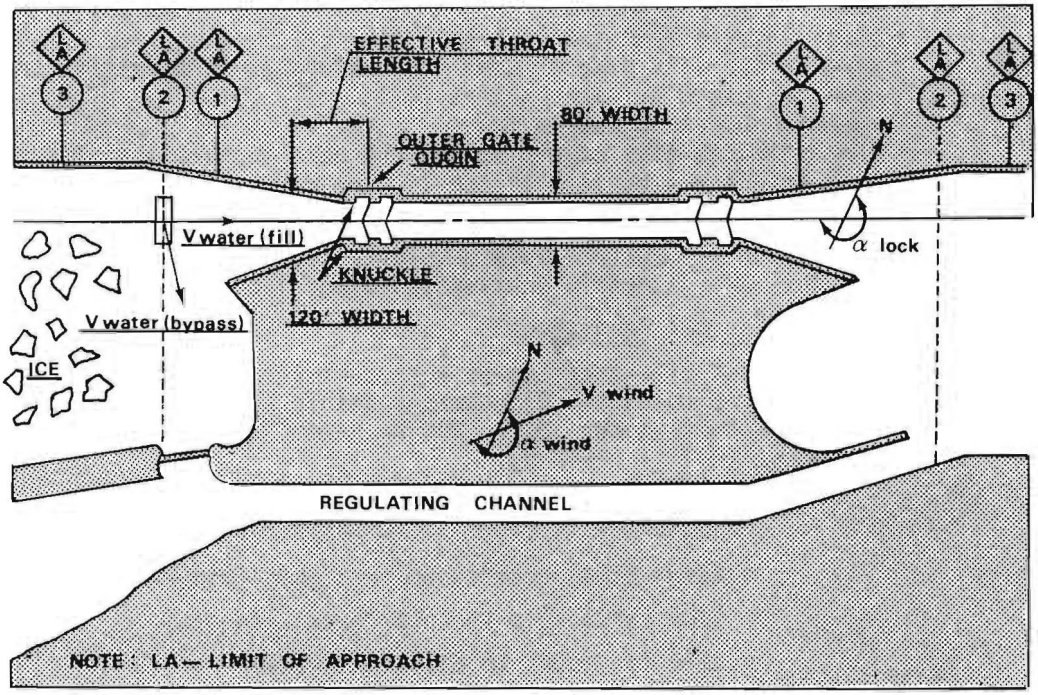

FIGURE 2

CONCEPTUAL BLOCK DIAGRAM OF LOCK MODEL

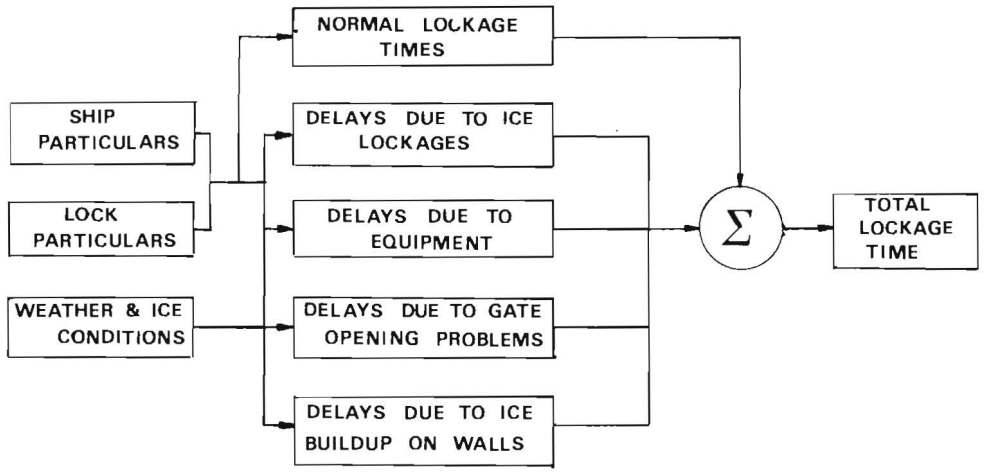

5. Tandem lockages are permitted provided the sum of the ships' lengths is 45 feet less than the usable length of the lock.

6. A ship will not be locked through if any of the following conditions occur between the lock and the next anchorage or lock wall:

   - visibility is less than one-half mile
   - wind velocity is greater than the designated wind restriction
   - next anchorage or lock wall is full
   - another ship is stuck in ice
   - the estimated time of arrival at the next anchorage or lock wall is after nightfall if the lighted navigation aids have been pulled from the river

While these rules and assumptions were developed specifically for locks in the Seaway, they are generally applicable to any lock.

Ship Lockage During Normal Conditions

The locking process of a ship begins when the stern of the ship passes LA2 (Limit of Approach No. 2) entering the lock and ends when its stern clears LA2 exiting the lock. During normal conditions, the lock processing time (t_ℓ) is given by:

$$t_\ell = t_{enter} + t_{gate\ closing} + t_{dump/fill} + t_{gate\ opening} + t_{exit} \quad (2)$$

where t_ℓ = total time required to lock ship (minutes)

t_{enter} = time for a ship to enter lock (minutes)

$t_{gate\ closing}$ = time for gates to close (minutes)

$t_{dump/fill}$ = time for lock to dump or fill (minutes)

$t_{gate\ opening}$ = time for gates to open (minutes)

t_{exit} = time for ship to exit lock (minutes)

While the gate opening and closing times and the dump or fill times are functions of the lock particulars, such as the required change in water elevation and the size of the filling and dumping culverts, the entrance and exit times are a function of the ship characteristics. For locks in the Seaway, with the exception of the Iroquois Lock:

$$t_{gate\ closing} = t_{gate\ opening} \cong 2 \text{ minutes}$$
$$t_{dump/fill} \cong 7 \text{ minutes} \quad (3)$$

during normal operating conditions. At Iroquois, because of its very small lift (0.5 feet), a walk-through procedure is used whereby a vessel proceeds, without securing, under its own power at a low speed. The lockage is therefore a smooth, continuous movement. An analysis of lock records from Cote St. Catherine Lock for December, 1971; April, 1972; and July, 1972, led to the following expressions for the entrance and exit times for inland ships (lakers) and ocean-going vessels (salties):

INLAND SHIPS

Direction	t_{enter} (minutes)	t_{exit} (minutes)
Upbound	$1.97 \cdot 10^{-4} \cdot (L \cdot B) + 6.58$	$1.04 \cdot 10^{-4} \cdot (L \cdot B) + 5.53$
Downbound	$2.59 \cdot 10^{-4} \cdot (L \cdot B) + 4.92$	$1.62 \cdot 10^{-4} \cdot (L \cdot B) + 4.07$

(4)

OCEAN-GOING SHIPS

Direction	t_{enter} (minutes)	t_{exit} (minutes)
Upbound	$1.50 \cdot 10^{-4} \cdot (L \cdot B) + 9.47$	$0.93 \cdot 10^{-4} \cdot (L \cdot B) + 5.88$
Downbound	$2.06 \cdot 10^{-4} \cdot (L \cdot B) + 5.86$	$1.99 \cdot 10^{-4} \cdot (L \cdot B) + 3.22$

where L and B are the length and beam of the ship respectively.

Ship Lockages During Winter Conditions

Winter operations generally bring about increased lock transit times because cold temperatures and ice interfere with normal lock procedures and machinery operations resulting in the following types of delays:

- increased equipment failures
- ice lockages
- increased fill time
- gate opening delays
- removal of ice build-up on lock walls

Because of these delays, the lock processing time during winter conditions can be expressed as:

$$t_{\ell} = t_{enter} + t_{gate\ closing} + t_{dump/fill} + t_{gate\ opening} + t_{gate\ delay} + t_{exit} + t_{ice\ lockage} + t_{wall\ scraping} + t_{equipment\ failure} \quad (5)$$

where: t_{enter}, $t_{gate\ closing}$, $t_{dump/fill}$, $t_{gate\ opening}$, t_{exit} are components of the normal lockage time given by equation (2)

$t_{gate\ delay}$ = additional time required to open lock gates in the presence of ice (minutes)

$t_{ice\ lockage}$ = time required to lock ice through ahead of a downbound ship (minutes)

$t_{wall\ scraping}$ = time required to scrape walls when ice buildup prevents further lockages (minutes)

$t_{equipment\ failure}$ = time required to repair equipment (minutes)

Each of these delays are discussed in the following sections.

Increased Equipment Failures: Equipment failure at a lock may be described by the Mean Time Between Failures (MTBF). The actual time between failures will occur in a normal distribution around the MTBF with a standard deviation of σ_{MTBF}. At each failure, there will be an asso-

ciated mean delay time of $\bar{t}_{fail}$. The value of MTBF decreases as temperature increases while the value of $\bar{t}_{fail}$ increases as temperature decreases. The probability of a failure occurring at any given time t_1 is highest when t_1-t_0 equals MTBF (where t_0 is the time of the previous failure) and decreases according to a normal distribution when t is greater than or less than t_1. If P_1 is a random number evenly distributed between 0 and 1 chosen at time t, then failure occurs at time t_1 if P_1 is less than or equal to P_0, where

$$P_0 = \frac{h}{\sqrt{\pi}} \int_{-\infty}^{t_1} e^{-h^2(t-\text{MTBF})^2} dt \tag{6}$$

$$h = 1/\sqrt{2}\ \sigma_{\text{MTBF}}$$

Thus:

$$t_{\text{equipment failure}} = \begin{cases} \bar{t}_{fail} : \text{if } P_1 \leq P_0 \\ 0 \quad : \text{if } P_1 > P_0 \end{cases} \tag{7}$$

Ice Lockages: In winter, brash ice will exist in the shipping channel above the lock. If the upstream throat of a lock is filled with some of this ice, a downbound ship will push a portion of the ice into the lock. If the length of the downbound ship plus the length of the plug of ice pushed into the lock is greater than the usable length of the lock, the ice must be locked through separately before the ship is locked through. To determine the need for an ice lockage, the amount of ice in the upstream throat of the lock and the portion that is pushed into the lock by the vessel must be determined.

The amount of ice in the upstream throat is a function of the amount and type of ice upstream of the lock and the wind speed and direction. For example, if there is a large amount of broken ice upstream of the lock and the wind is blowing from the upstream direction, the throat will be full of ice, whereas if the wind is blowing from the downstream direction, the throat will be free. The details for determining the amount of ice in the upstream throat of the lock are given in Reference [2]. To proceed with the analysis, if the amount of ice in the throat is defined as A_t, the percentage of ice pushed into the lock by a ship depends on the total clearance (d) between the sides of the ship and the lock walls. The following relation expresses the amount of ice (A_ℓ) pushed into the lock, based upon the qualitative experience of persons associated with the operation of locks in ice conditions:

$$A_\ell = P * A_t \tag{8}$$

where

$$P = \begin{cases} 0 : \text{when } d \geq \text{Lock Width}/2 \\ 1.0 - \dfrac{d^2}{(\text{Lock Width}/2.)^2} : \text{when } d < \text{Lock Width}/2 \end{cases} \tag{9}$$

An ice lockage is assumed to be required if the length of the ship (L) plus the length of the ice pushed into the lock (L_{ice}) is greater than the usable length of the lock (L_{usable}), where $L_{ice} = A_\ell$/Lock Width.

The time required for an ice lockage consists of the normal gate closing and opening times (2 minutes each, 8 minutes total), the normal dump time (7 minutes), a fill time appropriate for the upstream conditions, plus time required to flush the ice out of the lock chamber. A somewhat slower fill rate is required to avoid excessive turbulence at the water intake ports, since the ship to be locked through will be tied up close to the lock. An increase from 7 minutes to approximately 11 minutes is usually sufficient. When an efficient ice flushing system which feeds water from the upper gate sill is available, the ice may be flushed from the lock in 5 minutes. On the other hand, if the normal filling ports must be used, a flushing time of 20 minutes is required with 20 percent of the ice remaining in the lock because the filling ports feed only the center 50 percent of the lock. The flushing time (t_{flush}) can be expressed by:

$$t_{flush}(\text{minutes}) = 5 + (1-C) * 15 \qquad (10)$$

where C is a measure of the efficiency of the flushing system (0 to 1). A typical ice lockage therefore requires at least 31 minutes.

Increased Fill Time: During the filling of a lock, ice upstream of the lock is drawn into the upstream throat. The lock operator keeps an eye on the movement of ice, and if he judges the movement to be too fast he will cut back on the fill rate. In making this judgment, he considers the amount of ice in the throat and the length of the ship which is waiting for a downbound lockage. The model, in determining the increased fill time, begins by analyzing the amount of ice which will be drawn into the throat for a 7 minute fill. If this amount of ice will require an ice lockage, the program recycles itself using an 8 minute fill time and continues to recycle up to a maximum of 15 minutes until the amount of ice that would be in the throat is less than that requiring an ice lockage. In determining this slow fill time, the model considers the influence of wind velocity, water fill velocity, and water bypass velocity. The details of the iteration routine are given in Reference [2]. For the Seaway, a typical slow fill time is approximately 15 minutes.

Gate Opening Delay: Ice on the upstream side of both sets of gates may delay the opening of the gates if it becomes trapped in the gate recesses. A clearance of approximately 46 feet is required for the gates to swing freely. Surface flow developers such as air bubbler systems are used in the gate recesses to push out the ice. From quantitative discussions with lock operators, the following expressions for the gate opening delays were developed:

$$t_{\text{gate delay}}(\text{minutes}) = (D \times 30)e^{-2V_{surf}} \qquad (11)$$

where $$D = A_{ice}/(L_{avail.} \cdot W) \qquad (12)$$

$$A_{ice} = \text{area of ice to be moved } (ft^2) \qquad (13)$$

$L_{avail.}$ = length of area available for containing ice (ft)

W = width of lock (ft)

V_{surf} = surface flow velocity (ft/sec)

In actual operation gate opening delays occur with some randomness and therefore the lock model allows delays to occur only when a randomly generated number was less than D.

Ice Buildup on Lock Walls: A ship entering the lock from upstream will push some ice ahead of it. Part of that ice flows aft along the sides of the ship and adheres to the lock walls. Continued pressure from subsequent lockages causes the ice to build up to a thickness that will reduce the effective lock width and prevent the passage of large beam ships. The thickness of the ice adhering to the lock walls after a ship passage is dependent on the air temperature, the mean ice piece size (usually 6 to 12 inches), and the total clearance between the sides of the ship and the lock walls. Analytical data to support an equation was not available but the following equation is consistent with lock operators' experience [2]:

$$y = 9.77 * 10^{-9}\, d\left(\frac{W}{2} - d\right)^5 \left(1 - e^{-.03(32.1 - \theta_{air})}\right) e^{-\overline{X}} \qquad (14)$$

y = ice thickness on lock walls (ft)

W = lock width (80 ft)

d = effective lock width - beam of ship (ft)

θ_{air} = air temperature (°F)

$\overline{X}$ = average ice piece size (ft)

The lock model calculated y as if there was no ice on the wall and then added that amount to whatever ice was already on the wall. When the total thickness was found to be equal to or greater than the clearance required by a ship (d), lockages ceased until all of the ice could be scraped from the lock walls.

LOCK CAPACITY

As previously stated, one of the important measures of performance of a waterway system equipped with locks is the capacity in ships per day as expressed by equation (1). If the average daily slack and delay times are assumed to be zero, the capacity is given by

$$N(\text{ships per day}) = 1440/t_{\ell} \qquad (15)$$

where t_{ℓ} is the average time to process a single ship. Expressed mathematically

$$t_{\ell} = \frac{N_d * t_{\ell_d} + N_u * t_{\ell_u} + t_{\text{ice lockage}} * \frac{N_d}{R} + t_{\text{turnback}} * |N_d - N_u|}{N_d + N_u} \qquad (16)$$

where: $N_d : N_u$ = mix of downbound ships : upbound ships

t_{ℓ_d}, t_{ℓ_u} = downbound and upbound lockage times

R = number of downbound ship lockages per ice lockage

In equation (16) delays due to gate openings and slow fill are included in t_{ℓ_d} and t_{ℓ_u}. However, delays due to equipment failure and lock wall scraping have been neglected.

To illustrate the effects of winter operations, consider an inland ship with a length of 730 feet and a beam of 75 feet with the following locking time components:

	NORMAL OPERATIONS		WINTER OPERATIONS	
	upbd	dwnbd	upbd	dwnbd
t_{enter}	17.4	19.1	17.4	19.1
$t_{gate\ closing}$	2.0	2.0	2.0	2.0
t_{dump}	0	7.0	0	11.0
t_{fill}	7.0	0	11.0	0
$t_{gate\ opening}$	2.0	2.0	2.2	2.2
t_{exit}	11.2	12.9	11.2	12.9
t_{ℓ}	39.6	43.0	43.8	47.2

$t_{turnback}$ = 11 minutes

$t_{ice\ lockage}$ = 31 minutes

Using equations (15) and (16), the effect on lock capacity of the ice conditions' severity can be investigated by varying R. The results are shown in Figure 3. The need for ice lockages, as seen in Figure 3, can reduce the capacity significantly. For all downbound traffic, the capacity can drop from 26.7 ships per day to 16.1 ships per day if an ice lockage is required for every ship. In terms of gross registered tonnage, 259,000 tons can be processed as opposed to 429,000 tons during normal conditions if each ship is assumed to be 16,065 gross registered tons.

SUMMARY

The model as developed provides a tool to be used for determining the effects of winter conditions on lock operation, ship transit time, and system capacity. The model can be used to identify problems associated with the lock and then to evaluate various proposed levels of improvements. The model can therefore play an important role in the process of planning for these improvements by providing a rapid and economical means of evaluating the impact of alternative levels of improvements.

FIGURE 3

CAPACITY VERSUS NO. OF DOWNBOUND TRANSITS / ICE LOCKAGE

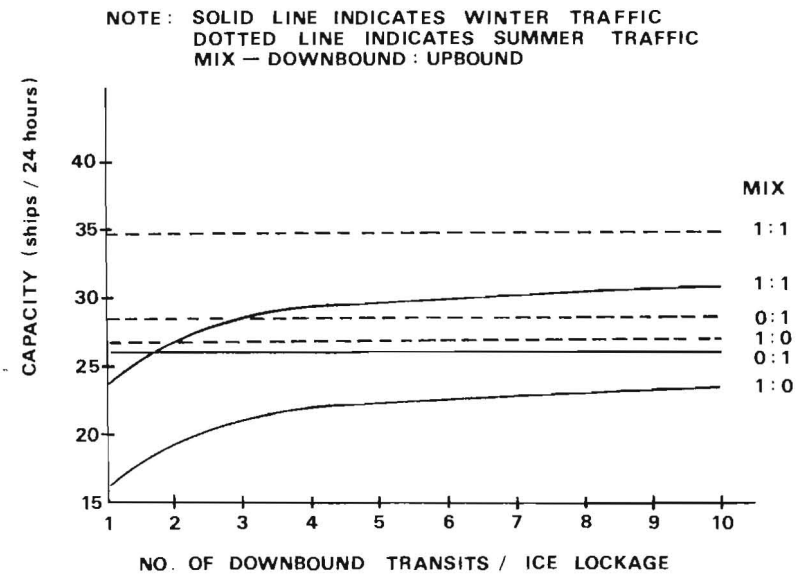

REFERENCES

1. Kotras, T., Lewis, J.W., and Robb, D.C.N., "St. Lawrence Seaway: A New Goal of Year-Round Navigation," Symposium on Modeling Techniques for Waterways, Harbors, and Coastal Engineering, September, 1975.

2. Lewis, J.W., "St. Lawrence Seaway System Plan for All-Year Navigation," St. Lawrence Seaway Development Corporation, TR105-7, July, 1975.

THIRD INTERNATIONAL SYMPOSIUM ON
ICE PROBLEMS
Hanover, New Hampshire, USA

COST COMPARISONS FOR LOCK WALL DEICING

Darryl J. Calkins	Research Hydraulic Engineer	USACRREL Hanover, NH
Malcolm Mellor	Research Civil Engineer	USA

ABSTRACT

Lock wall icing conditions on the Great Lakes and St. Lawrence Seaway are described, and possible solutions are listed. Operating assumptions are laid down as a basis for consistent cost estimates, and selected deicing methods are considered, using figures condensed from a more detailed report. The estimates cover wall heating by embedded electrical cables and embedded fluid circulation systems, repetitive surface coating with salt solutions, deicing with an inflatable boot, scraping with backhoes, cutting with large chain saws, and slicing with high pressure water jets.

Initial costs vary from zero for contract arrangements, to over $600,000 for a deicing boot. Average annual cost, which covers direct operating costs plus an allowance for amortization, ranges from less than $4000 for a salt dispenser to more than $80,000 for a deicing boot. The chain saw concept, which has not yet been tested, appears to be positive and economical, with average annual costs less than $10,000. The feasibility of deicing with salt solutions has not been investigated experimentally, but there is a strong economic motivation to make suitable field tests. The relative attractions of other methods will depend to some extent on the particular circumstances at various locks.

COST COMPARISONS FOR LOCK WALL DEICING

Darryl J. Calkins and Malcolm Mellor

INTRODUCTION

During the winter of 1974-75, USACRREL investigated three different methods for removing ice collars from lock walls, and gave some consideration to additional possible methods. In order to guide further development work, it was necessary to assess the relative merits of all methods which appeared practically feasible, and in particular to consider the economics of competing concepts.

It is hardly possible to make an absolute economic comparison, as different lock systems are situated with respect to climatic conditions, energy costs, and logistic circumstances. However, a representative situation can be defined for locks on the Great Lakes and the Saint Lawrence Seaway, and it was felt that this could be used as the basis for cost comparisons that would identify methods that are either inherently expensive or inherently economical. Because cost figures are strongly dependent on the assumptions made for the accounting exercise, the costs given in this paper should be taken in a comparative sense, and it should be recognized that different conclusions might be reached with radically different starting assumptions.

In a short paper, itemized costs cannot be covered in detail. For a more complete discussion, the reader is referred to Calkins and Mellor[1] (1975).

PROBLEM DEFINITION

During winter operation of locks, collars of ice form along the lock walls, reducing the effective width of the lock and restricting ship movement. The thickness of the ice collars has to be reduced so as to permit efficient operation of the lock throughout the winter season.

Two distinct processes contribute to the formation of ice collars: (i) direct freezing of water on a cold wall, and (ii) compaction and adhesion of ice debris on a cold wall during ship passage. There may also be combined processes: e.g. floating ice may freeze on to the wall, or adhering ice debris may be consolidated by infiltration and freezing.

---

[1] Calkins D.J. and Mellor M., "Preliminary Economic Analysis of Lock Wall De-icing Methods", USACRREL Internal Report 444, May 1975, Hanover, NH.

The operational requirement is for the walls to have a maximum of 3 in. of ice whenever a wide ship enters the lock. This requirement can be met either by preventing formation of ice collars, or by periodically removing the collars at a frequency determined by traffic, taking due account of weather conditions.

POTENTIAL SOLUTIONS

There are a number of possible solutions to the problem of lock wall icing. They include the following but not limited to:

1. Avoiding or minimizing ice collar formation by modification of operating procedures. The crucial point is that the lock wall must be cooled below 0°C before significant ice adhesion can develop, and it is unlikely that a submerged portion of the wall will undergo the necessary cooling. Thus there is a strong incentive to hold the lock at the highest feasible water level during the long intervals between ship passages.

2. Built-in wall heating. Ice adhesion can be prevented by maintaining wall temperature above 0°C, or ice collars can be shed periodically by raising the wall temperature intermittently. Possible arrangements include embedded electrical heating cables, conductive surfacing materials, and internal piping or ducts for warm fluids.

3. Surface coatings. There are a variety of surface coatings that are intended to minimize ice adhesion, but three broad classes of materials can be distinguished: (i) "ice-phobic" coatings, such as PTFE or polyethylene, that give low bond strength, (ii) "sacrificial" coatings, such as oils and greases, that shed part of their thickness and allow the ice to separate, (iii) ice-melting substances that have to be continually replenished.

4. Built-in mechanical devices. Inflatable deicing boots, once commonly fitted to aircraft, have been proposed for lock-wall deicing. There might conceivably be other types of built-in mechanical equipment capable of shedding ice collars, e.g. vibratory panels.

5. Mechanical removal with contact tools. At present, ice collars are removed by scraping the wall vertically with a backhoe. More effective mechanical tools could be built in the form of chain saws, slot millers, face millers, or possibly percussive tools, the object being to cut the ice close to the interface.

6. Removal with non-contact tools. At present, low pressure steam jets are used for limited deicing in the vicinity of lock gates. More rapid cuts near the interface can be made with flame jets or high pressure water jets. More exotic possibilities include lasers, plasma torches, or explosive jets.

7. Combination methods. In a practical operating scheme it is quite likely that two or more of the above concepts would be applied together. For example, if No. 3 were to be adopted, there might well be a need for a more positive device to complete the removal process. No matter what method is adopted, it would be foolish to ignore No. 1.

ASSUMPTIONS FOR PRELIMINARY COSTING

In order to compare capital costs and operating costs for the various methods that could be used for de-icing, certain assumptions have to be made and they are listed below.

1. Ice collar dimensions - A strongly bonded collar for the first 3.0 ft of vertical extent with an additional 3.0 ft of unbonded section, giving a total depth of 6.0 ft. The length of one wall is taken as 1000 ft and it is assumed that both walls are to be treated (ignoring orientation effects).

2. Formation rates - In the absence of any firm information, it will be assumed that complete ice collars can form or re-form within a few hours once the wall has been sufficiently chilled.

3. Frequency of ice collar removal - For present purposes it is assumed that the ice collar will have to be removed once a day during the ice season. The ice season is taken as 90 days.

4. Rate of removal - In the absence of information on required removal rates, it is assumed that a 6 hour period is available for cleaning the two walls of a lock.

5. Available facilities. It is assumed that electrical line power will be available at the lock at a cost of 3¢/kw-hr and that both lock wall esplanades will be accessible by vehicles. It is also assumed that the esplanades will be kept substantially free of snow.

6. Installation costs - Materials, labor, supervision and engineering are all included.

7. Operating costs - An annual maintenance figure, labor, and energy costs are considered.

DE-ICING SYSTEMS

Wall Heating:

The major expense for any built-in well heating system is likely to be the capital cost of installation. The writers have not attempted any detailed design work in wall heating systems, but the order of cost can probably be estimated from simple conceptual designs. Three methods were considered; i) embedded electrical heating cables, ii) hot

fluid circulation, and iii) conductive panels attached to the existing wall. The latter may be undesirable because of the potentially high shearing force caused by the ice and ship reacting with the panel (attachment problems).

One factor that has to be considered in a built-in system is variation of water level in the Great Lakes. It appears that, over long periods, maximum water level has changed as much as 2.6 ft, and therefore the datum for high pool elevation in a lock could change significantly. In the following estimates we have made a 2 ft allowance for changes in lake level, i.e. the heated belt of wall is 2 ft greater in vertical extent than it would need to be if the ice always formed at exactly the same level. The total depth of coverage on the wall is taken as 5.0 ft. A design power level of 30 watts/ft^2 is used in all calculations.

Surface Coatings:

There are current investigations of the feasibility of "abhesive coatings". There is a long history of study in this area for a variety of applications, but as far as the writers are aware, the only chemical treatment that has been used successfully on a large scale is repeated application of chemicals that depress the freezing point of water. As far as concrete surfaces are concerned, the classic treatment for ice removal is application of sodium chloride or calcium chloride.

While sprayed-on coatings of polymers would probably reduce the strength of adhesive bonds, it seems likely that a subsidiary mechanical system would be needed to actually dislodge the ice on a regular daily basis. Annual renewal of the coating would probably be required in view of scraping to be expected from ship hulls.

In our judgement, the only coating worthy of field study during the next winter season is a concentrated solution of sodium chloride or calcium chloride. We visualize a dispenser laid along the curbing of the lock wall, perhaps in the form of perforated hose wrapped with a burlap diffuser. The working fluid could be sodium chloride solution, which has a freezing temperature of -21°C at 32% concentration, or calcium chloride solution, which freezes at -51°C at 23% concentration. The object would be to repeatedly apply a thin coating, either holding a thin layer of solution in place by surface tension or slow flow, or by crystallizing salt on the wall by evaporation. A replenishment surge would be required immediately after each cycling of the lock. There would obviously be environmental objections, but we estimate that the dilution of the 30% calcium chloride by the average daily flow at Sault Ste Marie would amount to less than 3 parts per billion downstream -- certainly vastly less than the effect of runoff from salted roads.

Mechanical Systems:

Three different mechanical methods were considered; i) a de-icing inflatable boot, ii) backhoe scraper and, iii) chain saw cutting equipment. The removal rates for the backhoe were in the order of 3-5 hours for one lock wall. A de-icing boot system could be adjusted to a very short time cycle. The ice cutting equipment had a design removal rate of 10 ft/min while cutting through 6.0 ft of ice.

Two saw cutting units were considered; i) a soil trencher modified with an extended trenching ladder and offset from the unit, and ii) a special coal saw designed with ice cutting teeth, offset mounted on a small tractor, both traveling next to the lock wall on the esplanade.

Non-contact method:

The only concept evaluated was cutting with high pressure water jets. Previous field experience indicated that removal of ice for lock walls was feasible using this method. A 150 hp unit capable of developing 10,000 lb_f/in^2 would be able to cut 3.0 ft of ice at a traverse speed of 3.5 ft/min, for a total working time of 5 hours per wall.

Conclusions and Recommendations:

The cost figures for the various methods are summarized in Table I. The range for average annual cost is very large, from less than $4,000 for the salt dispenser to more than $80,000 for the de-icing boot. However, the range is considerably smaller when the consideration is limited to the more reasonable positive methods. Systems offering a guarantee of success could be mobilized at an average annual cost of $10,000 to $30,000.

If a new lock were to be constructed, electrical heating of some kind would be extremely attractive, and even as a retro-fit on an old lock electrical heating would have many advantages, provided the capital cost could be met. The fluid circulation alternative does not seem particularly attractive.

The backhoe scraper now used at some locks is not particularly economical, and damage caused to concrete walls would probably be unacceptable in extended operations. A chain saw cutter could probably do a better job at half the cost.

The high pressure water jet has some operational attractions, chiefly the ability to operate in awkward areas near the lock gates and it does not appear to erode the concrete wall. However, it is an expensive method and it involves technology that may be somewhat unfamiliar to lock operators.

Ice removal by salting the wall has interesting potential, if only because it appear to be very cheap. However, the concept has never tested and ideally air-entrained concrete should be used as the wearing surface on the lock wall to minimize the deteriorating effect of salt solutions.

The de-icing boot appears to be extremely expensive, and it seems to be an unnecessarily complicated solution to the problem.

These estimates are quite rough, but they probably establish general magnitudes of cost fairly well, at least in relative terms.

DE-ICING METHOD

COST BREAK-DOWNS	IMBEDDED ELECTRICAL	HOT FLUID	MECHANICAL DE-ICING BOOT	BACKHOE SCRAPER 2 UNITS	TRACTOR-MOUNTED COAL SAW	TRACTOR-MOUNTED SOIL TRENCHER	HIGH PRESSURE WATER JET 2 UNITS	SURFACE COATINGS
INSTALLATION COSTS	30 W/SF 6" spacing 5' depth cov.	100 BTU/SF 12" spacing 5' depth cov.	Inflatable Rubber-mounted Steel-protected	Lag-mounted 3/4 yd	Backhoe mounted	Side-mounted on trencher	150 hp 10,000 psi pump	Calcium Chloride
Labor	317,000	302,000	>150,000	-	3,000	3,000	-	1000
Materials	41,000	116,000	450,000	-	30,000	25,000	-	3000
Engineering	25,000	29,000	42,000	-	-	-	-	<1000
Sub-total	383,000	447,000	>642,000	70,000	33,000	28,000	74,000	5000
Amortization-yrs	20	20	10	10	10	10	7	7
Ave. Inst. Cost	19,000	22,000	64,000	7,000	3,300	2,800	10,500	<700
OPERATING COSTS								
Labor	400	400	2,000	5,000	6,500	2,500	16,000	1500
Energy	1,800	2,100	2,000	1,000	800	500	3,200	800*
Maintenance	3,800	4,500	16,000	3,500	600	2,400	3,700	500
Ave. Inst. Cost	6,000	7,000	20,000	9,500	8,000	5,400	23,000	2800
AVE. ANNUAL COST	25,000	29,000	>80,000	17,000	11,000	8,000	34,000	4000

*Calcium Chloride

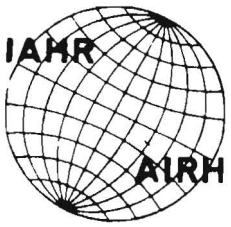

International Association of Hydraulic Research (IAHR)
Committee on Ice Problems
International Symposium on Ice Problems
18-21 August 1975
Hanover, New Hampshire

COMMENTS

Paper Title: Cost Comparisons for Lock Wall Deicing

Author: Darryl J. Calkins and Malcolm Mellor

Your name: Nabil AbdEl-Hadi

Address: Dept. of Civil Engineering
University of New Brunswick
Fredericton, N.B., CANADA

Comment:

It was noticed that the labour cost involved with the water jet technique is as high as $16,000 annually. How about using a mounted crane mechanism which allows for a convenient movement of the nozzle along the lock walls. This way you may only need one labourer to work the pump and the jet, which would decrease any degradation of lock walls after a long term use of this technique.

Author's Reply:

It is likely that a crane would cost much more than a small tractor, and its operator would probably be paid at a higher rate than a tractor driver. In any event, the high pressure pump would have to be tended by a suitably qualified mechanic.

As long as cuts are made within the ice, we would not expect the jet to harm the wall.

THIRD INTERNATIONAL SYMPOSIUM ON
ICE PROBLEMS
Hanover, New Hampshire, USA

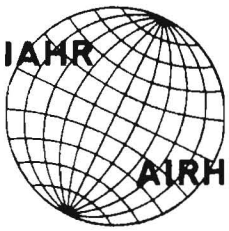

INLAND NAVIGATION AND MAINTENANCE OF HYDRAULIC STRUCTURES AT NEGATIVE AIR TEMPERATURE IN ICE-BOUND CONDITIONS

V.Aleksandrov	Ch.Eng.Wat.Trans. Department	M.R.F.	Moscow USSR
V.Balanin	Rector Wat.Trans. Institute	M.R.F.	Leningrad USSR
G.Onipchenko	Sin.Res.Hydroproj.	M.R.F.	Moscow USSR
V.Tronin	As.Prof.Wat.Trans. Institute	M.R.F.	Gorkyi USSR

Geographical position and climatic conditions of the Soviet Union are such, that during winter months water - ways of the country get icebound and this stops the navigation nearly on all waterways, though inland water transport plays an important role in the econimics of separate parts and regions of the country. That is why the prolongation of the terms of navigation on separate river sections and water reservoirs is very significant for economy not only on account of transportation costs but also because of its great influence on the development of national economy in a number of regions having no other developed means of communications as yet. Among these regions there are Northern Siberian regions and some regions of the European parts of the country.

It goes without saying, that prolongation of navigation in different regions of the country varies greatly and, naturally the prolongation of river fleet operation varies as well. For example, in Russian Federation average duration of self-propelled cargo fleet operation is about 180 days, on the Irtysh basin it is about 166 days, on the Enisey - about 155 days, on the Volga-Kamsky basin - about 210 days, on the Volga-Don - about 220 days. It is to be noted here, that in some years the duration of navigation may vary considerably. So, for instance on the Volga and the Enisey these deviations may account up to 30 days from average figures given above.

It should be noted, that the nature of breaking up the ice on waterways depends considerably upon its flow direc-

tion. Rivers flowing southward break from the mouth to the source calmly, but rivers flowing northward break up not because of the effects of thermal factor, but mainly on account of mechanical force of the flood water wave. Breaking up ice on such rivers is accompanied by heavy jams (as the ice was not effected by thermal action), which move down the river causing the water level rise about 20 metres and sudden water level fall.

Great changes in the navigation phases that are on the river in its natural state are caused by constructing water storages especially if they form the cascade of interconnected reservoirs, such as on the Volga, the Dnieper and the Kama.

The breaking up of water storages takes place 10-15 days later than that of on the rivers in the same geographical regions. This is due to weak action of mechanical factor while breaking up.

It should be noted, that more quiet nature of freezing on water storages than on rivers determines also more uniform structure of ice cover. Such ice almost entirely loses its mechanical strength while keeping considerable thickness and immobility. This process of ice cover weakening in spring under the influence of solar radiation takes place on the reservoirs even at negative temperatures. The above said proves the expediency of using mechanical means, ice-breakers for convoying ships along the icebound water storages in particular.

The freezing of deep water storages takes place somewhat later than that of the river-bed sections; the deeper and the larger this water storage is and the more heat it accumulates in summer, the greater is the delay. Water storages which are not very deep freeze simultaneously or even 7-10 days earlier than the rivers under the same geographical conditions.

As a result the period of navigation on such reservoirs may be shortened to 20-25 days compared to free river.

At the same time, below the hydroproject ranges, ice lanes (sometimes of considerable length) are formed. These are retained during the whole period of freezing and develop most intensively during the first one or two months after the beginning of freezing the river and at the same period in spring before the breaking up of the water flow.

It is very important for navigation that the bucket type creeks where ships winter, usually break up much later than the main water flow they are adjacent to, especially if this water flow is a river of high current.

Finally, it should be noted that many tributaries used for navigation during spring flood and discharging into the water storage break up much earlier than the water storage itself.

The features of the ice regimes of reservoirs given above stipulate the following principal trends and stages for prolonging the terms of navigation.

a) Complete usage of the whole period of physical naviga-

tion, that is the operation of the transport fleet during the whole period of navigation and distributing ships into creeks during autumn ice-drifting period and when the river starts to get ice-bound.
b) The determination and usage of the exact and guaranteed terms of the annual start and completion of using the transport fleet irrespectively of ice conditions in each year that improve immensely the usage of water traffic by users.
c) The prolongation of the navigation above mentioned quaranteed terms up to the year round navigation on some sections of the waterways caused by a special need of national economy and by high economic efficiency

In particular, the expedition voyages along the water storage to the tributaries in spring for cargo delivery along the tributaries in high flood period on them.

At present, the prolongation of the navigation takes place in general on account of the phase (a) and partially of (c). At the same time the work giving the possibility to use the phase (b) is being carried out.

In particular, as the result of the analysis of observation over the ice regime in the Volga basin carried out for many years are given as the first approach in figure 1. To provide the guaranteed terms of navigation is possible only taking into account the ice-breaking means at the disposal of the basin and their expected replenishment.

The navigation period may be prolonged both in autumn and spring. In solving this problem first of all it is necessary to take into account the specific features of the river and available technical means.

For rivers flowing northward, characterized by heavy jams, the prolongation of navigation in spring with the river itself remaining free, (i.e. without constructing hydroprojects) is unreal at present. On the contrary, when constructing cascades of storage basins on such rivers, the prolongation of navigation along those rivers in spring will be absolutely necessary and might be carried out. Most probable is the prolongation of navigation on such rivers in autumn. One should, however, take into account possible intensive sludging and foresee proper actions to overcome serious difficulties experienced by ships sailing in sludge.

On rivers flowing southward and especially on storage basins navigation is prolonged both in spring and autumn. The Volga, the Volga-Baltic waterway and other rivers may serve as examples.

It is expedient now to provide all-the-year-round navigation on separate comparatively short but having great goods traffic volume river sections in rather mild climatic conditions. For instance, one of the sections of the Dnieper where for a distance of 93 km the transportation of 5,5 mln tons of ore from the mining complex to the metallurgical works should be provided all the year round. The ore transportation by water when navigation is prolon-

ged is very effective from economical point of view.

The most widely used technical means for prolonging navigation are icebreakers and tugs having special support. Short technical data about them are given in the following table.

type of ship	Length m	Draft m	Power plant capacity h.p.	Maximum ice-thickness overcome when sailing
"Don" type icebreaker	44,7	2,3	1800	0,33
Harbour icebreaker	27,0	1,8	600	0,25
Icebreaker tug	13,5	1,4	300	0,20
Tugs	up to 46,0	up to 2,2	up to 1300	0,22

The "Don" type icebreaker is provided for convoying ships during autumn drifting ice and when rivers are ice-bound. It performs all kinds of ice-breaking, artificial breaking up of waterways including. The ship has icebreaking outlines strong hull and roll-trim system (tank capacity is about 42% of displacement).

The tests of harbour ice-breakers showed that they are able to sail c6ntinuously, their speed being 1,5 km/hour and the ice thickness - up to 0,25 m. With speed 0,5 km/hour the icebreaker overcomes ice of maximum thickness 0,4 m. and in spring up to 0,7 owing to reduced strength of ice during this period.

Technical potentialities of icebreakers both concerning maximum thickness of ice cover to overcome and the width of the channel broken up may be considerably improved on account of swinging installations giving the ship vertical oscillations like pitching. The oscillations are formed owing to rotation of unbalanced masses of high frequency.(120 - 180 oscillations/minute.)

To improve ship maneuverability in compact and broken ice and to de-ice the channel after the icebreaker, hydrowashing arrangements in the form of a pumping installation and a pipe-line with exit nozzles in the icebreaker hull below its water-line are used.

To improve icebreaker's ability to pass through those river sections where sludging takes place, it is necessa-

ry to provide the heating of their hulls.

Rather expedient icebreaking means are icebreaking attachments for pushers. Their advantages are: comparatively low cost of manufacturing and possibility to use such pushers during navigation according to their direct purpose. For push-boats with 1.340 h.p. capacity there is an attachment with swinging installation. Its displacement is about 400 tons. Its capacity is 140 kwt. The attachment is provided with hydrowashing arrangement. The push-boat of 1.340 h.p. equipped with such attachment breaks ice having thickness up to 0,8 m, rough ice including. With ice thickness of 0,4 m. the push-boat provided with the attachment moved at a speed of 3 km/hour and formed a channel 17 - 21 m. wide.

Another attachment having displacement 100 tons provided in its lower part with ski-cutters breaks ice when ship runs continuously up to 0,6 m , but when a ship goes by raids - up to 1,2 m.

Considerable improvements of traffic conditions for cargo ships following an ice-breaker are created when navigable routes are almost free of broken ice. This is achieved by keeping off the broken ice under the ice edge by proper devices on the ice-breaker or on a special ship in tow.

Effective means of facilitating the operation of ice-breakers when cutting channels in ice-field cover of considerable thickness is preliminary formation of deep furrows by means of ice furrows. The ice furrows are sharp wedges introduced horizontally into the ice cover and destroying it on the principle of cleaving. Ice-furrows form cuts having depth of 45 cm, its speed being 15 km/h. The necessary traction is 1250 kg. The wedge of the ice-furrow is fastened to the frame having runners and air capacities for providing buoyancy of the whole installation in case of its submerging into the water. Ice furrowing is advisable to carry out 10-15 days before breaking the route by the ice-breaker. Three lengthwise non-through furrows corresponding the width of the ice-breaker hull make it possible to increase her speed by 2-3 times.

For ice-breaking in back-water areas with the object of leading out the fleet into the river, ice cutting machines are used. Such machines are made with chain saws and milling cutting devices.

The ice cutting machine of the latest design is made on the principle of a tractor having rotor-spiral mover. It consists of two metal cylinders placed parallel in the direction of the machine run. On the cylinder surfaces there are spiral projections that round the cylinders by several turns. During rotation of the cylinders its projections cut into the ice or ground and make the machine move. Such tractor may easily pass through snow, ice, sand and swamps and has a large tractor effort. It may also

valve. This results in the wave formation, the front slope of which is greater than the water slope in the lock chamber that is registered at the end of the discharging process.

In the machinery rooms temperature not less than +5°C is maintained by electric heaters. To ensure safe lockage while dark, during snowfalls and snowstorms, the lighting of the lock is intensified, measures to heat the sensors of the automatic control system and to prevent ice formation in the float pits are taken. All auxiliary devices (ice-arresting booms, pneumatic installations and so on) are included into the automatic control system of the lock. The regime of the heating devices' operation and installations to prevent the water area from freezing is controlled automatically taking into account the temperature fluctuations of the ambient air.

The chamber and approach channels of the lock are regularly cleaned from ice by ice-breakers (if the ice thickness is above 15 cm) In the outer harbour the de-iced fairway is kept by the rise of warm deep waters under favourable temperature conditions.

The typical arrangement described above may be modified in accordance with climatic conditions, the required duration of the lock operation and negative air temperatures, arrangement and structure features of the lock, the type of feeding system and gate design being of the utmost importance. For example, with a distributive feed system supplying water to different parts of the lock chamber through various culverts, it is possible not only to eliminate the flow in the chamber towards the lower head during lock emptying but also to form the opposite direction flow. The installation of the ice-arresting boom in front of the lower gate becomes unnecessary, which essentially simplifies the whole complex of arrangements for tne lower head. In the shaft-type locks with a flat lifting gate in lower head and a concrete baffle in front of it the problem is much simpler. At present in the USSR a classification system of locks from the viewpoint of their operation at negative air temperature has been worked out.Locks are being equipped with proper installations.

The above mentioned stage to prolong navigation on the main waterways sections of the country has been realized by building both 12-line ice-breakers of 1800 h.p. and several types of transport ships fitted for ice-navigation.

All these installations essentially facilitated the fleet operation both at the beginning and at the end of navigation. They also ensure expedition cargo delivery on the tributary which was said above. On account of all these measures the navigation period has increased by 10-15 days. To ensure quaranteed terms of navigation in the Volga-Kama basin (which were given above) much more powerful means in considerably larger quantities are necessary. According to preliminary studies more than 10 line ice-

breakers of 4 000 - 5 000 h.p. each are necessary in this region, nearly the same number of ice-breakers of 2 400h.p. more than 25 ice-breakers of 600 h.p. with swinging installations and more than 45 pushers of 600 - 1 200 h.p. equipped with ice-breaking attachments.

The prolongation of navigation is a complex problem. It may be solved provided all the countries concerned take an active part in this work.

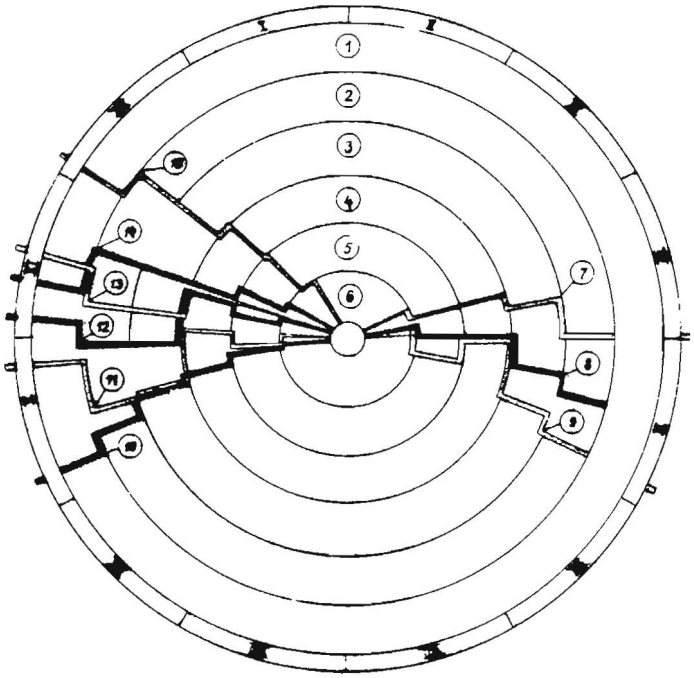

FIG. 1

Diagram of ice phenomena terms in navigation.

1. The mouth of the river Kama-Perm;
2. Rybinsk-Belomorsk;
3. Rybinsk-Leningrad;
4. Rybinsk-Moscow;
5. Kuibyshev-Rybinsk;
6. Astrakhan-Kuibyshev;
7. The dates of the start of icebreaker operation;
8. The reference dates of the transit shipping start;
9. The mean dates of ice clearance;
10. The early dates of ice drift;
11. The early dates of ice bounding;
12. The mean dates of ice drift;
13. The end of fleet decommissioning for winter (early formation of 30 cm thick ice cover);
14. The mean dates of the ice bounding;
15. The mean dates of 30 cm thick ice formation.

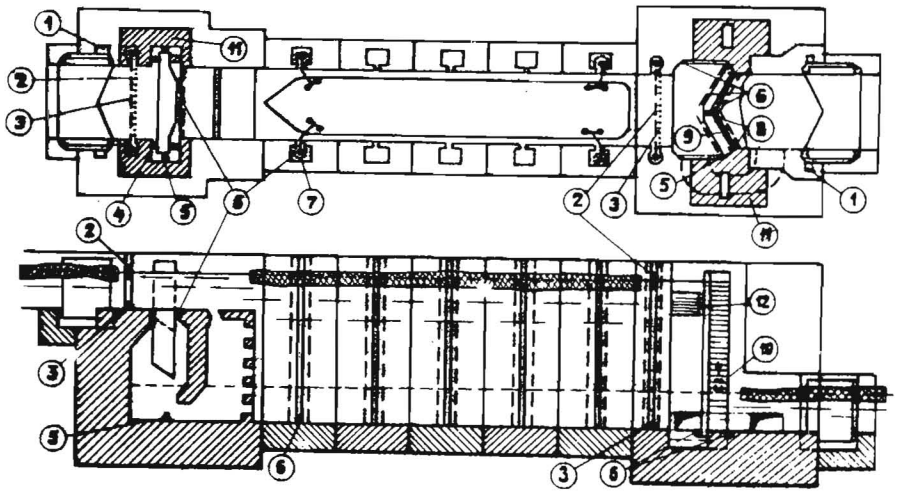

FIG. 2

Standard sketch of lock equipment for operation at negative temperatures.

1. Slots for flow generator;
2. Ice-arresting boom;
3. Perforated pipeline with nozzles;
4. Heating of the upper parts of gate seals;
5. Nozzles for air delivery to the main upper gate;
6. Perforated pipeline;
7. Mooring floating ring with heaters;
8. Heating of seals in the gate range pole and gate leaf abutment;
9. Heat coating;
10. Intercoat heating;
11. Heated rooms;
12. Heating of the raising water.

THIRD INTERNATIONAL SYMPOSIUM ON
ICE PROBLEMS
Hanover, New Hampshire, USA

ICE MOVEMENT CONTROL BY THE ARTIFICIAL ISLANDS IN LAC ST. PIERRE

J. V. Danys
Superintendent of Civil Engineering | Ministry of Transport Marine Aids | Ottawa Canada

SYNOPSIS

Icebreakers maintain an open channel across Lac St. Pierre, P.Q., throughout the winter for flood control and winter navigation purposes. In addition to other structures, artificial islands have been built to prevent ice from moving into the navigation channel.

GENERAL

Lac St. Pierre, located 50 miles (80 km) downstream from Montreal, is some 8 miles (13 km) wide and 20 miles (32 km) long with an average depth of about 10 feet (3 m). The navigation channel passes through the middle of the lake, is 800 feet (240 m) wide, and has been dredged to a depth of 35 feet (10.5 m) (Fig. 1). Lac St. Pierre is one of the most important river sections controlling ice conditions below Montreal. Until the early fifties the frozen lake stopped all navigation to and from Montreal.

The formation of the ice cover on Lac St. Pierre starts at the very restricted outlet of the lake. With the advent of cold weather, drift ice, frazil ice, slush and broken ice sheets drift downstream into Lac St. Pierre and form an ice bridge across the narrow outlet of the lake which acts as a bottleneck.

The low velocity of the current in the lake, approximately 1.7 f.p.s. (0.50 m/s) in the channel and approximately 1 f.p.s. (0.30 m/s) or less in the other parts of the lake, increases the effect

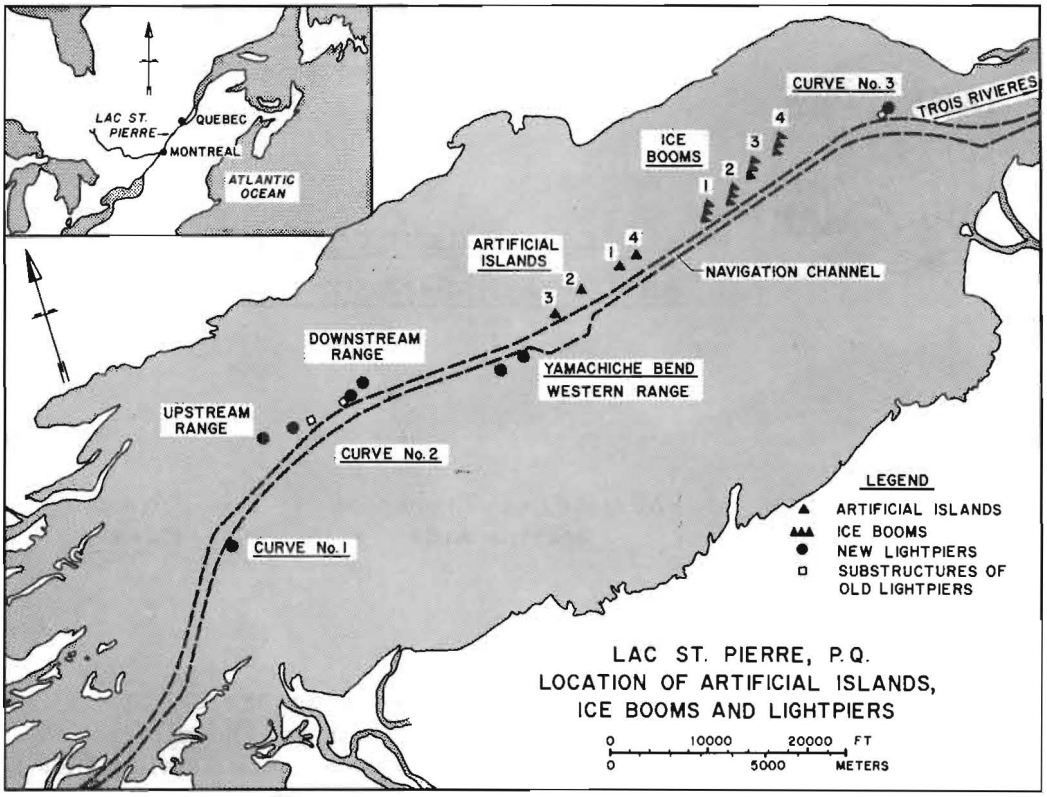

Fig. 1. General plan and location of artificial islands, ice booms and lightpiers.

of this bottleneck because ice cannot be evacuated fast enough. When there are strong northeasterly winds there may be no surface movement at all to carry the ice down. The ice then backs up until, first, the whole lake is covered and eventually the river itself as far as Montreal.

The combination of ice rafting, piling, frazil ice and heavy snow produces situations where the flow of water is so constrained that the level of the river can rise very quickly above its banks and cause disastrous floods in areas above Lac St. Pierre, including Montreal Harbour. Before the days of organized flood control by icebreaking, there was a long record of winter floods in these areas [1]. In 1865, fifty people lost their lives during the spring flood.

ICEBREAKING FOR FLOOD CONTROL

Icebreaking to control the formation of ice barriers was begun in 1906; the icebreakers "Lady Grey" and "Montcalm" were

given the task of breaking up the ice bridge at Cap Rouge, a few miles upstream of Quebec City. The operation was a success and has been continued since.

After a disastrous flood in Montreal in 1928, flood control operations were also initiated in the area between Trois Rivières and Montreal. Icebreakers were put to work opening a channel up the river in February. The objective was to reach Montreal before the time of the spring run-off, thus providing an escape channel for the spring flow. Such a programme was only partially successful because often large pieces of the ice cover break off through the action of wind and move into the shipping lane, effectively blocking it.

In 1953 the Ministry of Transport started icebreaking throughout the winter; these operations proved much more effective for flood control above Lac St. Pierre.

WINTER NAVIGATION

At first icebreaking between Montreal and Quebec City was carried out only for flood control and the maintenance of an icefree track for ferry crossings at Quebec, Trois Rivières and Sorel.

About 15 years ago a few ships from Sorel, located at the head of Lac St. Pierre, took advantage of icebreaking operations and started to sail to Montreal. They were more or less following the icebreakers. As the navigation channel was kept open throughout the winter, winter navigation increased so much that today the Montreal port is virtually open to year-round navigation. The closed season has been progressively shortened from about five months at the beginning of the century to several days in some current years. Although the major task of the icebreakers is still flood control, they now have the additional responsibility of also maintaining an open channel for the winter navigation.

ADDITIONAL ICE CONTROL MEASURES

When a solid ice cover forms over the lake, the currents in the open navigation channel move ice floes, slush and frazil ice through the lake successfully. But mild weather and winds loosen and break up the ice sheet in the lake, plugging the navigation channel. This may happen several times during the winter and each time it requires additional work by icebreakers. Of course, winter navigation is also stopped. It was observed that the ice sheet tends to stay longer not only on the shoals but also around the lightpiers and cribs in the lake.

In 1959-64 a study was carried out to regulate water levels in Montreal harbour and ice movement in Lac St. Pierre [1] . Among the various alternatives, a straight channel across Lac St. Pierre was considered. Earth dykes, pile clusters, ice booms and artificial islands were proposed for retaining and stabilizing ice cover in the lake. Subsequently, improvements of the navigation channel were carried out by dredging, but the proposed additional measures were tried out at various places.

In 1962 several timber clusters were installed along the navigation channel in Lac St. Pierre, but they failed early in the winter, mainly because of the very weak foundation and large ice forces.

Ice booms have been successfully used in Canada since 1949-50 in the Beauharnois Power Canal in the St. Lawrence River. Four of them were installed in 1967 in the northeastern part of Lac St. Pierre (Fig. 1). The installations proved successful [2] , although their maintenance is rather expensive because of the particular conditions in Lac St. Pierre. The installation is in open water and is exposed to several ice movements during the winter.

Four artificial islands were built in 1967-68 as part of an experimental programme. One island, No. 3, supports a light tower and its top is well above the high water levels in the lake (Fig. 2). Its design was quite elaborate because of a very weak foundation [3] . The weak foundation required a relatively wide base for the artificial island. The island was designed with two berms and varying slopes. It was thought that the ice floes should be grounded so that later an ice barrier would be created by the following floes. This reduces ice pressure against the island. Also, it was considered that piling of ice against the island should not damage the light tower. As a precautionary measure, the tower was made very light, of reinforced fibreglass, so that it could be replaced with another one by helicopter in the case of damages by ice.

Three other islands have been built only to the mean highest winter water level, so it is expected that sometimes ice floes would float over the islands. Their design and construction was much simpler (Fig. 2). Although their construction cost was lower, they require much more maintenance work and their effectiveness in ice retention is considerably smaller.

The lightpiers in Lac St. Pierre were built as early as 1905. While replacing the old lightpiers or building new ones in the lake during the last decade, consideration was given to their potential ability to retain ice floes and an ice sheet.

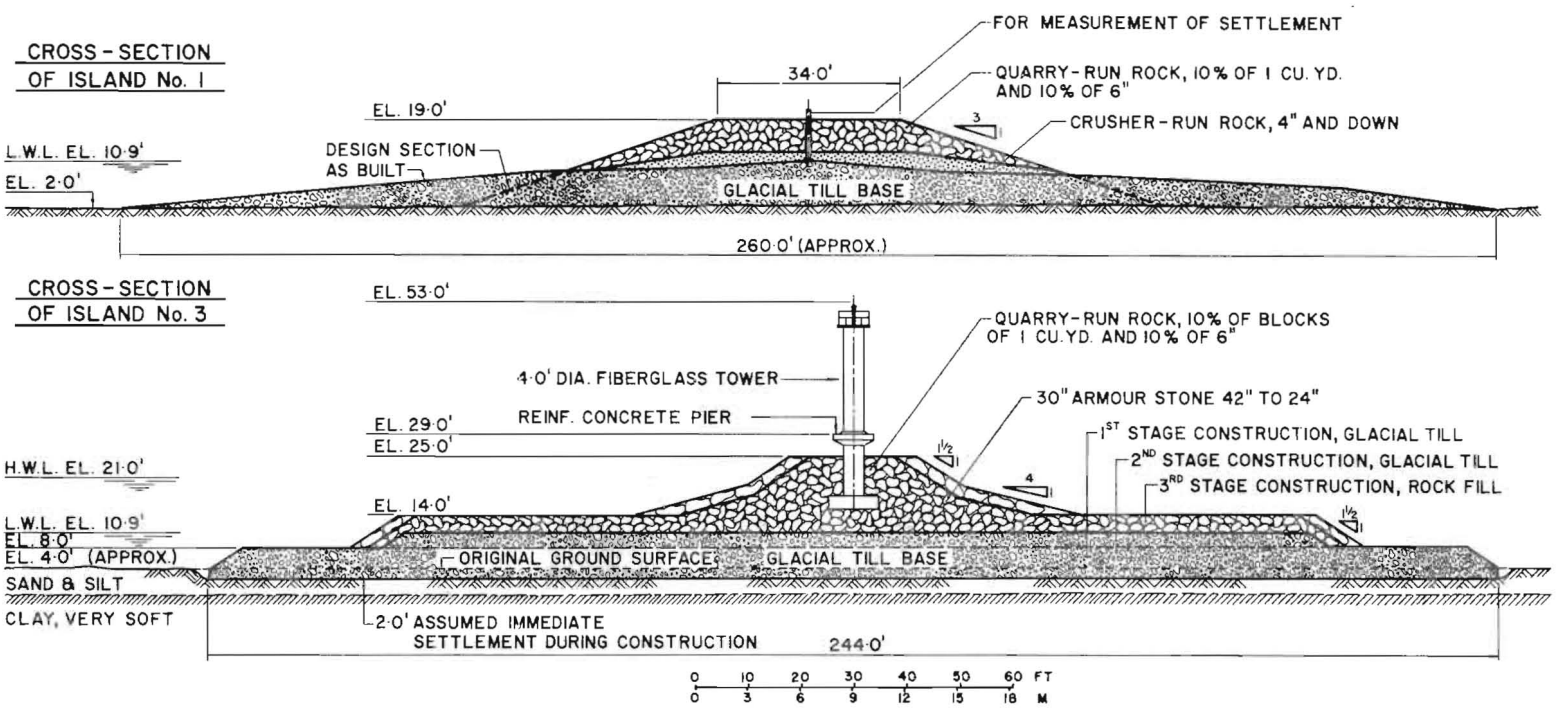

Fig. 2. Cross-sections of artificial islands.

Instead of completely demolishing the old lightpiers at Curve No. 2 and Curve No. 3 [1] their substructures were converted to artificial islands by placing rip-rap around them.

Fig. 1 shows the location of the four artificial islands, four ice booms, eight new lightpiers and three old substructures of the early lightpiers, converted to the small artificial islands.

The formation of the ice cover over the lake, as was mentioned, follows a certain pattern. The southern part of the lake is shallower and has several shoals; the ice cover is formed here relatively quickly. In the northern part of the lake, the formation of the shore ice is slower and a considerable quantity of ice floes moves downstream through the middle part of the lake along the navigation channel, to the outlet of the lake which is a kind of bottleneck. Artificial islands, ice booms and lightpiers help to retain the downstream moving ice floes, which by freezing together gradually extend the ice cover over larger areas until the entire lake is covered. Thus these artificial structures speed up the formation of the solid ice cover over the lake and reduce the danger of ice jams in Lac St. Pierre. Later they help to hold the ice in place.

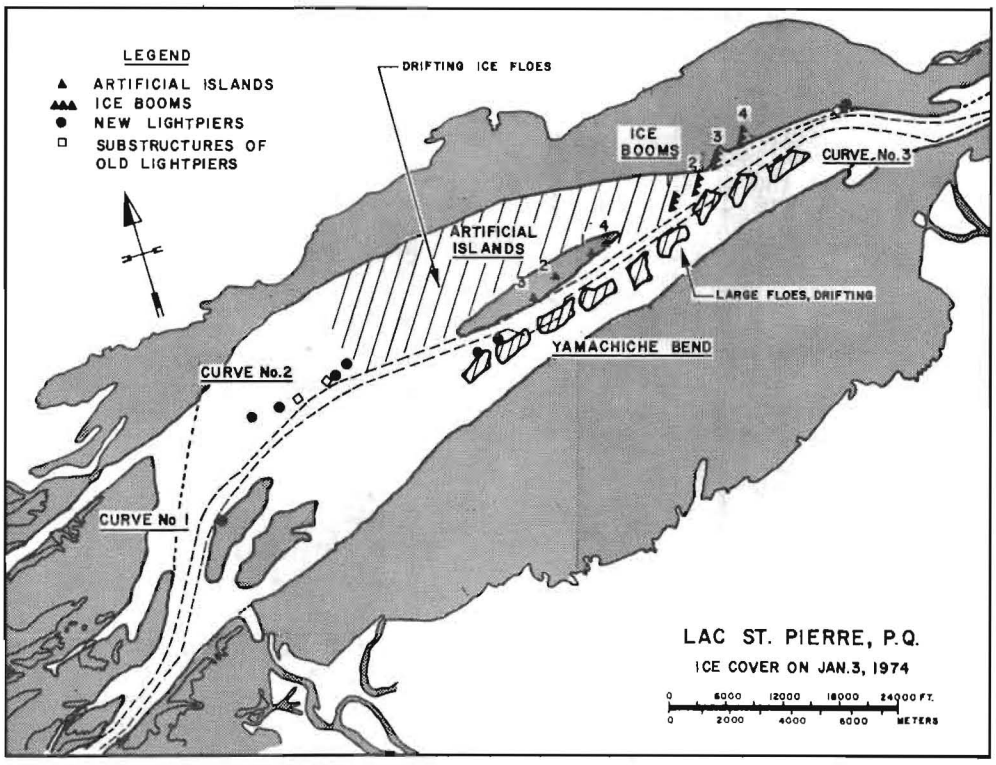

Fig. 3. Ice cover on January 3, 1974.

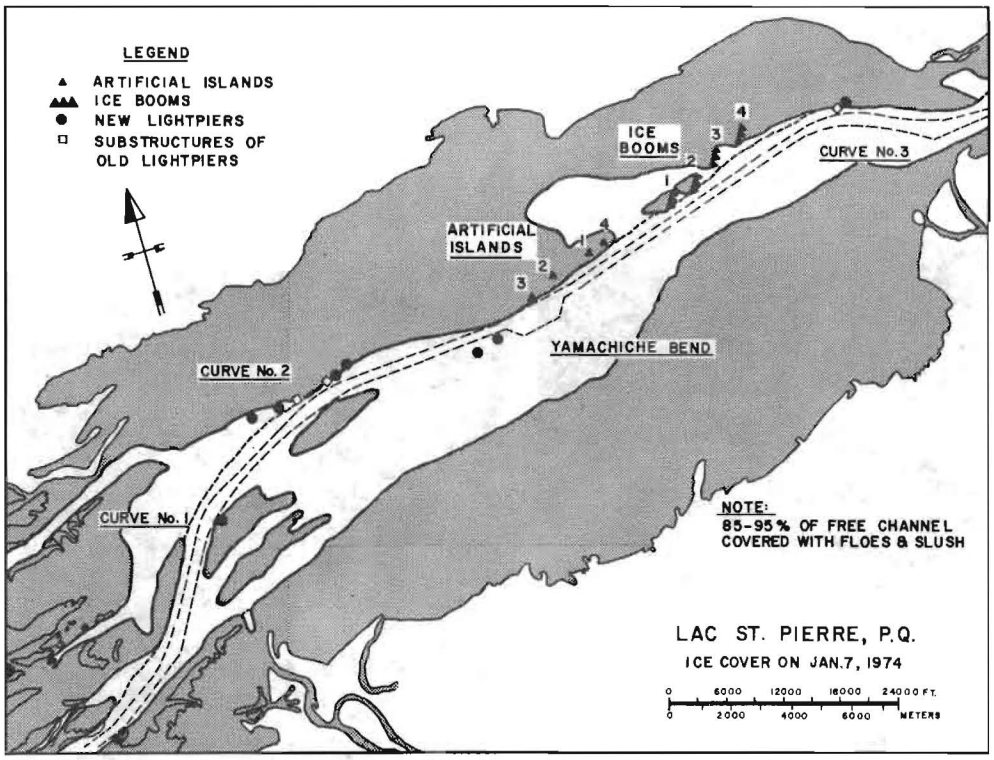

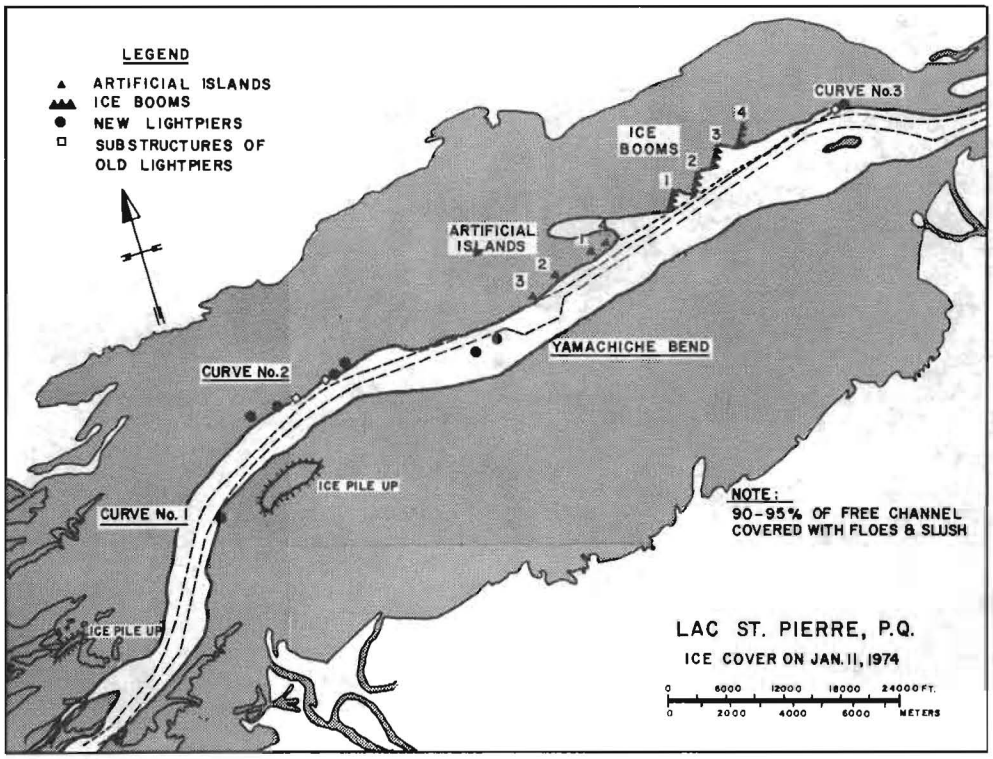

Fig. 4 and 5. Ice cover on January 7 and 11, 1974

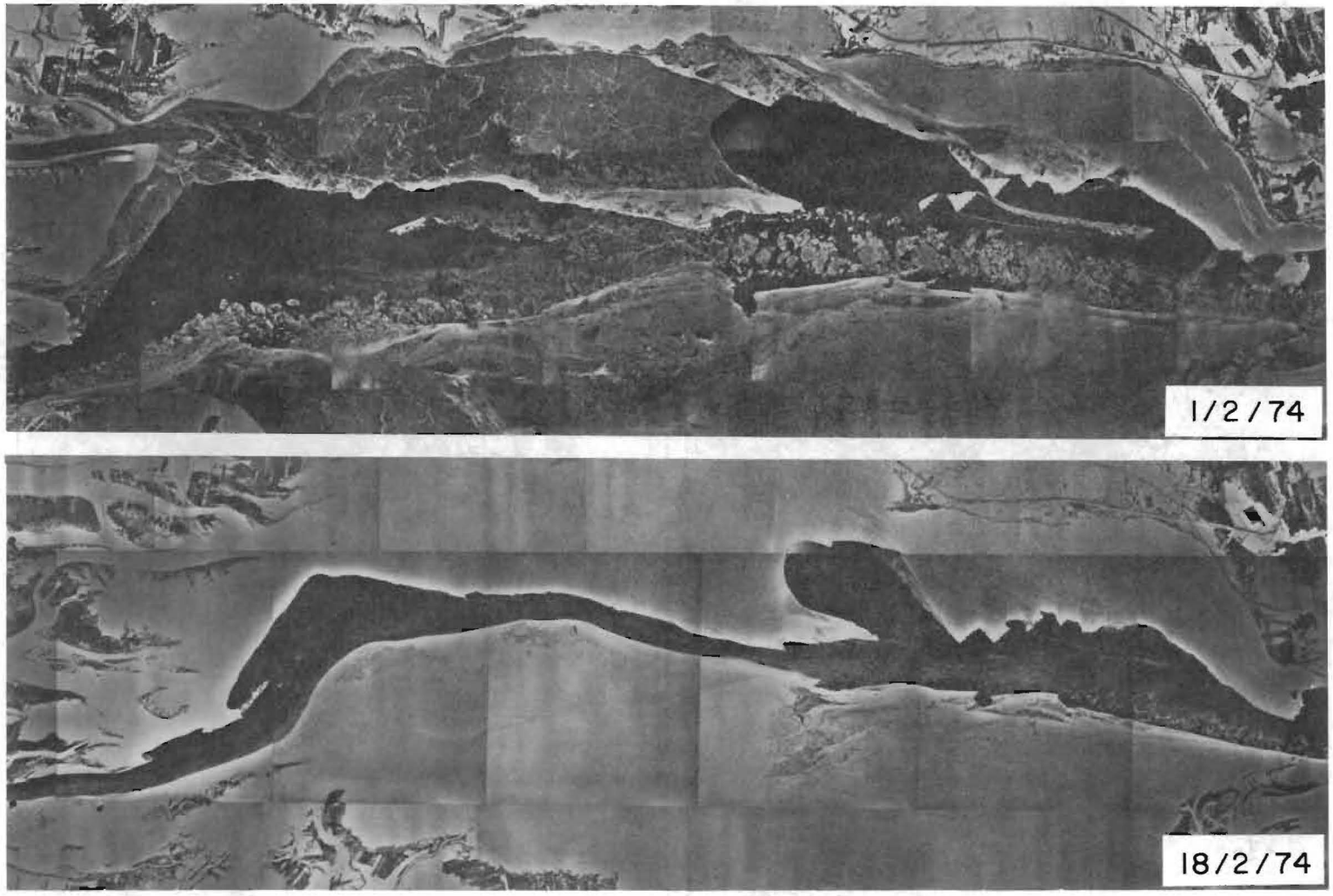

Fig. 6 and 7. Ice cover on February 1 and 18, 1974.

Fig. 3, 4 and 5 show the ice cover formation during the period from January 3 to 11, 1974. The anchoring effect of the artificial islands, ice booms and lightpiers is clearly shown. First the ice cover is formed along the shores. The artificial islands, ice booms and lightpiers start to accumulate the drifting ice and initiate formation of the ice cover upstream of these structures.

Two air photographs shown in Fig. 6 and 7 further illustrate ice cover formation and the effect of the structures.

When the navigation channel is opened by the icebreakers, the ice sheet anchored by the artificial structures resists wind and current forces much better and stays stable for longer periods, thus extending the period of winter navigation and reducing the work needed by icebreakers.

During the winter, frequent air reconnaissance flights are made to observe ice conditions on the lake and to report them to the sailing ships. Air observations are supplemented by air photographs. Other relevant hydraulic and climateologic data are also collected in order to evaluate the efficiency of the artificial structures in retaining ice.

Statistics about the closing time of winter navigation in Lac St. Pierre in the last 14 years indicate that the average navigation season has been extended by about 30 days since the construction of artificial islands and ice booms in 1967 and 1968:

Winter	Channel Closed	Average
1961/62	59 days	
1962/63	70	
1963/64	20	
1964/65	54	44 days
1965/66	39	
1966/67	43	
1967/68	26	
1968/69	18	
1969/70	6	14 days
1970/71	22	
1971/72	7	
1972/73	21	
1973/74	4	
1974/75	4	

The most unstable ice is in the northeasterly area of the lake near Curve No. 3 (Fig. 1) and therefore the first artificial struc-

tures have been built here.

The ice in the southern part of the lake is more stable. But sometimes southern winds break the ice deck here and push it into the navigation channel. Therefore, five artificial islands will be built on the south side of the navigation channel between Curve No. 2 and Yamachiche Bend adjacent to the two lightpiers to prevent ice movement into the channel from the south.

CONCLUSIONS

Artificial islands proved to be successful in forming and retaining a stable ice deck, thus reducing the icebreakers' work and extending the winter navigation season.

Because of the very weak foundation in Lac St. Pierre, they are economical only in shallow water depths.

They require maintenance work because of foundation settlement and erosion of the slopes by frequently moving ice.

ACKNOWLEDGEMENT

The assistance of Mr. R. Galarneau, District Manager, Mr. L. Grenier, District Engineer and Mr. C. Sabourin, Ice Control Engineer of Montreal District, Marine Services, Ministry of Transport in the preparation of this paper is gratefully acknowledged.

REFERENCES

1. Ministry of Transport of Canada, Marine Services. Records of Observations. Montreal.

2. Lawrie, C. J. R. Ice Control Measures on the St. Lawrence River, Eastern Snow Conference, Oswego, N. Y., 1972.

3. Danys, J. V. Earth and Rockfill Mound on Soft Clay in Lake St. Peter, P. Q. C. G. S., 25th Geotechnical Conference, Technical Note. Ottawa, 1972.

International Association of Hydraulic Research (IAHR)
Committee on Ice Problems
International Symposium on Ice Problems
18-21 August 1975
Hanover, New Hampshire

COMMENTS

Paper Title: Ice Movement Control by the Artificial Island in Lac St.Pierre

Author: J. V. Danys

Your name: W. E. Webb

Address: St. Lawrence Seaway Authority
5250 Ferrier Street
Montreal, P.Q., CANADA

Comment:

It was suggested that weather data be considered in evaluating the effect of the islands.

I would also suggest that the flow in the river and resulting levels and current velocities be incorporated in the evaluation.

THIRD INTERNATIONAL SYMPOSIUM ON
ICE PROBLEMS
Hanover, New Hampshire, USA

A FIELD STUDY ON ICE PILING ON SHORES AND THE ASSOCIATED HYDRO-METEOROLOGICAL PARAMETERS

Gee Tsang
Research Scientist
Ice and Hydraulics

Canada Centre for
Inland Waters

Burlington, Ont.
Canada

ABSTRACT

A field program was conducted on Lake Simcoe in Southern Ontario in the spring of 1974 to study ice pilings and the associated hydro-meteorological conditions. On site meteorological and hydrological parameters were recorded. The changes and the movements of the ice cover were monitored. The constant observation of the ice cover and its movement permitted the establishment of the exact time of the ice pilings that have occurred. It also permitted detailed observations of the ice behaviour during piling. The analysis of the hydro-meteorological data confirmed the earlier proposition that ice pilings are short duration events and are caused by the quick change in wind direction from offshore to onshore. A water gap is necessary for the ice field to build up its momentum. An impulse parameter was found to be a useful tool to predict ice piling. Static wind shear was found to have little effect on ice piling and the breakup of the ice cover. The field study also showed that until a large open water lead is developed, the lake current is weak and has little effect on ice piling. The piling of ice was influenced by the floe size and the physical state of the ice. Factors affecting the former are still not well known. More work in that area will help the calculation of the kinetic energy of a piling ice floe.

Introduction

In Winter, ice forms over lakes, reservoirs and sea. Under adverse hydro-meteorological conditions, the ice on the water surface will pile on shore and cause extensive damage to shoreline properties and coastal structures.

The problem of ice piling has been studied by Allen (1969), Bruun and Straumsnes (1970), Bruun and Johannesson (1971), Tryde (1972 a, b, 1973), Reeh (1972) and Tsang (1974). In the Soviet literature, ice piling has been mentioned by Korzhavin (1961). The overall picture of the past works shows that knowledge on ice piling is still at the pioneering stage. More has yet to be done for quantitative understanding the problem and the application of research findings to solve engineering problems.

In Tsang's work mentioned above, ice piles on Lake Simcoe in southern Ontario were studied and the meteorological data at the time of the ice pilings were analysed. From his study he concluded that ice piling is a short time event involving the conversion of energy. The primary cause of ice piling is the change of wind direction from off-shore to on-shore with the existence of an open water lead. The above conclusions were from post-event investigations. The meteorological data used were from two weather stations (Malton Airport and Muskoka Airport, See Fig. 1) 80 km to the south and 80 km to the north respectively of the ice piling site. The hydrodynamic data, which could be quite influential to ice piling, were not available for inclusion in the analysis. The field study reported here intended to substantiate and supplement Tsang's earlier findings by carefully monitoring and analysing the ice and hydro-meteorological parameters at the site.

Field Program

1. The Site

As a continuation of Tsang's earlier work, Lake Simcoe was again chosen as the studied lake for the field season 1973-74. The geographic location of Lake Simcoe is shown in Fig. 1.

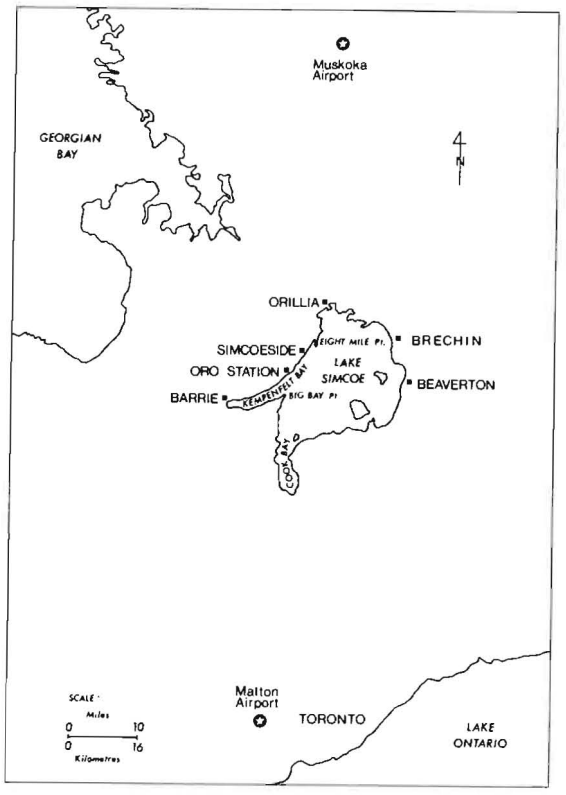

Fig.1. Geographic Location of Lake Simcoe

In the Winter of 1972-73, major ice piling took place at Big Bay Point and Eight Mile Point. With the same expectation, Big Bay Point was chosen as the studied site. The shoreline and the bathymetric lines at Big Bay Point are shown on Fig. 2.

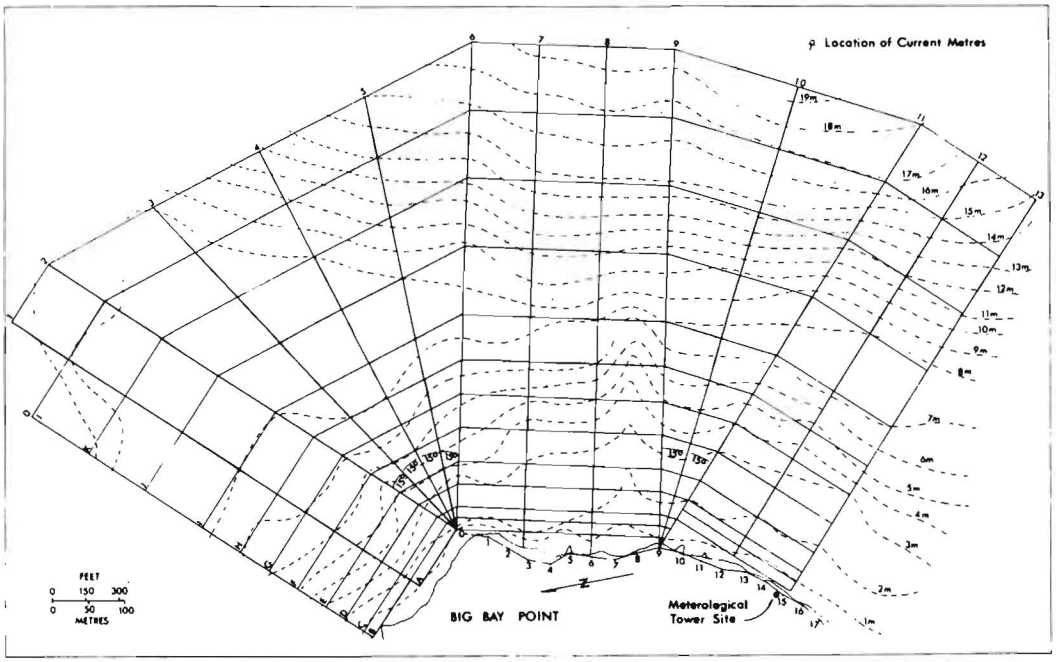

Fig.2. Grid, Bench marks and Flag markers at Experimental Site.

2. Instrumentation and site preparation

To study the movement of the ice cover, 17 bench marks 30.5 m (100 ft) apart were established along the shoreline and a grid was laid down on the ice cover as shown on Fig. 2. At the off-shore end points of the grid (points 1 to 13), flag markers were erected on the ice. By surveying the position of the flags from selected bench marks and observing the grid from the air at regular intervals, the movement of the ice cover could be detected.

Non-toxic black dye was used to mark the longitudinal grid lines perpendicular to the shoreline and red pigment was used to mark the latitudinal lines. To draw the grid, an all terrain vehicle was driven between markers. The coloured water stored in a container on the vehicle flowed and spread on the ice surface to mark the grid lines. The grid proved to be rain-resistant, remained visible except after new snow falls. The darker lines caused local accelerated melting, but the melting was insignificant to the total thickness of the ice cover. There was no evidence that the grid lines produced weak spots on the ice cover.

Local meteorological parameters were sensed by instruments atop a meteorological tower erected on the site at place shown on Fig. 2. Wind speed, direction, air temperature and humidity at the height of 20 m from the lake surface were recorded at 5-minute intervals. The readings

were also instantaneously displayed on a monitoring counter housed in the field office which was a mobile trailer parked under the tower. The real time knowledge of the meteorological condition permitted on the spot decision making. While the wind direction, air temperature and humidity were instantaneous readings, the wind speed was 5-minute average reading. The meteorological tower was about 10 m from the water edge and had no lake side obstructions. On the shoreside, there were cottages with trees up to 10 m high. Although the trees were bare in winter, off-shore winds would still be distorted and producing some error. However, since ice piling is mainly determined by onshore winds, the above meteorological sensing was considered acceptable in view of the mounting difficulties involved for a higher tower.

The limnological data were obtained at the point shown on Fig. 2. A series of 4 Geodyne current meters were attached to a vertical cable at the depths of 4, 9, 14 and 19 m in a total depth of 21 m as shown on Fig. 3. The first current meter was inverted to avoid possible ice damage. Water temperature, current speed and direction were recorded by the current meters at 10 minute intervals. The current direction and water temperature were instantaneous readings and the current speed was 10-minute average readings.

The period of weather recording was from Feb. 11 to April 22, 1974 and the period of limnological recording was from Feb. 19 to May 30, 1974. The grid was completed on March 7, 1974. The period of constant observation was from Jan. 28 to April 18, 1974, when ice piling was no longer a probable event.

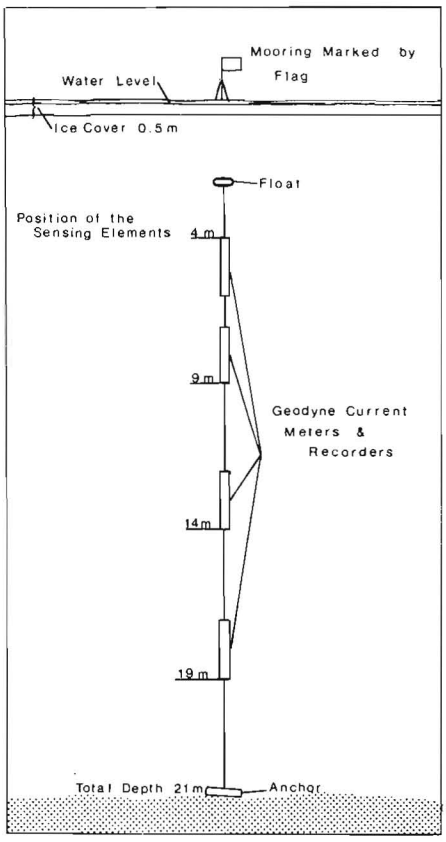

Fig.3. Installation of Current Meters.

Experimental Findings

1. Static effect of wind on ice

In the earlier studies of ice piling, it was the prevailing opinion of researchers that static wind shear is the primary cause of ice piling. The following field evidences disputed such a proposition:

For the studied period, a near hurricane scale wind of 31.8 m/s (71 m.p.h.) was recorded over Lake Simcoe on Jan. 28, 1974. The wind was from the easterly direction perpendicular to the shoreline at the site. At that time the lake was completely ice covered. On Jan. 29, when an inspection was made, the wind had subsided slightly, but was still strong enough that one slid with the wind when the gusts came. However, the inspection showed no piling of the ice cover.

Fig.4. Local Buckling along a Major Crack.

Fig.5. A Pile of Ice Crust.

The ice cover did buckle at places along some major cracks as shown on Fig. 4, but the buckling height was no more than 0.5 m (1.5 ft). A number of ice heaps up to a man's height were seen here and there at a short distance from the shore. By the first glance they gave the impression of the piling of the ice cover. However, a close examination of the ice heaps showed that they were composed of ice debris of 5 to 7.5 cm (2-3 in) thick (see Fig. 5) while the thickness of the ice cover on that day was roughly 0.5 m (20 in). On March 4, strong winds again caused the buckling of the ice cover along some large cracks and the formation of ice debris heaps. A study of the cross-section of one of the heaps produced Fig. 6. From Fig. 6 one sees that the ice heaps formed on January 28 and March 4 were piles of the ice crust only, not the ice cover itself.

An ice crust will form over an ice cover when the covering snow is melted by the sun or is sopped up by rain and subsequently freezes again into ice. The ice crust thickens as more rain or melted snow is frozen onto it. Before the ice crust is finally frozen to the ice cover and becomes part of it, there is a layer of snow or slush ice sandwiched between the ice cover and the ice crust. When the wind is strong, the static shear on the ice can be high enough to crush the ice crust and pile the debris into heaps although not high enough to crush the ice cover itself.

In the broader sense, the piling of the ice crust may be considered as one kind of ice piling. From a practical point of view, it is questionable whether this kind of ice piling would have much engineering significance. The field experiment showed that for crushing a relatively thin ice crust of 5-7.5 cm, a near hurricane wind was required. For crushing a reasonably thick ice cover that is capable of doing some practical damage, the wind will have to be so strong that it is doubtful whether the indirect

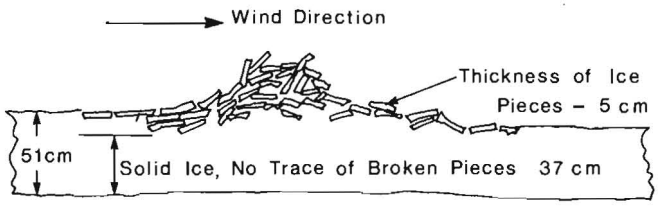

FIG. 6 CROSS SECTION OF AN ICE PILE FOPMED BY CRUST ICE.

damage by ice piling would be more severe than the direct damage by the wind.

2. Dynamic piling of ice

During the studied period, three pilings of the ice cover took place. Analysis of the weather data and on-the-site observations showed that the ice pilings were dynamic in nature. The physical revelation of the ice pilings is better shown by individually treating the ice pilings.

(i) First ice piling

The first ice piling occurred on March 11. The morning field inspection taken between 0830 and 0930 hour showed that the ice was 45-50 cm (18-20 in) thick, strong, and showed no sign of deterioration. At the edge, there was an open water gap of 30-38 cm (12-15 in) wide. A large crack on the ice cover was noted at the site extending from the point (bench mark 0) gradually turning South and maintaining a distance of 1.5 km (2/3 miles) from the shore. Another similar crack about 1.5 km (1 mi) to the south of the site was also noted. Both cracks were about 38 cm (15 in) wide and were covered by a thin ice of about 2 cm (3/4 in) thick.

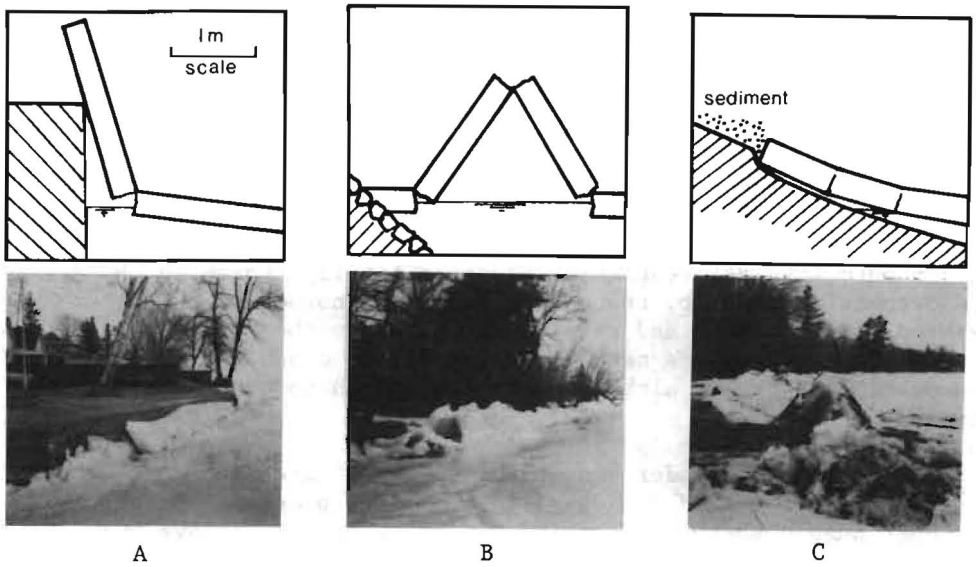

Fig.7. Ice Movement against the Shore - First Ice Piling.

In the afternoon, when the ice was again inspected at 1600 hour, ice had already moved in. Eyewitnesses estimated the time of ice movement to be around 1300 hour. There was no multi-layer piling of the ice cover. The ice cover either (1) pushed against an embankment or a rock protection, end first, then flexured upwards and broke (see Fig. 7,A), (2) pressed against the shore, then buckled upwards and failed (Fig. 7, B and C), or (3) slid on shores of small slope and pushed the sediment in

front of it, causing considerable shore erosion (Fig. 7,C, foreground in the photograph). As a result of the ice movement, the cracks were closed and the covering thin ice on the cracks was crushed and jutted out of the cracks as shown on Fig. 8. Although the incident involved only a small ice movement, much damage was done to the shore and the shoreline structures. At a marina, newly installed wooden piles of 30 cm diameter were pulled out from their positions. At another point, concrete slabs 3 m wide by 6 m long by 25 cm thick were lifted and moved.

Fig.8. Closed Crack Following the First Ice Movement.

From the recorded data, the wind speed, direction, current speed, direction and air temperature were plotted for the day of the ice piling as shown on Fig. 9. From Fig. 9 the meteorological factor responsible for the ice piling is immediately recognizeable. It is seen from the wind direction recording that prior to 1035 hr, EST, the wind had been persistently in the direction parallel to the shore. From 1035 to 1155 hr the wind gradually shifted to the onshore direction. Then in the next hour from 1155 to 1255, the wind quickly shifted from the onshore direction to the offshore direction and back to the onshore direction again. It was this sudden wind change that produced the ice movement. The offshore wind widened the cracks and the onshore wind following permitted the building up of momentum of the immense ice floe by closing the cracks.

The wind effect on ice piling or ice movement may be better seen by plotting the impulse of wind shear on the ice cover. The wind shear impulse on an ice cover in the direction normal to the shore-line over a time period t from the instant T is proportional to

$$I = \int_{T}^{T+t} V^2 \, \hat{v}.\hat{n} \, dt$$

where $\hat{v}$ is the wind unit vector and $\hat{n}$ is the unit vector normal to the shoreline in the onshore direction. The multiplication of I by the density of air and the drag coefficient of wind on ice gives twice the wind shear impulse per unit area in the onshore direction. From the wind data, I was calculated and plotted against time as shown on Fig. 9. In the plotting, EST 1000 was chosen as T.

It is from Fig. 9 that the plotting may be divided into three sections. In the first section from 1000 to 1208, I increased monotonously except for minor irregularities, indicating a gradually increasing windshear impulse in the onshore direction. However, this windshear impulse produced no momentum to the ice cover because it was pressed against the shore and the wind force was cancelled by the reaction from the shore.

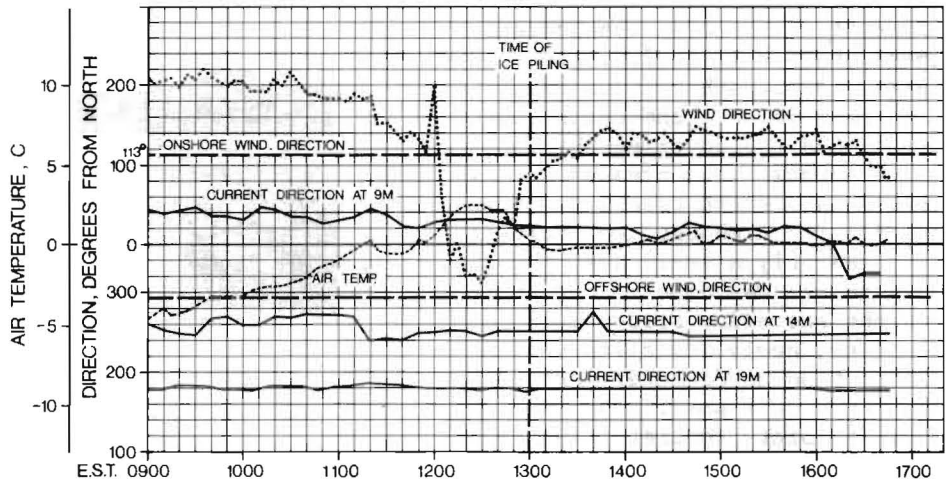

WIND DIRECTION, CURRENT DIRECTION AND AIR TEMP.

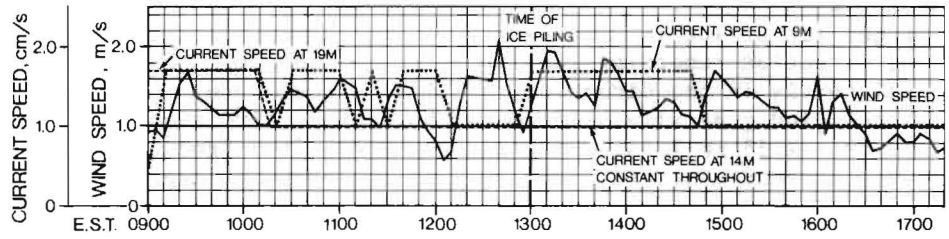

WIND AND CURRENT SPEED, MARCH 11, 1974

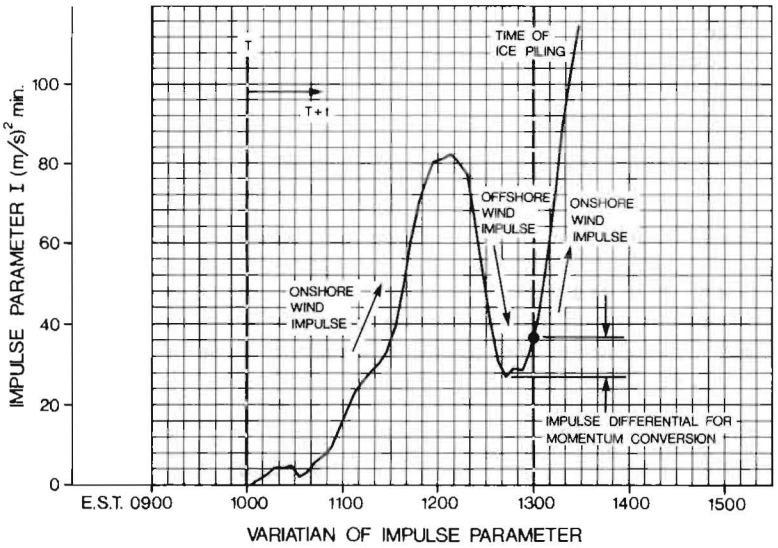

VARIATIAN OF IMPULSE PARAMETER

Fig.9. THE HYDRO-METEOROLOGICAL PARAMETERS ASSOCIATED WITH THE ICE PILING ON MARCH 11, 1974

For the second section, from 1208 to 1243, I decreased monotonously, indicating a continuing offshore windshear. For the first part of this period, the wind might have produced an offshore motion to the ice cover. However, this offshore motion would be short-lived because of the limitation of the narrow water gap. For the third section from 1243 hr on, I again increased monotonously, showing again an onshore wind shear. Under the onshore wind, the ice cover gathered momentum by closing the widened cracks caused by the preceeding wind. The sheer size of the ice floe itself; of the lake size or at least fractions of it, means it was quite capable of doing all the damage although the distance of momentum gathering was only a meter or two. The short time lag from I at its minimum at 1243 to the ice coming to the shore at 1300 also indicated the short distance of ice movement. From the I values at these two instants, the momentum of the ice floe at the time when it came to shore can also be calculated if the floe size is known.

Since a maximum in I also means a change in the windshear direction, one might expect a similar ice movement to the opposite shore following the maximum at 1208. Such an ice movement, however, was not reported. A study of the temperature recording shows that prior to 1200, the air temperature has been practically subfreezing all the time. The onshore wind shown in section 1 (the offshore wind to the opposite shore) therefore had to crush the still strong ice sheet over the cracks to create room for the later onshore ice (to the opposite shore) ice movement. Apparently, the mild wind recorded could not accomplish such a task. On the other hand, the above freezing temperature during the time period of section 2 considerably weakened the ice over the cracks and helped to promote the ice movement associated with the I minimum. An above freezing temperature was pointed out earlier by Tsang as one of the conditions required for ice piling.

The uppermost current meter, unfortunately, failed to work. The limnological data shown on Fig. 9 were from the bottom three current meters. An inspection of the current direction curves shows strong layering effects in the lake, but there was no evidence of correlation between the surface wind and the lake currents. The figure shows that the lake current were two orders of magnitude smaller than the wind speed. If the same drag coefficient is assumed for the air-water and ice-water interfaces, it can be shown that the wind shear was an order of magnitude greater than the water drag. The above analysis thus leads to the conclusion that for ice movements involved small water openings, the lake current plays no definite role and is not an important affecting factor.

The important finding from the first ice piling is that a wide water gap and a strong wind really are not necessary for damaging ice movements. When the meteorological combination are right, the ice is strong and the floe is huge, the momentum built up over a water gap of one or two meters under a wind of only 2 m/s (4.5 mph) is capable of doing much harm.

The ice movement discussed above really was not an ice piling because the ice did not pile up. Fig. 7 also shows that the ice floe failed by flexuring and the breaking off parts were solid slabs. On the other hand, for a typical ice piling, the ice fails by shearing as well as bend-

ing and the failing point is very close to the foot of the pile (see next section). The ice floe remains seemingly intact while piling, without breaking into slabs first. It may be pointed out that all the mentioned scientists except Tsang, in their treatment of the ice piling problem, considered the ice floe breaks into slabs first before piling. Therefore their treatments are only valid for ice movements similar to the first "ice piling" discussed above, but not for typical ice pilings with laminar structures metres high.

(ii) Second ice piling

The second ice piling took place on April 14, between 1215 and 1228 hour. In the morning when the ice was inspected at 1000, the ice cover was seen intact but ripe. It showed a dark green colour close to that of the lake water, indicating that water had soaked into the ice cover in the spaces between ice crystals. At the shore, a water gap of 2-5 m was noted. The edge of the ice cover showed signs of considerable deterioration or had disintegrated into small pieces. The distance of ice cover movement therefore would easily be twice the open water gap. From 1115 hour, the wind began reversing its direction. At 1200, the ice cover was noted to agitate and noises were heard. At 1215, the ice cover came to the shore and began to pile. The piling action came to an end at 1228 after the ice had piled to a height of about 2 m measured from the lake surface.

Fig. 10 is a record of the ice piling. The first picture shows the ice condition and the water gap in front of the meteorological tower at 1000 hr, roughly two hours before the ice piling. Frames 2 to 10 show the early stage of ice piling and frames 11 to 14 show the later stage of the ice piling. In between the camera was reloaded. Although the focus point was different, the same location was being filmed as may be recognized from the forked tree at the top left corner of both frames 5 and 11. The last picture on Fig. 10 shows the site at 1230, immediately after the ice piling.

Different from the first ice piling in which the ice showed much strength and rigidity, the ice cover this time showed considerable plasticity. As the ice cover came to the shore, it was deflected continuously up the slope. After overshooting the top of the slope, the overshot part fell off to the shore side and by so doing further increased the height of the basis of the ice pile.

From the change in colour of the ice sheet one sees from Fig. 10 that the failing point of the ice floe was at the foot of the pile. The arm of the moment produced by the reaction of the slope therefore was short and shearing would have been an important, if not the predominent, factor causing the failure of the ice floe.

Depending on factors yet to be determined, the ice cover might buckle upwards and break at the foot of the ice pile. As the up wind ice cover continued to proceed, multi-layer laminar ice piling would result. In a way, the buckling and breaking of the ice cover at the foot of the pile was similar to the rafting action classified by Tsang in his earlier work, only that now the rafting action took place within the same

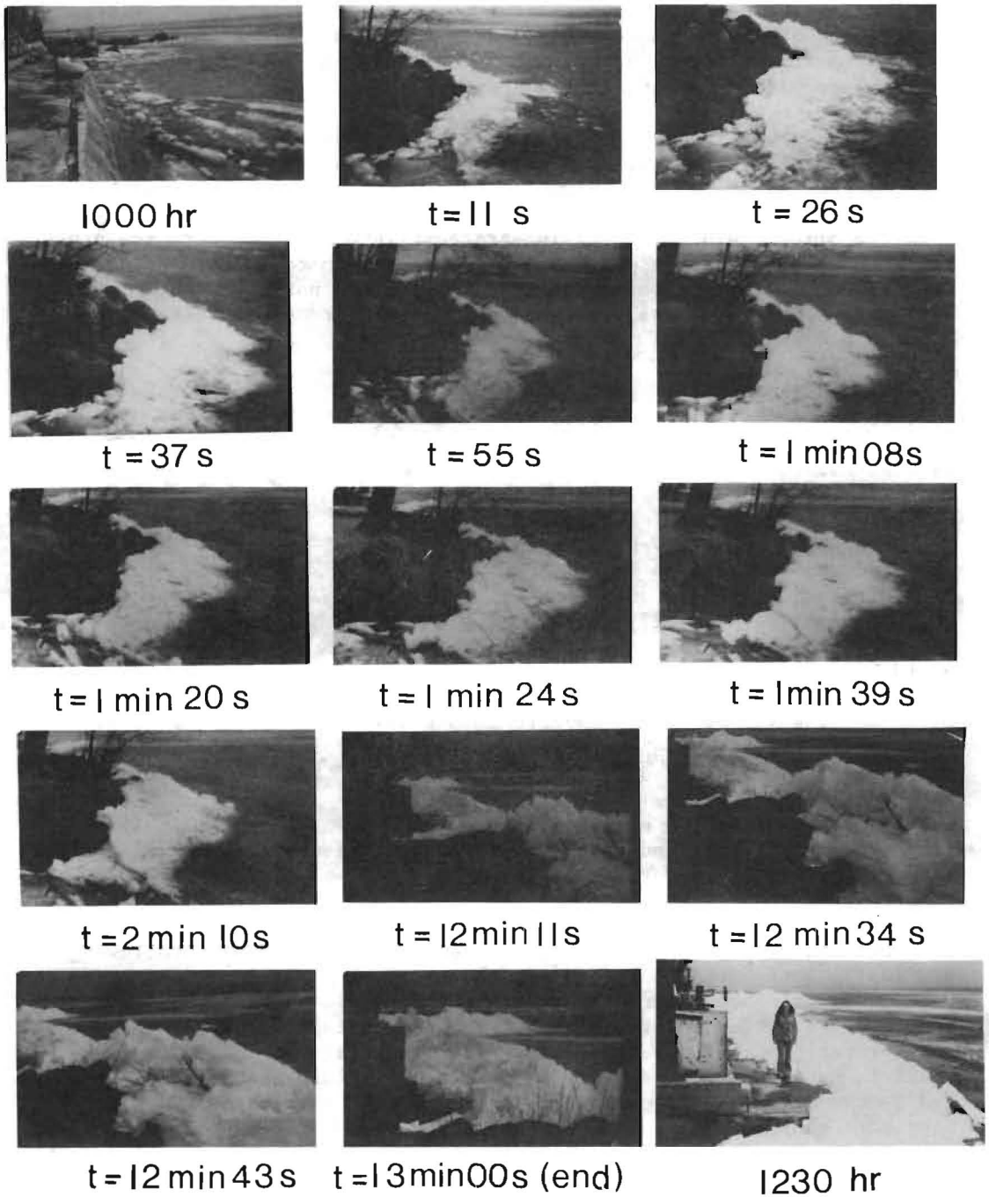

Fig.10. Time Sequence of Second Ice Piling (t = 0 at 1215 hr).

ice floe instead of at the contacting edges of two neighbouring floes. Telescoping of ice floes were also noted after the piling event. Since the ice cover was intact before the ice piling, the telescopings must have taken place within the intact ice cover.

The plasticity of the ice cover was caused by the ripeness of the ice. A close examination of the ice piles showed that the ice had decayed considerably. The columnar ice crystals in the ice could be clearly recognized. A kick by the foot on a large ice cube broken off from the piles could easily disintegrate it into the composing ice crystals. For the ice that did not pile, no strength test was made although it would be a little stronger because the ice had not been subject to failure. The ice crystals themselves, however, remained quite strong.

Substantial damage was done to the shoreline properties by the ice piling. Within the several hundred metres of water front at the site, several sundecks, boat rams and jetties were twisted and moved onshore. Many trees were uprooted and boulders up to 1 m in diameter were pushed up atop some of the piles (see Fig. 11). Had the ice been stronger, more damage would have been done.

Fig.11. Example of Shoreline Structure Damages by the Second Ice Piling.

The survey of the marker flags on the ice cover showed that the studied ice cover had moved as one piece for a distance of 17 metres at the direction of 176° from the north by the end of the ice piling. This gave an average piling velocity of the ice cover of 2.3 cm/s.

Figure 12 shows the meteorological and limnological data associated with the ice piling (as well as the 3rd ice piling, see following section). During the shown period, the meteorological recorder failed to work. The data shown were taken from the monitor. During the ice piling time and the subsequent field inspection time, displayed readings on the monitor were not taken because of manpower shortage, thinking that they would be automatically recorded anyway. The failure of the recorder thus led to two missing data periods as shown on Fig. 11. Estimated weather data were generated using the weather data from Malton airport as guides for the first period and from Muskoka airport for the second period. The estimated weather curves are shown by dashed lines on Fig. 12. The Malton weather station is close to Big Bay Point, the site of the second ice piling, and the Muskoka weather station is close to Brechin, the site of the third ice piling. The readings from these two stations were hourly readings.

Since the ice movement was in the direction of 176° from the north, in treating the hydro-meteorological data, 176° may be considered

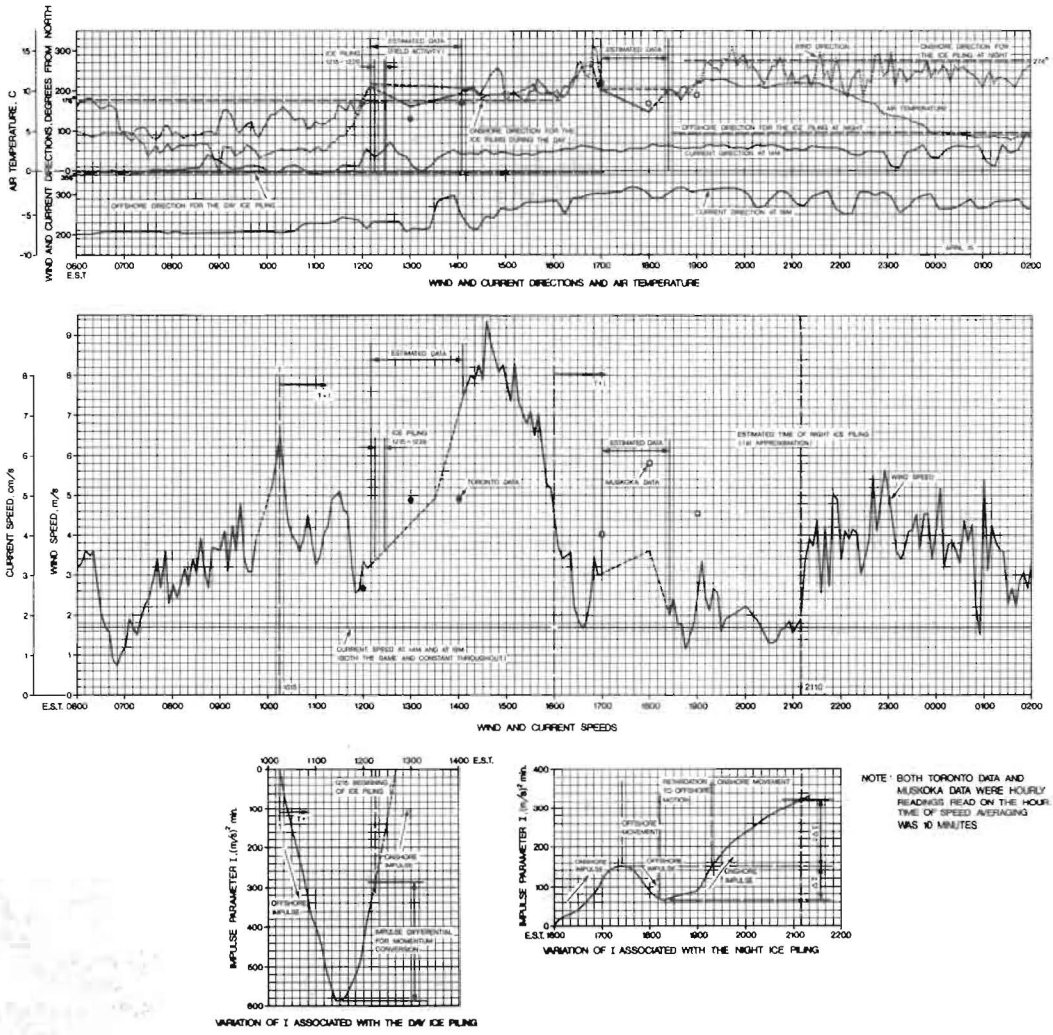

Fig.12. The Hydro-meteorological Parameters Associated with the Ice Piling on April 14, 1974.

as the offshore direction, as shown on Fig. 12.

From Fig. 12 and field observations, one again observes similar conclusions as from the first ice piling:

1. The ice piled not long after the quick wind reversal from 50^{o} to 210^{o} took place between 1115 hr to 1210 hr. Ice piled at a wind speed of 3.4 m/s (7.5 mph), the ebb of the wind speed curve rather than the crest of it. The static wind shear therefore was not responsible for the ice piling. It was caused by the shift in wind direction.

2. From the impulse parameter plotting, one again notes that the ice piled not long after the minimum in I. A greater time lag between the I minimum and the onset of the ice piling than that of the first ice piling means that the ice cover had drifted over a greater distance before piling. The difference in I in the time lag period is seen from Fig. 12 to be 285 $(m/s)^2$min, which is about 26 times the I differential involved in the first ice piling. Should the drifting ice floes be able to hit the northern shore, which is normal to the ice movement, great ice piles could have been resulted. However, such an ice piling was not reported. The northern shore was protected by an ice cover which had little movement. The kinetic energy of the ice floes from south of Kempenfelt Bay was largely spent on telescoping of the ice floes. For the experimental site, the shore was not protected by an ice cover so ice piling took place. Since the shoreline at the test site made an angle of 27^{o} to the direction of ice movement, the normal component of the I-differential to the shore is calculated to be 130 $(m/s)^2$min. The two-metre high ice piling was produced by this impulse differential.

3. For the shown period on Fig. 12, the second current meter from the top also failed to work. However, from the limnological data obtained by the bottom two current meters, one once again notes the absence of correlation between the surface wind and the lake current and the insignificance of the current speed in comparison to the wind speed. Lake current, therefore, is once again shown not an important factor in affecting ice piling on lakeshores.

4. Throughout the period, the air temperature was above 0^{o}C, showing again that an above freezing temperature promotes ice piling.

(iii) Third Ice Piling

Following the second ice piling, the wind shifted to the westerly direction that night and produced a major ice piling to the other side of the lake. Fig. 13 shows the shoreside and lake-side view of an ice pile and a crushed cottage at Brechin.

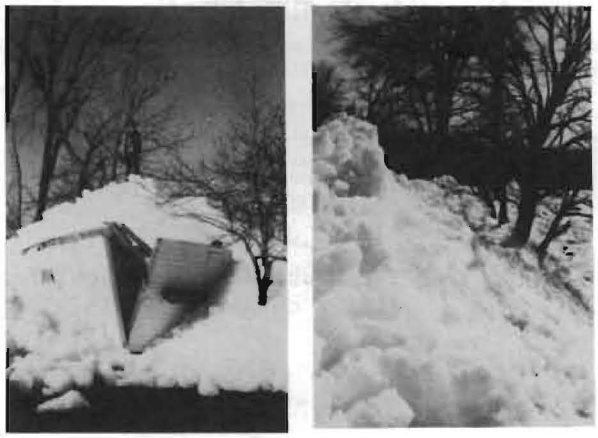

Fig. 13. An Ice Pile at Brechin.

The exact time of the event was not recorded as the east shore of Lake Simcoe was sparsely inhabited and most of the cottages were not occupied in Winter. The highest ice pile at Brechin Beach, where a field inspection was made, was 8 m high. Extensive damage was done to the shoreline properties. The piling ice floes were large, kilometres in linear dimensions. The examination of the ice piles showed the ice had piled the same way as in the second ice piling, and the ice floes had drifted in from the direction of 270° from the North. An aerial inspection of the lake showed that besides piling on the shore, the ice floes also telescoped one on the other, many times in the form of fingering. Following the ice piling, an open water gap of 0.5 to 1 km was noted the next morning at the Big Bay Point site.

It was unfortunate that the weather data in the crucial period of 1700-1825 (see Fig. 12) were missing. However, from the estimated wind data one sees that in the short period of 1650 to 1945 hr, the wind had quickly shifted from 310° to 150° and then back to 310° again, a wind change very similar to that responsible for the first ice piling. Based on the conclusions obtained from the last two sections, one can see that this change in wind direction was the cause of the ice piling.

The plotting of the impulse parameter I for the period beginning at 1600 again shows an I maximum and an I minimum. As in the first ice piling, the maximum in I might indicate an ice piling on the opposite western shore. Such an ice piling, however, was not observed. The duration of the onshore wind to the western shore was not long enough; the ice field changed its direction of motion before reaching the western shore.

The approximate time of the ice piling may be estimated from the I curve. If the impulse differential between the I maximum and the I minimum was for the westward, offshore motion of the ice field, an equal impulse differential is needed for stopping this offshore motion after the wind had changed its direction. If twice this impulse differential was again required to move the ice field to the shore, the time of ice piling would be around 2110 hours as shown on Fig. 12. The above estimate tends to be an overestimate. Since the later part of the ice movement did not involve acceleration, the ice field should arrive at the shore earlier.

From Fig. 12, one again notices that the ice piled at a time when the wind shear was at its ebb rather than at its peak. The lake current again showed no obvious bearing to the surface wind and had negligible effect on the movement of the ice cover. The air temperature was well above freezing at the time of the ice piling.

A study of the weather maps of the period showed that in the night of April 14, a low pressure storm centre had passed right over Lake Simcoe. The great fluctuation in wind speed and direction because of this storm centre as shown on Fig. 12 no doubt would have imparted a shuffling action to the ice floes and by which helped the floes to pile high. In Tsang's earlier study, he pointed out that the staying of a storm centre over an area is a promoting factor for ice piling.

3. Breakup Pattern of the Ice Cover

The capability of an ice floe in doing damage to shoreline properties depends on its momentum and mechanical strength. The momentum of the ice floe in turn depends on the windshear impulse parameter I and the floe size. Some observation was made on Lake Simcoe on the breakup pattern of the ice cover and the size of the piling floes. Following are what have been observed:

Prior to the spring breakup, thermal cracks first appeared on the ice cover. These cracks were few in number and occurred mostly (i) radially from points of the land mass, (ii) parallel to the shoreline at a distance of 0.5 to 2 km from the shore, and (iii) between islands and from the points of islands to points of the land mass. The thermal cracks occurred when the weather was still cold and there was no sign of deterioration of the ice cover. After cold spells, some cracks would refreeze but some, protected by a snow cover, would remain only covered by a thin ice on the surface through the rest of the winter. Rains on the ice cover and the melting of the snow cover produced surface runoffs that drained to the lake through the thermal cracks. The runoffs would substantially erode and enlarge the thermal cracks. Even so, the thermal cracks were all narrow, none of the observed was wider than 1 m.

As the weather warmed up, the ice cover melted at the shore as the land mass absorbed the solar radiation at a faster rate and warmed up faster. The water gap at the shore gradually widened as a result of further melting and the disintegration of the edge caused by the sloshing of water in and out of the water gap. The ice cover, however, remained intact and strong. When the meteorological conditions were right, the ice would move onshore and cause damage to the shoreline properties. The first ice piling discussed earlier was of this kind. During the ice movement, there was no telescoping of the ice cover and the ice floes were of the size of fractions of the surface of the lake.

As the warm weather continued, the ice cover deteriorated and the water gap at the shore further widened. The piling of the ice cover was preceeded by a noticeable movement of the ice cover. The long distance of travel and the weakened state of the ice permitted the breaking and the telescoping of the ice cover. The piling floes were thus of a smaller size than that of the preceeding case. The second ice piling discussed earlier was of this kind. It should be pointed out that although the ice has been weakened, it was still strong enough for walking on and although the ice floes were smaller, they were still kilometres in linear dimensions.

Following the first major ice piling associated with the above discussion, the water gap for free ice movement would be greatly increased. For the next ice piling, the ice floes would have a greater distance to acquire momentum. The greater movement also meant that the ice floes had more chance to break down and telescope. The third ice piling shown earlier was associated with ice movement of this kind. Fig.14 is a photograph showing the telescoped ice floes on Lake Simcoe immediately after the third ice piling. In the middle of the photograph, three longitudin-

al grid lines can be seen. Since the grid lines were roughly 100 m apart, the size of the ice floe showing the grid lines therefore was of the order of magnitude of 0.5 km in linear dimension. For the ice floes farther away from the shore, Fig. 14 shows that they could easily have a linear dimension of 2 to 3 km. The ice shown at the trailing edge of the ice field was in a much riper state. They were from Kempenfelt Bay and south of Big Bay Point which is shown on the top left corner of the photograph.

Fig.14. Broken down and telescoped ice floes.

The field observation also showed that as a large ice floe approaching the shore, it might pile directly while remaining intact (as did the ice floes at Brechin), or it might break into smaller floes first before piling as shown by Fig. 15. It is seen from Fig. 15 that there was a "chain action" in the breaking up process. The large floes broke into smaller floes and they in turn broke into even smaller floes. No attempt was made to quantitatively explain the size of the ice floes. Until such a question is answered, the calculation of the kinetic energy of a piling ice floe is greatly hindered.

Fig.15. The Chain Action of the Breakup of Ice Floes.

Conclusions

The new field evidences supported the earlier proposition that ice piling is a dynamic activity following a quick shift in wind direction from offshore to onshore. A water gap is necessary for the ice floes to gather momentum before piling. An above freezing temperature is also one of the conditions for ice piling. Static windshear is not the cause of ice piling on shores although a strong wind may crush the crust of an ice cover and produce heaps of ice debris. Great damage can be done by a mild wind with the closing of a small crack if the ice floe is immense. Lake currents under an ice cover are not influenced by the surface wind and have negligible effect on the movement of the surface ice. The impulse parameter I appears to be a good parameter for predicting ice piling. Ice piles not long after the I minimum. The prediction of ice piling by I minimum led to the successful filming of the second ice piling. To calculate the kinetic energy of an ice floe for ice piling, the size of the floe has to be known. Although it was found that the floe size decreases with the accumulated movement of the ice, much has yet to be learned before one can calculate the kinetic energy of an ice field for ice piling.

Acknowledgement

The author wishes to thank Messrs. Richard Hastings and Roger Foord for their kind permission to use their properties to conduct the study, to thank the Township of Innisfil for permission to erect the meteorological tower and for providing security coverage, and to thank the Toronto Weather Office for supplying weather maps for the studied period.

References:

1. Allen, J.L., 1969, "Analysis of forces in a pile up of ice", Proc. of Conf. in Ice Engineering and Avalanche Forecasting and Control, Oct., Calgary, pp 49-56.
   The Proc. was also published as N.R.C. Tech. Memo. No.98, Nov. 1970.
2. Bruun, P.M. and Johannesson, P., 1971, "The interaction between ice and coastal structures", Proc. of 1st Intern. Conf. on Port and Ocean Engin. under Arctic Conditions, Trondheim, Norway, Aug., pp 683-712.
3. Bruun, P. and Straumsnes, A.,1970, "Piling up of ice on seashore and on coastal structures", Proc. of I.A.H.R. Symp. on Ice and its Action on Hydraulic Structures, Reykjavik, Iceland, Sept., pp 3.8, 1-7.
4. Reed, N., "Impact of an ice floe against a sloping face", 1972, Prog. Rep. No.26, Inst. of Hydrodynamics and Hydraulic Engin., Tech. Univ. of Demark, Aug., pp 23-28.
5. Tryde, P., "A method of predicting ice pilings", Prog. Rep. No.25, Inst. of Hydrodynamics and Hydraulic Engin., Tech. Univ. of Demark, April, pp 17-23
6. Tryde, P., "A method of predicting ice pilings-impact of floe against inclined plane", Prog. Rep. No.26, Inst. of Hydrodynamics and Hydraulic Engin., Tech. Univ. of Denmark, Aug., 1972, pp29-33.
7. Tryde, P., "Forces exerted on structures by ice floes", Proc. of 23rd Navigation Congress, PIANC, Ottawa, July 1973, Section II, Subject 4, pp 31-44.
8. Tsang, G., "Ice piling on lakeshores-with special references to the occurrences on Lake Simcoe in the Spring of 1973", Proc. of Symp. on River and Ice, IAHR & PIANC, Jan., 1974, Budapest, Subject C, pp41-56.
   The paper in an improved form was also published as Scientific Series No.35, Inland Waters Directorate, Dept. of the Environment, 1974, Information Canada Cat. No. En 36-503/35.

THIRD INTERNATIONAL SYMPOSIUM ON
ICE PROBLEMS
Hanover, New Hampshire, USA

PLANNING THE GREAT LAKES-ST. LAWRENCE SEAWAY NAVIGATION SEASON EXTENSION PROGRAM

Carl Argiroff
Chief, Planning Branch
Engineering Division

Corps of Engineers,
Detroit District
Department of the Army

Detroit, MI

INTRODUCTION

The 95,000 square miles of water surface of the Great Lakes within the United States and Canada is the world's largest body of fresh water and provides the means of transporting over 100 billion ton miles of waterborne freight per year. The access to these waters for ocean vessels is the St. Lawrence River. The mean lake surface elevation (IGLD 1955) of the uppermost Great Lake (Lake Superior) is 600.39 feet. The five lakes (Superior, Michigan, Huron, Erie, and Ontario) which make up the Great Lakes, and the St. Lawrence River are located between latitude 41 and 50 degrees north, and are interconnected by improved transportation facilities of 27-foot controlling depth channels, canals, and locks. The length of vessel track from the Ports of Duluth-Superior, U.S.A., the westerly end of the system and halfway into the American continent, to the mouth of the St. Lawrence River at Father Point, Canada, is 1,684 miles. The present limit of year-round navigation is the Port of Montreal, Canada, 1,344 miles via water route to the Ports of Duluth-Superior. Lakes Superior, Huron, Erie, and Ontario and their connecting channels and part of the St. Lawrence River are boundary waters of the United States and Canada.

The Great Lakes have a tempering effect on the summer and winter temperatures of the Basin. Average annual temperatures in the Great Lakes Basin range from about 39 degrees Fahrenheit on Lake Superior to about 49 degrees Fahrenheit on Lake Erie. Minimum and maximum monthly temperatures occur in February and July, respectively, on all the lakes. The mean annual precipitation for the entire Basin ranges from

a minimum of 25 inches to a maximum of 37 inches. The annual snowfall within the Basin ranges from 30 inches to about 120 inches. Estimates of the annual rate of evaporation on the surface of the Great Lakes range from a minimum of about one and one-half feet on Lake Superior to about three feet on Lake Erie. The Lakes are generally ice-free from May to the early part of November. The dates of maximum freezing-degree-day accumulation for the Great Lakes area based on 10-year mean values are shown on Plate 1. This graph illustrates the time range for the maximum accumulation as well as the period of greatest ice cover across the Great Lakes. A freezing-degree-day is defined as a day with the average temperature 1 degree below 32 degrees Fahrenheit. The 20-year average value of the accumulated number of freezing-degree-days versus time is shown on Plate 2. Ice cover on the Lakes is made up of ice of various ages and type, but acts as a homogeneous ice sheet as long as air temperature remains below freezing. Ice cover on the Lakes is therefore two general types, sheet ice and agglomeratic ice. Ice formation usually begins about 1 December in the northerly portions of the Lakes and by 1 January is prevalent throughout the system. Ice thickness in excess of 40 inches are common in many harbor areas in Lake Superior. As ice cover moves, it rafts and forms ridges and in some Sections of the Great Lakes may reach a height of 25 feet above the surface and grounded on the bottom 30-40 feet below the surface. On the St. Lawrence River, the winter ice cover usually forms first along the south shore canal between Montreal and Lake St. Louis in early to mid-December and advances upriver to Lake Ontario. Mid-winter conditions usually consist of fast ice which is not generally subjected to breakup from wind or current conditions. Ice thickness in channel sections may average two to three feet while lake and river ice may only reach a thickness of one and one-half to two and one-half.

Navigation on the Great Lakes-St. Lawrence Seaway has been historically suspended every winter from about mid-December until early April because of adverse effects of weather and ice. This suspension requires stockpiling as an alternative method of operation, and less than full use of shore and terminal facilities and the Great Lakes fleet. Transportation cost for existing commerce reflect the more costly alternatives. Oceangoing vessels and oversea traffic are shut out of the Great Lakes Navigation System for one-third of every year. The impact on the economy of the Nation is significant. Although the Great Lakes Region within the United States covers only about four percent of the Nation's land areas, its 26 million residents comprise about 15% of the United States population and produce over 50% of the Nation's steel. This region is considered the industrial heartland of the country.

PROGRAM

In recognition of the potential benefits of an extended season, the United States Congress in 1965 authorized the U.S. Army Corps of Engineers, the principal water resources management agency of the Nation, to investigate and conduct a limited study of the feasibility of means of extending the season. This study completed in 1969, concluded that present technology is sufficiently advanced to make winter operations on the Great Lakes-St. Lawrence

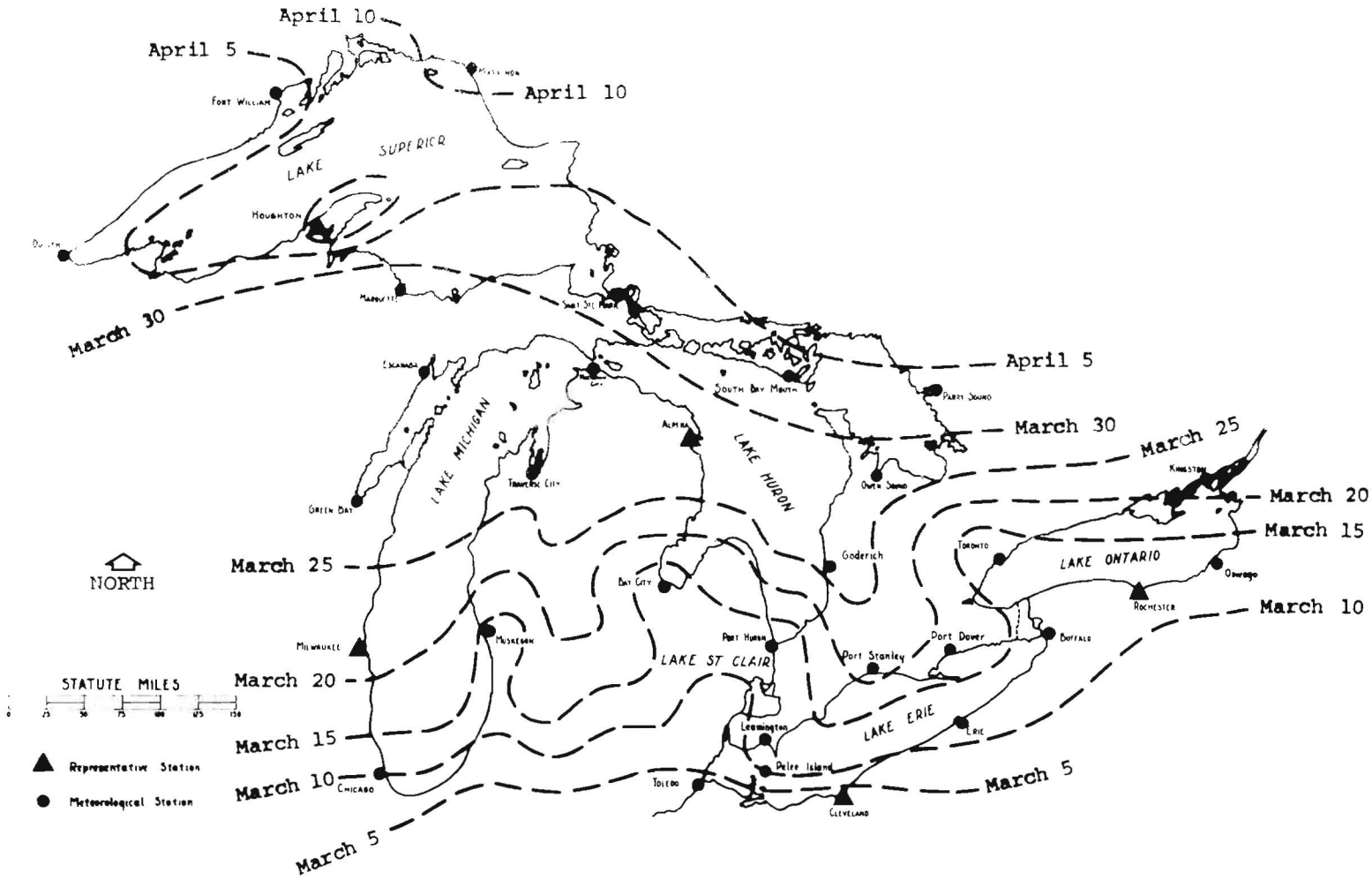

Plate 1. Average dates of maximum freezing degree-day accumulation.

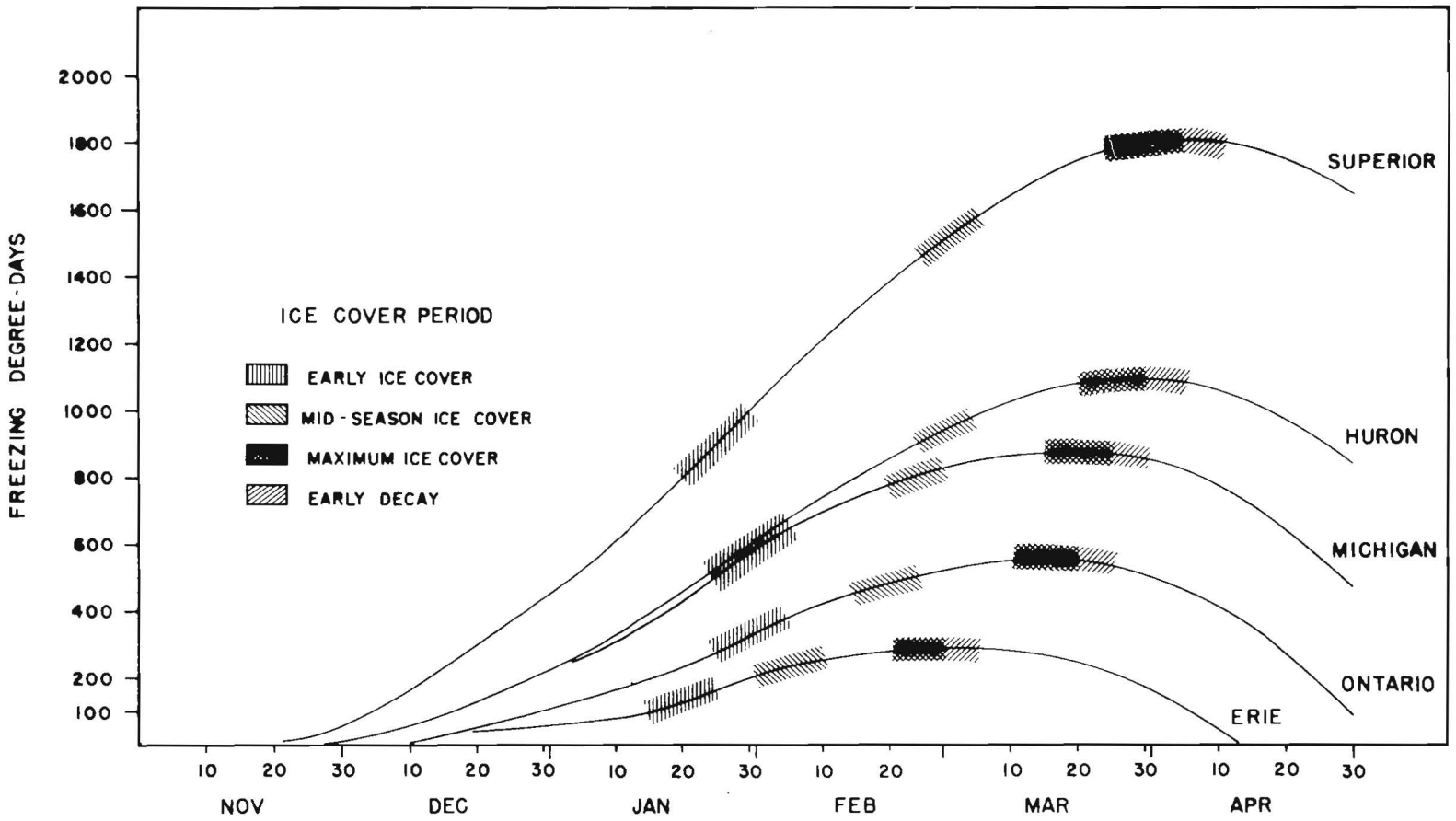

Plate 2. Twenty-year average accumulated freezing degree-days.

Seaway System physically feasible. The United States Congress subsequently authorized in 1970 a Winter Navigation Program, consisting of (1) a detailed survey study (investigation) to determine the economic, engineering, environmental, and social impact and feasibility of an extended season, (2) an action program aimed at demonstrating the practicability of extending the season, and (3) an insurance study to determine the ways and means for providing reasonable insurance rates to shippers and vessels operating during the extended navigation season. The insurance study was completed by the Maritime Administration in June 1972.

The product of the Winter Navigation Program will be a report to the United States Congress, recommending the advisability of Federal participation in improvements needed to achieve a guaranteed extended season, either partially or year-round, in all or parts of the Great Lakes-St. Lawrence Seaway System.

The Demonstration Program is a comprehensive plan of projects and activities to test and evaluate those engineering solutions which appear to have a high potential for success. All demonstration activities under the program are presently limited by Congressional authorization to a maximum expenditure of 9.5 million dollars. The organizational structure to conduct the Demonstration Program consists of a Winter Navigation Board composed of senior field representatives of participating Federal agencies and other invited organizations. The Board is composed of representatives from the U.S. Army Corps of Engineers (Chairman), U.S. Coast Guard (Vice Chairman), St. Lawrence Seaway Development Corporation, Maritime Administration, Federal Power Commission, Department of the Interior, Great Lakes Basin Commission, Great Lakes Commission, National Oceanic and Atmospheric Administration, and the Environmental Protection Agency. Members of an Advisory Group to the Board are from the Lake Marine Engineering Beneficial Association and the Great Lakes Task Force. Observers to the Board represent the St. Lawrence Seaway Authority, Canada, the U.S. Section of the International Joint Commission, and the U.S. Department of State, Office of Canadian Affairs. Technical advisors are represented from the National Aeronautics and Space Administration and the Atomic Energy Commission. There is also a special assistant to the Chairman, a coordinator from a local governmental agency, Chippewa County Commission in the St. Marys River, Michigan area. More recently a special Technical Review Panel consisting of three internationally known experts on ice problems from the United States and Canada have been added to the Board's structure as special technical advisors to the Board. The Board provides overall planning, programming, budgeting, and approval for execution and reporting of Demonstration activities. A Working Committee, similarly constituted, carries out the program activities approved by the Board. "Lead agencies" are responsible for carrying out activities under each of seven functional categories, as follows: Ice Information, (NOAA, Great Lakes Environmental Research Laboratory); Ice Navigation, (Coast Guard); Ice Engineering, (Corps of Engineers, Cold Regions Research & Engineering Laboratory); Ice Control, (St. Lawrence Seaway Development Corporation); Ice Management, (Corps of Engineers); Economic Evaluation, (Corps of Engineers); and Environmental Evaluation, (Environmental Protection Agency). A report on the Demonstration Program is scheduled to be provided to the United States Congress on 30 December 1976.

The Demonstration Program activities and findings will provide the principal basis for developing alternative plans of improvement for navigation season extension. These data will form the framework and essence of the Survey report to Congress. Findings, evaluations, and conclusions therein, together with economic and environmental analysis, will provide the Congress with information on which to base its decision for further improvements on the Great Lakes and St. Lawrence Seaway System. The Survey Study is being prepared by the U.S. Army Corps of Engineers and has been assigned to the Detroit District. The Survey Report is now scheduled for completion during 1977.

PROBLEMS

Major problems of winter navigation on the Great Lakes-St. Lawrence Seaway System are classified into four areas of primary consideration: channels, both interlake and on the St. Lawrence River; harbors; locks; and the open lake courses. Specific problem areas tested or proposed for testing or study are:

a. Maintaining vessel tracks in the Seaway, connecting channels, and lakes.
b. Maintaining stable ice covers in the connecting channels and the St. Lawrence River to reduce the threat of ice jams.
c. Maintaining access between the mainland and islands affected by winter navigation.
d. Potential shore erosion and shore structure damage as a result of vessel movement or broken ice movement in restricted channels.
e. Ice jams in the connecting channels and ice build-up on intake structures of power facilities which may effect power production.
f. Navigating tight channel turns and bends.
g. Navigating ice booms without disrupting the integrity of the ice field which the ice boom helps form.
h. Damage to vessels as a result of transiting various types of ice conditions.
i. Ice build-up on vessel superstructures.
j. Increased insurance rates for vessel operators.
k. Implementation of navigation aids and systems to withstand and operate in the winter environment.
l. Collection and dissemination of real-time winter data.
m. Effects of the winter environment on working personnel, both onboard vessels and onshore.
n. Environmental effects of all aspects of winter navigation.
o. Increased potential of oil spillage as a result of vessel operation during the winter months.
p. Broken ice in lock chambers.
q. Ice build-up on lock walls.
r. Ice accumulation in lock gate recesses.
s. Icing at harbor entrances, in harbor main channels and berthing areas, and at dock and terminal facilities.

ACCOMPLISHED DEMONSTRATION ACTIVITIES

The last winter navigation season, 1974-75, concluded the fourth of five scheduled years of demonstration activities, and was the first time year-round navigation was achieved at the St. Marys Falls Canal and Locks. The previous season's closing date at the St. Marys Falls Canal and Locks has been extended from the normal closing date of 16 December to 1 February 1972, 8 February 1973, and 7 February 1974. The extension of the season has been accomplished primarily through the effort of vessel operators, the U. S. Coast Guard's icebreaking efforts, and the operational units at the lock facilities, managed by the Corps of Engineers at St. Marys Falls Canal and the St. Lawrence Seaway Development Corporation at the St. Lawrence Canal. Seaway closing dates for the four years of the Demonstration Program were 12 December 1971, 23 December 1972, 22 December 1973, and 17 December 1974; compared to closing dates during the first week of December prior to the Program. Opening dates are also earlier at the Seaway during the last several years from the second week in April to late March due primarily to the impetus of the Program.

A full, or even a partial, discussion of all activities tested and the resulting conclusions is not possible here. However, a full summary on demonstration activities is provided in annual reports published by the Great Lakes-St. Lawrence Seaway Winter Navigation Board. Major activities accomplished include: expansion of an Ice Navigation Center; extensive aerial and ground surveillance activities of ice conditions, ice movements and ice effects on water levels, and shore and shore properties; field test of several marine navigation systems; increased icebreaking assistance including the added service of ice buoys and navigational aids; development and testing of ice booms with and without gates on the St. Lawrence River; installation of air bubbler systems as a means of retarding ice growth; test of vehicles to solve island transportation problems; ice force measurements; physical model tests to determine the most effective way to stabilize an ice field interrupted by a vessel track; and system studies of the St. Lawrence Seaway (American Sector) and the Lake Huron-Lake Erie connecting channel.

Several successful tests conducted as part of the ice management and control functional work groups are of interest. First bubbler tests were conducted two successive years in a navigation channel in the St. Marys River and proved successful in reducing ice thickness in a navigation channel. Air bubbler tests were also conducted in three separate locations in Duluth and Superior Harbors. The first pre-demonstration test in Duluth Harbor proved the system feasible. The second in Superior Harbor proved the ability of bubbler to facilitate vessel maneuvering into a loading area. The third, in Duluth Harbor proved the effectiveness of bubbler operating in a channel adjacent to a companion bubbler operating in a slip area where potential existed in exhausting the heat supply. Special environmental studies were also carried on during these demonstrations. These studies have not found bubblers to have any significant adverse environmental impacts. Effectiveness of bubblers in open lake conditions under a shifting ice field still remains to be demonstrated. Consideration of

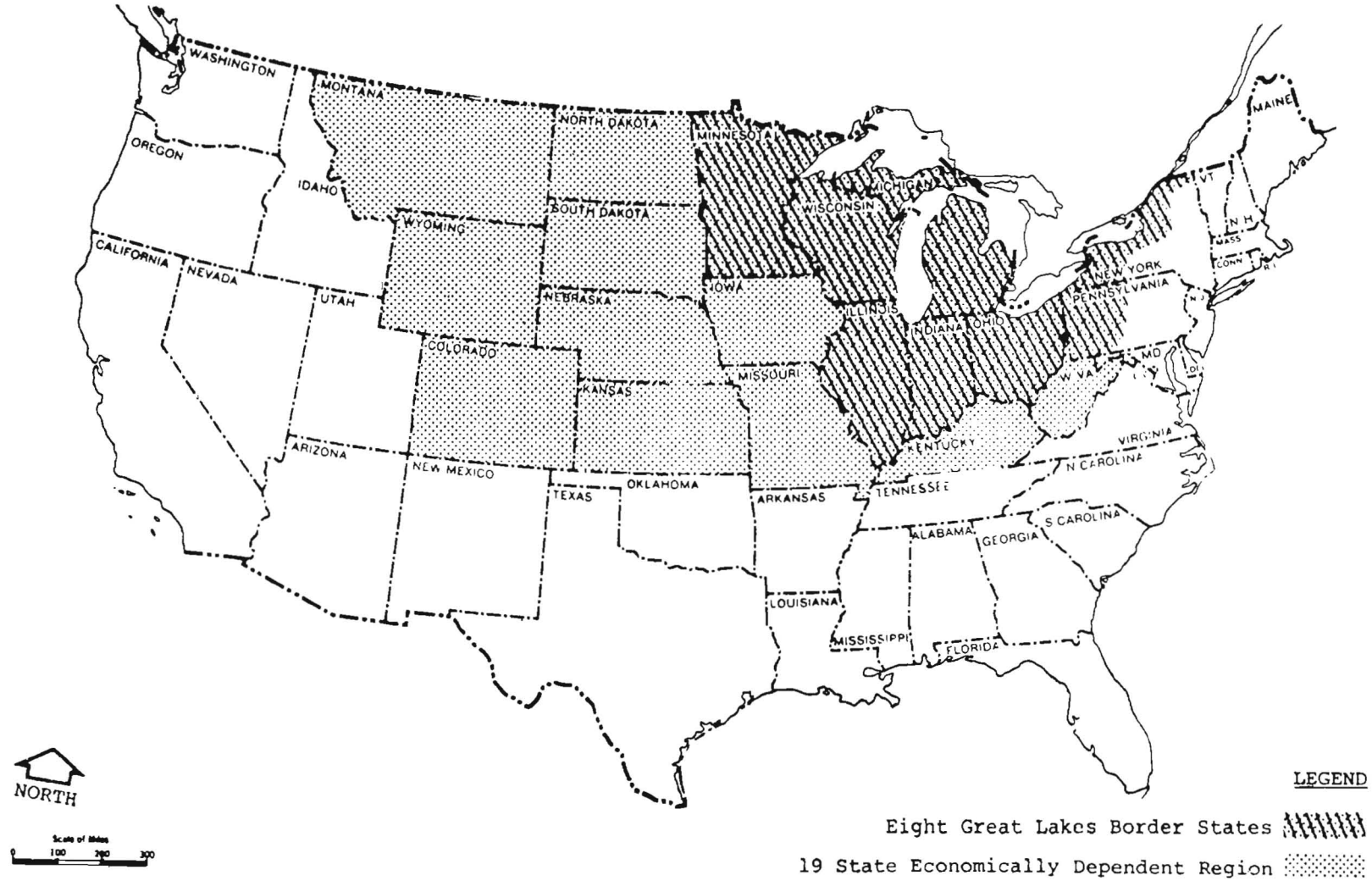

Plate 3. Great Lakes Economic Regions.

Environmental Plan, provided the benefit-cost ratio is favorable and the environmental and social impacts are acceptable. The National Economic Development objective is enhanced by increasing the value of the Nation's output of goods and services and improving national economic efficiency. The Environmental Quality objective reflects society's concern and emphasis for the management, conservation, preservation, creation, restoration and improvement of certain natural and cultural resources and ecological systems.

CONCLUSION

The demonstration activities and studies conducted to date have proven that extending the navigation season on the Great Lakes-St. Lawrence Seaway System is technically feasible. Preliminary studies also indicate that extending the season is environmentally and economically feasible on the Great Lakes and economically feasible on the St. Lawrence Seaway. There remains to be determined the extent of winter navigation in the various geographic areas of the System. Our report to the U.S. Congress will define specifics to any proposed improvements.

THIRD INTERNATIONAL SYMPOSIUM ON
ICE PROBLEMS
Hanover, New Hampshire, USA

ALGORITHM FOR ACCELERATED GROWTH OF ICE IN A SHIP'S TRACK

B. Michel, Dr.Eng., Professor of Ice Mechanics, Université Laval, Canada

D. Bérenger, M.Sc. Eng., Research Engineer, Arctec Canada Ltd, Canada

1. INTRODUCTION

One of the major problem of winter navigation in closed canals or quiescent water bodies, is the accelerated growth of ice in a limited ship's track with repeated ship passages. Because of the presence of water closer to the surface in the holes of broken-up ice accumulations, this growth may lead to unusual thickening of the ice, that would eventually close the passage to further navigation, unless the large volume of ice is cleared by some means.

We have developped an algorithm [1] to represent this phenomenum for navigation close to a wharf in Arctic waters and we are applying this method here to accelerated ice growth in a canal of the Saint-Lawrence Seaway in the Montreal area.

2. THE PHYSICAL REPRESENTATION

The appearance and distribution of ice pieces in the track of a ship depend very much on its form, the kind of ice the ship is going through, the propulsion system and other parameters [2] that cannot be discussed at length, here.

After observing the modes of accumulation of broken ice and ice growth in ship's tracks, we proposed the simple physical model shown on Figure I. It is made of a pile of superposed ice sheets of basic thickness ΔH with a residual ice thickness H_R at the bottom. Each unit layer contains an area full of water of surface ε, where ε is the ratio of water volume to total volume of the accumulation, that is, the

porosity of the accumulation.

The thickness of the basic layer has to be determined by the growth of a solid ice layer between successive passage of a ship in the same track. It is possible that the water hole be in any position per unit area in a layer. Part of a water hole in layer i may be indirectly under that of layer $(i-1)$. The probable distribution of ice and water inside the accumulation is shown on the following Table.

Layer number	Relative position and area of water				Area of continous ice
1	ε	ice	ice	ice	$(1-\varepsilon)$
2	ε^2	$(1-\varepsilon)$	ice	ice	$(1-\varepsilon)^2$
3	ε^3	$(1-\varepsilon)\varepsilon^2$	$(1-\varepsilon)\varepsilon$	ice	$(1-\varepsilon)^3$
4	ε^4	$(1-\varepsilon)\varepsilon^3$	$(1-\varepsilon)\varepsilon^2$	$(1-\varepsilon)\varepsilon$	$(1-\varepsilon)^4$
i	ε^i	$(1-\varepsilon)\varepsilon^{i-1}$	$(1-\varepsilon)\varepsilon^{i-2}$	$(1-\varepsilon)\varepsilon^{i-3}$ ...	$(1-\varepsilon)^i$

TABLE 1- PROBABLE DISTRIBUTION OF WATER AND ICE IN A BROKEN-UP LAYERED ACCUMULATION OF UNIT AREA.

In general it is not possible to produce ice in any water hole underneath solid ice thicker than two layers. Furthermore after a certain number of layers, water holes would have been seen in the mass covering the whole unit area so no residual ice of thickness H_R would be formed underneath.

3. THE ALGORITHM

A widely used engineering formula for ice growth of a solid cover [3] is:

$$H = \alpha \sqrt{D} \qquad (1)$$

where:

- H - ice thickness in inches
- D - number of degree-days of frost
- α - local heat exchange coefficient, always smaller than one

Applied to our case, this gives the thickness ΔH_{LN} of ice formed in a water hole at any level n :

$$\Delta H_{LN} = \left(\left[(n-1)\ \Delta H \right]^2 + \alpha^2\ \Delta D \right)^{-\frac{1}{2}} - (n-1)\ \Delta H \qquad (3)$$

where ΔD is the number of degree-days of frost between successive ship passages.

A complete analysis has been made to formulate the amount of ice produced in the holes at the surface, in the holes inside the pack itself and the residual ice formed under the pack. This gives an overall increase in thickness ΔH_T between the passage of each ship.

$$\left.\begin{aligned} \Delta H_T = {} & \frac{\varepsilon}{1-\varepsilon} \left\{ (\Delta H - \Delta H') + \xi \left[\sqrt{\alpha^2\ \Delta D} - (\Delta H - \Delta H') \right] \right\} \\ & + \varepsilon \sum_{i=2}^{K} \left[\sqrt{\left[(i-1)\ \Delta H^2 \right] + \alpha^2\ \Delta D} - (i-1)\ \Delta H \right] \\ & + \nu\ (1-\varepsilon)^{n-1} \left[\sqrt{(n\ \Delta H + H_r)^2 + \alpha^2\ \Delta D} - (n\ \Delta H + H_r) \right] \end{aligned}\right\} \qquad (4)$$

where:

K is the critical number of layers required to stop the formation of residual ice.

$$K = 1 \,/\, (1-\varepsilon)\,\varepsilon$$

and:

$$\xi = 1 \quad \text{for} \quad \sqrt{\alpha^2\ \Delta D} \leq (\Delta H - \Delta H')$$

$$\xi = \varepsilon \quad \text{for} \quad \sqrt{\alpha^2\ \Delta D} > (\Delta H - \Delta H')$$

$$\nu = 1 \quad \text{for} \quad n \leq K$$

$$\nu = 0 \quad \text{for} \quad n > K$$

$\Delta H'$ = distance between the top ice and the water surface.

A computer program was developped to solve the algorithm. It gives the writings and results and follow each step of the computation.

4. SOME APPLICATIONS

The initial application of the algorithm dealt with the growth of ice along a projected wharf in the Beaufort Sea that would be boarded at possible intervals of 1 to 5 days. The design was conceived in a manner such that the ice would be cleared in the quiescent area every-

time it would get to be 12 feet thick.

The computations were carried out for the coldest year on record at Inuvik in 1963-64. The total number of degree-days of frost was then 8318°F- days and the natural ice thickness growth in this aera is around 72 inches. The value of the coefficient α was computed to be 0.9, which is a very good heat exchange coefficient. The computations were carried for various values of the porosity factor ε. For a value of ε of 0.3 the results are shown on TABLE 2.

	Interval of passage (days)				
	1	2	3	4	5
total ice thickness inches	635	459	382	332	292
number of times of ice clearance	4	3	2	2	1

TABLE 2- ACCELERATED GROWTH AND ICE CLEARANCE ALONG WHARF IN BEAUFORT SEA.

This shows that a very large quantity of ice is formed approaching the wharf and that an ice management plan had to be developped to dispose of this ice.

This problem will also be an important one if winter navigation is to be opened in the St. Lawrence Seaway. We have made a computation of accelerated ice growth in the South Shore canal near Montreal for the winter temperatures of 1968-69 which can be taken as an average winter. Many ships would use the canal during daytime and the basic ice layer would form overnight. Thus an equivalent frequency of passage of one a day was taken for the computation with a porosity value of 0.3. The results are shown on Figure 2 where the accelerated growth can be compared with the static growth. It is clear that the ship generated ice grows almost linearly with degree-days while static growth depends on the square root of the variable. The large thickness of ice which is produced shows that there will be a problem of ice management if most ships are to make it for winter navigation.

1- MICHEL, B., LAFLEUR, P. (1971). Ice management at marine terminal, Herschel Island. Report to Dpt. of Public Works, Canada 212 p.

2- Transactions of the Society of Naval Architects and Marine Engineers Vol. 67, 1959. Seven papers on icebreakers, with discussions.

3- ASSUR, A. (1956). Airfields on floating ice sheets. USA-SIPRE, Technical Report 36.

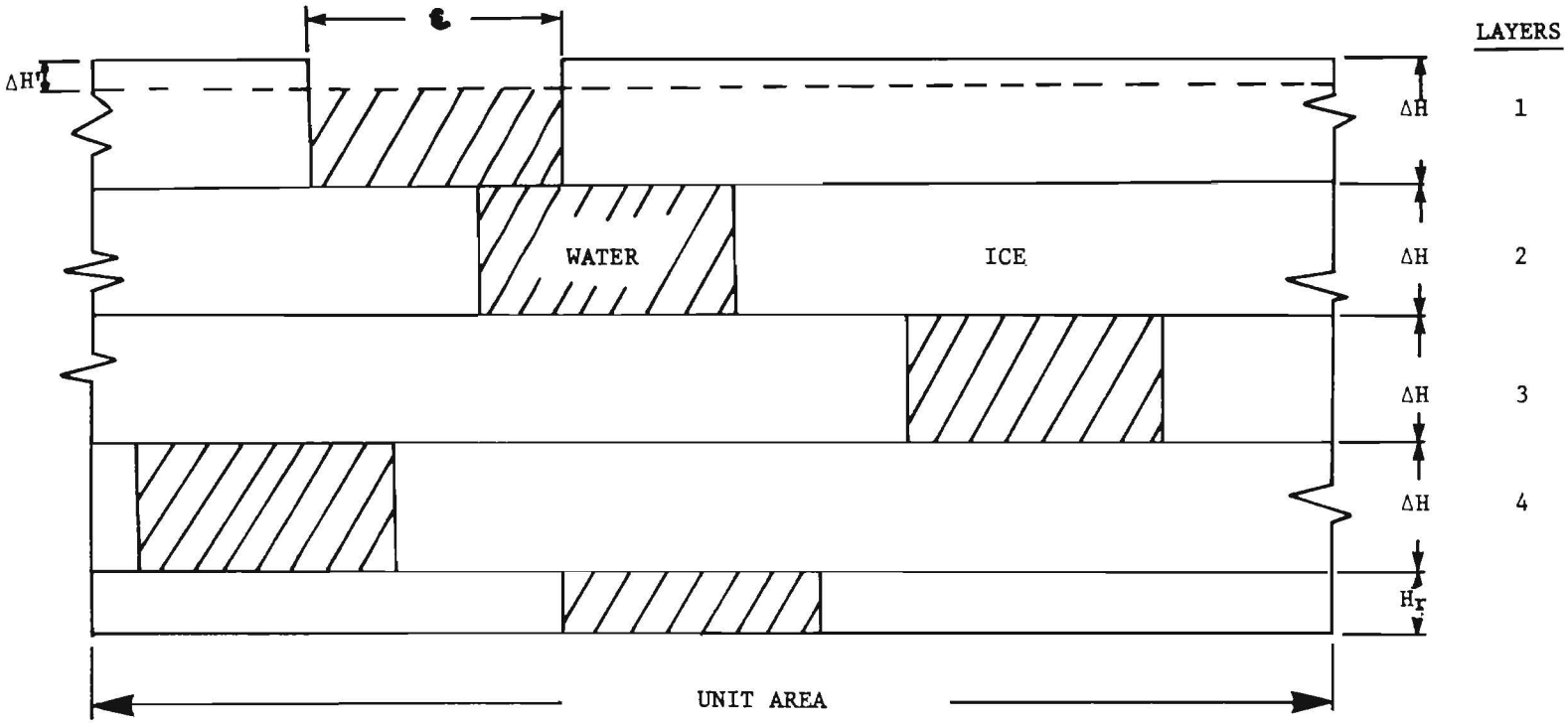

FIGURE 1

PHYSICAL MODEL OF ICE GROWTH IN SHIP'S TRACK

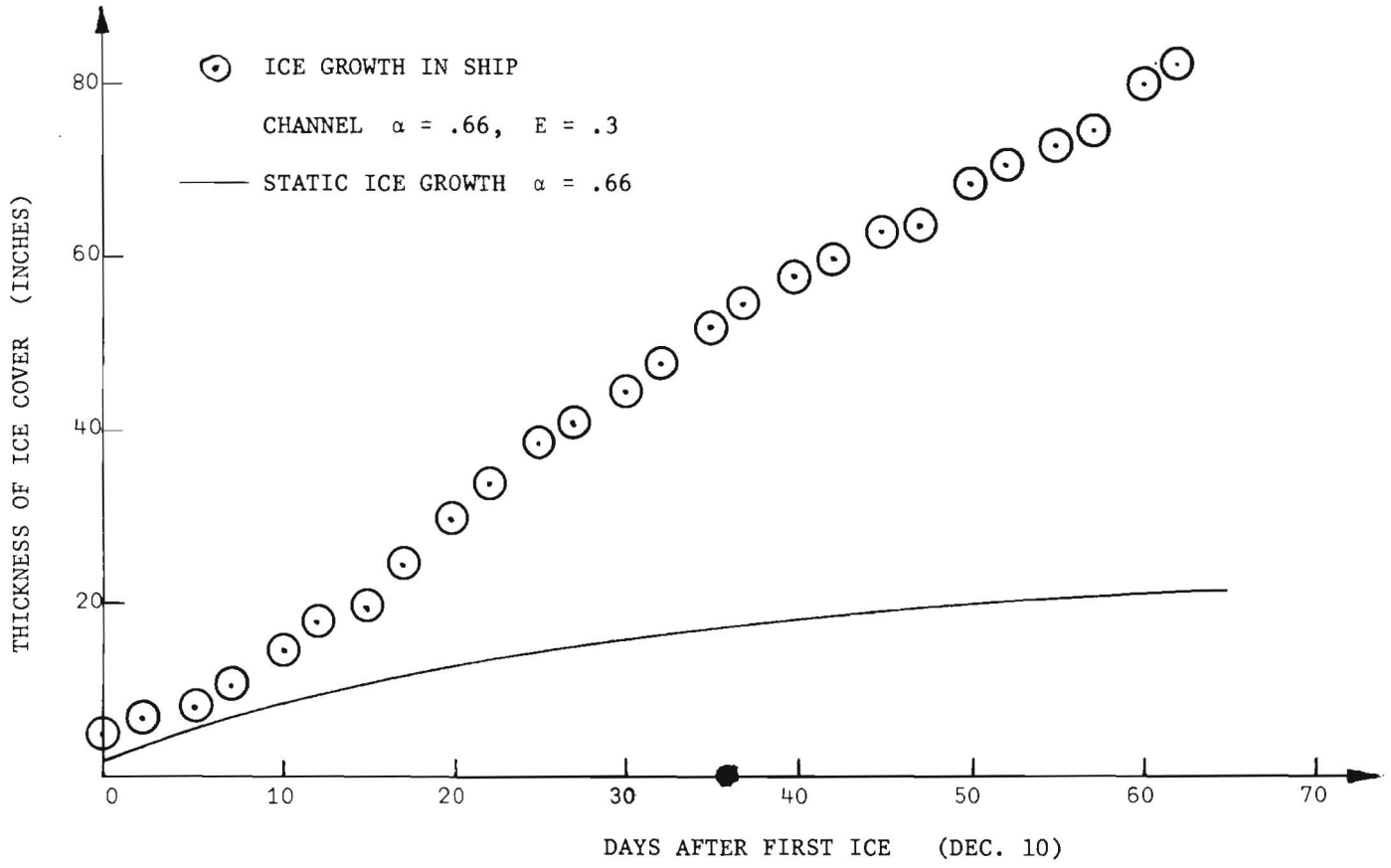
ICE GROWTH IN SHIP
CHANNEL α = .66, E = .3
STATIC ICE GROWTH α = .66
THICKNESS OF ICE COVER (INCHES)
80
60
40
20
0
10
20
30
40
50
60
70
DAYS AFTER FIRST ICE (DEC. 10)

THIRD INTERNATIONAL SYMPOSIUM ON
ICE PROBLEMS
Hanover, New Hampshire, USA

EXPERIMENTAL EVALUATION OF BUBBLER-INDUCED HEAT TRANSFER COEFFICIENTS

Dr. George D. Ashton
Hydrologist

Snow and Ice Branch
U.S. Army Cold Regions
Research and Engineering
Laboratory

Hanover, NH
U.S.A.

The results of laboratory experiments to evaluate the heat transfer coefficients associated with flow induced by a line source bubbler system are reported. The heat transfer coefficients, both in the impingement area and laterally outward from the axis of the impingement region, were evaluated by observation of melting rates induced at the underside of an ice cover formed in a large cold room. The experimental results are compared and interpreted in light of an analytical model previously developed. Implications for field applications of bubbler systems are discussed.

INTRODUCTION AND BACKGROUND

The use of air bubbler systems has frequently been considered as a means of suppressing ice formation. Until recently, however, the design and performance of such systems has been based largely on past experience with successful systems. Recently Ashton (1974) examined air bubbler systems from an analytical standpoint, with the ultimate goal of predicting the effectiveness of using bubblers to suppress ice formation under various field conditions. One of the parts of that analysis was an estimation of the heat transfer coefficient induced at the ice cover undersurface by the flow above a line-source bubbler. In that analysis the published results of small-scale experiments with air jets issuing from slots in an ambient air environment was used as the basis for predicting the heat transfer coefficient. Clearly, larger-scale two-dimensional studies using an air bubbler in water would provide a more sound basis for prediction. Herein the results of preliminary experiments in a laboratory situation are reported, and compared and interpreted in light of the analytical model previously developed. Implications for field appli-

cations of bubbler systems are discussed and the direction of future research efforts indicated.

DESCRIPTION OF EXPERIMENTS

The experiments were conducted in a cold room measuring 7.6 m by 7.6 m which contained water at a depth of 1.07 m. A total of six experiments were conducted, the first two of which were prematurely terminated because of a variety of operational problems. The bubbler line was on the bottom at approximately the centerline of the tank. Line diameter was 9.5 mm and orifices with a diameter of 1.0 mm were spaced at 0.30 m along the line. Air was supplied from laboratory lines at a nominal gage pressure of 4.2×10^5 Pa but was throttled between the supply and the diffuser line. The procedure in all experiments was as follows: With the air supply shut off, the cold room was brought to a temperature near -15°C and an ice cover allowed to form and thicken over a period of a few days or less. When the ice had thickened to about 0.12 m the room temperature was raised to 0°C and maintained overnight and for the duration of the experiment. This minimized the heat conduction through the ice cover and allowed the heat transfer rate induced by the bubbler operation to be interpreted from direct measurements of thickness changes in the ice cover.

Prior to starting the air bubbler the ice thickness was measured in a line transverse to the bubbler axis. Generally the ice was very uniform in thickness with maximum differences ordinarily less than about 4.0 mm. A thermal survey of the water below the ice was also made prior to bubbler operation with temperatures measured to a resolution of 0.1°C. The mean temperatures before bubbler operation were of the order of 2.5°C.

After the bubbler system was started, ice thickness measurements were made periodically in a line transverse to the bubbler line at about the midpoint of the tank. Water temperature measurements were also made periodically which were used later in the analysis of the data. The experiments were terminated either when melt-through had occurred above the bubbler axis or when the thermal reserve of the water had been exhausted. Air was collected in an inverted container above each orifice and the volume/time result used to determine the air discharge rate for each orifice. Due to variations between individual orifices there were some variations in the air discharges. In the analysis of the data the discharge rate of the orifice most proximate to the thickness measurements was used as the reference air discharge for that experiment. At the conclusion of each experiment a cut was made in the ice sheet and a profile of the ice measured. This information was also used to evaluate heat transfer rates.

DATA ANALYSIS

The energy balance at the ice-water interface assuming no heat conduction through the ice cover is

$$-\rho_i \lambda \frac{d\eta}{dt} = q_w \qquad (1)$$

where ρ_i is the ice density (kg m^{-3}), λ is the heat of fusion (J kg^{-1}), η is the ice thickness (m), t is time (s), q_w is the heat transfer rate to the under surface (W m^{-2}), and the negative sign means η is decreasing with time. In turn, the heat transfer rate may be described in terms of a heat transfer coefficient h (W m^{-2} $°C^{-1}$) applied to a temperature difference ΔT (°C) in the form

$$q_w = h \, \Delta T \qquad (2)$$

If it is assumed that h is independent of t and ΔT then equations (1) and (2) may be combined and integrated to yield

$$h = \frac{\rho_i \lambda \, (\eta_o - \eta)}{\int_{t_o}^{t} \Delta T \, dt} \qquad (3)$$

Thus the slope of the line of a plot of $\eta_o - \eta$ versus $\int \Delta T \, dt$ yields the product $h/\rho_i \lambda$ and hence h since ρ_i and λ are constant. In Figure 1 are presented data from a representative experiment showing measured values of $\eta_o - \eta$ and the associated values of $\int \Delta T \, dt$ for a centerline location, and for distances out from the centerline of 0.25 m, 0.51 m, 1.02 m, and 1.52 m. The results of calculations of h are presented in Figure 2a as a function of y/b where b is the width of the standard deviation of the assumed Gaussian profile of plume velocity and which is calculated (see Ashton, 1974, for details) from

$$b = (H + x_o) \, C_c \, Q_a^{0.15} \qquad (4)$$

In equation (4), H is the depth of submergence of the bubbler, x_o is an empirical correction to an analytic origin describing the induced water flow as a linearly spreading plume, C_c is an empirical constant gleaned from the data of Kobus (1968) ($C_c = 0.182$ $m^{-0.3}$ $s^{0.15}$), and Q_a is the line air discharge rate ($m^3 s^{-1} m^{-1}$). Similar results for three other experiments are presented in Figures 2b, 2c, and 2d. The solid line is that predicted assuming no entrainment of colder water in the spreading warm surface jet. The dashed line represents the effect of entrainment of 0°C water by the spreading surface jet with h referenced to the temperature of the impinging plume. These lines correspond to the analytical prediction of Ashton (1974). That analysis combined the empirical results of Kobus (1968) for the hydrodynamics of a bubbler-induced plume, with results of Gardon and

Akfirat (1966) for heat transfer rates induced by an impinging turbulent jet. The resulting prediction for the heat transfer rate at the impingement centerline (assumed to be constant out to a distance y=b) is

$$h_b = \frac{0.96\ k\ U_c^{0.62} b^{-0.38}}{\nu^{0.62}} \tag{5}$$

where k is the thermal conductivity of the water ($W\ m^{-1}\ °C^{-1}$), U_c is the centerline velocity of the induced plume at the undersurface of the ice, and ν is the kinematic viscosity of the water ($m^2 s^{-1}$). U_c was given by Kobus (1968) in the form

$$U_c = \left[\frac{-P_{atm}\ Q_a\ \log_e\left(1 - \frac{H}{H+10.3}\right)}{\sqrt{\pi}\ \rho_w\ U_b\ b}\right]^{1/2} \tag{6}$$

where SI units are implied, P_{atm} is the atmospheric pressure ($N\ m^{-2}$), ρ_w is the water density, and U_b is the mean rising speed of the bubbles. U_b was found by Kobus (1968) to be described by

$$U_b = C_b\ Q_a^{0.15} \tag{7}$$

where $C_b = 2.14\ m^{0.7}\ s^{-0.85}$.

Assigning the numerical values to the constants and properties and combining the equations yields (SI units)

$$h_b = \frac{17224\left[-\log_e\left(1 - \frac{H}{H+10.3}\right)\right]^{0.31} Q_a^{0.160}}{(H+0.8)^{0.69}} \tag{8}$$

If the wall jet is assumed to be constant temperature (assuming no thermal stratification of the ambient water body and negligible cooling of the jet due to transfer to the ice sheet) the distribution of h is then of the form (solid line in Figure 2)

$$\frac{h}{h_b} = \left(\frac{y}{b}\right)^{-0.38} \tag{9}$$

which is essentially the result implied by the air jet data of Gardon and Akfirat (1964). If the ambient water is at 0°C a turbulent entrainment model then yields (see Ashton, 1974) a distribution of h of the form (dashed line in Figure 2)

$$\frac{h}{h_b} = \left(\frac{y}{b}\right)^{-0.38} \left[\frac{1}{0.109\left(\frac{y}{b}\right) + 1}\right] \qquad (10)$$

where the reference ΔT for calculation of h (and h_b) is that of the impinging plume.

As noted earlier, at the termination of each experiment measurements of the ice thickness profile were made in a line normal to the axis of the bubbler line (and through a point above an orifice). The melted thickness distribution, when normalized by the melt thickness at the centerline, also gives an indication of the distribution of heat transfer rates. In Figure 3, data of $\Delta\eta/\Delta\eta_b$ versus y/b from 4 experiments are presented and compared to the predicted distributions of h/h_b.

DISCUSSION OF RESULTS

Examination of Figure 2 shows the predictions given by equations (8), (9), and (10) to be reasonable fits to the data. Particularly near the impingement area effects such as temporary entrapment of air (relieved in some experiments by drilling a hole), and deflections of the plume by secondary currents resulted in considerable scatter of the data. Within the accuracy of practical calculations and considering the highly unsteady ice conditions to which bubbler systems are subjected in practical usage, the predictions are considered reasonably accurate. Clearly, more work needs to be done to improve the analytical model and extend the available data base. Currently under development is a numerical simulation of the performance of bubbler systems which includes the unsteady effects of varying ice cover, varying meteorological conditions, and depletion of the thermal reserve of a water body. One of the preliminary results of that study and which is reinforced by the present results is that a bubbler system should not be expected to open a wide channel area free from ice. Rather, the advantage of a bubbler system is that it provides a line of weakness which allows vessels to more easily transit an otherwise intact ice cover.

ACKNOWLEDGEMENTS

In the conduct of the experiments and the data reduction the author was aided considerably by SP5 Jack A. Karalius and Mr. Howard Scott. The work was funded under the Ice Engineering Program of the Civil Works area of the U.S. Army Corps of Engineers, Project No. CWIS 31361 and 31362.

REFERENCES

Ashton, G.D., Air bubbler systems to suppress ice, U.S. Army Cold Regions Research and Engineering Laboratory (USACRREL), Special Report 210, September 1974, 35 p.

Gardon, R. and J.C. Akfirat (1966) Heat transfer characteristics of impinging two-dimensional air jets. Transactions, American Society of Mechanical Engineers, Series C, Journal of Heat Transfer, Feb., p. 101-108.

Kobus, H.E. (1968) Analysis of the flow induced by air-bubble-systems. Chapter 65 of Part 3. Coastal Structures, vol. II, Proceedings Eleventh Conference on Coastal Engineering, London, England. New York: ASCE, p. 1016-1031.

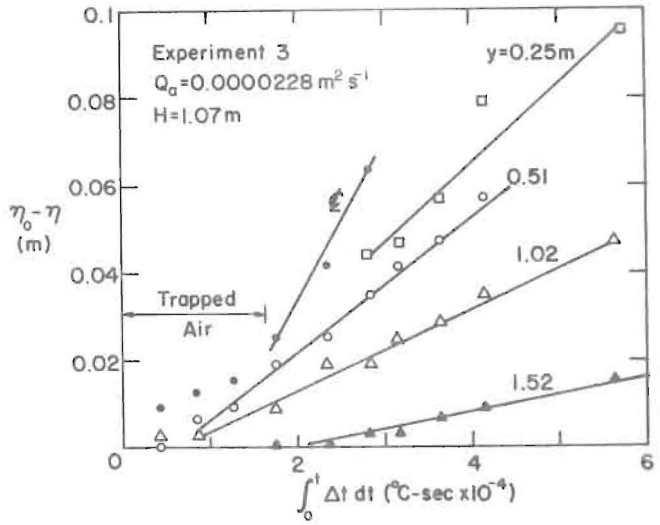

Figure 1 - Melting rates observed experimentally.

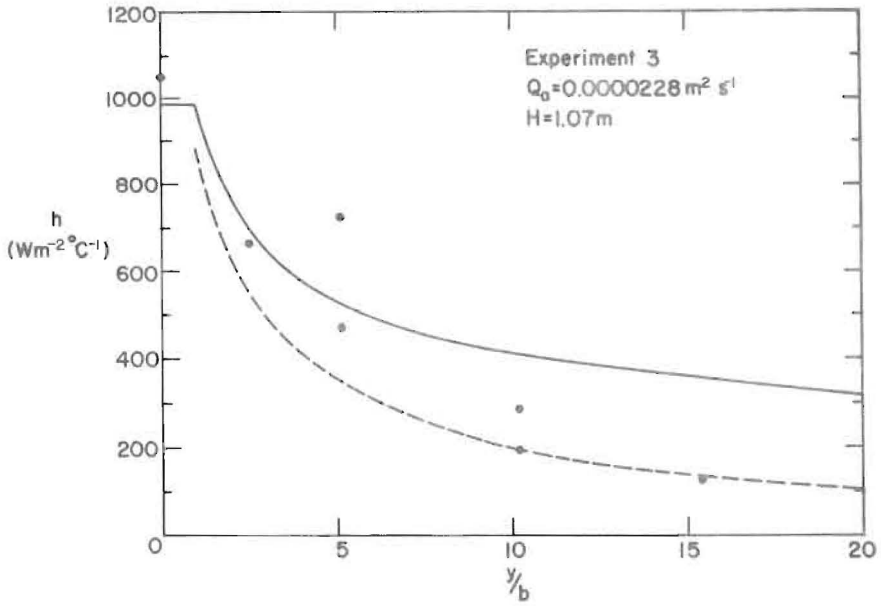

Figure 2a - Lateral distribution of h, Experiment 3.

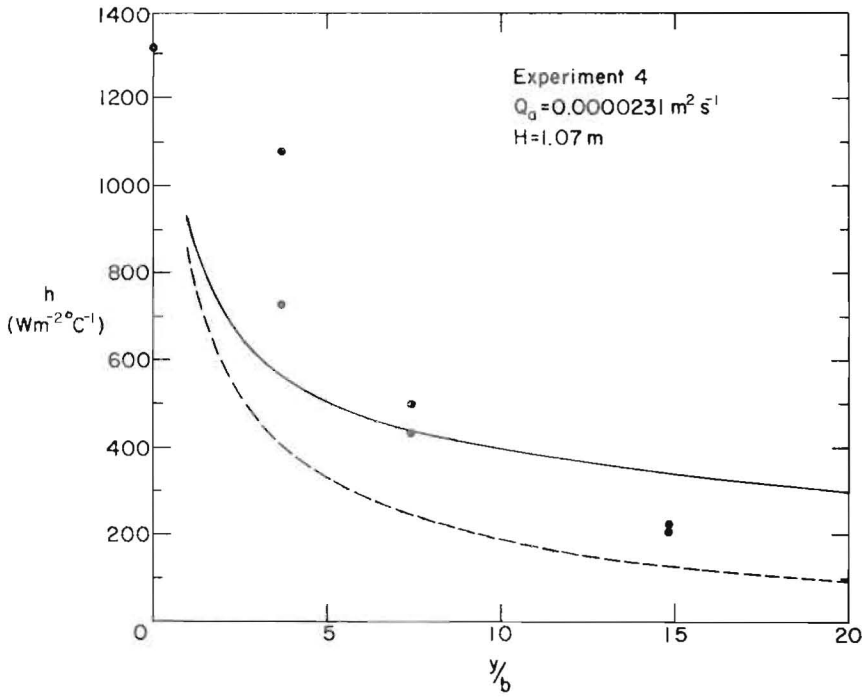

Figure 2b - Lateral distribution of h, Experiment 4.

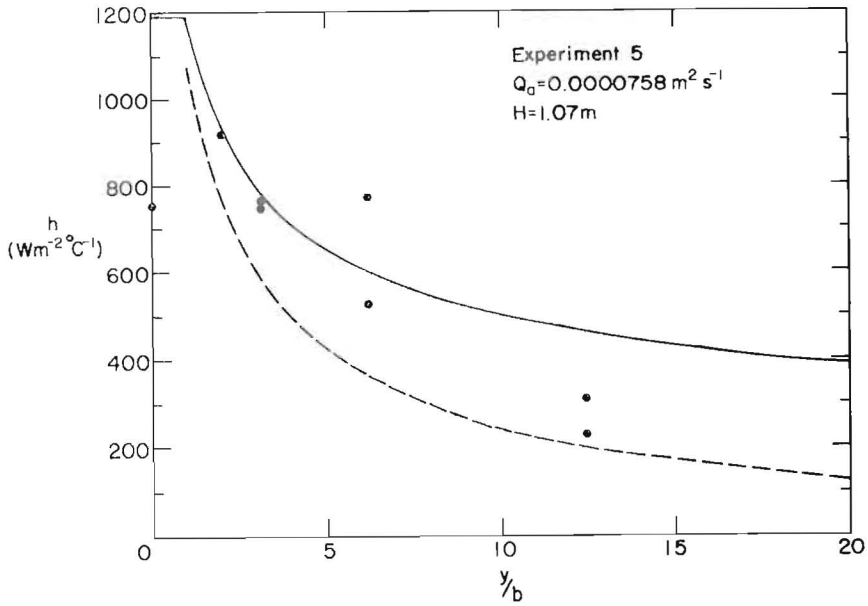

Figure 2c - Lateral distribution of h, Experiment 5.

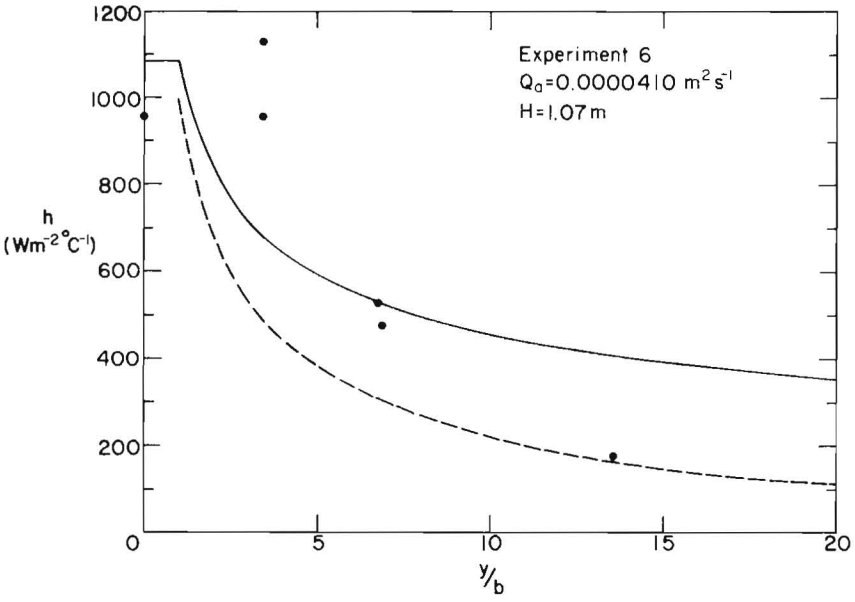

Figure 2d - Lateral distribution of h, Experiment 6.

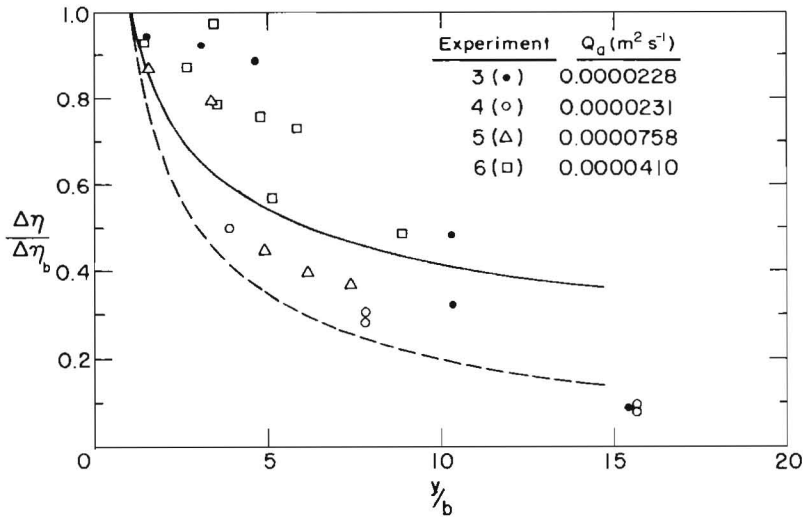

Figure 3 - Lateral distribution of melted thickness.

International Association of Hydraulic Research (IAHR)
Committee on Ice Problems
International Symposium on Ice Problems
18-21 August 1975
Hanover, New Hampshire

COMMENTS

Paper Title: Experimental Evaluation of Bubbler-Induced Heat Transfer Coefficients

Author: G. D. Ashton

Your name: Bruce D. Pratte

Address: Hydraulics Laboratory
National Research Council of Canada
Ottawa, Ontario, CANADA

Comment:

Observations of the width of ice melted by a 3-mile long air bubbler line in water varying from 20 to 150 feet in depth in Lake Ontario at Kingston, shows a relatively constant open width. This suggests that extrapolation of the theory to greater water depths with associated predictions of very large quantities of water brought up by the bubble columns, and therefore larger open widths, may be considerably in error. Field tests in deep water are sorely needed to corroborate the theory, or allow modifications to it.

Author's Reply:

Pratte's discussion centers around the assumption that has been made (Ashton, 1974) that the flow pattern induced by a bubbler spreads linearly with distance above the bubble source. While agreeing that this is still an open question, the author also wishes to point out that width of open area of ice does not serve as a sensitive measure of the induced flow width since the heat transfer coefficient is roughly proportional to the centerline velocity of the impinging flow and that velocity is nearly independent of depth. Nevertheless it is clear that detailed field tests are needed to resolve this and other questions related to bubbler performance as a means of suppressing ice.

THIRD INTERNATIONAL SYMPOSIUM ON
ICE PROBLEMS
Hanover, New Hampshire, USA

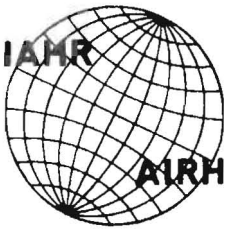

General Lecture on Theme 2

ICE-JAM MECHANICS

John F. Kennedy
Director

Iowa Institute of
Hydraulic Research
The University of Iowa

Iowa City, Iowa
USA

SUMMARY

This survey paper describes general features of the occurrence and behavior of river-ice jams. Some of the earlier work on ice-jam mechanics is reviewed. A new, simplified theory is developed for the prediction of the thickness and propagation velocity of ice jams, and for the increase in river stage the jam produces. The problem of the strength of ice jams is briefly reviewed. Finally, pressing research problems related to ice-jam mechanics are discussed.

I. INTRODUCTORY REMARKS

One of my senior colleages at The University of Iowa, Professor Enzo Macagno, has been heavily involved for the past several years in research on the fluid mechanics (pumping, and its relation to the motion, or "motility" in medical terminology, of the intestine wall; fluid velocity distributions; mixing; exchange processes; etc.) of the human small intestine. Needless to say, this is a very difficult research topic: more complex conduit geometry would be difficult to imagine; the fluid motion is produced by contractions of the intestine walls which are irregular in both space and time; the fluid (called chyme) is strongly non-Newtonian, and its properties change along the intestine and with time; and so on - the list of complexities is nearly endless. In a moment of frustration, Professor Macagno once remarked to me: "If one is going to do research on the fluid mechanics of the digestive tract, he never should look at a real intestine. If he does, he will become so discouraged at the outset that he will not pursue the problem further".

Professor Macagno's statement could as well have been made concerning river ice jams (also called embacles), as anyone who ever has studied a large, natural ice jam will attest. Figure 1 is a photograph illustrating several features that are all too common in jams. The jam is an agglomeration of irregularly shaped, random size ice fragments (or floes) packed together with haphazard orientation to form a mass that frequently undergoes buckling or shear failure that forms ridges or mounds of significant proportions. The surface of the embacle often is cluttered with assorted debris, such as tree trunks, empty oil drums, and pieces of car bodies, of generally unknown origin which is sprinkled over the surface of the jam as though it had been broadcast from a high-flying plane; this extraneous junk complicates the appearance of the ice cover, but probably plays no role in the jam's behavior. And the whole accumulation of ice and extraneous matter often undergoes continuous or sporadic deformation.

If jams seem complicated to the casual observer, they are even more so to one who examines their behavior in detail. Indeed, an ice-jammed river is among the most deranged of hydraulic phenomena. Let us consider some of the complexities. A jam is formed by concurrent flows of liquid water (hereinafter referred to simply as water) and ice; thus the flow is inherently two-phase (liquid-solid), a difficulty which is compounded by the possibility of phase change between water and ice. (In a sediment transporting flow, on the other hand, water remains water and sand remains sand; not so with ice-transporting water flows.) This phase change plays a very important role in the behavior of jams, as will be discussed later, because of its effects on the strength of the ice agglomeration. The flow that accompanies, and indeed produces, a jam is both unsteady and nonuniform. It is of the free-surface variety in that the position of the upper boundary is not fixed or known *a priori*, but of the confined type because of the existence of an upper boundary - the arrested ice - that is constrained against motion in the streamwise direction. The roughness of the underside of the ice cover is generally unknown; moreover, it changes with time. The general

problem of the strength of ice is one of the most difficult confronting ice engineers; even the relatively simple question of the correct procedure to be used in determining the compressive strength of monolithic ice is far from resolved, and the far more difficult problem of formulating the compressive and shear strengths of floating, fragmented ice - a problem of central importance to ice-jam analysis, as will be discussed below - is still in the early stages of investigation.

The foregoing discussion, albeit brief and incomplete, of the complexity of the constituent phenomena attendant to ice jamming should suffice to convince the reader that a generally applicable, wholly reliable, and relatively complete formulation of ice-jam mechanics likely will not be forthcoming in the forseeable future. However, this observation is equally applicable to many other current engineering problems. It appears to be the unhappy fate of researchers in the last quarter of the twentieth century that most of the easy problems have been solved. There is left for us, however, the possibility of making relatively smaller contributions to the understanding of more difficult problems, and this can be just as challenging and rewarding as obtaining complete solutions of simpler ones. (The latter, however, is surely more satisfying, and more often leads to the immortality of the investigator's name and work. One can but envy Osborne Reynolds, for example, for having had the good fortune (and alertness!) to encounter a relatively simple problem like lubrication theory, which he was able to solve almost in its entirety.)

This brief survey paper on ice-jam mechanics will not undertake to review all earlier work on this topic; for this the reader is referred to a recent report by Uzuner and Kennedy (1974), and to the references cited therein. Instead, the principal phenomena involved in ice jamming will be recounted and some of the noteworthy contributions to their elucidation will be reviewed. A simple analytical model of ice jams will be developed. Finally, the avenues of research that need to be pursued will be examined. Let the reader be warned at this early point that ice jams are too complicated to allow for generally acceptable interpretations and formulations of their behavior; complexity promotes dissension. This review inevitably will reflect the writer's views and opinions and biases on the jams - a common feature of most review articles.

II. THE GOALS AND THE MEANS

Many natural phenomena are so complex that it often is not readily apparent which of the variables involved are dependent and which are independent. For example, there still is considerable disagreement among river engineers on the question of what constitutes a complete set of independent variables for predicting the depth and sediment discharge of an alluvial stream. Therefore it seems reasonable at this early juncture to enumerate what one ideally would like to obtain from a mathematical model for ice jams, and which physical relations must be utilized in developing a theoretical analysis for their prediction. A reasonably complete list of goals is as follows:

1. The conditions for initiation of a jam (i.e., a relation between the geometry of a channel obstruction, ice discharge, flow properties, etc. for which jamming is incipient).
2. The speed of upstream movement of the leading end of the jam.
3. The thickness profile of the jam (i.e., the streamwise distribution of jam thickness).
4. The water surface profile upstream from the jam, especially the depth increase at the leading edge of the jam, and the streamwise distribution of flow depth beneath the jam.
5. The forces the jam can exert on stationary structures (e.g., bridge piers, ice booms, etc.).

Theoretically inclined hydraulicians have little to work with except relations expressing continuity, conservation of momentum and energy, kinematical restrictions (which often arise as boundary conditions), and constitutive relations for the fluid and solid materials involved. Specifically, the following relations must form the basis for an analysis of ice jams:

1. Continuity of motion of the ice and water.
2. The momentum (or energy) equation for the nonuniform flow approaching and beneath the jam.
3. Equilibrium among the static and dynamic forces exerted on the jam.
4. A relation between the depth and velocity of flow and the shear stresses exerted on the underside of the ice cover and the stream bed.
5. The "constitutive" relations which give the compressive and shear strengths of ice as functions of floe dimensions, jam thickness, rate of cover deformation, etc.
6. A boundary condition giving the thickness of the upstream end of the jam as a function of ice discharge, flow properties, floe dimensions, etc.

Needless to say, most of these relations are mathematically coupled. For example, the shear stress on the bottom of the jam is a function of the water discharge beneath the ice, which in turn is affected by the ice discharge approaching the jam and the jam thickness, which is related to the shear stress exerted by the flow on the ice. These mathematical complexities can be overcome in the age of the electronic computer. The principal stumbling blocks encountered in the analysis arise from inadequate knowledge of the strength of floating, fragmented ice, and of the forces exerted on the ice by the flow.

Before grappling with the mathematical expression of some of the relations enumerated above and solution of the resulting equations, it may be helpful to discuss some general characteristics of embacles.

III. SOME GENERAL FEATURES OF ICE JAMS

There would appear to be two requisites for the formation

of an ice jam: a large discharge of frazil or fragmented solid ice; and an obstacle in the channel which impedes the downstream passage of the ice. The character of the ice which initiates the jam will influence its early behavior, primarily because the strength of a frazil ice accumulation is much different from that of an agglomeration of solid ice floes, and because of differences between the vertical distributions over the flow depth of the two types of ice.

The variety of channel obstacles the flows of water and ice may encounter is almost boundless, ranging from changes in width (e.g., bridge piers and abutments), to changes in depth (e.g., sand bars), to man-made surface obstacles (ice-booms), to combinations of these. Only recently has research been conducted on the magnitude of lateral restriction which will initiate a jam. Calkins and Ashton (1975), for example, have undertaken a laboratory flume investigation using artificial ice (low-density polyethylene, with sp. gr. = 0.92) blocks to determine the conditions under which ice fragments will bridge the gap in a symmetrical surface obstacle (e.g., an ice boom with a navigable opening). They have found that the threshold of arching is a function of the surface concentration of ice on the approach flow and the ratio of gap width to floe dimension; an example of their results is shown in figure 2, in which a is the long dimension of the parallelepiped blocks they used, b is the gap width, Q_i is the plan-surface-area discharge of ice in the approach flow, and V is the mean velocity of the water flow. It is seen that as the floe size is increased, the ice discharge at which arching is incipient decreases. In experiments with mixtures of floe sizes, they found that the dimensions of the larger blocks are critical in determining if an arch will form. Similar experiments at the Iowa Institute of Hydraulic Research using both real and artificial ice have yielded results that are in general agreement with those of Calkins and Ashton. In the Iowa experiments on arching across gaps in obstacles which penetrate to the flume bed, it was observed that the floes are passed much more readily through the opening than in the case of a surface obstacle. In the former case, the velocities of the water and ice are increased by approximately the same relative amounts as they pass through the gap, and therefore no increase in surface-concentration occurs, whereas in the latter situation the ice must become more densely arrayed to pass through the gap while being transported at the velocity of the water, which increases little if any because the channel section is only very slightly reduced by the obstacle.

It is important to recall that an ice jam, like a stable ice cover, may not be formed upstream from an obstacle if the approach flow can submerge the blocks and transport them beneath the cover. The conditions for submergence of floes at the upstream end of an ice cover have been examined by Uzuner and Kennedy (1972) and by Ashton (1974), and a review of contributions to this problem is given by Uzuner and Kennedy (1974). A general field observation is that a stable ice cover will not form if the Froude number based on the depth and velocity of the approach flow is greater than about 0.06 to 0.14, depending on the ratio of floe thickness, t_i, to flow depth, H, (with the maximum Froude numbers for underturning generally

occurring at t_i/H in the range 0.2 to 0.4) or if the approach velocity is greater than about 2.0 ft/sec to 2.6 ft/sec.

Ashton (1974) developed a simplified and relatively reliable analysis for the prediction of incipient block submergence which gives the critical densimetric Froude number (based on floe thickness) as

$$\frac{V}{[g\, t_i (1-\frac{\rho'}{\rho})]^{\frac{1}{2}}} = \frac{2(1-t_i/H)}{[5 - 3(1-t_i/H)^2]^{\frac{1}{2}}} \qquad (1a)$$

where V is the velocity of the flow approaching the jam, ρ and ρ' are the densities of the water and ice, and g is the gravitational constant. In the development of (1a), the floe was treated as being initially at its level of hydrostatic flotation. Inclusion of the dynamic effect on the flotation level modifies (1a) to

$$\frac{V}{[g\, t_i (1-\frac{\rho'}{\rho})]^{\frac{1}{2}}} = \frac{\sqrt{2}(1-t_i/H)}{[3 - 2(1-t_i/H)^2]^{\frac{1}{2}}} \qquad (1b)$$

Figure 3 shows a comparison of (1a), (1b), a relation developed by Pariset and Hausser (1961) in which the floes are treated as sinking without rotating,

$$\frac{V}{[g\, t_i (1-\frac{\rho'}{\rho})]^{\frac{1}{2}}} = \sqrt{2}(1-t_i/H) \qquad (1c)$$

and experimental data on floe submergence. The analytical relations are seen nearly to bracket the data.

After an ice jam is initiated, the presence of a field of stationary ice produces an additional localized energy loss, by lengthening the wetted perimeter of the reach of channel occupied by arrested ice; clearly, the magnitude of the additional energy loss will increase as the jam lengthens, and, to a lesser extent, thickens. As this occurs, the flow beneath the jam will deepen, and reaches of nonuniform flow will be produced upstream and downstream from the jam. Thus the added resistance encountered by the flow because of the presence of the jam is overcome in two ways: the increased flow depth beneath the jam reduces the energy dissipation rate (compared to what it would be if the flow depth did not increase), and the energy gradient also is reduced along the channel reaches just upstream and downstream from the jam. It should be noted that, just as in the case of an isolated bend in a long channel, there is no net additional energy dissipation due to the presence of the jam, but only a redistribution of the rate of energy dissipation along the channel. The presence of the jam will diminish the velocity and Froude number at its upstream end, which in turn facilitates the accumulation of ice. Therefore, a flow which initially may be at the threshold of submerging floes and transporting them beneath the cover will tend, as ice accumulation occurs, toward conditions

favorable to formation of an embacle.

If the supply of ice to the jam is continued for a sufficiently long time, quasi-steady conditions eventually will be reached. The situation depicted in figure 4 will then prevail. Ice arriving at the upstream end of the jam will be arrested and will cause the cover to extend upstream. Some distance downstream from the leading edge of the jam, uniform conditions will be attained, with the cover thickness and flow depth at the equilibrium values of t_{eq} and h_{eq}, respectively. The force balance that exists in the cover along this equilibrium reach and in the nonuniform portion of the jam upstream from it will be discussed in Section V, below. After the quasi-steady situation is reached, the jam front will propagate upstream with constant velocity, V_w. The jam and the flow then will appear steady when viewed in a coordinate system attached to the upstream end of the jam. The kinematics of the jam are then comparitively simple; these are examined in the following section.

IV. CONTINUITY RELATIONS FOR QUASI-STEADY JAMS

In general the nonuniform reach of a jam is relatively short, and the time required to reach quasi-steady conditions is not great. Therefore, if the water and ice discharges remain constant and if the channel is uniform, or reasonably so, results derived from a quasi-steady analysis will be applicable to most of the period of embacle formation.

The quantity V_w may be determined from consideration of the continuity of ice movement in the moving coordinate system, which is expressed by

$$V_w t_{eq} (1-p) = q_{in} + (C_c t_i)_n V_w \qquad (2)$$

where t_{eq} is the equilibrium thickness of the jam, determined as discussed below; p is the jam's porosity; q_{in} is the volume discharge per unit width and C_c represents the surface concentration of ice; and t_i is floe thickness. The subscript n denotes conditions far upstream, where the flow has normal depth and velocity. Equation 2 yields

$$V_w = \frac{q_{in}}{t_{eq}(1-p) - (C_c t_i)_n} \qquad (3)$$

The backwater curve upstream from the jam will move upstream as a monotonic wave, with the depth at a fixed location increasing until the maximum depth at the upstream end of the jam, H, is reached. Water storage will occur in the moving backwater reach, and therefore the water discharge (measured in fixed coordinates) beneath the jam will be reduced. The unit discharge in moving coordinates, q', is constant and is expressed by

$$q' = (V_n + V_w)h_n \qquad (4)$$

The corresponding velocity is

$$V' = \frac{q'}{h} = (V_n + V_w)\frac{h_n}{h} \tag{5}$$

The discharge measured in fixed coordinates at any point is then

$$q = (V' - V_w)h = q_n + V_w(h_n - h) \tag{6}$$

Since $h > h_n$, q is reduced below q_n.

Finally, although it is really not a kinematic feature of the flow, it is in order here to examine h_{eq}. The boundary shear stresses exerted on the lower and upper boundaries, $\tau_{1,2}$, are, respectively,

$$\tau_{1,2} = \frac{f_{1,2}}{8}\rho\left(\frac{q}{n}\right)^2 \tag{7}$$

where $f_{1,2}$ are the friction factors for the two boundaries. In the equilibrium reach the slopes of the energy grade line and the channel must be equal, or nearly so. Equating the boundary shear stresses to the streamwise component of the gravity force on the water gives

$$h_{eq} = \left[\frac{q^2}{8gS_o}(f_1 + f_2)\right]^{1/3} \tag{8}$$

where q is given by (6), with h replaced by h_{eq}, is to be used in solving (8), and $S_o = \sin\theta$ is the channel slope.

The far more difficult question of determining t_{eq}, which is needed for the simultaneous solution of (3), (6), and (8), will be taken up in the next section.

V. THE FORCE BALANCE IN ICE JAMS

Consider an elemental control volume of rectangular planform taken from and extending over the full thickness of an ice jam, as shown in figure 5. The forces acting on the element in the streamwise direction are:

1. The streamwise component of the weight of the ice and the pore water it contains.
2. The shear stresses, τ_{xy}, acting on the lateral sides of the element.
3. The normal stresses exerted on the ends of the element.
4. The shear stress, $\tau\tau_2$, applied by the flow to the bottom of the cover.

Note that the seepage force exerted by the water discharge q_p percolating through the ice agglomeration, as shown in figure 4, is just equal to the streamwise component of the weight of the pore

water, and that the x-components of the hydrostatic forces acting on the ends of the volume are themselves in balance. If $\alpha \ll \theta$ (i.e., the phreatic surface and the stream bed are nearly parallel), the static balance of forces in the x direction is expressed by

$$\frac{\partial}{\partial x}(\sigma_x t) - t\frac{\partial \tau_{xy}}{\partial y} - \tau_2 + \rho g t \sin\theta = 0 \qquad (9)$$

for a two-dimensional configuration [i.e., $\frac{\partial}{\partial y}(t,\tau_2) = 0$]. In this case neither the first, third, or fourth term is a function of y, and therefore the second term also is y-independent. Consequently, τ_{xy} is linearly distributed across the channel and, because of symmetry, is zero at mid-channel and has its maximum, $(\tau_{xy})_M$, at the sides of the stream. This explains why shear lines in ice jams generally occur near the banks. If the jam is undergoing shear failure along the banks,

$$\tau_{xy} = -\frac{2y}{W}(\tau_{xy})_M \qquad (10)$$

where W is the width of the stream.

Before proceeding with consideration of the solution of (9), to obtain t as a function of x and the quantities describing the properties of the ice and flow, it is necessary to consider the boundary conditions on t. At large x, the flow and jam are uniform in the case of quasi-steady jam, $\frac{\partial}{\partial x}(\sigma_x t) = 0$, and (9) and (10) yield

$$\frac{2t_{eq}}{W}(\tau_{xy})_M - \tau_2 + \rho' g t_{eq} \sin\theta = 0 \qquad (11)$$

in which τ_2 is to be computed from (7) using the reduced discharge given by (6). If $(\tau_{xy})_M$ can be related to t, for example by the simple relation suggested by Uzuner and Kennedy (1974),

$$(\tau_{xy})_M = C_o \gamma_e t + C_i \qquad (12)$$

where C_o and C_i are constants and

$$\gamma_e = \tfrac{1}{2}\left(1 - \frac{\rho'}{\rho}\right)(1-p)\rho' g \cos\theta \qquad (13)$$

is an effective unit weight of the floating ice cover, then the mathematical problem of solving for the equilibrium conditions is closed: four equations [(3), (6), (8), and (11)] are available to

solve for the four unknowns (t_{eq}, h_{eq}, V_w, and q) in the equilibrium reach. The downstream boundary condition on t for quasi-steady conditions is the value of t_{eq} so obtained.

Now consider the upstream end of the jam, and the conditions that determine its thickness, a question that is far more difficult to resolve. Two reasonable physical situations come to mind. Experiments presently underway at the Iowa Institute of Hydraulic Research with small ice parallelepipeds demonstrate that over a wide range of conditions, the floes reaching the end of the jam submerge immediately and accumulate to form a jam that has nearly constant thickness over its whole length; in other words, the upstream end of the jam is very blunt, and $t = t^*_{eq}$, say, over most of the length of the jam. In this case, t^*_{eq} is determined not by the jam thickening until the embacle's shear strength is great enough to balance the applied forces, as described above, but by the depth to which the floes can be submerged upon reaching the cover. An estimate of this depth can be obtained as follows. The kinetic energy of the arriving floes is

$$KE = \frac{1}{2}\rho' \forall (\alpha V)^2 \tag{14}$$

where $\forall$ is the volume of the floe and αV is the water and floe velocity at the surface. The potential energy of a floe (relative to its equilibrium floating position) whose center of gravity has been displaced vertically a distance t^*_{eq} below its position when the block is floating on the surface, is

$$PE = (\rho - \rho')g\forall \left[\frac{t_i}{2}\left(1 - \frac{\rho'}{\rho}\right) + t^*_{eq}\right] \tag{15}$$

Equating the kinetic and potential energies given by (14) and (15), which assumes there is no energy transfer from the flow to the ice during submergence, and solving for t^*_{eq} yields

$$\frac{t^*_{eq}}{t_i} = \frac{(\alpha V)^2}{2\frac{\rho - \rho'}{\rho'} g t_i} - \frac{1}{2}\left(1 - \frac{\rho'}{\rho}\right) + 1 \tag{16}$$

in which the unity on the right hand side arises from the floating floes arriving at the jam having thickness t_i, while the change in potential energy results from submergency below the equilibrium level of the individual floating floes. The quantity t^*_{eq} is a rough measure of the thickness of accumulation in this case. Actually, the thickness can be expected to be slightly greater, because of energy imparted to the submerging ice floes from the flow. It should be kept in mind that the depth of flow was not introduced into the foregoing energy analysis; therefore, the result can be expected to apply only to cases in which the flow depth is much larger than t_i

and t^*_{eq}. Figure 6 presents a comparison of (16) and experimental data obtained from the Iowa experiments with ice parallelepipeds, mentioned above. The quantity C is a measure of the ice surface-concentration, defined by

$$C = \frac{1}{1.2} \frac{q_{in}}{q_n} \frac{h_n}{t_i} \tag{17}$$

where, in addition to the quantities defined in figure 4, q_{in} and q_n are the unit discharges of ice and water far upstream, and $\alpha = 1.2$ has been utilized. The quantity α is related to the Darcy-Weisbach friction factor, f, through the logarithmic velocity-defect law (Schlichting 1968), with the result

$$\alpha = 1 + 4.07\sqrt{(f/8)} \tag{18}$$

For the flows used in the Iowa experiments, f was approximately 0.025. The values of t^*_{eq}/t_i presented in figure 6 show general agreement with the form of (16), but are slightly larger, as anticipated in the discussion above.

A second possible upstream boundary condition states that the leading edge of the jam thickens until its strength is adequate to withstand the momentum of the arriving floes. This condition, which was utilized by Uzuner and Kennedy (1974), requires knowledge of the relationship between the thickness and compressive strength of floating fragmented ice covers, which is one of the most difficult and incompletely resolved questions related to ice jams.

The foregoing remarks have been directed primarily to the equilibrium and leading edge thicknesses of ice jams. In a long jam, there exists the possibility that the gradient of $(\sigma_x t)$ [the first term in (9)] and the bank shear initially are inadequate to support the applied loads. The ice cover may then thicken by failure or "collapse" of the ice cover (generally not fracture of the individual floes), until its shear and compressive strengths become great enough to balance the externally applied forces. There then again arises the difficult question of the strength-thickness relation of the cover. Uzuner and Kennedy (1974) utilized some heuristic arguments to arrive at the relation

$$\sigma_x = k_x \gamma_e t \tag{19}$$

where k_x is a coefficient to be determined from experiments. They introduced (10), (12), and (19) into (9) and numerically integrated the resulting equation to obtain t as a function of x. They present a computer program to accomplish this calculation, as well as the determination of the corresponding values of t_{eq}, h_{eq}, V_w, and q. Their technical report gives some complete solutions, in graphical form, for specific conditions. It must be emphasized, however, that their results are heavily dependent on the ice-strength relations

they utilized, (12) and (19).

In the analysis developed above, two different equilibrium thicknesses, t_{eq} and t^*_{eq}, given by (11) and (16), respectively, were considered. The former occurs when the cover thickens by internal collapse until its shear strength is great enough that bank shear balances the applied external forces. In the latter case, the jam thickness resulting from the arriving floes being submerged by conversion of their kinetic energy to potential energy is sufficiently great that bank shear can balance the forces applied externally to the ice cover. It follows, therefore, that $t^*_{eq} \geq t_{eq}$. The equilibrium thickness to be expected in a given situation depends on several factors, principally the channel width and the shear strength of the ice cover. The latter question poses the greatest hurdle.

VI. A SIMPLIFIED SOLUTION

If the thickness of accumulation at the upstream end of a jam given by (16) produces ice-cover strength which is great enough to support the applied loads, the jam thickness will be constant along its length and it becomes relatively simple to calculate the four unknowns, t^*_{eq}, h_{eq}, V_w, and q from a simultaneous solution of (3), (6), (8), and (16). For a numerical example, consider a channel and flow with the following properties:

S_o	$= 2.5 \times 10^{-4}$	h_n	$= 10$ ft
f_1	$= 0.025$	t_i	$= 0.50$ ft
f_2	$= 0.10$	$(C_c)_n$	$= 0.50$

Pertinent computed quantities are:

$V_n = 5.07$ ft/sec [from (8)]

$\alpha = 1.23$ [from (18)]

$F_n = V_n/\sqrt{gh_n} = 0.282$ (flow Froude number)

$q_n = (5.07)(10) = 50.7$ ft^2/sec

$q_{in} = (1.23)(5.07)(0.50)(0.50) = 1.56$ ft^2/sec

Simultaneous solution of the four equations listed above gives:

t^*_{eq}	$= 2.15$ ft	V_w	$= 1.50$ ft/sec
h_{eq}	$= 15.26$ ft	q	$= 42.81$ ft^2/sec

The flow depth just upstream from the end of the cover will be (refer to figure 4), approximately,

$$H = h_{eq} + \frac{\rho'}{\rho} t^*_{eq}$$

$$= 17.23 \text{ ft}$$

and the corresponding velocity and Froude number are

$$V = 42.81/17.23 = 2.48 \text{ ft/sec}$$

and

$$F = 2.48/\sqrt{(32.2)(2.48)} = 0.105$$

It is seen that the Froude number is reduced from a relatively high value to one which can produce a stable ice cover.

In closing this section it must be emphasized that the line of analysis followed in this section is applicable only after the jam has reached the quasi-steady state. During the early stages of formation, the velocity of the floes reaching the jam will be greater, the local jam thickness produced will be larger, and t will be reduced to t^*_{eq} along the jam as the depth of flow is increased and flow velocity decreased by the ice accumulation. One point should be noted: the dynamics of the flow as it passes under the jam have not been considered. This needs to be introduced into the analysis, using a method of analysis similar to that of Uzuner and Kennedy (1972) which utilizes the momentum or energy relation for the flow. The effect on the ice jam characteristics likely is minor.

V. THE STRENGTH OF ICE JAMS

One of the dominant traits of human nature is the desire to avoid confrontation with difficult problems, or at least to postpone the moment of truth as long as possible. And so it is in this review that the matter of the shear and compressive strengths of floating, fragmented ice covers is deferred until it precedes only the summary and conclusions. The major stumbling block encountered in the problem arises from the fusion of the ice fragments to form a monolithic mass. If the plane surfaces of two pieces of ice surrounded by air at a temperature well below the melting temperature of water are brought into contact and pressed against each other, the bond that forms between the two, as measured by the tensile or shear strength of the interface, forms very slowly; even after long-time exposure to a relatively high compressive stress, the two particles are readily separated. If, on the other hand, the two ice fragments are submerged in water, even very small contact pressure between the ice pieces will result in surprisingly fast formation of a strong bond. Indeed, after two ice cubes are pressed together just by hand while submerged for only a few seconds, it may be impossible to separate them by hand. The phenomenon of bond formation or fusion has been explained by Merino (1974) as resulting from the facts that the ice-water interface is at the melting point, and the melting temperature of ice decreases as pressure is increased. He argues that the applied pressure produces some melting at the interface which is followed by re-freezing and attendant bond formation when the pressure is relieved. Bond formation also is promoted by certain physical-chemical processes that occur in water at its solid-liquid transition

temperature. All of these processes occur at certain rates, rather than instantaneously, with the result that the shear and compressive strengths of ice covers are heavily dependent on the strain rate of the ice accumulation. This has been revealed in strength tests at the Iowa Institute of Hydraulic Research, (Merino 1974; Uzuner and Kennedy 1974) with the results shown in figures 7 and 8. In figure 7, U_c is the relative velocity of the two components of the direct-shear apparatus utilized, L is the length of the shear plane, and d_e is the average plan-form dimension of the fragments. It is seen in these figures that both the shear and compressive strengths decrease as the inverse of the strain rate. At higher strain rates, for which the inter-particle bonds do not have time to form, the shear stress results primarily from inter-granular friction and becomes nearly constant at about 2.0 lb/ft^2. Merino proposed the relation

$$\tau_M = \frac{1}{2}\gamma_e t \frac{d_e}{U_c} + 2.0 \text{ (lb-ft-sec)} \qquad (20)$$

to predict the shear strength of fragmented ice covers; (20) is compared with experimental data in figure 7.

Figure 8 presents data on the relationship between the compressive strength of floating fragmented ice covers and the velocity of the plate used to compress the ice. Again, the strong dependence of the compressive strength, σ_x, on the rate of ice-cover deformation is apparent.

VII. SUMMARY AND CONCLUSIONS

The preceding discussion of the many gaps that exist in our understanding and formulation of phenomena that arise in the ice-jamming of rivers should make it apparent that much research remains to be done before the problem can be regarded as solved. For even the very simple case of steady, uniform flows of ice and water in a uniform channel considered herein, the mathematical analysis encountered several major obstacles, principally the formulation of the shear and compressive strengths of fragmented ice covers. Additionally, the question of the shear strength of the ice-bank interface remains to be solved. In a real-world situation, one seldom has steady, uniform flows or uniform channels, and the characteristics of specific jams vary widely with local conditions from site to site. Research on the problem of prediction of the conditions for initiation of ice jams is in its infancy, and much remains to be done to develop reliable predictors for the onset of jamming. This topic is very important to river engineers; the best way to handle ice jams is to prevent their formation! The matter of the ice forces exerted by jams on structures, (e.g., ice booms) is still far from solved, and is deserving of considerable additional research attention. And so on; the shopping list of research needs related to river ice and ice jamming is indeed a long one.

The analytical considerations developed herein were based,

to the extent possible, on generally applicable principles of mechanics. The results developed in this survey and in the more extensive analysis of Uzuner and Kennedy (1974) provide at least a minimal analytical framework for the analysis and prediction of ice jams, and for presentation of field and laboratory data on jams. The more complete analysis contains several coefficients, notably k_x, C_i, C_o, and f_2 which arise in the strength and stress relationships. As is the case in many analytical models of complicated phenomena, these must be regarded at present as free parameters which may be adjusted in order to bring the mathematical predictions of ice-jam behavior into conformity with measured data; in a sense, they act as "tuning knobs" for adjustment of the theoretical model. There is now a pressing need for good laboratory and field data on ice jams for the purpose of determining the adequacy of the existing mathematical models, and to provide quantification of the several coefficients any ice-jam theory likely will contain.

The next research steps in the study of ice jams should be directed toward elucidation of the nature of the shear and compressive strengths of embacles, and determination of the aforementioned coefficients. It must be pointed out that the heavy dependence of ice-jam behavior on the strength properties of the fragmented ice, which results from the formation of cohesive bonds between ice fragments, suggests that model studies of ice jams should be conducted with real ice, since artificial materials, such as wax, polyethylene, and wood, generally do not exhibit this cohesive behavior, at least not to the extent that ice does.

It generally is not a good idea to close on a pessimistic note. Nevertheless, the writer's experience during the past 15 years with the somewhat similar problem of sand transport by rivers, and the slow rate of progress that has characterized that area of research, suggest that the engineer will not have a complete and reliable set of analytical tools for dealing with ice jams in the foreseeable future. Although this observation may be unhappy news for river engineers who must deal with ice jams, it has the bright aspect of promising to provide researchers in the area of ice engineering with ample outlet for their analytical and experimental energies for many years to come.

No paper on ice jams would be complete without some comment on the problem of what to do after a major ice jam has been formed. Various techniques have been tried to break up ice jams, including coal-dusting to increase the uptake of solar energy and thereby hasten melting, blasting of jams with explosives placed in them, and aerial bombing. None of these has proved to be particularly effective. The last two have the advantage of giving one a certain sense of vindictive fulfillment; he at least feels that he is striking back at the jam, even though his effort may be to little avail. Nature ultimately takes care of the jam, by providing warmer weather. Eventually the ice returns to its liquid form and runs off, but all too often after having done considerable damage to river training-works and other man-made structures, not to mention that caused by the jam-produced flooding. Unlike sediment, however, the ice does not remain after the flood of water has retreated; for at least this small

favor, one can but be thankful.

ACKNOWLEDGMENTS

Preparation of ths survey paper and much of the work reported in it were supported by the U.S. Army Corps of Engineers, Cold Regions Research and Engineering Laboratory, under Contract No. DAAK 03-75-C-0030, and by the National Science Foundation under Grant No. GK-35918.

REFERENCES CITED

Ashton, G.D., "Froude Criterion for Ice-Block Stability", J. of Glaciology, Vol. 13, No. 68, 1974.

Calkins, Darryl J. and Ashton, George D., "Arching of Fragmented Ice Covers", Special Report 222, Cold Regions Research and Engineering Laboratory, U.S. Corps of Engrs., Hanover, New Hampshire, April 1975.

Merino, M.P., "Internal Shear Strength of Fragmented Floating Ice Covers", M.S. Thesis, Dept. of Mechanics and Hydraulics, The University of Iowa, Iowa City, Iowa, 1974.

Pariset, E., and Hausser, R., "Formation and Evolution of Ice Covers on Rivers", Trans. Eng. Inst. of Canada, Vol. 15, No. 1, 1971.

Schlichting, H., Boundary Layer Theory, McGraw-Hill, New York, 1968.

Uzuner, M.S. and Kennedy, J.F., "Stability of Floating Ice Blocks", J. of the Hyd. Div., Proc. ASCE, Vol. 98, No. HY12, Dec. 1972.

Uzuner, M.S. and Kennedy, J.F., "Hydraulics and Mechanics of River Ice Jams", IIHR Report No. 161, Iowa Institute of Hydraulic Research, The University of Iowa, Iowa City, Iowa, May 1974.

Figure 1. Blasting of ice jam on Iowa River near its confluence with Mississippi River, January, 1975.

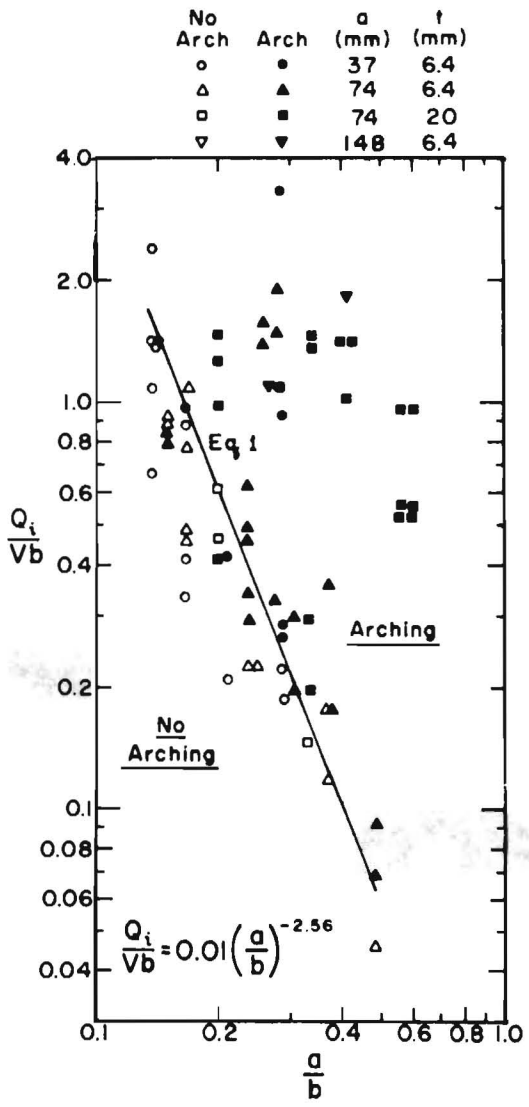

Figure 2. Arching criterion developed by Calkins and Ashton (1975) in their experiments with symmetrical surface obstacles with gap of width a.

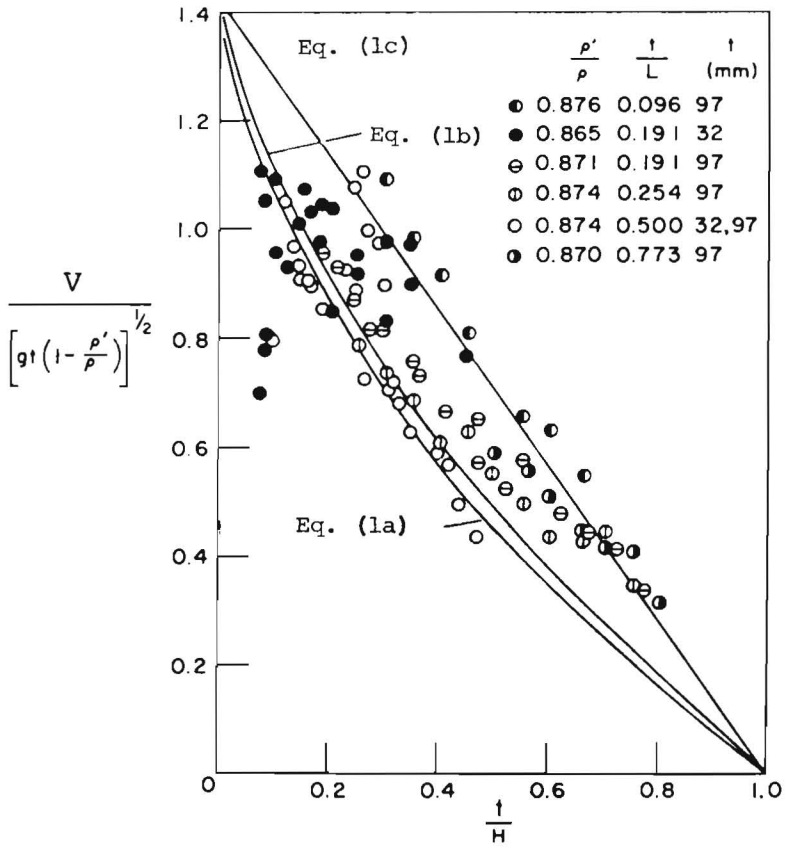

Figure 3. Submergence criterion for floes (Ashton 1975).

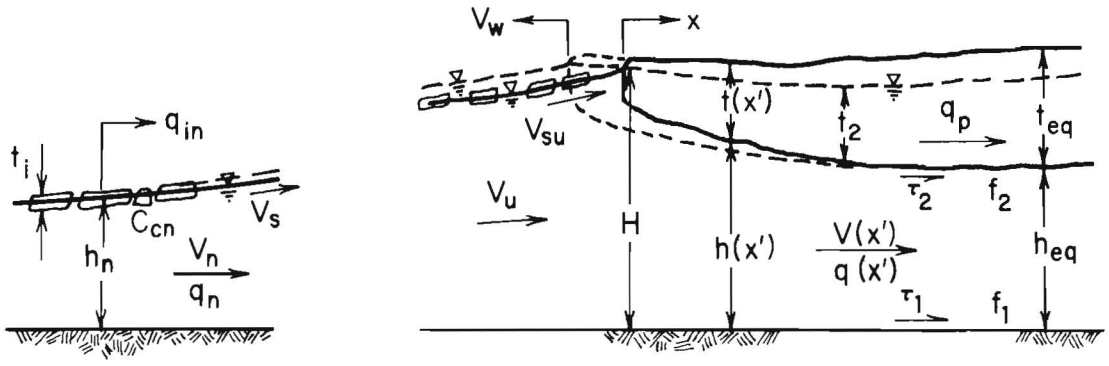

Figure 4. Definition sketch for ice jams (Uzuner and Kennedy 1974).

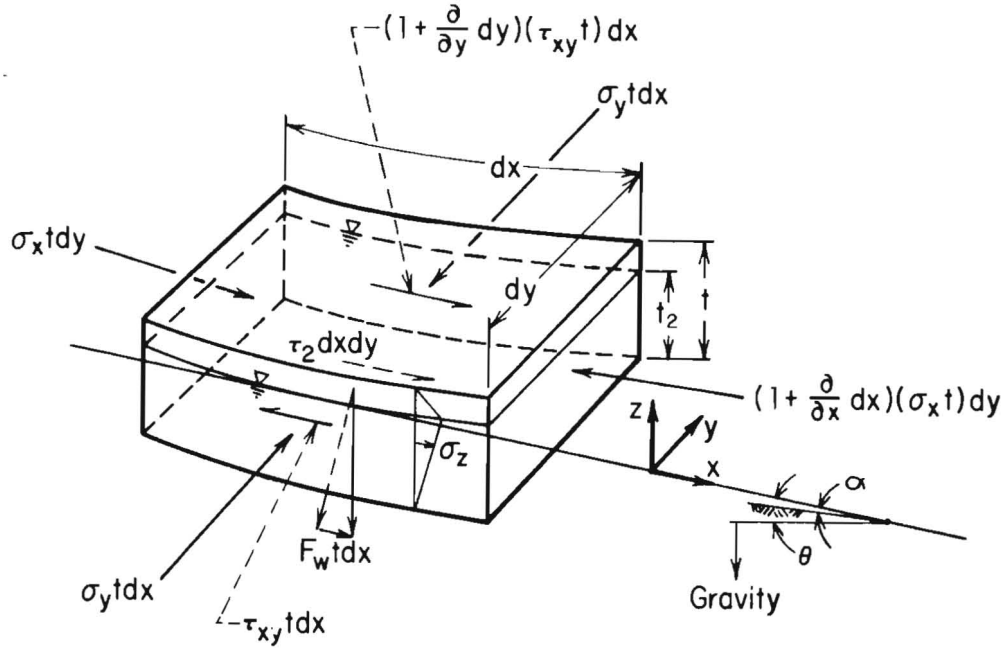

Figure 5. Elemental control volume taken from an ice jam (Uzuner and Kennedy 1974).

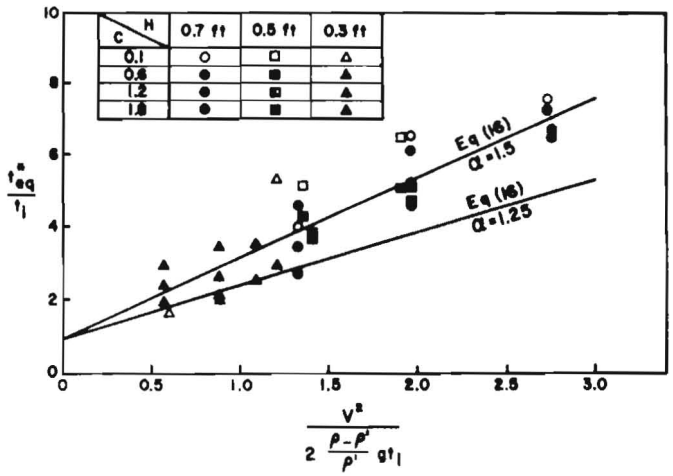

Figure 6. Comparison of (16) with ice-jam depths measured in laboratory. (Data by Wang and Tatinclaux.)

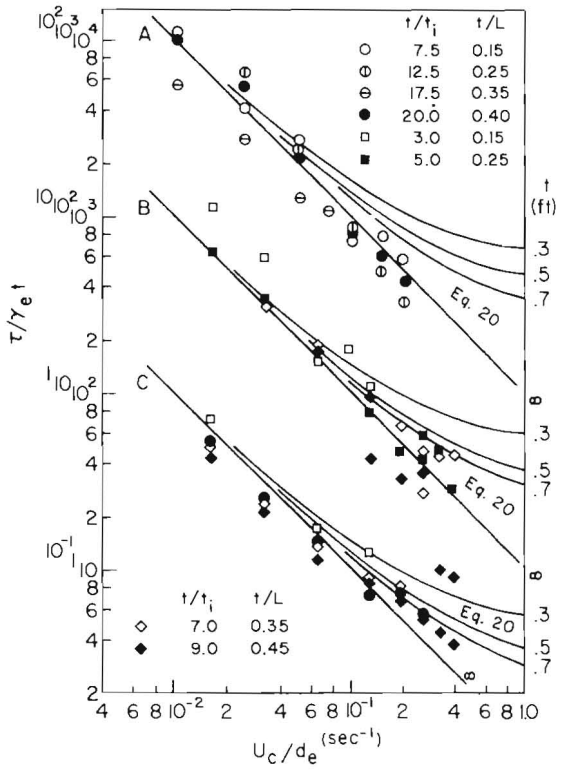

Figure 7. Shear strength of floating ice (Merino 1974). (Note: Curves A, d_e/t_i = 1.3, L = 2.0 ft, γ_e = 1.19 lb/ft^3; Curves B, d_e/t_i = 1.0, L = 2.0 ft, γ_e = 1.47 lb/ft^3; Curves C, d_e/t_i = 1.0, L = 1.2 ft, γ_e = 1.47 lb/ft^3)

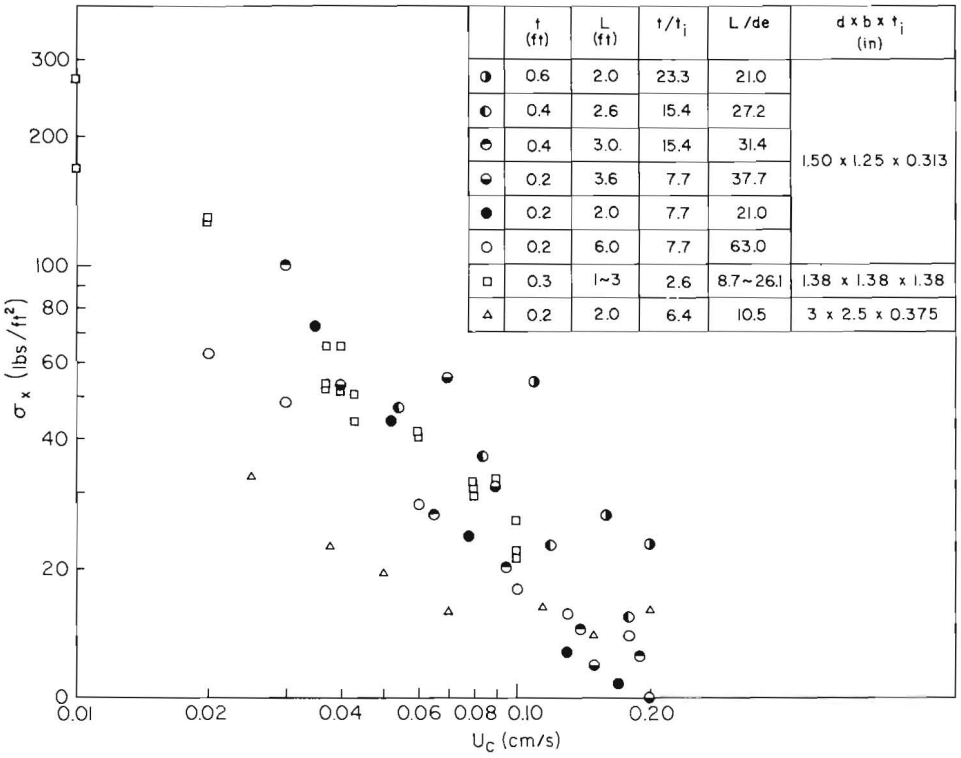

	t (ft)	L (ft)	t/t_i	L/de	d x b x t_i (in)
◑	0.6	2.0	23.3	21.0	1.50 x 1.25 x 0.313
◐	0.4	2.6	15.4	27.2	
◔	0.4	3.0.	15.4	31.4	
◒	0.2	3.6	7.7	37.7	
●	0.2	2.0	7.7	21.0	
○	0.2	6.0	7.7	63.0	
□	0.3	1~3	2.6	8.7~26.1	1.38 x 1.38 x 1.38
△	0.2	2.0	6.4	10.5	3 x 2.5 x 0.375

Figure 8. Compressive strength of floating, fragmented ice. (Data by Nakato, Govil, and Karim.)

International Association of Hydraulic Research (IAHR)
Committee on Ice Problems
International Symposium on Ice Problems
18-21 August 1975
Hanover, New Hampshire

COMMENTS

Paper Title: Ice Jam Mechanics

Author: J. F. Kennedy

Your name: Nabil AbdEl-hadi

Address: Dept. of Civil Engineering
University of New Brunswick
Fredericton, N.B., CANADA

Comment:

You used the friction factor of the ice undersurface, f_z, in your analysis. Since the ice undersurface changes with time, velocity, and temperature, it is expected to have a variable friction factor. Have you used an average value for f_z? Was it based on measurements?

Author's Reply:

In the absence of better information, one should use an estimated, average value of f_2. Determination of f_2 is very difficult, and generally involved measurement of velocity profiles under an ice cover. Perhaps it is most reasonable to view f_2 as one of the "tuning knobs" the model contains, the others being the various strength coefficients, which can be varied as needed to achieve conformity between experimental results obtained to verifu the mathematical model. Then, the mathematical model can be used with the value of f_2 so determined to make predictions about other ice jams.

THIRD INTERNATIONAL SYMPOSIUM ON
ICE PROBLEMS
Hanover, New Hampshire, USA

HYDRAULIC MODEL STUDIES OF ICE BOOMS TO CONTROL RIVER ICE

Philip H. Burgi
Hydraulic Engineer
U.S. Bureau of Reclamation Denver, Colorado

Ice jams frequently occur on rivers in the western United States. Many of the jams are small and may even go unnoticed in sparsely populated areas. Some occur infrequently and are caused by unusual meteorological conditions or temporary unsteady river hydraulics. However, others reoccur on a somewhat frequent basis and at the same locality. Although there are many factors involved, there are several which play a major role in creating an ice jam. These major factors include control sections in a river such as a channel constriction or a lake or reservoir, ice covered river systems where the ice in the headwaters melts before the downstream river ice melts, and river reaches where large quantities of frazil ice are produced (figure 1).

The North Platte River flowing through Casper, Wyoming, experiences ice cover formation every winter and at times ice jams are formed. Storage reservoirs upstream and downstream have permitted increased river discharges during winter months. The frequency of ice jam formation has reportedly increased due to the increase in winter river discharges above the native flow. In the fall of 1966, the Casper Project Office of the U.S. Bureau of Reclamation initiated an experimental ice boom study on the North Platte River. The major objective of the study was to develop a structure capable of containing the slush ice upstream from a small residential area west of Casper, Wyoming, affected by ice jams. The operation of the ice boom was expected to trigger an artificial ice cover by capturing slush ice thus creating an ice cover which would progress upstream from the boom in an area where a flood easement was established. The prototype log boom was installed 11 kilometers upstream from Casper, Wyoming, as shown in figure 2. The ice boom consisted of two 25-millimeter cables with 3.66-meter timbers attached to the cables by 1-meter lengths of chain. The timbers had spikes extending 305 millimeters above and

below on 225-millimeter centers. Several prototype ice boom configurations were tested on the river; however, due to time and cost limitations, the Project requested a model investigation of the ice boom to optimize the design of the existing structure.

Modeling Hydrodynamic River Ice Phenomenon

Groat 1/, as early as 1918, used a hydraulic model to study ice diversion using paraffin to simulate float ice. Several investigators 2/ 3/ 4/ have since used hydraulic models as a tool to better understand ice processes on rivers. Materials such as wax, paraffin, wood, and polyethylene have been used to simulate river ice. There are two areas of similitude considered in modeling ice processes. One involves the modeling of individual ice floes in a river system where the internal properties of the ice are neglected and the similitude is based on hydrodynamic considerations. The other area involves modeling of the ice properties per se. This investigation considered only the hydrodynamic forces and therefore the Froude model laws were used to scale the model.

North Platte River Model

A 1/2-kilometer reach of the North Platte River was modeled in the laboratory study at a 1:24 undistorted scale (figure 3). The model riverbed was constructed of concrete using river cross sections taken at 30-meter intervals along the river reach. River ice was simulated in the model using 3.2-millimeter hemispherical particles of low density polyethylene plastic with a specific gravity of 0.92 (figure 4). A 2.7-meter-long hopper with a 0.25 m^3 capacity was used to drop the plastic ice onto the water surface at the upstream end of the model. Since the laboratory has a recirculating water supply, a wire screen basket was installed at the downstream end of the model to collect the plastic used in the study.

A uniform test procedure was followed throughout the test program. Each test was operated with a discharge representing 26.6 m^3/s in the prototype river. To keep the absorptive properties of the plastic stable, the plastic model ice was stored in large drums containing water which kept the plastic wet at all times. The plastic model ice was applied to the water surface across the width of the model river. Discharge and water surface elevations were recorded during each test. The tests were normally terminated when the ice cover ceased progressing upstream. This was usually accompanied by a significant amount of model ice passing under the ice cover and boom. The quantity of model ice that had accumulated in the screen basket at the downstream end of the ice model during each test was removed from the basket and measured as "ice lost" by the boom.

Model Test Results

Initial ice boom. - The model test results indicated that the initial field location for the ice boom did not provide ideal flow conditions for proper operation of the ice boom. Due to a bend in the river, the

flow concentrated on the right side resulting in a considerable amount of ice flowing under the ice boom as shown in figure 5. Establishment of a uniform approach flow was further aggravated by a rock protrusion on the left side of the riverbed. The average flow velocity at the ice boom section was 0.5 m/s with an average depth of 1 meter. Several investigators 5/ 6/ recommend slower velocities for proper ice retention at this flow depth.

Modifications to the ice boom. - Several modifications to the initial ice boom structure were tested in the model including ice boom cable sag (4.3 and 14 meters), spacing between booms (24, 47, and 88 meters), timber spikes, and cable configurations.

In general, the least amount of cable sag resulted in the best ice retention by the boom. The spacing between ice boom cables was not critical. The use of one ice boom should be all that is required when properly located.

Several timber spike designs were tested as shown in figure 6. The boom timbers with 152-millimeter bottom spikes on 225-millimeter centers retained more ice than timbers without bottom spikes. Larger, 305-millimeter bottom spikes showed little improvement over the 152-millimeter bottom spikes and collected large amounts of debris when initially installed in the field.

Test with an "upstream V" configuration resulted in a more stable ice cover and better ice retention than the simple parabolic design. The ice boom was anchored to the model riverbed to form a 45° upstream angle with the river shoreline. This boom configuration wedges the slush ice between the boom and the river shoreline thus increasing the ice cover stability at the boom (figure 7).

To determine the effect of field shore ice on ice cover stability at the ice boom, large sheets of polyethylene were cut to simulate shore ice in the model (figure 8). The model shore ice produced a more stable ice cover which progressed upstream further than the tests without shore ice. The absence of any cohesive property in the polyethylene plastic resulted in a less stable model ice cover than what would occur in the field.

Artificial channel modifications. - To decrease the flow velocity and thus improve the ice retention capability of the ice boom, two artificial constrictions were tested in the model. The constrictions were located some 15 meters downstream from the ice boom and caused an increase in the water surface of approximately 0.3 meter reducing the flow velocity to 0.4 m/s. The first constriction was created by an opposing jetty which reduced the river width from 64 meters to 15 meters for the winter discharge of 26.6 m^3/s (figure 9). The model jetties were designed to overtop at a discharge of approximately 42 m^3/s. The second constriction consisted of a submerged overflow sill. The sill had a crest width of 0.3 meter and 2:1 side slopes. For the ice boom to function properly, the water surface at the ice boom site should be increased by 0.49 meter and the rocky

protrusion on the riverbed as shown in figure 10, should be removed. This will reduce the river flow velocity to 0.30 m/s.

Although this investigation was limited to a specific reach of the North Platte River, the results can be applied to other rivers flowing through alluvial valleys. The results are encouraging; however, more investigations related to river ice jam formation are needed to better control their occurrence.

REFERENCES

1. Groat, B. F., "Ice Diversion, Hydraulic Models, and Hydraulic Similarity," Transactions of American Society of Civil Engineers, Vol. 82, 1918

2. Cebertowicz, R., "Hydraulic Engineering Structures in the Light of Tests with Models," Institute of Hydraulic Engineering, Gdnask, 1968

3. Pariset, E., Hausser, R., Gagnon, A., "Formation of Ice Covers and Ice Jams In Rivers," Journal of Hydraulics Division, ASCE, Vol. 91, November 1966

4. Taubmann, Christian, "Model Tests for the Design of Ice-Retaining Basin on the Sihl River," Schweizerischen Bauzeitung, 1971

5. Kivisild, H. R., "Hanging Ice Dams," International Association for Hydraulic Research, Vol. 3, Eighth Congress, Montreal, Canada, 1959

6. Michel, B., "Analysis of Hypotheses Relative to the Formation of Ice Covers in Winter," Department of Civil Engineering, Laval University, Quebec, Canada, 1966

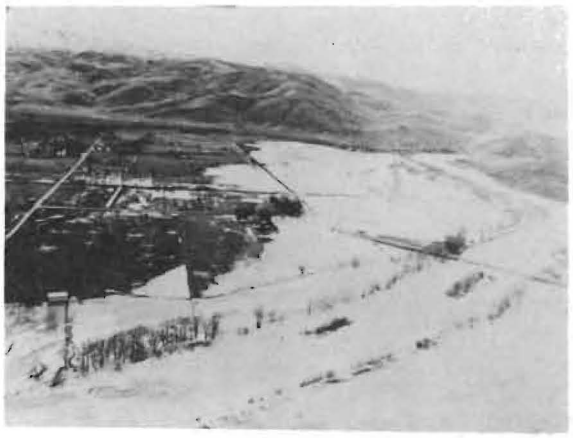

a. Ice jam on the Payette River upstream from Black Canyon Reservoir

b. Ice jam on Yellowstone River due to ice melt in the headwaters

c. Ice jam on Gunnison River due to upstream frazil ice production

Figure 1

Figure 2

View of initial ice boom on the
North Platte River

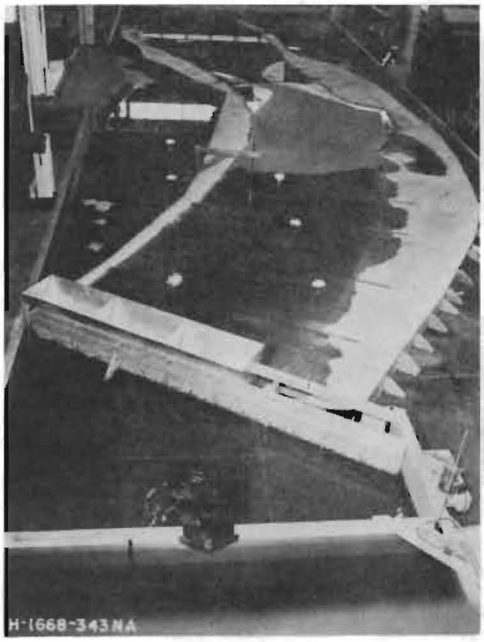

Figure 3
1:24 scale model of
North Platte River

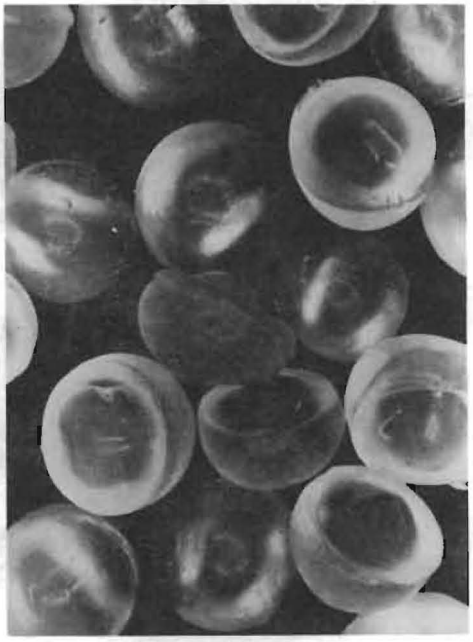

Figure 4
3.2 millimeter polyethylene
plastic - model river ice

Figure 5

View of North Platte River
with ice passing by ice boom

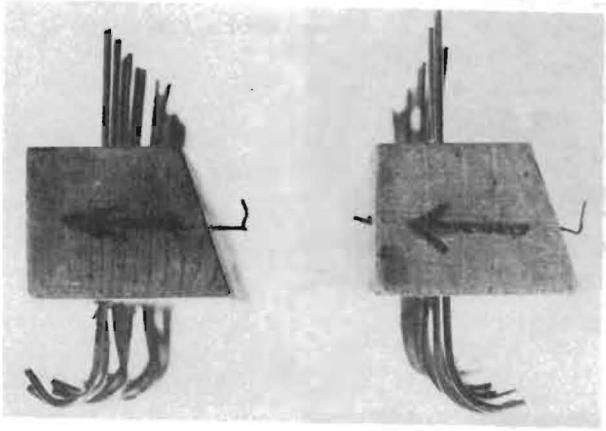

Figure 6
Spike configurations
tested in the model

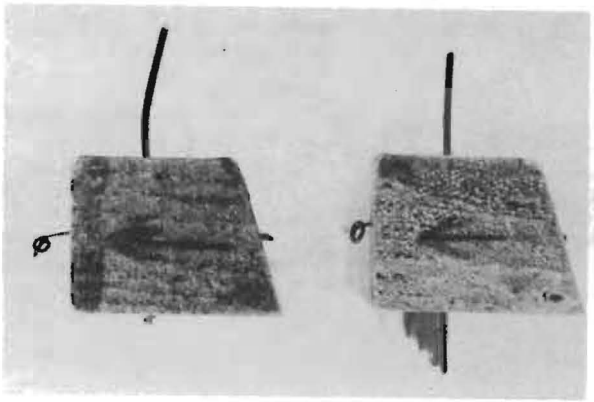

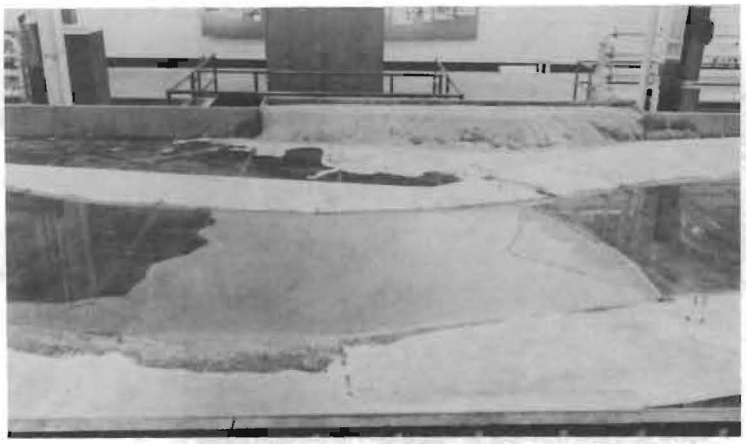

Figure 7
"Upstream V"
configuration
tested in model

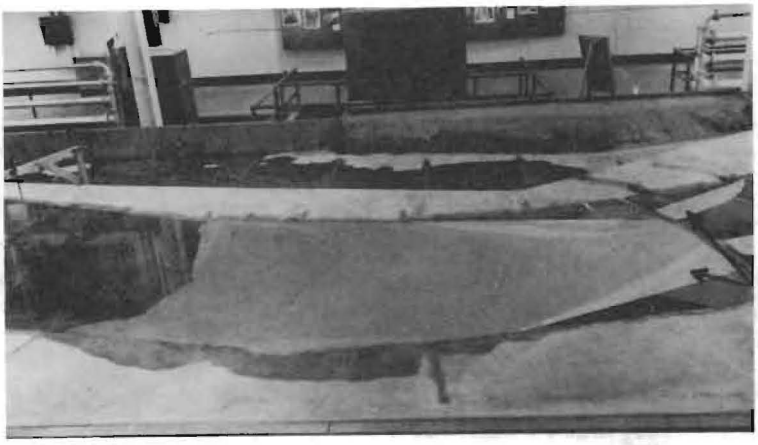

Figure 8
Simulated model
shore ice

shore ice

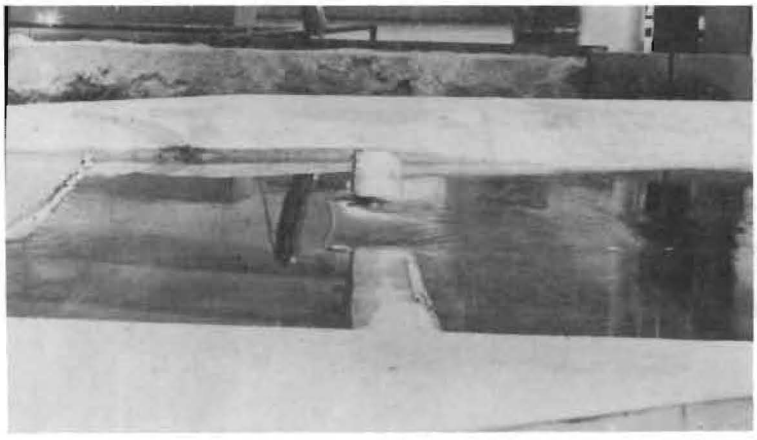

Figure 9
Opposing jetty
constriction in
model river

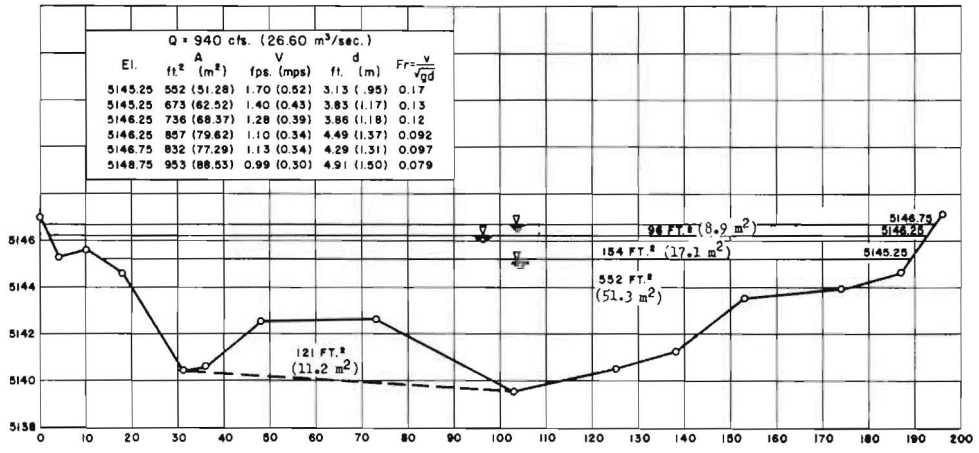

Figure 10
River cross section at ice boom

THIRD INTERNATIONAL SYMPOSIUM ON
ICE PROBLEMS
Hanover, New Hampshire, USA

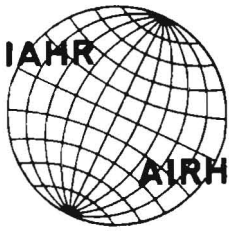

ICE JAM CONTROL UPSTREAM AND DOWNSTREAM FROM HYDRO POWER PLANTS

I.N.SOKOLOV, M.Sc.(Eng.) The B.E.Vedeneev VNIIG Leningrad, U.S.S.R.

Ya.L.GOTLIB, M.Sc.(Eng.) The "Hydroproject" Institute Moscow, U.S.S.R.

Ice jamming is a natural phenomenon observed on many rivers. Occurrence of ice jams is more or less a characteristic feature of most rivers freezing up in winter.

In the Soviet Union ice jams occur predominantly on rivers flowing through cold regions of the North, Siberia and Far East, e.g. on the Northern Dvina, Ob, Yenisei, Lena etc. which are closed with ice cover up to 1.5 m thick due to extended winter periods of very low air temperatures.

It should be noted that under milder weather conditions of comparatively short and warm winters in the Western and Southern regions of the country and even in the Central Asia the ice jams also develop in rivers, such as the Western Dvina, Neman, Dniester, Danube, Syr-Darya, Amu-Darya etc., covered by ice about 0.5 m thick.

More frequent and severe ice jams form on the northward-flowing rivers, because here during spring breakup the drifting accumulates against the thick solid ice cover that has not yet started to melt.

The sites susceptible to frequent ice jamming are as follows /R.1/:

1. Sudden transition zones from high to low river slopes, where the river enters the backwater of a reservoir, the sea or the lake.
2. Areas immediately below rapids, where the flow velocity is retarded.
3. Confluence sections of rivers carrying large amounts of ice.
4. Restrictions of flow caused by sharp bends (over 110-115°).

Additional potential jam areas include sharp bends, abrupt narrowings of ice passage, shallows with islands, river stretches closed with stable and thick ice cover, the areas of frazil ice accumulation during the late fall or winter months.

The developments of an ice jam is affected by the following fac-

tors: the amount and density of ice masses approaching an ice jam, the rate of water level rise during spring breakup, obstacles available in a river channel, flow discharge, air temperature, solar radiation, sequence of a breakup etc.

The volume of an ice jam and resulting height of water levels /R. 2, 3/ depend primarily on the amount and density of floating ice.

Once the jam is formed two situations are likely to be encountered depending on flood discharges and the intensity of ice breakup. Under the conditions of large discharges and intense breakup jams are generally of lower strength. They exist for a short time of 12-18 hours and break up readily. Sometimes a chain of jams forms, when breakout of a jam followed by destroying of an ice cover in a downstream reach leads to the formation of a new jam and so on.

In contrast, when a flood discharge is not large and almost constant an ice jam does not break up but extends downstream. The length of such jams can be from 10 to 15 km and even to 35 km on the Siberian rivers. The long jams are very stable, their duration is from 3 to 5 days for the European part of the U.S.S.R. and for 8 to 10 days for the Northern regions of Siberia.

Below control of ice jams in a river with a cascade of hydro power plants is discussed. The construction of a hydro power plant may result in ice jamming in its tailrace and at the end of backwater zones.

Appreciable jamming is likely to occur below an existing hydro power plant when further downstream the river channel is heavily constrained by structures of the next step of a cascade under construction. On a number of power plants the ratio of the ice passage front to the width of a natural channel is as low as 0.03-0.12. Under these conditions the probability of severe ice jamming is greatly increased.

Preventive measures against ice jams on rivers with a cascade of hydro power plants call for not only the successful control of river breakup and motion of ice masses upstream and downstream of a plant, but also for the control of ice during the formation of ice cover.

The efficiency of above measures depend upon gate manoeuvring at hydro power plants, reservoir parameters (length, depth, flowage, the drawdown volume) and the length of a river reach not effected by backwater of a succeeding reservoir.

When a deep reservoir with high winter temperature of water of 2 to 3° (for example, the Bratsk reservoir) is available in a cascade it is possible to reduce the amount of ice downstream of the dam by maintaining an area of open water ~100 km long, melting ice by warm water released from the reservoir in the spring, by keeping ice masses transported from the upper reaches of a river within a reservoir.

Ice jams and resulting rises of water levels downstream from a hydro power plant during the freeze-up period and spring breakup may be reduced by decreasing turbine discharges. The experience gained in operation of plants on the Angara provides support for this view.

At a hydro power plant with a small reservoir, as a rule, mechanical breakup of ice cover is performed and drifting ice is diverted to downstreams along a special channel up to 100 m wide cut by an ice-breaker through ice cover surface. Effective operation of ice-breaker in combination with adequate gate manoeuvring ensures ice motion. Sometimes, to lessen intensity of ice movement to dam site ice masses are

deposited to bottom and after partial melting are discharged downstream. This was accomplished at the Kegumskaya power plant before commissioning the Plyavinis power plant erected further upstream /R. 5/.

Ice jam formation downstream from a power plant can be alleviated or even eliminated by certain releases from a reservoir at which rise of water levels and temperatures of ice cover provide the conditions when ice cover is weakened but not broken.

For example, in 1967, in the vicinity of the Ust-Ilim hydro plant located on the Angara 300 km downstream from the Bratsk hydro plant massive ice jamming formed resulting in 5.66 m raise of water level. As a consequence, the first-stage cofferdam was flooded and partly eroded. The ice jamming was induced by vast quantities of fragmented ice drifting from the Ilim to the Angara closed by stong ice cover. During the years which followed in order to prevent ice jamming at the Ust-Ilim plant spring floods were controlled by varying turbine discharges at the Bratsk plant.

When general meteorological data permitted forecasting the earlier ice breakup at the reach of the Angara from the Bratsk to the Ust-Ilim hydro plants (before the Ilim breakup) water releases from the Bratsk hydro plant in March and April were increased to 3500-4000 m^3/sec. When the specific conditions (cold extended spring, drawdown of a reservoir and limited power production) predeterminate the later breakup of the Angara ice cover the releases from the Bratsk reservoir were minimized to 2000-2500 m^3/sec providing decrease in water levels due to jamming. Decrease in water releases from the Bratsk reservoir during the fall freeze-up prevented jam formation and raise of water levels due to jamming in the spring.

Jam control at the end of the backwater curve can be examplified by measures taken at the Kaunass hydro plant (at the Neman) and the Dubossary hydro plant (at the river Dniester). At the end of the backwater zone of the Kaunass hydro plant the ice jams formed initially in the river channel and transported to the reservoir may result in an intensive rising of water level. Drawdown of the reservoir preceding the spring flood allowed preventing accumulation of huge ice masses.

At the end of the backwater curve of the Dubossary hydro power plant (at the Dniester) ice jams occur almost annually. Bombing is one of the preventive measures taken here. However, it is not always a success, since sometimes breakup of a jam by blasting resulted in the formation of a new severe ice jam further downstream (1967) Control of water levels and current velocities in a reservoir proved to be the most effective measure of jam control downstream and upstream from hydro power plants, the end of the backwater zone being included.

REFERENCES

1. Methodological recommendations on preventing ice dams and jams. - Ed. "Energia", 1970.

2. Gotlib Ya.L.. Razzorenov F.F., Gorina M.V., On ice conditions in the Angara at the Ust-Ilim hydro power plant. - Trudy koordinatsionnykh soveshchanii po gidrotekhnike , Ed. "Energia", 1970, Vyp. 56.

3. Sokolov I.N., Ice regime control upstream and downstream of hydro power plants. - Trudy Gosudarstvennogo Gidrologicheskogo Instituta, Gidrometeoizdat, L., 1972, Vyp. 192.

4. Balanin V.V., Control of ice jam formation and methods for preventing ice jams. - Trudy koordinatsionnykh soveshchanii po gidrotekhnike, Ed. "Energia", 1972, Vyp. 56.

5. Gotlib Ya.L., Koren'kov V.A., Korzhavin K.N., Sokolov I.N., Sokolnikov N.M., Ice passage through hydro power plants under construction and in operation. - Ed. "Energia", M., 1973.

THIRD INTERNATIONAL SYMPOSIUM ON
ICE PROBLEMS
Hanover, New Hampshire, USA

STABILITY OF ICE BLOCKS BENEATH AN ICE COVER

Mehmet Secil Uzuner
Consulting Hydraulic Engineer

ARCTEC, Incorporated Columbia, Maryland, U.S.A.

INTRODUCTION

Problems associated with the extension of the navigation season to winter months in inland waterways and damage caused by ice jams have increased interest in and research on the understanding of evolution of ice jams. It is important to understand the behavior of individual ice blocks in addition to the understanding of the behavior of the whole cover. The latter behavior has been studied recently by Uzuner and Kennedy (1975) analytically and experimentally. Their theory was based on the force equilibrium of a fragmented ice cover, continuity equations for the liquid water and ice, the momentum relation for the flow, and strength thickness relations for the jam. There is, however, a possibility that ice jams thicken by means of floes being transported as "cover load" (after being submerged at the leading edge) for a distance, then being deposited there.

The goal of the ensuing analysis is to develop an analytical framework for the incipient motion of an ice block resting under a floating ice cover, and to compare this with the submergence criterion at the leading edge to determine which mode of transport occurs at a lower velocity and/or Froude number. The critical conditions obtained from the analysis presented here are also compared to those for streamwise force balance (Ashton, 1974) of an ice block beneath the ice cover.

TRANSPORT MECHANISM

Flume experiments using wooden and paraffin blocks have shown that the blocks resting beneath the ice cover generally move by

rotation or "under-turning," rather than by sliding or saltation, due to the irregular nature of fragmented ice cover bottom. This is also reported by Allen (1942) for the prisms resting on the river bed. Hence, it is necessary to examine the moment equilibrium of a floe resting under a floating, fragmented ice cover. The moments acting per unit width of the block, shown in Fig. 1, may be summarized as follows:

a. The moment due to the drag on the block may be expressed

$$M_D = C_d \frac{\rho V^2}{2} t_b^2 \tag{1}$$

in which C_d is a moment coefficient, t_b is the block thickness, and V is the mean flow velocity under the cover.

b. The moment from the shear force on the bottom of the floe can be written

$$M_S = \frac{f_i}{8} \rho V^2 t_b \ell \tag{2}$$

where f_i is a friction coefficient for the underside of the block and ℓ is the length of the block.

c. The moment due to the local pressure reduction under the block near its upstream end, is of the form

$$M_L = C_\ell \rho \frac{V^2}{2} \ell^2 \tag{3}$$

in which C_ℓ is the moment coefficient.

d. The moment of the submerged weight has the form

$$M_B = (\gamma - \gamma') t_b \frac{\ell^2}{2} \tag{4}$$

where γ and γ' are the specific weights of the liquid and solid phases of water, respectively. For static equilibrium, the destabilizing moments M_D, M_S, and M_L, should be balanced by the restoring moment M_B. Equating the sum of Eqs. 1, 2, and 3 to Eq. 4 and rearranging terms results

$$\frac{V}{\sqrt{\frac{\gamma-\gamma'}{\gamma} g t_b}} = \left(C_d \frac{t_b}{\ell} + \frac{f_i}{4} + C_\ell \frac{\ell}{t_b}\right)^{-1/2} \left(\frac{\ell}{t_b}\right)^{1/2} \tag{5}$$

Dimensional considerations indicate that the moment coefficients C_d and C_ℓ must both be functions of t_b/ℓ.

The problem of ice block stability beneath an ice cover is closely related to that of the initiation of motion of prisms resting on a river bed. The relation developed analytically and quantified experimentally by Novak (1948), for the incipient motion of a prism resting on the bottom of a river can be adopted, with the slight modification to the situation depicted in Fig. 1. In nondimensional form this relation is given by

$$\frac{V_e}{\sqrt{\frac{\gamma-\gamma'}{\gamma} g t_b}} = \left[1.596 - \frac{1.277}{\left(5.8 + \frac{h_e}{t_b}\right)^{1/3}} \right] \frac{\ell}{t_b} \qquad (6)$$

in which h_e is the flow depth, where the fragmented ice cover has reached uniform thickness. The form of Eq. 5 and Eq. 6 are identical if the friction and lift terms are small enough to be neglected. In the derivation of Eq. 6, both lift and drag were accounted for by introducing a single coefficient. The shear force on the underside of the block was not taken into consideration. Because of having the right general form and being quantified by means of experiments, Eq. 6 will be adopted in this analysis.

Introducing the continuity relation between sections 1 and 2 in Fig. 1, Eq. 6 takes the form

$$F_t = \frac{V_u}{\sqrt{\frac{\gamma-\gamma'}{\gamma} g t_b}} = \left[1.596 - \frac{1.277}{\left(5.8 + \frac{h_e}{t_b}\right)^{1/3}} \right] \frac{\ell}{t_b} \frac{h_e}{H} \qquad (7)$$

where F_t is the Froude number for incipient transport, V_u and H are the flow velocity and depth of flow upstream from the leading edge. The quantity, h_e in Eq. 7 is given by

$$h_e = H - \left(1 - \frac{\rho'}{\rho}\right) t_e \qquad (8)$$

in which t_e is the fragmented ice cover thickness where it has achieved uniform thickness. Eliminating h_e in Eq. 7 using Eq. 8 yields

$$F_t = \left[1.596 - \frac{1.277}{\left(5.8 + \frac{H}{t_b} - (1-\frac{\rho'}{\rho}) \frac{t_e}{t_b} \right)^{1/3}} \right] \frac{\ell}{t_b} \left[1 - (1-\frac{\rho'}{\rho}) \frac{t_e}{H} \right] \quad (9)$$

where all the terms are depicted in Fig. 1.

COMPARISON OF SUBMERGENCE AND TRANSPORT CRITERIA

Ashton (1974) and Uzuner and Kennedy (1972) have developed theories for and data on the submergence of ice blocks at the leading edge of an ice cover for different t_b/ℓ ratios of various specific gravities. Because of its simpler form and adequate description of extensive experimental results of both investigations, Ashton's relation is used here as the submergence criterion. The critical thickness-densimetric Froude number defined by him is given by

$$F_s = \frac{V_u}{\sqrt{\frac{\gamma-\gamma'}{\gamma} g t_b}} = \frac{2(1 - \frac{t_b}{H})}{\left[5 - 3\left(1 - \frac{t_b}{H}\right)^2 \right]^{1/3}} \quad (10)$$

in which F_s is the Froude number for incipient submergence.

Equations 9 and 10 can not be easily compared because of the number of variables contained in Eq. 9. The quantities h_e and t_e in Eq. 9, can be determined from the analytical investigation of ice jams by Uzuner and Kennedy (1975). The procedure to obtain h_e and t_e is complex and beyond the scope of this paper. For simplicity, the comparison of Eqs. 9 and 10 is made for uniformly thick solid ice cover of one block thickness (i.e., $t_e \cong t_b$). For this case Eq. 9 takes the form

$$F_t = \left[1.596 - \frac{1.277}{\left(5.8 + \frac{H}{t_b} - (1-\frac{\rho'}{\rho}) \right)^{1/3}} \right] \frac{\ell}{t_b} \left[1 - (1-\frac{\rho'}{\rho}) \frac{t_b}{H} \right] \quad (11)$$

which now involves similar terms as Eq. 10.

Ashton (1974) also analyzed the same problem using streamwise and vertical force balance on the block. Introducing continuity into this analysis, the critical Froude number for block transport obtained by equating drag force and friction between the block and the ice cover takes the form

$$F_t = \left[\frac{2\mu}{C_D \frac{t_b}{\ell} + \mu \frac{C_L}{C_D}} \right]^{1/2} \frac{h_e}{H} \qquad (12)$$

where C_D and C_L are the drag and the lift coefficients, respectively, and μ is the friction coefficient. The magnitude of the coefficients C_D and C_L are reported on the order of 1.2 and 0.5, respectively. Because of the uncertainty regarding its magnitude, the friction coefficient, μ is assumed to vary between 0.03 and 0.1. Equations 10, 11, and 12 are compared graphically in Fig. 2. As it is seen from this figure, a higher V_u is required to transport the floes by rotation than to submerge them. Ashton (1974) also reached this conclusion on the basis of his analytical work and a limited series of experiments using polyethylene blocks with various t_b/ℓ ratios. It is also seen in Fig. 2 that as t_b/ℓ increases, the critical thickness densimetric Froude number for transport decreases. This can be explained physically by the increase in the length of moment arms for drag and shear force (both overturning) and at the same time, by the decrease in the moment arm for buoyancy (restoring force). This result is apparent in Eq. 13. Also shown in Fig. 2 is Eq. 12 with $C_L = 0.5$ and $C_D = 1.2$ for different values of t_b/ℓ and μ. Note that the values of C_D and C_L are assumed to be constant for a range of t_b/ℓ for calculation purposes.

SUMMARY AND CONCLUSION

The stability of ice blocks beneath or at the leading edge of an ice cover is important in the understanding of thickening phenomena in ice jams. The result of this investigation shows that, fragmented, floating ice covers generally thicken by internal collapse rather than by transport of floes beneath the ice cover. This conclusion is reached by comparing the critical thickness, density Froude number for submergence (Eq. 10) developed by Ashton (1974) with that for the transport criterion (Eq. 11) obtained from the moment equilibrium of the block. Equation 11 is recommended for ice jams and ice covers with ripples at the ice-water interface and Eq. 12 can be used for consolidated ice covers with plane underside with appropriate coefficients. It should be kept in mind, however, that the comparison is made here for an ice cover of one block thickness. Recent experiments with various artificial ice materials indicate that floe transport does occur under the fragmented ice covers. This can be attributed to the developing boundary layer in the vicinity of the upstream end of the cover. Near the leading edge (where the boundary layer is thin) the high shear stress exerted on the floes resting under a floating ice cover may be able to move the floes along quite steep slopes of the underside of the cover, resulting in the formation of a hanging dam.

The formation of "hanging dams" still remains to be investigated. Thus, one of the next research topics in the understanding of the nature and the mechanics of fragmented ice covers should be the analytical and experimental investigation of formation of "hanging dams", and establishing the critical conditions under which they occur.

REFERENCES

Allen, J., (1942) "An Investigation of the Stability of Bed Materials in a Stream of Water," Journal of the Institute of Civil Engineers, Paper No. 5288.

Ashton, G. D., (1974) "Entrainment of Ice Blocks - Secondary Influences," International Association of Hydraulics Research, Proceedings, Symposium on River and Ice, Paper A-11, Budapest, Hungary.

Ashton, G. D., (1974) "Evaluation of Ice Management Problems Associated with Operation of a Mechanical Ice Cutter on the Mississippi River," U. S. Army Corps of Engineers, CRREL, Special Report 214.

Novak, P., (1948) "Experimental and Theoretical Investigation of the Stability of Prisms on the Bottom of a Flume," International Association for Hydraulic Structure Research, Proceedings, Second Meeting, Appendix 4, pp. 77-91, Stockholm.

Uzuner, Mehmet S. and Kennedy, John F., (1972) "Stability of Floating Ice Blocks," Journal of the Hydraulics Division, ASCE, Vol. 93, No. HY12, Proc. Paper 9418, pp. 2117-2133.

Uzuner, Mehmet S., and Kennedy, John F., (1975) "A Theoretical Model of River Ice Jams," Journal of the Hydraulics Division, ASCE, (Submitted for publication).

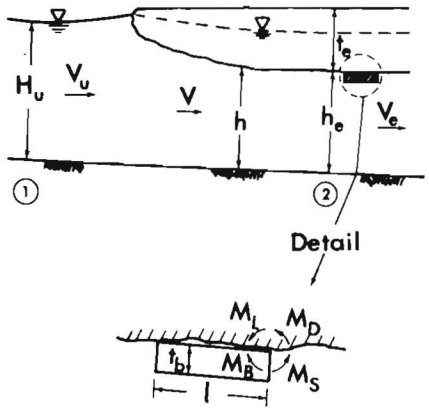

Figure 1. Schematic representation of an ice block at rest beneath a fragmented ice cover

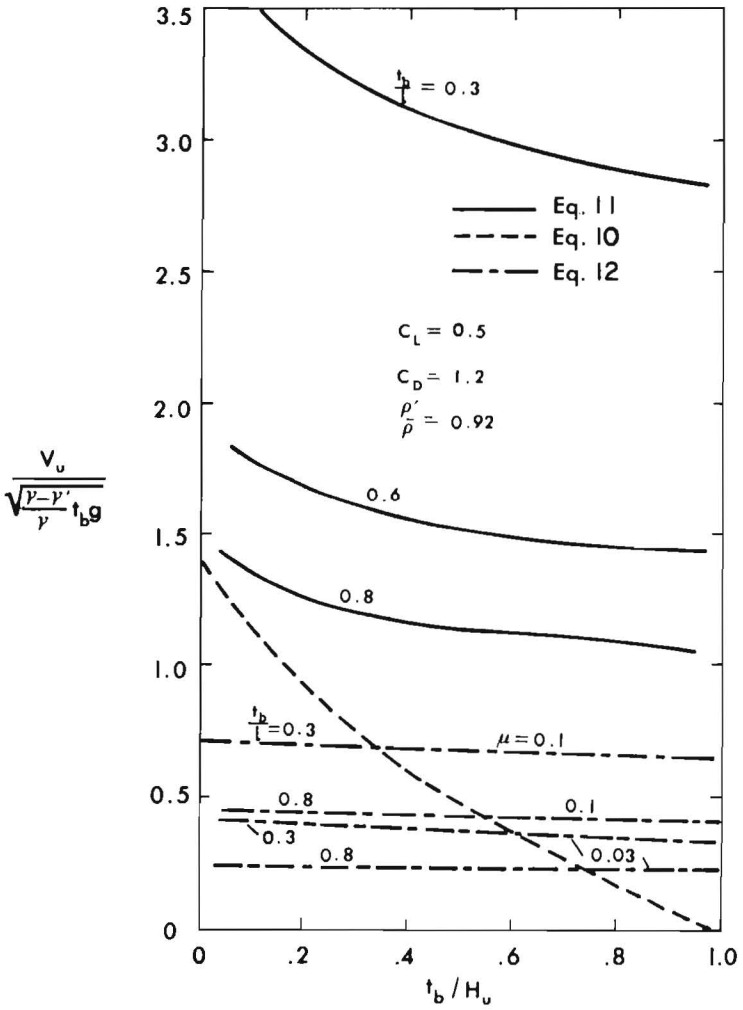

Figure 2. Graphical representation of eqs. 10, 11, and 12.

1. Velocity distribution equations for open and ice covered streams

To characterize the velocity conditions in a river, the hydraulic radius or the mean depth is mostly used. The formulas of the Chezysk type are simple, but insufficient. (Ref. 1). Eg.: a rectangular cross-section of breadth (b) and depth (h) gives a hydraulic radius $\mathcal{R} = \frac{b \cdot h}{b + 2h}$ and if R is kept constant, there will be many cross-sections with

$$h = \mathcal{R} \cdot \frac{b}{b - 2\mathcal{R}} \qquad \text{producing} \qquad b = 2\mathcal{R} > 0$$

Devik (Ref. 2) recommends the following Velocity equation, based on Matakiewiz's investigations:

$$V_m = k \cdot \alpha \cdot d \cdot j^{0.5} = \frac{q}{b \cdot d}, \text{ or: } k \cdot \alpha \cdot d^2 \cdot j^{0.5} = \frac{q}{b}; \quad q = V_m \cdot b \cdot d;$$

$k \cdot \alpha$ - composite roughness

k - characterizes friction against the bottom and $\alpha = f(d)$ is somewhat dependent on the mean depth. Fig. 1 shows the relation between q/b, j and V_m:

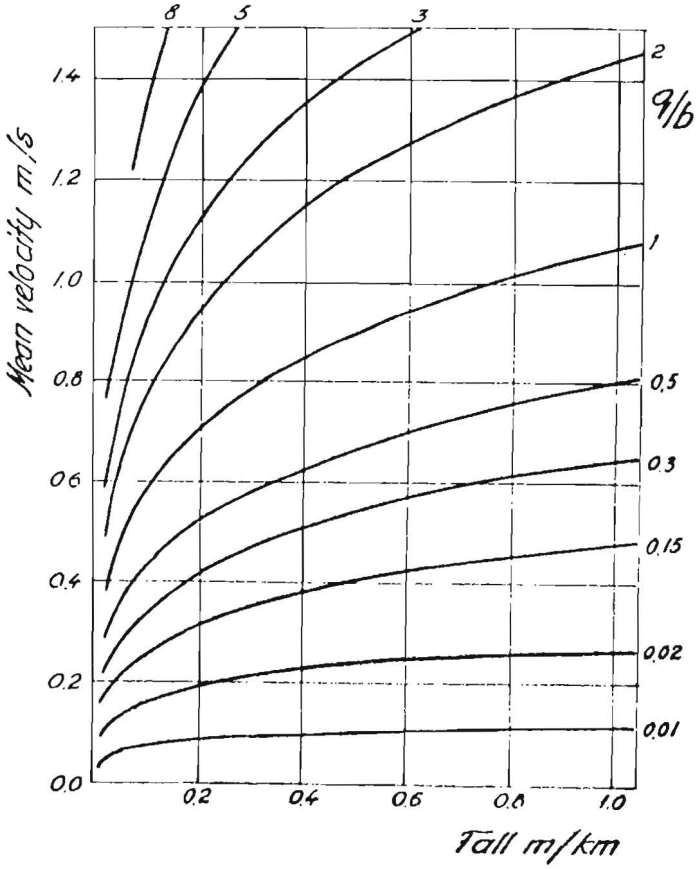

Fig. 1

Vitols (Ref. 3) maintains that the present hydraulics will not give a satisfactory solution, and does not advise using them for calculations of the composite roughness in rivers with dissimilar characters. To calculate the neccessary hydraulical coefficients he suggests the use of an expanded Bernoulli equation in the following form:

$$y_n - y_o = h_{kw} + h_{kg} + h_{rw} + h_{rg}:$$

$$y_n - y_o = \left(1 - \frac{q_n}{Q}\right)\frac{V_n^2}{2g} - \left(1 - \frac{q_o}{Q}\right)\frac{V_o^2}{2g}$$

$$+ \frac{\varepsilon}{2gQ}\left(V_n^2 q_n - V_o^2 q_o\right) + \frac{1}{Q}\int_{S_o}^{S_n} \frac{V^3 \gamma_w B}{C^2_{wB}}$$

$$+ \frac{(V_s - V)^3 b}{C^2_{wg}}\Big) ds + \frac{(\varepsilon - \alpha) \cdot w\Omega}{Q}, \text{ or:}$$

$$\frac{y_n - y_o}{S_n - S_o} = i = \frac{i_{kw} + i_{kg} + i_{rw} + i_{rg}}{}$$

This means that the absolute height on a given section of a river is equal to the konetic height of the water stream + the kinetic height of the sediment stream respective to ice drift + the magnitude of the loss of energy from the water stream + the loss of energy from the sediment respective to ice drift.

Vitols makes clear that the section $s_n - s_o$ of the river must be large enough in order to calculate to coefficients with accepted accuracy. The cross sections must be shosen so close to each other that the geometrical form of the river bed, on the section of importance, emerge. In practice this turns out to be very difficult.

Under Norwegian circumstances the safest method is to use direct measurement in order to determine a relation between discharge, ths cross section of the river, and the average velocity of the stream as shown in Fig. 2[a] and 2[b].

Fig. 2[a]

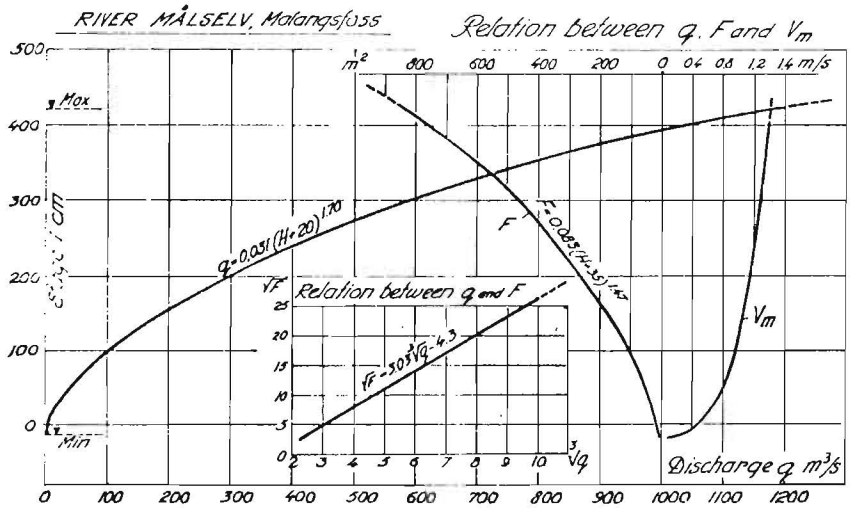

Fig. 2[b]

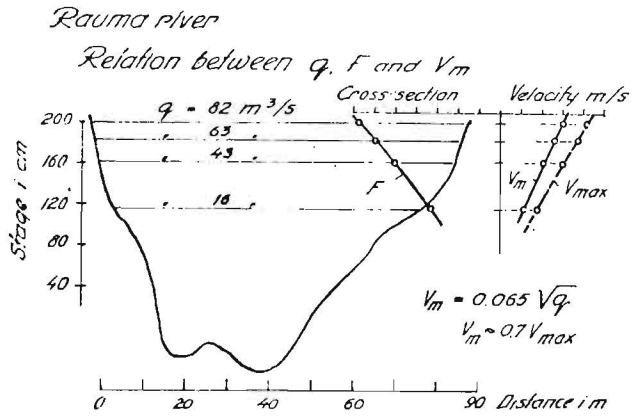

The cross sections of the rivers depends on the breadth b and depth h. This can be expressed approx.: $b = b_0 \cdot h^n$

where b_0 is the bredth of the river, when h=1 and n characterize the geometrical shape of the riverbed.

For a rectangular cross-section n=0 and a triangular shaped cross-section, n=1. Usually, the cross section of the rivers are approximately parabola shaped, and n is a number between 0 and 1.

A consideration of direct measures, Fig. 2[b], shows that in most cases mean velocity is approximately proportional to the square root of the discharge.

It is our experience that Devik's equation for open rivers can also be applied to ice-filled water and to partly or completely frozen rivers in the following form:

For ice-filled water, without ice cover (Ref. 2):

$$V_i = k \cdot k_i \cdot \alpha \cdot d_i \cdot j^{0.5} = q/b \cdot d_i; \text{ or: } k \cdot k_i \cdot \alpha \cdot d_i^2 \cdot j^{0.5} = q/b$$

Here k_i characterizes the friction in the water masses related to the normal conditions, and for ice-filled waters, this coefficient is presumed to be $\sim 0,8$

$$\frac{k \cdot \alpha \cdot d^2 \cdot j^{0.5}}{k \cdot 0.8 \cdot \alpha \cdot d_i^2 \cdot j^{0.5}} = 0.8 \left(\frac{d_i}{d}\right)^2 = 1, \text{ or: } \frac{d_i}{d} = \sqrt{1.25} = 1.12$$

In an ice-filled river (without ice cover), with an unaltered discharge, and an unaltered breadth and slope, the mean depth increases by approximately 12 %.

For partly and completely ice-covered rivers (without accumulated ice sludge), (Ref. 4):

$$V_n = k \cdot a_n \cdot d_n \cdot j^{0.5}, \text{ or: } V_n^2 = k \cdot a_n^2 \cdot q_n / b_n \cdot j^{0.5}$$

In this case for an ice-free river n=0, a_0 31, for partly covered, not ice-filled water, n=0,5, $a_{0,5}$ 24, and for a frozen river n=1, a_1 18.

Devik's equations give sufficient results in those cases where the river has an equal depth. The most frequent cross-sections in Norwegian rivers show a deeper main stream in the middle with more shallow parts at the sides. This formula is mostly used for each section of the river seperately to determine the relative velocities.

E. g.: a river with a cross-section of three parts: b_1, b_2, b_3 and d_1, d_2, d_3, where the midle part is the deepest, $v_2/v_0 = 3\ p/p+2$, and if p=2, the main stream is twice as deep as at the two sides of the river: $v_2 = 1,5\ v_0$.

In parts of rivers with pack ice and especially with accumulated sludge under the ice cover, it is not possible to use Devik's equation.

E. g.: in Fig. 3, current velocity measured in Bardu river just before and just after the covering with ice.

From a hydraulic point of view formation of an ice jam, breaking up of ice and the floating of ice process are so chaotic that they are almost impossible to analyse.

Fig. 3

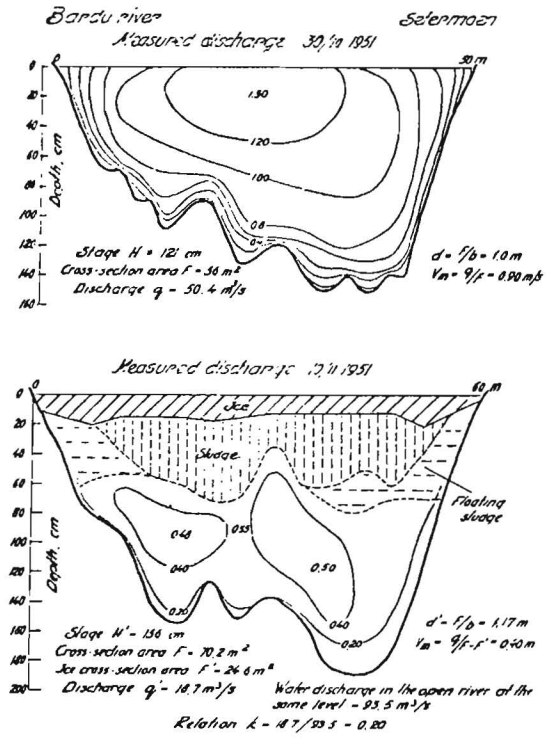

Fig. 4[a]

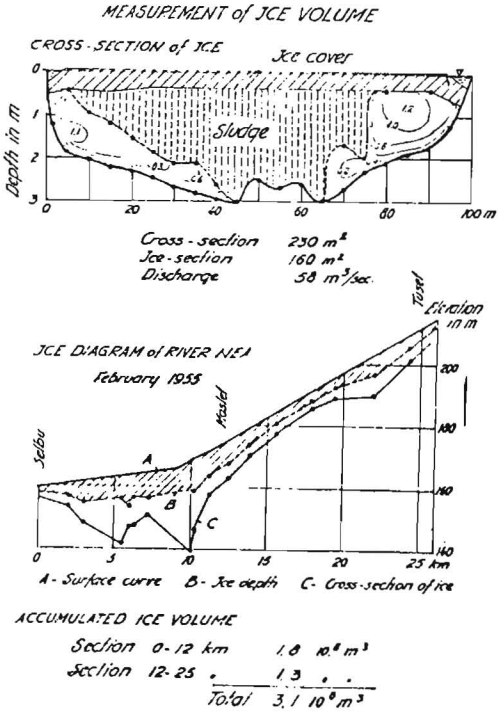

Fig. 4[a] shows the distribution of ice-masses in the river Nea and Daugava. By means of this longitudinal profile, we can ascertain the following two facts: 1) that ice stored in a river can reach gigantic quantities and 2) that the water stages of a rapid river like the Daugava or the Bardu, cannot be utilized forthwith for determining the mass of winter discharge. Therefore great care should be taken in choosing the site for a hydrometrical station outside the influence of ice.

Fig. 4[b]. River Daugava at the Koknese.

The enormous water pressure which ice-jams are capable of with standing can be seen from observations. E. g.: On Nov. the 20, 1941 the water level in the river was 298 cm, but next day with ice-jam it rose to 627 cm, a difference of 327 cm. Discharge was ca. 200 m^3/sec.

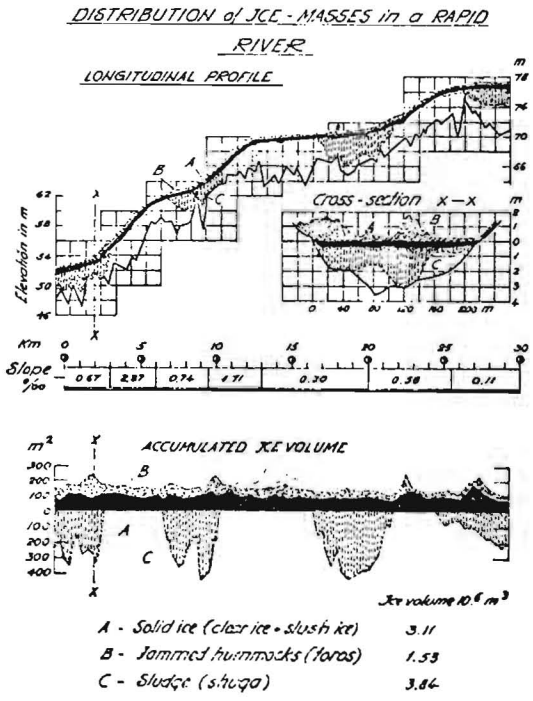

2. Control of ice production

Ice formation in rivers can only take place when the water is cooled to the freezing point. When this condition is present, ice production is related to water velocity and the nature of the river bed.

There exist critical combinations of water temperature on surface velocity, as shown in Fig. 5.

Ice production in rivers is much more complicated than in lakes. Fig. 6 shows ice formation in still water and in turbulent running water.

In turbulent waterstreams, supercooled elements of the surface film move in an irregular way through the water and may just as often sweep the bottom as be moving along the surface. On the way down, the supercooling of the element will decrease and a slight supercooling of the surrounding water will result. It ought to be emphasized that as long as the heat loss continuous from the water surface, there will be a stationary stability in the exchange of heat between the growing individual crystals and the surrounding supercooled water stream. Evidently the chance of crystal growth will be the greatest in the surface film, and the smallest at the bottom, where the chance will depend upon the time which the moving water film element will take on its way from surface film to bottom, i. e. upon the water velocity and the depth. The formation of bottom ice will thus be more frequent at shallow sections than at deep ones.

Fig. 7 shows typical situations for the formation of ice cover in the Glomma river and Fig. 8 - stabilization of ice conditions in the rapid section of the Glomma.

Fig. 5

CRITICAL COMBINATION of WATER TEMPERATURE and SURFACE VELOCITY

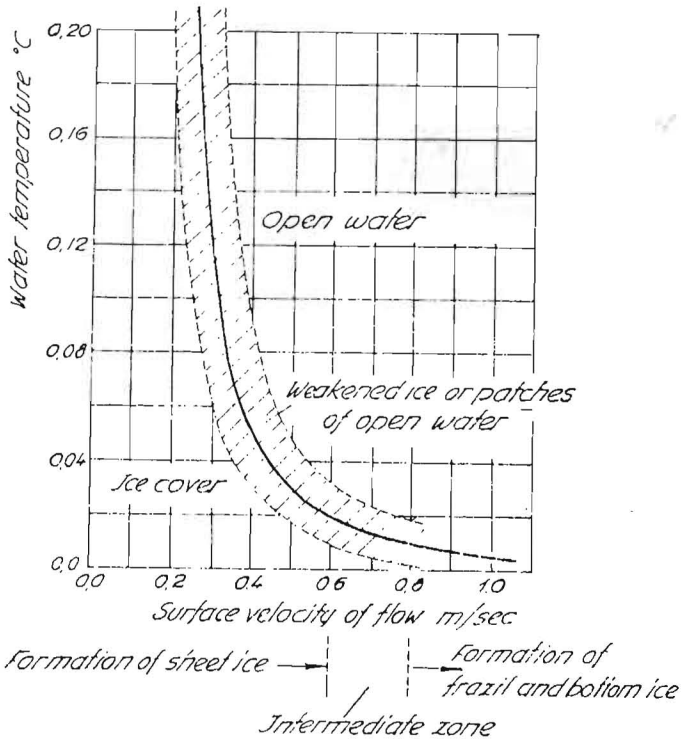

The buoyancy will be sufficient to keep the clusters floating if the stream velocity is lower than a certain critical value, which according to our preliminary measurements is about 1.2 m/s.

Combination of frazil ice floating in slightly supercooled water with incessantly new formed supercooled water film elements whirling down and gradually "dying" represents a most potent factor in the ice formation in rapid rivers. It may be called "active sludge" in contrast to sludge in water which is not supercooled can be classified as "passive sludge".

When the water transport is illustrated by stream lines, the following consequences will appear for the relation between surface areas covered by clusters of sludge ice and open areas between:

a. Where stream lines are diverging, open surface areas will be increased. In such places the supercooling will produce conditions for bottom ice production e. g. where the river is expanding. Another important case is the water surface just in front of an obstacle placed in the stream, e. g. a stone or a pilar, and similary for the water surface just behind the obstacle.

b. Where streamlines are converging, for instance near an obstacle the open areas will be reduced. As long as the velocity of the water is below the critical value mentioned above, the chance for bottom ice production will also be reduced.

If the convergence should increase, the velocity above the critical value, however, the sludge ice would be immersed in the water, leaving the surface open to the production of a supercooled water film, the elements of which would follow the converging water stream which would be sweeping along the obstacle on its way. This case is of importance when the obstacle is a pillar placed in the stream.

A. Formation of sheet ice (clear ice) Fig. 6

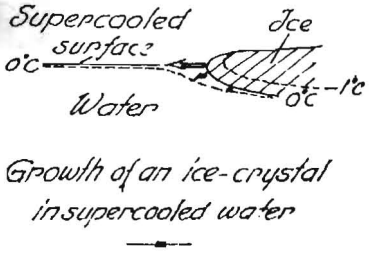

Growth of an ice-crystal in supercooled water

An ice cover will start with the supercooling of a thin surface film where ice crystals will grow from nuclei suspended in the water. The heat of crystallization is lost to the air. It is a slow continuous procedure, which may be called static ice production.

B. Formation of underwater ice (frazil and bottom ice-sludge)

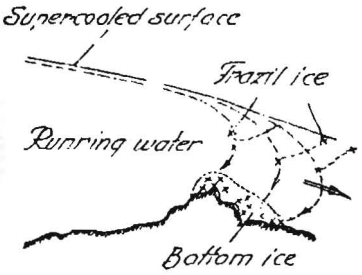

In this case, the heat of crystallization is lost in the water masses, which may generally be called dynamic ice production.

Ice crystals have a tendency to from clusters. This is active frazil ice. Sludge ice has a very loose structure. However, when we pick up a portion of such ice we can easily squeeze it in to an ice ball, quite similar to a snowball. This is due mainly to the combination of dynamic compression and the regelation effect.

The most important means of reducing ice production in rapid rivers is the reduction of the cooling surfaces.

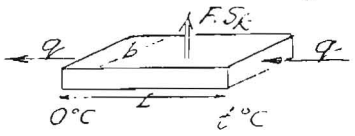

The cooling surface:

$$f = b \cdot l = \frac{1000\, q\, t}{S_k}$$

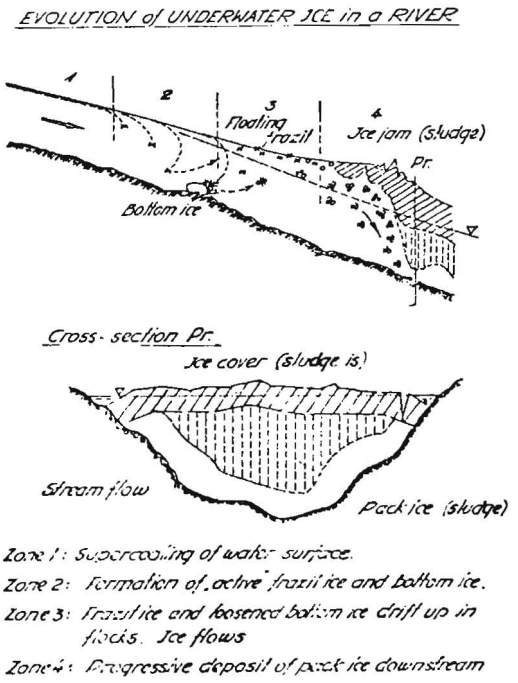

Fig. 7[a]. A survey of ice production by a river's longitudinal view.

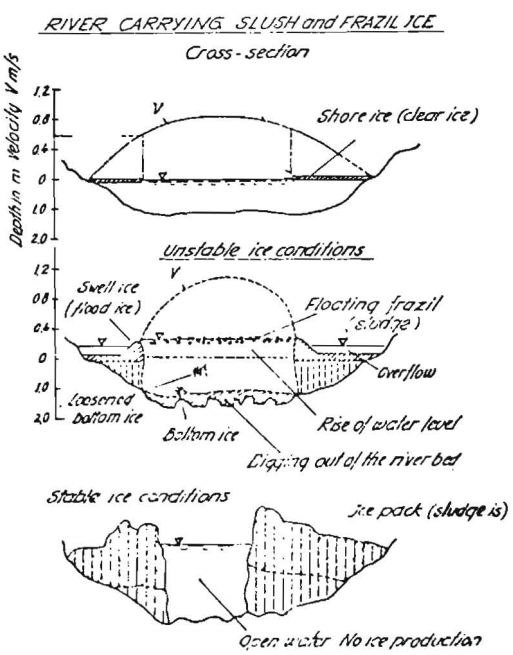

Fig. 7[b]. The different phases of ice production in a cross section.

Fig. 8. The flow is concentrated in a narrow main channel. The supply of heat from the falling energy is a contributing cause to this kind of flow.

When the heat transport (S_k) is known and constant within a period of time, and there is a complete mixing of the water along the distance L, the cooling of the water masses can be estimated:

$$-\Delta t q = S_k \cdot L \cdot b, \text{ or: } -\Delta t = S_k \cdot L \cdot b/q$$

The proportional coefficients are to make the equation simpler, included in S_k.

A reduction of the cooling surface is possible in many ways and under Norwegian conditions the following means are used:

a. To establish a continuous ice cover over the ice producing river sections by use of different booms or groins (Ref. 5).

b. Prevent the formation of artifical ice bridges and stabilize ice dams (Ref. 6).

c. A favourable combination of these.

By these means a rapid river can be transformed into a series of ice dams, each with a comparatively still water surface (surface velocity 0,6 m/s), which is very quickly covered by a growing ice sheet.

Fig. 9, 11 and 12 gives examples of stabilization of ice conditions in the rapid rivers.

For practical use, the relation between velocity 0,6 m/sec and the slope at different discharges in open rivers is given in Fig. 10.

Fig. 9. Stabilization of the ice condition in Kvina river

Threshold of gravel rises waterlevel approx. 500 m upstream.

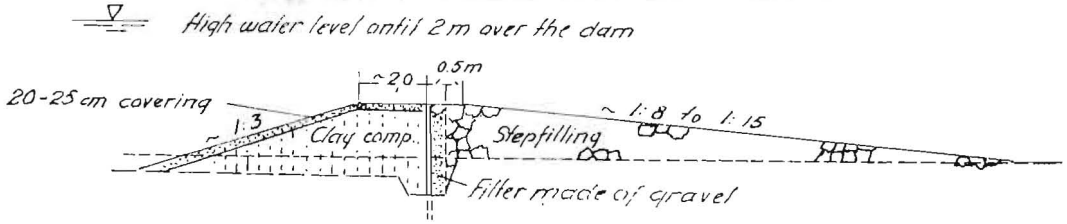

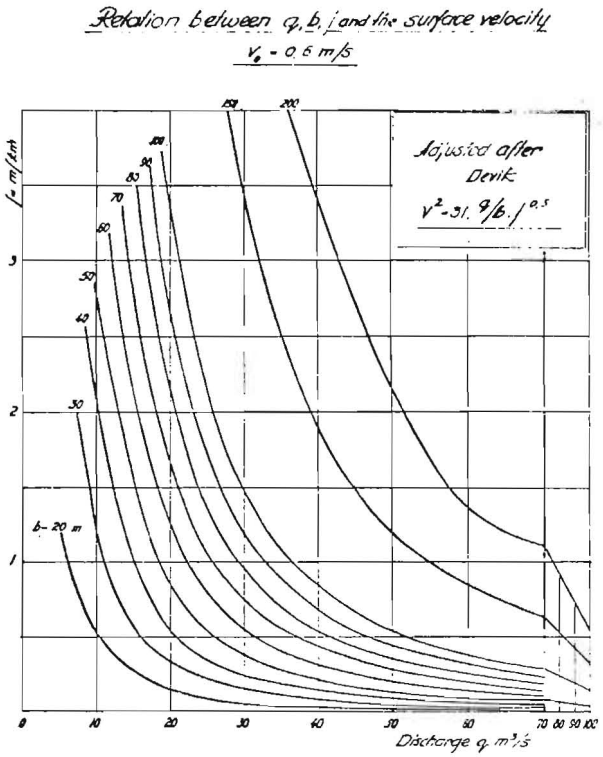

Fig. 10.

Fig. 11 shows an arrangement, which has until now been effective to stabilize an ice dam.

Present experience on ice problems connected with the utilization of water power in Norway are given in Ref. 7 and 8.

Fig. 11. Experiments to stabilize an ice dam

River Unsetåa, Øvre Rendal, 10. Dec. 1957. During 24 hours ca. 50 000 m^3 of sludge was accumulated on the front side of the bridge.

Øksna river. This arrangement stopped the ice-flow for a while.

Ice problems naturally, can be considered best and brought to an effective solution by an intimate cooperation between engineers and physicists.

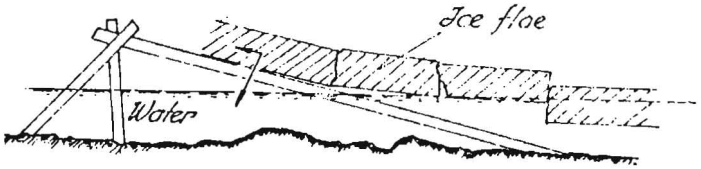

References

1. VITOLS, A., 1938: Beiträge zur Frage des Ungleichförmigkeitsgrades der Flussbetten. Hauptbericht 5 d. VI Hydr Konf. d. Baltischen Staaten, Lübeck-Berlin.
2. DEVIK, O., 1933: Über die Eisbildung eines Wasserlaufes und ihren Einfluss auf das Längenprofil Deutsche Wasserwirtschaft, Heft 10/11, Stuttgart.
3. VITOLS, A., 1942: Beitrag zur Erweiterung des Gesichtskreises der heutige Hydraulik. Wasserkraft und Wasserwirtschaft, H. 4, München.
4. DEVIK, O., 1938: Über Wasserstandsänderung eines Flusses bei Eisbildung, auf Götaälv angewandt, VI Hydr. Konf. d Baltischen Staaten, Lübeck-Berlin.
5. KANAVIN, E. V., 1944: Eisverhältnisse in Osteuropa und die angewandten Massnahmen zu Beeinflussung der Eisbildung und des Eisganges in der Daugava, Riga.
6. KANAVIN, E. V., 1970: Experience with Ice Problems in the Pasvik River, IAHR, Reykjavik
7. DEVIK, O., 1964: Present experience on ice problems connected with the utilization of water power in Norway, IAHR, Vol. 2 no. 1.
8. KANAVIN, E. V., 1972: Problems with Sludge ice connected with the Planning an Utilization of Water Power in Norway, IAHR, Leningrad.

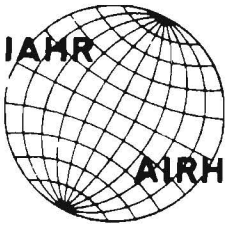

International Association of Hydraulic Research (IAHR)
Committee on Ice Problems
International Symposium on Ice Problems
18-21 August 1975
Hanover, New Hampshire

COMMENTS

Paper Title: Water Velocity in Open and Frozen Rivers - Control of Ice Production

Author: E. Kanavin

Your name: Kartha, V. C.

Address: Manitoba Hydro, 820 Taylor Avenue,
Winnipeg, R3C 2P4, CANADA

Comment:

The author presented an interesting paper on the practical aspects of river-ice engineering. The problems described by Prof. Kanavin are somewhat similar to those encountered in the Nelson River Development Program currently undertaken in Manitoba, Canada.

The author resorted to field-measurements as the first step in tackling specific river-ice problems. However, in the sixties several investigators combined field observations with analytical techniques and developed useful guidelines for the engineering design of regulating the river-ice regime. Lately more scientists are working in the theoretical field. Unless the theoreticians try to refine their analysis to match the results of field observations, the theory will be of little or no use to the practicing engineers dealing with hydro-power generation, navigation and oil-exploration. This This will definitely require a break-through in the analytical techniques, perhaps, deviating from the conventional one-dimensional approach and investigating the two-dimensional velocity and thermal boundary layers preferably in the framework of a two-phase fluid motion. This is because of the fact that the design engineers can no longer be contented with the understanding of the gross phenomenon of the fluid motion but often they are called upon to predict the local phenomena and design for those conditions subject to the constraints stipulated by environmentalists and other resource-users.

THIRD INTERNATIONAL SYMPOSIUM ON
ICE PROBLEMS
Hanover, New Hampshire, USA

OBSERVATIONS OF TANANA RIVER ICE

Thomas E. Osterkamp
Associate Professor of
Physics and Geophysics

Geophysical Institute Fairbanks, Alaska
University of Alaska United States

ABSTRACT

The ice in the Tanana River near Fairbanks, Alaska, has been observed each winter since 1971. When frazil ice was present in the river the water temperature was usually < 0.05°C. Approximately 10-15 km may be required for frazil ice crystals to evolve into meter sized frazil ice pans. Frazil ice pans > 1 m in thickness were observed. Snow slush balls were finer grained and more strongly bonded than frazil ice pans. Anchor ice formations were common and floating anchor ice was observed to transport fine grained sediments and gravel. The ice discharge of the tributaries was time dependent with the Delta River being the major contributor. The maximum estimated ice discharge was 33 $m^3 sec^{-1}$ (∿ 22% of the flow). There was general agreement between changes in the specific electrical conductance of the water and the ice discharge but the details of this relationship were not clear. Turbidity decreased by more than an order of magnitude during the freeze-up period and was inversely related to ice discharge. Frazil ice jams formed in narrow and/or curved parts of the river by consolidation of frazil ice pans and floes. These jams were the first ice cover to form on the river and were separated by open water areas which froze over by the process of border ice growth. The frazil ice jams produced during freeze-up may become strong points in the river ice cover during break-up and thus initiate ice jams at this time. Internal decay of the river ice results in liquid 3-grain boundaries at temperatures near the melting point of the ice. These liquid 3-grain boundaries may provide channels for water flow and may be expected to modify the thermal, mechanical and electrical properties of river ice near its melting point.

INTRODUCTION

The Tanana River begins at the confluence of the Chisana and Nabesna Rivers in Eastern Alaska on the northern side of the Wrangell Mountains and flows ∿ 800 km in a northwesterly direction to the Yukon River. Upstream from Fairbanks, the river is braided with many fast-flowing channels and downstream from Fairbanks the channel is fairly well-defined. The primary study site was ∿ 2 km downstream of the Chena River although some ground and aerial observations were also made from the city of Nenana upstream to the Johnson River (∿300km). The observations have been primarily qualitative in nature; however, measurements include the dimensions of frazil ice pans and snow slush balls; ice discharge; water temperature and characteristics (specific conductance and turbidity); and ice thickness. River ice structure was examined using thin section techniques and a photographic history of freeze-up and break-up was also made each year.

ICE FORMATION

Water temperature measurements were made daily during the 1974 freeze-up and showed that when frazil ice was present in the river the water temperature was usually < 0.05°C. The first ice was observed in the river on October 2, 1974 and no other exact dates for the appearance of the first ice are available, although these first ice forms were usually observed in the river at Fairbanks ∿ 3-5 weeks prior to the time of freeze-up and were either frazil ice pans or border ice. The frazil ice pans were 0.1 - > 1.0 m thick and 0.5 - 3 m in maximum horizontal dimensions. Ice floes were formed by consolidation of several pans and occasionally a few very large ice floes (100 x 100 m or larger) were observed. The ice particles in the pans were usually granular, up to 1 cm in maximum dimensions, although ice particles with a planar form were sometimes observed. A few leaves, sticks, sediment and gravel were observed in some of the pans. The ice particles in the pans were poorly bonded and the smaller pans were sometimes destroyed or mixed in with larger pans by collisions with them. Evolution of frazil ice crystals into frazil ice pans appears to occur over a fairly long distance on the river. Aerial observations indicated that 10-15 km may be required for frazil ice crystals to evolve into meter-sized frazil ice pans in the Tanana River above Fairbanks although the number of observations were limited.

Snow slush balls were observed in the river whenever snow fell during the freeze-up period. These slush balls were more equidimensional than frazil ice pans and ranged up to ∿ 0.5 m in maximum dimensions. They were composed of granular ice particles a few millimeters in size and were much better bonded than frazil ice pans.

Anchor ice has been observed at numerous places on the river bottom during freeze-up, however floating anchor ice has not been observed in the river at Fairbanks. Aerial observations 10-20 km upstream from Fairbanks showed that ∿ 1% of the ice pans were anchor ice (as indicated by their dark color from the entrained sediments and gravel) and ∿ 150 km upstream ∿ 5% of the ice pans were anchor ice. On November 14, 1974,

at the Richardson Highway bridge (∿150 km upstream from Fairbanks) the ice pans covered ∿ 10% of the river surface and were all anchor ice. While these observations of floating anchor ice differ it should be noted that the amount of floating anchor ice in the river depends on the time of the season, the time of day and position in the river. Also, continued reshaping of the floating anchor ice by very turbulent water and collisions with border ice and other floating ice may cause the entrained sediments and gravel to be released and fall to the bottom. This process may be a significant mass transport mechanism capable of transporting fine grained sediments, gravel and even rocks (Benson and Osterkamp, 1974).

Aerial and ground observations during the freeze-up period indicated that the ice discharge of the river at Fairbanks consisted of ice formed in the river and ice from its tributaries. While all of the tributaries contributed some ice discharge it appeared that the Delta River was the major contributor. On one occasion, during 1974, the Delta River contributed ∿ 50% of the ice discharge of the Tanana River at their confluence. However, ice discharge from tributaries was time dependent, and just before freeze-up it appeared that almost all of the ice discharge of the Tanana River was produced in the river.

The ice discharge at Fairbanks was estimated from the river width, percent ice coverage, thickness of the pans and velocity of the pans (see Figure 1). These estimates are somewhat crude due to the difficulties of estimating (visually) the percent ice coverage, variations in the shape of the pans and the velocity differences of the pans (pans along the bank moved slower than pans near the center of the flow). The estimates were not corrected for the porosity of the pans. A maximum ice discharge of 33 m^3 sec^{-1} (∿ 22% of the flow) was estimated for the day before the 1974 freeze-up.

It has been shown that changes in the specific electrical conductance of stream water during periods of ice formation in a small stream may be related to the volume of ice produced (Osterkamp et al., 1975). Figure 1 shows the specific conductances of water collected on a daily basis from the Tanana River and the ice discharge (as estimated above) during freeze-up. There was general agreement between changes in specific conductance of the river water and ice discharge except for one time period from October 11-14th when the ice discharge decreased substantially while the specific conductance of the water remained nearly constant. The reason for this deviation is not clear although it should be noted that, in large rivers, the effects of tributaries, snowfall and different ice and water velocities may modify the specific conductance of the water and mask its relation to ice discharge.

Alaskan rivers (glacial and non-glacial) undergo a transition from cloudy to clear during freeze-up although there do not appear to be any data on this point. The turbidity of the water samples (collected for specific conductance measurements) was measured and Figure 2 shows the results of these measurements. Turbidity decreased by more than an order of magnitude during the freeze-up period and when turbidity was compared to ice discharge an inverse relationship was found. The

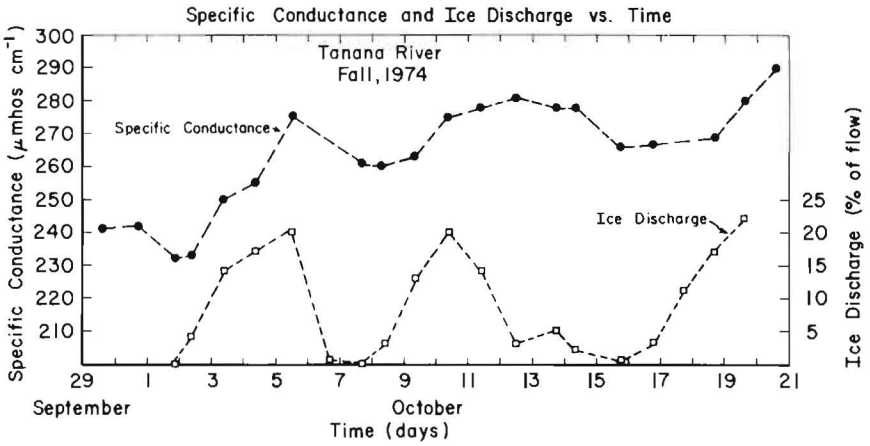

Figure 1. Specific conductance of the river water and ice discharge vs time for the Tanana River at Fairbanks during the freeze-up period in 1974.

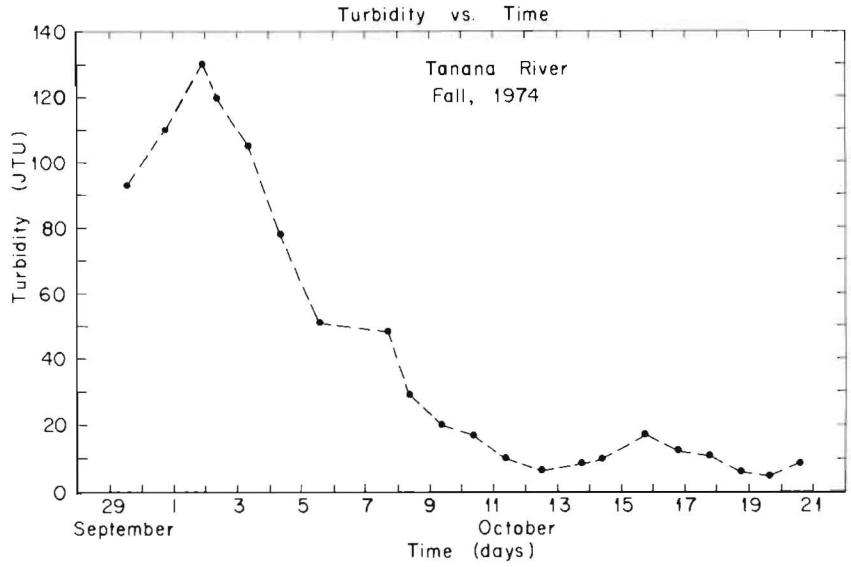

Figure 2. Turbidity of the river water vs time for the Tanana River at Fairbanks during the freeze-up period in 1974.

reduced turbidity during periods of ice discharge may be partially due to a reduction of turbulence by frazil pans on the surface of the flow. Since the Tanana River is primarily a glacial river, some of the turbidity decrease may be attributed to a decrease in water flow from glaciers during this time of year which leads to a low and generally decreasing stage during freeze-up.

ICE COVER

The ice cover of the river during the 1971-1974 winter seasons was initiated when frazil ice pans and large floes jammed in narrow and/or curved portions of the river. These large frazil floes were produced in the river and were sometimes 30 m or more in maximum dimensions. Under some conditions, they may play a key role in initiating the frazil ice jams in the river. Limited observations suggest that these frazil ice jams form at the same place each year and that the site of the jam can be modified by man. For example, during 1971, 1972 and 1973, a frazil ice jam formed in a narrow and curved place in the river below Fairbanks. During the summer of 1974, the curve was partially filled and straightened and during the 1974 freeze-up a frazil ice jam formed at the beginning of the straightened section $\sim$ 1 km upstream from the former jam site.

When frazil ice jams form in the river the resulting ice cover consists of a series of frazil ice jams with frazil ice pans and floes packed against the jams and extending upstream a few hundred meters to several kilometers with a series of open water areas between the frazil ice jams. Only a small amount of frazil slush has been observed to pass beneath these jams. Sheet ice forms on the open water areas by growth of the border ice toward the middle of the river. This process may involve 2 months or more before a continuous ice cover forms on the river. One site $\sim$ 150 km upstream from Fairbanks remains open through the winter when air temperatures may be -50°C or colder.

The surface topography of the ice cover formed from frazil ice was usually rough compared to the smooth sheet ice formed by border ice growth. In some cases, ice piles > 1 m high have been observed in the frazil ice cover. The ice thickness in the frazil ice cover may also be much greater than in the sheet ice formed by border ice growth. For example, on March 25, 1974, the frazil ice cover was 1.5 m thick near the center of the river and the sheet ice cover $\sim$ 100 m downstream was 0.76 m thick.

ICE DECAY

Several river ice cores were obtained from the frazil ice cover in March, 1974, and horizontally oriented thin sections were prepared from these cores and examined under a microscope at temperatures near the melting point of the ice. At 3-grain boundaries, channels of liquid were observed (see Figure 3) which appear to be similar to those that occur in pure ice (Nye and Frank, 1973), in ice lenses in the soil (Osterkamp, 1975) and in lake ice (Osterkamp, unpublished research). These liquid 3-grain boundaries in the river ice are important since

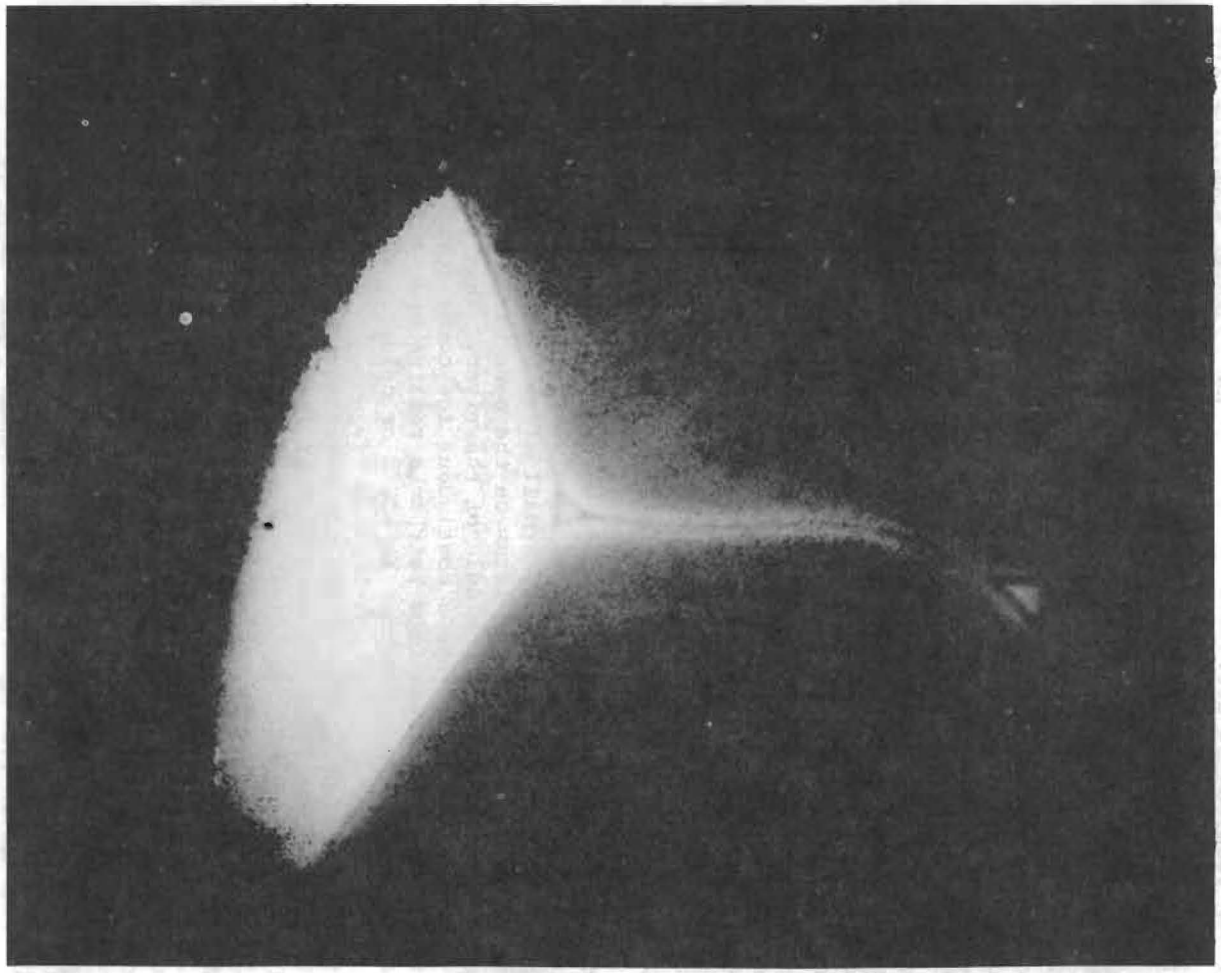

Figure 3. River ice thin section showing a 3-grain boundary.

they provide channels for water flow in the ice and may be expected to modify the thermal, mechanical and electrical properties of river ice near its melting point.

During the 1973-74 winter the history of a frazil ice jam was followed. This frazil ice jam began on October 26, 1973 during freeze-up. As mentioned above, this led to an ice thickness at the jam site which was nearly twice as thick as the sheet ice just below the jam. As the air temperature increased during April, 1974, the sheet ice below the jam and some of the frazil ice cover in the high-velocity flow areas above the jam were the first to melt. This melting appeared to progress from below since the snow cover remained on the ice surface. By April 25th, the high-velocity flow areas were free of ice, except for border ice and an ice bridge $\sim$ 40 m in width at the frazil ice jam site, and by April 27th, the ice bridge was reduced to $\sim$ 20 m in width. Ice floes in the river at this time were 0.3-1.5 m in thickness and 1-10 m in maximum dimensions. The ice floe velocity and water depth were estimated to be $\sim$ 1.4 m s^{-1} and $\sim$ 6 m, respectively, and the water level was $\sim$ 1 m higher above the dam. These ice floes were observed to strike the jam and to ride up on the ice on the upstream edge of the jam. The current then pushed them down at their upstream end and the floes rotated and were incorporated into the front edge of the jam, disappeared beneath the jam or continued to rotate at the front of the jam. Only small pieces of ice were observed to pass under the jam and it appears that ice floes which disappeared under the jam were either lodged there or were broken into smaller pieces.

The ice jam was destroyed sometime during the evening on May 1st and on the following day ice chunks up to 0.5 m in thickness were observed on the far bank and were found up to 2 m above the water level on the near bank above the site of the jam. Ice floes and slush ice were observed in the river for 5 days after the jam was broken.

ACKNOWLEDGEMENTS

I wish to thank Mr. R. Jurick for his help in the field and laboratory. This research was partially supported by the Earth Sciences Section, National Science Foundation, NSF Grant GA-30748.

REFERENCES

Benson, C.S. and T.E. Osterkamp, Underwater ice formation in rivers as a vehicle for sediment transport. Oceanography of the Bering Sea (D. W. Hood and E. J. Kelley, ed.), Inst. of Marine Sciences, University of Alaska, 1974.

Nye, J. F. and F. C. Frank, Hydrology of intergranular veins in a temperate glacier. Pub. No. 94, Int. Assoc. Sci. Hydrology, 1973.

Osterkamp, T.E., Structure and properties of ice lenses in frozen ground. Rept. No. UAG R-233, Geophysical Institute, University of Alaska, February 1975.

Osterkamp, T. E., R. E. Gilfilian and C. S. Benson, Observations of stage, discharge, pH and electrical conductivity during periods of ice formation in a small Sub-Arctic stream. Water Resources Research, 11(2), 268-272, 1975.

International Association of Hydraulic Research (IAHR)
Committee on Ice Problems
International Symposium on Ice Problems
18-21 August 1975
Hanover, New Hampshire

COMMENTS

Paper Title: OBSERVATIONS OF THE TANANA RIVER ICE

Author: T. E. OSTERKAMP

Your name: R.S. ARDEN

Address: ONTARIO HYDRO

Comment: Your description of ice formation in the Tanana River closely parallels observations made in the Upper Niagara River. Anchor ice in the Niagara forms only at night and usually lifts from the bottom the following day, bringing with it sand, gravel, and small boulders; and in the early part of the winter (early January) plant and algal material is included. The water in the early part of the winter is very murky, secchi disk readings being in the order of 50cm. As the season advances, the water clarifies and by mid-February secchi disc readings of 3m or more have been observed. The best period to observe ice formation in-situ was therefore, in the later part of February and early March,

THIRD INTERNATIONAL SYMPOSIUM ON
ICE PROBLEMS
Hanover, New Hampshire, USA

TEMPERATURE PATTERNS DURING THE FORMATION OF BORDER ICE AND FRAZIL IN A LABORATORY TANK.

T. O'D. Hanley, Dept. of Physics, Wheeling College, Wheeling, West Virginia 26003, U.S.A.

B. Michel, Ice Mechanics Laboratory, Laval University, Quebec, P.Q., Canada G1K 7P4

Studies of ice growth in rivers and lakes have addressed themselves to many aspects of the process. Two recent examples are those by MARCOTTE (1974) and McFADDEN (1974). Such studies are complicated by variations in air temperature, wind velocity, stream discharge, and so on. Flow conditions were controlled by MICHEL (1963) in his study of frazil production in an outdoor flume. Investigations under the controlled conditions available in a laboratory cold room have been less frequent; noteworthy among these is that of CARSTENS (1966).

Ice formation at several air temperatures and water speeds has been studied in a cold room of Laval University, Quebec, Canada. The purpose of this paper is to present several temperature patterns observed during these experiments, especially the effect of air temperature and water speed on (1) the maximum supercooling observed, (2) the rate of change of water temperature, and(3) the temperature gradient in air adjacent to the air-water interface. Another pattern, observed in still water, is an evolution with time of the temperature profile in the water. In conjunction with these patterns the terms of the energy balance are presented.

EXPERIMENTAL DETAILS

Water from the city mains was contained in a cylindrical tank of stainless steel 120 cm in diameter and 76 cm deep, surrounded at the sides by a plywood box containing fiberglass wool to a thickness of 30 cm or more. Four paddles of 2 cm plywood 51 cm long and 5 cm wide were bolted horizontally on a steel shaft which was mounted along the vertical axis of the tank and rotated by a variable speed motor. The paddles were positioned 25 cm above the bottom of the tank. A current meter was used to measure water speeds at various depths and radii,

and thereafter the desired water speed was obtained by setting the motor to the required rate of rotation.

Temperatures were measured by 21 thermistors with a time constant of 0.8 seconds in still water, which were set into the leading edge of a plastic wand shaped to minimize disturbance of the water flow. The thermistors were spaced so that when the wand was mounted vertically with the middle thermistor at the air-water interface, the temperature was monitored at positions 0.5, 1.0, 1.5, 2, 3, 4, 5, 7.5, 10, and 30 cm above and below the interface. The thermistors were calibrated at 0°C by immersing the wand in a tank full of frazil slush. A second parameter obtained for each thermistor by measurements at higher temperatures made it possible to compute the temperatures from the recorded resistance measurements. Small corrections, usually a few hundredths of a degree, to the temperatures computed from resistance data were made by reference to experiments in which frazil was produced.

The thermistor wand was clamped in a vertical position and was always placed 4 cm from the wall of the tank, since the experiments were intended to study the growth of border ice to a width of about 6 cm. Likewise the water speeds to be listed in this paper are those measured at 4 cm from the tank wall and 2.5 cm below the air-water interface. Water speeds from zero to 73 cm/sec were used, at air temperatures of -2°C, -5°C, -10°C, and -20°C.

The heat exchanger in the cold room recirculated the air in such a way that the net air velocity was not more than 1.5 m/sec. However, since the tank was surrounded by the insulating box and since the water level in the tank was about 10 cm below the top of the box, the wind speed at the water surface was effectively zero.

RESULTS AND DISCUSSION

a. Supercooling as freezing began

Frazil was never observed in tests performed at water speeds less than 24 cm/sec but was always formed at this and greater speeds, regardless of cold room temperature. In all experiments conducted with water speeds other than zero, even those in which frazil was not produced, the water temperature behaved in the manner characteristic of frazil production; that is, it decreased steadily until it was slightly below the freezing point, and then rose toward the freezing point as freezing began. An interesting value among these temperatures is the maximum supercooling. In the forty-five experiments which showed this characteristic behavior, the supercooling did not exceed 0.06°C. This is in contrast with the results of CARSTENS (1966), who shows supercoolings as great as 0.15 degrees.

The supercooling appears to be a function of both air temperature and water speed, as is seen in Figures 1 and 2. The origin is to be included as a point in both of these graphs -- in Fig. 1 because no supercooling was observed at zero water speed, and in Fig. 2 because supercooling could not occur with an air temperature of 0°C.

It is worth noting that in Fig. 1 the points at speeds less than 20 cm/sec represent experiments in which no frazil was produced.

The time rates of change of water temperature just before supercooling are shown in Fig. 3 as a function of water speed and air temperature. The points at speeds greater than 20 cm/sec suggest a linear relationship for each air temperature, but at speeds less than 20 cm/sec the points fall below their respective straight lines. It is difficult to assign values to the cooling rates at zero water speed, but they are clearly greater than zero.

b. Energy balance

Some modes of heat exchange found in nature do not occur or are negligible in the cold room, such as precipitation and advected groundwater. In the laboratory the net rate Q^* of heat loss per unit area from the water can be expressed by the equation

$$Q^* = Q_e + Q_c + Q_i + Q_t + Q_w - Q_a - Q_r - Q_f \qquad (1)$$

where the heat fluxes are denoted as follows:

Q_e, evaporation
Q_c, conduction across the air-water interface
Q_i, conduction through the insulation
Q_t, conduction upward in the tank wall
Q_w, long-wave radiation from the water
Q_a, long-wave radiation from the air
Q_r, short-wave radiation from the cold-room lamps
Q_f, frictional heat from the paddles.

Q_e, evaporation. MICHEL (1971) (Fig. 24 in the reference) put into one graph the results from several investigators for the coefficient of evaporative heat transfer H_e as a function of wind velocity. His graph yields a value of 38 cal/(cm^2 day mm Hg) for the coefficient at wind velocities between zero and 1.5 m/sec. This can be used in the equation

$$Q_e = H_e(p_a - p_w) \qquad (2)$$

where p_a and p_w are the vapor pressures of the air and water respectively.

Q_c, conduction across the air-water interface. Q_c was evaluated by using the relation of BOWEN (1926), $Q_c = R\,Q_e$, in which the dimensionless ratio R is

$$R = 0.46\ (T_w - T_a)/(p_w - p_a) \qquad (3)$$

when T_w, T_a are the Celsius temperatures of water and air, and p_w, p_a are vapor pressures in mm of mercury.

Q_i, insulation losses. DROUIN's (1966) equations for calculating heat loss through the walls of our cold room were adapted to obtain losses through the floor and the insulation around the wall of the tank, as a function of the temperatures of air and water.

Q_t, conduction through the tank wall. The heat flux Q_t' upward

within the metal wall can be converted to heat flux per unit area of water surface by multiplying by a factor 2 dr/r where r is the tank radius and dr is the thickness of the metal wall. Then

$$Q_t = - K \left(\frac{dT}{dy}\right)_t \cdot \frac{2\ dr}{r} . \qquad (4)$$

For stainless steel at 0°C the thermal conductivity K is 518 cal/(cm^2 day °C). From the temperature profile in the air and from the shape of the border ice at the tank wall, a good approximation for the temperature gradient in the wall is

$$\left(\frac{dT}{dy}\right)_t = \frac{T_a - T_w}{20\ cm} . \qquad (5)$$

Q_w, long-wave radiation from the water. For a water emissivity ϵ of 0.97, the Stefan-Boltzmann relation yields

$$Q_w = \epsilon \sigma T_{wK}^4 = 1.14 \times 10^{-7}\ T_{wK}^4\ cal/(cm^2\ day) \qquad (6)$$

where T_{wK} is the Kelvin temperature of the water.

Q_a, long-wave radiation from the air. Long- wave radiation toward the water was calculated as follows:

$$Q_a = f' \epsilon' \sigma T_{aK}^4 \qquad (7a)$$

$$= 0.95\ (0.74 + 0.022 \sqrt{p_a})(1.17 \times 10^{-7} cal/cm^2 day\ ^\circ K^4) T_{aK}^4$$

$$= 1.11 \times 10^{-7}(0.74 + 0.022 \sqrt{p_a})\ T_{aK}^4 \qquad (7b)$$

where f' is the reflectance of the water and T_{aK} is the Kelvin temperature of the air. The expression for the emissivity was adapted from the equation of MARCOTTE (1974) so that p_a is in mm of mercury. Emissivities for the painted walls of the cold room and for the masonite ceiling were at least no greater than the emissivity of air, and so it was decided to use simply the emissivity for the air.

Q_r, radiation from artificial lighting. Illumination in the cold room was provided by six 150-watt incandescent lamps enclosed in diffusing globes. Two lamps were located at a distance of 1.6 m from the water surface, two at 3.0 m, and two at 3.7 m. Assuming that 60% of the electrical energy is radiated into a hemisphere of area $2\pi r^2$, and using 0.85 as the absorptivity of the water, results in a short-wave radiation flux of $Q_r = 28$ cal/(cm^2 day).

Q_f, frictional heat from the paddles. Measurements were made of the electrical power drawn by the motor at various paddle speeds with the tank both empty and full of water; these measurements furnish values of the power needed to keep the water moving at any chosen speed. The values of the power divided by the area of the air-water interface give the flux rate Q_f. This is the only heat flux term which depends to an important degree on the water speed. Its values do not exceed 5 cal/(cm^2 day), and so they will be neglected in what follows.

The experiments were not usually continued after the border ice attained a width of a few centimeters. Therefore the terms of the energy balance have been evaluated for the beginning of ice production,

assuming a water temperature of 0°C, and are listed in Table I.

Table I. Heat flux terms. Water temperature 0°C.

T_a Air temp. °C	HEAT LOSSES in cal/(cm² day)					HEAT GAINS		
	Evaporation Q_e	Conduction Q_c	Insulation Q_i	Tank wall Q_t	Water Rad'n Q_w	Air Rad'n Q_a	Lighting Q_r	Net LOSS Q^*
- 2	69	40	5	0.3	631	478	28	239
- 5	90	87	6	0.8	631	451	28	336
-10	117	174	7	1.6	631	418	28	485
-20	149	351	9	3.2	631	349	28	766

c. Temperature gradients

The temperature gradient in the air at the air-water interface can be evaluated directly from the data. The best method found was to compute $\Delta T/\Delta y$ between pairs of data points, and plot the logarithm of these values against the cube root of the vertical distance y above the air-water interface. The cube root was chosen because it resulted in a nearly straight line and the points were well spread. Fig. 4 contains representative plots. The series of points drawn as triangles exhibits a hump which is typical of experiments done at the faster water speeds; this anomaly occurs among the thermistors close to the water, and is due to splashing of water on the thermistors. For thermistors located closer to the water surface, points obtained for a given air temperature lie along substantially the same line, independent of water speed.

The temperature gradient in air at the interface can also be evaluated from the conductive heat flux Q_c by using the equation

$$Q_c = - K_a (dT/dy)_{y=0} \qquad (8)$$

where K_a is the thermal conductivity of the air.

Table II. Temperature gradient in air at the air-water interface. Mean values of the gradients, obtained by two methods.

Air temp. °C	Q_c cal/cm² day	K_a cal/cm² day (°C/cm)	$-(dT/dy)_{y=0}$ in °C/cm	
			from eq. (8)	from data
- 2	40	4.93	8	6
- 5	87	4.89	18	8
-10	174	4.81	36	30
-20	351	4.65	76	200

Table II presents temperature gradients in the air at the interface, as obtained both from Q_c and directly from the temperature measurements. Extrapolation to an intercept on a logarithmic scale leads to a wide margin of error, perhaps even a factor of two. Substantially the same intercept was obtained from a dozen sets of data for each air temperature; this engenders confidence in gradients obtained from the data.

A comparison can be made also between values obtained from the experimental data and from the net heat flux Q*. The stirring by the paddles kept the water nearly isothermal, so that Newtonian cooling continues until the water temperature descends even to 0°C. Consequently a heat transfer coefficient H_o can be computed, following the discussion of ice cover formation by MICHEL (1971), both from the net heat loss Q* using the equation

$$Q^* = H_o(T_w - T_a) \tag{9}$$

and from the equation

$$dT_w/dt = H_o(T_a - T_w)/\rho_w c_p Y. \tag{10}$$

With the water density ρ_w equal to 1 gm/cm^3 and the specific heat c_p equal to 1 cal/gm °C, the volumetric heat capacity $\rho_w c_p$ has the value 1 cal/cm^3 °C; the mixing depth Y is simply the depth of water in the tank, 66 cm. The correspondence between the two approaches is fairly good, as Table III illustrates, although the values from the heat flux term seem excessive at the higher temperatures.

Table III. Heat transfer coefficient at the interface. Mean values, obtained from the net heat flux and from the rate of cooling.

Mean air temp. °C	Q* cal/cm^2 day	dT/dt °C/hr	H_o in cal/(cm^2 day °C) from eq.(9)	from eq.(10)
- 2.4	239	- 0.071	99.6	56.4
- 5.4	336	- 0.155	62.2	49.9
- 9.9	485	- 0.244	49.0	38.7
-19.7	766	- 0.552	38.9	43.7

d. Border ice growth

Two patterns have emerged in the temperatures associated with growth of border ice. One is the occurrence of a curve of supercooling at the onset of freezing, similar to that commonly observed during frazil formation. This effect is seen in Fig. 5 in the nonzero supercooling at speeds of 10 and 15 cm/sec.

The second pattern is an evolution of the temperature profile in the water. At most water speeds the water temperature was the same

at all depths except within a few millimeters (less than 5 mm) of the air-water interface. But in tests conducted when the water was still, a knee developed in the graph of water temperature versus depth. The knee delineates a non-convective layer adjacent to the air-water interface, a layer which thickens as the temperature continues to fall. Fig. 5 illustrates this effect. The non-convective layer will retard the cooling of the water farther from the upper surface. It will be an interesting problem to develop a model of convection and conduction in the tank, and to compare these temperatures with the model.

CONCLUSIONS

The following patterns have been considered in this paper:

1. The water supercooled by a few hundredths of a degree just prior to freezing, in all experiments performed at nonzero water speeds.
2. The maximum supercooling depended on both air temperature and water speed.
3. The rate of cooling of the water depended strongly on air temperature and weakly (at least at air temperatures down to -10°C) on water speed.
4. The magnitude of the temperature gradient in the air adjacent to the air-water interface was greater at colder air temperatures, but did not depend significantly on the water speed.
5. At zero water speed the development of a non-convective layer in the water just below its upper surface was identified in the water-temperature profile at successive times.

REFERENCES

BOWEN, I. S. 1926. "The rate of heat losses by conduction and by evaporation from any water surface." Phys. Rev. 27, 779-787.

CARSTENS, T. 1966. "Experiments with supercooling and ice formation in flowing water." Geofys. Publ. XXVI, 9, 1-18.

DROUIN, M. 1966. "Conception d'un laboratoire pour la recherche en mécanique des glaces." Thèse de maîtrise, Université Laval.

MARCOTTE, N. 1974. "Heat transfer from open-water surfaces in winter." Proceedings: Research Seminar on Thermal Regime of River Ice, (NRCC Technical Memorandum no. 114), 2-17.

McFADDEN, T. 1974. "Radiation and evaporation heat loss during ice fog conditions." Proceedings: Research Seminar on Thermal Regime of River Ice, (NRCC Technical Memorandum no. 114), 18-27.

MICHEL, B. 1963. "Theory of formation and deposit of frazil ice." Proceedings of the Eastern Snow Conference, 8, 129-149.

_____ 1971. Winter Regime of Rivers and Lakes. CRREL Monograph III-B1a.

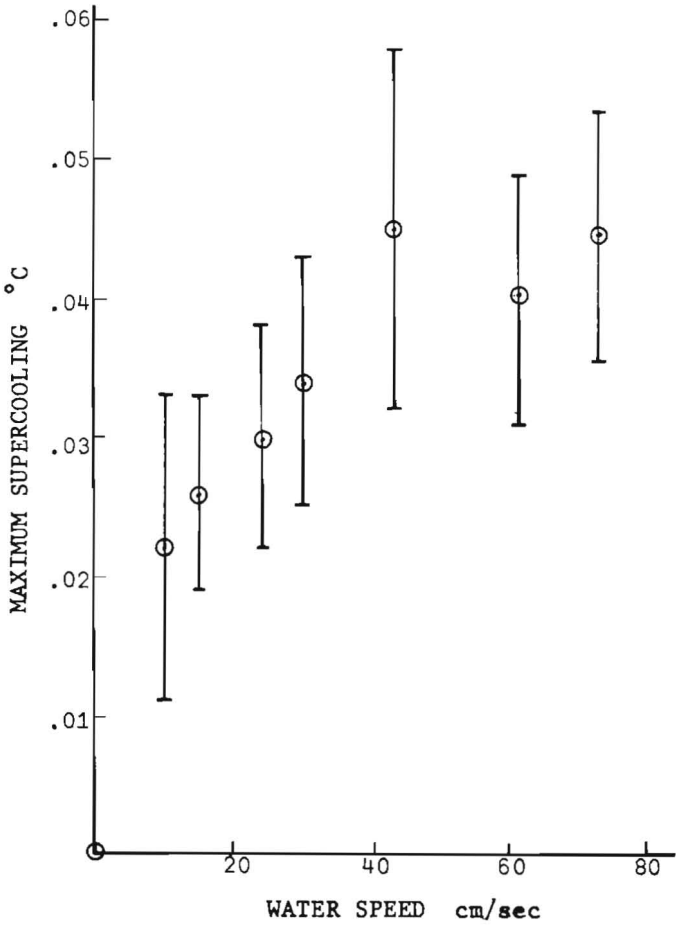

Fig. 1. Supercooling: Mean values for each water speed

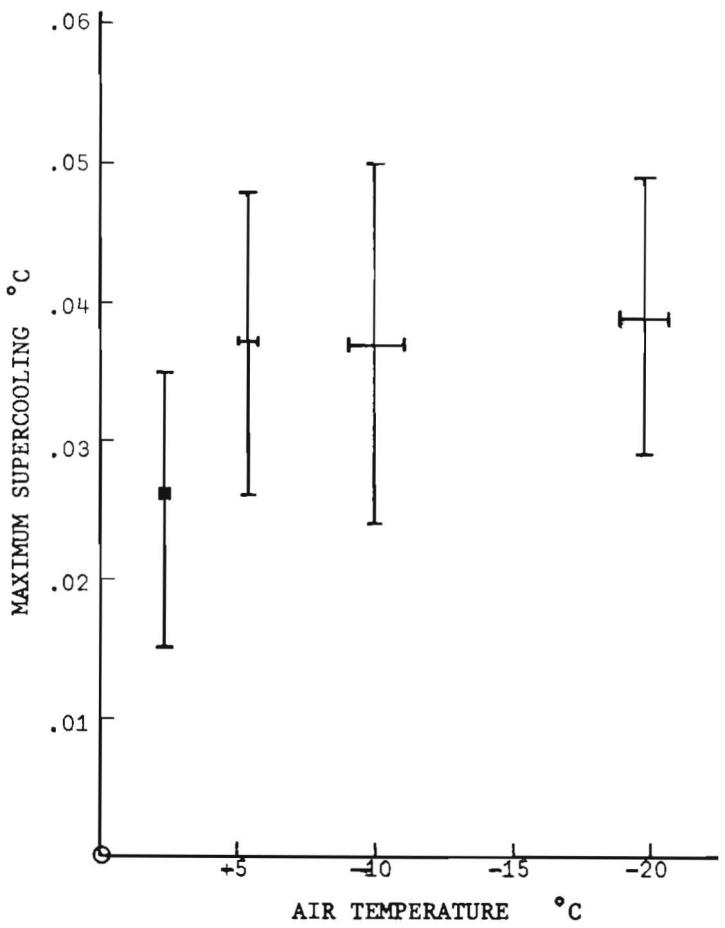

Fig. 2. Supercooling: Mean values for each air temperature

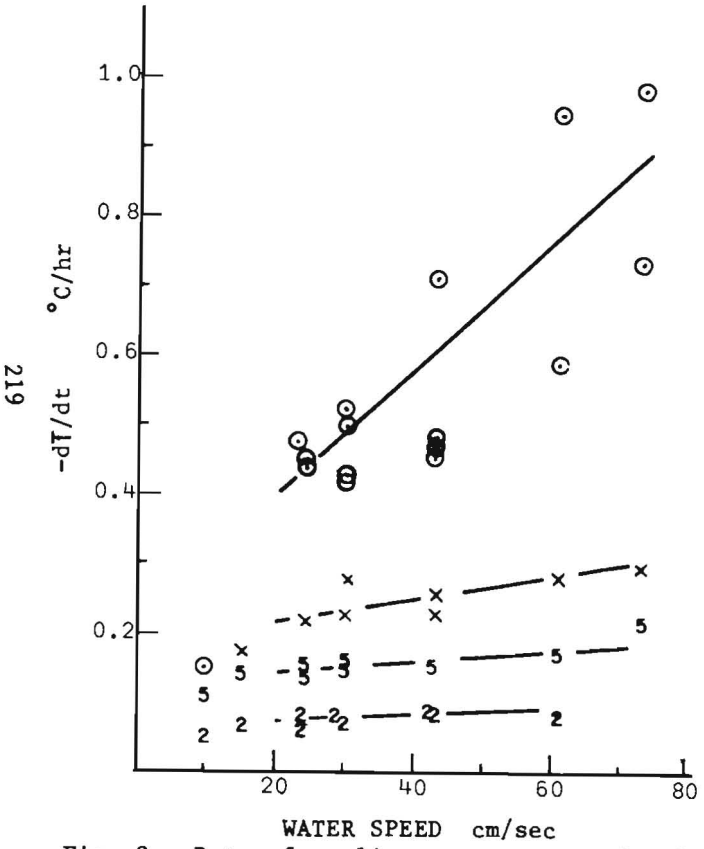

Fig. 3. Rate of cooling vs water speed and air temperature. Symbols: 2: -2°C; 5: -5°C; x: -10°C; θ: -20°C.

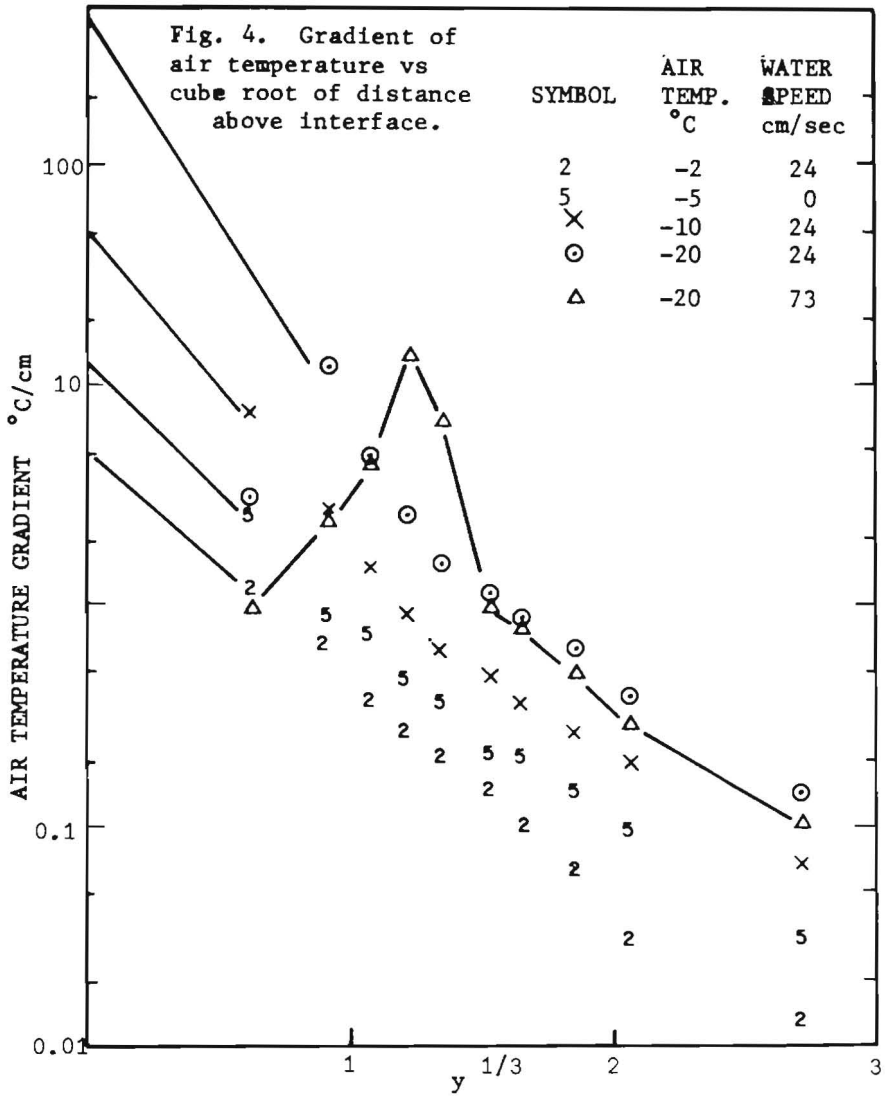

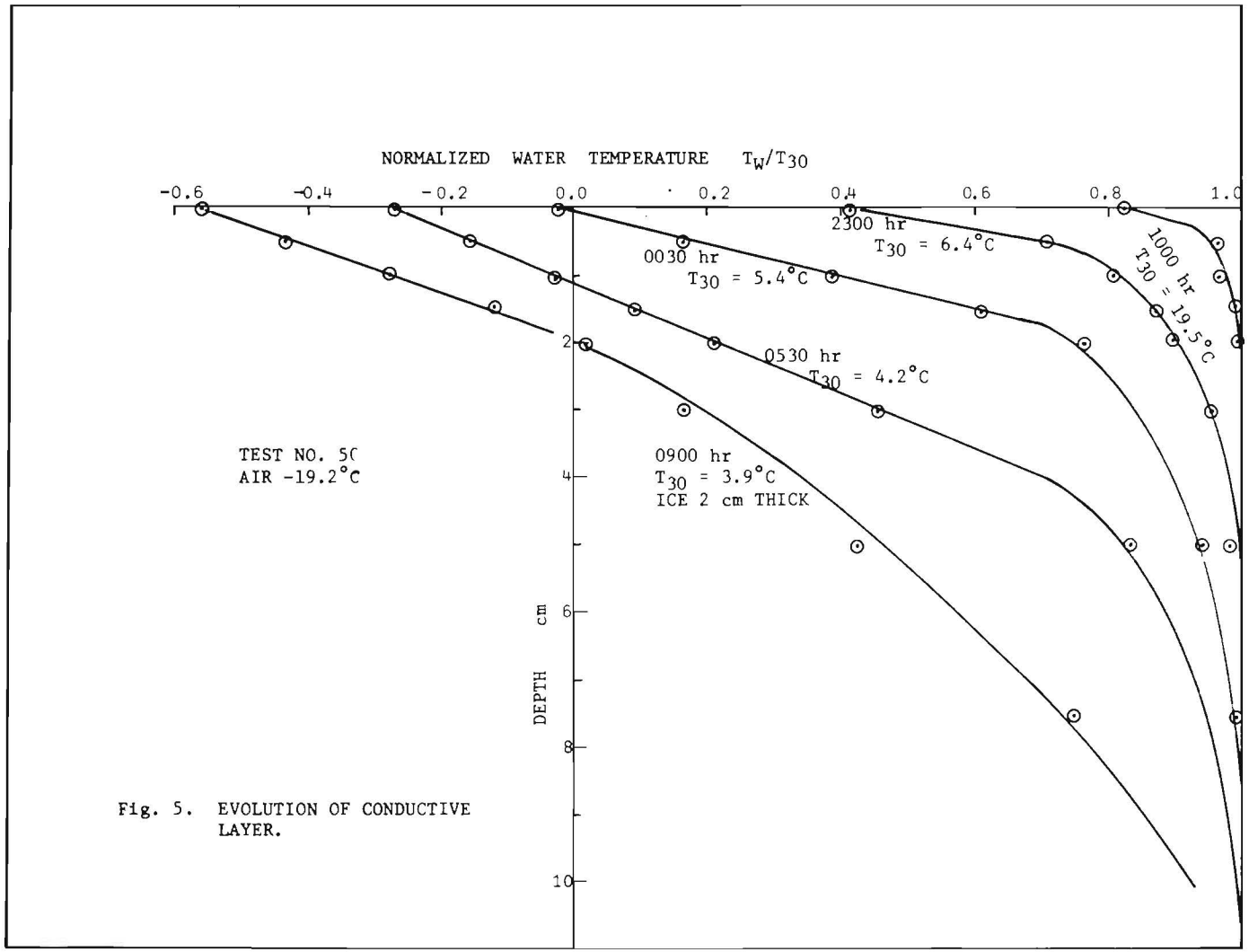

Fig. 5. EVOLUTION OF CONDUCTIVE LAYER.

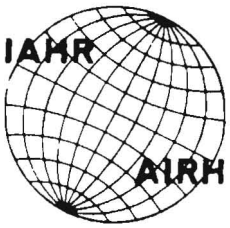

International Association of Hydraulic Research (IAHR)
Committee on Ice Problems
International Symposium on Ice Problems
18-21 August 1975
Hanover, New Hampshire

COMMENTS

Paper Title: Temperature Patterns During the Formation of Border Ice and Frazil in a Laboratory Tank

Author: T. Hanley, B. Michel

Your name: Question from unidentified attendee

Address:

Comment:

Couldn't pressure be considered as a third coordinate instead of the Reynold's number.

Answer:

Since pressure is a customary thermodynamic variable whereas Reynold's number is not. This recommendation is a priori attractive and merits further consideration.

THIRD INTERNATIONAL SYMPOSIUM ON
ICE PROBLEMS
Hanover, New Hampshire, USA

INVESTIGATIONS OF ICE JAMS ON THE SIBERIAN RIVERS AND MEASURES TAKEN TO PREVENT THEM.

V.V.Degtyarev,Professor. Novosibirsk The Soviet
I.P.Butyagin, M.Sc. Water Transport Union
V.K.Morgunov,M.Sc. Engineering Inst.
The Water Transport
Engineering Institute

In the USSR the ice jams of the greatest depth are formed on the Siberian rivers flowing in meridional direction to the north and breaking up from the headriver towards the mouth. It is this fact that differs them from the most of the rivers in the European part of the country which, as a rule,flow from the north to the south and in spring are broken up comparatively quietly starting from the lower river towards the upper ones.The rivers Northern Dvina, Dnestr and some others, which are also characterized by great ice jams under breakup, are an exception.

As everywhere else,ice jams on the Siberian rivers essentially depend on ice drift conditions and patterns under freeze-up and break-up.

The delay of the breakup in the lower sections of the river usually causes spring ice jam formation.This delay may occur due to meteorological conditions of the region, as well as due to the formation of thicker and more solid ice on these sections.

Ice jam formations also often occur in the upstream of sharp bends and branching of the river which reduce the conveying capacity therein for transit motion of drifting ice.

Thus,ice jam depth on the Siberian rivers may be controlled by two main factors. The first one is the

large thickness and strength of ice cover due to low air temperatures in winter, the second one is that spring flood wave, spreading along the current, outruns the coming of warm weather in the northern riverain areas resulting in intensive effect of the mechanical factor under river breakup. River stages and current velocities increasing, the flow has to destroy still solid ice which has not yet been subjected to heat destroying.

Ice jam depth on the Siberian rivers being very great, these ice jams influence the channel up to the 500km long section upstream (e.g. the Yenisei river at the city of Igarka-), herein river stages may rise to 15 m and the length of ice jam accumulation may reach scores of kilometres.

. Ice jams impede operating the country's river fleet and developing other branches of national economy. As a consequence of ice jams one can observe hereat the degradation of stream channel which disagrees with the direction of the shipping course. Water stage rising due to ice jams often favours the aggradation of channel shallow crests. All these effects change for the worse the navigable conditions and considerably increase the volume of dredging. The ice jams having been broken, the ice moving at great velocities destroys banks and bank protection works. Ice jams are of great danger to the fleet berthing in winter even in backwaters with good facilities.

If ice jam break occurs below the entrance to the backwater, the ships laying up there can be pushed out of it into the river covered with drifting ice. Ice jams formed above the backwater may cause the ships laying up there to go down to the bottom. Sharp fall of water stages due to ice jams results in flooding bank stream-side areas and damaging buildings and river port structures.

The aforementioned facts require that proper measures should therefore be taken to fight ice jamming on a number of sections of the Siberian rivers.

To destroy the accumulations of ice jams already formed various methods were used: air bombing, gun firing and more often blasting.

Experience has shown the bombing to give some beneficial effect only at the start of ice jam formation. Air bombing used in later periods proved to be almost useless.

Gun firing, as a rule, destroys only such ice jams that have been formed as a result of the stoppage of giant ice floes and provided that the river section in the downstream of ice jam is free of ice.

Ice blasting not always gives some beneficial effect either. The helicopters being used for placing charges, the efficiency and safety of ice blasting would increase, but explosions result in great damage to fisheries and must be resorted to only in exceptional circumstances.

All these measures only accelerate the destroying of ice jams but do not eliminate their harmful consequences as a whole, besides, they are too expensive and often dangerous to bank structures.

Moreover, ice jams of considerable length, often formed on the rivers of Siberia, can't be eliminated at all when using above mentioned methods under low water discharges.

Preventive ice measures appeared to be more effective as they lead to the prevention of ice jam formations or reduce ice jam depths and decrease the dangerous effect thereof on structures of importance for national economy.

Beneficial effect as well could be achieved due to artificial destroying or weakening the ice cover in case of probable ice jam formation on the river section in the downstream. The length of the river section with the ice cover to be destroyed (or to be weakened) depends on freeze-up pattern, winter temperature regime and hydrological conditions of the year considered.

Regular observations on ice phenomena, being widely carried out now by hydrometeorological service of the country and other authorities, as well as the study of ice - thermal regime of water bodies, permit the locations of ice jam formations in the river channel to be determined with high accuracy. The investigations carried out have shown, in particular, that spring ice jams are often formed in locations of their debacles when freezing starts and, especially, in locations of autumn ice jam formations. These phenomena favour the formation of thicker and more solid rough ice. As already mentioned, of is this process that often causes spring ice jam formation.

For a long time blasting was the major artificial method used to destroy the ice cover in locations of probable ice jam formations. On the rivers of the European part of the USSR the icebreakers were also used hereat. As experience has shown, blasting proved to be not very effective for this purpose. Besides, blasting being used to prevent ice jam formations is now prohibited by fishery inspection almost everywhere. The icebreaker fleet in Siberia has not almost been used for this purpose due to large ice thickness.

Ice can be weakened by blackening it using the method of pulverization of powdered materials (coal, slag).

Hereat ice absorbs more solar radiation and melts quicker.

Ice blackening tests had been carried out on the river Irtysh and on the Novosibirsk reservoir but they failed to give good results. Good effects could only be obtained in artic conditions.

The weakening of the ice cover section can be reached by cutting it with the aid of ice-cutting machines To prevent ice jam formation usually two or three parallel rills, that follow the channel, are cut in the ice cover. To date the ice-cutting machines have been seldom utilized for this purpose but the organization of production of ice-cutting machines equipped with cutterheads in the country does present wide prospects for utilization such mechanisms having operational ice-cutting speeds up to 500 m p h and higher.

The utilization of machines for ice removal and sloping knife-planes to be used for the same purposes appears to become even more economically expedient " Knife-planes" can cut rills in the ice cover of 30-40 cm deep at the speed of up to 15 km p h. Prototype machines had been tested and approved and their commercial production would considerably increase the ice-cutting capacity.

The utilization of impulse water jets designed in the Siberian Branch of the USSR Academy of Sciences for ice destroying might also be of great help in the future. These impulse water jets have been tested on the Novosibirsk reservoir and their working capacity appeared to be more than 6.700cu.m. of ice per hour.

The method of shifting ice jam into a safe location proves to be effective in case the ice jam is expected to be formed on this particular river section. Follow this purpose, an artificial ice jam can be formed in the upstream in the form of an ice dam using installations of boom type or some other means for ice anchoring at the banks.

Ice motion creating no ice jams on certain river sections can also be ensured in case the complex of regulation works is developed channel cutoff, cutting of bank projections, cutting of spits and isles the utilization of structures made of artificial ice is expected to be effective under aforementioned regulation works too.

Finally, the most reliable means to fight ice jam formations proved to be the regulation of hydrological river regime by erecting the cascade of hydropower stations on the river.

However, the erecting of such cascades of hydropower stations on all Siberian rivers is a matter of rather distant future. Therefore in the near future the major method to prevent ice jam formations in dangerous locations, obviously,will be the method of ice distroying and weakening with the aid of mechanical means as well as regulation works to be developed on some river sections.

The elaboration and perfection of measures for fighting ice jams require that special investigations on ice drift regime should be carried out as well as those on peculiarities of river breakup and freezeup, and physico-mechanical properties of the ice cover. To carry out such investigations a number of new devices has been designed in Novosibirsk.

I.P.Butyagin has designed installations for determining alterations of ice cover strength and thickness in field conditions.

The installation for studying ice strength (see App.I) permits us to carry out in the field numerous tests on bending prismatic specimens at constant temperature,being equal to 0°C, that corresponds to the river breakup conditions.

The specimens are tested while being submerged into water by using the scheme of one-span,freely-supported beam immorsing by vertical concentrated load in the middle of the span. Their cross section values may vary from 6x6 up to 10x10 cm, and the bearing(effective)length (the distance between supports) is 50 cm. These specimens are prepared with the aid of a light ice-cutting machine specially designed for this purpose. The effort for immersing ice specimen is created with the aid of a tank being filled with water and is transmitted to the specimen by leverage.

The method considered permits us to carry out more than 50 tests a day, hereat one obtains sufficiently reliable information on alterations of ice cover strength in various ice strata in terms of time.

Another installation has been designed to carry out tests on bending large ice cover specimens having cross-section height as large as their thickness. The specimens can be tested by using the schemes of double-seat (supported) beam, having been submerged (immersed) by one or two efforts, or the console. Hereat the specimens are prepared and tested just in the ice cover without taking them out of water.

The functioning of the installation for precision measuring ice thickness in spring is based on using electric current for heating a thin high-resistant conductor,having a little suspended load supported in the upper part. The heating of conductor permits us to raise the load up to its thrust in the underside surface of the ice cover. Hereat the changes (alterations) of its thickness are accurately read off from a rigidly-fixed stick from both surfaces. Current is supplied to the installation from a portable.

As a consequence of experimental investigations carried out, analytical and graphical dependences have been elaborated. The results of ice specimen tests provided the data for estimating the design strength of the ice cover in field conditions taking into account the scale effect.

The reducing of ice strength in spring under the influence of solar radiation has also been investigated.

The original photogrammetric devices for estimating motion velocities, trajectories and sizes of ice floes under ice drifting have been designed by V.K.Morgunov.

The crosshairs-slotted device (see App.3) is used for determining motion velocities of ice floes. This device permits us to reproduce successive images of a drifting floe on a single glass,large-sized negative. The camera shutter is spring-controlled. In case stereophotogrammetrical survey by two cameras is needed, the camera shutters are provided with electromagnetic synchronizers.

Camera magazine is provided with two elastic blinds located in front of a photographic plate. These blinds are moving by means of two pairs of rotating rollers in reciprocal perpendicular directions. These light-tight blinds have vertical and horizontal slots which form a movable film gate under intersection. The rollers,that direct the motion of blinds, are kinematically linked with a sighting device,herein a telescope.

During the survey the camera shutter operates automatically and you can observe a moving body (a floe) continuously with the aid of a telescope. Hereat, the image of an object on a plate will constantly be placed in the film gate shifting along the surface of this plate. If necessary, the phototransformation of a picture can be made (the reduction of a perspective image to a horizontal surface).

Synchronical photogrammetrical survey by means of two cameras described above, which are located in both ends of a basic line,permits us to plot three-dimensional coordinates of successive positions of the floe in the function of time.

Portable photogrammetrical camera (see App.4) permits to obtain easily the plan of ice field contour by means of a single perspective picture, hence, one can determine the sizes thereof with sufficient accuracy. The device is provided with a rigid camera fixed at the proper angle to the horizon on a theodolite-type support permitting its rotation only around a vertical axis. The camera magazine is designed for a rolling film with frame sizes of 6x9 cm.

While printing the picture of the ice field, the image of perspective coordinate grid, corresponding to the angle of the optical axis of the device to the horizon under surveying, is being simultaneously projected thereon. The perspective picture is easily transformed on the horizontal surface (plan) by means of this grid. Successive pictures made with a fixed device permit also to plot trajectories of drifting floes or floats set out on purpose.

The investigations carried out with the aid of the devices described above in addition to the study of ice jam phenomena, have also been applied for evaluating the methods of calculation of ice loads on hydrotechnical structures.

Приложение 1

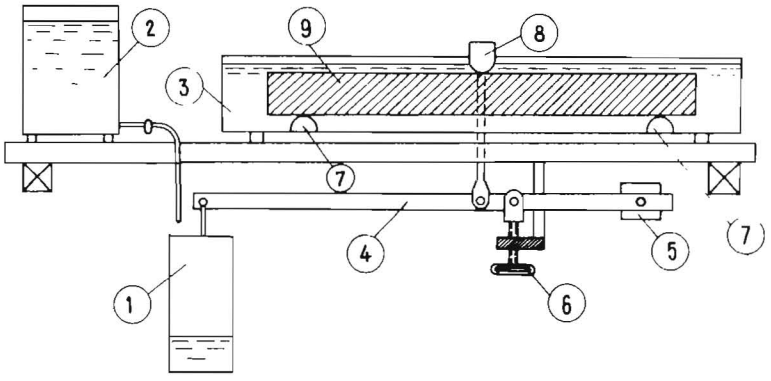

Appendix 1.

The installation to investigate the strenth of the ice

1 - in load tank;
2 - water - inlet tank;
3 - water basin;
4 - in - load lever;
5 - counterweight of the lever;
6 - support control screw;
7 - supports for a specimen;
8 - in - load stirrup;
9 - specimen.

Приложение 2

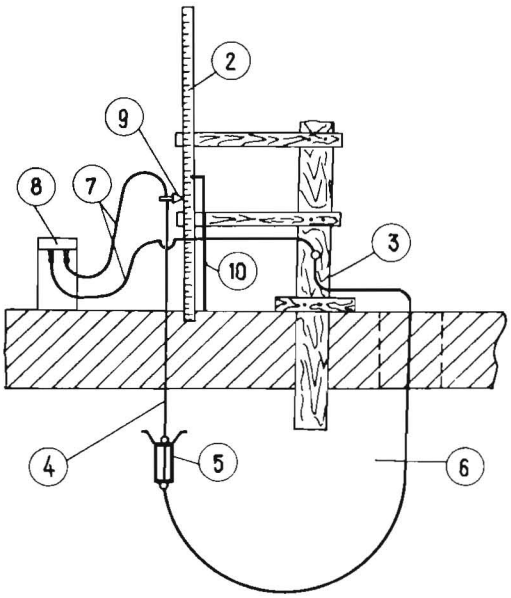

Appendix 2

Electro - icemeter device

1 - ice cover;
2 - stationary meter batten;
3 - fasten bar of the batten frozen into the ice;
4 - large resistance conductor heated by the current;
5 - load with the rests;
6 - flexible copper conductor;
7 - joining conductor;
8 - accumulator;
9 - reckon indicator of the batten;
10 - a snow - thickness sound.

Приложение 3

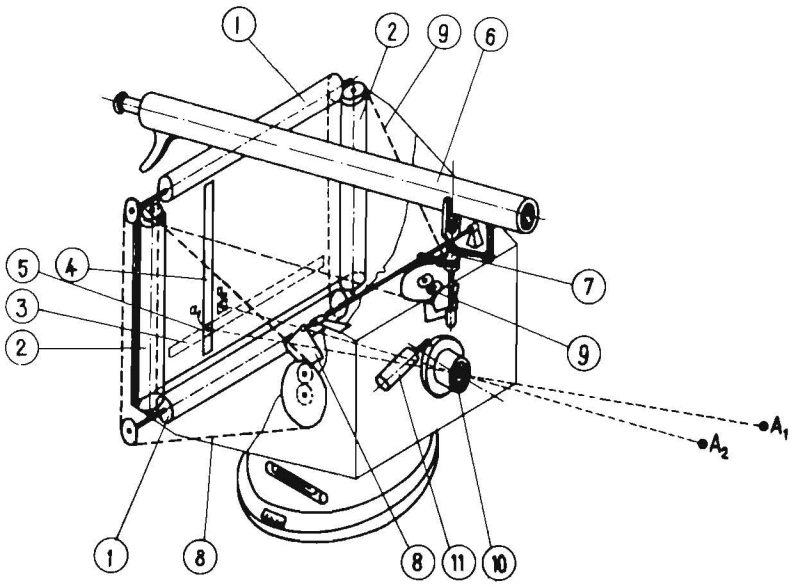

Appendix 3

Crest-peep-hole photo chamber for determination of the velocity of the motion of the pieces of ice.

1 - cylinders for the blind of the vertical motion;
2 - cylinders for the blind of the horizontal motion;
3 - horizontal peep-hole in the blind;
4 - vertical peep-hole in the blind;
5 - cardo movable opening;
6 - optical tâbe of the vising device;
7 - mechanism for kinematic connection of the vising device with cylinders of the blinds;
8 - mechanism for rotation of horizontal cylinders;
9 - mechanism for rotation of vertical cylinders;
10 - objective;
11 - control mechanism for objective lock.

There has not been a shortage of water for ice flushing after construction of the storage at Lake Thorisvatn.

The operation of the ice flushing has been satisfactory under normal conditions which is to say most of the time. However, it happens now and again that the ice flushing breaks down and an ice bridge is formed between the upper end of the ice trough and the rock jetty, see Fig. 1. An unavoidable cause for the formation of this ice bridge is an increase in the ice discharge which exceeds the ice flushing capability of the structures. Other causes are unfavourable currents in the pool or too limited flushing water. Temporary increases in the ice discharge occur in combination with the so-called step-bursts, or flash floods, which result from the break-up of ice dams or anchor ice restrictions consecutively one after another. The large concentrations of ice in the step-bursts can be difficult to handle, even though a warning system signals their coming. The operators have been gaining experience over the years, but it is not likely that the formation of the ice bridge in the pool (see Fig. 1) can be avoided at all times. The ice bridge can often be removed by manipulating with the water level and the gates. If the ice bridge can not be removed, it may stay there with the ice going under it and mostly surfacing downstream so that ice flushing can be continued, but some of the ice will go into the diversion canal to the power station.

With heavy ice runs it is more likely that the ice will build up a jam upstream of the ice bridge and this has happened several times every winter. The formation of the ice jams has followed the same pattern ever since the first winter of operation, see Figures 1 through 5. In the beginning the ice accumulates in the river channel and the jam grows upstream. This is followed by rise in water level and the jam is more or less unstable. After some time, usually 2 to 6 hours, the jam starts moving downstream and can then be flushed down through the spillway flap gates. If this flushing fails, and that has happened one or more times every winter, the jam will build up to about 1 1/2 km upstream of the dam and completely clog the river channel. The water is forced along the left bank and out of the river channel to that side (see Fig. 2 and 3). This was what happened during the first ice jam in November 1969. Much of the water was then temporarily lost over the ungated spillway but later it opened up a channel to the pool through an opening that was excavated in the rock jetty (Fig. 1). This situation, with the water coming through the opening in the rock jetty almost perpendicular to the ice trough, has recurred and may last for weeks. It is unfavourable for ice flushing, as much of the ice is suspended in the water and goes into the diversion canal to the power station. In November and December 1973 during an unusually long frost period this resulted in the formation of an extensive hanging ice dam under the ice cover on the diversion canal and the intake pond which seriously restricted the flow to the power station. The volume of the ice accumulation in the diversion canal and intake pond was estimated approx. 2 million m^3. This was the main cause for the

many days of ice troubles during that winter as tabulated in Table I. The situation improved gradually with warmer weather in January to March 1974.

The channel on the left bank of the river may fill up with ice during step-bursts or heavy ice runs. This results in renewed growth of the ice jam with further rise in water levels. Large areas on the left bank of the river have been covered with water and ice during this second stage of the ice jams and much water has been temporarily lost. The ice edge has moved up to about the upstream end of the Klofaey island, or about 3 km upstream of the dam, and the river has found a new channel up on the right bank (Fig. 4 and 5).

The second stage ice jam is often unstable during the build-up, just like the initial ice jam. In December 1973 it shoved down the channel on the left bank and almost overtopped the left bank dike. The channel on the right bank is usually narrow and of limited capacity. This results in overflow out on the ice jam and the river frequently erodes a gorge through the jam in the original channel. In prolonged cold spells the channels may get filled with ice alternately and the river moves between the banks and out on the jam several times. Further growth of the jams upstream other than a short distance upstream of Klofaey has not been observed as yet.

During warm spells the river erodes a gorge through the ice jam in the river channel. This has often been favourable for ice flushing but more ice is suspended in the water than under normal conditions. Remnants of the ice jams may last throughout the winter.

When the ice jams have been most extensive they have covered an area of 6-8 km^2 and the rise in water levels has amounted to 3-4 meters. Detailed surveying of the extent and elevations of the jam has not been carried out and would be difficult to perform. It can even be difficult to get a view of the situation except by air reconnaissance.

The most rational approach to remedy the critical ice situations and reduce the flushing water would be to reduce sufficiently the area of the active zone upstream of the diversion dam. Canalization of the river upstream was foreseen in the original project planning and has been undertaken to some extent. The left channel at the Klofaey island has been closed by a rock dike and two distributory channels farther upstream have also been closed.

The opening that was cut in the rock jetty during the first ice jam in November 1969 has been left there and the river has repeatedly come that way to the diversion intake when the main channel has been clogged by ice jams.

The danger of losing the water over the ungated spillway when jams were building up became obvious already the first winter. Fill and rock was dumped above the spillway. In the summer of 1970 this

fill was improved and the rock jetty was extended by a low dike to the left bank and an embankment was made on the left bank all the way up to Klofaey island. These dikes and embankments were overtopped during ice jams the following winter, and were further strengthened in the summer of 1971. The next two winters were rather mild and without serious difficulties and little was done except repairs of minor damages. The first part of the winter 1973-74 was cold and with serious troubles due to ice jams.

After that, it was decided to build the present system of embankments as shown on Fig. 1. Now the river must overtop or break through three barriers before it will go over the ungated spillway. The winter 1974-75 was cold but the operation was generally smooth and without serious ice jams. This may not least be due to better approach flow conditions to the ice trough and the gates after construction of the groin from the left bank. Previously the flow to the ice trough under normal conditions was converging somewhat unfavourable (Fig. 6). Now the flow is much more parallel and in the right direction (Fig. 7) and the ice flushing capacity of the structures seems to have greatly increased. The approach flow conditions along the wall upstream of the ice trough have often been troublesome. A recess is formed where the wall bends up on the bank. When this recess is not ice covered an eddy will stay there and collect ice that will partially go into the diversion canal. An attempt to close the recess with an ice boom was not successful. The first ice bridge tore the ice boom away.

The use of explosives to open up water passages through the ice jams in the river channel upstream of the dam has been tried but without success. On the other hand explosives have been successfully used to improve channels that the river itself has eroded through the ice jams.

Ice jams during break-up have not occurred at the Burfell dam. Ice floes from shore ice and ice covers farther upstream can occur in great quantities but the discharge is higher and the ice concentration less than during the heaviest frazil ice runs. Ice floes and ice cakes are often mixed with the frazil, expecially in the step bursts. Impact forces from ice floes have damaged the spillway flap gates and flap gates on the ice trough were totally wrecked the first winter in operation. Icing on the downstream side of the spillway flap gates has put these gates out of operation for extended periods.

In summary it can be concluded that the Burfell ice flushing facilities have thus far proved to be of successful design except for the spillway and the ice trough gates which should have been of stronger construction.

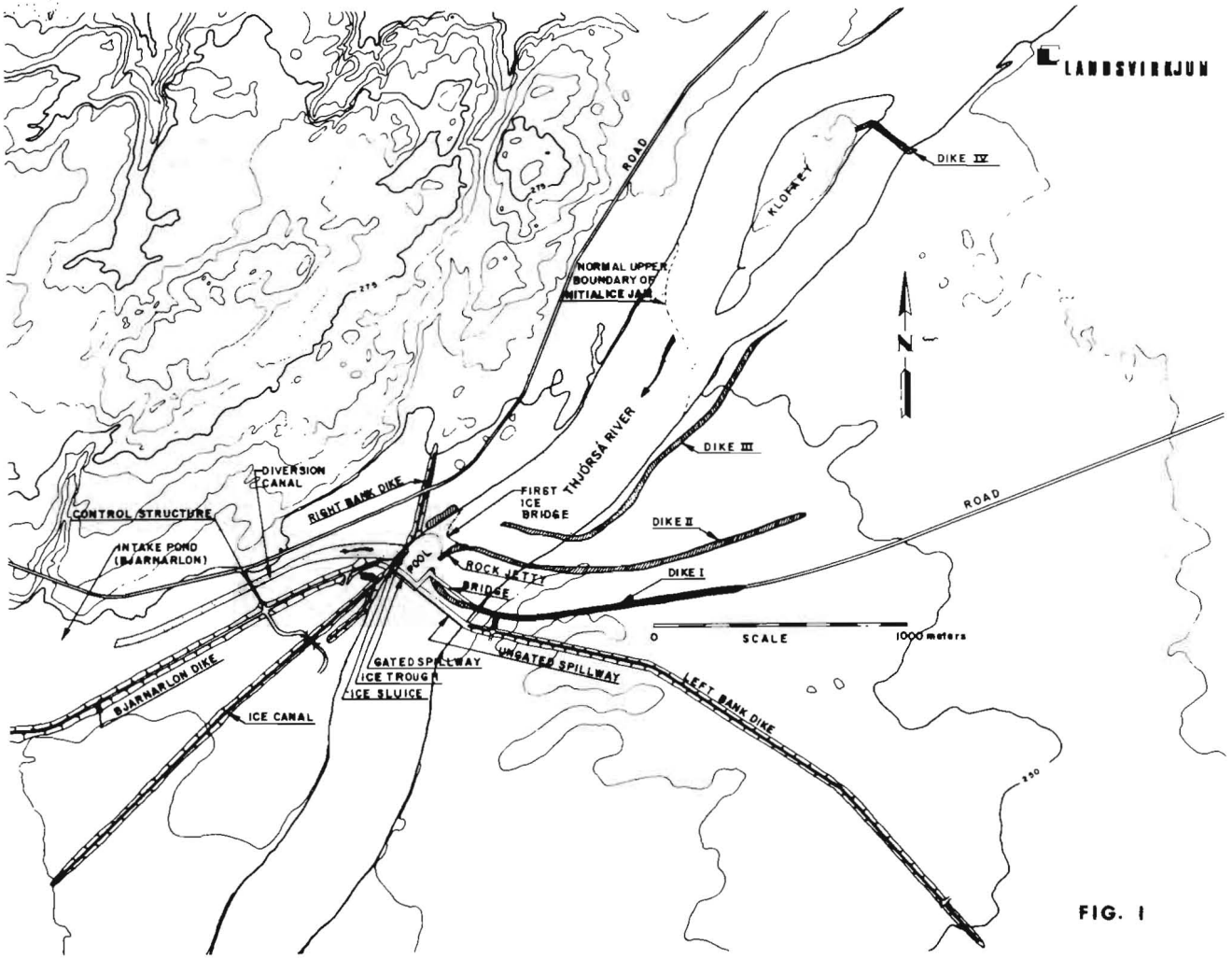
LANDSVIRKJUN
DIKE IV
KLOFAKEY
ROAD
NORMAL UPPER BOUNDARY OF INITIAL ICE JAM
N
DIKE III
FIRST THJÓRSÁ RIVER
ICE BRIDGE
DIKE II
ROAD
DIVERSION CANAL
RIGHT BANK DIKE
CONTROL STRUCTURE
INTAKE POND (BJARNARLON)
ROCK JETTY
BRIDGE
DIKE I
0 SCALE 1000 meters
GATED SPILLWAY
ICE TROUGH
ICE SLUICE
UNGATED SPILLWAY
LEFT BANK DIKE
BJARNARLON DIKE
ICE CANAL

FIG. 1

Fig. 2 (Nov. 27, 1969)

Fig. 3 (Dec. 6, 1973)

Fig. 4 (Jan. 8, 1970)

Fig. 5 (Dec. 21, 1973)

Fig. 6 (Nov. 25, 1970)

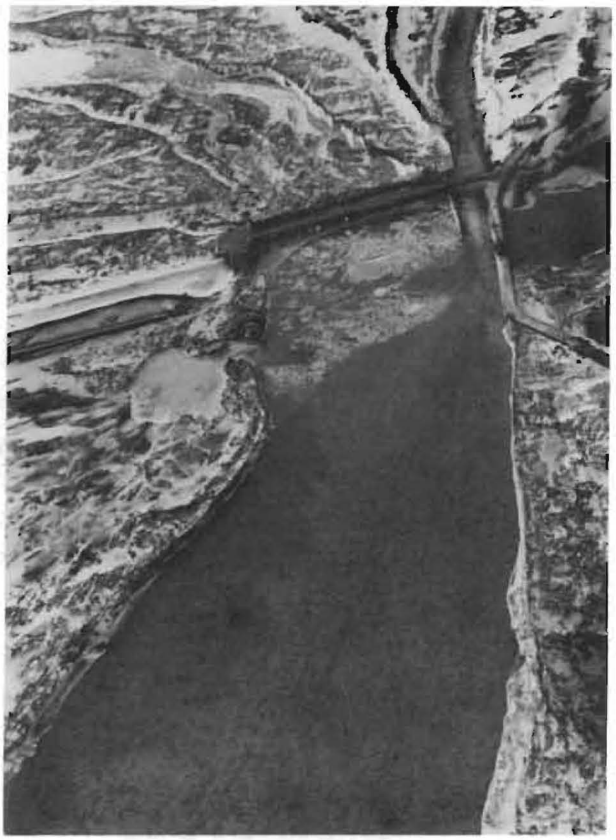

Fig. 7 (Jan. 7, 1975)

THIRD INTERNATIONAL SYMPOSIUM ON
ICE PROBLEMS
Hanover, New Hampshire, USA

SOME NEW RELATIONSHIPS OF THE JAMMED ICE MOTION

ENDRE ZSILÁK
CIVIL ENGINEER,
HYDRAULIC SENIOR DESIGNER

VIZITERV
INSTITUTE FOR HYDRAULIC PLANNING

BUDAPEST
HUNGARY

ABSTRACT

A part of the tasks concerning winter operation of low head barrages is connected with ice motion of highly covered river surfaces, termed saturated ice motion. This paper deals with permanent, rectilinear, uniform ice motion. The results draw attention to a few new features of ice motion.

The first part of the paper introduces the concept of the so-called effective distance. This is a suitable parameter for characterizing ice conditions of rivers.

The second part of the paper deals with the thrust distribution inside a moving ice body, assuming that water velocity is changing linearly. The results draw attention to a few new explanations of the forming of blocks of ice in the sorroundings of the upper limit of backwater reaches.

SOME NEW RELATIONSHIPS OF THE JAMMED ICE MOTION

1. A former paper of the same author presented to the IAHR-PIANC Symposium /Budapest, 1974/ introduced a physical-mathematical model of the saturated, rectilinear, gradually changing ice motion. The model consists of the dynamic basic theorem deduced from Newton's second axiom as well as of the condition of continuity expressing the principle of conservation of material. On the basis of Fig. 1. the following two equations can be set up:

$$\left(\frac{\gamma_i}{g} d \cdot B dx\right)\left(\frac{\partial v_2}{\partial x} v_2 + \frac{\partial v_2}{\partial t}\right) = B d i \gamma_i dx +$$

$$+ sgn(v_1 - v_2)\beta B (v_1 - v_2)^2 dx - P_r dx - B d \frac{\partial p}{\partial x} dx +$$

$$+ B\beta_w v_w^2 \cos\xi dx \ldots \qquad 1.$$

$$v_2\left(\frac{\partial n}{\partial x} + \frac{n}{B}\frac{\partial B}{\partial x}\right) + n\frac{\partial v_2}{\partial x} + \frac{\partial n}{\partial t} = 0. \qquad 2.$$

Designations:

d /m/	Thickness of ice
g /ms^{-2}/	Acceleration of gravity
i	Grade
n	Coverage
p /Mpm^{-2}/	Thrust
t /s/	Time
v_1/ms^{-1}/	Mean velocity of water of a cross-section
v_2/ms^{-1}/	Mean velocity of ice of a cross-section
v_w/ms^{-1}/	Velocity of wind
B /m/	Average width of river
P_r/Mpm^{-1}/	Resisting force for a unit length of flow
β /Mps^{2}m^{-4}/	Velocity coefficient for friction between water and ice
β_w/Mps^{2}m^{-4}/	Velocity coefficient for friction between wind and ice
γ_i/Mpm^{-3}/	Gravimetric density of ice
ξ /radian/	Angle included between the direction of ice motion and that of the wind

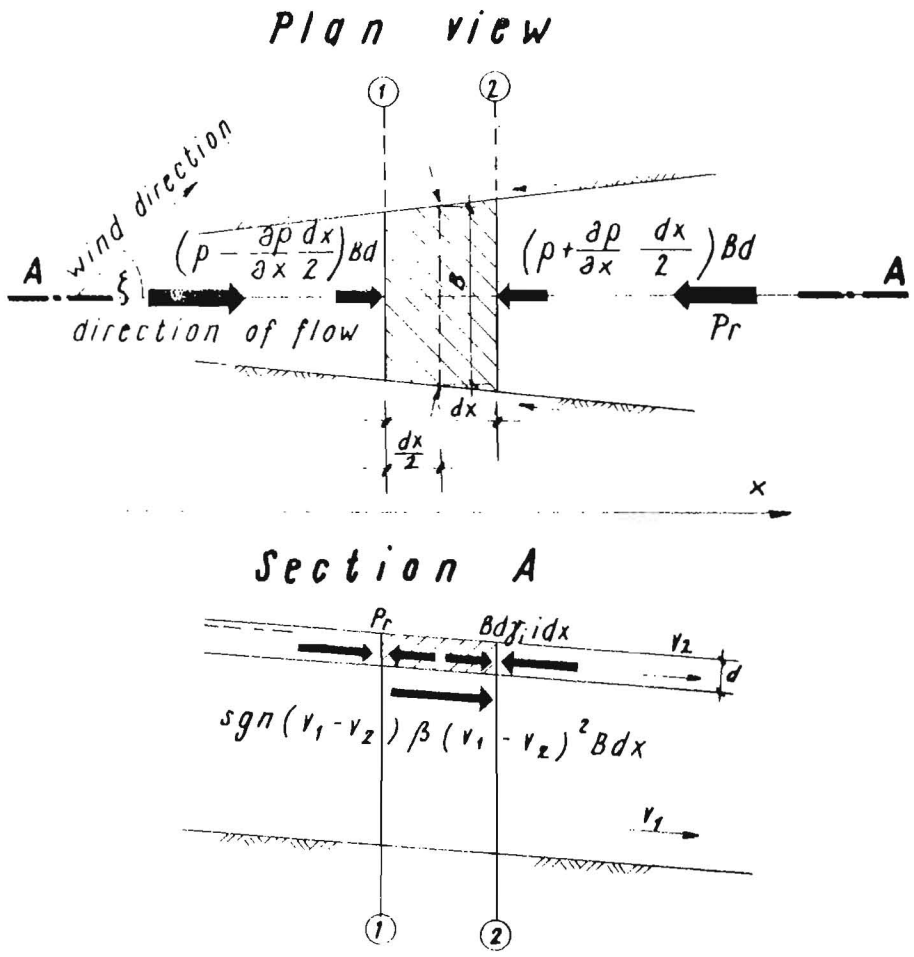

Fig. 1 Scheme to the differential equations of saturated, linear, gradually varying ice motion

In the case of p = 0 the ice motion is termed free from congestion; in the opposite case it is termed jammed ice motion.

In the above mentioned paper the permanent, rectilinear, uniform, jammed ice motion has been investigated. In that case $\frac{\partial v_2}{\partial t} = 0$, $\frac{\partial n}{\partial t} = 0$, $\frac{\partial v_2}{\partial x} = 0$ and, due to the condition of saturation, $\frac{\partial n}{\partial x} = 0$. As a consequence of Equ. /2/, B = constant. Assuming

that the resisting force is a linear function of thrust the formula

$$p = F(x, v_2) * e^{-\omega x} \qquad 3.$$

has been deduced, enabling to calculate the thrust. In the paper the concept of effective distance is deduced from Equ. /3/.

Designations:

$F\ /x,\ v_2/$	A function governed by the parameters of water and ice motion
e	Base of natural logarythm
$\omega = \frac{2\mu z}{B}\ /m^{-1}/$	A characteristic constant for jammed ice motion
z	Proportionality factor between tangential stress and thrust
μ	Quotient of longitudinal and lateral thrust

Since $F\ /x,\ v_2/_{min} \leq F\ /x,\ v_2/ \leq F\ /x,\ v_2/_{max}$ and since the exponential function is always positive, one can write:

$$\int_0^x F(\xi, v_2)_{min}\ e^{-\omega(x-\xi)}\, d\xi \leq F(\xi, v_2) * e^{-\omega x} \leq$$

$$\leq \int_0^x F(\xi, v_2)_{max}\ e^{-\omega(x-\xi)}\, d\xi\ ,$$

$$\frac{F(x, v_2)_{min}}{\omega}\left(1 - e^{-\omega x}\right) \leq F(x, v_2) * e^{-\omega x} \leq$$

$$\leq \frac{F(x, v_2)_{max}}{\omega}\left(1 - e^{-\omega x}\right)$$

If $x \geq \frac{3}{\omega}$, then $1 - e^{-\omega x} \simeq 1$. In this case, however,

$$\frac{F(x, v_2)_{min}}{\omega} \leq p \leq \frac{F(x, v_2)_{max}}{\omega}\ .$$

By introducing $\frac{1}{\omega} = l_h\ /m/$,

$$F(x, v_2)_{min}\ l_h \leq p \leq F(x, v_2)_{max}\ l_h\ .$$

From a practical viewpoint, l_h might be termed as <u>effective distance</u>. This is a length, along which any effect decreases

to its e-th part. As a matter of course, the concept of effective distance can be interpreted for standing ice, too. Thus, both for standing and moving ice the extreme values of thrust can be determined as the product of effective distance and a function of the parameters of water and ice motion. The less the effective distance, the less the thrust and, at the same time, the change in thrust. Thus, the danger of ice congestion and of jamms are also less. Effective distance is a suitable parameter for characterizing the ice conditions of rivers.

Assuming $\mu = 0{,}30$ /a very low value/, and for $z = 0{,}30$, too, the values of ω and $\frac{1}{\omega}$, depending on the width of the river, are shown in Table 1:

B	ω	$\frac{1}{\omega} = l_h$
m	m^{-1}	m
50	0,0036	277
150	0,0012	831
300	0,0006	1662

Table 1.

From the date of this table it is apparent that ice phenomena of a given cross-section are determined by the hydraulic parameters of only a very short river reach.

2. Thrust distribution inside moving ice body

As a matter of general experience, blocks of ice often form above low head barrages, near to the upper limit of dammed water. The forming of blocks of ice is generally explained by the collision of arriving ice tables against a standing ice sheet. Obviously, these phenomena also have a role in the forming of blocks of ice.

It often happens, hovewer, that ice sheet formed or just forming, occasionally slips and piles up. This phenomenon is going to be analyzed in this paper on the basis of pressure distribution inside the ice sheet. For the sake of generality, the results of investigations of moving ice are here discussed. The conclusions are relevant, of course, also for standing ice sheets.

By setting forth in detail Equ. /3/, thrust can be calculated from the following formula:

$$P = \int_0^x A_0(\xi)\, e^{-\omega(x-\xi)}\, d\xi + v_2 \int_0^x A_1(\xi)\, e^{-\omega(x-\xi)}\, d\xi + v_2^2 \int_0^x A_2(\xi)\, e^{-\omega(x-\xi)}\, d\xi \qquad 4.$$

Designation:

$A_o / \xi /$, $A_1 / \xi /$.... functions of water and ice motion characteristics, arranged according to the powers of ice velocity.

Equ. /4/ has been solved for the backwater reaches of low head barrages, assuming a linear change in water velocity along the reach. The model assumed is shown in Fig. 2.

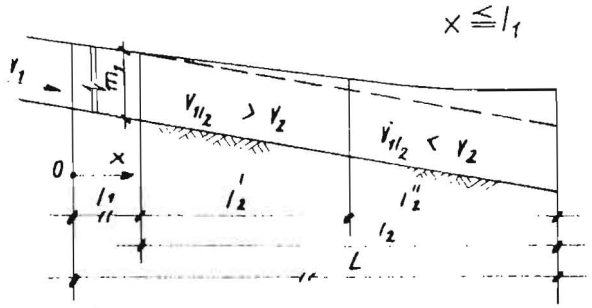

Fig. 2 A model for examining the ice motion developing within the reach

In the following, the solution of Equ. /4/ will be described, pressed for space, only for the reach l_2''. The force resulting from the grade is taken into account. The effect of grade can, according to our results, be neglected. On the other hand, the functions valid for the other reaches can be deduced from Equ. /5/.

$$P = \frac{\beta}{d\omega} \left[-(v_{1h} - v_2)^2 - 2v_1 s (v_{1h} + v_1 s - v_2) + \right.$$
$$+ e^{-tv''} \left\{ (v_1 - v_2^2) - (v_{1h} - v_2)^2 + v_1 s \left[-2v_{1h} (tv'' + 1) \right.\right.$$
$$\left.\left. - v_1 s (tv''^2 + 2tv'' + 2) + 2v_2 (tv'' + 1) \right] \right\} +$$
$$+ e^{-tv_2''} \left[2(v_{1h}^2 + v_2^2 - 2v_2 v_{1h}) + 4(tv_2'' + 1) v_1 s (v_{1h} - v_2) + \right.$$
$$\left. + 2v_1^2 s^2 (tv_2''^2 + 2tv_2'' + 2) \right] \Big]_L^r \qquad 5.$$

Designations:

c /$m^{1/2}s^{-1}$/	The Chézy velocity factor
k	Ratio of entrache to exit water velocity within the reach
$s = \frac{1-k}{\omega l_2}$	Auxiliary value for calculations

$t_v'' = \omega / l_2' + l_2'' /$ — Auxiliary value for calculations

$t_{v2}'' = \omega l_{2v}''$ — Auxiliary value for calculations

l_{2v}'' /m/ — The length of the backwater reach along the stretch l_2'' up to section examined

V_{lh} /ms^{-1}/ — Mean velocity of water in the cross-section examined:

$$V_{lh} = k V_1 + \frac{1-k}{l_2} V_1 (L - x)$$

In order to solve Equ. /5/, one has to know the value of ice velocity. The paper presented to the Symposium in 1974 of IAHR-PIANC has dealt with ice motion within backwater reaches of low head barrages, in the case of linear change of water velocity. On the basis of the results given in that paper /Fig.3./ the valocity of ice can be determined.

Neither Equ. /5/, nor the pressure distributions as shown in Fig. 3. include the effects of cohesion along the banksides and those of the wind, since now primary interest is given to the distribution of pressure and not to its actual value.

One can see from Fig. 3., that the maximum value of pressure arises in the surroundings of grade-breaks. From here to the barrage the pressure decreases first intensively and then moderately.

According to what has been said in Chapter 1, the following relationship is valid for the thrust, in any section:

$$\frac{F(x, v_2)_{min}}{\omega} \leq \rho \leq \frac{F(x, v_2)_{max}}{\omega} \; ; \; if \; x \geq \frac{3}{\omega}$$

According to the model assumed the function F /x, v_2/ is constant along stretch l_1, and at the same time, maximum for the whole stretch L.

As a consequence, the value of pressure is maximum at l_1, whenever the length of the ice sheet above the backwater reach: $l_1 \geq \frac{3}{\omega}$.

Besides the causes known till know, the pressure distributions as shown in Fig. 3., give additional explanation for the forming of blocks of ice in the sorroundings of the upper end of backwater reaches. The ice-floes arriving from the upper reach of the river first form an ice sheet of loose construction within the backwater reach. As soon as the upper end of the ice sheet reaches the limit of dammed water, the ice sheet will be subject to growing pressure. The causes of slippings can be identified as the condensation of ice sheet under increasing pressure as well

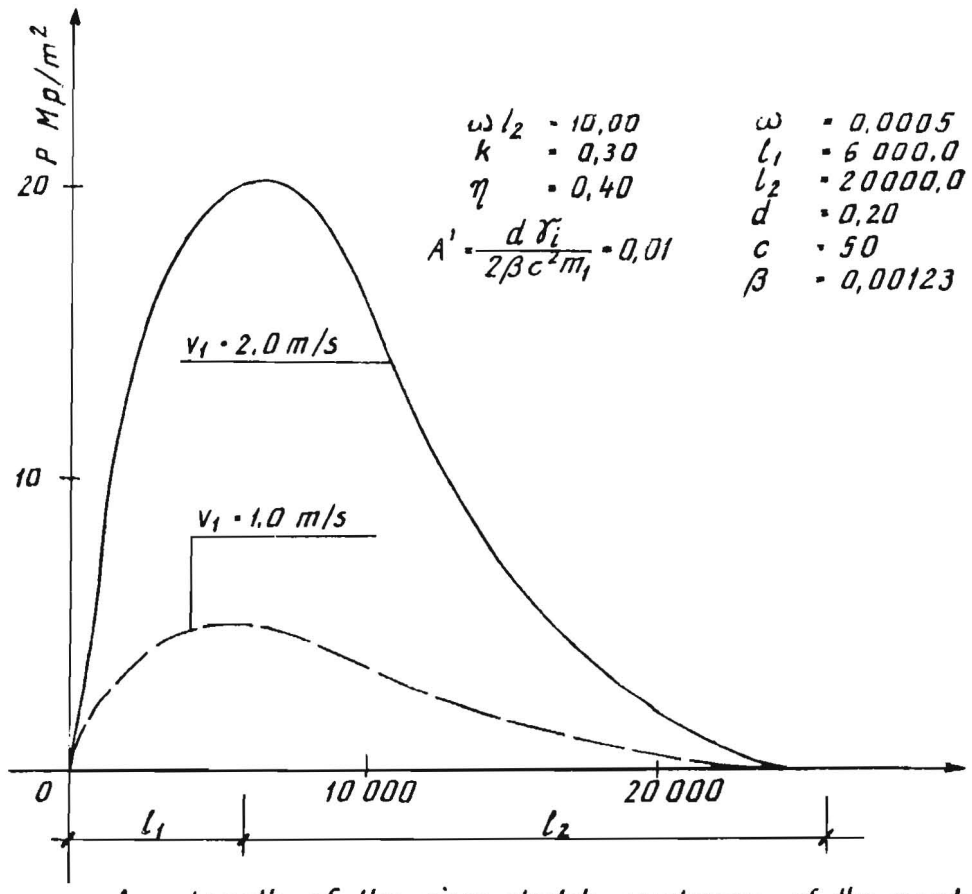

l_1 - Length of the river stretch upstream of the reach
l_2 - Length of the reach

Fig. 3. Distribution of pressure in the reach of low-head barrages

as its insufficient leaning onto the banksides. The power resulting of thrust diminuition has to be supported by the banksides. Is the force of reaction insufficient, the ice sheet collapses, becomes thicker till an equilibrium state is achieved.

In the case of shorter backwater reaches connected with river

stretches of relatively higher grade, the danger of forming blocks of ice is even higher, than it the case of longer backwater reaches. Namely, the change of pressure is more intensive in the case of shorter reaches. A redaction of the maximum of thrust must be achieved by means of riverbed regulation, as a consequence of which the change of thrust will decrease, too.

References

1. Beccat, R. - Michel, B.: Thrust exerted on a retaining structure by unconsolidated ice cover. Proc.VIII.Congress of IAHR, Vol.III.11.Si. Montreal 1959.

2. Pariset, E. - Hausser, R.: Formation and evolution of ice covers on rivers.Transaction of ice. Engineering of Canada.Vol.5 No.1. 1969.

3. Pariset, E. - Hausser, R. - Cagnon, A.: Formation of ice covers and ice jams in rivers.Proc.of ASCE. Journal of Hydraulic Division. Nov. 1966, Hy 6.

4. Starosolszky,Ö.: Ice in Hydraulic Construction Work. VITUKI. Studies and Research Schievements. 1969.

5. Zsilák, E.: A few problems of ice motion which covers a major part of the water surface, termed saturated motion. IAHR-PIANC. Symposium River and Ice. Subject A. Budapest 1974.

6. Zsilák, E.: Some theoretical problems of the motion of ice, covering a major part of water surface. Vizügyi Közlemények. 1974/1. Budapest.

THIRD INTERNATIONAL SYMPOSIUM ON
ICE PROBLEMS
Hanover, New Hampshire, USA

BREAK-UP OF A SOLID RIVER ICE COVER

B. Michel, Dr-Eng., Professor of Ice Mechanics, Université Laval, Canada
R. Abdelnour, M.Sc. Eng., Arctec Canada Ltd, Canada

SUMMARY

This paper gives the results of an experimental study made in a laboratory flume to determine the stability of a river ice cover. This cover was simulated with a wax whose properties were similar to those of ice at an average scale of about 1/25.

The main objective of the study was to determine the hydraulic conditions for which the solid ice would break and be carried along with the flow.

It was found that the phenomenon of failure of the ice cover could be interpreted with a non-dimensional number characterizing the flow velocity and the strength of the ice in function of the relative thickness of the ice. A power law was found to relate these two numbers and the correlation coefficient is acceptable.

These laboratory results may be extrapolated to nature in many cases to compute the river discharge and water levels necessary to destroy an ice cover of variable resistance.

1. INTRODUCTION

Until now, research on stability of ice covers has been made only on broken-up ice accumulations with no or very little cohesive strength. Two cases have been clearly distinguished: the formation and the break-up of the ice cover. During the formation of the ice cover, there is an accumulation of ice pieces in front of a cover which freeze together behind the edge. The hydrodynamic stability of these pieces is given in function of a Froude number by many authors [1-6]. At break-up, the laws of stability of ice covers are quite different. Large volumes of ice pieces accumulate in front of solid ice reaches and the only case which has been studied is that of the stability of such a long accumulation under the hydrodynamic thrust [7].

This latter case has often been considered to be typical of break-up conditions. But it is quite possible that an early flood might occur when the ice cover is still very strong. It is then necessary that the tangential stresses caused by the flow be high enough to destroy the cover and this may lead to the worst flooding conditions. This is the case we have simulated in a laboratory flume.

2. THE EXPERIMENTAL SET-UP

The tests have been carried out [8] in a flume 6 ft wide, 46 ft long and 12 inches high. The bottom roughness was $n = 0.0115$ and the canal was fed from the pumping station of the hydraulics laboratory. At the lower end of the flume an ice retaining structure was built, made of a metallic grid with 1/2 inch square mesh set inside a frame in a way such that the thrust on the grid could be measured.

A model ice wax was used for the tests which simulates to scales of 1/20 to 1/40 the properties of real ice [9]. It has the same density as ice. Its flexural strength was measured with small cantilever beams, ten times for each test. The averages varied from 3.0 to 7.0 psi from one test to the other. The Young's modulus was measured three times for each test and it varied from 4 000 to 25 000 psi. The ratio of the preceding properties varied from 700 to 5 000 and this would cover possible combinations of brittle behavior of real ice. The wax was mixed in a tank and poured on warm water in the flume so it would spread evenly and form a uniform ice cover, 24 ft long. The standard deviation on measured thickness was 5 to 10% in any one test. The roughness of the ice and canal varied between 0.022 and 0.033.

Each test consisted essentially in increasing the discharge until complete failure of the ice cover and its accumulation in front of the retaining structure.

3. RESULTS AND THEIR INTERPRETATION

The condition of failure was defined as that for which the first plates of ice would detach and begin to accumulate in front of the grid. The mechanism of failure varied from one test to the other depending mainly on the number and position of initial fractures in the ice, the state of attachment to the flume walls and the state of submersion of the cover. In all casse, submersion happened before failure and the cover became unstable and started to oscillate in the flow.

Twenty five tests were carried out and the basic results are given in TABLE 1.

A dimensional analysis was made of the parameters affecting this phenomenon and the following numbers came out:

$$f\left(\frac{V}{\sqrt{\sigma/\rho}}, \frac{h}{B}, \frac{h}{y}, \frac{\sigma}{E}\right) = 0 \qquad (1)$$

where:

- V - velocity underneath the cover
- σ, E - flexural strength and elastic modulus of the ice
- h, y, B - thickness of ice, depth of water and flume width
- ρ, ρ' - density of water and ice

Regression analysis were made on all these factors and it was found that the highest correlation coefficient was obtained with only the first two numbers. The first number had however to be corrected for a velocity at the origin:

$$M = \frac{V - Vo}{\sqrt{\sigma/\rho}} \qquad (2)$$

It was found that Vo could well be represented with a simplified law of stability of single ice blocks [1]:

$$Vo = \sqrt{\frac{2g\,(\rho-\rho')\,h}{\rho}} \qquad (3)$$

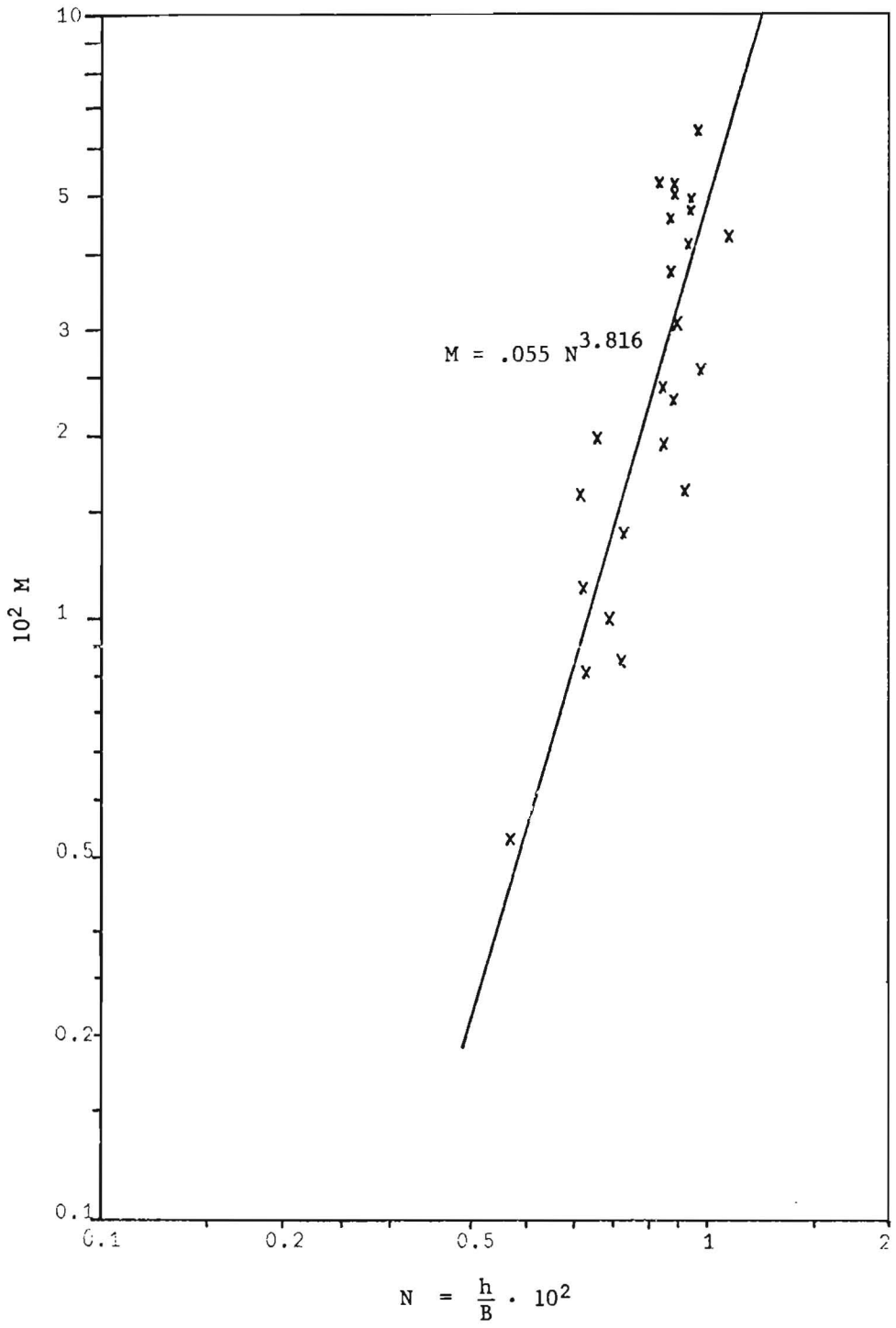

Fig. 1.

The final regression gave a best fit with the power law:

$$M = .055\left(\frac{h}{B}\right)^{3.816} \qquad (4)$$

where B is counted in hundred units of h. The correlation coefficient for this law is r = 0.79 and the standard deviation on h/B is 0.128. The regression line is shown with the experimental data on Figure 1.

4. DISCUSSION AND CONCLUSION

The proposed relationship shows that the velocity required to destroy a solid ice cover varies very quickly with the ice thickness, as should be expected, the power exponent to h being 3.816. For a zero ice thickness the velocity also reduces to zero.

The velocity does not vary as quickly with the ice strength as shown by dimensional analysis. It is however interesting to see that for $\sigma = 0$ the critical velocity is given by relation [3] corresponding to that of a thin unconsolidated ice cover.

Finally, it has not been possible in these tests to determine clearly the role of the water depth, the canal width and the Young's modulus. The depth did not appear as such, probably because we were measuring the velocity underneath the cover and this is related directly to the hydrodynamic forces. Because we had only one canal width it was not possible either to study the influence of this parameter. It is thought however that there must be a limiting width in equation [4] that may be related to a number of times the characteristic length of the ice cover. Otherwise, for a very large river M would reduce to zero corresponding to the case of an unconsolidated ice cover.

We believe that the knowledge of a law expressing the stability of a solid ice cover may be useful in many cases related to power production, navigation and flood control. In particular it would give the highest discharge that may be passed safely underneath a cover of given state without breaking it up.

REFERENCES

(1) MICHEL, B. (1957). Note sur les vitesses d'entraînement des corps flottants. La Salle Hydraulic Laboratory, Report NC108, La Salle, Montréal.

(2) KIVISILD, H. (1959). "Hanging Ice Dams" IAHR, 8th Congress, 2, Paper 23-F-1/30, Montreal.

(3) PARISET, E. & HAUSSER, R. (1961). Formation and Evolution of Ice Covers in Rivers". Trans. Eng. Institute of Canada, Vol. 5, no. 1, p. 40-49.

(4) MICHEL, B. (1965). Criterion for the Hydrodynamic Stability of the Frontal Edge of an Ice Cover. Proc. IAHR, 11th Congress, 5, p. 1-11, Leningrad.

(5) UZUNER, M.S. & KENNEDY, J.F. (1972). Stability of Floating Ice Blocks. Journal of the Hydraulics Division, ASCE, Vol. 93, No. HY12, Proc. Paper 9418, pp. 2117-2133.

(6) ASHTON, G.D. (1974). Entrainment of Ice Blocks, Secondary Influences. IAHR, Proc. Symposium on River and Ice, A-11, Budapest.

(7) MICHEL, B. (1965). Static Equilibrium of an Ice Jam at Break-up. AIRH, 11th Congress, Proc. Vol. 5, p. 71-76, Leningrad.

(8) ABDELNOUR, R. (1975). Caractéristique de la débâcle hâtive d'un couvert de glace encore résistant. Thèse M.Sc.A. en préparation, Dépt. Génie Civil, Université Laval.

(9) MICHEL, B. (1969). Nouvelle technique de simulation totale de la glace flottante. L'Ingénieur 248, pp. 16-20.

TESTS RESULTS								
	BASIC PARAMETERS				FAILURE OF COVER			
Test	Mean ice thickness	Flexural strength	Elastic modulus	Global roughness Manning's	Water depth under cover	Velocity under cover	$M.10^2$	$\frac{h}{B}.10^3$
Number	inch	psi	psi	n	ft	ft/sec	—	—
1	0.445	6.66	5194	0.026	0.156	0.79	1.62	6.18
2	0.473	7.44	6367	0.024	0.161	0.92	2.00	6.57
3	0.448	7.87	13607	0.028	0.189	0.71	1.12	6.22
4	0.670	6.62	19478	0.024	0.190	1.46	4.20	9.30
5	0.522	5.04	12231	0.029	0.166	0.74	1.39	7.25
6	0.452	5.77	12716	0.027	0.195	0.61	0.82	6.28
7	0.517	6.51	14154	0.022	0.186	0.66	0.86	7.18
8	0.492	4.48	7302	0.024	0.192	0.63	1.00	6.83
9	0.647	3.53	7481	0.030	0.198	1.01	3.04	8.98
10	0.342	6.73	16256	0.020	0.173	0.48	0.43	4.75
11	0.362	5.70	8773	0.032	0.188	0.56	0.83	5.03
12	0.362	5.61	5641	0.030	0.177	0.57	0.88	5.03
13	0.332	5.86	4101	0.026	0.179	0.56	0.86	4.62
14	0.668	2.99	15789		0.200	0.70	1.14	9.28
15	0.626	4.77	13750	0.025	0.183	0.95	2.28	8.70
16	0.613	5.28	15770	0.029	0.261	0.99	2.42	8.52
17	0.656	4.68	14760	0.028	0.211	0.83	1.61	9.12
18	0.606	5.31	13020	0.030	0.187	0.90	1.95	8.42
19	0.700	4.24	21113	0.028	0.194	1.00	2.59	9.72
20	0.770	5.15	20595	0.025	0.193	1.41	4.30	10.70
21	0.666	4.95	20324	0.027	0.248	1.46	4.79	9.75
22	0.691	5.30	17317	0.033	0.265	1.83	6.46	9.60
23	0.667	6.56	24955	0.028	0.230	1.64	4.95	9.27
24	0.627	6.77	20535	0.027	0.243	1.65	5.04	8.72
25	0.619	6.41	21761	0.029	0.227	1.34	3.80	8.60

TABLE 1

THIRD INTERNATIONAL SYMPOSIUM ON
ICE PROBLEMS
Hanover, New Hampshire, USA

PRELIMINARY OBSERVATIONS OF SPRING ICE JAMS IN ALBERTA

Robert Gerard
Research Officer

Highway and River
Engineering Division,
Alberta Research Council

Edmonton,
Alberta,
Canada

Synopsis

A programme of ice jam observations in selected reaches of rivers in Alberta is described. In the first year of operation of this programme four ice jams were observed in various parts of the province, three of which could be called major. The salient features and effects of these jams are described and summarised, and information is provided on the antecedent meteorological conditions and geomorphic characteristics of the jam sites.

The four jams illustrate the ability of ice jams to cause severe perturbations in the natural regime both upstream and downstream of the jam site. After their formation water levels much higher than are reached by summer floods can be generated and, on failure, these high water levels may be propagated downstream accompanied by very high velocities and, possibly, significant scour.

Introduction

Ice jams are one of the most striking of natural phenomena in a northern river environment. Unfortunately they also cause floods, high ice levels, fast velocities and an unknown amount of scour. Despite this capacity for catastrophe they have rarely been systematically studied in North America and are poorly understood. They therefore remain largely an unknown in the design of bridges, pipeline crossings and flood protection.

The problem in Alberta, past and present, is exemplified by the following extracts:

> *"... The winter of 1874-75 was a bitter one, with deep snow and never a thaw until April. On the 2nd or 3rd of that month, however, a further heavy fall of snow was followed by a sudden rise in temperature. The change of weather and weight of melting snow caused the ice for the 85 mile stretch of rapids above the fort [Fort McMurray] to break-up, and it came down the Athabasca with terrific force. On striking the turn in the stream at the post it blocked the river and drove the ice 2 miles up the Clearwater in piles 40 or 50 feet high. In less than an hour the water rose 57 feet, flooding the whole flat and mowing down trees, some 3 ft diameter, like grass ..."* (1); or, more recently:
>
> *"... an unusual feature about the [bridge] design is the extreme ice force that the piers have to resist, amounting to 1,600,000 lbs on each pier at the level of ice jams, which occur 60 ft above streambed ..."* (2).

Less apparent features of ice jams are their ability to cause very high floe velocities when they fail, and to scour the stream bed either after the jam fails or during the formation of a hanging dam.

The prime motivation for the present ice jam investigation in Alberta is the need for knowledge of ice levels for bridge design. Also of interest is the effect of jam-induced water levels on stage-frequency distributions and the scour caused by ice jams. To provide this information a programme of ice jam documentation and observation was instigated in 1974. The documentation includes the compilation of ice jam history in Alberta from newspapers, diaries, archives, hydrometric records and resident interviews. The objective of the observations is to develop an increased understanding of the causes, mechanics and consequences of ice jams and to build up a statistical record of the severity of break-up and the occurrence of ice jams in the chosen reaches. The methods and initial results of this second part of the programme form the subject of this paper.

Break-up in Alberta rivers

As shown in Figure 1(3) the dominant drainage direction of the major rivers is to the east and north. In southern Alberta break-up, on the average, progresses upstream. The contrary is true in the north. Although there is little doubt that the worst ice jam problems occur in rivers flowing 'with' the break-up progression, the fact that rivers flow against this progression is no guarantee that they will be free of break-up jams.

The locations of the ice jams detected in 1974 and discussed in this paper are shown in Figure 1. Of five areas monitored, ice jams were found in four of them. Three of these jams could be called major.

Observation programme

The reaches selected for observation offer one or more of the following features: a typical reach of which the character of the ice run is of interest (e.g. channel pattern, size); 'frequent' ice jams have been reported; historical records for a significant period of time; frequent ice jams can be expected; access, at least by river, after break-up; nearby hydrometric gauge; and a bridge.

To serve the main purpose of the ice jam observations the major requirement is to document the cause, location, length, maximum water level and mode of failure of the ice jams. Other information collected in the field or from other sources is indicated in the ice jam summaries given with the figures.

The primary means of surveillance is by fixed-wing aircraft and begins after break-up has begun on the chosen reach. When located photographs are taken of the complete jam, with closer photographs of the head and toe, and of the water level against each bank or island at selected locations along the jam. Time permitting, an attempt is then made to obtain ground access to the jam to carry out similar documentation from this vantage, including observation of floe entrainment at the jam head, evidence of buckling in the jam and water levels along the jam. When this is complete, or if it is not feasible, the aerial reconnaissance is repeated after an appropriate interval of time. Alternatively, if access is good, observations may be continued from the ground. The process is continued until the reach is clear of ice. Finally, the ice debris along the reach is sampled for ice type, thickness and strength. As soon as possible after the ice moves from the river a survey at the jam site should be carried out. This would include surveys of the thalweg, cross sections, water surface slope, bed material, high water marks and water levels recorded in the photographs taken from the air. In the office records from the gauging station, if one exists, should be procured, as should those of antecedent meteorological conditions near the jam location and in the catchment. An effort should also be made to note any independent observations or photographs of the break-up or ice jam by other persons who may have witnessed the event (farmers, residents, reporters).

Needless to say the above is a more or less ideal set of observations for our available facilities. They are rarely all carried out because of time constraints. However, as stated before, the major objective of the observations is to document the jam location, length, maximum water level and mode of failure. This information is provided by the aerial or ground reconnaissance, an analysis of the hydrometric gauge record, and later surveys of, or estimates from, the photographically recorded water levels or high water marks.

Ice jam classification

There are few systematic attempts at this reported in the literature. The only universally accepted classification seems to be that of

winter or spring ice jams. Despite their obvious individuality, ice jams in various locations can have features in common and it would seem advantageous to have such a classification. The jam classification used in the ice jam summaries given below considers the following features:

(i) Initiation of the jam : free or forced. The term free denotes a jam formed by the accidental jamming or locking of ice floes on the river surface. Forced denotes ice floes forcibly halted by some obstruction. This latter group could be subdivided on the basis of the obstruction - for example, geomorphic features (shoals, sharp bends), ice cover, hanging dam, ice bridge, structures, etc.

(ii) Jam extent - vertical : surface, thickened or dry. The first term refers to a jam of ice floes which remain on the surface, with no floe entrainment or buckling of the jam. The last term applies when the channel has been more or less blocked completely by jam buckling or floe entrainment. Thickened refers to situations between these extremes. This feature of a jam has a strong influence on the behaviour of the water level and indicates whether scour under the jam is a possibility.

- Horizontal : partial or complete cover. This refers to whether the channel surface and/or flow is partially or completely blocked by the jam. It is particularly pertinent in reaches with islands or multiple channels and will have significant effect on scour and water level behaviour.

(iii) Failure mode : complete or partial failure. This denotes whether the jam fails instantaneously across its whole width or whether just a portion of the channel is cleared. The latter condition indicates that severe scour and high velocities may have occurred just after failure because of the large hydraulic head and constricted channel. High velocities can also be associated with complete failure.

(iv) Jam importance : Two groups are suggested for this - major or minor - based on the maximum stage achieved by the water level behind the jam, using the 2-year summer flood level or bankfull, whichever is less, as that dividing the two groups.

Ice jam observations, 1974

Details of the four ice jams observed are given in Figures 2 - 25 and in the summaries accompanying the figures. The details listed under 'Stream' in these summaries were obtained from (4).

Winter 1973/74 was characterised by above normal snowfall over most of the Province and reasonably normal spring temperatures. At all observed locations break-up occurred close to the average date.

South Saskatchewan River upstream of Sandy Point. The jam at this site was apparently a surface jam of minor proportions (Figures 2 - 8) and probably formed under gentle circumstances as 3 km downstream the ice cover was intact. It is debateable whether the side floes at the toe had moved at all, or whether the jam was 'forced' by the floes grounding on the bar in the widened section or accidentally locked in place. However no matter how they form such jams are well defined and should be a source of valuable information on the hydraulic roughness

of fragmented ice covers. They also illustrate the fact that large water level increases upstream can be generated by jams merely by the large roughness of the ice conglomeration, without the drama of thickening or hanging dams. The surge generated by the failure of this jam was the cause of noticeably high floe velocities at the bridge 12 km downstream.

Peace River at Peace River. The details given in the summary are for the second of three jams which were observed to form in the 26 km reach downstream of Peace River. The last of these was probably the largest, being some 10 km long and causing about a 4 m rise in local water level. The first jam was approximately 3 km long, with the toe 5 km downstream of the town. This latter location coincides with the end of the reach of ice artificially weakened prior to break-up in an attempt to reduce the intensity of the expected ice jams. Considerable effort was also expended by the authorities in blasting the first two jams immediately after their formation.

The second jam was against the solid ice cover between the island shown in Figure 10 and the right bank, with a strong flow moving out from under the jam around the left side of the island. Previous river surveys show a gravel bar across this line of flow. The first movement in the jam was of ice moving with this flow. This allowed the remaining ice to move and gain enough momentum to begin a crushing front moving downstream on the right of the island as shown in Figure 14. This front eventually caused the ice sheet to fail and release the jam. It is nearly impossible for summer floods to cause the water level increases generated by this jam.

Athabasca River at Fort McMurray. Unfortunately break-up at this location was missed and the formation of the ice jam was not observed. However reports were that break-up had been unspectacular. At 0800 on April 21 the concentration of broken ice from the 150 km reach of rapids upstream of the town moving towards the jam was quite high. It is possible that the jam was caused by the combination of such high ice concentrations and the shallow channels between the islands downstream. At the bridge the broken ice was packed along the sides of the stream with well-developed shear lines. This packed ice and its level suggested the water had been at least 2 metres higher and that the jam may have extended back beyond this location.

Athabasca River ice had pushed back a few kilometres up the Clearwater River, which is a substantial tributary. Remnants of the jam, shown in Figures 17 and 21, were holding the initial ice cover in on this river and blocking the confluence (Figure 22). This was the cause of flooding on the outskirts of Fort McMurray. Despite the partial failure of the jam on the Athabasca River this obstruction continued to block the Clearwater for several days, as shown by the water levels at Draper (Figure 20). These, and the levels on the Athabasca, are again much higher than those normally caused by summer floods.

The first flight over the jam site was taken only a relatively short time after the surge released by the partial jam failure had crested at the hydrometric gauge downstream of the jam site. The failure had concentrated the total release into a small side channel

near the left bank (Figures 17 and 21). One result was the formation over a half kilometre reach of the large, approximately 3 metre high, standing waves shown in Figure 23. An hour later these waves were gone. Based on crude estimates of the wave length taken from the photographs, and the literature on standing waves, the associated velocity was estimated to be between 4 and 7 m/s. If correct, this is an extremely high velocity for such a large sand bed river. The accompanying sand wave was estimated to be 2 m high and the depth of flow, given that the flow must presumably be beyond critical to form standing waves, to be from 2 to 4 metres.

The amount of general scour caused in this channel by the high velocities and concentrated flow could not be determined at the time but would have been of much interest. There would seem to be considerable potential for such scour, while that for local scour around an obstacle such as a bridge pier, given its quicker response to velocity changes, may be even more considerable. The whole question of ice jam (dam) failure, and the resultant velocities and scour, requires more work than has been done to date. Indeed downstream effects of such failures seem to have been largely ignored in favour of investigations of ice jam formation and its upstream effects.

Christina River (see Figure 16). The situation observed on this river is evidence that small rivers are not exempt from large ice jams. Unfortunately its difficult location prevented adequate documentation but sufficient can be seen in Figure 25, which shows water and ice extending well back into the trees, to appreciate that the increase in water level was considerable.

Conclusion

A programme of break-up ice jam observations has been described and the results of the first year of operation (1974) reported. These demonstrate that simple and relatively inexpensive aerial reconnaissance of selected reaches can provide valuable information on the formation, character and consequences of ice jams. The more dramatic of the four ice jams described provide examples of their ability to cause extremely high flood levels and high velocities, and an indication of their capacity for scour. The latter two features are examples of the downstream effects of ice jam failure - an important, but in this context, largely unexplored subject.

Acknowledgements

Thanks are due to Dr. S. Beltaos of this Division for the field observations of break-up on the Peace River. The scope of his observations at that location was extended considerably by the hospitality of B. C. Hydro personnel, particularly Mr. F. Sampson, who were using a helicopter to monitor break-up in the area.

This work was carried out as part of continuing research in river engineering under the auspices of the Alberta Cooperative Research Programme in Highway and River Engineering. The support of this programme by Alberta Transportation, Alberta Environment and the University of Alberta is gratefully acknowledged.

References

1. Moberly, H. J. and Cameron, W. B., 1929. "When fur was King", J. M. Dent and Sons Ltd.; Toronto, p. 151. This extract was brought to the writer's attention by Dr. T. Blench.

2. Sanden, E. J. (Chief Bridge Engineer, Alberta Transportation), 1974. Remarks made at the opening of the Fort Vermilion Bridge over the Peace River.

3. Anonymous, 1974. 'Ice thickness and break-up data for selected rivers in Alberta', Calgary Branch, Water Survey of Canada, Inland Waters Directorate, Environment Canada.

4. Kellerhals, R., Neill, C. R. and Bray, D. I., 1972. "Hydraulic and geomorphic characteristics of rivers in Alberta", River Engineering and Surface Hydrology Report 72-1, Alberta Research Council, Edmonton, Alberta; 54 p.

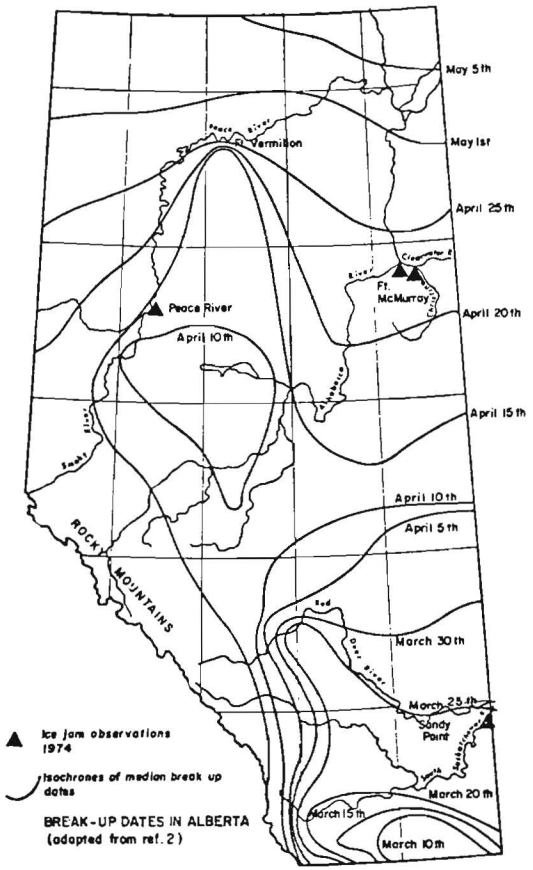

Figure 1. Break-up dates in Alberta

ICE JAM SUMMARY

Stream

Stream name: *South Saskatchewan River* Location: *12 km upstream Hwy. 41 at Sandy Point*
2-yr discharge (m^3/s): *1,060* Surface width (m): *235* Average depth (m): *3.5* Slope: *0.00036*
Sinuosity: *1.01* Bed material: *Sand with some gravel*
Reach description: *Entrenched single channel.* Geodetic elev. WSC gauge zero: *583.10 m.*
Gauge reading at zero flow: *0.61 m.*

Meteorology

°C-days to break-up at site: *48* from *27 March 74* Snowfall (m) at site: *1.3* *(av. 1.0)*
in catchment: - from - in catchment: *3.5* *(av. 1.9)*

Ice

Thickness (m) average: *0.5* Strength (KPa): *220* Type: *0.2 m clear ice, remainder snow ice.*
maximum: *0.7*
Freeze-up date: *n.a.* Discharge (m^3/s): *n.a.* Gauge reading (m): *n.a.*
Break-up date: *~ 11 April 74* Discharge (m^3/s): *200* Gauge reading (m): *3.5*
Break-up description: *Water level had risen ~ 1 m gradually from early March (Q ~ 80 m^3/s). Break-up upstream of jam site seems to have been precipitated by an ice jam failure upstream of Medicine Hat.*

Ice Jam

Jam classification: *Free, surface, complete, complete, major.*
Date of jam failure: *14 April 74* Time: *~ 1800 hrs* Discharge (natural) (m^3/s): *~ 250*
Jam length: *6 km* Height: *~ 2.1 m (surge measured at 1.7 m, 12 km D/S).*
Return period of summer flood of equal maximum stage: *> 3 yr.*

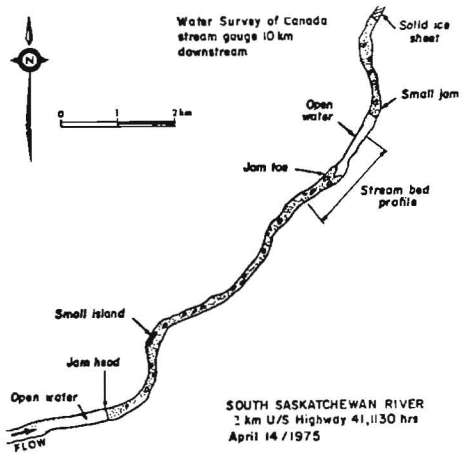

Figure 2. Plan of ice jam location, South Saskatchewan River

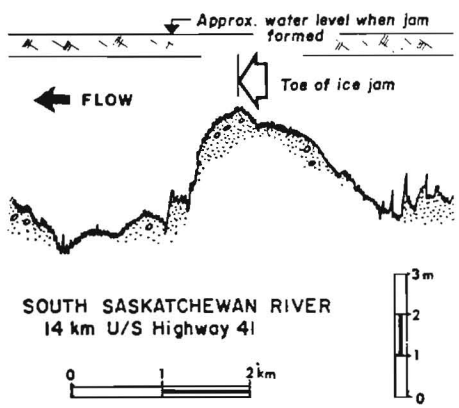

Figure 3. Stream bed profile across jam site, South Saskatchewan River

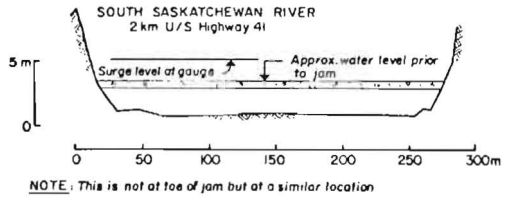

Figure 4. Cross-section at site similar to jam site, South Saskatchewan River

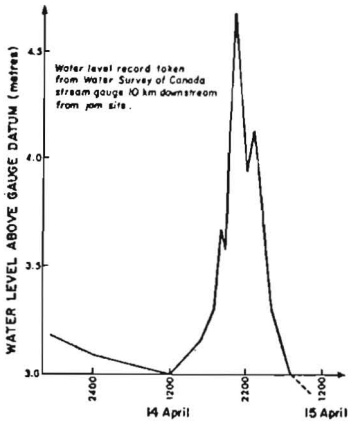

Figure 5. Hydrograph of flood wave caused by jam failure, South Saskatchewan River

Figure 6. South Saskatchewan River ice jam looking downstream, 1200, 14 April 1974

Figure 7. Toe of South Saskatchewan River ice jam looking downstream, 1200, 14 April 1974

Figure 8. South Saskatchewan River ice jam site looking upstream, 15 April 1974

ICE JAM SUMMARY

Stream

Stream name: *Peace River* Location: *10 km downstream of Peace River town.*

2-yr discharge (m^3/s): *8,900* Surface width (m): *570* Average depth (m): *5.7* Slope: *0.00035*

Sinuosity: *1.1* Bed material: *Gravel*

Reach description: *Irregular meanders with occasional islands and mid-channel bars. Entrenched and partly confined.*

Geodetic elev. WSC gauge zero: *304.96 m.* Gauge reading zero flow: *5.18 m.*

Meteorology

°C-days to break-up at site: *48* from *6 April 74* Snowfall (m) at site: *2.4 (av. 1.5)*

in catchment: - - in catchment:

Ice

Thickness (m) average: *0.8* Strength (KPa): *1,100* Type: *Mainly clear ice.*

maximum: *1.2*

Freeze-up date: *n.a.* Discharge (m^3/s): *n.a.* Gauge reading (m): *n.a.*

Break-up date: *19 April 74* Discharge (m^3/s): *2,000* Gauge reading (m): *9.6*

Break-up description: *Water level had risen gradually by 0.8 m since the beginning of April (when Q ~ 850 m^3/s). Break-up was initiated by that on Smoky River which in turn was associated with an ice jam failure several km upstream. Ice on the Peace River upstream of Smoky confluence stayed in until 22 April when the break-up front from upstream reached that location.*

Ice Jam

Jam classification: *Forced (ice cover, gravel bar), thickened, partial, complete, major.*

Date of jam failure: *20 April 74* Time: *~ 1600 hrs* Discharge (natural) (m^3/s): *~ 2,000*

Jam length: *4.8 km.* Height: *~ 5 m.*

Return period of summer flood of equal maximum stage: *> 100 yr.*

Remarks: *This was the second of three jams which formed in the 25 km reach downstream of Peace River.*

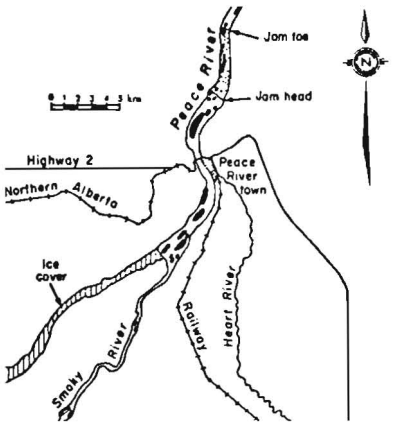

Figure 9. Location of Peace River ice jam

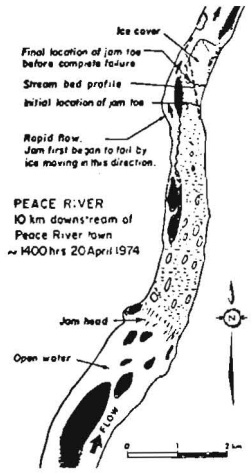

Figure 10. Plan of ice jam, Peace River

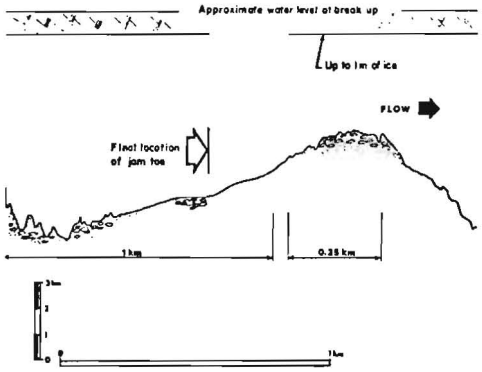

Figure 11. Stream bed profile across ice jam site, Peace River

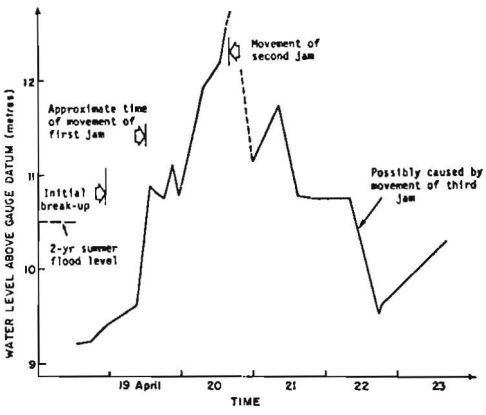

Figure 12. Water level fluctuations at Peace River town

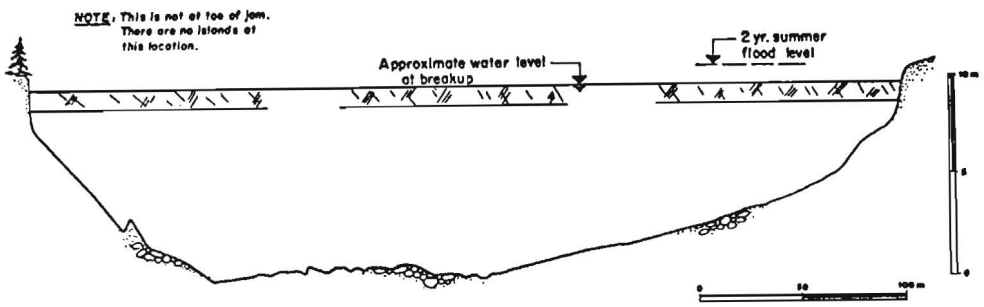

Figure 13. Cross-section of Peace River near jammed reach

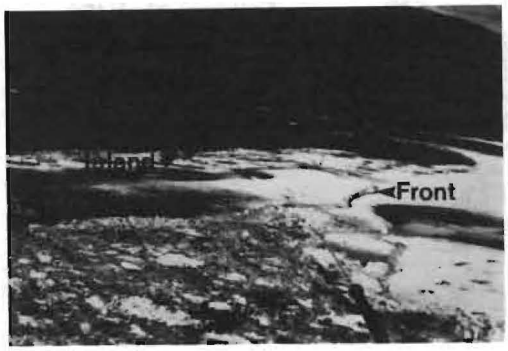

Figure 14. Toe of ice jam on Peace River, looking downstream ∿ 1230, 20 April 1974

Figure 15. Looking upstream from near toe of Peace River ice jam ∿ 1240, 20 April 1974

ICE JAM SUMMARY

Stream

Stream name: *Athabasca River* Location: *at Clearwater River confluence.*
2-yr discharge (m^3/s): *2,200* Surface width (m): *540* Average depth (m): *3.1* Slope: *0.00014*
Sinuosity: *1* Bed material: *Shallow fine sand with local gravel.*
Reach description: *Straight with islands and mid-channel bars. Entrenched.* Geodetic elev. WSC gauge zero: *235.97 m.*
Gauge reading at zero flow: --

Meteorology

°C-days to break-up at site: *74* from *7 April 74* Snowfall (m) at site: *2.2 (av. 1.4)*
in catchment: - from - in catchment: *2.6 (av. 1.8)*

Ice

Thickness (m) average: *0.8* Strength (KPa): - Type: *Approx. 0.4 clear ice; remainder snow ice.*
maximum: *0.9*
Freeze-up date: *6 November 73* Discharge (m^3/s): *∿650* Gauge reading (m): *3.5*
Break-up date: *20 April 74* Discharge (m^3/s): *1,680* Gauge reading (m): *4.6*
Break-up description: *Normal break-up triggered by ∿ 3 m rise from 23 March (when Q ∿ 180 m^3/s). Ice from upstream is well broken up when passing over 80 mile reach of rapids upstream.*

Ice Jam

Jam classification: *Forced (sand bars), thickened/dry, complete, partial, major.*
Date of jam failure: *21 April 74* Time: *∿ 1100 hrs* Discharge (natural) (m^3/s): *∿ 2,200*
Jam length: *Difficult to determine ∿ 5 km.* Height: *4.1 m.*
Return period of summer flood of equal maximum stage: *> 100 yr.*
Remarks: *(i) At upstream end of this reach (near Horse River) there is a sudden change in slope from 0.00095.*
(ii) After partial failure the jammed ice continued to block the Clearwater River until 23 April.

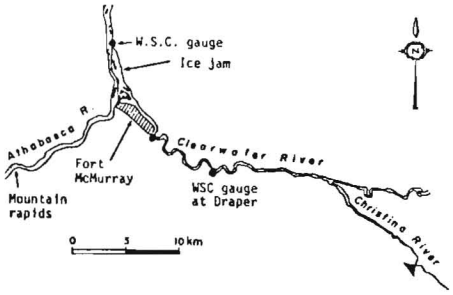

Figure 16. Location of Athabasca and Christina River ice jams

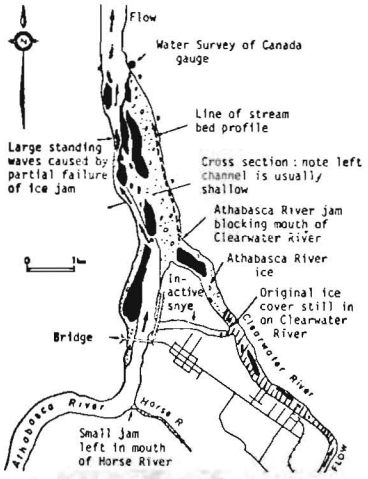

Figure 17. Plan of ice jam, Athabasca River

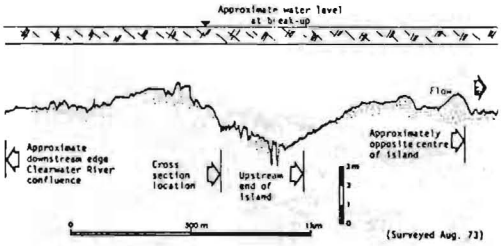

Figure 18. Stream bed profile across ice jam site, Athabasca River

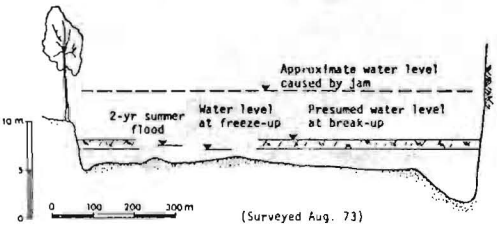

Figure 19. Cross-section across jam site, Athabasca River

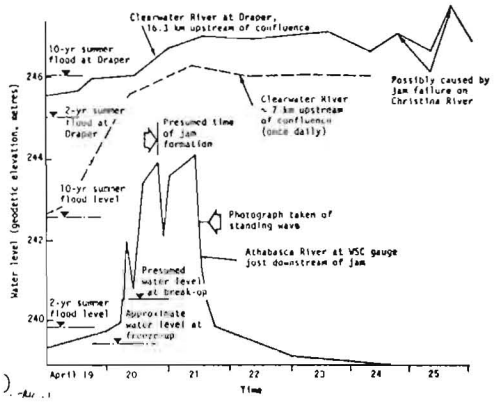

Figure 20. Water level fluctuations downstream of Athabasca River ice jam and upstream on Clearwater River

Figure 21. Ice jam on Athabasca River below Fort McMurray ~ 0930, 22 April 1974

Figure 22. Looking downstream along Clearwater River to Athabasca River ice jam. Note outskirts of Ft. McMurray and flooding, ∿ 0930, 22 April 1974

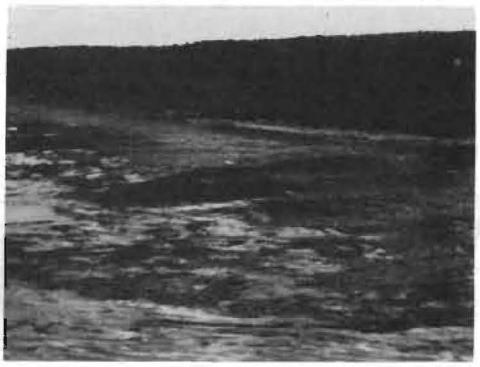

Figure 23. Large standing waves generated on Athabasca River after partial failure of ice jam ∿ 1215, 21 April 1974

ICE JAM SUMMARY

Stream

Stream name: *Christina River*

Location: *12.5 km upstream from mouth.*

2-yr discharge (m^3/s): *∿ 250*

Surface width (m): *∿ 70*

Ice jam

Jam classification: *Forced, unknown, complete, n.a., major.*

Jam length: *5 km.*

Height: *5 - 10 m.*

Figure 24. Ice jam on Christina River, ∿ 0930, 22 April 1974

Figure 25. Toe of ice jam on Christina River. Note large amount of flooding, ∿ 0930, 22 April 74

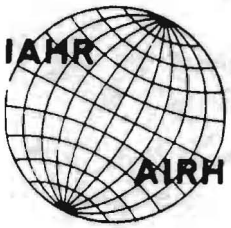

International Association of Hydraulic Research (IAHR)
Committee on Ice Problems
International Symposium on Ice Problems
18-21 August 1975
Hanover, New Hampshire

COMMENTS

Paper Title: Preliminary Observations of Spring Ice Jams

Author: R. Gerard

Your name: Kartha, V. C. Tel. (204) 474-3542

Address: Head, Hydrologic Studies Section,
System Planning Division, Manitoba Hydro,
820 Taylor Avenue, Winnipeg, R3C 2P4, CANADA

Comment:

You have recorded three or four ice jams in rivers of Alberta. Would you please attempt to establish the values of Froude Number at the site of each of the winter ice-jams when they appeared? Further, the same information on the spring ice-jams with estimates of the instantaneous maximum flood volumes at each of these locations would also be desirable.

Response to discussion of paper titled 'Preliminary Observations of Spring Ice Jams in Alberta' by Robert Gerard

Some thought was indeed given to including values of Froude number in the ice jam summaries but the idea was discarded because the estimate that could be derived from the information available (which didn't include velocity observations) would be very rough. In addition the discussion of the method of calculating the Froude number and its justification and limitations would consume more text than was available. Instead sufficient information was included in the summaries and figures to allow the reader to obtain an estimate of Froude number if he so desired.

Presumably the discusser is interested in the Froude number as being the parameter governing floe entrainment, an event which would possibly contribute to the formation of a hanging dam and influence the severity of flow obstruction by the jam. Conditions for such entrainment are probably worst at the instigation of the jam when velocities are largest and flow depths smallest. If so, some indication of the velocity to be used in calculating the Froude number would be given by the average flow velocity calculated from the discharge and area of flow at breakup. It is of course realised that this velocity gives only a lower bound. The more relevant velocity is that at the surface. However what this will be when the ice has begun to move, or when the flow is modified by a surge released by jam failures upstream, is difficult to say.

The velocities used to determine the Froude numbers given below were calculated from the discharge and water level at breakup. The depth used to calculate the ice thickness/depth ratio was the average depth of flow at this water level (i.e. flow area divided by surface width).

Location	Gauge reading for 2-yr flood	Froude number $V/\sqrt{g(1-\rho'/\rho)t}$ *	Ice thickness/ average depth t/H
South Saskatchewan River near Hwy. 41	4.3	0.54	0.19
Peace River at Peace River	10.3	0.90	0.16
Athabasca River at Fort McMurray	4.2	1.17	0.23

* Based on an assumed average value of $\rho'/\rho = 0.89$.

It should be noted that the length scale used in the Froude number is the ice thickness rather than the more usual flow depth. This point was the basis of some general discussion at the Symposium. For very large depths the pertinent length scale is obviously the ice thickness,

and the relevant parameter the 'ice thickness' Froude number. This can be demonstrated theoretically. For smaller depths the effect of this ice thickness Froude number is modified by the thickness/depth ratio and two dimensionless parameters are required to define the instigation of floe entrainment. Hence for large depths only one parameter is required - the ice thickness Froude number - and for moderate to small depths two parameters are required - the thickness Froude number and the thickness/depth ratio. There would seem to be no situation where the entrainment depends on the *flow* Froude number *alone* and its use in this context therefore seems irrelevant and should be discouraged.

International Association of Hydraulic Research (IAHR)
Committee on Ice Problems
International Symposium on Ice Problems
18-21 August 1975
Hanover, New Hampshire

COMMENTS

Paper Title: Preliminary Observations of Spring Ice Jams in Alberta

Author: R Gerard

Your name: Philip Burgi

Address:
U.S. Bureau of Reclamation

Comment: I am encouraged to see field observations as reported in this paper. Dr. Gerard and the Alberta Research Council are to be congradulated on their efforts. This is a difficult task to initiate since the return on project costs may not be realized for many years.

As more field observations are reported, it is evident that standardized field observation terminology and testing procedures should be adopted as soon as possible in the field of Ice Engineering

THIRD INTERNATIONAL SYMPOSIUM ON
ICE PROBLEMS
Hanover, New Hampshire, USA

REGULATION OF THE DEVELOPMENT OF ICE-BARRIERS IN THE REACH OF THE TISZA RIVER ABOVE THE BARRAGE OF TISZALÖK FOR A SECURE WINTER OPERATION OF THE BARRAGE

P. Rozsnyói, civil engineer — National Water Authority, Budapest, Hungary

I. Pados, civil engineer — Regional Water Authority, Miskolc, Hungary

Abstract: The paper deals briefly with ice-conditions of the Hungarian reach of the Tisza River above the barrage of Tiszalök and with the aspects of winter operation of the barrage. The overdeveloped curve above the barrage must be regulated in such a way that besides navigation an artificial stop of ice masses is also possible in order to protect the barrage.

A short characterization of the ice-regime of the Tisza River

The second largest river of Hungary, the Tisza is not a dangerous flow according to specialists when ice-floods are considered.

The cut-through of over developed curves and other regulation activities in the river bed in past decades promoted the smooth passage of ice, decreased the possibility of the development of ice jams, however, the danger of ice floods has not been eliminated completely.

Despite of less probable ice floods, a new situation has been created through two already existing dams and by perspectively

planned river-canalization.

By investigating the factors influencing ice-condition, the following statements can be made:

- climatic conditions are different along the upper and lower reach of the Tisza River. Daily average temperatures are higher in the lower than in the upper reach;
- there is a significant difference in slope-conditions of the upper and the lower reach;
- in winter, primarily small discharges are characteristic. Even early spring floods which help melting do not exceed 50 percent of the standard discharge and stay, in general, in the main river bed;
- river beds and curves became more favourable due to man's influence, primarily to river regulation.

The biggest interference in the life of the river was the construction of the barrage at Tiszalök after general regulation of the river.

Compared to previous situations the stop of ice occurred 3-4 days earlier, the start of ice motion and the disappearance of ice 8-10 days later than earlier in the river reach above the barrage.

Due to climatic and slope conditions early ice development is usually observed in the Tisza and its stay is pretty long. The frequency of drifting above Tiszalök is 100 percent and that of an ice stop between 70 and 91 percent. There is a 50 percent probability that in average, standing ice will exist over 40 days along the discussed reach.

Ice-conditions of the backwater-reach of the river-barrage of Tiszalök

After completion of the dam not only the time of ice stop and of motion has changed compared to the previous situation but the ice development itself has been altered.

Considering an average icy period, usually about 2.5-3 million m³ of ice can be found in the backwater reach.

From a security point of view, the development of a continuous ice cover above the dam must not be hindered with regard to the protection of the sluice-system of the barrage against the mechanical effects of floating ice, and to the decrease of the development of clumpy ice which may cause problems in the turbines of the power-station.

Special care should be paid to the operation of moving parts especially during the winter season. Above the hinged doors an iceless strip of 30-50 cm must be secured and maintained in order to help moving these doors and to prevent deformation due to the influence of frozen ice cover.
Due to security of the dam and the continuity of energy production deicing of the backwater reach should be scheduled according to a certain system.

In the first step the lower reach canal must be deiced. Meanwhile, above the dam and on the side of the power-plant ice should not be broken, in order to prevent motion of drifting ice at the rack before the turbines.

In the second step a 20 m wide corridor should be opened along the streamline, which may be even wider in curves. Special attention should be paid to the timing of the beginning of ice-breaking with consideration to the operation of ice-breakers, to expected serious frosts and to the thickness of ice.

It is an important requirement that the once broken ice should pass through the dam. During the initial stage of ice-breaking ice will move over the doors. Possibly,only one hinged door should be lowered to the proper level because a water column of at least 1.2-1.5 m must be maintained over the door to prevent damages.

A rapid increase of the temperature and in the meantime the beginning of a flood on the upper reach of the river and its tributaries will cause large and extended ice masses to move.

$$tg\ \alpha = \frac{v^2}{R\ g}$$

where, v - the average velocity of the cross-section /m/s/

R - the radius of the curve /m/

g - acceleration due to gravity: 9.81 m/sec^2

α - the angle between the direction of the gravitational force and the resultant of the gravitational force and the centrifugal force affecting the water masses moving in the curve.

Alternative 1. Minimum radius, short through-cut. Demands of navigation are satisfied even in a long-term range; in the same time it offers still a favourable opportunity to hold back ice. It is most favourable from an economic point of view.

Alternative 2. A transition between alternatives 1. and 3. To hold back ice it is less favourable than alternative 1. The longer through-cut is more expensive.

Alternative 3. From a river regulation point of view this alternative is the most favourable because the uncharacteristic reach between river kilometres 542.0 and 543.0 is left out, its tracing and the junctions are adequate. A drawback is that the long through-cut is expensive and it does not satisfy the requirement to hold back ice.

Alternative 1. seems to be best and presumably it is the most economic.

An artificial ice trap

Indices L, R, $\frac{L}{R^2}$ and $tg\ \alpha$ of the selected alternative differ only in a limited way from those of the present situation. Still the stopping of ice in the new, regulated river bed must be helped presumably by a floating, artificial ice trap.

The task of this floating ice trap is to promote the development of an ice arch and if the ice-load on this floating structure becomes too large - similarly to the ice-trap used

in Lake Erie and described by Bryce and Foulds - it submerges and allows the ice to move above it.

When the pressure of ice is calculated which affects the floating structure a static pressure of dynamic origin of the standing ice cover integrated from parts is assumed where self-arching has not yet been developed.

No consideration was given to the dynamic ice pressure originating from temperature changes and consequently from a collision of the standing and drifting ice.

According to an equation recommended by a Soviet standard /the force working on surface F in the direction of the flow/:

$$P = /p_1 + p_2 + p_3 + p_4/F$$

where p_1 - the effect of water friction

p_2 - the hydrodynamic pressure affecting the upper end of the ice cover distributed along the length of the cover

p_3 - the slope-direction component of the weight of ice

p_4 - the friction due to wind.

According to the quoted standard:

$$p_1 = k_1 \cdot v^2 = /5\text{-}20/ \cdot 10^{-4} \cdot v^2$$

/for 5 smooth and 20 rough surfaces/

$$p_2 = k_2 \cdot \frac{h}{L} \cdot v^2 = 5 \cdot 10^{-2} \cdot \frac{h}{L} \cdot v^2$$

$$p_3 = k_3 \cdot h \cdot I = 0.92 \cdot h \cdot I$$

$$p_4 = k_4 \cdot w^2 = 2 \cdot 10^{-6} \cdot w^2$$

where v - the average velocity of water /m/sec/

h - the thickness of ice /m/

I - the slope of the water surface

L - its limit is the triple width of the water flow /m/

w - wind speed with a probability of occurrence of 1 percent

p_1, p_2, p_3, p_4 - /t/m/

According to calculations made for the problem reach specific ice pressure /for 1 m width/ was set to 1 t/fm. This approximated nicely the emperical value obtained earlier at the same place.

The floating trap will be constructed from wooden beams connected elastically to each other and bound to a steel cable stretched between the two banks. Its final shape will be worked out during the starting experiments.

Literature

1. Árvizvédekezési Kézikönyv. Budapest, 1974.
2. Brachtl, J.: Ice control structures on Slovak rivers. International Symposium on River and Ice, A. Budapest, 1974.
3. Csoma, J.: Jégjelenségek a Tiszán, a Sajón és a Hernádon. VMGT. 52.sz. Budapest, 1973.
4. György, J.: Vizügyi létesitmények kézikönyve. Budapest, 1974.
5. Horváth, S.: A folyószabályozás hatása a folyók jégjárására. VMGT. 52.sz. Budapest, 1973.
6. Korzhavin, K.N.: Conditions of the ice passage through bridge openings free of jams on Siberian rivers. International Symposium on River and Ice, A. Budapest, 1974.
7. Lászlóffy, W.: Folyóink jégviszonyai, különös tekintettel a Dunára. Vizügyi Közlemények. 1934/4. Budapest
8. Lászlóffy, W.: Folyóink jégviszonyai. Mérnöki Továbbképző Intézet. Budapest, 1954.
9. Michel, B.: Winter regime of rivers and lakes.
10. Sipos, B.: A jégvédelem kézikönyve. Budapest, 1973.
11. Starosolszky, Ö.: A jég a vizépitésben, Budapest, 1969.
12. Török, L.: A vizi mütárgyakra ható jégnyomás számitásának módszerei. Vizügyi Közlemények.1955/3-4.Budapest

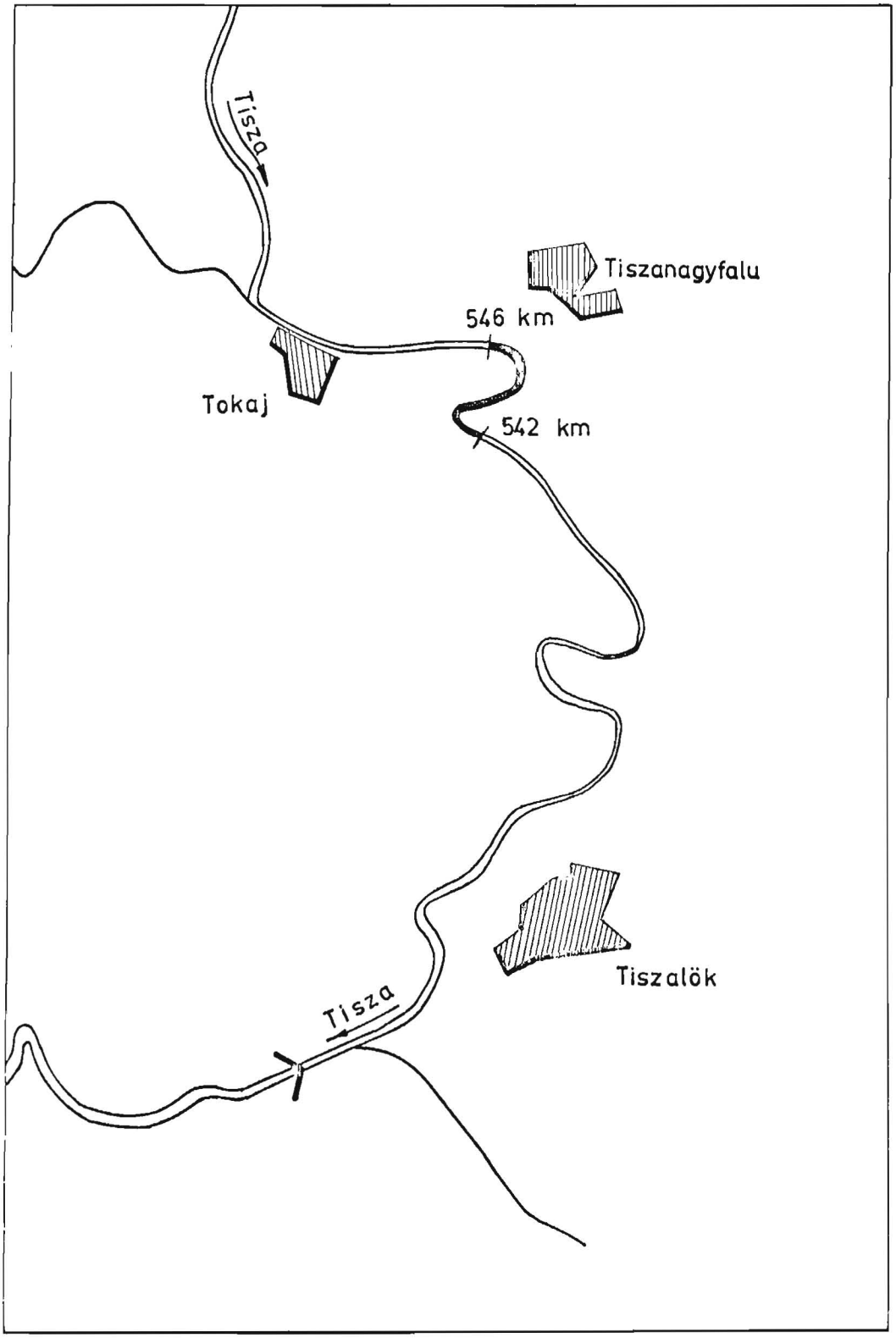

Fig. 1.

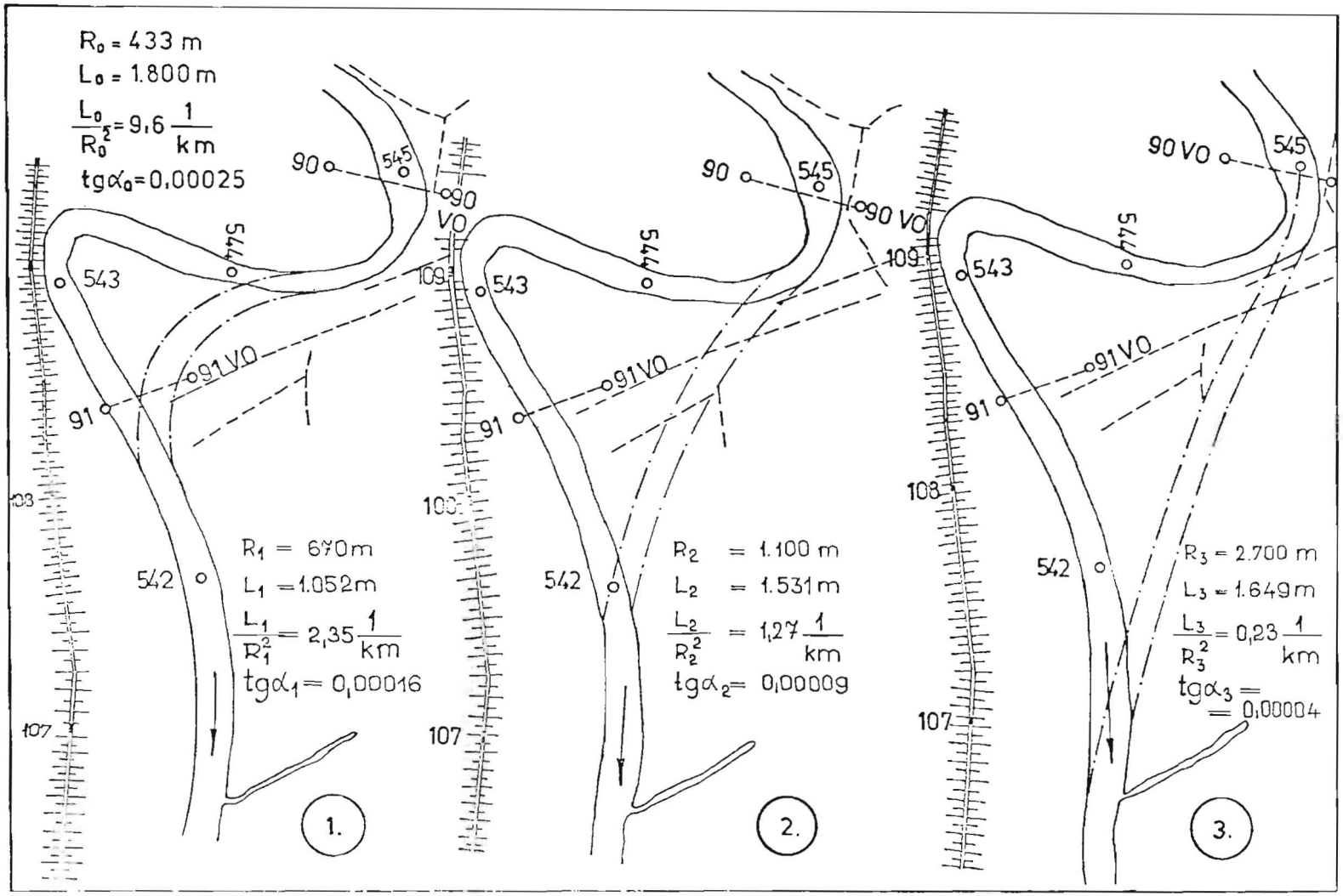
R_0 = 433 m
L_0 = 1.800 m
$\frac{L_0}{R_0^2}$ = 9,6 $\frac{1}{km}$
$tg\alpha_0$ = 0,00025
90
545
90 VO
544
543
109
91 VO
91
108
542
107
R_1 = 670 m
L_1 = 1.052 m
$\frac{L_1}{R_1^2}$ = 2,35 $\frac{1}{km}$
$tg\alpha_1$ = 0,00016
1.
R_2 = 1.100 m
L_2 = 1.531 m
$\frac{L_2}{R_2^2}$ = 1,27 $\frac{1}{km}$
$tg\alpha_2$ = 0,00009
2.
R_3 = 2.700 m
L_3 = 1.649 m
$\frac{L_3}{R_3^2}$ = 0,23 $\frac{1}{km}$
$tg\alpha_3$ = 0,00004
3.

Fig. 2.

THIRD INTERNATIONAL SYMPOSIUM ON
ICE PROBLEMS
Hanover, New Hampshire, USA

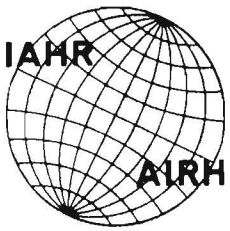

EFFECTS OF LAKE ERIE-NIAGARA RIVER ICE BOOM ON THE ICE REGIME OF LAKE ERIE

Ralph R. Rumer, Jr. Professor	State Univ. of N.Y. at Buffalo	Buffalo, N.Y. U.S.A.
Charles H. Atkinson Executive Engineer	Acres Consulting Services Ltd.	Niagara Falls, Canada
S.T. Lavender Senior Engineer	Acres Consulting Services Ltd.	Niagara Falls, Canada

INTRODUCTION - In 1964 the International Joint Commission granted temporary authority to the Hydro-Electric Power Commission of Ontario and the Power Authority of the State of New York to install an ice boom in Lake Erie near the entrance to the Niagara River. The purpose of this boom is to: accelerate the formation of a stable ice cover at the eastern end of Lake Erie; reduce movement in the ice cover while it is being formed; and help to stabilize the downstream edge of the ice cover so that erosion and breakoff of ice is reduced. The boom provides added resistance to breakage of the natural arch under storm conditions.

The boom has been designed to submerge and allow passage of ice over it if, during a storm, the arch breaks and the ice forces on the boom become very great. Towards the end of a storm, as the wind subsides, the boom returns to the floating position and the flow of ice into the Niagara River is again cut off.

The boom provides a distinct advantage in achieving optimal hydroelectric power generation on the Niagara River by significantly reducing ice flows at the water intake structures located downstream of the boom. Additionally, property damage due to massive ice runs has probably been reduced along the entire Niagara River.

In the spring of 1971, the recorded last day of ice in Lake Erie was May 31. This marked the third time in recent history when ice remained in Lake Erie to such a late date. The earlier events occurred on May 31 in 1926 and 1936. After the severe winter of 1971, concern developed as to whether or not the ice boom was: (a) increasing the volume of ice in Lake Erie during the winter season; and (b) prolonging the period of ice cover in Lake Erie toward the end of the ice season. The possible consequences of the above effects led the International Niagara Board of Control to study the effects the ice boom may have on: the thickness or extent of the ice field, the rate of dissipation of ice in Lake Erie, navigation, recreation, and weather. This report

presents the results of that study.

The study involved an examination of the historical record of ice growth and dissipation in Lake Erie for preboom and postboom years. A statistical analysis was made of water temperature data proximate to the ice boom for preboom and postboom years. Ice melt models were reviewed and a simplified mathematical model simulating the ice dissipation process in Lake Erie was developed. The study was hampered by the sparsity of field data available that could be used to quantify the physical processes occurring during the dissipation period, with or without the boom in place.

The physical setting for the Lake Erie-Niagara River ice boom study is depicted in Figure 1. Meteorological data collection stations are shown and the surface area of the lake can be estimated from the table provided in the Figure.

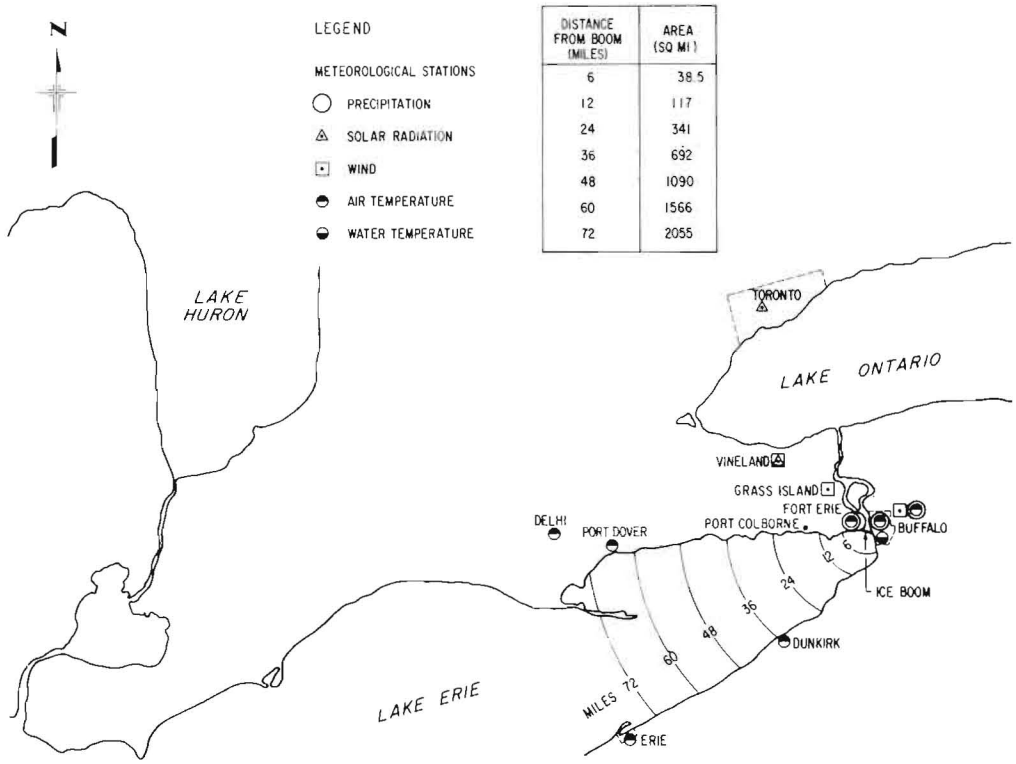

Figure 1 – Eastern End of Lake Erie

ICE DISSIPATION PROCESSES - Ice dissipation in Lake Erie occurs through melting resulting from heat exchange with the air and water environment and by transport of ice out of the lake into the Niagara River. The two principal observational records pertaining to the first of these

processes are the areal extent, or coverage, of ice during the dissipation period and the reported day of last ice in the lake. Observations of ice discharge down the Niagara River are available from the power entities. These observational records, along with meteorological information and lake water temperature records, provided the data bank on which the analysis of ice boom effects was based.

Using published methodologies (Edinger and Geyer, 1965; Ryan and Stolzenbach, 1972) for computing heat exchange due to long and short wave radiation, evaporation, condensation, and conduction and convection, the net heat exchanged at the ice-air interface in Lake Erie was computed for the period April 12 to May 5, 1972 (see Figure 2).

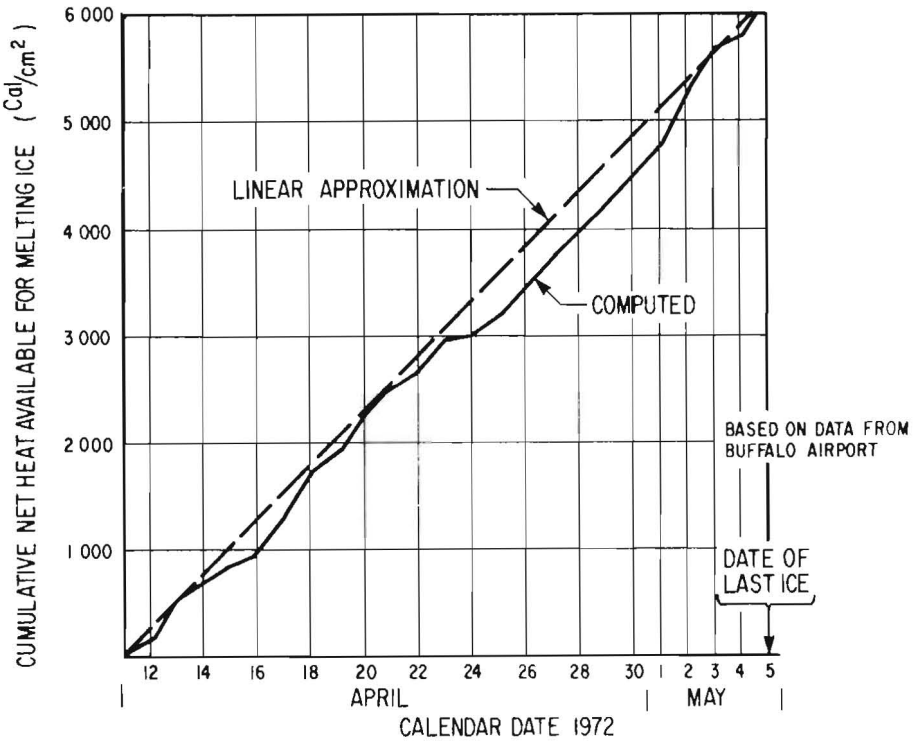

Figure 2 – Accumulated Net Heat Exchange at Air-Ice Interface During Dissipation Period, 1972

The sum of the daily net heat exchange represents the accumulated heat available either for melting ice or warming the water body. The linear approximation shown in Fig. 2 represents an average daily net heat exchange of 260 cal/sq. cm, or an average ice melt rate of 3.25 cm/day. The daily variation in this melt rate ranged from 0.61 cm/day (on April 24, 1972) to 6.1 cm/day (on May 2, 1972) during this period.

No systematic record exists of the quantity of ice discharged down the Niagara River during the ice melt season. Estimates of the maximum ice discharge capability of the Niagara River vary widely from approximately 50 square miles per day (130 km^2/day) to something less than 20 square miles per day (52 km^2/day). What ice discharge can be sustained

in the Niagara River without jamming and stoppage of ice flow from the lake is not known and cannot be estimated with confidence at this time.

The ice melt at the ice-water interface can be estimated with knowledge of observed water temperatures, speed of water movement beneath the ice cover, extent of the ice field, and assumed values for the vertical heat diffusivity. One estimate so obtained revealed that the melt rate due to heat exchange at the ice-water interface was of the order of .003 ft/day (0.1 cm/day) on 10-11 April 1972. At that date the surface area of ice was approximately 1500 square miles (3885 square kilometers). This estimated melt rate at the ice-water interface is considerably smaller than the computed melt rate of 3.25 cm/day at the air-ice interface.

MATHEMATICAL MODEL FOR ICE DISSIPATION - A simplified mathematical model representing ice dissipation in eastern Lake Erie was formulated taking into consideration the ice melt at the air-ice interface and ice discharge down the Niagara River. This dissipation process is depicted in Figure 3.

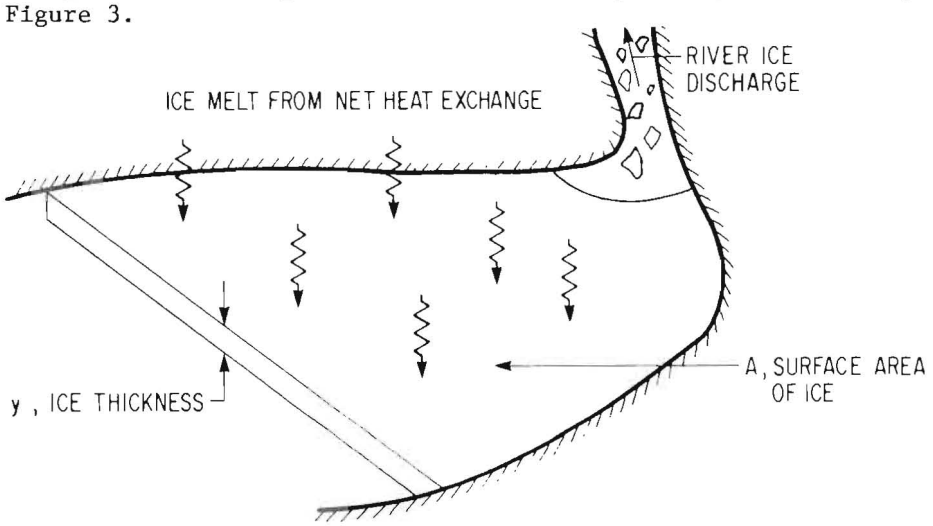

Figure 3 – Ice Dissipation Process

The model is formulated on the basis that: the ice dissipation period is underway; no new ice is being produced; and the thickness of the ice cover is constant in space and dependent on time only.

With these simplifying assumptions, the volume of ice, V, in the lake expressed as a function of time, t, is

$$V = (A_o - at)(y_o - rt) \qquad (1)$$

where A_o and y_o are the ice area and ice thickness respectively at the beginning of the period of interest (note that $A_o y_o$ is the initial ice volume), a equals the Niagara River ice discharge in square miles per day, and r denotes the rate of ice melt at the air-ice interface in feet per day. The time, T, to completely dissipate the ice in the lake is obtained by setting V = 0 in equation (1). After rearranging, this

gives

$$T = \frac{1}{2}\left[(T_r + T_a) \pm (T_r - T_a)\right], \qquad (2)$$

where $T_r = y_o/r$, and is the time it would take to melt all the ice in place; $T_a = A_o/a$, and is the time it would take to discharge all of the ice in the lake down the Niagara River. Equation (2) indicates that there are two possible lengths to the dissipation period. If the positive sign is chosen, $T = T_r$; if the negative sign is chosen, $T = T_a$. The smaller of the two indicates which of the two dissipation processes is the controlling factor in determining the date of last ice.

At any given time during the dissipation period, the date of last ice can be forecast on the basis of estimated values for the two dissipation rates; the dissipation rate due to ice melt in place, $dV/dt = -rA$, and the dissipation rate due to ice discharge down the river, $dV/dt = -ay$. It can be seen that the ratio of these two dissipation rates provides a dimensionless parameter, $T' = (rA)/(ay)$, which, if evaluated, allows the determination of the relative importance of each of the two dissipation processes in reducing the ice volume and in setting the date of last ice. Accordingly, whenever T' is less than one, the discharge of ice by the river would lead to a shortening of the dissipation period. The reduction of ice volume during the dissipation period incorporating the parameter T' is depicted in Figure 4.

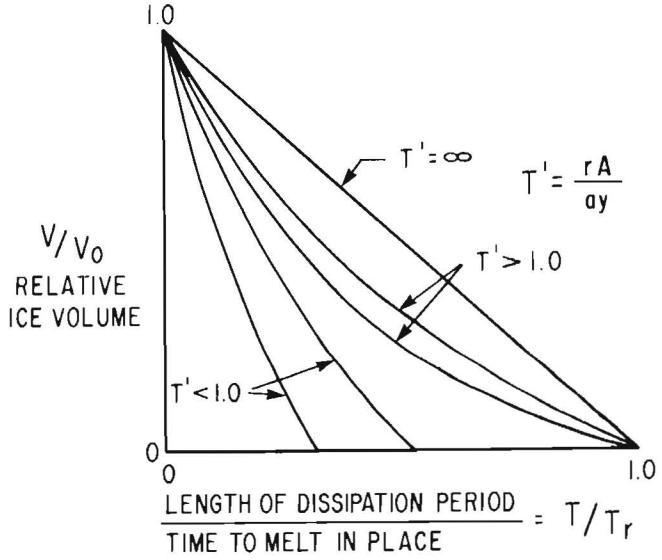

Figure 4 – Ice Volume Reduction During Dissipation Period

The mathematical model can be used to estimate the effect that reduction of ice discharge down the Niagara River would have on the length of the ice dissipation period and the water temperature depression that would result from an extension of the ice dissipation period. If the presence of the boom had the effect of reducing ice discharge down the river to zero (a = 0), then the dissipation period would have been extended a time increment given by $\Delta T = T_r - T_a$. In this case, T_a would be based on the expected ice transport capability of the river if the

boom had not been in place. In dimensionless terms, this becomes

$$\frac{\Delta T}{T_r} = 1 - T' \tag{3}$$

For T' less than one, river ice discharge would have shortened the ice dissipation period. For T' equal to or greater than one, river ice discharge would not have altered the date of last ice in Lake Erie, but it would still have contributed to a reduction in ice volume in the lake at any specific time in the dissipation period (see Figure 4).

An extension of the ice cover in eastern Lake Erie by ΔT days prevents the addition of heat to the water body for the same increment of time, since this heat would be utilized to melt the remaining ice. If the daily net heat exchange at the lake surface is H_n, then the corresponding water temperature increase, ΔF, in degrees F, that would have occurred (assuming complete vertical mixing in the water body and neglecting advection) is given by

$$\Delta F = \frac{H_n}{17D} \tag{4}$$

in which H_n is in cal/sq cm per day and D is the water depth in feet. The factor 17 has the units (cal cm^{-2} F^{-1} ft^{-1}) and is required for dimensional homogeneity. Therefore, as a first approximation, the effect of an extended ice cover by ΔT days will be to prevent the lake from warming up an amount F, given by

$$F = \frac{(\Delta T)H_n}{17D} \tag{5}$$

Since H_n gradually increases during the warm-up period, an extension of the ice cover period in early April would have a lesser effect on water temperature than an extension in early May.

The relative importance of the factors affecting ice dissipation in Lake Erie can be estimated only, since the model is an idealization of the actual physical phenomena that it represents, and the information required to use it is lacking. The simulation model is being further developed to permit ice thickness to be variable in space as well as time. This model, when developed, should be calibrated to: (a) determine any limitations inherent in the model as a consequence of the simplifying assumptions used; (b) verify the suitability of the model as a predictor for planning boom operations; and (c) make the model operational. These can be achieved if observations of melt rates, rates of ice discharge down the Niagara River, and the areal extent and thickness distribution of the ice cover are observed at regular intervals during the dissipation period.

HISTORICAL ANALYSIS - The historical analysis of the ice regime in Lake Erie encompassed the period 1956 to 1973 plus the winter of 1935-36. The annual ice cover cycle was divided into five basic calendar periods (see Figure 5) to reflect the sequential nature of the winter heat budget of Lake Erie and to facilitate the historical analysis. These periods were separated by the following dates:

(a) Date of maximum summer water temperature;
(b) Date of 39°F water temperature in the fall
(c) Date of 32°F water temperature (signalling the beginning of

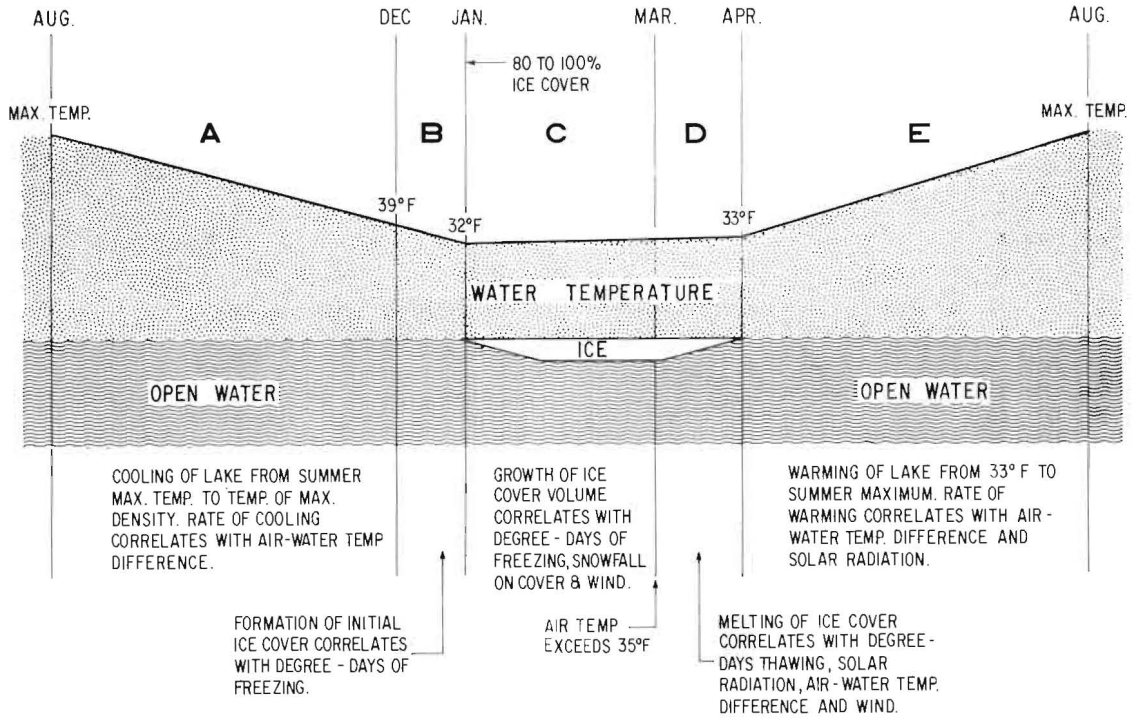

Figure 5 – Annual Ice Cover Cycle

the ice production period);

(d) Date of 5-day average air temperature greater than 35°F (signalling the end of the ice production period);

(e) Date of 33°F water temperature in the spring.

Water temperatures at a depth of 18 feet in Lake Erie at the entrance to the Niagara River and approximately 1000 feet downstream from the boom have been observed by the Buffalo Department of Public Works since 1926. Inspection of this record showed anomalies which precluded the use of data collected prior to 1956. There remained 17 years of temperature data of which 8 were preboom and 9 were postboom (see Figure 6).

The historical analysis revealed that a very high correlation existed between the first occurrence of 32°F water temperature in the near-boom vicinity and the appearance of first ice. A similar high correlation existed between the occurrence of 33°F water temperature in the spring and the disappearance of last ice. It was concluded that water temperatures in the vicinity of the boom remain very close to 32°F until all lake ice has disappeared from the eastern end of Lake Erie. This was further substantiated by the field measurements of Stewart (1973). Furthermore, the historical analysis revealed that the climatic factors affecting the ice cover processes are numerous and highly variable and that these factors must be considered sequentially in order to interpret their effects. A direct comparison of the climatic factors for 2 years having similar late spring dates of last ice (1936 and 1971) provided no conclusive evidence as to whether or not the ice boom contributed sig-

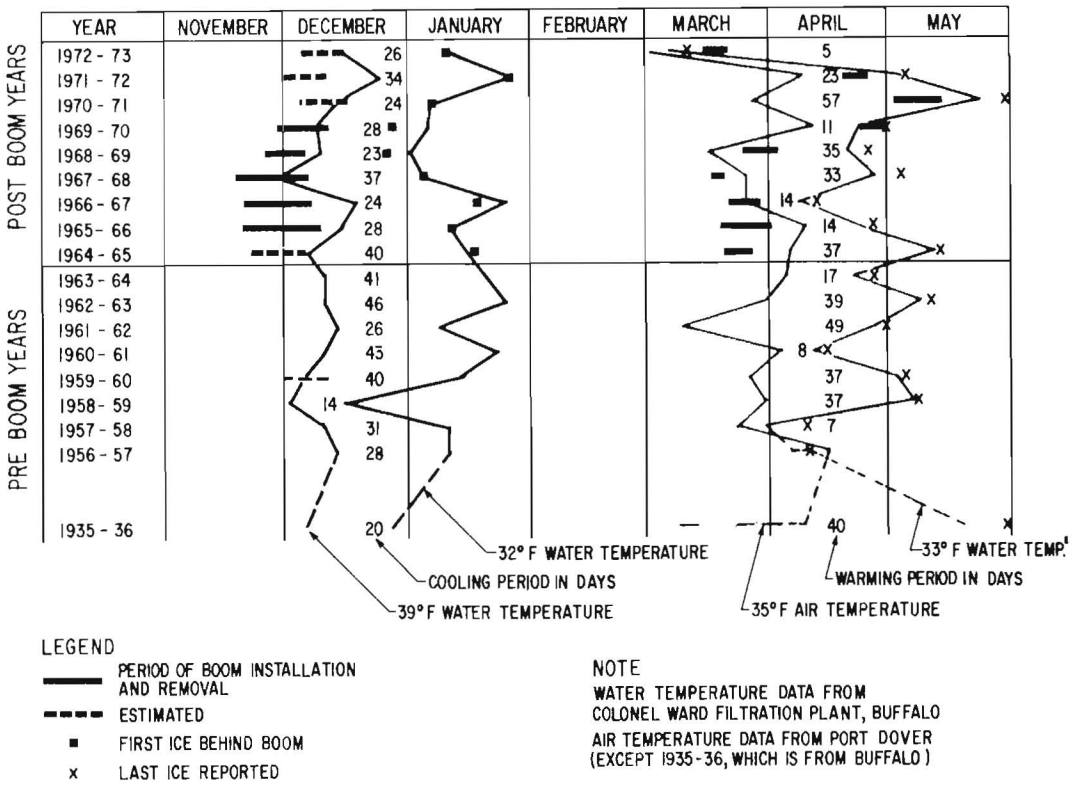

Figure 6 – Ice Cover Events on Lake Erie

nificantly to the late date in 1971.

TEMPERATURE ANALYSIS - The purpose of this analysis was to compare the water temperature regimes which existed before the installation of the boom with those prevailing subsequent to installation. This comparison was accomplished by means of an inspectional analysis of the temperature record and a detailed statistical analysis of the temperature data.

The preboom and postboom water temperatures are shown in Figure 7. In all cases, the late May temperatures tend to be near 50°F. The downward trend of late May and early June temperatures is consistent with the higher lake levels experienced in the postboom period. Once the ice has departed from the eastern end of the lake and no longer holds the local temperature at 32°F, the water mass warms as a result of the net heat exchange at the air-water interface. The later dates of departure from 32°F result in a more rapid warming of the water mass because of the greater heat exchange that occurs later in the spring period.

The statistical analysis revealed that the water temperature regimes at the eastern end of Lake Erie during similar calendar periods for preboom and postboom years were different. The differences, which indicate colder postboom temperatures, vary throughout the ice dissipation period. The probabilities of the observed maximum temperature differences being due to causes other than chance exceeded 50%, reaching a maximum of 94%. Physical reasoning and sensitivity of certain of the observed differences

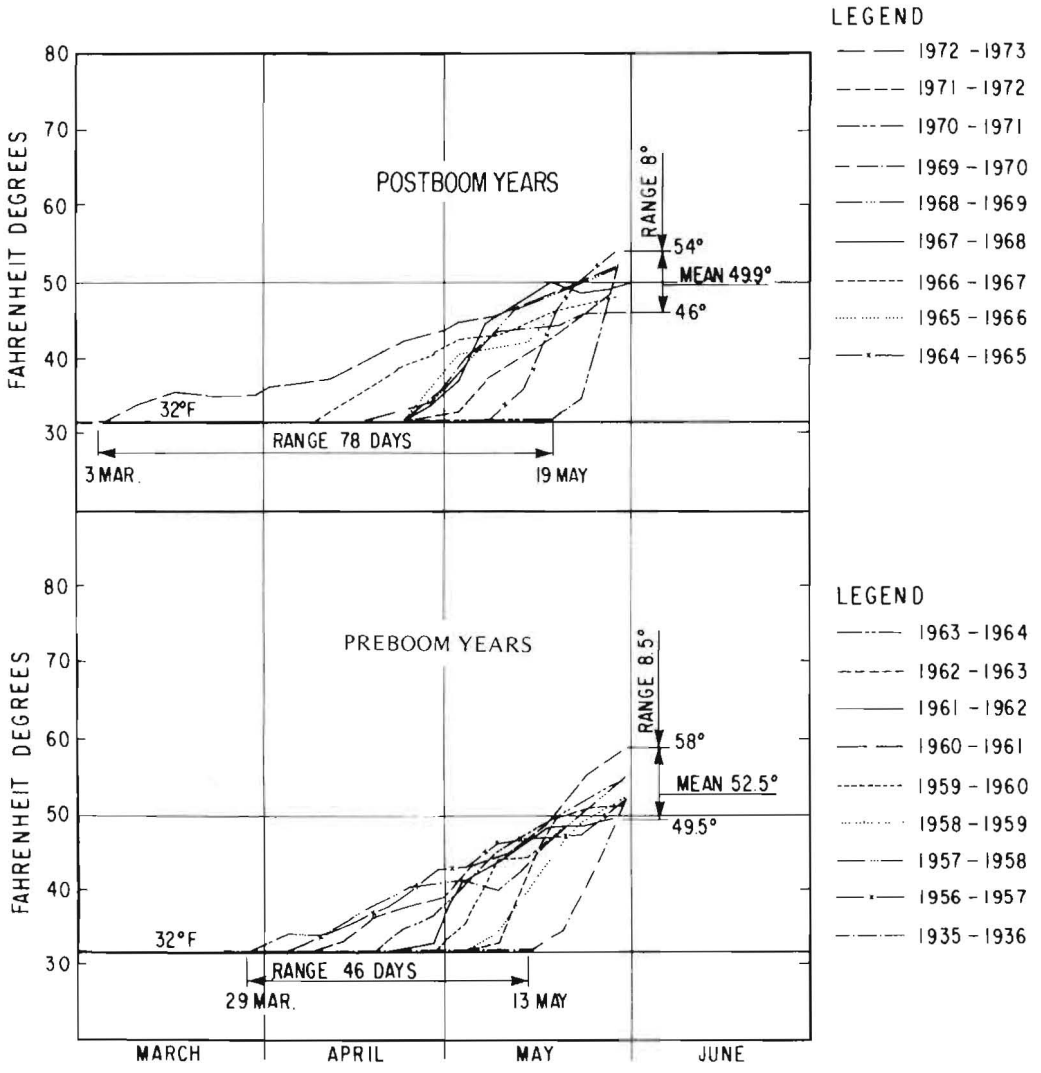

Figure 7 – Comparison of Preboom and Postboom 5-Day Average Water Temperature

to sorting according to the boom removal date suggest that the boom contributed to the observed differences. There are, however, other factors (e.g., rising lake levels) which may contribute to the observed differences.

SUMMARY AND CONCLUSIONS - It is certain that the boom affects the ice cover by stabilizing the initial ice cover formation at the beginning of

THIRD INTERNATIONAL SYMPOSIUM ON
ICE PROBLEMS
Hanover, New Hampshire, USA

A NOTE ON THE MECHANISM OF FRAZIL INITIATION

Thomas O'D. Hanley Wheeling College Wheeling, WV
USA

There has been a problem of explaining the nucleation of frazil at supercoolings of a tenth of a degree or less, when it is well known that samples of the same water can be supercooled several degrees without nucleation. The problem can be illustrated by a free energy barrier separating the liquid state from the ice state. Experiment has indicated that the activation energy required for surmounting this barrier can be as much as $k\Delta T = 40k = 0.003$ electron-volts.

I suggest that frazil formation may be initiated by a mechanism other than nucleation. By way of example, one such mechanism which has received much attention from metallurgists is called spinodal decomposition, which Schwartz et al (1975) have characterized as follows:

> "Spinodal decomposition refers to the process whereby a single-phase system separates into two phases via spontaneous growth of fluctuations in composition or density. It differs from nucleation in that the latter process relies on the existence of a local fluctuation to surmount a thermodynamic barrier to phase separation thus allowing the formation of droplets or bubbles of the new phase; in spinodal decomposition this thermodynamic barrier is absent."

The spontaneous growth of fluctuations occurs in that portion of a graph of free energy vs concentration, where $\partial^2 G / \partial C^2 < 1$. In this

region, spinodal decomposition is described by Cahn (1968) as a diffusional process in which the diffusion coefficient is negative, so that diffusion occurs toward a higher concentration. But spinodal decomposition in metals is subject to other conditions which may inhibit it.

The nucleation temperature of a water sample has usually been measured with the water motionless. Yet it is well known that a condition for frazil formation is that the water must be notably turbulent.

So I propose that the mechanism for initial formation of ice is dependent on turbulence or, equivalently, on the Reynolds number Re, in such a way that at sufficiently high values of Re the transition from water to ice is effected by a mechanism other than nucleation, so that the nucleation barrier need not be surmounted.

While I am not at present prepared to espouse spinodal decomposition as the operative mechanism, it has this interesting characteristic, that it results in production of the new phase in small zones distributed throughout the samples. This is interesting because, in watching carefully the initiation of frazil during several dozen experiments, I had the impression that its formation began throughout the liquid, and not merely at the surface.

This indicates the need, as G. D. Ashton pointed out to me (private communication) of several investigations such as, first, watching frazil formation through a window on the side of the tank in order to ascertain whether frazil is produced at the surface or throughout the body of water, and secondly, attempting to produce frazil in a chamber without an air-water interface in order to show whether frazil production involves the interface.

A thorough investigation of the mechanism by which frazil is initiated might have very practical results, such as affording an unequivocal means of frazil detection. For example, one property peculiar to spinodal decomposition in optically transparent substances is a scattering of light that is time-dependent and angularly distributed in such a way that a ring of scattered light is observed contracting slowly toward the unscattered beam.

To sum up, the mechanism of frazil initiation ought to be investigated theoretically and experimentally without overlooking mechanisms other than classical nucleation.

REFERENCES

A. J. Schwartz, J. S. Huang and W. I. Goldburg (1975), "Spinodal decomposition in a binary liquid mixture near the critical point," J. Chem. Phys. 62, 1947-52.

J. W. Cahn (1968) "Spinodal decomposition," Trans. AIME, 242, 166-180.

G - free energy

C - "concentration;" ice-like-ness

Re - Reynolds number

W - water

I - ice

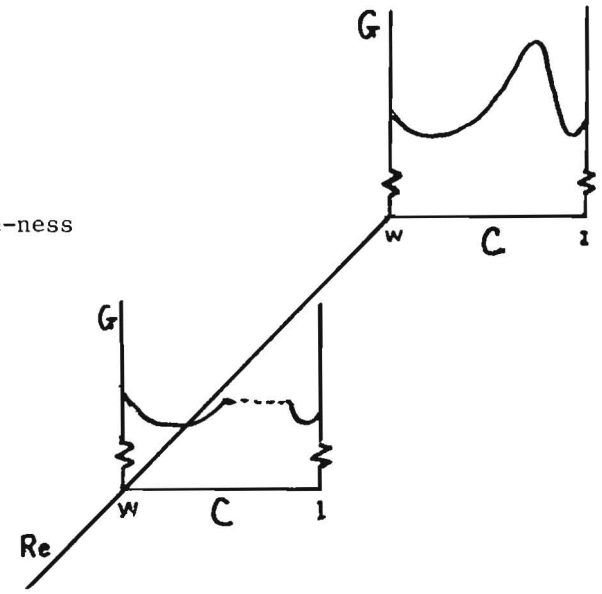

Figure 1. Proposed free energy vs ice content and Reynolds number, not to scale.

International Association of Hydraulic Research (IAHR)
Committee on Ice Problems
International Symposium on Ice Problems
18-21 August 1975
Hanover, New Hampshire

COMMENTS

Paper Title: A Note on the Mechanism of Frazil Initiation

Author: Thomas O'D. Hanley

Your name: T. E. Osterkamp

Address: Geophysical Institute
University of Alaska
Fairbanks, AK 99701

Comment:

The nucleation of turbulent water has been studied experimentally by many investigators. In general, when the possibility of nucleation at the air-water interface was prevented the amount of supercooling was large (several degrees Celsius) and when nucleation at the air-water interface was possible the degree of supercooling was small (usually $< 0.1^{o}C$). These results imply that frazil nucleation may be associated with the energy and/or mass exchange processes at the air-water interface. If a process analogous to spiroidal decomposition is responsible for frazil nucleation then it must somehow be related to these energy and/or mass exchange processes. At the moment, it is difficult to understand how this proposed frazil nucleation process is related to these processes that occur at the air-water interface.

THIRD INTERNATIONAL SYMPOSIUM ON
ICE PROBLEMS
Hanover, New Hampshire, USA

NOTES ON THE STABILITY OF FLOATING ICE BLOCKS

Peter Larsen, Director of Research, Dept of Water Resources Eng
Lund Institute of Technology / University of Lund, Sweden.

The stability of ice floes arrested at the upstream edge of an ice cover has been studied by a number of investigators both in the field and in the laboratory. Limiting velocities for stability have been noted as early as in the 1920ies while actual studies of the mechanics governing stability date back about 20 years. Among early work on this problem is that of Pariset and Hausser reported at the IAHR Seminar on "Ice Problems in Hydraulic Structures" in Montreal in 1959. Since then Uzuner and Kennedy, Michel, Ashton among others have reported on experiments and analytical work on this subject. Stability of ice floes transported from upstream is an ingredient of the mechanics of ice cover formation.

This note is a brief summary of results obtained as part of a master's thesis (Johansson, Nilsson 1975) carried out at Lund Institute of Technology.

Test procedure

Fig 1 shows a simulated ice floe (paraffin, ρ = 0.89) resting against the upstream edge of a simulated ice cover in a hydraulic flume. (Flume dimensions and range of test conditions are given in Table 1). The solid ice cover - simulated by a sheet of plyform - was free to move vertically and the thickness so adjusted as to obtain the same level of the underside as that of the floe underside. Discharge was set at a predetermined rate and then kept constant. Flow velocity was increased by gradually opening a downstream gate until instability occured. Flow depth was then measured and velocity computed based on discharge and cross sectional area. Tests were repeated several times and average

values computed. Little scatter in obtained instability conditions with a specific floe indicated that instability was well defined.

No spill condition and modes of submergence

The vertical position of the floe is governed by forces due to weight and pressure. Taking moments about the line of support, i.e. the lower, downstream edge of the floe, the weight of the flow produces a destabilizing moment. Static plus dynamic pressure on the upstream face produce a stabilizing moment while static pressure on the downstream face accounts for a destabilizing moment.

In still water the constant pressure on the underside of the floe exactly balances the weight of the floe (buoyancy = weight). If the floe is forced down at the upstream end buoyancy increases and a stabilizing moment is created. Assuming that the line of support is unchanged the stabilizing moment increases until the upstream end of the floe becomes submerged and remains thereafter nearly constant.

When a flow is established the pressure distribution on the upstream face and notably on the underside of the floe is changed due to local acceleration of the flow. The flow pattern and hence the modified pressure distribution depends on the floe geometry and to some degree on the turbulence level of the approaching flow. The pressure reduction under the floe causes its upstream end to sink and instability occurs when water starts spilling onto the floe (the "no spill condition"). This mode of instability has been called "submergence by underturning". Figures No 1, 2 and 3 show this sequence of events resulting in the floe being swept down-stream under the cover.

A different mode of submergence has been observed both in laboratory and field in which the floe sinks in a horizontal position until the downstream upper edge is below the solid cover. The floe then slides under the cover. This mode has been termed "vertical submergence".

A third mode was observed in the present studies of floes with a rounded upstream face. The sequence of events is shown in Fig 4. With the rounded face flow separation is prevented and the pressure center is moved downstream.

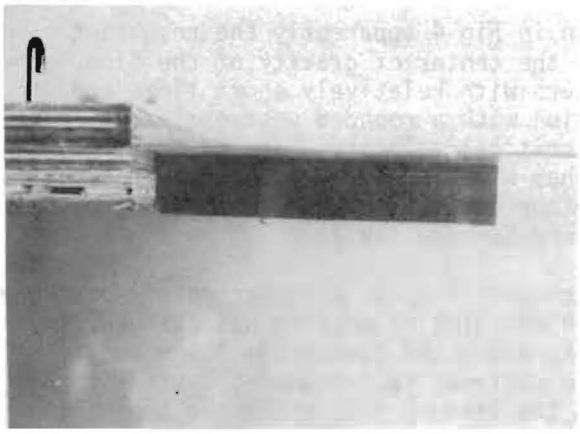

Fig. 1. Sequence showing submergence by underturning.

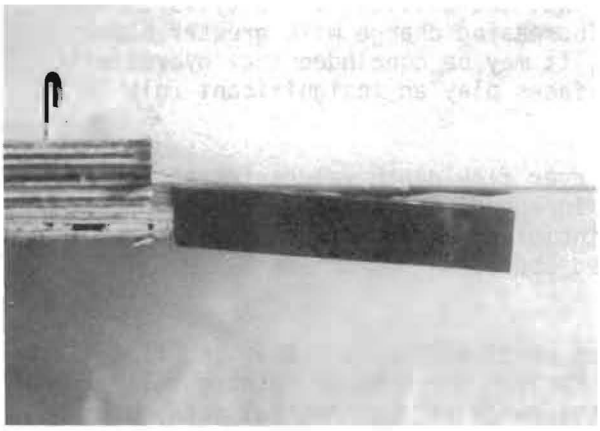

Fig. 2. Sequence showing submergence by underturning.

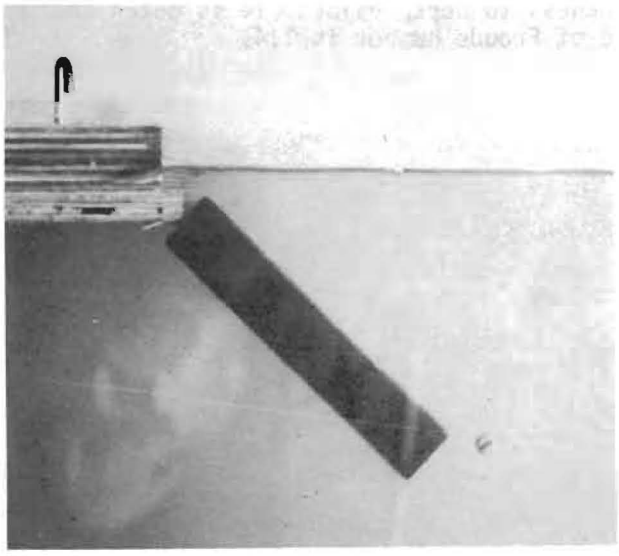

Fig. 3. Sequence showing submergence by underturning.

With the mode of submergence shown in Fig 4 apparently the resultant pressure force acts downstream of the center of gravity of the floe. This mode of submergence only occurs with relatively short floes and has been observed only in connection with a rounded upstream face. Also it should be noted that the critical velocity - the velocity at which submergence occurs - is higher with this floe geometry stressing the importance of the local behaviour of the flow. These findings have been indicated earlier by Uzuner and Kennedy (1972).

In order to determine the effect on stability of pressure on the upstream face tests were performed in which the line of support was changed. In underturning the line of support is along the downstream lower end of the floe and pressure force on the upstream face produces a stabilizing moment about this line. By mowing the line of support to the top of the floe the corresponding moment becomes destabilizing. Similarly the moment of pressure force on the downstream end changes sign. Test results, shown in Fig 5, indicate that the critical velocity is changed only little with a tendency of increasing change with greater block thickness, as would be expected. It may be concluded that hydrostatic and dynamic pressure on the end faces play an insignificant role in determining the floe stability.

For the range of floe thickness over flow depth values tested Fig 6 shows that critical velocity is independent of flow depth. In other words the force equilibrium at incipient instability depends on local properties of the flow as assumed above.

Stability of thin floes

Fig 7 shows relationships between critical Froude number and floe thickness to depth ratio as given by Pariset and Hausser (straight line) and by Ashton. Vertical lines show the range of experimental data obtained by Uzuner and Kennedy. The Froude number is a type of densimetric Froude number with the length parameter chosen as the floe thickness. It is seen that fair agreement between theoretical and experimental results is obtained over an extensive range of thickness to depth values. It is noted that theoretically the maximum value of Froude number is 1.4.

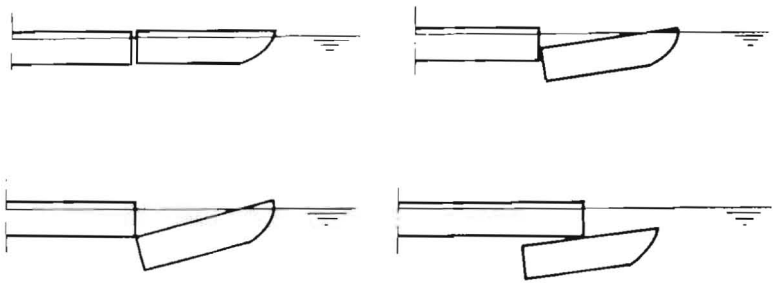

Fig. 4. Submergence of blocks with rounded upstream face, $3 < \frac{L}{t} < 15$.

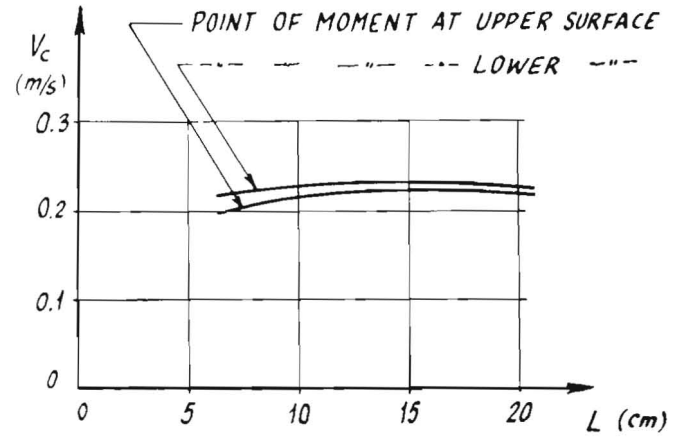

Fig. 5. Effect of changing the point of support from lower to upper level of block.

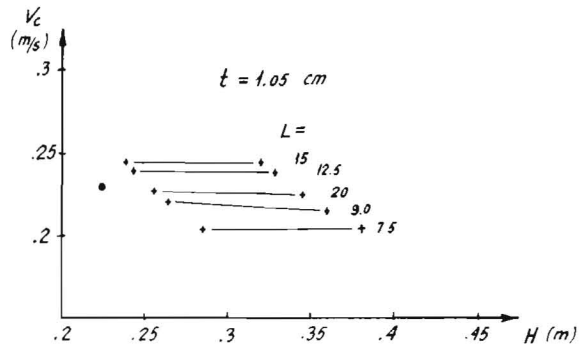

Fig. 6. Critical velocity versus depth for blocks of various thickness and length.

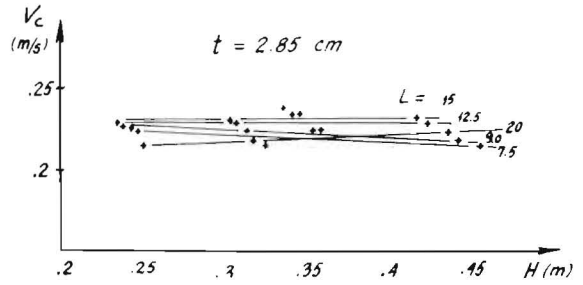

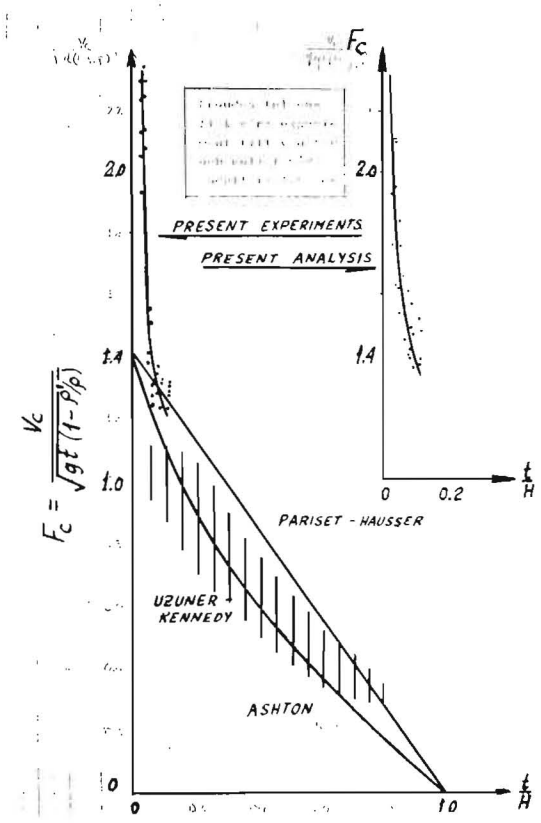

Fig. 7. Froude number at instability as a function of block thickness over flow depth.

Ashton (1974), however, found in experiments that thin floes were stable at Froude numbers exceeding 1.4, a result noted also by Pariset and Hausser and by Cartier although expressed by them in a different way.

The present tests were carried out with floe thickness varying between 2.5 and 15 % of flow depth. Froude numbers as high as 2.4 were obtained.

Theoretical determination of stability

In an attempt to theoretically determine the floe stability of floes with small thickness compared to water depth it was assumed that the flow may be treated as potential. Using a Schwarz-Christoffel transformation velocity distribution and hence pressure distribution was computed along the floe underside. Fig 8 shows an example of plotted pressure distribution in nondimensional format. The moment equation for equilibrium was solved taking into account the previously mentioned forces. The resulting velocity at incipient submergence was combined with actual values of floe thickness and density to form a critical Froude number. Fig 9 shows a comparison between Froude numbers obtained in this way and Froude numbers based on experiments. It is seen that the agreement is fair, that better agreement is obtained for floes having a rounded upstream end and that Froude numbers as high as 2.4 are obtained for the thinner floes.

Concluding remarks

There has been considerable discussion about the validity of the "no spill condition". Observation of the behaviour of floes in the laboratory gives visual support to the relevancy of the assumption that instability occurs when the upstream end of the floe becomes submerged. However, it does not seem correct to equate the upstream velocity head to the "freebord" of the floe. For example the floes of 1.05 cm thickness in the present experiments had a "freebord" in still water of (1 - 0.89) 1.05 = 0.12 cm. The velocity head of the approaching surface flow at instability was about 0.26 cm or greater by a factor of two.

Conventionally drawings of water surface profiles upstream of a blockage show an upward curvature at the blockage with the surface profile terminating at an elevation of one velocity head above the upstream water level. This is the case in most textbooks on hydraulics showing a channel with a bottom sluice. Observation in the laboratory seems to contradict this behaviour of the water surface.

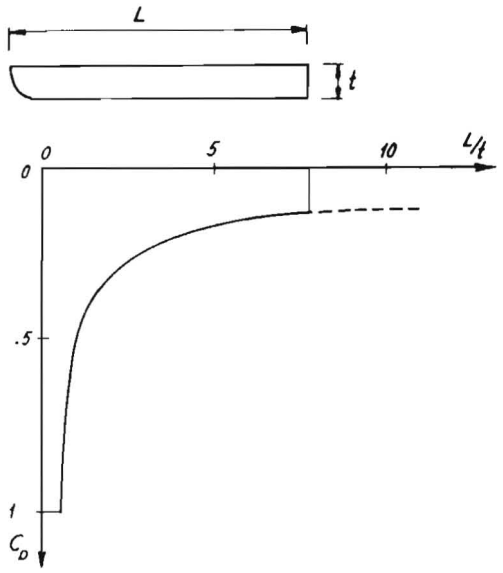

Fig. 8. Dimensionless pressure distribution along floe underside based on potential flow theory.

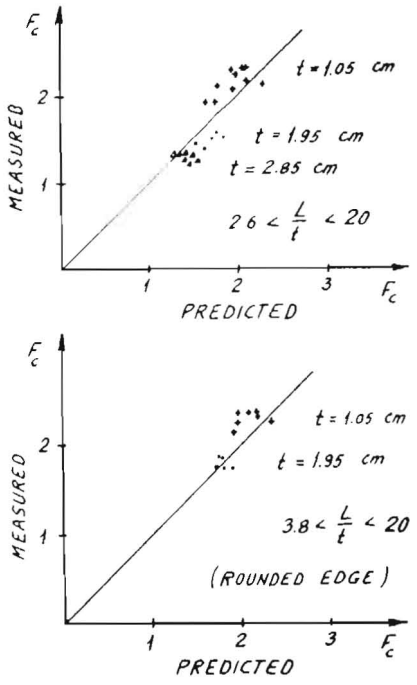

Fig. 9. Comparison between computed Froude number and experimental.

In experiments with different materials simulating ice floes surface tension may affect the test results. The ability of the floe to become wetted or indeed its ability to repell water may to some degree affect the condition of "no spill". In the present experiments surface tension was reduced in some tests by spraying liquid soap on the approaching flow. No significant change in equilibrium conditions was observed, however.

References

Ashton, G D: "Entrainment of Ice Blocks-Secondary Influences". IAHR/PIANC International Symposium on River and Ice. Budapest 1974.

Johansson, A; Nilsson, K: "Stabilitet av flytande isblock" thesis presented to the Lund Institute of Technology in partial fulfillment of the requirements for the degree of Master of Engineering.

Pariset, E; Hausser, R: "Formation and Evolution of Ice Covers on Rivers". Transactions of The Engineering Institute of Canada. Vol 5, No 1, 1961.

Uzuner, M S; Kennedy, J F: "Stability of Floating Ice Blocks" ASCE Journal of the Hydraulics Division, HY 12, 1972 (Proc Paper 9418).

Table 1. Range of variables and equipment data

Flume 0.5 x 0.5 m Length 4 m

"Ice" blocks of paraffin, square

$\rho'/\rho = 0.89$

Block lengths L 7.5, 9.0, 12.5, 15.0, 20.0 cm

Block thickness t 1.05, 1.95, 2.85 cm

Depth of flow $20 < H < 45$ cm

Discharge $25 < Q < 50$ l/s

$$2.6 < \frac{L}{t} < 20$$

$$0.03 < \frac{t}{H} < 0.12$$

$$1.2 < F_c < 2.4$$

Tilting angle at incipient instability small

THIRD INTERNATIONAL SYMPOSIUM ON
ICE PROBLEMS
Hanover, New Hampshire, USA

ICE FORCES ON MARINE STRUCTURES

K.R. Croasdale
Engineer

Imperial Oil Limited

Calgary, Alberta,
Canada

INTRODUCTION

Organizations responsible for the supply of fossil fuels and minerals regard the arctic regions as being potentially bountiful, but difficult to explore and produce from. The difficulties are even greater in the offshore regions of the arctic because of the presence of ice. Whether or not these regions will ever contribute to our energy needs will depend to a large extent on the work being done by people attending this symposium. The technical feasibility and cost of operating in the arctic will be governed by our understanding of the environment and of ice forces on marine structures, which is the title of this theme paper.

In general, to make a meaningful assessment of ice forces on marine structures, we first have to know the types of ice features common to the area, and second, be able to predict how these ice features interact with various shapes of structures under consideration.

Although the title of this paper is general enough to allow discussion of a wide variety of marine environments, I will concentrate on one particular area, that of the South Beaufort Sea, which is, of course, currently receiving much attention as a potential area for oil and gas production.

To orient my paper to one particular area will allow the inclusion of more detail than would be possible in a general coverage of global marine environments. It will also allow me to

avoid areas which I am not qualified to describe. In any case, the ice features native to this area are common, with a greater or lesser severity, to other ice-infested marine environments.

THE SOUTH BEAUFORT SEA

The Beaufort Sea is just one of the many coastal seas of the Arctic Ocean; it is generally defined as that sea immediately adjacent to the northern coast of Alaska, the Yukon, the Mackenzie District of northwest Canada, and the western isles of the Canadian Archipelago.

Conditions vary from complete ice coverage for nine months of the year to open water along a narrow coastal strip during the brief polar summer. Ice drift is dominated by the Beaufort Gyral which circulates in a clockwise direction.

Typical winter ice features are shown in Figure 1. Landfast ice extends out to about sixty feet of water, but has a smooth surface only out to about the fifteen-foot depth. Beyond that there are usually numerous first-year ridges which are formed during the early winter before the ice becomes landfast. Many of these ridges are grounded, forming anchor points for the landfast ice. The grounding action by these and the occasional multi-year ridge probably causes the seabed scours which are numerous in the area. The active shear zone, between the fast and pack ice, is often characterized by an open lead. Further offshore, the ice gradually changes from first-year to multi-year ice, and there will be the occasional one-hundred foot thick ice island.

Ice Ridges

The annual ice reaches a maximum thickness of six to seven feet by late April, but is heavily covered by ice ridges.

Few of these ridges have sails greater than ten feet and measurements of selected first-year ridges show that ridge keels are about four times the sail heights. However, first-year ridges are largely an accumulation of unconsolidated ice blocks and as such do not present as severe a loading condition for marine structures as the multi-year ridges.

Multi-year ridges are fully consolidated (KOVACS et al, 1971) and although rarer in the coastal zones, they do appear to govern the ice loads on marine structures in this area. Multi-year ridges with thicknesses of up to fifty feet are relatively common in the Beaufort Sea. Statistical techniques can be used to define the extreme ridge at a particular location. However, in the shallow areas the water depth will probably determine the design ridge thickness.

For structures in water deeper than about fifty feet, the risk of collision by massive ice islands has to be considered.

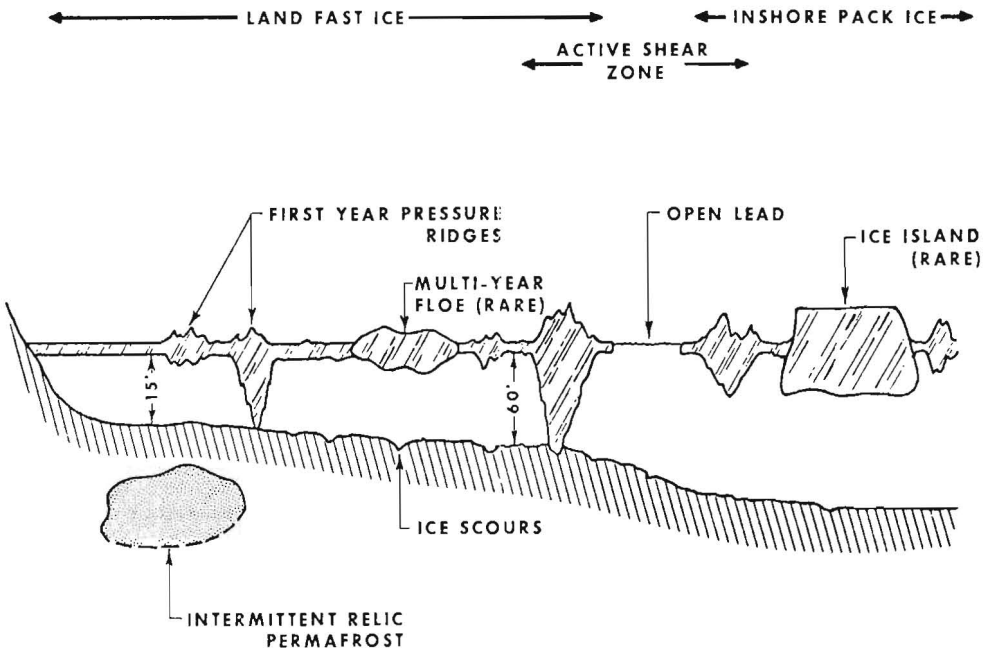

FIGURE 1. TYPICAL WINTER ICE FEATURES, BEAUFORT SEA.

Ice Movement

Patterns of ice movement affect ice forces in several ways for several reasons. First, ice strength and modulus are a function of loading or strain rate. Second, ice movement can cause ice rubble and ridges to form around a structure which can then influence future ice/structure interaction. And third, there may be stationary periods during which the ice can freeze to the structure to form an intimate contact condition which can result in high ice forces when movement starts up again. In the South Beaufort Sea, tidal variations in water level are too small to prevent this frozen-in condition.

The so-called landfast ice which covers much of the coastal zone is relatively stable but movements of several feet can occur due to deformation of the ice under the action of wind stress (Table 1).

TYPICAL LANDFAST ICE MOVEMENTS

BEAUFORT SEA - 1970

WATER DEPTH (FEET)	FIRST TIME INTERVAL (DAYS)	GROSS MOVEMENT (FEET)	SECOND TIME INTERVAL (DAYS)	GROSS MOVEMENT (FEET)
56	33	63	28	15
28	20	97	39	62
30	14	20	27	7

TABLE 1

Measurements we have conducted during the last few years lead us to conclude that the ice behaves like an elastic plate which is fixed at one end (the shore). Under the action of onshore winds, the plate is subject to an edge pressure from the polar pack and a wind stress along its upper surface, which causes the ice to deform and move relative to the seabed (Figure 2). Typical observed movements of fifty feet or so, which occur generally during storms, can be explained by such a model.

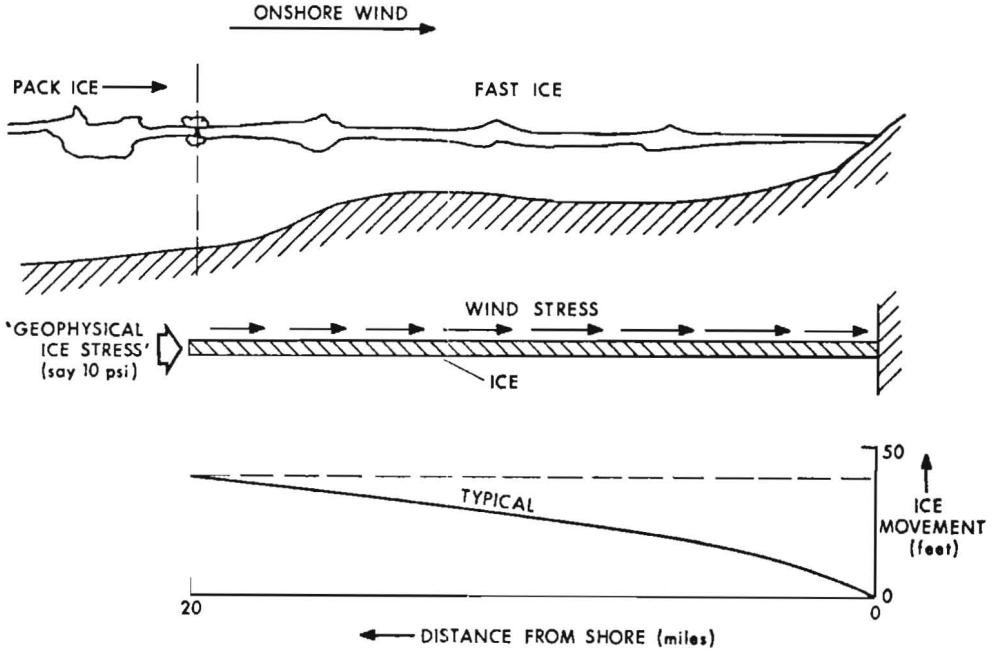

FIGURE 2. LANDFAST ICE MOVEMENT MODEL.

It is during break-up of the ice in the coastal zones of the Beaufort Sea that the largest ice movements will occur. Such movements may lead to ice rubble forming around stationary structures.

Ice Strength Parameters

In addition to thickness and geometry, ice strength obviously governs the forces exerted on arctic marine structures. It is beyond the scope of this paper to discuss the intricacy of ice physics as it affects strength; in any case this topic has been well covered at previous symposia and is the subject of several papers to follow. So it will perhaps be sufficient to just highlight a few key points.

The strength of the ice in the Beaufort Sea, as expected, is a function of crystal structure, temperature, salinity, area under stress, and rate of loading.

In these respects, the annual ice of the Beaufort Sea appears to be typical columnar sea ice with a horizontal c-axis. In the coastal zones, particularly near the Mackenzie River, ice salinities are extremely low, and in certain areas, the ice can be considered fresh. The multi-year ridge with its low salinity and random crystal orientation in the refrozen zones, probably represents the toughest ice in the region, a fact well known by arctic mariners.

TYPES OF MARINE STRUCTURES FOR THE SOUTH BEAUFORT SEA

In order to discuss ice loads on marine structures, we should first of all look at the kinds of offshore drilling concepts that might be possible in the area (Figure 3).

Artificial islands are an obvious choice for shallow water and their design can be optimized to suit local materials and construction equipment. The oil industry has already built several islands in the Mackenzie Delta area of the Beaufort Sea in water depths from five to fifteen feet.

The water depth limit for islands has not yet been defined and is likely to be a function of economics and the short summer for construction. It appears that islands can be built to withstand the worst ice features. But in deeper water, mobile gravity structures of either conical or cylindrical shape may have the advantage.

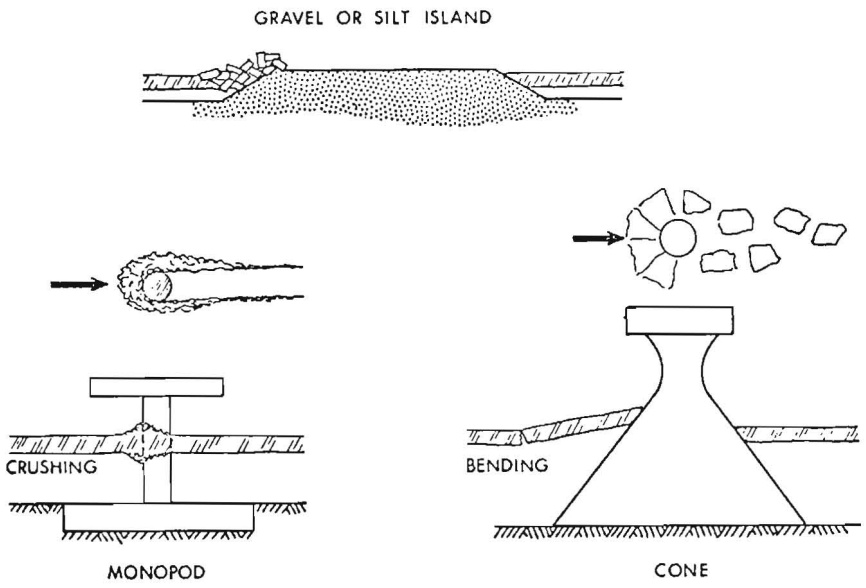

FIGURE 3. TYPES OF ARCTIC OFFSHORE PLATFORMS.

ICE/STRUCTURE INTERACTION

The problem of ice interaction with structures will be discussed in relation to three basic types of structures, namely:

1. structures of narrow cylindrical form, against which the ice fails in crushing,

2. structures of narrow conical form, against which ice fails in bending,

3. wide structures, such as islands, where the presence of an ice foot or refrozen ice rubble may lead to a mixed mode failure involving both crushing and bending.

Ice Action on Narrow Cylindrical Structures (Monopod)

The problem of ice crushing against a narrow circular pile has become a classic problem in the field of ice mechanics. A proper review of previous work on this topic would constitute a lengthy thesis, so the best I can do in the time available is present a few comments to stimulate your thoughts and encourage discussion. But I will also look at the problems in the context of structures for the Beaufort Sea.

For the engineer, the range of recommended values for ice pressure on piers is confusing and obviously unsatisfactory. In a recent paper, DANYS (1975) reports that in Canada, recommended ice pressures during the last twenty years have ranged from 40 to 400 psi.

The platforms in Cook Inlet were apparently designed for a maximum ice pressure of 300 psi. PEYTON (1968) recommends a design ice pressure of 475 psi for arctic ice.

Actual measurements of ice forces on platforms and piers generally indicate lower pressures. In the Cook Inlet, to my knowledge, the maximum measured ice pressure has been less than 200 psi (BLENKARN, 1970). Measurements conducted by NEILL (1970, 1972) on Alberta bridge piers have yielded pressures up to 375 psi, but these were of short duration. SCHWARZ (1970) measured ice pressures on a Baltic pier and obtained pressures up to 150 psi for weak sea ice.

An empirical load correlation for ice crushing against a pier was developed by KORZHAVIN (1971).

$$p = Imk\sigma \qquad (1)$$

where p = ice pressure across the structure diameter and ice thickness

I = indentation factor, which is a function of the structure width (D) to ice thickness (t) and varies from 2.5 for a narrow structure to 1.0 for a wide structure

m = shape factor (equals 1.0 for flat face)

k = contact factor which equals 1.0 for intimate contact

σ = ice strength in crushing.

The usefulness of the equation to the engineer is limited because of the need to input a value for the ice compressive strength (σ). Compressive strength measured on small ice blocks is notoriously variable, being highly sensitive to crystal orientation, degree of confinement, temperature, strain rate and size of sample.

However, despite this limitation, equation (1) includes some useful concepts for ice pressure on piles. It tells us that for wide structures, with $I = 1$, the maximum pressure approaches the uni-axial ice crushing strength (σ_c), and for narrow piers, the ice pressure could be 2.5 times greater. The equation also tells us that the ice pressure is a function of the "goodness" of contact between the ice and pier.

Similar conclusions can be reached from theoretical considerations; the ice can be assumed to behave as an elasto-plastic material with a Tresca yield criterion. MORGENSTERN and NUTTALL (1971)

used this approach, and concluded that an upper bound solution for a flat pier (or indenter) could be represented by the wedge-type failure shown.

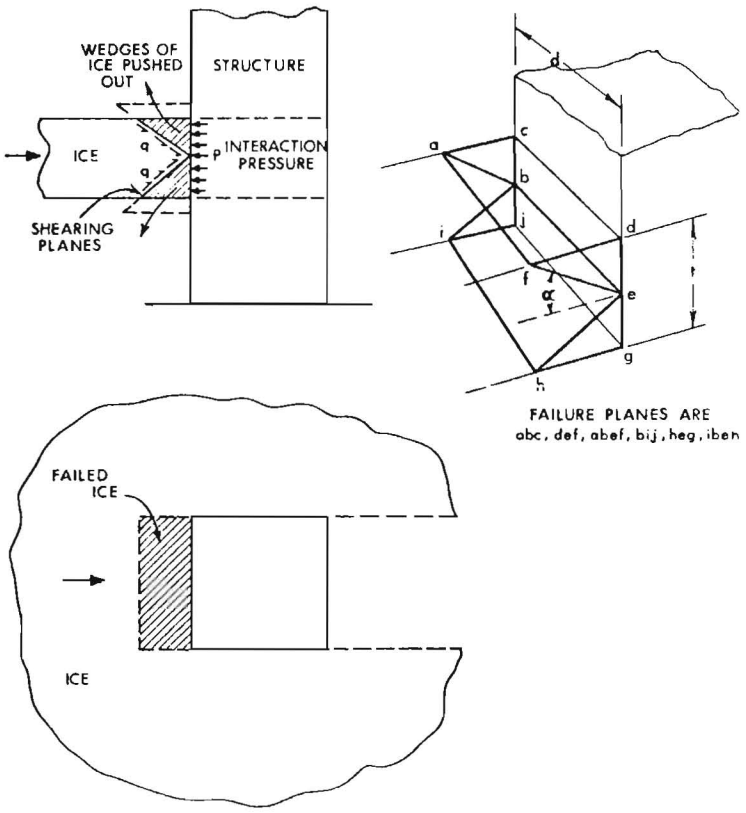

FIGURE 4. WEDGE-TYPE FAILURE (UPPER-BOUND SOLUTION).

This failure concept neatly explains the size effect (I in Korzhavins equation). If the material has a uniform shear strength (q) clearly, for the geometry shown, with 45° wedges.

$$p = 2q + 0.707q\,(t/d) \qquad (2)$$

As the structure width increases relative to ice thickness, the second term becomes negligible and the equation becomes:

$$p = 2q = \sigma c \text{ (for Tresca yield criterion)} \qquad (3)$$

Obviously the model can be used with other failure criteria, such as the Mohr-Coulomb if, as some investigators have detected, ice strength is a function of confining pressure. (ROGGENSACK, 1974)

The failure model can also easily be modified to take account of ice anisotropy and other pier geometries.

The double wedge failure is obviously only applicable to the initial failure peak for ice in intimate contact with the pier. However, similar reasoning can be used to look at subsequent pressure peaks. (Figure 5)

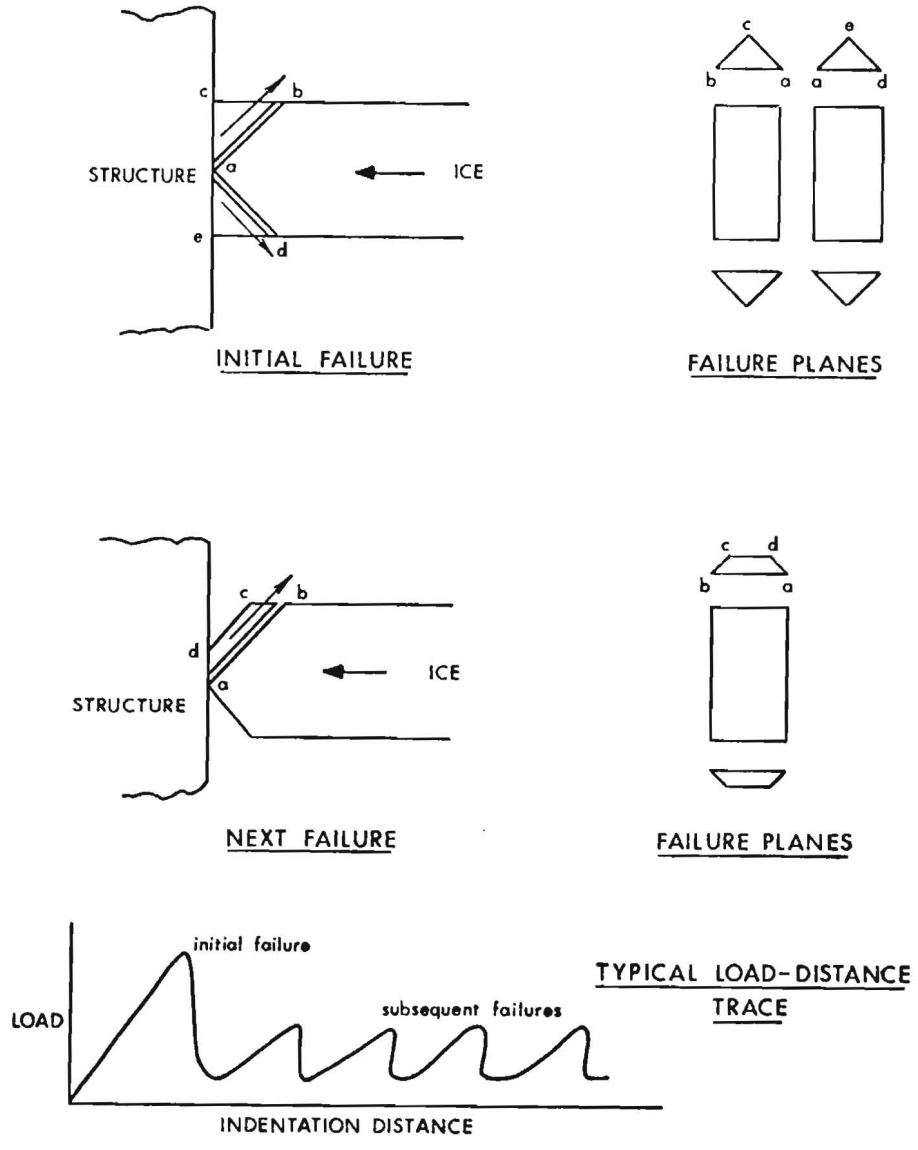

FIGURE 5. UPPER-BOUND SOLUTIONS.

It can easily be shown that for subsequent failures (or continuous crushing) the pressure peaks are about half the initial peak. Also that the ice pressure for continuous crushing is less sensitive to structure width.

To my knowledge, the only published data on the crushing strength of Arctic ice is that obtained by CROASDALE (1970, 1974). In these tests, an active system was used to push piers up to 5 feet wide through the ice. The tests gave ice pressures in the range 600 to 1000 psi except for one low value in the creep regime.

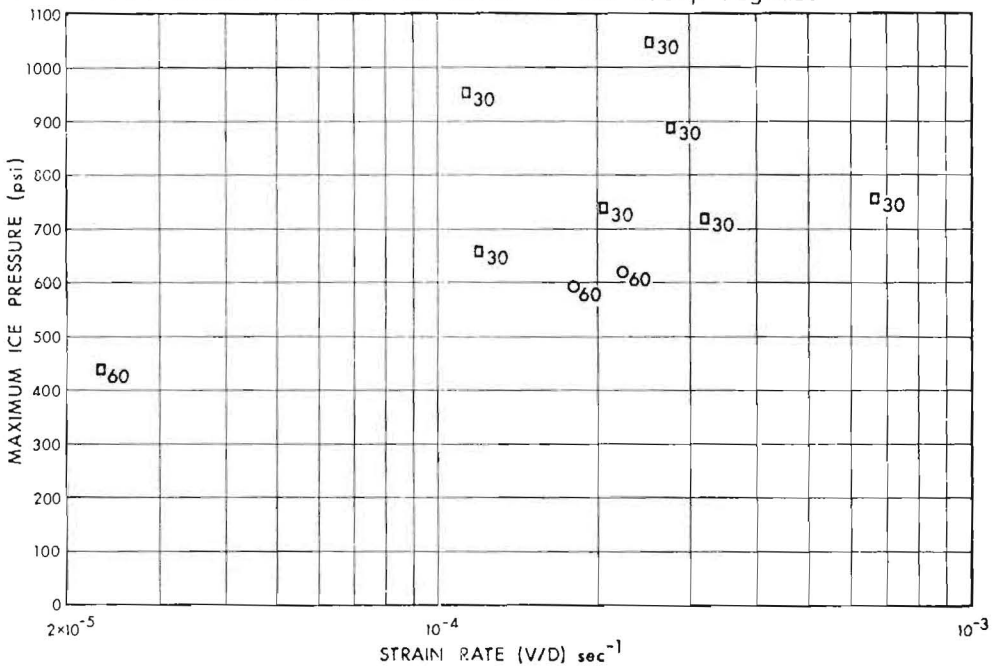

FIGURE 6. RESULTS OF ARCTIC ICE CRUSHING TESTS.
(PIER DIAMETERS SHOWN IN INCHES.)

The pressures obtained on the 60 inch piers were always lower than those obtained for the 30 inch piers. But there is insufficient data to confidently draw a size-effect curve.

However, it is of interest to draw curves through the two groups of tests points based on various theories. (Figure 7)

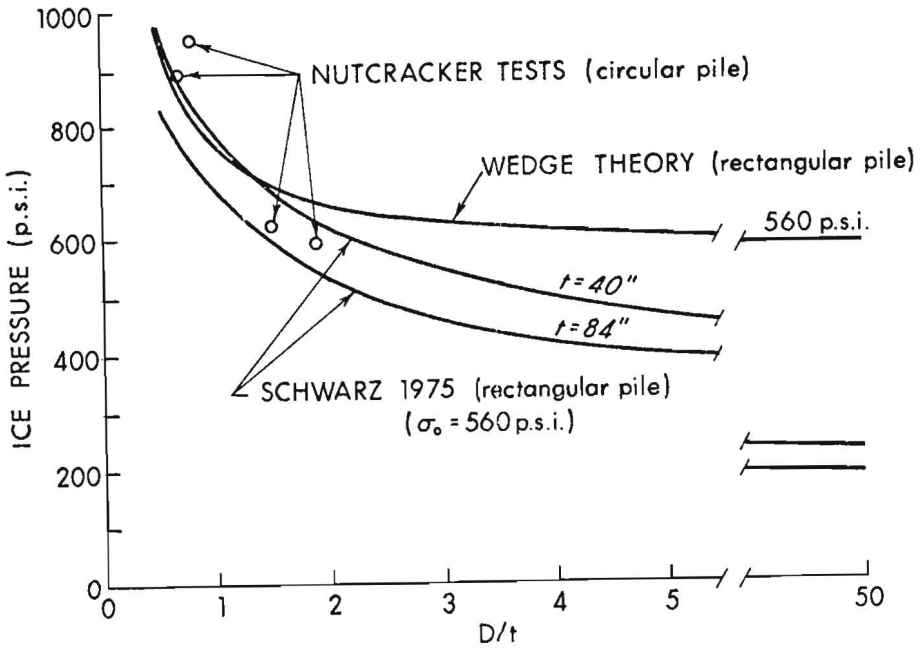

FIGURE 7. COMPARISON OF THEORIES FOR ICE CRUSHING.

Using the wedge theory for a rectangular pile, the best fit we can get is shown as the upper curve. The theory suggests an asymptote of about 560 psi. This would then be the design ice pressure for a wide structure, if we were confident of the data and the theory. However, such confidence is not justified in this example because of the sparse data base.

The correlation quoted by SCHWARZ (1974) and his colleagues for a rectangular pile in complete contact with the ice has also been considered.

The correlation fits our data well for the appropriate test ice thickness of 40 inches. However, for 7 feet of ice, as is appropriate to design of structures in the Beaufort Sea, Schwarz's correlation would give lower pressures. This is especially so at high ratios of D/t.

You can see from the above, that the problem of creating a theory to explain ice crushing loads on structures, remains unsolved.

Getting back now to the problem of predicting ice forces on a cylindrical type structure in the Arctic, JAZRAWI and DAVIES (1975) have described the design of a Monopod type structure for the use in the shallow waters of the Beaufort Sea.

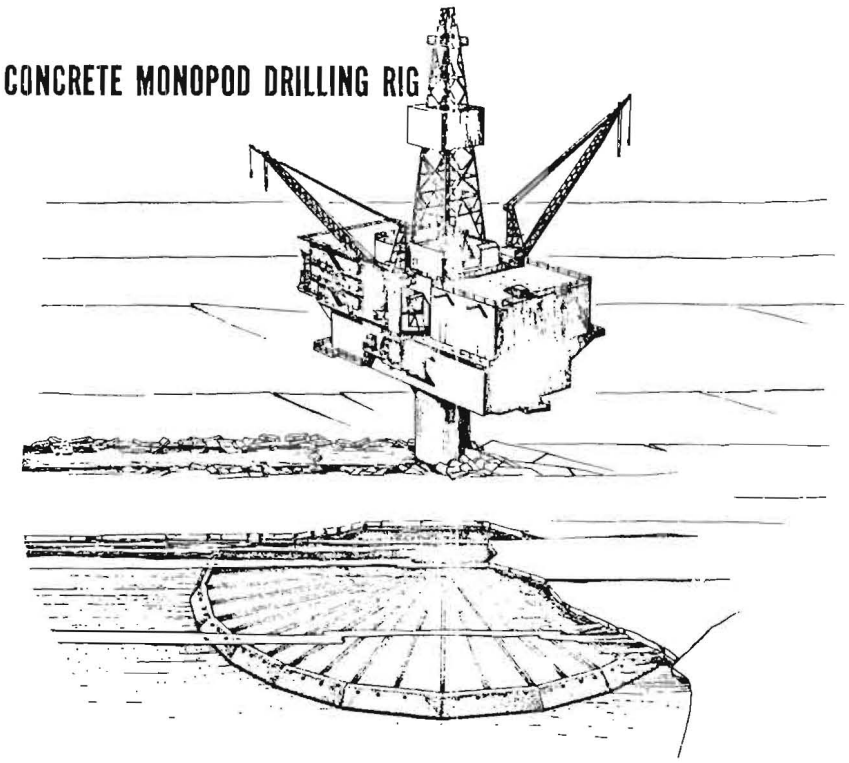

FIGURE 8.

This structure has a 30 foot diameter shaft and is held on location by the friction between the large diameter (320 ft.) hull and the sea bed.

It is designed for a lateral load, 22.5 million pounds, due to a uniform ice sheet crushing against the shaft. But this load is only valid for very shallow water where ice ridges can be ignored.

If such a structure was to be used in deeper water, the loads due to a multi-year pressure ridge would have to be considered. Even if we consider a modest crushing pressure of, say, 300 psi, the load due to a 50 foot thick ridge, would be about 65 million pounds, which is about three times greater than that due to uniform ice.

Clearly, for arctic marine structures of cylindrical shape, the problem of predicting the ice pressure caused by a local ice thickening such as a ridge has a higher priority than the study of interaction with a uniform ice sheet.

Where multi-year ridges are a possibility, the use of a sloping surface to fail thick ice features in bending rather than crushing may lead to lower ice forces.

Ice Action On Narrow Conical Structures

Ice will fail against a conical structure in bending unless the angle of the structure is so steep that crushing occurs at a lower load.

The ice and geometrical parameters governing loads on a concial structure are obviously quite different from those governing the ice pressure due to crushing action.

For ice not frozen to the structure, the total horizontal force on a cone (R) can be separated into two basic compounds.

(1) The force necessary to break the ice. (R_1)

(2) The force necessary to move the broken ice up and around the structure. (R_2)

$$R_1 = f(\sigma_f, t^2, b, \beta, \mu)$$

$$R_2 = f(\varrho_{ice}, d, t, \beta, \mu, E)$$

where
- σ_f is the flexural strength of the ice
- t is the thickness of the ice (or ridge)
- b is the width of the ridge if applicable
- ϱ is ice density
- d is the cone diameter
- β is the cone angle
- μ is the ice-to-structure friction
- E is the elastic modulus of the ice

Actual load equations can be derived mathematically, by model tests, by near full-scale tests or by measurement of forces on an instrumented structure. A combination of all these techniques seems desirable.

(a) Math Models

For math models, the theories developed for plates and beams on elastic foundations can be used to predict the vertical forces necessary to fail the ice.

As an example, some possible ridge loads, calculated from published theories (HETENYI, 1946), are shown in Figure 9.(for a 45° cone)

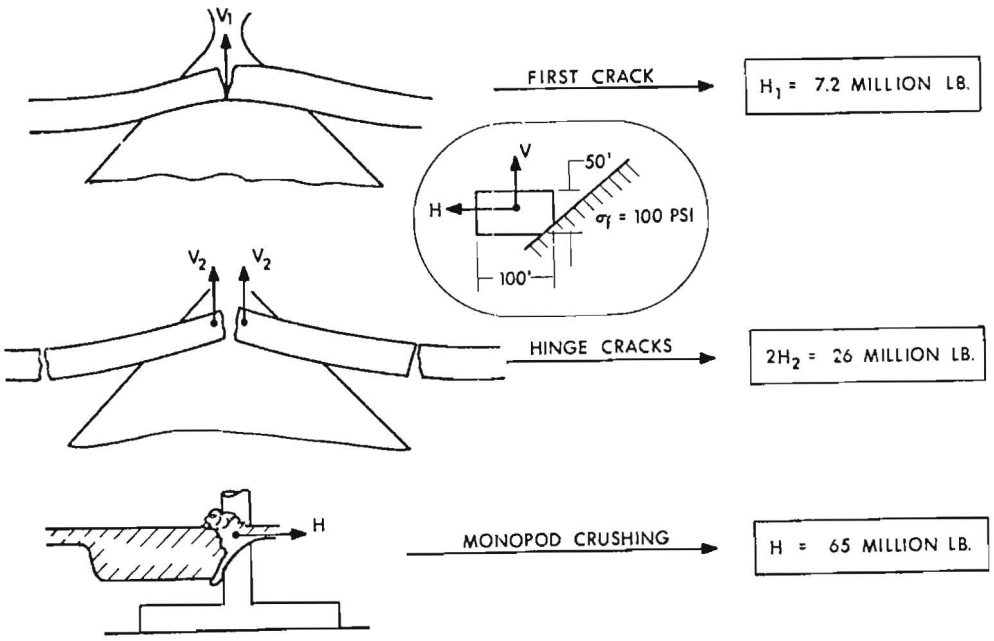

FIGURE 9. TYPICAL RIDGE LOADS.

For a 50 foot thick ridge, 100 feet wide, a centre crack is first formed when the load on the cone is about 7 million pounds. For the ridge to clear around the cone, additional hinge cracks are needed, and their formation requires the cone to sustain a load of about 26 million pounds. (if both cracks occur simultaneously).

This is only an example; obviously better math models should be used to account for the effect of the surrounding ice sheet and for ice ride-up components.

Math models do rely heavily on physical tests for insight into the appropriate failure mechanisms of the ice. Physical tests can be conducted on a model scale or full scale.

(b) Modelling Techniques

It is well known that to properly model ice breaking in bending, the ice flexural strength and ice modulus has to be scaled by the linear scaling factor. Density and friction coefficient should be the same as full scale.

Model basins exist in Europe and North America where such tests can be performed, using either high salinity ice or synthetic ice. For improved confidence, it is obviously desirable to compare model predictions with full scale data.

(c) Full Scale Tests

ROBBINS et al (1975) has described an open-air test facility in Calgary, where such comparisons can be made. The test basin is 200 feet long by 100 feet wide with a towing system that allows ice sheets up to two feet thick to be pulled into an instrumented structure.

FIGURE 10. OUTDOOR ICE TEST BASIN IN CALGARY.

During the past two winters, we have measured the forces acting on 45° cone with a 10 foot waterline diameter, subject to a variety of ice sheets and ridges. This was a cooperative industry program through APOA and the results of this work have not yet been published.

The facility is not a model basin as real ice is used, but the results have been used to confirm and refine math and physical model techniques. It is a cheaper alternative to a full scale instrumented structure. In some ways it is better, because parameters such as

movement rate, ice thickness, and strength can be controlled and adjusted. Also, its much easier and cheaper to work in Calgary than in the Arctic.

Several conical lightpiers have been instrumented in Canada (DANYS, 1975), but so far only preliminary results are available. The lightpiers are unmanned, so the difficulty of obtaining ice thickness and strength to associate with specific force measurements will always be a problem. However, in the long term, the measurements will be very valuable.

Ad Freeze Forces

A cone is only a good shape for ice breaking as long as the ice slides over its surface, if the ice remains stationary long enough for it to freeze to the structure, an adfreeze bond will develop. When ice movement starts again, this adfreeze bond will have to be broken before ice can continue to fail in bending on the structure.

Obviously the adfreeze force is a function of the area of contact and the bond strength between ice and steel (or concrete). Little data has been published on ice bond strengths. But if we assume a nominal (100 psi), a conical structure 80 feet diameter at the ice line and an ice sheet 7 feet thick frozen around it; the adfreeze force works out to be greater than 30 million pounds.

Obviously to reduce adfreeze forces, the cone diameter should be minimized. The use of heat, or anti-friction coatings currently being considered for ice breakers (MÄKINEN, 1975) are other possible ways of reducing these potentially high forces to manageable values.

Local Ice Pressures

Regardless of the total load on a structure, its outer surface will have to be designed for high ice crushing pressures. Experience gained in the use and design of ice breaking vessels should be applicable here.

The ice breaker design codes suggest local ice pressures for design of up to 1200 psi for the bow plating. To my knowledge, no failures have occured in the plating of ships designed to this pressure.

For many structures conceived for the Beaufort Sea, the design thickness of the outer shell is controlled by local ice pressure criteria; and leads to considerably more structural material than would be required to resist the total ice force. So the incentive to refine the prediction of local ice pressures is, therefore, high.

Ice Action on Wide Structures (Islands)

Artificial islands are being used to conduct exploratory drilling in the shallow water of the Beaufort Sea.

RILEY (1975) describes construction of these islands, which takes place in the summer using dredging equipment. Geotechnical aspects of island stability have been described by HAYLEY and SANGSTER (1974).

An island has only three designer controlled variables:

- height (freeboard)
- beach slope angle
- surface area

These three parameters combine to give the dredged fill volume which, for low cost and construction time, should be minimized.

The lateral ice pressure on an island, if high enough, will control the island freeboard for a particular diameter, which in turn is usually determined by the required operational space.

For low ice pressures the island freeboard will be determined by the wave height or ice ride-up.

Clearly there is an incentive to determine ice pressures on these islands.

We can consider the problem of ice action on islands in the context of two distinct ice environments, namely:

- extensive continuous ice motion
- intermittent restricted ice motion

For extensive continuous ice motion, the ice will initially fail in bending on the sloping beach of the island at low loads. In subsequent failures, there are then two possibilities.

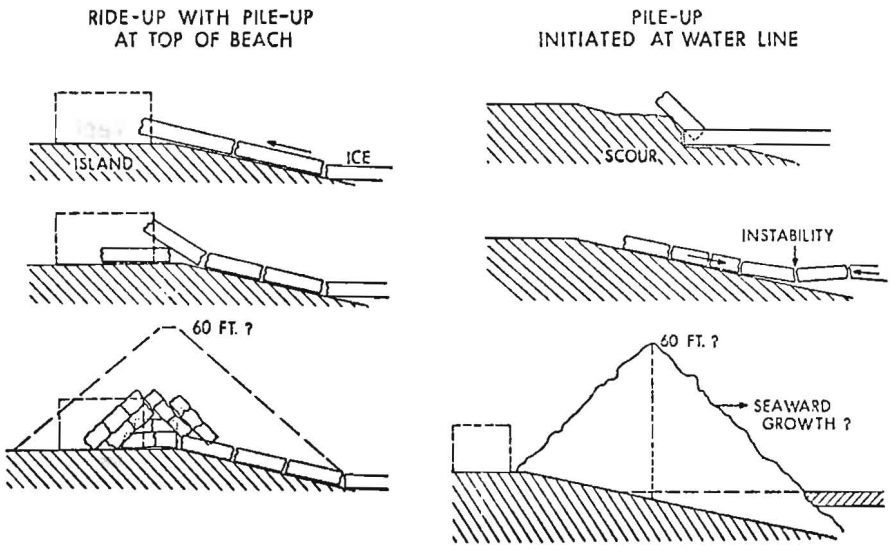

FIGURE 11. ICE PILE-UP ON ISLANDS.

First, the ice is pushed up the beach to the island surface where the change in slope causes the blocks to pile-up on each other. The pile-up will continue to grow symetrically and encroach into the island until a stable height of perhaps 60 feet has been reached, when the rubble will then grow seaward.

The second possibility is that the ice will start to pile-up at the water line so that encroachment onto the island is less likely, and is a function of the height of the pile-up.

So far in our experience these situations are hypothetical as Imperial's artificial islands have not been exposed to extensive ice motion. As we go further offshore, the hazard will increase particularly during break-up when sheets of ice, several miles in extent and several feet thick, can move many miles.

To my knowledge, very little good data exists to examine this phenomena of pile-up on wide structures with sloping beaches. BRUUN and JOHANNESSON (1971), have reported experience with lighthouses in the Baltic where extensive pile-up has been observed. But we are not sure how to apply this experience to the Beaufort with its thicker ice condition.

ALLEN (1970) proposed a theory to predict pile-up height,

$$H = \sqrt{\frac{2pt\sigma}{(1 + 0.25)\tan \beta}}$$

where H is the pile-up height (feet)

p is the effective unit ice pressure (kips/ft^2)

ρ is the density of the piled up ice (kips/ft^3)

t is the ice thickness (feet)

0.25 is the ice to ice friction

β is the angle of the slope of the pile-up

Using this formula, a pile-up height of 80 feet is obtained for 7 feet of ice.

Further examination of this problem by theory, model test and field observations is desirable.

Once a rubble pile has formed around an island, the ice forces will be generated by a stochastic process involving a mixture of ice crushing and bending. This process has been discussed by ASSUR (1972), but no definite solution exists. In any case, a high rubble pile may protect the island against extreme ice forces.

For islands situated in the landfast ice, expecially near shore, the ice will freeze to the island perimeter and form a continuous surface with the frozen crust of the island. If ice movement then occurs and the ice is strong enough, the ice sheet and frozen crust of the island would move as one, resulting in a shear failure of the island through the fill.

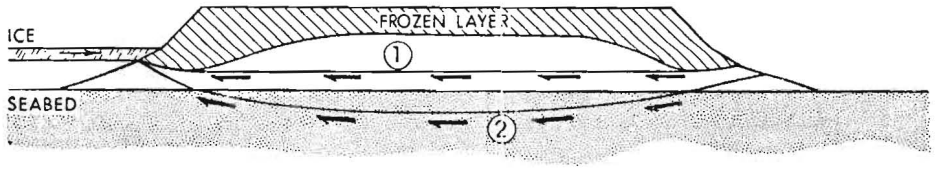

① FAILURE THROUGH ISLAND FILL

② FAILURE THROUGH SEABED

FIGURE 12. POSSIBLE ISLAND FAILURE MODES.

No such island failures have occurred, but then on many of our islands we have defended them against this extreme condition by creating a zone of weakness by slotting the ice around them. These slots are designed to fail at ice pressures much less than that required to cause ice crushing.

The problem of predicting ice crushing pressure across a wide monolithic structure remains unsolved. For the frozen-in condition which I've just described, I know of no precedents or current work which can be used to derive ice pressure.

Our current approach is considered conservative, for we are basing our design ice pressures on crushing tests performed on indenters up to only 12 feet wide. This extrapolation assumes that the ice will fail simultaneously across the width of the island which intuitively seems unlikely.

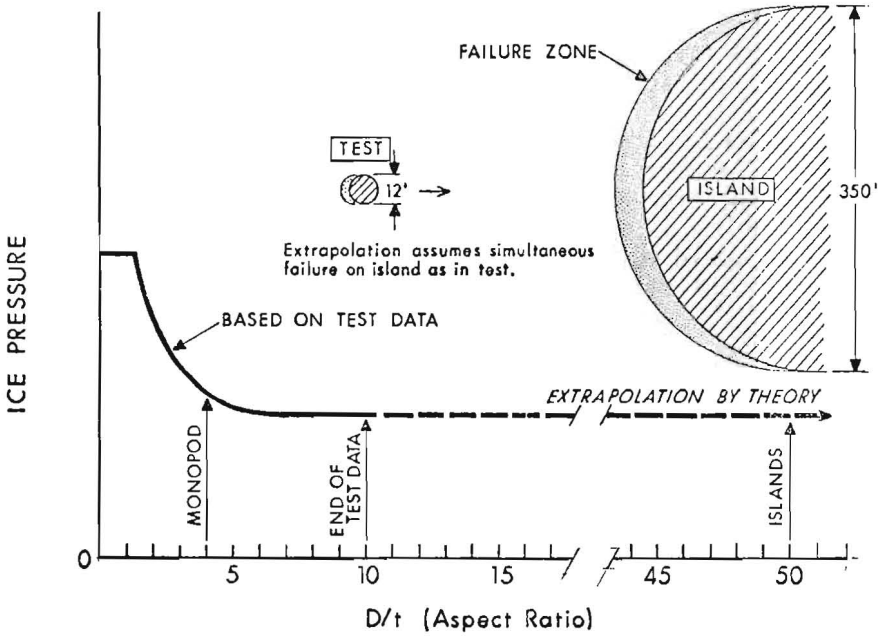

FIGURE 13. DERIVATION OF DESIGN ICE PRESSURE FOR ISLANDS.

In addition to this conservative approach we are, as I mentioned, cutting slots around some of the islands to improve factors of safety.

To better understand ice pressure on islands, we have a programme to measure in-situ the stresses in the ice around them. METGE et al (1975) will be describing a pressure sensor developed for this application, during this symposium.

If slots are used to avoid the potentially high initial ice pressure associated with complete contact, the subsequent ice pressure is that appropriate to ice crushing across a wide structure in a more random fashion. This so called 'continuous crushing' mode may also involve bending failures and may only be amenable to analysis based on a stochastic method. However, the field measurements of in-situ pressures will also provide an insight into this process.

SUMMARY

The coastal zones of the Arctic Ocean are subject to severe ice conditions, and marine structures will experience high ice loads. Except in the very shallow areas, ice ridges will govern the design ice load. Sloping structures are able to withstand the extreme loads due to ice ridges, better than vertical sided structures. However, this advantage may be minimized if ice adheres to the structure and/or if ice rubble interferes with the optimum ice failure and ride-up process. In some areas, the impact by massive ice islands, may threaten the survival of permanent marine structures.

ACKNOWLEDGEMENTS

I would like to thank Imperial Oil Limited, for permission to present this paper.

Many of the projects mentioned were conducted through cooperative research programmes (APOA); the support of the participating companies is acknowledged.

Finally, I would like to thank colleagues and co-workers who have contributed to the topics discussed in this paper.

REFERENCES

ALLEN, J.L., (1970), Analysis of Forces in a Pile-Up of Ice NRC Technical Memo No. 98, Ottawa, November, 1970.

ASSUR, A., Forces in Moving Ice Fields, POAC Conference, Trondheim, 1971.

BLENKARN, K.A., Measurement and Analysis of Ice Forces on Cook Inlet Structures, Offshore Technology Conference, Houston, 1970.

BRUUN, P.M. and JOHANNESSON, P., The Interaction Between Ice and Coastal Structures. POAC Conference, Trondheim, 1971.

CROASDALE, K.R., Crushing Strength of Arctic Ice. The Coast and Shelf of the Beaufort Sea, the Arctic Institute of North America, 1974.

DANYS, J.V., Effect of Ice and Wave Forces on the Design of Canadian Offshore Lighthouses, Canadian Journal Civ. Eng. 2 138(1975).

DANYS, J.V., (1975), Offshore Installations to Measure Ice Forces on the Lightpiers in Lac St. Pierre, IXth Inte. Conference on Lighthouses and Other Aids, Ottawa, 1975.

HAYLEY, D.W., and SANGSTER, R.H.B., Geotechnical Aspects of Arctic Offshore Drilling Islands, 27th Canadian Geotechnical Conference, November, 1974, Edmonton, Canada.

HETENYI, M., Beams on Elastic Foundation, University of Michigan Press, 1946.

JAZRAWI, W. and DAVIES, J.F., A Monopod Drilling System for the Canadian Beaufort Sea. SNAME "Ice Tech 75", Montreal, 1975.

KORZHAVIN, K.N., Action of Ice on Engineering Structures, CRREL Translation 260, September, 1971.

KOVACS, A., WEEKS, W.F., HIBLER, W.D., Pressure Ridge Characteristics in the Arctic Coastal Environment, POAC Conference, Trondheim, 1971.

MÄKINEN, E., LAHTI,A., RIMPPI, M., Influence of Friction on Ice Resistance, Search for Low Friction Surfaces. SNAME 'Ice Tech 75', Montreal, 1975.

METGE, M., STRILCHUK, A. and TROFIMENKOFF, P., On Recording Stresses in Ice. IAHR Symposium, Hanover, U.S.A., 1975.

MORGENSTERN, N.R., and NUTTALL, J.B., The Interpretation of Ice Strength from In-situ Indentation Tests. (Report to Imperial Oil Ltd., March 1971)

NEILL, C.R., (1970), Ice Pressure on Bridge Piers in Alberta, Canada. IAHR Symposium, Reykjarik, 1970.

NEILL, C.R., (1972), Force Fluctuations During Ice Floe Impact on Piers. IAHR Symposium, Leningrad, 1972.

PEYTON, H.R., Ice and Marine Structures. Part 3 Ocean Industry Vol. 3, No. 12, December, 1968.

ROBBINS, R.J., METGE, M., TAYLOR, T.P., VERITY, P.H., Test Techniques for Study of Ice Structure Interaction. POAC 3rd Conference, Fairbanks, 1975.

ROGGENSACK, W.D., Large Scale Laboratory Direct Shear Tests on Ice. University of Alberta, Edmonton, January, 1974.

SCHWARZ, J., (1970), The Pressure of Floating Ice Fields on Piles. IAHR Symposium, Reykjavik, 1970.

SCHWARZ, J., HIRAYAMA, K., and WU, H.C., An Investigation of Ice Forces on Vertical Structures. Iowa Institute of Hydraulic Research Report No. 158, June, 1974.

THIRD INTERNATIONAL SYMPOSIUM ON
ICE PROBLEMS
Hanover, New Hampshire, USA

INTERMITTENT ICE FORCES ACTING ON INCLINED WEDGES

P. Tryde
Assoc.Prof.

Institute of Hydrodynamics
and Hydraulic Engineering
Technical University of Denmark

Lyngby
Denmark

1. INTRODUCTION

A theoretical and experimental investigation of the rupture pattern in front of an inclined wedge has been performed in order to determine the force fluctuations during the impact of a drifting ice floe.

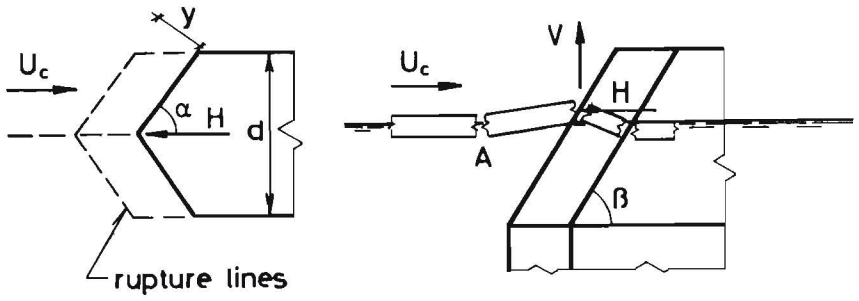

Wedge with inclined faces

The present work is based on the pioneering studies and recommendations made by K. N. Korzhavin, presented in his thesis 'Action of ice on engineering structures'. A theoretical determination of the rupture pattern has, to the knowledge of the author, not previously been presented.

The forces acting are of an intermittent nature since they increase abruptly each time a parallelogramic piece is about to break off, after which the force decreases until the next encounter takes place. The distance y in the figure has been observed and theoretically determined at approx. 2-6 times the thickness of the ice.

2. SYNOPSIS

The maximum force on a given section in front of a structure with vertical faces can be written

$$F_{max} = r_c \; e \; d \quad \text{(kNewton)}$$

where

r_c is the compression strength (in kN/m^2)
e is the thickness of the ice (in meters)
d is the width of the structure (in meters)

The actual force acting on the inclined wedge will be reduced

$$F = C_F \; F_{max}$$

C_F is a function of the system data

$$C_F = \phi \; (E/\rho \; u_c^2, \; e/d, \; y/e, \; r_b/r_c, \; \alpha, \; \beta, \; \mu)$$

where E is Young's modulus (in kN/m^2), ρ is the density of ice (in t/m^3), u_c is the velocity of the floe (in m/sec), y is the characteristic breaking off distance (in meters), r_b is the flexural strength (in kN/m^2), 2α is the included angle at the point of wedge in horizontal plane, β is the inclination of wedge to horizontal, and μ is the coefficient of friction.

An approximate formula of C_F, valid in the interval $0 \leq C_F \leq 0.4$, can be written

$$C_F = \frac{6.4 \sqrt{\frac{r_b}{r_c}}}{\sqrt{C}} \tag{1}$$

where

$$C = 0.16 \sqrt{\frac{E}{\rho \; u_c^2 \; \sin^2\alpha}} \; \frac{C_1}{C_2} \; C_3^2 \tag{2}$$

$$C_1 = 1 - \mu \frac{\tan \beta}{\sin \alpha} \qquad C_2 = \mu + \frac{\tan \beta}{\sin \alpha} \qquad C_3 = 6 \frac{C_1}{C_2} + 6 \frac{e}{d} \cos \alpha$$

Formula (1) is derived by dynamic considerations and it is assumed that no other exterior forces are acting on the floe. Therefore the velocity should not be less than approx. 0.1 m/sec with an upper limit of approx. 4 m/sec in order to maintain the assumed type of rupture. The practical interval of α is from 30^o to 60^o and for β from 45^o to 70^o. The friction coefficient will seldom exceed 0.1, but in some cases it may be considerably higher.

The realistic value of the factor C_1/C_2 will vary from 0.1 to 1.0, depending on the combination of α, β, and μ. Graphs showing the relationship will be presented in Diagram I. The factor e/d can vary from zero to 0.3 limited by the assumptions made for the rupture patterns. The ratio between the flexural strength and the compression strength may vary from 0.2 to 0.5.

Looking at the formulae it can be seen that

(1) The influence of ρ, u_c, and E is not appreciable, since it is in the fourth root. However, an increase in velocity should give a slight increase in the force. Low values of E should also result in higher values of C_F.

(2) The increase of β will result in a decrease in C_1/C_2 giving higher values of C_F. The increase of α results in an increase of C_1/C_2. For low values of μ, C_1/C_2 approaches 1.0. For $\mu \to 0.3$, C_1/C_2 can obtain rather low values - resulting in values of C_F up to 1.0, i.e. no reduction at all.

(3) r_b/r_c may vary from 0.2 to 0.5, increasing C_F for increasing values of r_b/r_c, but only with the square root of the ratio.

(4) Finally the influence of e/d shows that for $e/d \to 0$ greater values of C_F are obtained. The upper limiting value of 0.3 will produce lower values of C_F. This is due to the eccentric, combined bending and axial loading along the rupture line, producing high stresses.

Example:

$\rho = 0.9 \quad (t/m^3), \quad E = 2 \cdot 10^5 \quad (kN/m^2), \quad u_c = 1.0 \quad (m/sec),$
$\alpha = 50^o, \quad \beta = 60^o, \quad \mu = 0.1, \quad r_b/r_c = 0.3, \quad e/d = 0.1,$
$C_1/C_2 = 0.32, \quad C_3 = 6 \cdot 0.32 + 6 \cdot 0.1 \cdot 0.64 = 2.3.$

From formulae (2) and (1)

$$C = 0.16 \sqrt{\frac{2 \cdot 10^5}{0.9 \cdot 0.77^2}} \; 0.32 \cdot 2.3^2 = 166 \qquad C_F = \frac{6.4 \sqrt{0.3}}{\sqrt{166}} = 0.27$$

It should be noted that formula (1) is an approximation, and that the preliminary form presented in this paper may be revised as the findings of the investigation proceed. The formula is valuable, when planning model tests in order to verify the much more complex theoretical formulae.

3. EXPERIMENTAL VERIFICATION

In order to verify the theory presented, model tests have been performed with an artificial material developed at the ISVA-institute. This material consists of plaster of Paris, plastic granulate and several additives, which will be described in detail in article 5. The bending strength of the material is approx. 150 kN/m^2 and its Young's modulus approx. 10^5 kN/m^2, but these parameters can be adjusted to suit the Froude model law, which apply in this case.

The tests have been performed in a 2 m wide flume with a water depth of 0.3 m. A floe of the artificial material approx. 4 m long is floated to strike an 0.16 m wide inclined wedge. Velocities of the floe ranging from 0.1 to 0.7 m/sec have been used.

The forces acting on the wedge, horizontal as well as vertical, have been electrically recorded. The results for various combinations of the parameters have been plotted, using the dimensionless parameters

$$C_{\cdot} = 0.16 \sqrt{\frac{E}{\rho\, u_c^2 \sin^2\alpha}}\ \frac{C_1}{C_2}\ C_3^2 \quad \text{and} \quad C_F$$

to characterize the wedge parameters.

The results of the tests are shown in Diagram I represented by the dots. Various system constants have been used in the tests in order to obtain a wide range of C_F values. The strength parameters of the artificial material correspond to $\varepsilon = 0.2$.

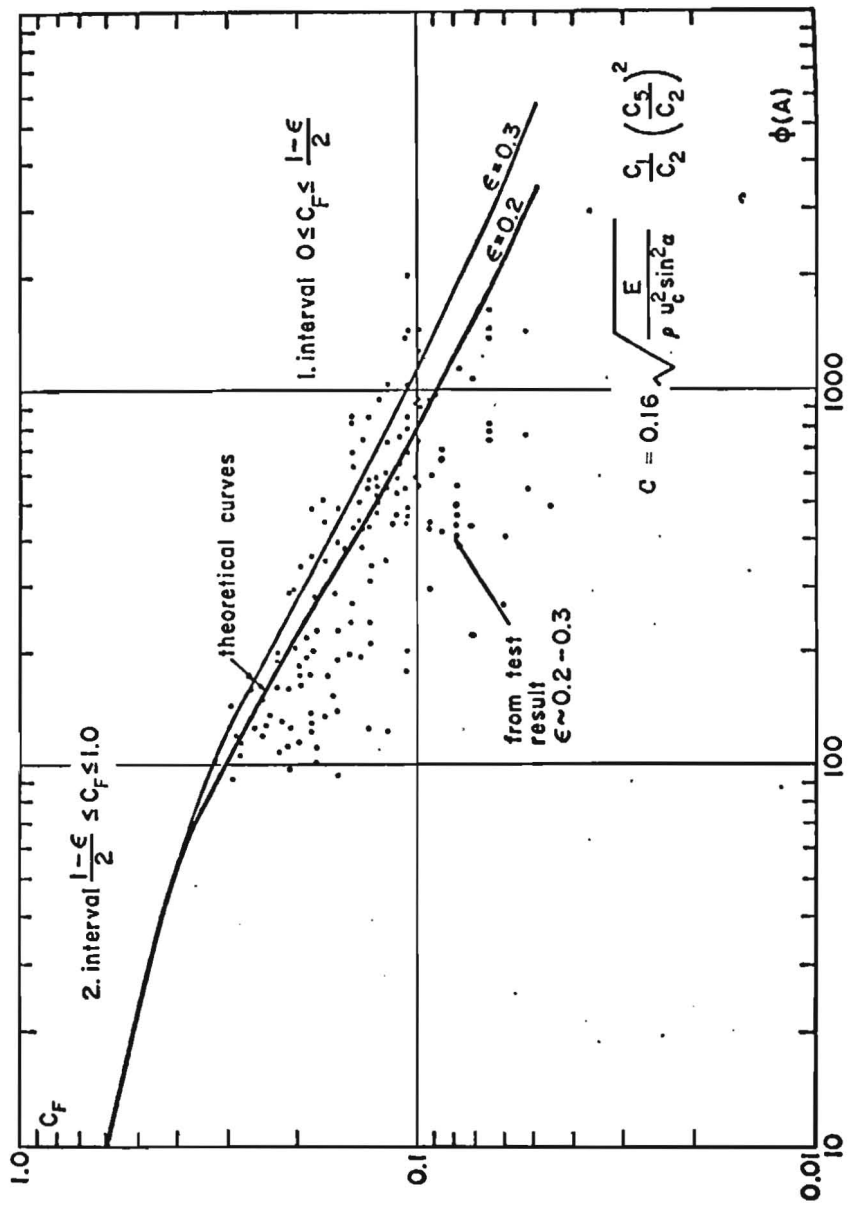

Diagram I

4. INTERMITTENT NATURE OF FORCE

It should be noted that the forces are of an intermittent nature, which should be considered when using the results in engineering design. The period of time between each peak force can be expressed

$$T_c = \left(\frac{\gamma}{e}\right) \frac{e}{u_c \sin \alpha}$$

which will normally be from approx. 0.5 to 5 sec in the prototypes. Each peak of force is taking place within 1/5 to 1/50 of a second.

5. ARTIFICIAL ICE

The artificial material consists of: Plaster of Paris: 100 gr., Plastic granulate (diam. 1 to 2 mm): 9 gr. (bulk weight 70 gr. per liter), NaCl (ordinary salt): 17 gr., Borax: 0.25 gr., Air-entraining agent: 2 gr., and Water: 50 gr. The salt solution acts as a strength reducer. The compression strength is approx. 500-1000 kN/m^2 and the bending strength approx. 100-200 kN/m^2 (shear strength approx. 250-500 kN/m^2). Density of the material: 0.94 gr/cm^3.

6. CLOSING REMARKS

The formulae given above are based on a theoretical investigation verified by model tests with artificial and natural ice.

Since the investigation is not completed, revisions may be introduced in the formulae given in this paper.

7. REFERENCES

Engelund, F.: 'Added moment of inertia for a rotating plate', Progr. Rep. 12, pp. 11-15, Coastal Engrg. Lab. and Hydraulic Lab., Tech. Univ. Denmark, Sep. 1966.

Korzhavin, K.N.: 'Action of ice on engineering structures', Novosibirsk 1962. TL 260, Draft transl. 260, Corps Engrs., U.S. Army Cold Reg. Res. and Engrg. Lab. (CRREL), Hanover, New Hampshire, Sep. 1971.

Nevel, D.E.: 'A semi-infinite plate on an elastic foundation', Res. Rep. 136, U.S. Army Cold Reg. Res. and Engrg. Lab. (CRREL), Hanover, New Hampshire, March 1965. DA Task IV025001A13001.

Reeh, N.: 'Impact of an ice floe against a sloping face', Progr. Rep. 26, pp. 23-28, ISVA, Tech. Univ. Denmark, Aug. 1972.

Tryde, P.: 'A method of predicting ice pilings - Impact of floe against inclined plane', Progr. Rep. 26, pp. 29-33, ISVA, Tech. Univ. Denmark, Aug. 1972.

Tryde, P.: 'Forces exerted on structures by ice floes', 23rd Int. Nav. Congr., S.II-4, pp. 31-44, Ottawa, July 1973.

THIRD INTERNATIONAL SYMPOSIUM ON
ICE PROBLEMS
Hanover, New Hampshire, USA

ICE FORCES AND VIBRATIONAL BEHAVIOUR OF BOTTOM-FOUNDED STEEL LIGHTHOUSES

Mauri Määttänen
Associate Professor

University of Oulu
Department of Mechanical Engineering

Oulu
Finland

Abstract

The bottom-founded tubular steel cylinder type lighthouse is very sensitive to ice-crushing induced vibrations. The structure tends to vibrate to the frequencies of its natural modes. Resonant condition is always possible for an ice force with a suitable ice drifting speed. To bring the vibration level down low enough for conventional types of lantern equipment it is more economical to arrange vibration isolation for the overwater structures than to stiffen underwater structures. An efficient vibration isolation system has been developed and tested using a scale model. Design work is in process for the first full-scale vibration isolated lighthouse.

1. Introduction

During summer 1973 two lighthouses, Kemi I and II, and 17 other smaller route markers were constructed at the northernmost end of the Gulf of Bothnia. All of them vibrated

violently during ice action, some secondary structural failures occurred and the Kemi I lighthouse collapsed totally. The structures of these new lighthouses were steel cylinders: the foundation pile was hammered deep into the sand of the sea bottom and the underwater pile narrowed conically to the waterline in order to minimize ice forces. The above-water structures were widened to accommodate conventional types of lighthouse rooms, app. 1a. The basic idea of this low-weight steel lighthouse was a cheap and simple structure with a minimal amount of construction work at sea.

The University of Oulu was requested by the Finnish Board of Navigation to study the causes of the vibrational behaviour of the Kemi I lighthouse as soon as lantern equipment failures were discovered at the beginning of winter 73/74 after ice formation and drifting had begun. Already the crushing of a relatively thin ice sheet had caused severe vibrations. Very soon fatigue failures appeared in the secondary structures. However, the final collapse in the spring was caused by static ice loads.

Measurements and observations showed the sensitiveness of this type of lighthouse to vibrations. An approximate formula was yielded to find the resonant condition. A mathematical FEM model was made to simulate the vibrational response of ice forces. The results verified the measured data and made it possible to check design calculations for future lighthouses.

It was realized that it is not possible to construct a steel cylinder-type lighthouse that is both cheap and also rigid enough to withstand ice-load induced vibrations without an effective vibration isolation system for the above-water structures. A system with springs and shock

absorbers - comparable with the car suspension system - was developed, simulated by the computer and tested with a scale model. The results verified the expected behaviour and now it seems that the low-weight steel lighthouse with vibration isolation will be a very competitive alternative.

2. Measurements and observations of vibrations and ice forces

During measurements ice 10 to 55 cm thick including pressure ridges drifted 200...300 meters per hour in an air temperature of -16 ^{o}C. Vibrations were measured by acceleration transducers and registered on an oscillograph plotter.

Three typical types of vibrations were observed but measurements could be performed only on the 10 cm thick ice. While the 55 cm thick ice or pressure ridges were crushing, vibrations were so violent that it was not safe to stay in the lighthouse.

Most common was the vibration type in which the ice force resonated according to the second natural mode of the structure. This might go on unchanged for several minutes while the 10 cm thick ice was crushing. Measurements at the waterline showed a frequency of 3.85 Hz, an acceleration level mean of 0.3 g with max. 1.2 g and displacement amplitudes of 1.3 cm. The acceleration values were mean 0.7 g with max. 1.8 g at a point 8.8 m above sea level.

While the 55 cm thick ice or a pressure ridge was crushing the ice load tended to resonate according to the first natural mode of the structure. According to visual observations frequency was 0.8...0.9 Hz and the amplitudes at the top of the lighthouse reached up to 20 cm. A frequency

of 0.83...0.85 Hz was also registered on the oscillograph plotter. This yields an acceleration of 0.58 g at the top of the lighthouse if the vibration is taken to be sinusoidal. Displacement amplitudes at the waterline were about 5 cm. Values of twice this amount would be expected with maximum ice thicknesses in the Gulf of Bothnia.

While the drifting ice cover was thickening a vibration type existed consisting of a combination of the first two natural modes. At the beginning of the cycle, when the ice failed and crushed, the sudden release of the load caused the structure to spring out of its deflection with all its natural modes. Of these the first two are most dominant, and as the second is much faster crushing will start with the second mode. During the return phase of the second mode the foundation pile came loose from the ice edge and later hit against it. At this stage all the energy of the second mode was dissipated and the crushing continued next only by the first mode for the remaining half cycle. A typical double blow crushing noise was heard during this type of vibration.

In March 74 when the above-water structures came loose from the foundation pile a fourth type of displacement response due to ice loads was observed. The thickness of the fast ice cover varied from 53 to 93 cm and the air temperature was -1 ^{o}C. The foundation pile stuck to the edge of the ice, the displacement grew linearily with the ice drifting speed until the resistance of the structure exceeded the crushing strenght of the ice and the ice crushed. The displacement was very quickly reduced to zero after which the foundation pile stuck to the edge of the ice,

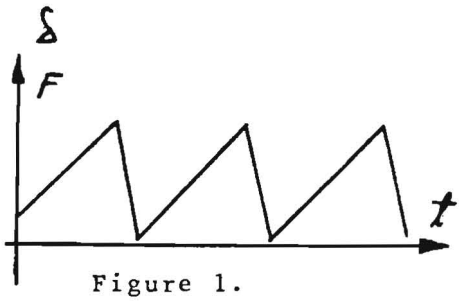

Figure 1.

starting a new cycle without any additional vibrations, fig. 1. In 93 cm thick ice the displacement average, peak to peak, varied around 10 cm while the max. values reached 20 cm. This means a max. pulsating ice force of 3.5 MN or a mean ice crushing strength of 350 N/cm^2.

The ice load which brought down the foundation pile at the beginning of May was calculated to be at least 4.4 MN or a mean ice crushing strength of more than 425 N/cm^2 in the case of a 93 cm thick fast ice cover. More evidently pressure ridge loads caused the foundation pile to collapse.

3. Resonance condition

The vibration measurements and observations showed that the frequency of the ice load tends towards the natural frequencies of the structure. The shape of the ice force function is similar to the displacement function, fig. 1. This is also verified by measurements /1/. The critical dynamic loading for the structure will be the one resonating with the natural frequencies.

The properties of structure and ice may be approximately interrelated for the resonant condition. The maximum deflection δ_c can be approximated

$$\delta_c = \frac{F_c}{k} \qquad (1)$$

where k = foundation pile stiffness coefficient (the spring constant for the ice load). This follows from the fact that during low frequency resonation the dynamic inertia forces for the maximum deflection of the foundation pile are negligible compared to the ice force, usually less than 10 % as stated by computer runs. The maximum ice force F_c just before crushing begins is

$$F_c = \sigma_c h d \qquad (2)$$

where σ_c = ice crushing strength, h = ice thickness and d = diameter of pile.

Since the mean crushing length per cycle is almost the same as δ_c it may be calculated by referring to fig. 1. using the ice drifting speed v and crushing frequency f_c

$$v = f_c \delta_c \qquad (3)$$

Eliminating δ_c and F_c yields the resonant condition

$$f_c = \frac{kv}{\sigma_c h d} \qquad (4)$$

Evidently it is always possible to have such an ice drifting speed that the resonance is achieved. This is true regardless of the simplifications in the above equations. Also the measurements verify the equation 4. The data v = 200-300 m/hour, h = 10 or 55 cm, σ_c = 350 N/cm^2 (t = -16 $^{\circ}$C), k = 256 kN/cm, d = 110 cm give

$$f_c = 0.67...1.01 \text{ Hz} \quad (h = 55 \text{ cm})$$
$$f_c = 3.70...5.54 \text{ Hz} \quad (h = 10 \text{ cm})$$

These values coincide very well with the first two natural frequencies 0.85 and 3.85 of the Kemi I lighthouse.

More stringently the properties of structure and ice can be interrelated using the theory of self oscillations. The discretized dynamic equations of motion

$$[k]\{\delta\} + [d]\{\dot{\delta}\} + [m]\{\ddot{\delta}\} = \{F(t)\} \qquad (5)$$

have a loading term dependent on the ice crushing strength rate which in turn may be expressed using the velocity vector $\{\dot{\delta}\}$

$$\{F(t)\} = \{F_0\} + \{F_1(\dot{\sigma})\} = \{F_0\} - [\lambda]\{\dot{\delta}\} \quad (6)$$

Here $\lambda = \lambda(\dot{\sigma})$ but it is linearized for convenience. The equation (5) may now be written

$$[k]\{\delta\} + ([d] + [\lambda])\{\dot{\delta}\} + [m]\{\ddot{\delta}\} = \{F_0\} \quad (7)$$

Since $\{F_0\}$ = constant the possibility for vibrations depends on the sign of determinant

$$\det([d] + [\lambda]) \quad (8)$$

The equation (7) is stable and no resonant vibrations are to be expected when the ice drifting speed is low, while determinant 8 remains positive. As ice drifting speed increases the curve of ice crushing strength will have a negative slope /2/ and in case the negative damping due to stress rate dependent ice crushing strength becomes greater than positive structural damping the determinant 8 becomes negative. This gives theoretical basis for the oscillations during ice crushing.

The equation 7 interrelates the properties of ice and structure during vibrations. In any case the most important parameters are those in equation 4. In addition there will be the mass and damping effects of the structure and ice. The $\dot{\sigma}$ will also be dependent on ice drifting speed v and pile diameter d with the usual ice properties. Also it should be mentioned that ice properties are random variables and so the response of the lighthouse due to ice forces will be a random variable.

4. Computer simulation

A beam FEM model was constructed to simulate the vibrational behaviour of the steel lighthouse under pulsating ice forces according to figure 1. The structure, app. 1a, was divided into 12 elements with distributed masses. In all 26 degrees of freedom were used. The dynamic response was calculated using the principal mode presentation with at least five lowest natural modes. The integration was carried out by the fourth order Runge-Kutta method.

The support rigidity of the sand at the bottom of the sea was first taken to be distributed triangularly according to Blum's model, fig. 2a, but it had to be tuned trapezoidally, fig. 2b, in order to obtain the same first natural frequencies by the computer run as measured. The support rigidity of the topmost layers of sand was less than 10 % compared to the deepest layers, but it had a significant effect on the first two natural frequencies.

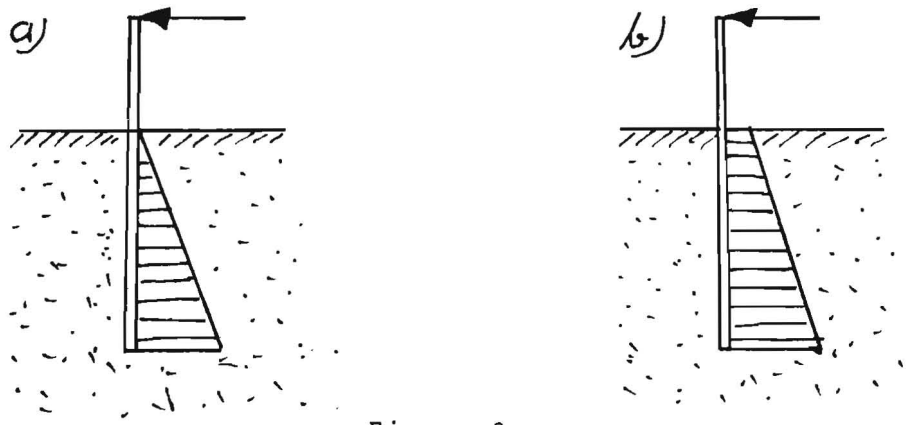

Figure 2.

The relative damping coefficients for the principal modes varied from 0.1 to 0.5. The effects of structural damping, hydrodynamic losses and the foundation damping

are small compared to energy dissipation during ice crushing. The above high damping values had to be used in order to obtain results that matched the aperiodic damping observed during crushing, fig. 1.

The computer simulations verified the sensitiveness to vibrations of the low-weight steel lighthouse. Ice forces due to a relatively thin ice cover would already cause too severe vibrations to the above-water structures for occupation or even for conventional types of lantern equipment.

5. Refined design and vibration isolation

For future purposes a more stringent desingn criterion was adopted. Structures have to be stressed against both a maximum pressure ridge statically and a resonant ice force dynamically. The resultant pressure ridge load will be four times the maximum ice force of the fast ice cover. The dynamic pulsating ice force will also be selected using the maximum ice thickness and the ice crushing strength will be adjusted unlinearily with the pile diameter/ice thickness ratio according to Tryde's formula /3/.

In order to obtain vibration levels low enough at the above-water structures for lighthouse purposes it is more economical to arrange a vibration isolation system rather than to stiffen underwater structures. Dimensioning only against ice forces yields a too flexible structure with great acceleration values at the top of the lighthouse.

The new steel lighthouse design, app. 1b, consists of a tubular underwater structure similar to the earlier Kemi I but the above-water structures are supported by special springs and shock-absorbers on the foundation

pile. The stiffness of the springs is so low that sharp displacements during ice crushing cannot contribute to high acceleration values in the upper structures. A damping greater than 30 db may be achieved. The shock absorbers must be capable of dissipating sufficiently vibrational energy during the resonant condition so that the relative movement between the upper and lower structures will not become too large.

The operation of the vibration isolation system was first simulated by computer runs. As the results were encouraging a scale model 1:2 was made and tested in a hydropulsator using load functions according to figure 1. The tests verified the computer results. Now design work is in process for a full-scale vibration isolated test lighthouse. The selected construction site will be in the southern part of the Gulf of Bothnia with a water depth of 11 meters and maximum ice thiknesses of 70 cm. The construction is planned to be completed before winter 76/77.

References

1. Peyton, H.R.: "Ice and Marine Structures, Part 2 - Sea Ice Properties" Ocean Industry, (December, 1968), Vol 3, No. 9.

2. Weeks, W. and Assur, A.: (1967) The Mechanical Properties of Sea Ice. USA CRREL Science and Engineering Report 11-C3.

3. Tryde, P.: "Iskrafter virkende på slanke konstruktioner og på kile med skrående forside." Symposium kring isfrågor, Ingengörsvetenskapsakatemien, Meddelande 190, Stockholm 1974.

Appendix 1.

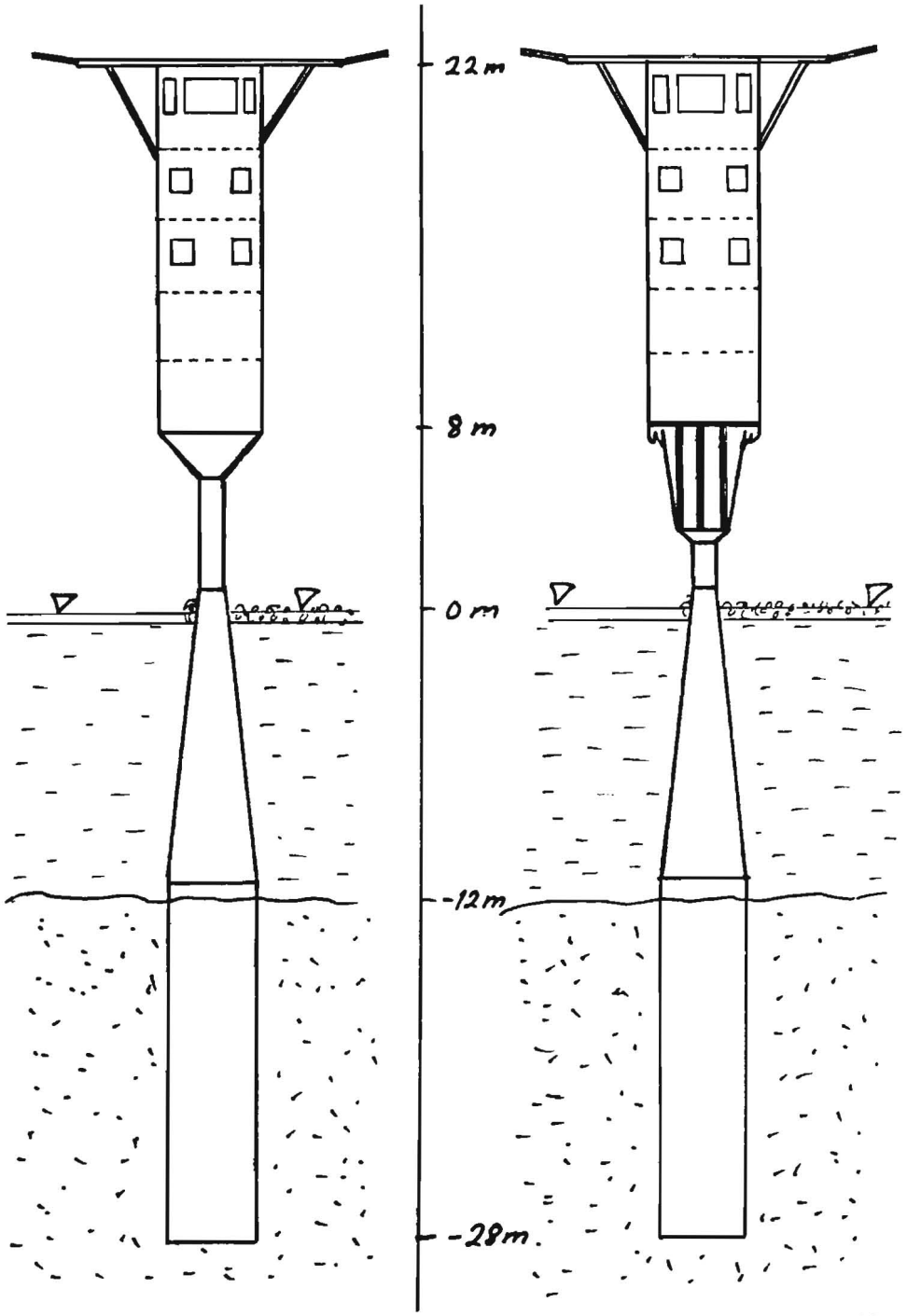

a) Kemi I

b) A lighthouse with vibration isolation system.

THIRD INTERNATIONAL SYMPOSIUM ON
ICE PROBLEMS
Hanover, New Hampshire, USA

THE OSCILLATING ICEBREAKING PLATFORM

CARSTENS, T. Head of Research	River and Harbour Laboratory	Trondheim, Norway
BYRD, R.C. Res. Asst.	Univ. of California	Berkeley, California, USA

While there are diverging results, both empirical and theoretical, on the effect of penetration rate on load when an ice-field hits a pile, there is unanimous agreement that the maximum force occurs if the pile is allowed to freeze into the ice and the ice subsequently begins to move (KIVISILD, 1969, FREDERKING and GOLD 1971, ASSUR 1972).

In Arctic waters with weak tides there is a good chance that adfreezing of ice to a structure occurs. Whether the ice-field is intact or consists of broken ice, the regular forces caused by a slow drift will then govern the design of the structure. This design strategy presumes that the arrival of ice-bergs, ice islands or certain pressure ridges is an unlikely event. If attacks by such ice forms that will undoubtedly cause destructive forces are imminent, the endangered platform must be removed, or perhaps allowed to drift.

In order to reduce the maximum horizontal force on a floating platform in a slowly drifting ice-field, the following scheme is proposed:

On the leg (or legs) of the platform is mounted a collar (Fig. 1), providing the icebreaking slopes that are part of most structures designed to stand in moving ice.

To secure that bending failure actually occurs, the platform is forced into a heaving motion. The ice is either lifted up or pressed down, by the collar on the leg, until the bending strength is exceeded.

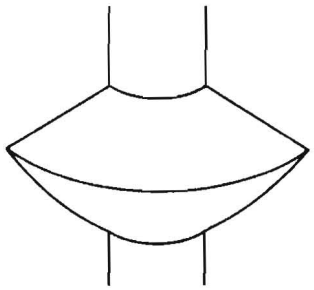

Fig. 1. Icebreaking collar

The forcing of a heaving motion is done by weighting and unweighting the platform at its natural period for this mode. For the size of platform under consideration, the natural period of heave is about 30 seconds. Oscillations at such periods with an amplitude of the order of 1 m will hardly be noticed by the crew, except on the instrument panel.

Excitation at or close to the resonance frequency is probably the only practical way to oscillate these heavy structures without excessive power requirements. The change in weight is accomplished by pumping water in and out of suitable compartments in the platform hull. Compressed air can also be used for these ballasting/deballasting operations.

The scheme is based on the assumption that a heaving motion of one or two metres is accepted by the drillers. Except during upstart of the hole, a gentle periodic heave does not affect the drilling operation significantly.

The concept described above is presently being studied for a bottle-shaped, one-legged platform. The investigation will include model tests at The Ship Research Institute of Norway with an artificial ice as a supplement to computations. This case study is primarily intended to serve as an example, and the purpose is to develop a relation between excitation power requirements and icebreaking capacity of an oscillating platform.

ASSUR, A. 1971: Forces in moving ice-fields.
Proc. 1st POAC Tech. Univ. of Norway, Trondheim.

FREDERKING, R. and GOLD, L.W., 1971: Ice forces on an isolated circular pile.
Proc. 1st POAC Tech. Univ. of Norway, Trondheim.

KIVISILD, H.R., 1969: Ice impact on marine structures.
Ice Seminar, Vol. 10, NRC Canada.

THIRD INTERNATIONAL SYMPOSIUM ON
ICE PROBLEMS
Hanover, New Hampshire, USA

PROBLEMS IN ICE ENGINEERING

Andrew Assur
Chief Scientist

USA Cold Regions
Research and
Engineering Laboratory

Hanover,
NH 03755
U.S.A.

SUMMARY

The design of large structures in ice infested water such as piers, off-shore terminals and platforms is subject to considerable uncertainties due to lack of suitable data and experience. However, observations on ships provide clues for some of the most serious problems to be solved. This paper discusses the effect of friction, adfreezing, side pressure and forces on random ice agglomerations. Horizontal ice pressure can stop ships, so can "ice pillows" under moderate ice conditions.

INTRODUCTION

Waterbodies covered with ice were always formidable obstacles for navigation and engineering structures. Only recently ice engineering is beginning to develop into a discipline, being pursued by many interests and countries. There are abundant natural resources in the Arctic regions, including energy, so that ice covered waters are indeed becoming our newest frontier. Let us discuss some of the critical aspects for which solutions should be improved or as yet no reliable solutions are available. We will refer to some observations made on ships, which also can be usefully applied to structures at sea.

and R = 3.268 x 23.66 x 0.60 = 46.39 to

With 3 m/sec or 5.8 knots we have to add

$$438 \left(\frac{23.66}{20}\right)^{2/3} \times \frac{3}{1} \times \frac{1}{5.960} = 246.6 \ to/m^2$$

to the parentheses in equ (2)

$$\frac{R}{Bh} = 3.268 + 0.824 = 4.092 \ to/m^2$$

and R = 58.09 to or 56.97 10^4 N.

This is somewhat less than observed but here we only want to demonstrate an interesting point regarding friction due to increased side pressure.

What additional horizontal pressure is needed to get the Finncarrier stuck?

The force P_f due to additional friction is

$$P_f = 2 f_r \sigma_n L h \qquad (3)$$

since two sides of the ship are involved.

If the ice resistance at V=3 m/sec is 58.09 to and at V=0 m/sec 46.39 to than an additional resistance of 11.70 to will bring the ship to a standstill provided it develops only 58.09 to of thrust (water resistance is neglected).

From equ (3) this would require

$$\sigma_n = \frac{11.70}{2 \times 0.1 \times 130 \times 0.6} = 0.75 \ to/m^2$$

This is an astonishingly small value for horizontal pressure to develop and just serves to illustrate a point. It takes but little horizontal pressure to beset a ship. This is especially true for icebreaking tankers which are much longer than conventional ships.

Now, the crushing strength of sea ice on small objects can reach 750 to/m^2. On large objects it is much less, perhaps the horizontal pressure an ice sheet can exert may be even as low as 75 to/m^2. Under any circumstances it is important to size up horizontal pressure. The ice, of course, will not exert more pressure than it can stand itself, therefore the horizontal

pressure which leads to formation of pressure ridges or the pressure which can be transferred through pressure ridges is of utmost importance. Nevertheless virtually no attention is devoted to this important problem.

Bradford (1972) has communicated qualitative information derived from the second voyage of the Manhattan, but we need quantitative data to make more progress. Ultimately we should be able to estimate overall horizontal pressure from satellite observations. This capability is close to the state of the art and would significantly propel our technological opportunities.

Eventually the approach could be refined. The third term of equ (2) should be nonlinear in V. f(B) also should be better defined. We could introduce a velocity dependent friction term and set

$$f(B)\,f(V_m)\left[1+2\alpha_m f_r(\sigma_0+\sigma_n)\frac{L}{B}\right]-f(B)\,f(V)\left[1+2\alpha f_r(\sigma_0+\sigma_n)\frac{L}{B}\right]= \quad (4)$$
$$= 2 f_r\,\sigma_n\,\frac{L}{B}$$

V_m - maximum speed, ship is capable under given ice conditions

α - multiplier for f_r due to velocity

α_m is α for V_m

First term of left side shows ice resistance component due to V_m (maximum ship is capable of) including increased friction due to velocity. Second term of left side shows velocity resistance at actual speed reduced due to the presence of horizontal pressure σ_n . Right side of equation shows increased resistance due to horizontal pressure σ_n . The function and parameters can be easily obtained from model tests. Then plot V/V_m versus σ_n as solution of equ (4) showing actual operating speeds affecting transit times for various ships as the result of horizontal ice pressure. This would be an operational tool for a well recognized difficulty.

Since considerable work has been conducted on the icebreaker problem, incl. equ (1) and many others which give us the capability to consider shape, it may appear that a solution for ice forces against a structure may be within easy reach. Above we have mentioned but one problem with icebreaker equations. There are many more. In the field a ship, beset by ice, simply yields and drifts; it is, of course, designed not to be crushed. A structure cannot yield, it must withstand the forces.

The phenomenon, analyzed above, concerning horizontal pressure is known to every seasoned icebreaker captain although ignored

in conventional icebreaker equations: under certain conditions, in particular with wind pressing against a shore, every icebreaker may be stopped even in relatively thin ice.

For long cargo ships this effect is even more important. Nevertheless few model tests deal with the effect of the length of the ship assuming the same frontal resistance. The controlled introduction of horizontal ice pressure in laboratory experiments is still in the future.

EFFECT OF ICE PILLOWS

Another difficulty is possible adfreezing of ice to structures or ships with tremendous increases in forces which must be handled. This is of considerable concern to the designers of structures since a mathematically well defined surface, such as a cone, suddenly would present a chaotic surface of random ice pieces. There are several schools of thought regarding this problem. One group maintains that no ice can be allowed to adfreeze under any circumstances, therefore such methods as heating are called for with high capital investment and operational cost.

Another group maintains that natural forces take care of this problem. As experienced Arctic travelers have noticed tidal forces produce a broken collar around rocks and steep walls, why not around structures? The natural movement of ice provides a self-cleaning process. However, one cannot deny that adfreezing indeed can occur with severe consequences.

Again we return to observations made by seasoned icebreaker personnel but not followed up by scientists or engineers. I am referring to the phenomenon of "ice pillows" which under certain ice conditions can form preferentially at the sides of the bow of an icebreaker, thus dramatically reducing its ability to proceed. Strangely this occurs with relatively modest pliable ice, usually covered with snow under cold weather conditions. It usually occurs when freezing mush achieves excellent compliance of broken ice pieces to the ship usually under high pressure created by the forward thrust of the ship. Fig. 1 shows the sketch of such an ice pillow.

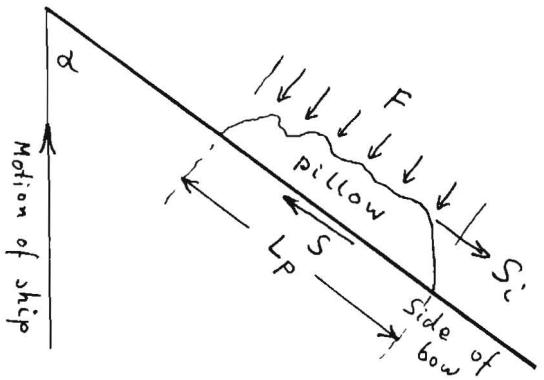

Fig. 1

The total shear force which could remove the ice pillow is

$$S = c\sigma_a L \cdot h \tag{5}$$

Its component in the direction of the ship is

$$S_t = c\sigma_a L \cdot h \cdot \cos\alpha \tag{6}$$

σ_a - adfreezing strength of ice to ship
L_p - length of ice pillow
h - ice thickness
c - constant of proportionality since vertical thickness of ice pillow is not necessarily equal to h.

The maximum pressure which the surrounding ice can exert on the ice pillow, which is a random aggregrate of ice pieces, can be calculated following an approach given by Assur (1971). Note: the integral sign $\int_0^{\Theta_1}$ was inadvertently omitted from his equ (10).

Developing Assur's suggestions somewhat farther for this application we obtain

$$F = C_2 \frac{2\Theta_1}{\pi} F_1 + (1 - \Theta_1) F_2 \tag{7}$$

F - overall force per unit width
C_2 - coefficient, somewhat below 1, accounting for the fact that simultaneous breaking does not occur everywhere but some pieces simply slide against each other.
$\Theta_1 = \operatorname{arctg}(\Theta_1 + \phi) - \phi$
$\operatorname{tg}\phi$ - friction coefficient ice to ice.

$$\operatorname{tg}(\Theta_1 + \phi) = \frac{6c}{\sqrt{2}\, e^{\pi/4}} \frac{\sigma_c}{\sigma_f} \frac{l_1}{h}$$

Θ_1 - limiting angle in chaotic mass of ice breaking against ice above which crushing rather than bending occurs.

$$\frac{\sqrt{2}\, e^{\pi/4}}{6} = 0.51696$$

$\frac{\sigma_c}{\sigma_f}$ - ratio of crushing to flexural strength

$\ell_1 = L_1 h^{3/4}$ with $L = \sqrt[4]{\frac{E}{3k(1-\mu^2)}}$

E, μ - Young's modulus and Poisson's ratio of ice

$$F_1 = \frac{2\Theta_1}{\pi} \frac{\sigma_f h^2}{6\ell_1} \sqrt{2}\, e^{\pi/4} \ln \cos(\Theta_1 + \phi) \quad . \quad . \quad . \quad (8)$$

Average bending force

$F_2 = c\,\sigma_c\, h$ - crushing force

For thinner ice sheets buckling may be a factor and $F_3 = \kappa \ell_1^2$ may be substituted for F_2. By setting $F_2 = F_3$ the critical ice thickness can be found below which buckling occurs satisfying the condition

$$c\sigma_c h = \kappa L_1 h^{3/4} \quad . \quad . \quad . \quad . \quad . \quad (9)$$

In that case, however, the critical angle Θ_1 must be re-defined.

In any case whether we assume crushing or buckling we find that there is a critical ice thickness below which ice pillows can form and survive but above which S_1, the shear force between the ice pillow and the surrounding ice sheet, is sufficient to break the ice pillow away providing the self-clearing feature postulated above. We can set

$$S_i = \sigma_s h L_p + F \operatorname{tg} \eta \cdot L_p \quad (10)$$

and $S_i \cos\alpha$ its component with the ships axis.

σ_s - cohesive strength of broken ice masses
η - angle of internal friction for broken ice masses
F - normal force exerted against the pillow as per equ (7)

Thus in the presence of an ice pillow the additional thrust needed to move the ship will be

$$\Delta R = \cos\alpha\,(\sigma_s h + F \operatorname{tg}\eta) L_p \quad . \quad . \quad . \qquad (11)$$

Occasionally the additional thrust will not be available and the icebreaker will stall much to the surprise of the unsuspecting crew. It has happened that ships following in convoy could not be warned sufficiently in advance which resulted in rear collisions.

It is quite evident that the phenomenon just described bears also on our first problem, the maximum side pressure ice can exert. This in the presence of pressure ridges will be F from equ (7). If sufficiently reliable observations are available about the critical ice thickness above which F is able to remove ice pillows than we will have a better handle upon the magnitude of F and will also have solved our first problem.

It is also evident that if reliable proof and quantitative parameters can be obtained about the phenomena described than considerable capital investment funds and operational energy could be saved since adfreezing would not occur at the highest ice forces the structure is designed against.

Now let us devote a few words about other problems in ice engineering.

ARTIFICIAL ISLANDS

Artificial islands are one of the choices to protect structures. Inevitable such islands will surround themselves with pressure ridges. But ice forces from surrounding pack ice will be largely absorbed by these pressure ridges. Again we see the utility of introducing and further developing stochastical methods such as those shown above for F. These forces will be absorbed by grounded ridges at the bottom unless the ridges move. Tremendous ridges can pile up in the process and threaten structures or roads. Suitable criteria have been derived for such cases but space does not allow to dwell upon it.

CONICAL STRUCTURES

Cone-like structures are probably a solution for offshore terminals and platforms. The calculation of ice forces can proceed by bracketing idealized cases.

a. Perfect non-adhering ice sheet surrounding the cone. Rigidly connected wedges. This actually is a somewhat fictitious

assumption since a rigorous solution is not available for a circular hole in a plate on a liquid foundation which is being attacked by a sloping cone.

Assume for the purpose of this exercise that tips of truncated wedges are rigidly connected and lifted at once over a semicircle. This should exaggerate the actual force required.

The force P_w required to lift one wedge vertically is given by

$$\frac{6 P_w}{b_0 \sigma_f h^2} = f(\varrho) \tag{12}$$

$f(\varrho)$ - given by Nevel (1972)

$\varrho = r/\ell$ $\quad b_0 = b/r$ $\quad r$ - radius of cone

$b = \frac{\pi r}{n}$ $\quad b_0 = \pi/n$ $\quad \ell = \sqrt[4]{\frac{E h^3}{12 K}}$

n - number of wedges per semicircle

The total vertical force required to lift the semicircle of wedges is

$$P_v = n P_w = \pi \frac{\sigma_f h^2}{6} f(\alpha) \tag{13}$$

Considering the friction of ice to surface material of the cone as $tg\phi$ we have for the horizontal force an estimate as

$$P_h = tg(\Theta + \phi) P_v = \pi \frac{\sigma_f h^2}{6} f(\alpha) tg(\Theta + \phi) \tag{14}$$

Just for the purpose of illustration let us assume sea ice with

$\sigma_f = 40\ to/m^2$ $\quad E = 200\,000\ to/m^2$

$\Theta = 45^\circ$ $\quad tg\phi = 0.2$ $\quad arctg\phi = 11.31^\circ$

Then $L_2 = \sqrt[4]{\frac{E}{12K}} = 11.362$

and $\ell = L_2 h^{3/4}$

and we obtain for various ice thicknesses (subtracting 1" = 2.5cm for skeleton layer) and for a 20 m diameter cone.

$h + 2.5$ cm	1 m	2 m	3 m
ℓ	11.148	18.929	25.738
ϱ	0.90	0.53	0.39
$f(\varrho)$	3.19	2.35	2.04
P_h [to]	95.3	288.0	567.3

Here $P_h = 31.42\, f(\alpha)\, h^2$

and $P_h = 31.42\ f(\alpha)\ h^2$

Values of $f(\varrho)$ for $\varrho > 1$ are available but have not been published as yet.

This simplified approach, of course, distorts the actual process and should be checked and calibrated in model tests. The actual values should be somewhat higher; the reasons for which cannot be explained in a short paper.

b. Perfect non-adhering ice sheet surrounding the cone. Unconnected wedges. This is the case when the ice sheet breaks into a number of wedges which then break off as they are lifted to the required height for the bending stress to reach bending strength. This problem can be solved rigorously considering the angle of wedge axis to direction of motion but would give a lowered estimate of horizontal forces.

Another possibility is to assume overall horizontal pressure in the ice sheet sufficient to cause failure on all wedges and then to calculate force needed to start to move cone in such a field.

c. Perfect adhering ice sheet. Here the force required to break the bond must be compared with the force required to break the sheet. Assumption of wedges and possible buckling is useful.

d. Ride-up of pieces. After the initial breaking, resulting ice ride up the cone, partially enveloping it.

e. Envelope of adfrozen broken pieces. This necessitates the use of a stochastical approach and in this, the severest case we return right to the problem discussed above. If, in addition, we consider that the cone does not have to be in a neutral situation but can be affected by overall horizontal pressure in addition to the forces created by the motion of the ice sheet we realize that the solution of the problems discussed above, indeed, represent a key to further progress in this unexplored field.

CONCLUDING REMARKS

We are standing barely at the beginning of properly developing ice engineering as a discipline which requires international cooperation between specialists in ice physics and chemistry, ice engineering and technology, deterministic and stochastic mechanics, supported by extensive testing in suitable laboratories and expensive field tests to calibrate the relationships thus

obtained.

REFERENCES

Assur A. (1971): Forces in moving ice fields. 1 Intern. POAC Conf. 1:112-118

Bradford J. D. (1972): Preliminary report of the observation of sea ice pressure and its effect on merchant vessels under ice-breaker escort. Intern. Conf. Sea Ice Reykjavik

Enkvist E. (1972): On the ice resistance encountered by ships operating in the continuous mode of icebreaking. Swed. Acad. Eng. Sci. Finland report 24, Helsinki

Mookhock A. D., Bielstein W. J. (1971): Problems associated with the design of an Arctic marine transportation system. Offshore Technology Reprint paper 1426

Nevel D. E. (1972): The ultimate failure of a floating ice sheet. IAHR Ice Symposium Leningrad

Kashtel'ian V. I., Pozniak I.I., Ryvlin A. I. (1968): Soprotivlenie l'da dvizheniiu korablia/Ice resistance to motion of a ship/ Sudostroenie, Leningrad

THIRD INTERNATIONAL SYMPOSIUM ON
ICE PROBLEMS
Hanover, New Hampshire, USA

ON THE FLEXURAL STRENGTH AND ELASTICITY OF SALINE ICE.

Dr. Joachim Schwarz — Hamburg Model Basin — Hamburg,
Head of Ice Tank — (HSVA) — West-Germany

Synopsis

Small scale cantilever beam tests on structurally simulated (seeded) freshwater and saline ice have been performed at the Hamburg Model Basin (HSVA) in order to elucidate the relation between flexural strength, elasticity, salinity and temperature. The tests have shown a considerable increase of the E/σ_f - ratio if saline ice was warmed up before tested. Furthermore the results of warm - ice tests seem to prove a theory constructed by Weeks and Assur (5) on the relation between flexural strength, elasticity, and brine volume.

Based upon the findings of present investigations a new ice testing technique was developed and is presently being utilized at HSVA. Besides obtaining a more natural E/σ_f - ratio several other similarity conditions are being improved by the new testing technique.

Introduction

Model tests for icebreaking ships or for investigations of ice forces on inclined structures require the reduction of strength and elasticity of the ice. Two methods are presently in use to achieve this similarity requirement :

(1) Artificial ice obtained from wax plus some additives and

(2) real ice from saline water.

The artificial ice generally has a too high friction coefficient (0.5 against 0.1 for real ice). Since friction is one of the most important parameters within the icebreaking performance, a non-similarity of the friction coefficient is almost eliminating artificial ice from practical use.

Therefore most of the existing ice model basins including the HSVA are working with saline ice in order to meet the requirement of strength reduction. Saline ice, however, has - so far - the disadvantage that strength and elasticity cannot be reduced simultaneously by the same scale ratio. At $\lambda = 40$, for example, saline ice has almost no elasticity but shows a too plastic behaviour. The ratio between elasticity E and flexural strength σ_f is only 200 to 500, compared with 2000 to 5000 of sea ice in nature.
Since σ_f and E govern the size of ice pieces broken by the icebreaker bow and since this size and also the shape of the ice slabs effect the total resistance, it is indispensable to simulate the ratio E/σ_f as proper as possible.

One possibility of improving the simulitude of the E/σ_f - ratio is to use low saline ice and to apply the temperature effect in order to reduce the ice strength in addition to the influence of brine.

This idea was investigated at HSVA by a special test program in which the relationship between flexural strength, elasticity, salinity and also temperature was examined on cantilever beam tests of constant beam dimensions and strain rate.

Theoretical aspects

Based on their model of saline ice Weeks and Assur (5) have suggested the following relationship between flexural strength and elasticity

$$\frac{\sigma_f}{\sigma_o} = \left(1 - \sqrt{\nu_b}\right)^2 \qquad (1)$$

$$\frac{E}{E_o} = \left(1 - \nu_b\right)^4 \qquad (2)$$

where

σ_f = flexural strength of saline ice

σ_o = flexural strength of freshwater ice

ν_b = brine content

E = Elastic modulus of saline ice

E_o = Elastic modulus of freshwater ice

Both equations can be combined and written in the form

$$\frac{\sigma_f}{\sigma_o} = \left(1 - \sqrt{1 - \left(E/E_o \right)^{1/4}} \right)^2 \qquad (3)$$

This relation between normalized strength and normalized elasticity (of saline ice) was plotted on log-log scale in Fig. 1.

Besides the theoretical curve of Assur and Weeks also results of present HSVA experiments are shown in Fig. 1. They will be discussed later. Assur's and Weeks' theoretical curve is in accordance with the experience with high saline model ice, i.e., a too low elasticity compared with the reduction of strength. This curve , however, indicates also that in a certain range of brine content E and σ_f could be reduced by the same scale ratio. Even though this hint is very important for the ice model technique Weeks' and Assur's theoretical curve has never been verified experimentally.

Determining the flexural strength and the elastic modulus a bundle of problems is involved :

It certainly is incorrect to calculate the flexural strength of ice simply by the elastic beam equation.

$$\sigma_f = \frac{6Pl}{b\,h^2} \qquad (4)$$

There are several reasons for this statement :

First, the neutral axis is located not in the center but is shifted towards the compressed fibre due to the different elastic modulus E_1 for compression and E_2 for tension.

Second, the elastic modulus E of floating ice fields varies with the thickness h due to temperature and salinity changes and also due to the nonhomogenity of the ice cover. This causes $E = E(z)$, where z is the distance from the surface.

Suggestions for considering these different conditions in the calculation of σ_f have been made by Weeks and Assur (5), Lavrov (3), and Kerr and Palmer (2).

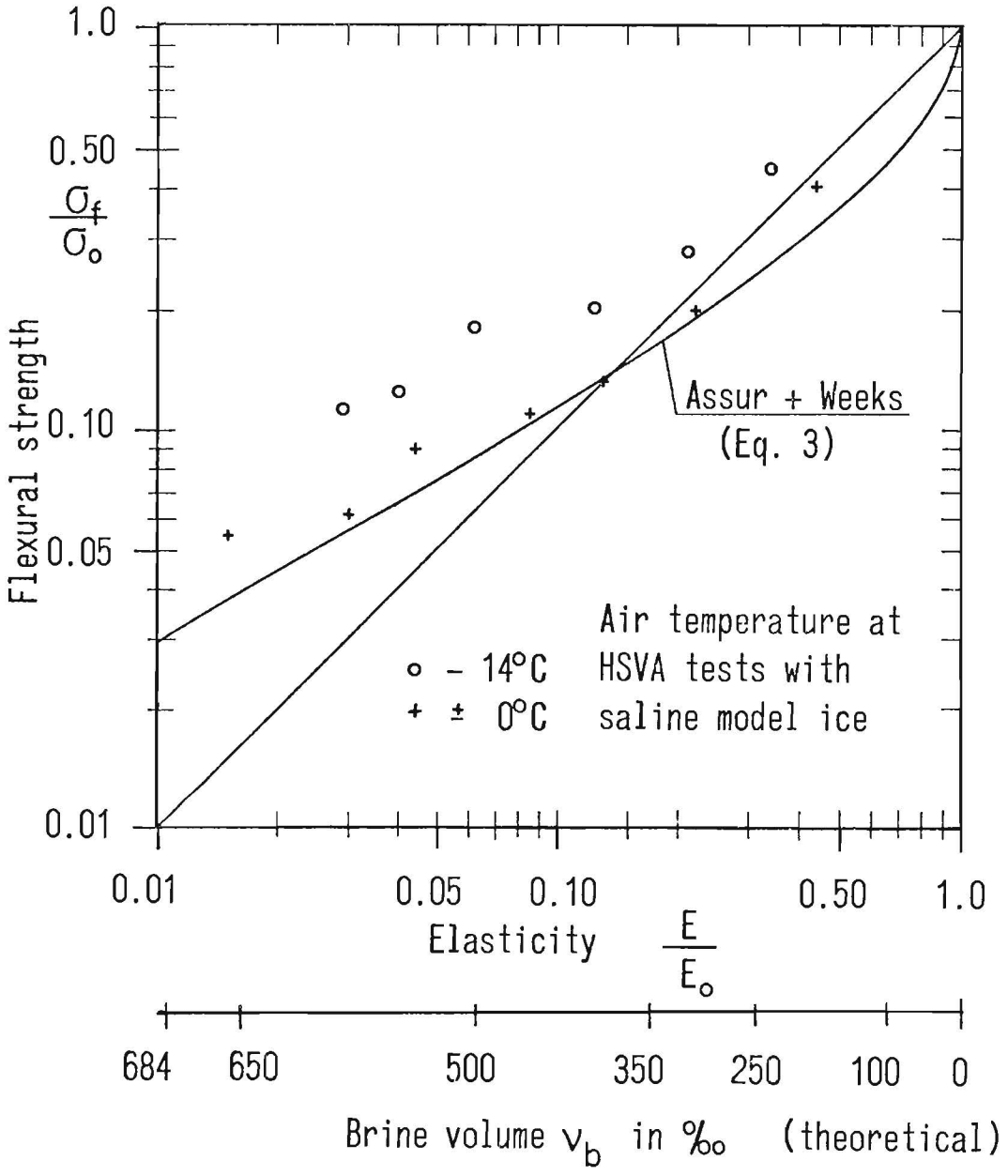

Fig. 1 Normalized strength vs. normalized elasticity of saline ice

Theoretically the problem is easy, the difficulty arises with the practical performance of obtaining the correct function of E versus z. Measuring salinity and temperature in various depths and using Eq. (2) for the determination of E is generally feasible if this equation is correct. This procedure can not be used here, since Eq. (2) is intended to be proved by the present studies. Any other direct measurements of E in various depth of the ice plate are almost impossible in case of small scale cantilever beam tests especially when the temperature and within the brine content changes rapidly. Therefore, the flexural strength of the present investigation has been calculated again by Eq. (4), knowing that the result is a relative and not an absolute strength value. For the purpose of comparing similar tests this procedure might even be justified.

The force-deflection record (Fig. 2) indicates a linear stress-strain relationship due to the fairly high loading rate (about 1 kg/s). From this point of view the application of the elastic theory is correct.

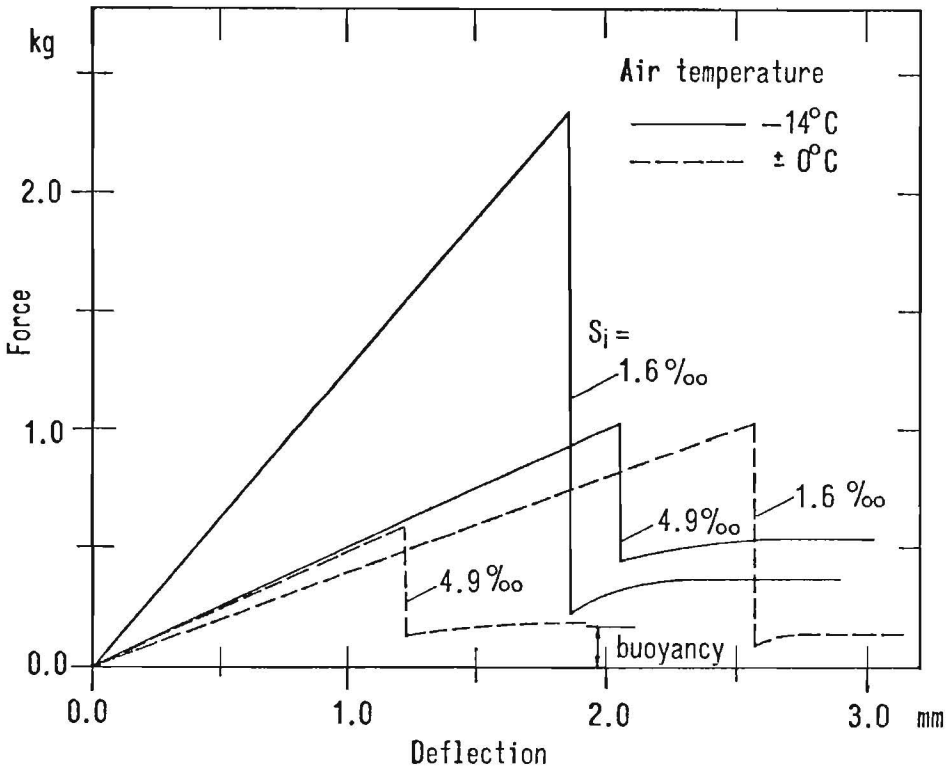

Fig. 2 Force - deflection curves for saline model ice of 2 different salinities and at 2 different temperatures

Test Facility and Procedure

The bending strength tests have been performed on cantilever beams of structurally simulated ice of various salinities. The beams were prepared from an ice cover grown in a 200 cm long, 80 cm wide and 60 cm deep ice tank located in the ice room at HSVA.
The ice formation was initiated by the water-spray-method in order to obtain uniform, fine-grained, columnar ice (S-2 ice). The tests were started with freshwater ice and continued with ice of various salinities (up to S_i = 6.7 o/oo).
Preparing the ice cover it was particularly important to have the water in the tank well mixed in order to guarantee water of uniform temperature and salinity.

The cantilever beams were about 30 cm long, 10 cm wide and 4 cm thick; these dimensions as well as the deflection rate were kept about constant throughout the experiments in order to avoid scale and rate effects (the deflection speed varied between 1.5 and 2.0 mm/s).

The long sidewalls of the wooden ice tank carried a steel frame on which the load apparatus and the deflection-meter were mounted. The free end of the cantilever beams were loaded vertically by a motor driven screw punch, at which an electronic load cell and a linear motion potentiometer were incorporated.

This set-up provided the measurement of the load versus deflection and time. One advantage of testing the flexural strength and the elasticity in the small ice tank instead in the large ice model basin was that the deflection at the fixed end of the beam was negligible small because the ice cover was narrow and frozen to the sidewalls of the tank while the deflection of the whole ice cover in the large ice model basin is significant which causes false results of E.

Presentation and discussion of results

If mechanical properties of materials are being investigated the stress-strain or as in this case the force-deflection relation is of fundamental importance.

Replotted records of this relation are shown in Fig. 2 for model ice at 2 different ice salinities (S_i = 1.6 o/oo and 4.9 o/oo) and temperatures (air temperature T_A = -14°C and 0°C).

The force-deflection curves of low saline ice (S_i = 1.6 o/oo) at both temperatures are very similar to natural ice. The residual force after the failure of the beam is mainly due to buoyancy. Its value is only about 15 % of the breaking force. With increasing salinity the residual force increases significantly due to the more plastic deformation of the ice and the coherence of ice crystals in the vertical plane of rupture.

In case of S_i = 4.9 o/oo and low temperature (T_A = -14°C) the residual force is about 50 % of the breaking force, at higher salinities even more. This false result is being suppressed if the ice is tested at 0°C.

The unnatural fullness of the force-deflection curves of high saline, cold ice obviously causes a too high energy required to break this model ice by bending. Enkvist (1) already reported about this distorting effect of the residual plasticity on model test results. He justified, however, the application of high saline ice for model tests on icebreakers with the reference that the pure breaking resistance is only a small portion of the total resistance of an icebreaking ship.

This statement or excuse might be acceptable for model tests on large icebreaking ships and at high velocities but not for model investigations on engineering structures and small icebreakers, because in these cases the pure breaking resistance is <u>not</u> small.

The main results of the present investigation i.e. the flexural strength and the elasticity of structurally simulated (seeded) freshwater and saline ice have been plotted in Fig. 3 and 4 as a function of time. All data points represent mean values of several single tests. The different curves are for various ice salinities, S_i, ranging from 0 to 6,7 o/oo. The flexural strength σ_f and the elasticity E of saline ice have been normalized by σ_o = 8 kg/cm^2 and E_o = 17 200 kg/cm^2. These values have been obtained from tests on freshwater ice under corresponding test conditions. The time t was nondimensionalized by the time t_{st} which is the time when the ice temperature reaches the steady state. At time t/t_{st} = 0 the air temperature was -14°C.

Besides the strength and the elasticity also the temperature rise with time was plotted in Fig. 3 and 4 in nondimensional form,

$$\frac{T_i\ (t)\ -\ T_f}{T_i\ (0)\ -\ T_f}$$

where

$T_i\ (t)$ = temperature at the ice surface at time t

T_f = ice temperature at freezing mark

$T_i\ (0)$ = temperature at ice surface at time t = 0 (air temperature T_A = -14°C)

Figs. 3 and 4 show the decrease of the flexural strength and of the elasticity with rising temperatures. It is not shown in Fig. 3 that the strength would decrease further if the temperature T_f would last for a long time. In this case the melting of the crystallographic bonds would cause an additional weakening of the ice strength.

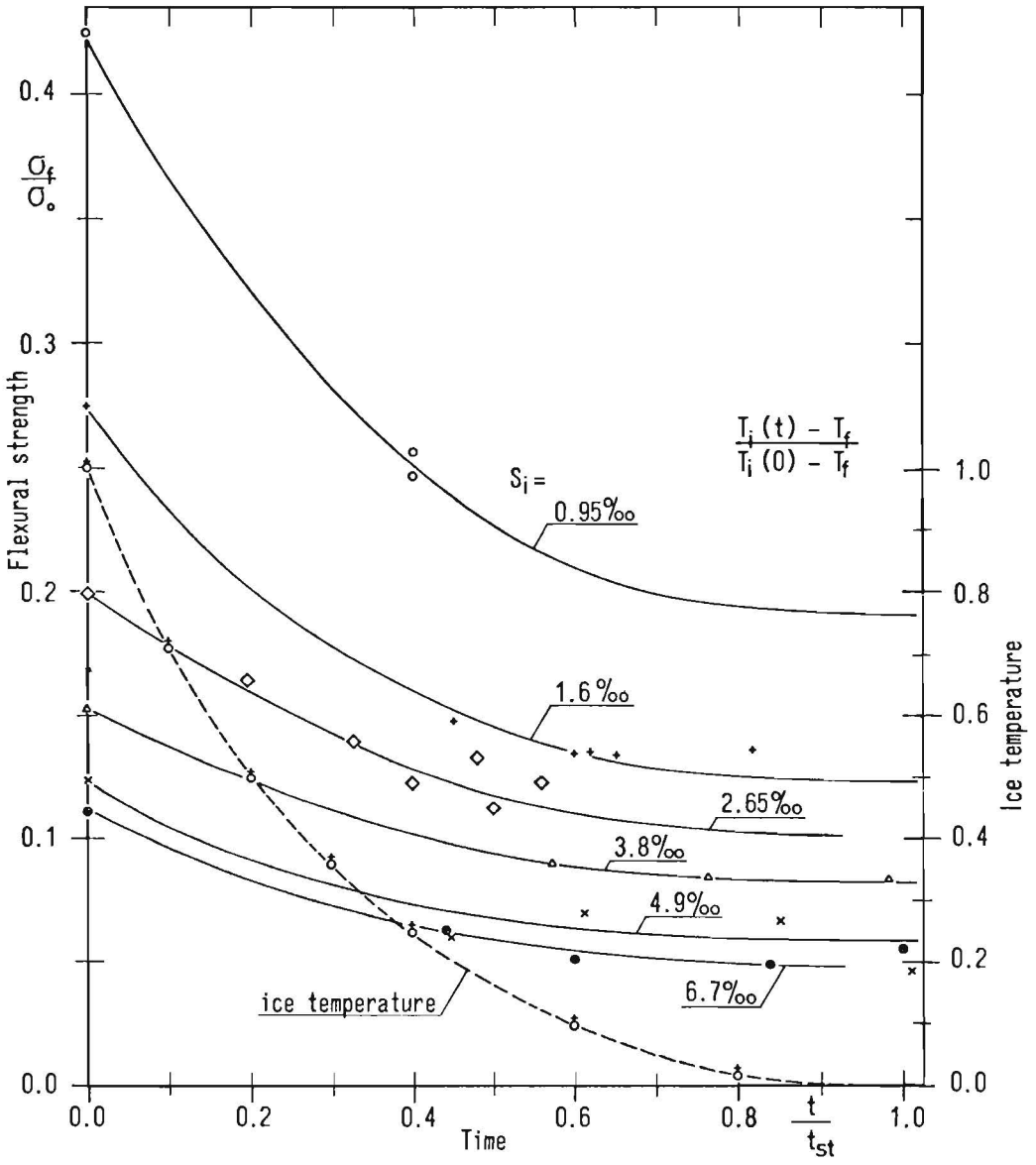

Fig. 3 Flexural strength and ice temperature vs. time for different salinities (ice)

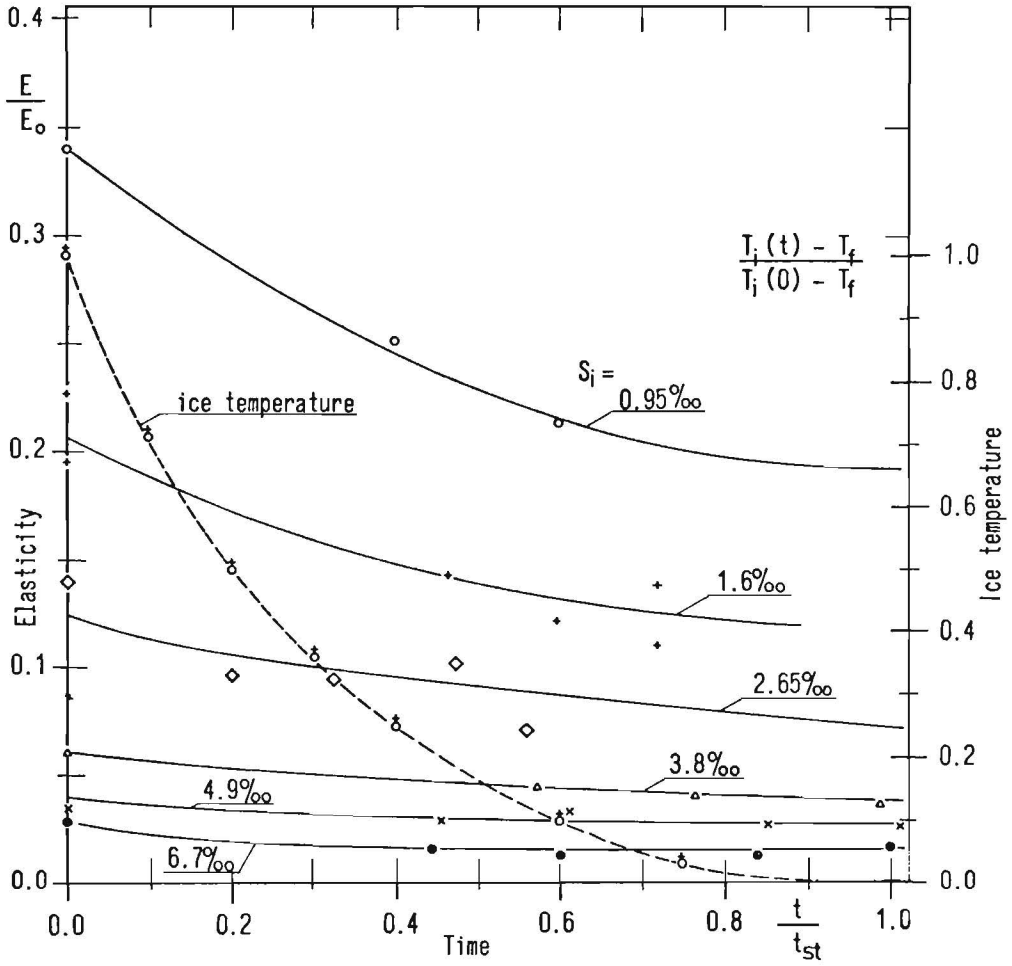

Fig. 4 Elasticity and ice temperature vs. time for different salinities (ice)

The ratios E/σ_f of different saline ice increase with rising ice temperatures (Fig. 5). The maximum of this ratio occurs before the freezing temperature T_f is reached. This is especially pronounced at low salinities.

Before the influence of this finding on the saline ice model technique will be discussed the results will be compared with Weeks' and Assur's theory, given by Eqs. 1 and 2 and demonstrated in Fig. 1. In addition to the theoretical curve of Weeks and Assur the normalized flexural strength of the present tests has been plotted versus the corresponding normalized elasticity for cold ice (air temperature $-14^{\circ}C$) and also for warmed-up ice (air temperature $0^{\circ}C$).

The test results of the warmed-up saline model ice seem to confirm the theory of Weeks and Assur, which means that there is indeed a range of salinity at which the ratio between normalized elasticity and normalized flexural strength is equal.

The E vs. σ_f - data of cold ice tests, however, are far above the theoretical curve, even though they seem to be shifted parallel to it. This disagreement between theory and results of cold ice tests can be explained as follows :

It is known(Poznyak (4)) that the top layer of cold saline model ice is about twice as strong as it should be according to the strength distribution across the thickness of ice in nature. Since the top layer is governing the flexural strength in case of cantilever beam tests (pushed downwards), this strength is too high compared with the corresponding elasticity, which causes the data points of the cantilever beam tests to lay above the theoretical curve.

Russian scientists try to overcome this disadvantage of saline model ice by spraying a certain brine solution on the ice surface in order to reduce the strength at the top layer of their model ice.

HSVA has also experimented with this method but found it very difficult to obtain equal ice properties across the entire tank area. Instead HSVA developed the warm-up technique of the ice cover and achieved a similar effect i.e. reducing especially the strength at the surface of the model ice cover.

Application of present test results

The results of small scale cantilever beam tests on the flexural strength and elasticity of ice in relation to salinity and temperature have been applied for the testing technique in ice at the Hamburgische Schiffbau Versuchsanstalt.

Tests in which the flexural strength and the elasticity of ice are important parameters(icebreaker tests and investigations on ice forces on inclined structures) are being carried out after low saline ice, originally frozen at about $-14^{\circ}C$ air temperature, has been warmed up and attains the freezing temperature of

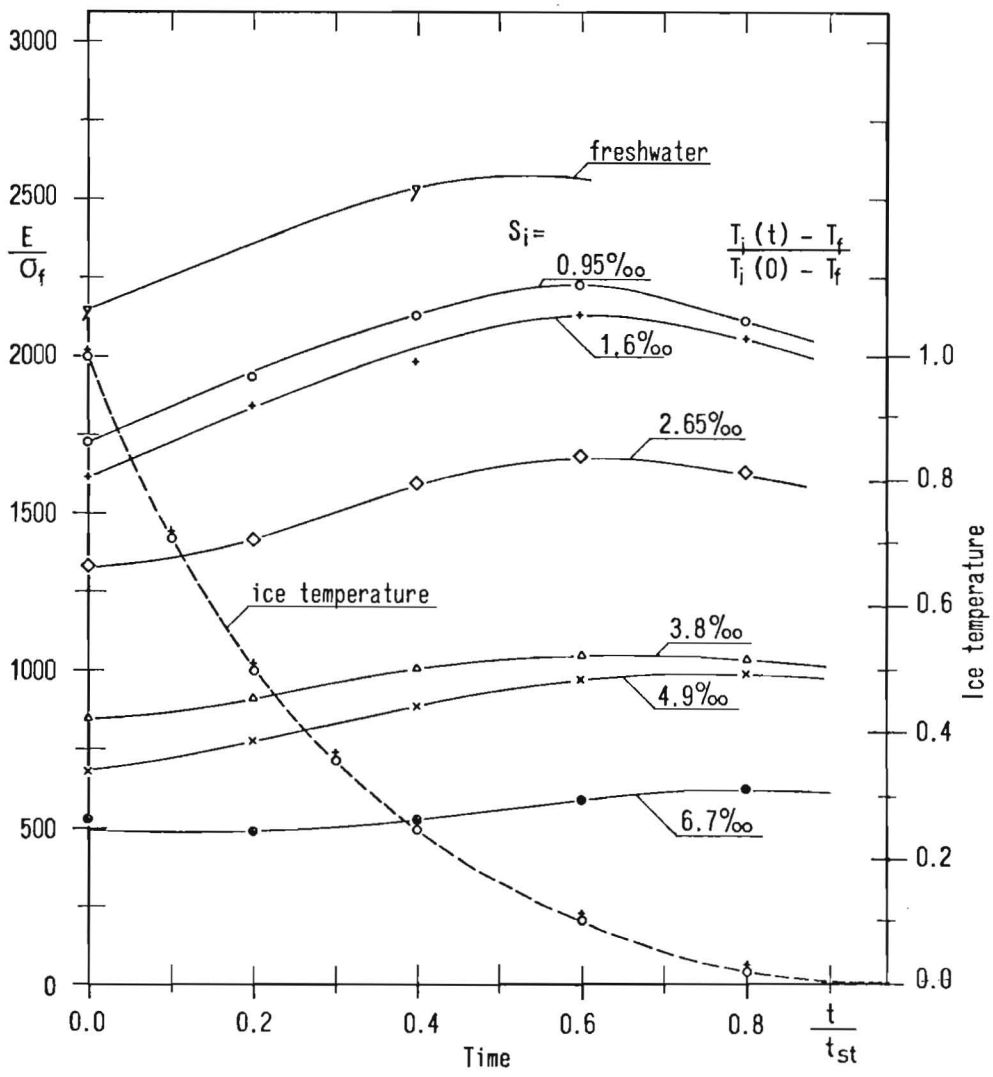

Fig. 5 E/σ_f and temperature vs. time for different salinities (ice)

water. This method which provides actually a new model ice has several advantages :

1. The flexural strength is being reduced by the ice warming technique which causes the brine volume to increase and the ice strength-even without brine - to decrease. In order to obtain a certain strength reduction ice of lower salinity can be used which provides better elastic properties.
2. For the same strength reduction but at different salinities and temperatures the E/σ_f-ratio increases, for example from 680 (S_i = 4.9 o/oo, T_A = -14°C) to 2060 (S_i = 1.6 o/oo, T_A = 0°C). By this increase the lower E/σ_f range of sea ice is reached, which improves the similarity of the breaking pattern of the model ice cover.
3. The residual plasticity which remains after the ice breaks and which causes significant scale effects in case of conventional cold, saline model ice is suppressed when the ice is tested at 0° C air temperature. The still remaining residual force is due to buoyancy. The force - deflection curve of warm saline model ice is similar to the one of natural sea ice.
4. The too strong surface layer of cold, saline model ice, commonly in use, is being weakened by rising the air temperature to 0°C which provides a more natural strength distribution across the thickness of the ice cover.

Even though the new ice testing technique (warm ice technique) requires a higher degree of temperature and strength control the improvements of the similitude of ice model tests justify the higher efforts.

Acknowledgement

The investigation was carried out within a research program sponsered by the German Ministry of Research and Technology. The tests were carried out by Mr. Lemke to whom the author is grateful for his assistance.

References

1. Enkvist, E. On the ice resistance encountered by ship operating in the continuous mode of ice breaking.
The Swedish Academy of Engineering Sciences in Finland. Report No. 24, Helsinki 1972

2. Kerr, A.D. and Palmer, W.T. The deformations and stresses in floating ice plates
Acta Mechanica, 1972

3. Lavrov, V.V. Deformation and strength of ice.
Gidrometeorologicheskoe Isdatel stvo.Leningrad 1969.
NSF-Translation TT 70 50130.

4. Poznyak, I. Improvement of the Method of Preparation of Model Ice.
in CRREL Translation
TL 417, Hanover N.H. 1973

5. Weeks, W. and Assur, A The Mechanical Properties of Sea Ice
CRREL Monograph II C 3
Hanover N.H. 1967

International Association of Hydraulic Research (IAHR)
Committee on Ice Problems
International Symposium on Ice Problems
18-21 August 1975
Hanover, New Hampshire

COMMENTS

Paper Title: On the flexural strength and elasticity of saline ice.

Author: Dr. Joachim Schwarz

Your name: Jack L. Lewis

Address: Arctec. Inc., U.S.A.

Comment: How important is, in your opinion, the elasticity on the icebreaking resistance?

Answer: If we consider elastic deformation in the process of breaking an ice cover by ship, Young's Modulus effects the characteristic length "l" only by the power of 1/4. Since the elasticity of cold-high and war-low saline ice differs strength, the characteristic length "l" changes up to about 50% and the volume of the broken ice pieces, which have to be moved by the icebreaker, of course, much more.

Besides, we know that the dimensionless numbers, so far in consideration, do not describe the icebreaking problem completely. Atkins (1975) just recently has proposed a so called "Ice Number" in which E is represented by the power of 1/2 and investigations at HSVA suggest an even higher involvement of E within the breaking portion of the total resistance. This shows that doday we are not sure yet about the quantitative influence of E on the total resistance of icebreaking ships. Therefore it is suggested to simulate the material properties of ice as proper as possible.

Practically speaking, several model tests cannot be performed properly, if the E/σ-ratio is not simulated close to natural conditions. The side-pressure-unit of HSVA for the investigation of ships or structures under lateral compression, for example, was only operational by using the new warm-ice-technique.

THIRD INTERNATIONAL SYMPOSIUM ON
ICE PROBLEMS
Hanover, New Hampshire, USA

ICE FORCES ON SIMULATED STRUCTURES

L. J. Zabilansky
Research Civil Engineer
D.E. Nevel
Research Physical Scientist
F. D. Haynes
Materials Research Engineer

U.S. Army Cold Regions
Research and
Engineering Laboratory

Hanover, NH
USA

Abstract

Simulated structures mounted on a portable apparatus were used to investigate ice forces on marine structures. Various geometric shapes of simulated structures or piles were pushed against natural lake ice. Parameters varied were size, shape, pile velocity, friction, initial pile-ice contact and slope of the pile.

Introduction

The design of a marine structure in a cold region requires the determination of the load exerted on the structure by a moving ice sheet. Factors which influence the design load are the geometry of the structure and the mode of ice failure. The purpose of this investigation was to identify the influence of the various parameters.

Test Apparatus and Procedure

To simulate forces at the structure-ice interface, independent of natural ice movement, an active system was used to push the simulated structures or piles against the ice. In preparing the test hole for the majority of the sloping and vertical pile tests, the pile-ice interface was cut to the contour of the pile. Forces developed during a test were transmitted via a baseplate to the ice sheet.

The key component of sloping pile apparatus is the telescoping support tower, shown in Figure 1. By means of a pin, the tower's height could be varied in three inch increments between 110 and 147 inches. A hydraulic ram, with a ten inch stroke, was used for fine

adjustment of the pile's height after placement of the tower in the water. A bearing pad attached to the base of the tower transmitted the vertical load to the lake bottom. A pin was used to attach the two sections and provided a moment free connection. The tower was placed such that it would be vertical midway through usable stroke of the ram, this minimized the change in pile elevation, due to tower's rotation. A 5.5-inch round pile was used to examine the effect of slope. By interchanging the angle block, Figure 1, the pile could be mounted at 15°, 30° or 45° from vertical. It is hypothesized that by reducing the pile's friction a smaller force would be required to initiate sliding on the pile. To explore this a stainless steel shroud was used to cover the rusty 5.5 inch steel pile.

The variables investigated with the vertical pile apparatus, shown in Figure 2, were size, shape, pile velocity, friction and the initial pile-ice contact condition. Piles used during this phase varied in size from 5.5 to 12.5 inches and were either flat or round. The stainless steel shroud was also used to study friction.

The energy required to push the pile through the ice was achieved by precharging a hydraulic accumulator to 6000 psi with an electric pump. By presetting flow control valves and opening a manual shutt-off valve, the pressurized fluid was released at the desired rate. The storage capacity of the accumulator was sufficient to drive the pile six inches or half of the available rod stroke. By recharging the accumulator, a second test was conducted in the same hole.

Analog output signals of the load cells and of the distance transducer were recorded on magnetic tape. The force records were later transferred to a digital computer for data reduction and analysis.

Test Results

During the three weeks in which sloping pile tests were conducted, a water-snow layer covering the lake was freezing. This condition has complicated the analysis due to interaction between the layers during a test.

Field observations of the sloping pile tests agree with a laboratory investigation done by Zabilansky, Nevel and Haynes (1975). For the 15° sloping pile test, ice failure was typical crushing-splitting, which is to be discussed later in the paper. Piles at 30° and 45° caused the ice to fail in bending. A typical bending failure initiated with local crushing, which seats the pile. Obtaining more uniform contact, radial cracks propagated straight ahead and at about 45° on either side. Radial cracks were followed by the formation of a circumferential crack resulting in failure of the ice sheet in front of the pile. Since data is still being analyzed, it is not known where the peak load occurred.

In the vertical pile test, failure was usually a crushing-splitting type. A typical failure of this type occurred in the following manner. Like the sloping tests, some local crushing and pressure melting at the pile-ice interface seats the pile. Then radial cracks propagate straight ahead and on either side at 45°. Simultaneously, the granular ice in front of the pile is being compressed into a shallow pressure bulb. As the pile advances, irregularities of the pressure bulb act like wedges to initiate horizontal cracks. The cracks divide the ice thickness into thin layers, typical one to two inches. As the pile advances the outer layes are spalled off to expose a thin edge which is easily crushed. Figure 3 shows a block of ice removed from in front of a 5.5-inch flat pile, after the second test. Figure 4 is a cross-section in the center of ice specimen. The tapered ice left by the spalling action in the first test was crushed up during the second test. Studying the specimen it appears that the pile made sufficient contact with the ice to start the spalling action. Figure 4 also reveals the compressed granular ice, which forms the shallow pressure bulb.

After a 12 inch round pile test, an ice specimen which was spalled off by a horizontal crack was recovered from under the ice sheet. The specimen is show in Figure 5. Although they cannot be seen in the figure, the surface adjacent to the horizontal crack has concentric ridges originating at the pile. The ridges spaced approximately a half an inch, have slight circular depressions between them. It is believed that the ridges are formed by the incremental propagation of the horizontal crack. Other specimens examined during the test program suggest that the spacing of the ridges is related to the temperature of the ice.

Moment and forces measured on the vertical pile test are shown in their positive sence, with their symbols in Figure 6. The eccentricity factor e, which locates the net thrust from the neutral axis, is a fraction of half the ice thickness. Referring to Figure 6 and taking moment, e can be expressed as $e = 2 (V \ell - M) / (T h)$. The distance ℓ is measured between the center of respective strain gages and the centroid of the contact area. Figure 7 is a computer analyzed force record of a 5.5-inch round pile. The short duration loading is typical of the majority of the force records. It is believed that the spike in the eccentricity trace is due to sudden spalling off of ice.

The results of the limited data reduction show considerable scatter, this makes it difficult to draw any rational conclusion. An example of this is the investigation of the initial pile-ice contact condition. It is hypothesized that decreasing the stress concentration, i.e. ridges on the ice contact face, will increase the nominal ice pressure. To examine this phenomenon, the hole drilled as the contact face was prepared in one of the following manners: (1) with an unguided auger with flights, resulting in a non-vertical face ($\pm$ 10°) with flight ridges, (2) a vertical guide

coring auger, leaving a smooth vertical face, or (3) allowing the apparatus to freeze in place. The resulting peak nominal ice pressures were 1200, 900 and 800 psi respectively for the three methods of preparation. The eccentricity trace at the thrust peak indicates that the net force was applied at a quarter point of the ice thickness. Further evaluation of the data will determine the validity of this hypothesis and other concepts. Further analysis and evaluation of the data will be published in a forthcoming CRREL report.

Acknowledgements

The authors express their appreciation for the work done by many member of the technical staff at the U.S. Army Cold Regions Research and Engineering Laboratory, especially D. Garfield, F. Gernhard, J. Kalafut, J. Karalius and C. Martinson. The authors also appreciate the cooperation of the Town of Canaan, NH.

References

Zabilansky, L. J.; D.E. Nevel; and F.D. Haynes (1975) Ice Forces on Model Structures. Presented at the 2nd Canadian Hydrotechnical Conference, Burlington, Ontario.

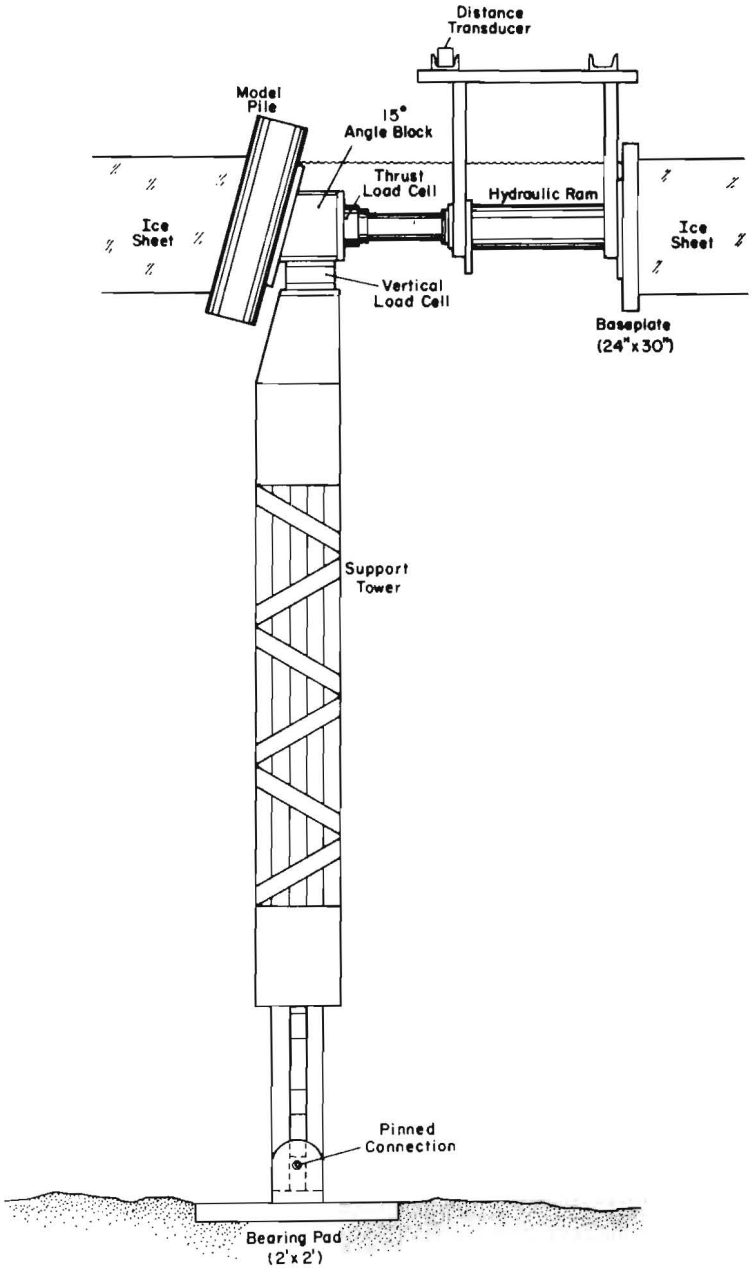

Figure 1. Sloping pile apparatus.

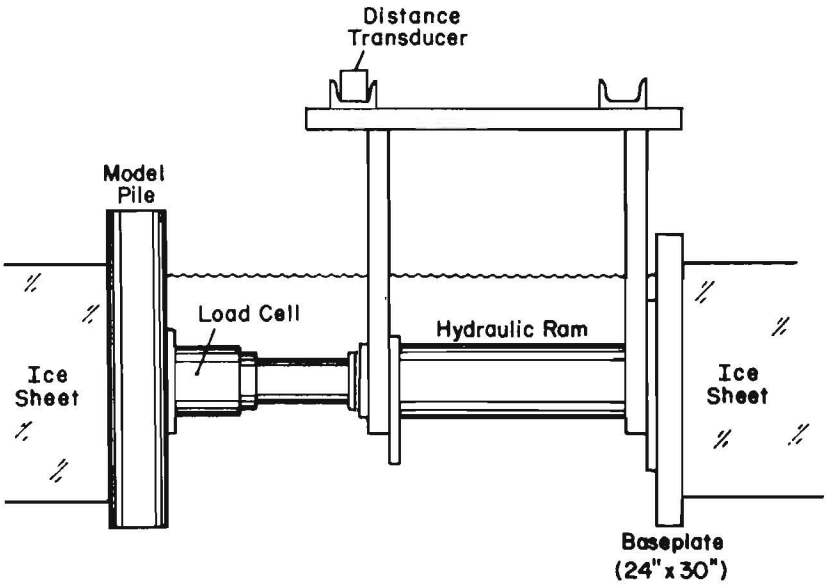

Figure 2. Vertical pile apparatus.

Figure 3. Ice specimen from in front of a 5.5-inch flat pile.

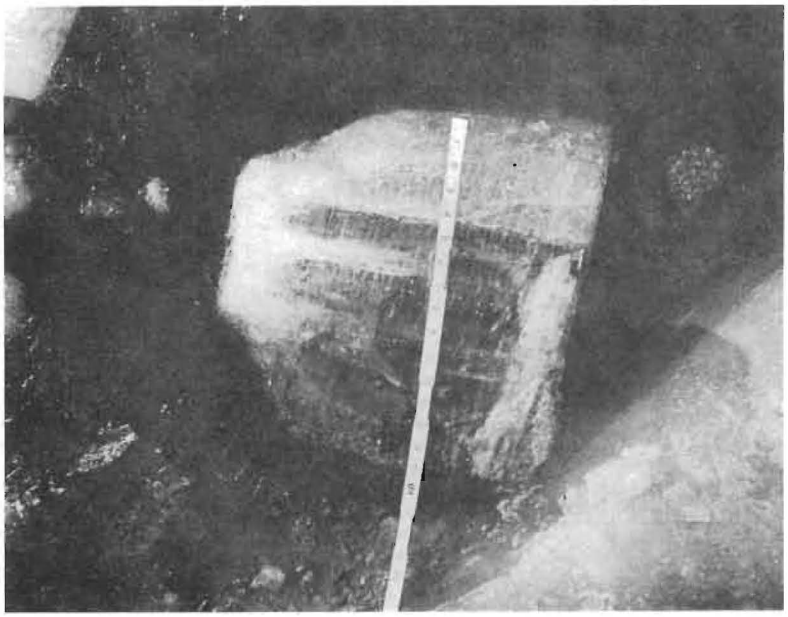

Figure 4. The cross section of the center of the specimen shown in Figure 3.

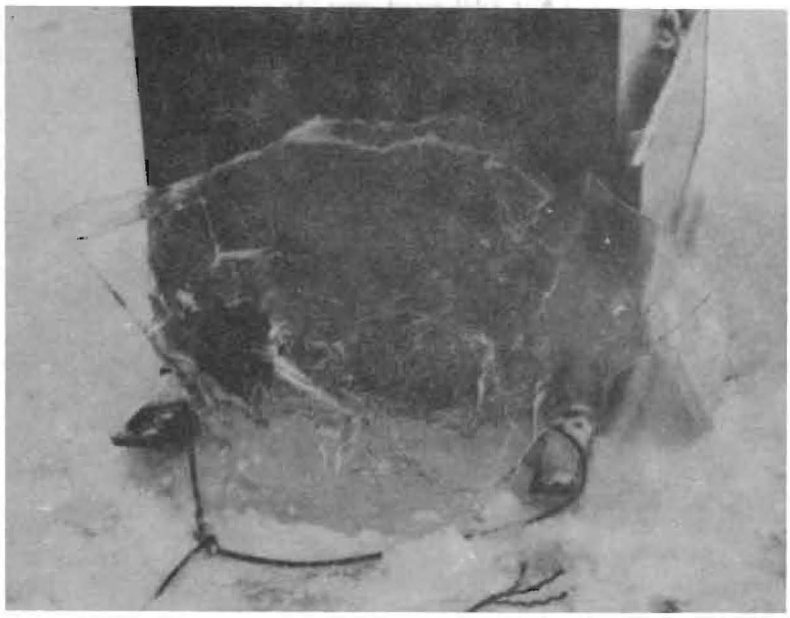

Figure 5. Ice that was spalled off the bottom of the ice sheet by a horizontal crack.

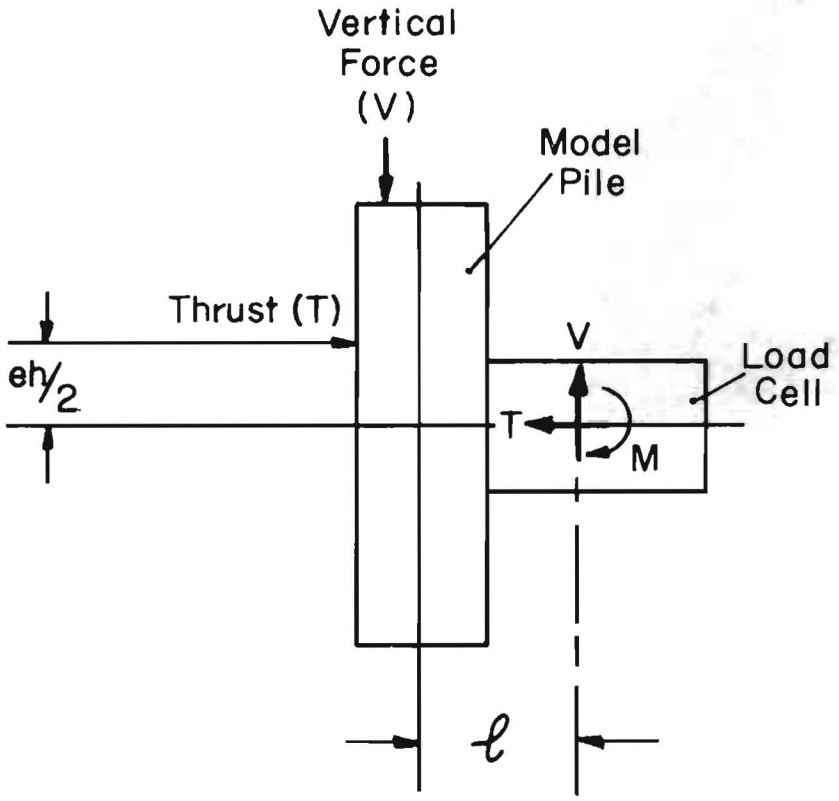

Figure 6. Vertical pile force diagram.

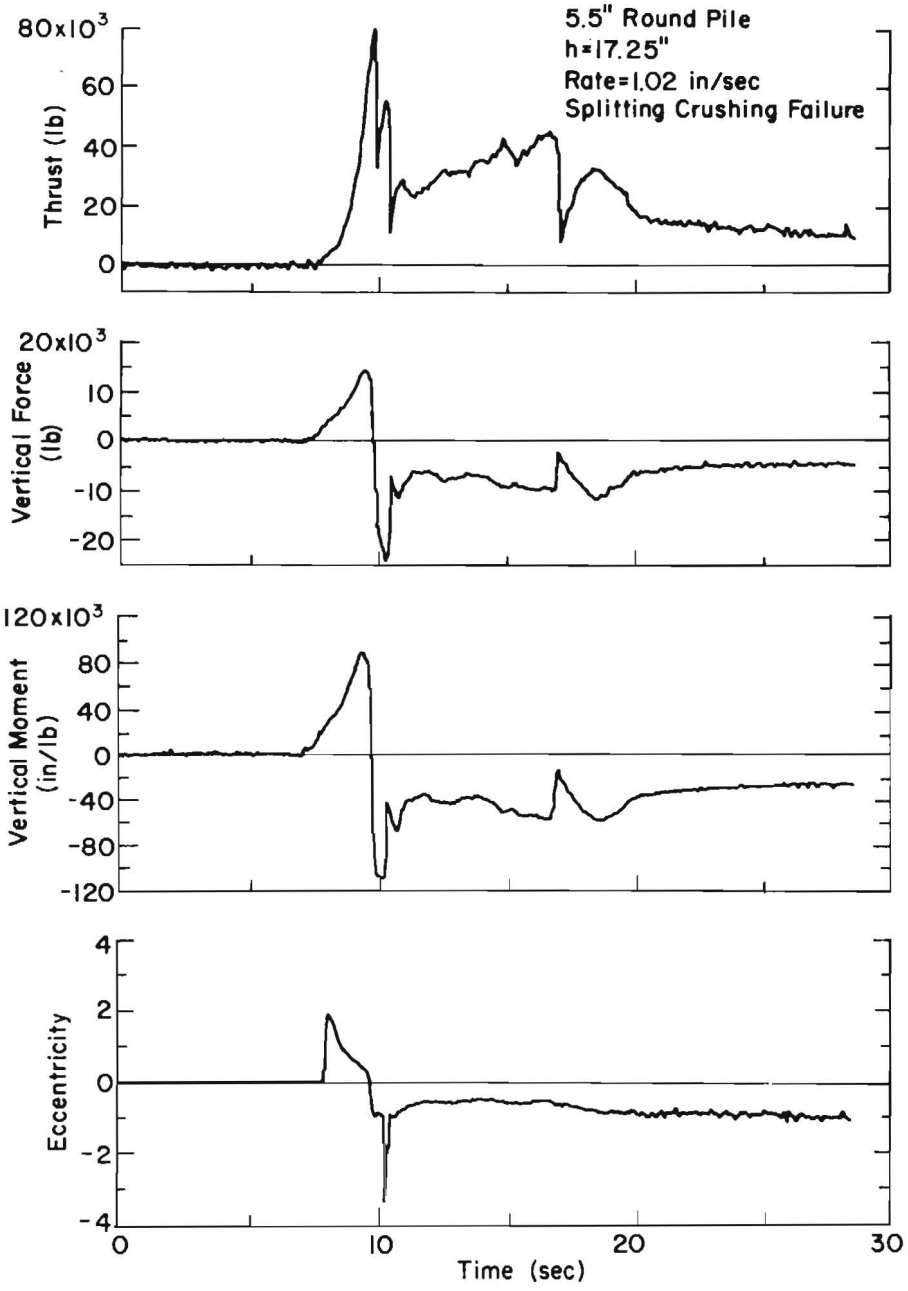

Figure 7. Computer analyzed force record of a 5.5-inch round pile.

THIRD INTERNATIONAL SYMPOSIUM ON
ICE PROBLEMS
Hanover, New Hampshire, USA

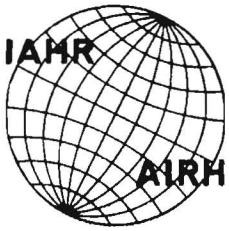

FORCES ON AN ICE BOOM IN THE BEAUHARNOIS CANAL

Roscoe E. Perham, Mechanical Engineer — U.S. Army Cold Regions Research and Engineering Laboratory — Hanover, NH

Leo Racicot, Chef de Division — Hydro-Quebec — Montreal, Que.

Ice booms are used to hasten the formation of a stable ice cover in early winter. Their main function is to reduce the area of open water where large amounts of ice floes and frazile ice can be generated. This ice, if uncontrolled, can cause an ice jam or blockage at power house intakes and restrict its generating capacity. A particular function of the forebay ice boom of the Beauharnois Power House is to prevent any ice upstream from moving down into the forebay.

In 1973, the U.S. Army Cold Regions Research and Engineering Laboratory (USACRREL) assisted the Hydro Electric Power Commission of Quebec (Hydro-Quebec) in making three electrical force measuring systems for installation in the forebay ice boom upstream of the Beauharnois Power House. These systems were installed in the winter of 1973-74 to measure the longitudinal, or downstream push, forces of the ice cover acting on the boom. The main function of the systems was to indicate the level of force in the ice boom structure as a reference for controlling the flow at critical periods of ice cover stability.

The following winter (1974-75) USACRREL installed three of its own systems to measure the corresponding lateral, or cross stream forces, in the forebay ice boom. Force information was obtained from both sets of measurement systems throughout the winter.

The purpose of this paper is to report these forces and their variations. A limited amount of supplemental data such as water flow, ice thickness, and canal dimensions is provided. All of the information should help in the understanding of interaction between an ice boom and its ice cover.

Latyshenkov (1946) studied the force buildup in an ice boom across a small canal due to the collection of ice floes. He found that at first the force increase was proportional to the length of the unconsolidated ice cover behind the boom. But when the length of the cover became equal to 2 1/2 to 3 times the canal width a maximum force was reached which remained constant. Any additional increase in the length of the ice cover is held in place by resisting forces at the shoreline. Kennedy (1958) in his study of forces in the booms used to contain pulpwood explained this phenomenon in terms of a granular material contained between two parallel walls. The longitudinal force is transferred by friction to the shore through an arching effect. This aspect of ice cover formation is quite an important factor in the forces developed in the forebay ice boom. An excellent description of the various factors involved in ice cover formation is given by Pariset and Hausser (1961). Some of the factors are water and air temperature, velocity and depth of water flow, ice floe dimensions, canal configurations, ice friction and cohesion, etc. Also their reply to a paper by Morton (1963) provides further illumination to the subject. Michel (1966) addresses the specific subject of forces in ice booms due to an unconsolidated ice cover and also considers the effect of wind on the cover.

Beauharnois Canal

The Beauharnois Canal is a river diversion canal of the St. Lawrence River about 25 miles (40 km) west of Montreal, Canada. It is a power canal for the Beauharnois Power House and also a part of the St. Lawrence Seaway. The canal and its location are shown on Figure 1(a).

The canal has distance or location markers which are used for navigation reference, ice cover reference, etc. and which show the distance in hundreds of feet from its beginning at Lake St. Francis. See Figure 1(b). The instrumented ice boom is at location 745. The next ice boom upstream is at location 690 or 5500 ft (1.68 km) away. These booms and the canal walls are boundaries for the ice cover that acts on the instrumented boom. The surface area is approximately $16(10)^6$ ft^2 ($1.4(10)^6$ m^2), the average flow area is 107,000 ft^2 (9950 m^2) and the average width is 3050 ft. (930 m). An important feature of this location is the lock entrance which is an irregularity that makes an analysis of forces on the ice boom less reliable.

Forebay Ice Boom

The plan of the forebay ice boom is shown on Figure 1(b). The ice boom structure is comprised of lengths of 2.0 inch (5 cm) diameter steel wire rope and is held in place by anchors on the canal bottom and on shore. The bottom anchors are spaced 118 ft (36 m) apart and each anchor rope supports one section of ice boom. There are four floating ice barrier elements attached to each section. Each barrier is constructed of two parallel steel pontoons and structural steel bracing with a heavy timber lattice on the upstream face. A partly obscured view of the units, and the ice boom, is shown on Figure 2.

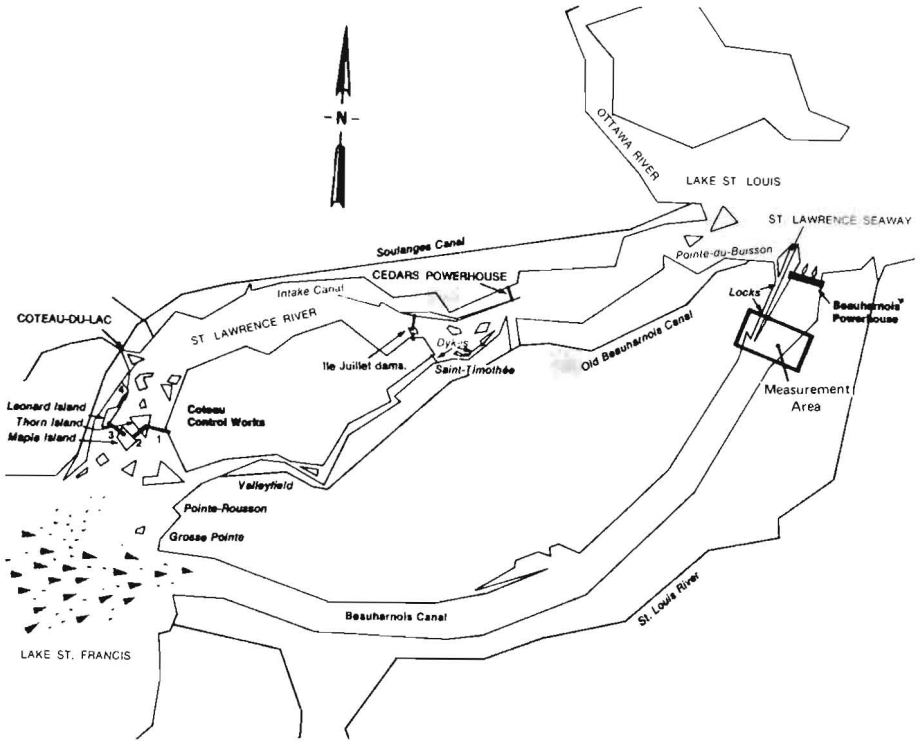

Figure 1(a). Location of the Beauharnois Canal and measurement area.

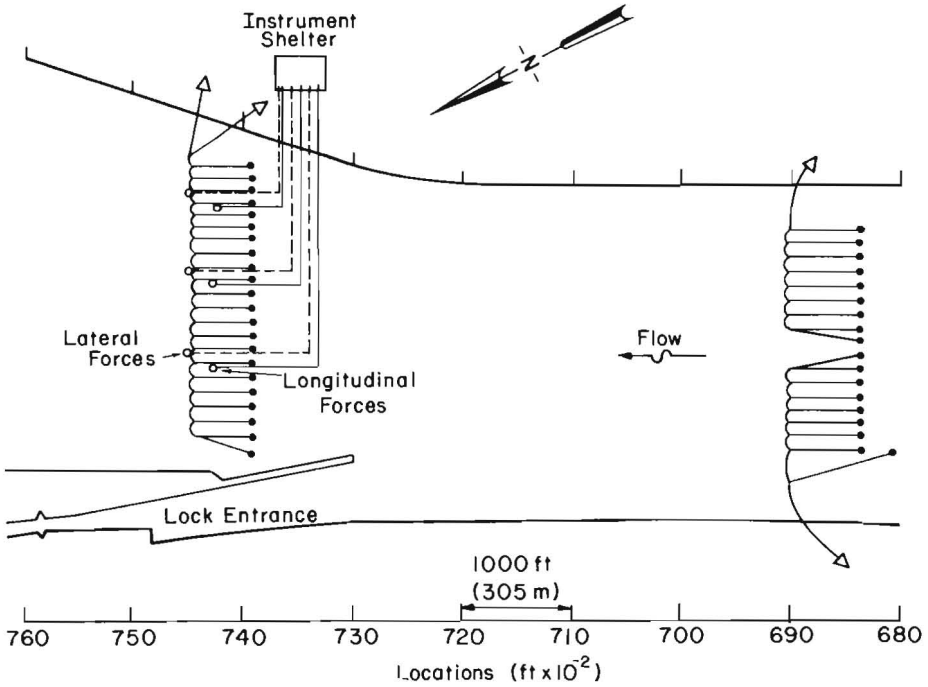

Figure 1(b). Plan of ice booms and measurement systems.

Figure 2. Loaded ice boom indicating sag of 118 ft (36 m) long section.

Measurement System

The primary element of the measurement system is the tension link which is an oblong steel plate with reinforced holes at each end and a centrally positioned strain gage circuit which senses the load on the link. The average sensitivity for each tension link is 6.30 millivolts per volt at the rated load of 300,000 lbs (1.33 MN). It is fully described by Perham (1974). The circuit is connected to shore by an armored cable which contains several electrical conductors. A lateral force link is shown in the installed position in Figure 3. It is put in series with the wire rope that holds the ice barrier units and receives contact from moving ice. The longitudinal force links were located deep under water away from the ice cover. The circuit excitation supplies and strip chart recorders were located in a shelter adjacent to the site on shore. The general arrangement of the lateral and the longitudinal force measuring systems is shown on Figure 1(b).

Supplemental Measurements

The volumetric flow rate Q of water is used to calculate an average water velocity, v, and it is obtained from the power house records. The

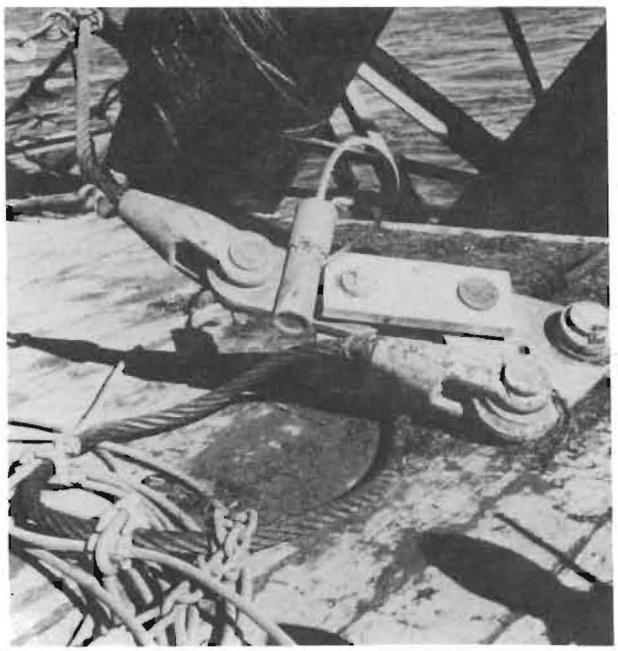

Figure 3. Tension Link and ice boom cable connections.

flow rate is given on Figure 4. A record of the hydraulic levels is also kept and some of the values have been converted to slope as shown on Figure 5. The wind can have a substantial effect on the ice cover; and a rotating cup anemometer, direction indicator and strip chart recorder were located at the shelter shown on Figure 1. Temperature records were kept to permit calculation of a freezing index called degree days below freezing (of water) or (day-degrees fahrenheit). The index is given on Figure 6. The average values of ice thickness at two different cross stream locations are shown on this latter figure.

The ice thickness measurement program was started as soon as the ice cover was thick enough to support a light helicopter. It was discontinued after the start of the navigation season on March 24th.

The freezing index shows that cold weather was present until after the ice left the canal. The ice thickness data shows that there was no excessive thickening of the cover at least not before March 24th.

The size, or area, of the early ice cover progression is shown on Figure 5. It is based on ground and airborne estimates but not aerial photographs.

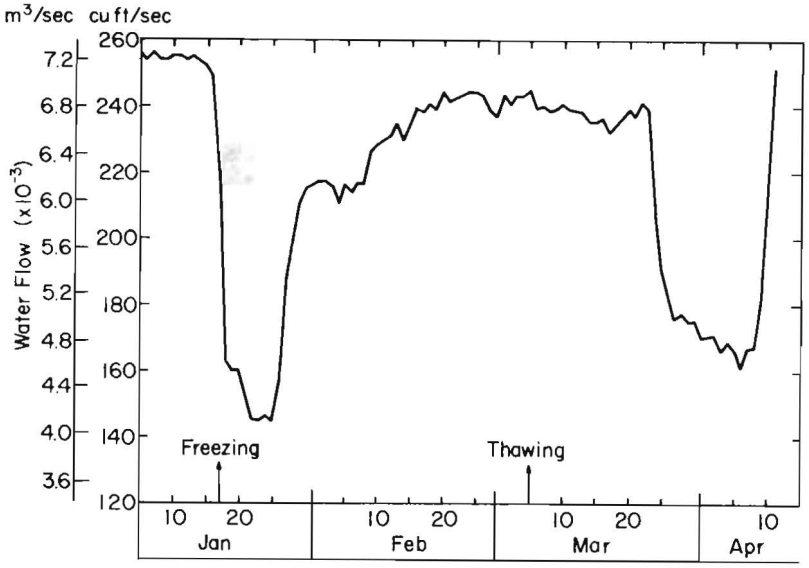

Figure 4. Average Water flow Beauharnois Canal 1975.

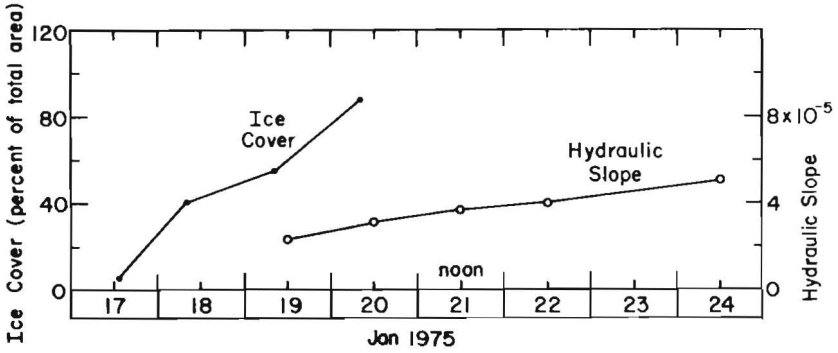

Figure 5. Early ice cover growth and hydraulic slope.

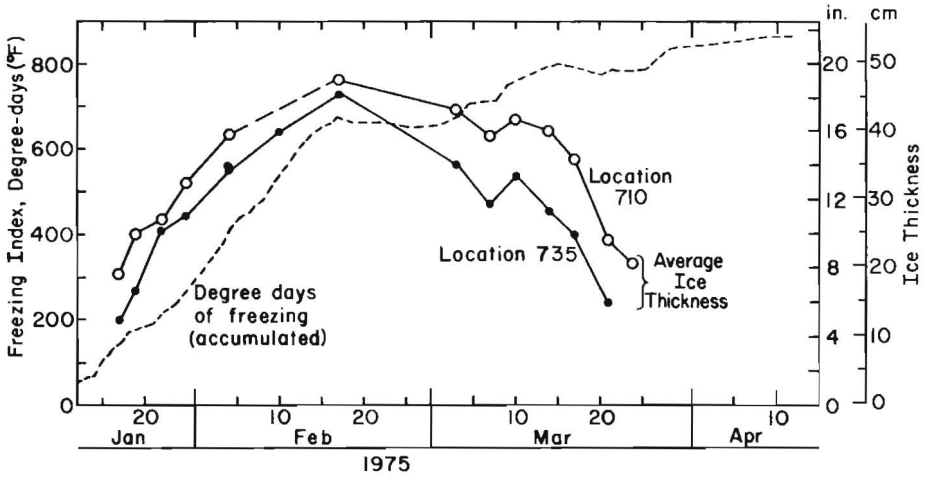

Figure 6. Average ice thickness and freezing index.

Results of Force Measurements

The winter of 1974-75 was rather mild and the ice cover did not begin to form until the 17th of January. Figure 6 shows that there had been an accumulation of only 50 degree days (Fahr) by that date. The freezing index levelled off in mid February but started to rise again in early March and continued to rise slowly even after the ice left the canal on April 11th. The navigation channel was opened up by ice breaker on March 24th. The north end of the forebay ice boom was also opened then.

The results of the measurement program are presented in graphical form as averages of all readings or of sets of readings. The values come from tables of readings and several readings were taken each day. Continuous data from each recorder were also available for reference.

Figure 8 gives the average force for all systems during each day of winter 74-75. The only deviation made in treating the data was applied to the data for the first few days in April. During this time the most southerly longitudinal force system gave values substantially higher than the other five; as high as 300,000 lbs (1.33 MN).

As Figure 8 shows there are three distinct periods or phases for the ice boom forces. The first one is when the unconsolidated ice cover is forming. The middle period is when the ice cover is solid and stable and the last period seems to include solid, partly solid, and unconsolidated ice cover conditions.

The average forces on the forebay ice boom during the unconsolidated ice cover phase are given on Figure 8. The lateral force levels are substantially higher than the longitudinal forces, but both curves are nearly parallel. The lateral force level starts to rise on January 17th to a definite level of 22,000 lbs on the 18th where it remains for one day. It then moves to a level of 36,000 lbs and remains there most of the following day. It then gradually drops to an intermediate level around 23,000 lbs (102 kN) until the 25th. On that day the lateral force drops rapidly from 25,000 lbs (111 kN) to about 2000 lbs (8.9 kN).

The average forces remain nearly equal to each other during the period of solid ice cover and Figure 7 should suffice.

Part of the period of ice breakup is shown on Figure 9. It starts on March 22nd when the average lateral force increases from 8000 lbs (36 kN) to 19000 lbs (84 kN). The longitudinal force remains unchanged for about two more days. March 24th is a day of force fluctuation. The northerly end of the ice boom was opened then and the breaking of ice in the navigation channel began. Reference to Figure 5 indicates that the water flow was reduced on that day. This was done to stop a flow of ice over the boom.

A high average longitudinal force of 96,000 lbs (430 kN) was registered on March 26th. This is the equivalent of over 800 lbs per linear foot of span (11.3 kN/m). From the evening of March 26th through the 29th the forces fluctuate from about 26,000 lb (116 kN) to 51,000 lb

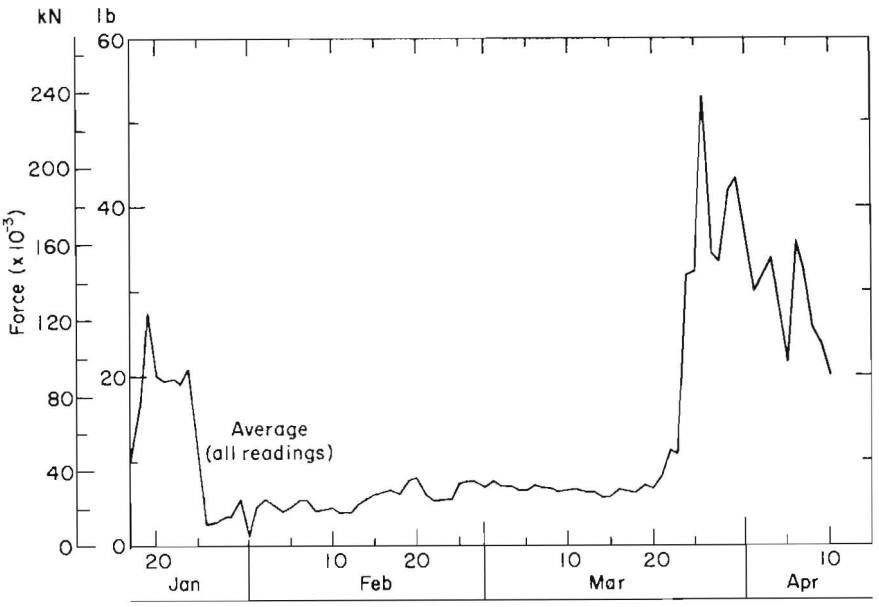

Figure 7. Average forces in the forebay ice boom.

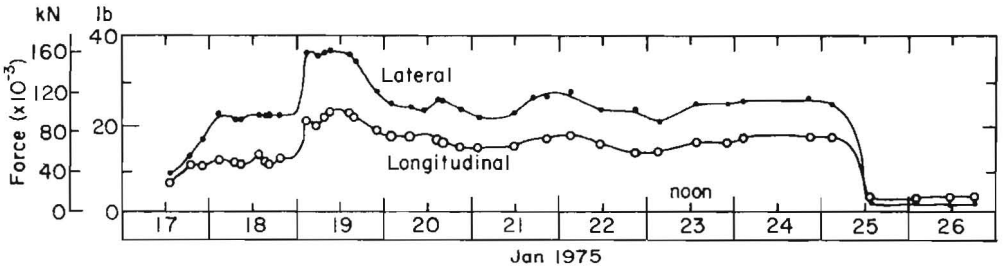

Figure 8. Average forces from unconsolidated ice cover.

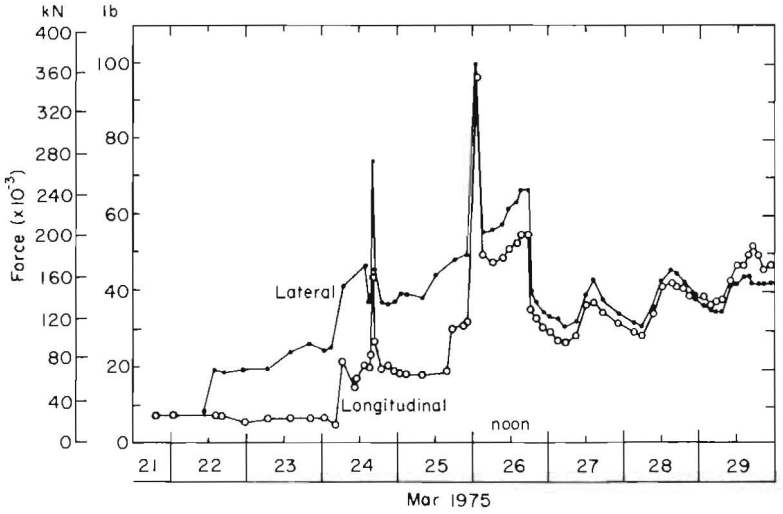

Figure 9. Average forces - early ice break-up period.

(227 kN). It should be noted that from the 24th through the 25th the ratio of lateral forces to longitudinal forces remained about the same as it was during the unconsolidated ice cover phase. After the high forces of the 26th, however, the forces were nearer to being equal. By March 29th the lateral forces were even lower than the longitudinal ones.

The full period lasted from March 20th until April 11th. The maximum average force from the tabular results (Fig. 8) was 53,000 lbs (240 kN) but this should not be thought of as the maximum average force developed in the boom. For example, a check of the strip charts from the recorders shows that the peak average force at 1700 hrs on April 2, 1975 was 84,000 lbs (370 kN).

Shear Stress Estimate

The forces on the ice cover are the hydrodynamic force of water at the upstream edge of the ice cover, the shear force of water flowing by the underside of the cover, the downstream component of the weight of the ice cover and the wind drag. That portion of the force which is not carried by the canal shore is carried by the ice boom structure.

Because the wind drag varies in intensity and direction, it will be given brief consideration in the concluding section with respect to one particularly interesting phenomenon. The force on the upstream edge of the ice cover is expected to become negligible when that edge reaches the next ice boom. This occurred on January 20th. The gravity force, the shear force, and the shore line forces are the only ones that continually affect the boom load throughout the winter. Of these, the gravity force would have the least effect. An estimate of the gravity force under the maximum conditions (see Fig. 5, 6 and 10) present during the unconsolidated ice cover period is 1500 lbs (6.7 kN), which is a relatively small value.

A rough estimate of the level of shear stress under the ice cover due to water flowing past it can be made in two ways. In the first way the value for longitudinal force is divided by the area of ice held back by one anchor rope. This value is called σ. In the second way the data on water flow, canal geometry and hydraulic head losses are converted to friction loss terms that are described in most fluid flow text books (Rouse, 1946). These are: The mean shear stress $(\tau_o)m$, sometimes called wall shear stress; the Manning boundary roughness factor n; and the Chézy flow coefficient C. The expressions for these terms are not given here because they are assumed to be well known in the field of hydraulics. Values for each term for several dates are given in Table I.

The values for σ would only be good indicators of the shear stress condition when the shoreline force on the ice cover is negligible. This occurs when the length of ice cover behind the boom is short and during spring ice breakup when the cohesion between the ice and shore can become negligible (Pariset and Hausser, 1961). Calculation of $(\tau_o)m$, n, and C assumes that the boundary roughness of the ice is the same as that of the canal bottom, that the flow area is constant and that the ice covered canal is a conduit.

One more term or parameter that is frequently used when discussing ice booms, ice covers and ice jams is the Froude number N_{Fr}. Values for N_{Fr} are also given on Table I. The Froude number is a dimensionless ratio of inertia force and gravity force in the fluid flow system. In this case, it refers to under ice velocities and depths.

Table 1. Values of shear stress and reference factors for selected dates

Date	Stress from forces σ lb/ft^2	Pascal	Mean stress from flow effects $(\tau_o)_m$ lb/ft^2	Pascal	Average flow coefficient or roughness Chézy C	Manning n	Froude No. N_{Fr}
Jan 17-18	0.028	1.3	-	-	-	-	-
18 Jan	0.049	2.3	0.027	1.2	70	0.034	0.029
19 Jan	0.069	3.3	0.037	1.8	59	0.041	0.030
19 Feb	0.011	0.53	0.216	1.0	42	0.063	0.053
29 Mar	0.079	3.8	0.043	2.1	63	0.038	0.036
2 Apr	0.129	6.2	0.045	2.2	59	0.040	0.033

Discussion and Conclusions

It was unexpected to have the longitudinal force achieve three different levels of force before the solid ice cover was established. There may be some type of interaction between the newly forming ice cover and the rapid increase in wideness of the river as the ice cover progresses upstream past the navigation lock entrance. A more plausible reason may be an influx of frazil ice which is known to increase the drag between water and ice. This effect may or may not be noticeable each year. Therefore, it may take several years of data evaluation before it is understood.

A second unexpected result was that the lateral loads were higher than the longitudinal loads as is shown on Figures 4 and 5. This was resolved as being caused by the anchor cables at the outer most ends of the ice boom which did not allow each ice boom section to sag (Fig. 3) as much as their geometry would ordinarily permit. This general relationship, that was started in early winter, was continued in late winter as the ice cover started to push more heavily against the boom. The northerly end of the forebay boom was opened on March 24th but the difference between the two did not change noticeably until March 26th when some peak loads occurred. By March 29th the lateral load was less than the longitudinal load which was the expected relationship.

The abrupt drop in force level on Jan 25th of 13,000 lbs (58 kN), longitudinal, was probably due to the effect of a strong NE wind which had an upstream component of 19 mph (8.5 m/s) at the 10 meter height.

The wind force on the ice was estimated to be 3000 lbs (13 kN). The estimate was based on a field estimate of 6 inches (15 cm) average ice roughness height and the Karman-Prandtl equation for turbulent flow near rough boundaries (Rouse, 1946). This force level, however, is not enough to account for the drop shown. The drop is thought due to the cooling effect of the 25°F (-4°C) wind which caused the ice cover to generally solidify and become fast to shore.

By March 29th the ice cover seemed to have become unconsolidated again. The ice cover also seemed sensitive to warming conditions. A look at the force levels from March 26th through the 29th (Figure 9) show that the ice cover seems to relax its hold on shore and push more strongly against the boom during the afternoon.

The values for apparent roughness of the Beanharnois canal in this area seem to be quite high. The reason for it may be the proximity of the lock entrance. This factor will need further investigation before much effort at separating ice cover roughness from canal roughness is made.

The ice boom load indicating systems were operated successfully throughout the winter. They are useful as an operational reference and as research tools. The only recommended change that would make them more useful as a research tool would be to move them to a location where the channel width is more uniform.

Bibliography

1. Latyshenkov, A.M. (1946) "A study of protective ice booms." Gidrotechnicheskiye Stroitel'stvo in Russian, vol. 15, no. 4, p. 13.

2. Kennedy, R.J. (1958) Forces involved in Pulpwood holding grounds. The Engineering Journal of Canada, January.

3. Pariset, E. and R. Hausser (1961) Formation and Evolution of Ice Covers on Rivers. Trans. Eng. Inst. Canada, vol. 5, no. 1, p. 41.

4. Morton, F.I. (1963) Criteria for the stability of ice covers on rivers. Proceedings of the 1963 Annual meeting, Eastern Snow Conference, Quebec City.

5. Michel, B. (1966) Thrust exerted by an unconsolidated ice cover on a boom. Ice Pressures against structures (March 1968), National Research Council Technical Memorandum #92, NRC No. 9851, Ottawa. Proceedings of a conference held at Laval University, Quebec 10-11 November, 1966.

6. Rouse, H. (1946) Elementary Mechanics of Fluids. John Wiley and Sons, Inc. New York.

7. Perham, R.E. (1974) Forces generated in ice boom structures. Special Report SR 200, U.S. Army Research and Engineering Laboratory, Hanover.

THIRD INTERNATIONAL SYMPOSIUM ON
ICE PROBLEMS
Hanover, New Hampshire, USA

INSTRUMENTED PILES FOR THE MEASUREMENT OF ICE-UPLIFT FORCES

R. J. Hodek,
Associate Professor of
Civil Engineering

J. O. Doud,
Graduate Asst.

Michigan Technological University

Houghton, Mich.
USA

INTRODUCTION

Ice-induced loads on pile supported marine structures have been recognized as significant under some conditions, and structures designed for high lateral loads or heavy vertical loads in compression have usually performed adequately in recent years. However, dock facilities at recreational harbors along the Great Lakes have not fared as well. Unless ice-free conditions are maintained around each pile, the governing pile design parameter will probably be the tensile or uplift force. Failure to properly estimate this force results either in an unnecessarily high first-cost or annual repairs.

The estimated uplift force on a pile caused by a floating ice sheet frozen to this fixed pile when the water level rises requires an estimate of the ice thickness, rate of loading, failure model, and the appropriate ice or ice-pile interface strength. Various plate models or bearing capacity theories (6, 8) are available, and ice strength relations (3, 4, 5) as well as ice-pile shear strength values (2, 7) have been determined. However, the time-dependent nature of the strength relation indicates the need to determine realistic loading rates and these are not generally available.

Large scale outdoor laboratory tests of artificially loaded timber piles which had been frozen into an existing floating ice sheet have been reported by Frederking (1), and similar model tests using concrete piles are currently underway at USACRREL in attempts to better develop the ability to predict the vertical loads which will act on a fixed pile

frozen to a floating ice sheet. Full scale field observations are necessary to provide actual loading rates, peak loads sustained by the pile, and visual failure patterns in the ice surrounding the pile.

This paper describes instrumentation which was developed to measure ice uplift forces acting in the field under natural conditions.

INSTRUMENTATION PACKAGE

Two general alternatives are available for instrumenting marine piles to observe ice-induced vertical loads. The first is to attach mechanical or electrical strain gages or load cells at a distance below the depth of maximum ice thickness. For existing marine piles this approach is all but impossible due to the working environment. If instrumentation can be provided before pile driving, these piles should enjoy the same success as instrumented onshore foundation piles have shown.

The second alternative, the one chosen, merely uses the existing pile as a support or reaction. A sleeve of slightly larger diameter than the pile is installed around it, suitably instrumented, and allowed to freeze in. The measured loads are those acting on the sleeve. This system offers the advantages of portability, relatively low cost, reusability elsewhere, and repairability. In addition, the metal sleeve may be given any of a variety of surface treatments to examine this variable.

Pile Sleeve

The system designed for this study consists of a two-piece vertically split cylindrical sleeve which surrounds the pile and extends from above the high water line to below the depth of maximum ice thickness. It was supported from above the water or ice line by a pair of strap load transducers, 180^{o} apart, attached to a mount which was free to rotate in the horizontal plane. Each half sleeve had a 45^{o} rosette of 350 ohm strain gages mounted on its inner surface at the approximate ice line to monitor ring compression. Figure 1 shows the support mount, a half sleeve, and one load transducer. The reaction for the support mount was provided by the structural steel dock skeleton which was integral with the pile.

This sleeve had an inside diameter of 14", a 3/8" wall thickness, a total length of 48" and was made of mild steel. It was designed to accommodate a 12" diameter spiral-weld pipe pile, and was coated with red lead oxide paint to approximate the finish of the insitu piles at the Ontonagon Marina.

Before installation the inner surface of each half sleeve was completely coated with a ½" thick layer of water resistant grease to insure that water freezing between the sleeve and pile would not cause them to act as a unit. Installation and underwater bolting was accomplished with the aid of a diver. After installation, additional grease was

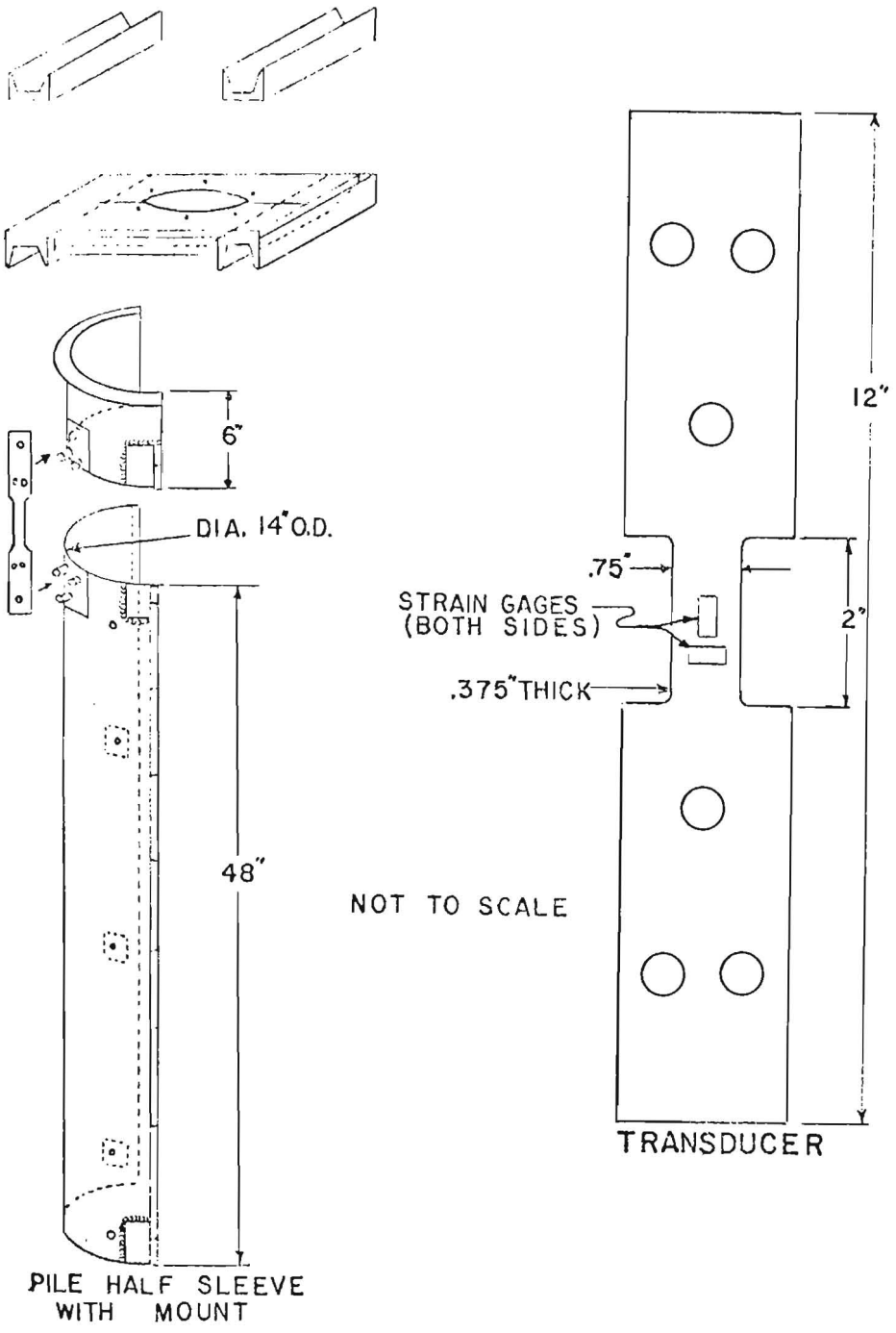

FIGURE 1. SUPPORT MOUNT, HALF SLEEVE, AND TRANSDUCER

added through grease fittings in the sleeve to drive out as much water as possible.

Force Transducers

For this application custom transducers, as shown in Figure 1, were fabricated. The transducers were made of Grade 6061-T6 aluminum. They were weatherproof, showed no noticeable hysteresis, were compensated for bending in the weak axis, and were temperature compensating. Each transducer had two 350 ohm strain gages at 90^{o} on each side wired into a full bridge.

Weatherproofing of the gages was provided by an oven-cured four-layer coating consisting of an acrylic moisture barrier, a nitrile rubber coating, a polysulfide epoxy coating, and finally a nitrile rubber outer coat. This four-layer coating was used for the strap load transducers located above the ice line as well as the rosettes on the half sleeves which were submerged.

Since the recording system would be required to operate for a period of several months with no opportunity to make external checks on the amplifier's zero drift, a full bridge drift block was incorporated at the pile for corrections to the output.

Figure 2 shows the response of one of the load transducers in the laboratory at -18^{o} C. This calibration check was made after the transducers were removed from the field after three months' service. It showed no change from the initial calibration.

FIELD PERFORMANCE

Two instrumentation packages were fabricated and installed at a marina on Lake Superior in late January, 1975. The site chosen for the evaluation was the Ontonagon Marina at Ontonagon, Michigan, which is about eighty miles east of the Wisconsin-Michigan border on Lake Superior's south shore.

This marina has a history of ice-uplift problems and was recently completely rebuilt and upgraded. It consists of a main service pier with a series of finger piers on each side.

Two existing piles were chosen for instrumentation. These 12-inch diameter concrete-filled steel pipe piles support finger piers and since their installation in 1972 they have not moved due to ice uplift. At the time of installation the ice thickness was approximately 30 inches. This ice was subsequently cut and removed from a radius of about seven pile diameters to partially remove the boundary effects of the existing ice sheet.

Power was continuously supplied to the strain gage bridges which were automatically scanned and read at five-minute intervals by a

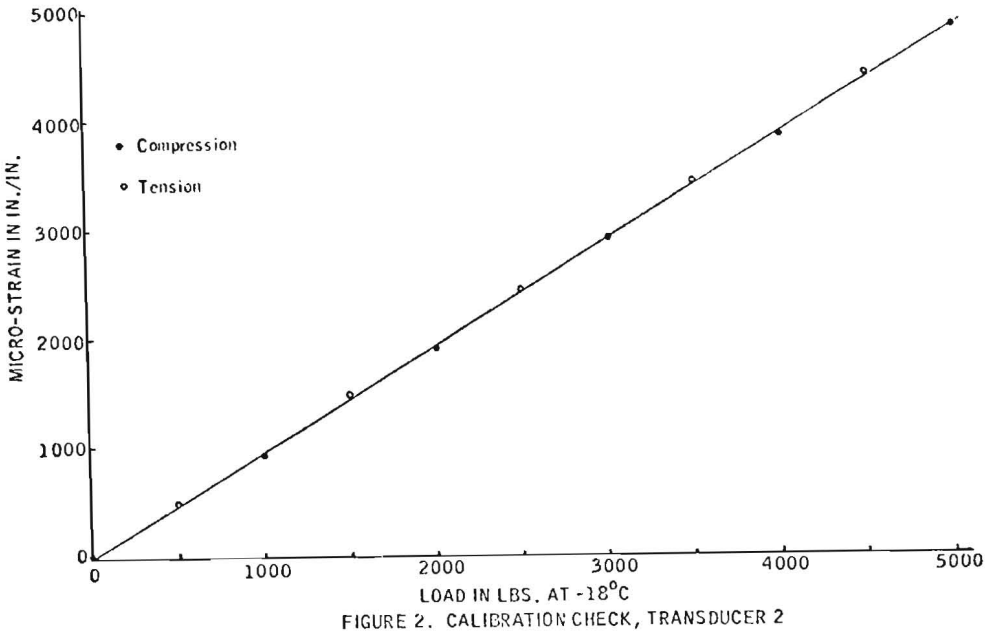

FIGURE 2. CALIBRATION CHECK, TRANSDUCER 2

B & F strain recorder. In addition, the air temperature and water level adjacent to the instrumented piles were continuously recorded on separate and independent recorders. Pile load and air temperature data were collected from early February through mid-April, and water level records were kept from mid-February through mid-April.

Typically there was an almost constant fluctuation of the water level. The amplitude varied to an observed maximum of 0.8 feet and the major period varied from 5 minutes to more than 10 hours. The tensile and compressive loads on the piles varied in direct response to this change in the elevation of the floating ice sheet.

Figure 3 is a plot of the loads measured on one of the instrumented piles in the early morning of February 11, 1975. At this time there were 8 inches of clear lake ice at the pile and a crack pattern had already formed. At 0305 hours a 7,500 pound tensile load was recorded for this pile. The same general pattern as shown in Figure 3 continued throughout the season. However, due to the mild winter only slush ice developed after this time and no larger uplift loads were recorded. At no time during the observation period were significant ring compression loads recorded.

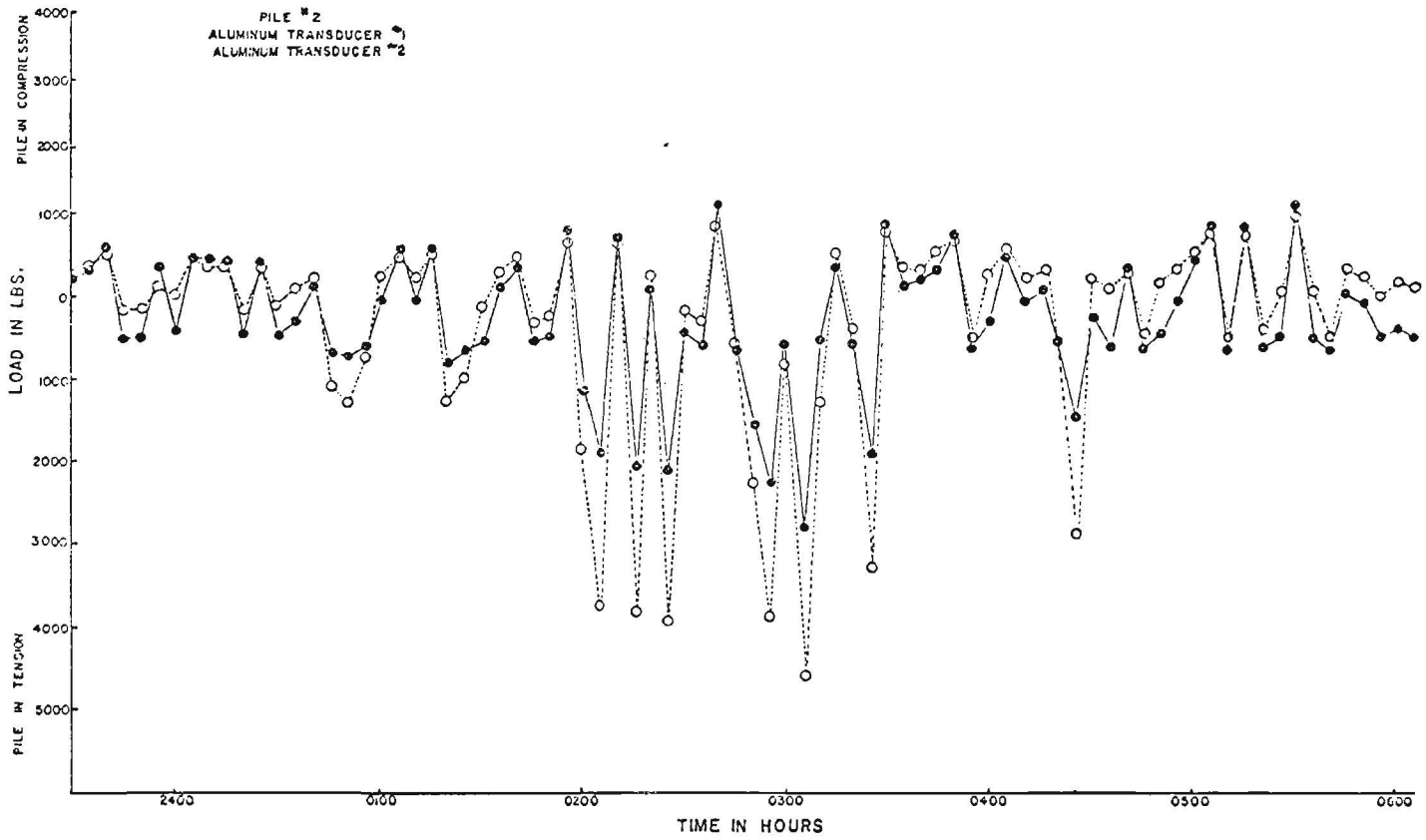

FIGURE 3. VERTICAL ICE LOAD ON PILE #2, FEB. 10-11, 1975

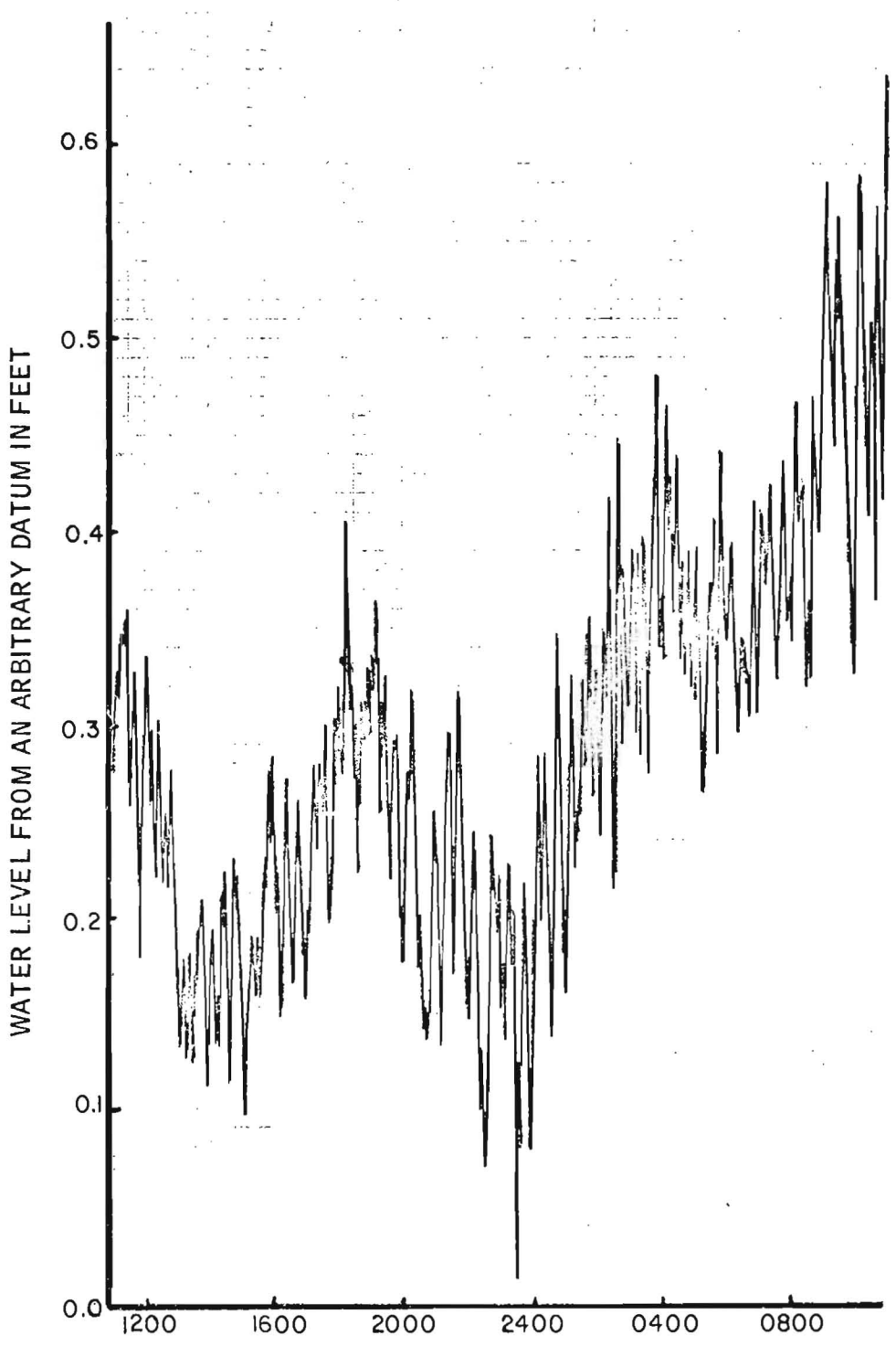

FIGURE 4. WATER LEVEL AT ONTONAGON MARINA, FEB. 21-22, 1975

Figure 4 shows the typical water level fluctuations observed at the Ontonagon Marina. It indicates the superposition of a high frequency water level oscillation on an oscillation whose period is measured in hours rather than minutes. Observations in other locations indicate that this condition is quite common on Lake Superior and is not confined seasonally or geographically.

SUMMARY

A relatively simple system has been developed to measure the vertical force developed by a floating ice sheet on a static pile due to water level fluctuations. The instrumentation has been field tested and appears to yield reliable results.

An analysis of the results of this initial field program indicates that the ice-pile failure mechanism may change as the winter season progresses and in response to the relation between rate of increase of the ice thickness and the amplitude and frequency of vertical movement of the floating ice sheet.

ACKNOWLEDGMENTS

This research was conducted with the financial support of the U.S. Army Cold Regions Research and Engineering Laboratory. Their interest and support are gratefully acknowledged.

REFERENCES

1. Frederking, R., "Downdrag Loads Developed by a Floating Ice Cover: Field Experiments," Canadian Geotechnical Journal, Vol. II, No. 3, August 1974, pp. 339-347.

2. Freiberger, A., and Lacks, H., "Ice-Phobic Coatings for Deicing Naval Vessels," Proceedings of the Fifth Navy Sciences Symposium, 1961, pp. 234-237.

3. Gold, L. W., "Elastic and Strength Properties of Fresh-Water Ice," Proceedings of the Conference on Ice Pressures Against Structures, Quebec City, November 1966, pp. 13-23.

4. Gold, L. W., "Process of Failure in Ice," Canadian Geotechnical Journal, Vol. 7, No. 4, November 1970, pp. 405-413.

5. Gold, L. W., and Krausz, A. S., "Investigation of the Mechanical Properties of St. Lawrence River Ice," Canadian Geotechnical Journal, Vol. 8, No. 2, May 1971, pp. 163-169.

6. Kerr, Arnold D., "The Bearing Capacity of Floating Ice Plates Subjected to Static or Quasi-Static Loads - A Critical Survey," Research Report 333, U. S. Army CRREL, March 1975, 43 pp.

7. Michel, B., Ice Pressure on Engineering Structures, U. S. Army CRREL Monograph III-Bib, June 1970, 71 pp.

8. Timoshenko, S., and Woinowsky-Krieger, S., Theory of Plates and Shells, Second Ed., McGraw-Hill, New York, 1959, pp. 259-281.

THIRD INTERNATIONAL SYMPOSIUM ON
ICE PROBLEMS
Hanover, New Hampshire, USA

ICE FORCES ON STRUCTURES

DUE TO A CHANGE OF THE WATER LEVEL

Dr. Arnold D. Kerr
Visiting Professor Princeton University Princeton, N.J.
U.S.A.

SUMMARY

The determination of vertical forces a floating ice cover exerts on a frozen-in circular pier or pile, due to a change of the water level, is discussed and analyzed. Since for engineering purposes the knowledge of the largest possible force is often sufficient, the analysis is restricted to the assumption that the ice plate responds elastically. In order to reduce the necessary calculations in the field to a minimum, the obtained results were evaluated numerically for a wide range of geometrical and material parameters which occur in practice and are presented graphically.

INTRODUCTION

When the water freezes over a river or a lake, the formed ice plate adheres to the structures it surrounds or adjoins to. Subsequently, any change of the water level creates forces between the ice plate and the structure. Examples of such structures are shown in Fig. 1.

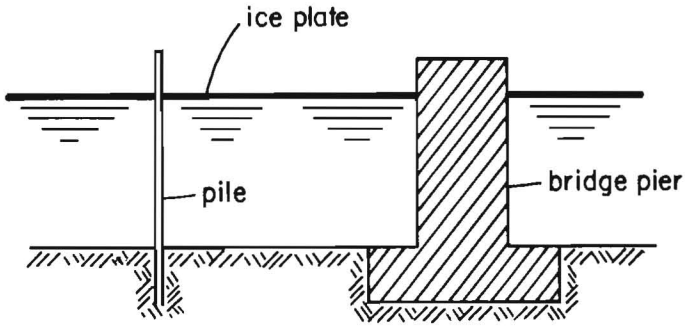

Fig. 1

In case the ice plate surrounds a bridge pier, a *rise* of the water level generates an upward force on the pier that, under certain conditions, may be sufficient to lift the pier off the base. In the case of a pile, the force may be sufficient to pull the pile out of the ground.

When the water level *drops*, the ice plate exerts a downward force on these structures. In the case of a slender pile the induced compression force may be sufficient to buckle it.

To prevent lift off, pull out, or buckling of such structures, the designer has to know the forces an ice plate will exert on the structure due to the anticipated changes of the water level.

Early attempts to determine these forces were made by A. N. Komarovskii [1], B. Löfquist [2], and A. P. Kuznetsov [3]. In view of the assumptions made by these authors, their results should be used with extreme caution.

It is well known that ice exhibits a viscoelastic response. Thus, when the water level is changed abruptly by Δ, the vertical force that the ice cover exerts on a structure is largest at the instant of change, because of the inherent relaxation of stresses in the ice. For the same reason, if instead of an instant change the water level changes slowly to the same fixed value Δ, the resulting vertical force will always be smaller than the force that corresponds to the instantaneous change. This conjecture is in agreement with results of the special cases analyzed by D. E. Nevel [4].

Noting that for design purposes of interest is often only the *largest* vertical force, the analysis may be simplified by considering only the elastic case. An attempt to solve this problem, for a circular pier, was recently made by A. I. Gamayunov [5], who based it on the bending theory of elastic plates. However, Gamayunov introduced a number of simplifying assumptions which make his results questionable. Gamayunov's results were recently included in a book on the action of ice on engineering structures by K. N. Korzhavin [6].

Some of the simplifying assumptions introduced by Gamayunov are not necessary, since the elastic problem under consideration may be solved exactly. The purpose of the present paper is to derive the exact solution for the circular pier and then to present the results graphically. The presented graphs greatly simplify the use of the obtained results and make possible their utilization also by those not familiar with Bessel functions.

LARGEST LIFTING FORCE DUE TO A RISE IN WATER LEVEL

Consider an infinite elastic plate rigidly attached to a circular pier of radius a, as shown in Fig. 2. Assume that at a certain instant the water level is raised by Δ.

Far away from the pier the plate follows the rise of the water level. However, at the pier the plate is rigidly attached and hence along the contact area it cannot move up or rotate. The resulting deflection surface is schematically shown in Fig. 2. Due to the constraints at the pier, the ice plate will exert on the pier a vertical upward force.

The resulting stresses in the plate, and the axial force induced in the pier, are the same as for the case when the water level remains unchanged but the pier is displaced downward by Δ. Because this second problem is easier to analyze, its formulation is used for the analysis of the problem under consideration.

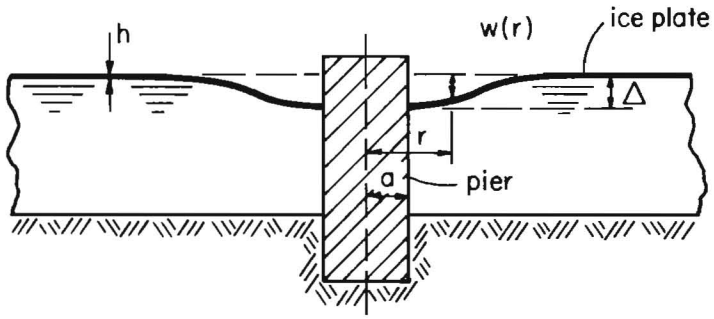

Fig. 2

In the following it is assumed that the floating ice field is of uniform thickness h and that Young's modulus E varies along the thickness of the plate. It is also assumed that the resulting motions of the plate and liquid base are so slow that the inertia effects are negligibly small.

With the notation shown in Fig. 2, the problem reduces to the solution of the differential equation (Ref. [7])

$$D\nabla^4 w + \gamma w = 0 \qquad \text{in } a < r < \infty \tag{1}$$

subjected to the boundary conditions

$$\left.\begin{aligned} w(a) &= \Delta \\ \left.\frac{dw}{dr}\right|_{r=a} &= 0 \end{aligned}\right\} \tag{2}$$

and the regularity conditions at $r=\infty$. In the above formulation w is the vertical deflection of the plate reference plane, a is the radius of the pier cross section, and γ is the specific weight of water. Since the posed problem is rotationally symmetrical it follows that

$$\nabla^4 = \left(\frac{d^2}{dr^2} + \frac{1}{r}\frac{d}{dr}\right)^2 \tag{3}$$

The flexural rigidity of the ice plate is

$$D = \frac{1}{1-\nu^2}\int_{-z_o}^{h-z_o} z^2 E(z)\,dz \tag{4}$$

The position of the reference plane, z_o, shown in Fig. 3, is determined from the condition

$$\int_{-z_o}^{h-z_o} zE(z)dz = 0 \qquad (5)$$

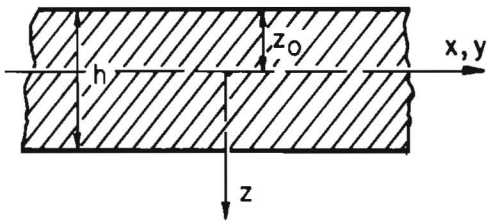

Fig. 3

Note that if E is assumed to be an averaged constant E_{av}, as it is often done in the literature, then the D in eq. (4) reduces to the customary $D = E_{av}h^3/[12(1-\nu^2)]$ and condition (5) is satisfied by $z_o = h/2$.

The general solution of equation (1) is ([8], p. 265)

$$w(r) = A_1 ber(\lambda r) + A_2 bei(\lambda r) + A_3 ker(\lambda r) + A_4 kei(\lambda r) \qquad (6)$$

where ber, bei, ker, and kei are Bessel functions and

$$\lambda = \sqrt[4]{\gamma/D} \qquad (7)$$

From the regularity conditions at $r = \infty$ it follows that

$$A_1 = 0 \quad ; \quad A_2 = 0 \qquad (8)$$

The remaining two constants are determined by substituting w(r) into the two boundary conditions shown in (2). The resulting constants are

$$A_3 = \frac{-\Delta\, kei'(\lambda a)}{\kappa_1} \quad ; \quad A_4 = \frac{\Delta\, ker'(\lambda a)}{\kappa_1} \qquad (9)$$

where

$$\kappa_1 = kei(\lambda a)ker'(\lambda a) - kei'(\lambda a)ker(\lambda a) \qquad (10)$$

Thus, the ice plate deflections are

$$w(r) = \frac{\Delta}{\kappa_1}\left[-kei'(\lambda a)ker(\lambda r) + ker'(\lambda a)kei(\lambda r)\right] \qquad (11)$$

The corresponding axial force induced in the pier is obtained by considering the vertical equilibrium of the free body diagram shown in Fig. 4

$$P + 2\pi a Q_{rr}(a) = 0 \qquad (12)$$

Thus

$$P = -2\pi a Q_{rr}(a) \tag{13}$$

Noting that ([8], p. 6)

$$Q_{rr} = -D \frac{d}{dr}\left(\frac{d^2w}{dr^2} + \frac{1}{r}\frac{dw}{dr}\right) \tag{14}$$

it follows that

$$P = -2\pi aD\left[\frac{d}{dr}\left(\frac{d^2w}{dr^2} + \frac{1}{r}\frac{dw}{dr}\right)\right]_{r=a} \tag{15}$$

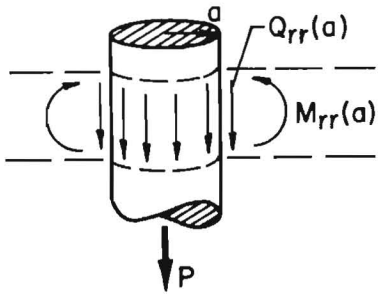

Fig. 4

Substituting the w(r) expression shown in (11) into eq. (15), it follows that the induced axial force is

$$P = 2\pi aD\lambda^3\Delta \frac{[ker'(\lambda a)]^2 + [kei'(\lambda a)]^2}{\kappa_1} \tag{16}$$

To facilitate its use, the above equation was numerically evaluated for a variety of parameters. The results are shown in Fig. 5.

To illustrate the resulting simplicity of the lift force determination by utilizing the graph presented in Fig. 5 consider, as an example, a pier of radius a = 100 cm frozen-in by an ice plate of thickness h = 40 cm. Assume that E_{av} = 30,000 kg/cm^2. Thus a/h = 2.5 and Fig. 5 yield the relation

$$P = 3.7\ \Delta \tag{17}$$

where P is in metric tons and Δ is in centimeters. Hence for a rise of Δ = 2 cm the largest axial lifting force in the pier is

$$P_{max} = 3.7 \times 2 = 7.4 \text{ tons} \tag{18}$$

provided that the plate does not break before this load is reached.

This reservation points out the need for a failure criterion for an ice plate-pier interaction problem, which will limit the P-force given in (17). Gamayunov [5] used

$$M_{max} = M_{rr}(a) = h^2\sigma_f / 6 \tag{19}$$

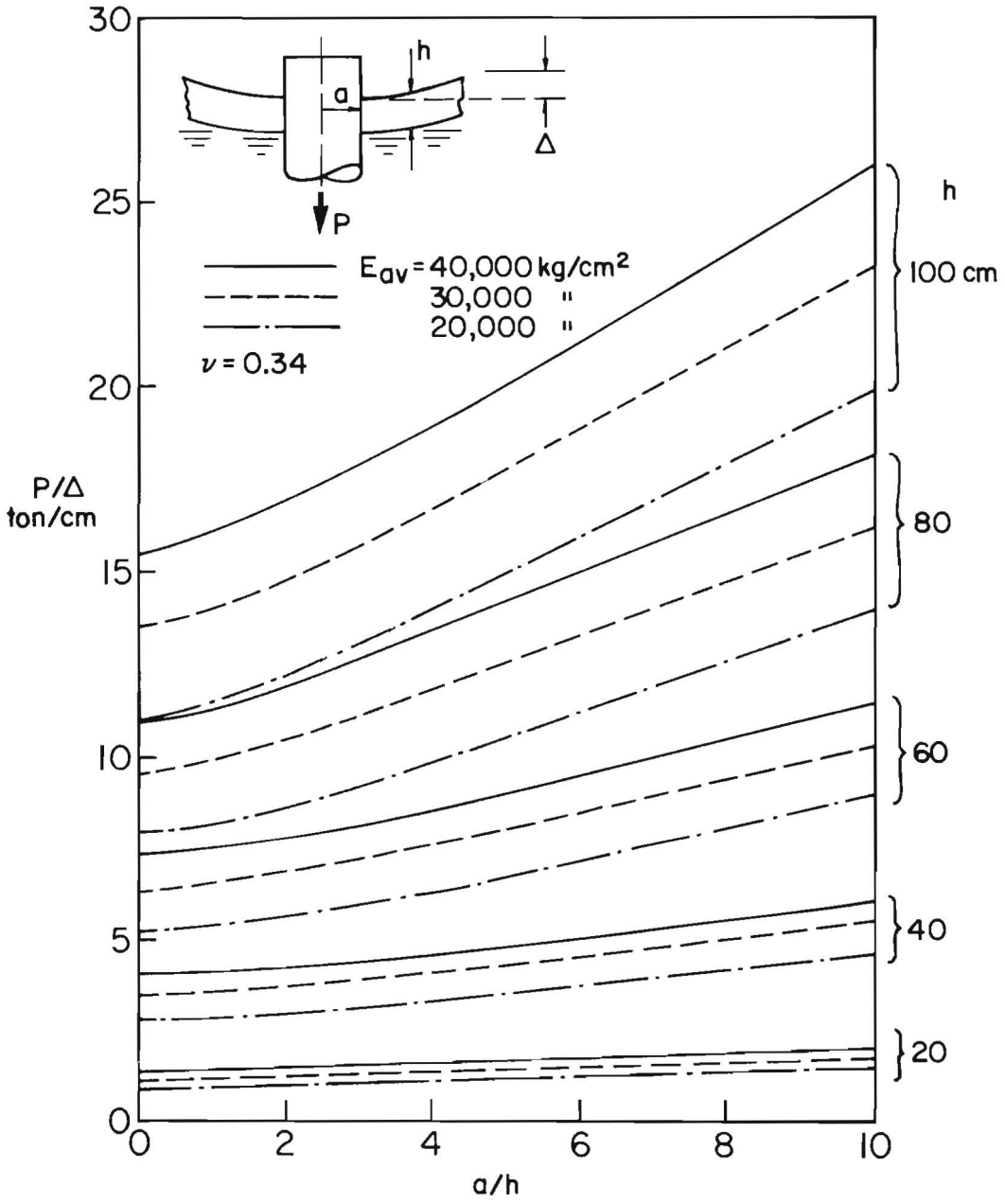
30
25
20
15
10
5
0
P/Δ
ton/cm
h
a
Δ
P
E_{av} = 40,000 kg/cm²
30,000 "
20,000 "
ν = 0.34
h
100 cm
80
60
40
20
0
2
4
6
8
10
a/h

Fig. 5

as failure criterion, where σ_f is defined as the failure stress shown in Fig. 6. He did not prescribe values for σ_f, nor did he suggest a method for its determination. Korzhavin [6] in his presentation of Gamyunov's method assumed that $\sigma_f = 11 + 35 \times |t°C|$ in kg/cm^2; an expression which he proposed earlier, in connection with another problem.

Note that because of the simplifying assumptions made by Gamayunov, his moment expression $M_{rr}(a)$ may not be accurate enough. Also, because of the temperature gradient in the plate, the stress distribution may not be linear along the plate thickness. Furthermore, there is a question whether failure criterion (19) is valid for the problem under consideration.

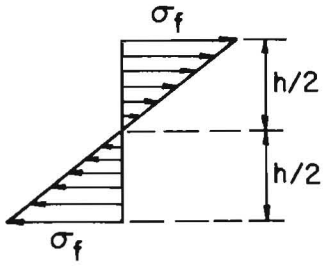

Fig. 6

Recently A. D. Kerr [9] surveyed various criteria proposed for the bearing capacity of floating ice plates subjected to vertical loads. One conclusion of this survey was that additional test results are needed to establish which of the proposed failure criteria are valid.

The failure mechanism of the plate-pier problem is even more complex, because of the plate-pier boundary and the possibility that failure may start there. No test results could be located in the literature which establish: (1) the failure pattern for different ratios a/h, (2) the effect on the failure load P_f when P is a tension or a compression force, and (3) the effect of ice temperatures on the failure pattern and the failure load P_f. Such test results are necessary for the formulation of a meaningful failure criterion for the ice plate-pier problem.

For the determination of the weight of a pier against lift-off, or the embedding depth of a pile against pull-out, the graphs in Fig. 5 may often be sufficient. This is so because the P-force determined from Fig. 5 is always larger than the actual lifting force, since viscoelastic effects and a failure criterion can only diminish the determined P value. Thus, if for a given pier the weight of the structure is larger than the corresponding P value obtained from Fig. 5, then the pier is safe against lift-off; a result often sufficient for engineering purposes.

LARGEST VERTICAL FORCE DUE TO THE LOWERING OF THE WATER LEVEL

Consider, as in the previous section, an infinite elastic plate rigidly attached to a circular pier of radius a, but assume that at a certain instant the water level drops by Δ.

The resulting stresses in the plate, and the axial force induced in the pier, are the same as for the case when the water level remains unchanged and the pier is displaced upward by Δ. Thus, for formulation of the problem under consideration for rotationally symmetrical deformations is the same as in the previous section, namely equations (1) and (2), except that now in the first boundary condition in (2) Δ is replaced by $(-\Delta)$. Therefore, except for a negative sign, the resulting solution w(x) and the axial force P are the same, as shown in eq. (11) and eq. (16).

According to the above argument, the graphs of Fig. 5 can also be used for the determination of the axial compression force in the pier, caused by a drop in the water level.

For the case of a slender pile, as shown in Fig. 1, the induced compression force may be sufficient to buckle it. If this is an undesirable situation and has to be prevented, then the buckling load of the pile, P_{cr}, has to be determined. This requires a separate analysis.

In conclusion it should be noted that if for the ice plate Young's modulus is given as $E = E(z)$, then the E_{av} which occurs in Fig. 5 may be determined from the equation

$$D = \frac{E_{av}h^3}{12(1-\nu^2)} = \frac{1}{1-\nu^2}\int_{-z_o}^{h-z_o} z^2E(z)dz \qquad (20)$$

Namely

$$E_{av} = \frac{12}{h^3}\int_{-z_o}^{h-z_o} z^2E(z)dz \qquad (21)$$

In this connection it should be noted that for the determination of the deflection surface, bending moments, and shearing forces (hence P) the use of E_{av} is admissible, whereas for the determination of the stresses in the plate [if needed in conjunction with a stress failure criterion, as the one shown in eq. (19)], the actual E(z) has to be used.

ACKNOWLEDGMENTS

This research was supported by the Cold Regions Research and Engineering Laboratory (CRREL), U.S. Army.

The author expresses his thanks to G. E. Frankenstein, Dr. A. Assur, and D. E. Nevel from CRREL USA for helpful discussions on the various aspects of ice forces.

REFERENCES

[1] Komarovskii, A. N., "Effect of an ice cover on structures and ways to combat it," (in Russian), Energoizdat, Leningrad, 1932.

[2] Löfquist, B., "Lifting force and bearing capacity of an ice sheet," (in Swedish), Teknisk Tidskrift, Nr. 25, Stockholm, 1944. Translated into English by the National Research Council of Canada.

[3] Kuznetsov, A.P.,"Effect of ice on structures of sea ports and the defense against it,"(In Russian) Leningrad 1939. Also, collected papers of Leningradskogo Oblastnogo Otdelenya Nauchnogo Inzhenerno-Tekhnicheskogo Obshchestva Vodnogo Transporta, Rechizdat, 1948.

[4] Nevel, D. E., "Lifting forces exerted by ice on structures," Proc. Conference on Ice Pressure Against Structures, Laval University, Quebec 10-11 November 1966. NRC No. 9851, Ottawa, 1960.

[5] Gamayunov, A. I., "The vertical pressure of an ice cover due to a change of the water level," (in Russian), Gidrotekhnicheskoe Stroitelstvo, Nr. 9, 1960.

[6] Korzhavin, K. N., "Action of Ice on Engineering Structures," (in Russian), Izd. Sibir, Otd. AN SSSR, 1962. Translated into English by U.S. Army CRREL, Draft Translation 260, Sept., 1971.

[7] Kerr, A. D. and Palmer, W. T., "The deformations and stresses in floating ice plates," Acta Mechanics, Vol. 15, 1972, pp. 57-72.

[8] Timoshenko, S. and Woinowsky-Krieger S., "Theory of Plates and Shells," McGraw-Hill, New York, Second Edition, 1959.

[9] Kerr, A. D., "The bearing capacity of floating ice plates subjected to static and quasi-static loads," CRREL Report No. 333, 1975. Accepted for publication in the Journal of Glaciology.

THIRD INTERNATIONAL SYMPOSIUM ON
ICE PROBLEMS
Hanover, New Hampshire, USA

ICE FORCES ON VERTICAL PILES: INDENTATION AND PENETRATION

Dr.Ken-ichi Hirayama	Iwate University	Japan
Dr. Joachim Schwarz	Hamburg Model Basin	West Germany
Dr. Han Chin Wu	The University of Iowa	U.S.A.

Synopsis

Experimental investigation of ice forces on vertical structure have been performed at the Iowa Institute of Hydraulic Research of the University of Iowa since 1970. Details and finding of the research, such as model test facility, similarity considerations,scale effect,and fracture mechanism of the ice in front of the pile were already reported (Schwarz and Hirayama [1], Hirayama, Schwarz and Wu [2], Schwarz, Hirayama and Wu [3]). This paper describes the further progress of the research. The fracture mechanism of the ice cover in front of the pile was thoroughly investigated by an application of strain gages frozen in the ice cover. Experimental results of the effective ice pressure on rectangular and circular piles of various diameters are shown for the indentation type of ice-pile interaction. The difference between the indentation and penetration ice pressure is thus clarified and an empirical power relation between indentation ice pressure and pile diameter is proposed. Measurements of indentation depth corresponding to the occurrence of the maximum ice pressure showed little dependency on the pile diameter. This led to the application of a theory proposed by Carothers [12] for the relationship between ice pressure and pile diameter. The effect of the degree of contact between ice and structure on the effective ice pressure was also investigated and found to be a function of strain rate, pile diameter, ice thickness and shape of the pile as well as of the ice temperature.

Introduction

A basic formula for the calculation of ice forces on vertical piles obtained from preceding research is given by equation (1) (Schwarz, Hirayama and Wu [3]) ;

$$F/\sigma_0 dxh = 3.57\, d^{-0.5}\, h^{0.1} \qquad (1)$$

where F is the total ice pressure on the pile, σ_0 is the compressive ice strength from unconfined compressive tests of the same ice, d and

h are the diameter of the pile and the thickness of the ice cover expressed in cm respectively. Results of field measurements by Schwarz [4] and other small scale investigations by Afanas'yev [5], Frederking [6], and Tryde [7] are in good agreement with this equation. However, the validity of equation (1) is restricted to certain conditions such as (a) ice temperature of 0°C or freezing mark, (b) circular pile and (c) penetration type of ice-pile interaction. Additional investigations of the problem described in this paper cover other conditions of indentation type of ice-pile interactions, the effect of pile shape and the effect of contact between ice and pile.

Fracture mechanism

In previous works on ice forces on structures the failure of the ice cover was considered to be caused by shear stresses (Tryde [7], Assur [8]), which in turn has led to the application of shear strength for the calculation of indentation forces. Other investigations (e.g. Korzhavin [9]) use the crushing strength, which has never been defined in terms of basic stress or strain components. Frederking and Gold [10] assumed a compressive failure of ice immediately adjacent to the pile. However this compressive failure has not been established and this failure mode was not consistent with observations made in the present study. In addition to fundamental visual observations and photograpy, strain gages were used to measure the strain in the ice sheet in front of the pile. Fine grained sands were glued on both sides of the strain gages in order to have a better contact between ice and gage. Due to the high roughness of the strain gage surface, the bond between ice and gage remained intact ; the loss of bonding could be detected easily from sudden drops of the strain records.
When circular piles were pushed into the ice sheet, vertical micro cracks started to form immediately in front of the pile.
These cracks developed vertically, and along the grain boundaries.
The numerous micro cracks spread over a distance of about one half pile diameter and resulted in a milky appearance of the ice in this region.
In spite of these cracks ice sheet did not collapse and the stress did not reach its maximum value. After attaining a certain compressive stress level, which caused a critical tensile strain in the z-direction (see Fig.1 for the definition of coordinate system for pile indentation or penetration cases), a horizontal plane crack (cleavage crack) formed at the midplane of the ice sheet in front of the pile.
This horizontal plane crack spread radially outward from the pile, cutting the ice crystals perpendicular to the longitudinal direction of their columnar structure. Maximum forces occured concurrently with the developement of this horizontal cleavage crack.
A similar fracture mechanism was observed in the field tests at Sault St. Marie in January, 1974.
In these field tests where the ice was about 25 cm thick additional short cleavage cracks developed at the quarter points and occasionally down to one inch intervals over the thickness of the ice sheet.

The horizontal plane crack as described above can be explained in terms of a strain failure criterion proposed by Wu [11]. According to this criterion, cleavage fracture occures when a function of strain reaches a critical value. In addition, the plane of fracture is normal to

the direction of the maximum tensile strain. This criterion of fracture has been shown to describe the fracture behaviour of brittle materials such as plain concrete. It has also been shown to be applicable to columnar grained ice in the case of unconfined compression test by Wu, Chang and Schwarz [12]. The horizontal plane crack discussed above was indeed normal to the direction of maximum tensile strain.
The strain ε_z was tensile, because ε_y was very small due to lateral confinement and ε_x was compressive.

This failure process was investigated further using strain measurements in the three principal strain directions. The strain gages used for this investigation were arranged as shown in Fig.2. These positios avoided cuts througth the grains. The strain behavior along the principal directions in the ice cover in front of the pile was obtained with strain gages in positions (1) and (2) as shown in Fig.2.
In these experiments, a pile of d=3.75 cm was pushed against the plane, vertical edge of a 1.5 cm thick ice cover. The strain gages were located 2 cm in front of the pile when the experiment started.
The velocity of the pile was 0.05 cm/sec which corresponds to a strain rate of $\dot{\varepsilon} = 0.08\ sec^{-1}$. Based on about 30 measurements the following statements can be made :
(1) In the far field reach in front of the pile, where the elastic deformation is expected, the ratio $\varepsilon_z/\varepsilon_x$ (ε_x : strain in the x-direction, ε_z : strain in the z-direction) remained about 0.3 as shown in Fig.3.
(2) When the ice started to deform plastically, the strain in the x- and z-direction increased rapidly. Simultaneously the strain ratio $\varepsilon_z/\varepsilon_x$ increased and reached values of about 0.8 to 0.9. This high strain ratio is possible because the strain in the y-direction remains nearly zero due to the lateral confinement of relatively large ice sheet. Thus the compressive strain in the x-direction and tensile strain in the z-direction was approximately of the same magnitude.
(3) A jump in the value of the strain shown on the strain record for ε_z (Fig.3) indicates the occurrence of the cleavage crack and coincides with the occurrence of the maximum force againt the pile.
It was therefore concluded that cleavage fracture of the ice sheet was caused by the tensile strain in the z-direction. The stress σ_x and strain ε_z along the centerline in front of the pile is schematically plotted in Fig.4. Regardless of the high density of the cracks the fractured ice adjacent to the pile transmit the stress σ_x forward. The strain ε_z, there, is restricted due to friction between ice and pile. As the shear stress caused by this friction decreases with the distance from the pile, the strain ε_z first increases, reaches a maximum at some distance, x_1, and then decreases monotonically.
Thus, it is reasonable to assume that the cleavage crack developes wherever the strain ε_z exceeds a certain critical value.

In summary,it was shown that the failure of the ice cover in front of a vertical pile occures due to the tensile strain in the unconfined z-direction and not due to shear or crushing, as has been commonly assumed.
Preliminary investigations on ice forces against frozen-in piles have shown a different failure mode due to the locally thicker ice around the pile (higher heat conductivity). Instead of cleavage failure

the ice cover around the frozen-in pile failed by shear as has been observed also by Croasdale [13] in the field tests and is sketched in Fig.5.

Effective penetration ice pressure

The effective ice pressure on circular piles penetrating with a constant speed through uniform ice cover has been discussed in previous paper ([1], [2], [3]). Model piles of 0.6 cm to 11.8 cm diameter were pushed through the ice cover at velocities ranging between 0.004 cm/sec and 2.75 cm/sec. The ice thickness was varied from 1.0 cm to 3.0 cm. The piles were oriented perpendicular to the plane of ice sheet, and the temperature of the ice was kept at the freezing point.
Forces acting on the pile were measured by a dynamometer, and the output signal was sampled with IBM 1800 computer by using a reasonable sampling interval depending on the penetration velocity. After the statistical treatments of the data, the effective ice pressure F/dxh, for which 99% of the data showed lower strength, was used for the analysis. The results of this investigation are summarized in Eq.1.
By the same testing procedure the effective ice pressure on rectangular and wedged piles has been investigated. The width of the rectangular piles ranged from 0.6 cm, to 5.0 cm and wedge angles of 120°, 90°, and 60° were tested.
From these experimental investigations, the relation between the effective ice pressure and the width of rectangular piles was found to be ;

$$F/dxh \propto w^{-0.43} \qquad (2)$$

where w is the width of the rectangular piles. The magnitude of the effective ice pressure on circular and rectangular piles were almost the same (see Fig.6).
Further, as will be shown in a later section, the penetration ice pressure is almost independent of the shape of the pile.

Effective indentation ice pressure

At the beginning of the ice-pile interaction, the pile meets the unfractured ice sheet with a vertical plane edge which is called the indentation type of ice-pile interaction. Investigations of the indentation ice pressure was performed for both circular and rectangular piles with various diameters. The ice thickness of 1.5 cm and a penetration velocity of 0.1 cm/sec, which corresponds to the maximum ice pressure related to the velocity, were used.
The dependency of the effective ice pressure for circular and rectangular piles on the width of the pile is shown in Fig.6 and can be expressed by Eq.3 and Eq.4 respectively.

$$F/dxh \propto w^{-0.51} \quad \text{for circular pile indentation} \qquad (3)$$

$$F/dxh \propto w^{-0.32} \quad \text{for rectangular pile indentation} \qquad (4)$$

In case of circular piles the effective pressure are almost for both indentation and penetration cases. However, for rectangular piles indentation ice pressure was much larger than the penetration ice pressure due to the practically 100% contact between ice and pile in case of indentation (Fig.6). The difference between the indentation and penetration ice pressure inceases with the pile diameter (Fig.6).

Other important results concerning the pile diameter effect have been obtained from pile indentation tests. It was found that the indentation depth l_0 , at the instant that the ice pressure reaches its maximum is almost independent of the pile diameter for both circular and rectangular piles as indicated by the data presented in Table 1. The data for circular piles show that the maximum pressure occures prior to full penetration of the pile while for rectangular piles the maximum pressure always corresponds to the full width contact between ice and pile. Therefore if the ice forces on circular piles are related to the effective width of contact between pile and ice, a similar relationship between width and effective ice pressure was obtained as has been found for rectangular piles.

$$F/cxh \quad \propto \quad c^{-0.25} \qquad (5)$$

where c is the chord length.

Effect of pile width

One major factor in determining the effective ice pressure is the width of the structure. It has been shown that the ice forces per unit area decrease with increasing width. This effect has been expressed by Assur [8], Afanas'yev [5], and Tryde [7] in terms of the dimensionless parameter d/h. However, in the present investigation it was found that, instead of d/h dependency, the effective ice pressure shows a power law relation of the pile width and ice thickness (Eq.1).

A theoretical approach for investigating this effect was made by adopting the analytical solution of stress distribution in linearly elastic solids, which was first solved by Boussinesq for the case in which a concentrated single load acts on the surface of a semi-infinite medium. This solution was modified by Carothers [14] to a plane strain case in which a unform strip load acts on the surface of a semi-infinite medium, which leads to expressions in the x- and y-direction at a point (x,y) in the form,

$$\sigma_x = \frac{p}{\pi} [\alpha + \sin\alpha \cos(\alpha + 2\delta)] \qquad (6)$$

$$\sigma_y = \frac{p}{\pi} [\alpha - \sin\alpha \cos(\alpha + 2\delta)] \qquad (7)$$

where the angle α and δ are expressed in terms of x, y and the indentor width 2a by the relationship (refer to Fig.7).

$$\tan (\alpha + \delta) = y/x \qquad (8)$$

$$\tan \delta = y-2a/x \qquad (9)$$

According to this solution, the stress σ_x, which is the stress at a distance x_c from the surface under the midpoint of the indentor, increases with increasing width 2a, due to the effect of supperposition of single loads. This implies that a critical stress at a certain point can be achieved by smaller load per unit width as the indentor becomes broader. The relation between the ratio p/σ_x, where p is the load intensity and the ratio a/x_c (x_c : the distance from the surface). can be derived from the theory (Fig.7). This theory can be adopted for indentation problems of ice when the stress σ_x is assumed to cause the critical strain in the z-direction.
Under this assumption, x_c corresponds to the distance from the pile to a point at which the cleavage crack originates. The distance x_c is very difficult to define but it is obvious that the cleavage crack can not start immediately at the pile-ice interface because of the three dimensional state of stress caused by friction between ice and pile. Experimental measurements of x_c, which scattered between 0.5 cm and 1.0 cm, and a value of x_c=0.75 cm was used in the analysis for the first approximation.
Since it seems reasonable to assume that the extent of x_c increases with the pile diameter, a second calculation of the load intensity as a function of the pile diameter was made for an estimated variation of x_c as follows,

$$x_c = 0.1d + 0.5 \qquad (10)$$

The results of both computations are plotted on log-log scales in Fig.8, showing the necessary load intensity for the failure of the ice sheet with an increase in the pile width w. The trend in the relationship between the indentation pressure and the pile width by this theoretical approach is similar to results obtained from present indentation model tests with rectangular piles. The slight difference between the results for the model tests and the theoretical approach is considered to be caused by the assumption of linear stress-strain relationship and by insufficient information concerning the length x_c in the model investigation.

Shape factor

The cross-sectional shape of a pile has been considered as one of the major factors affecting the ice forces on structures. Korzhavin [9] investigated the effect of different shapes in punch-type tests and found that the largest ice force occures when the pile is rectangular. For structures with wedge-shaped noses (e.g. bridge pier), Korzhavin explained this result as an effect of higher stress intensity at the tip of the wedge. Afanase'yev [5] found the same trend in his model experiments but no distinction was made between the indentation and penetration of the pile. In the present study the shape effect of

rectangular, circular and wedged piles with wedge angle of 120°, 90° and 60° was investigated in both the penetration and the indentation type of the ice-pile interaction.

From indentation tests with circular and rectangular piles of different diameter, it was found that the decrease in the ice pressure with pile diameter is greater when the shape is circular instead of rectangular as can be seen in Eqs.3 and 4. If the effective ice pressure exerted on piles of various shapes are related to the force on a rectangular one, a shape factor can be obtained. For the indentation type of ice-pile interaction, the shape factor is, for example, 0.77 for a circular pile of 1.25 cm diameter. The results of the present indentation tests are plotted on Fig.10 together with the result of Korzhavin's punch tests. His result shows roughly the same trend as present data, but the magnitude of the shape factor is smaller. This difference can be explained as a consequsence of Korzhavin's experimental procedure, where splitting of the ice sample was observed due to the lack of confinement against lateral deformation. In the present study the ice sheet was confined to prevent splitting ($\varepsilon_y = 0$).

For the case in which circular and rectangular piles penetrate into the ice cover, the shape factor is approximately independent of the pile width as shown in Fig.9. This result is different from Korzhavin's predictions.

Contact coefficient

The effect of the degree of contact between ice and pile on the ice pressure has not been investigated thoroughly. Korzhavin [9] defined a contact coefficient k as the ratio of the ice pressure in penetration phase to the ultimate resistance force of ice sample tested in compression.

According to the results of the present investigation, the contact coefficient k is not constant since the penetration ice pressure varies with strain rate, pile diameter, ice thickness, and shape of the pile as well as with the ice temperature. Since k is already incorporated into the relationship between ice pressure, pile diameter, ice thickness and penetration velocity, this coefficient does not need to be considered as an additional parameter, when the effective ice pressure is being calculated.

The reason for studying the contact coefficient in the present investigation is to obtain a better understanding of this effect as a part of the ice force problem. For this purpose the contact coefficient was defined as the ratio of the ice pressure in which the contact between ice and pile is incomplete and the indentation or penetration ice pressure, where the contact is assumed to be 100%. The 100% contact between ice and pile can be achieved by fitting the circular pile into a pre-drilled hole of the same diameter or by pushing the rectangular pile against a parallel, plane, vertical edge of the ice cover.

Using this definition, the dependency of the contact coefficient on the strain rate was investigated for a circular pile (Fig.10).

As expected, the coefficient is strongly strain rate dependent. It decreases with the strain rate and approaches a constant value of 0.7

at a strain rate of $\dot{\varepsilon} = 1.0\ \text{sec}^{-1}$. At the strain rate $\dot{\varepsilon} = 0.2\ \text{sec}^{-1}$, where the maximum effective ice pressure was obtained, the coefficient is about 0.75. This indicates that the ice force calculatedby Eq.1 is 33% too low when the pile is in complete contact with the ice. For rectangular piles the effect of width on the contact area can be seen from Fig.6. Further investigations related to the contact coefficient are being conducted at the Iowa Institute of Hydraulic Research.

Acknowlegement

The authers wish to express their gratitude to Drs. John F. Kennedy and Fred A. Locher of the Iowa Institute of Hydraulic Research.
This study was supported by the National Science Foundation under Grant GK-35918X, the U.S.Army Cold Regions Research and Engineering Laboratory, Hanover, New Hampshire under DA ENG-27021-72-G36, and the Deutsche Forschungs-Gemeinschaft Schw.166.

Reference

1. Schwarz and Hirayama, "Experimental Study of Ice Forces on Piles and the Corresponding Ice Deformation", IIHR Report, 1973.
2. Hirayama, Schwarz and Wu, "Model Technique for the Investigation of Ice Forces on Structures", Proceedin s of 2nd Int. Nat. Conf. on Port and Ocean Engineering under Arctic Conditions, Iceland, 1973.
3. Schwarz, Hirayama and Wu, "Effect of Ice Thickness on Ice Forces", Proceedings of 6th Annual Offshore Tech. Conf., Houston, 1974.
4. Schwarz, J., "The Pressure of Floating Ice Fields", Proceedings of 1st IAHR Symposium on Ice and its Action on Hydraulic Structures, Reykiavik, 1970.
5. Afanas'yev, Dologoplov and Shrayshteyn, "Ice Pressure on Separate Supporting Structures in the Sea", CRREL Translation TL346, 1972.
6. Frederking, R., Personal Communication.
7. Tryde, P., "Ice Research in Denmrak", Symposium Krig Isfragor Stockholm, 1974.
8. Assur, A., "Structures in Ice Infested Water", Proceedings of 2nd IAHR Symposium on Ice and its Action on Hydraulic Structures, Leningrad, 1972.
9. Korzhavin, K. N., "Action of Ice on Engineering Structures", CRREL Translation, TL 260.
10. Frederking and Gold, "Ice Forces on an Isolated Circular Pile", Proceedings of 1st Int. Nat. Conf. on Port and Ocean Engineering under Arctic Conditions, Norway, 1971.
11. Wu, H. C., "Dual Failure Criterion for Plain Concrete", Journal of the Enginrering Mechanics Division, ASCE, 1974.
12. Wu, Chang and Schwarz, "Fracture in the Compression of Columnar Grained Ice", Journal of Engineering Fracture Mechanics (in press)
13. Croasdale, K., "The Nutcracker Ice Strength Tester and its Operation in the Beaufort Sea", Proceedings of 1st IAHR Symposium on Ice and its Action on Hydraulic Structures, Reykjavik, 1970.
14. Carothers, "Plane Strain : Direct Deformation of Stress", Proc. HRB 35,773, 1956.

POAC, 1973
— POAC 1975

IAHR — 1970
IAHR — 1973

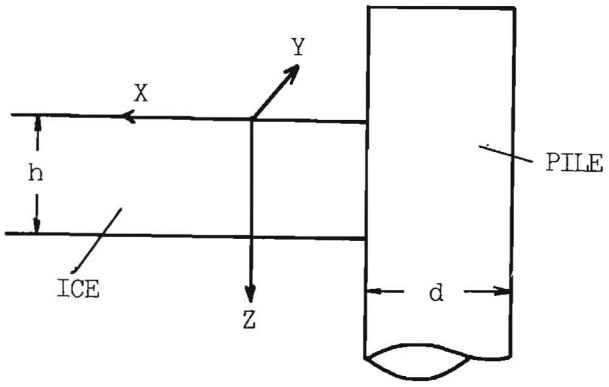

Figure 1 Definition of Coordinate System

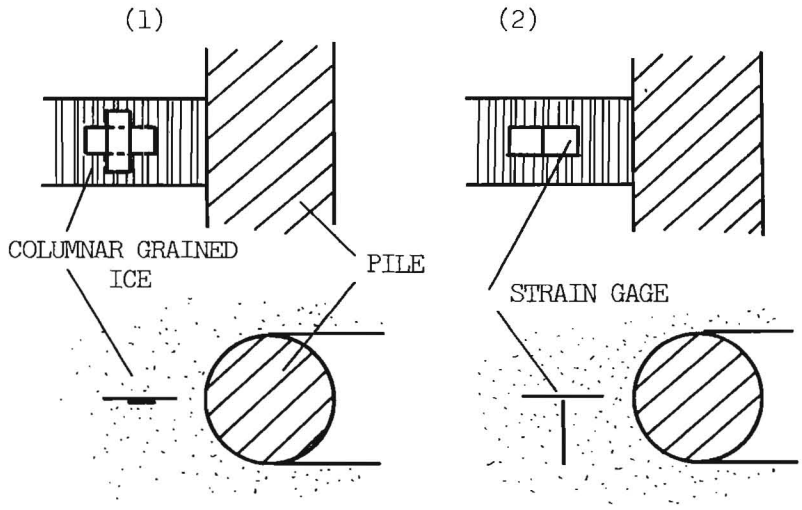

Figure 2 Positions of the Strain Gages.

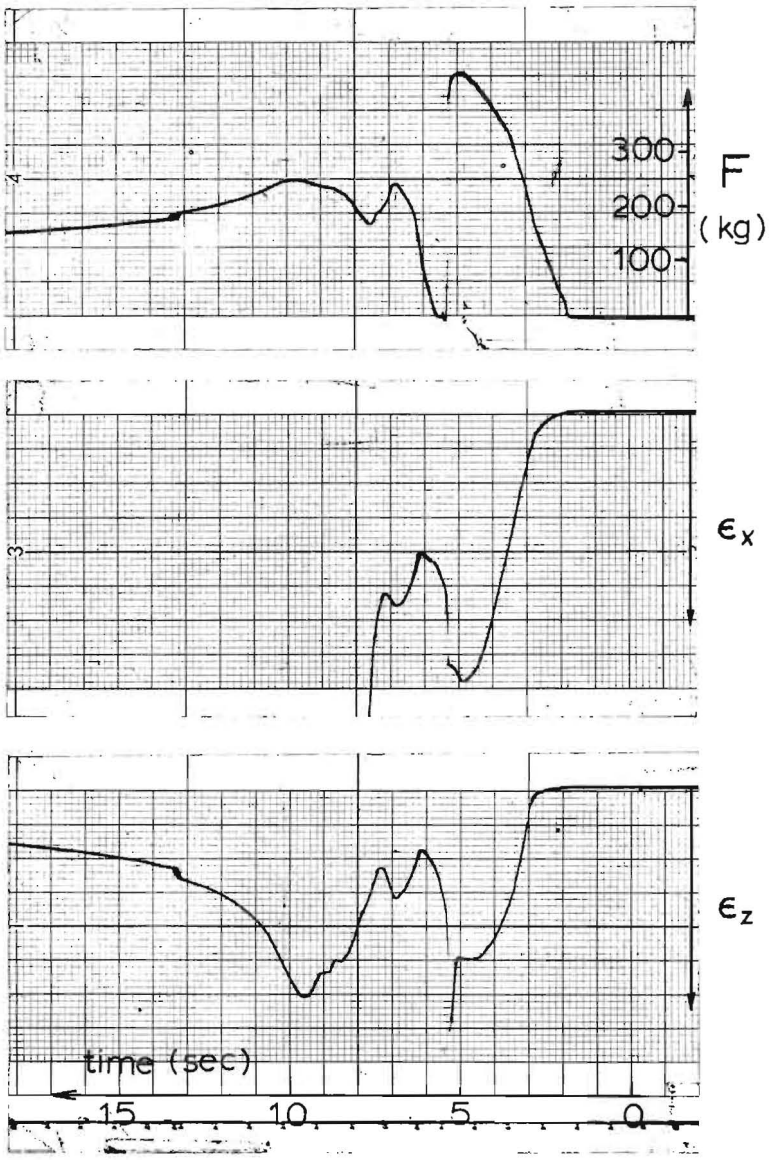

Fig.3 Record of Force F and Strains ε_x, ε_z.

w (cm) Pile Width	l_0 (cm) Circular Pile	Rectangular Pile
1.25	0.5	0.4
2.50	0.5	0.4
3.75	0.6	-
5.00	0.6	0.4

Table 1 Depth of Indentation l_0.

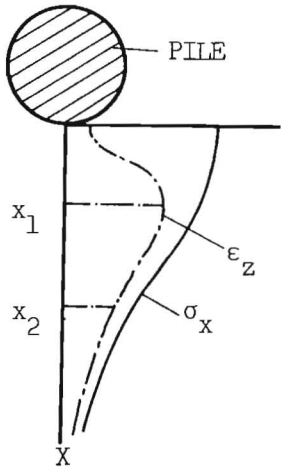

Fig.4 Schematic Distribution of σ_x and ε_z along the Centerline.

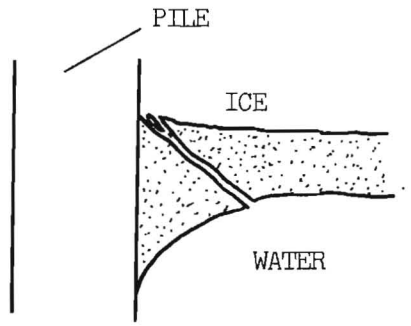

Fig.5 Sketch of the Failure Pattern around a Frozen-in Pile.

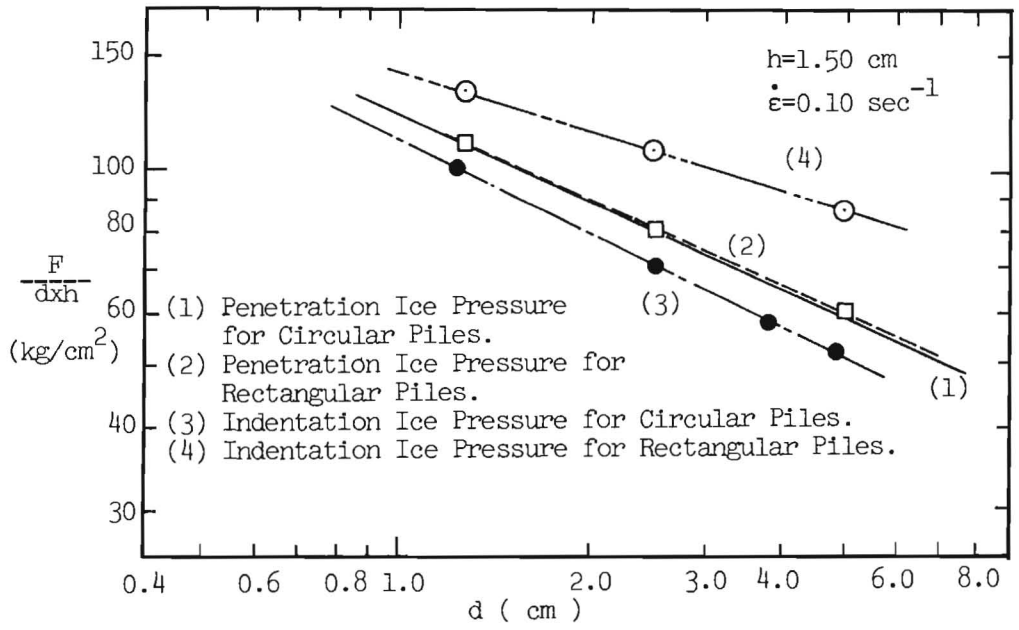

Fig.6 Variation of Effective Ice Pressure with Pile Diameter(Width).

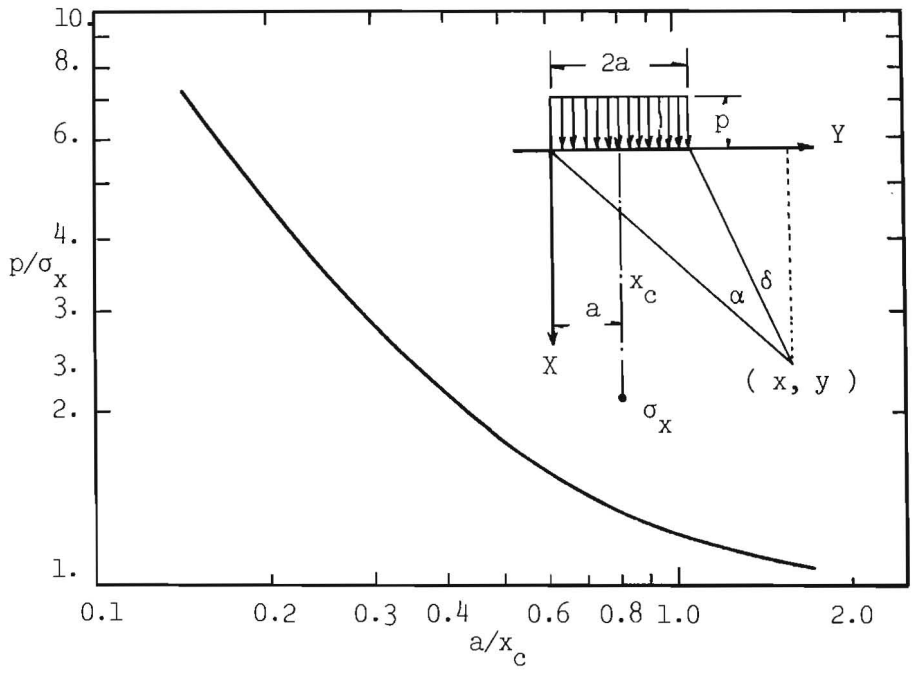

Fig.7 Relationship between p/σ_x and a/x_c

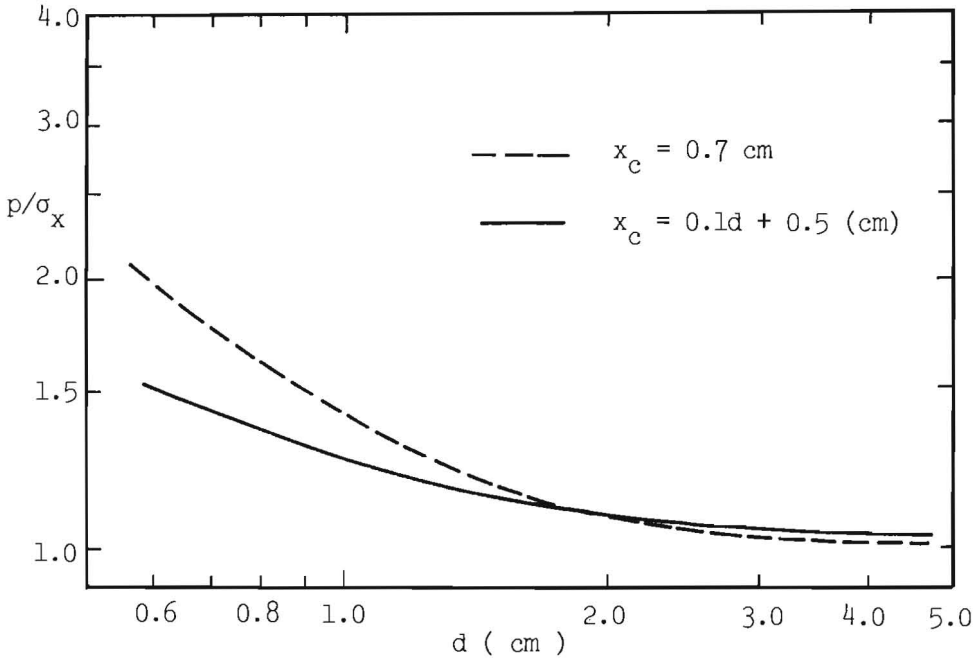

Fig.8 Relationship between p/σ_x and d.

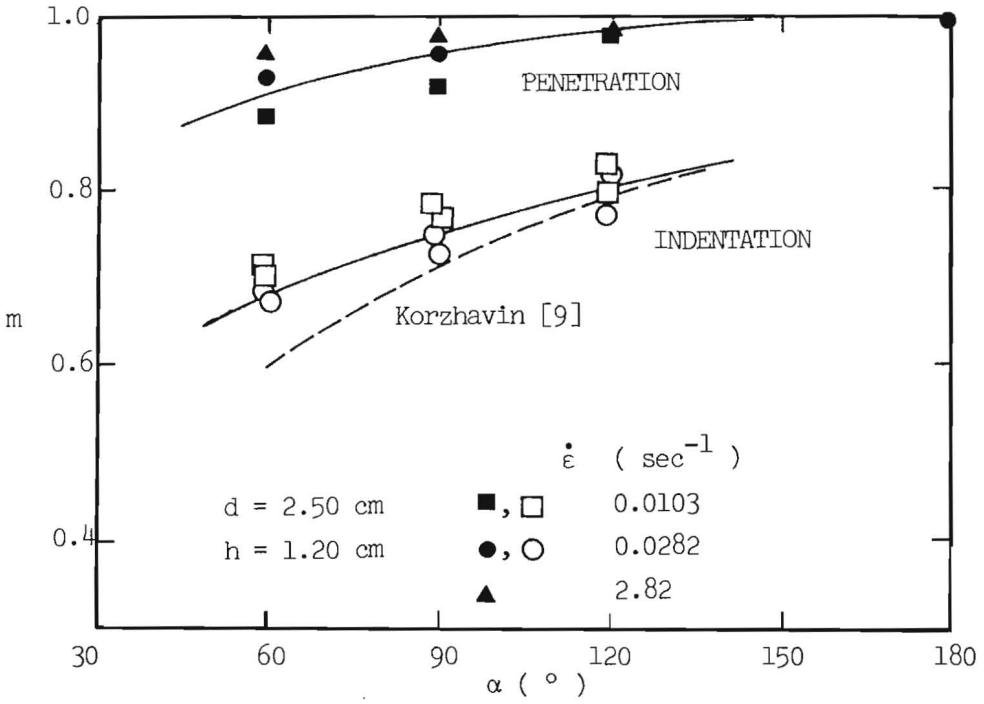

Fig.9 Variation of Shape Factor with the Wedge Angle.

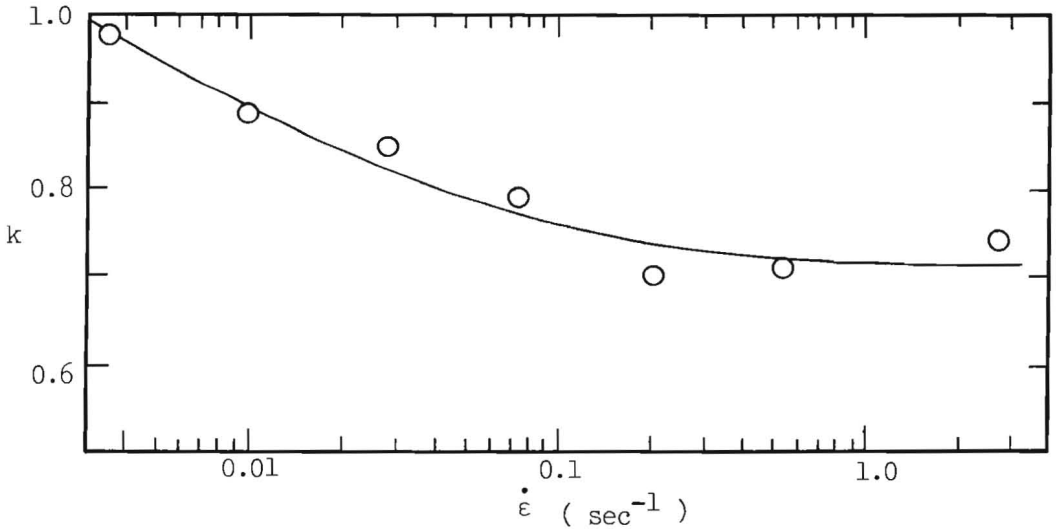

Fig.10 Variation of the Contact Coefficient with Strain Rate.

International Association of Hydraulic Research (IAHR)
Committee on Ice Problems
International Symposium on Ice Problems
18-21 August 1975
Hanover, New Hampshire

COMMENTS

Paper Title: ICE FORCES OF VERTICAL PILE INDENTATION AND PENETRATION

Author: K. Hirayama, J. Schwartz and H.C. Wu

Your name: B. Ladanyi,
Professor, Dept.of Mineral Engineering,
Address: Director, Northern Engineering Centre,
Ecole Polytechnique,
P.O.Box 6079, Station A,
MONTREAL, H3C 3A7, CANADA

Comment:

Most experimental investigations of ice forces on structures carried out to date both in the laboratory and in the field, lead to the conclusion that average pressure of ice on a vertical structure decreases with the aspect ratio B/t (where B is effective current structure width in contact with the ice, and t is the ice thickness), following a curve of a concave shape, as shown schematically in Fig. 1(a), (e.g., Korzhavin, 1962; Croasdale, 1972; Zabilansky et al. 1975). It was also observed that, while this general trend remains, it is often blurred by other factors, such as the effects of size, shape and imperfect contact.

A similar trend can also be seen in the authors' results where it appears combined with the size effect. For example, if their formulas for ice pressure on vertical piles are put in a dimensionless form, they become (in our notation)

$$q_f/C_o = K\,(B/t)^{-\alpha}\,(B/B_o)^{-\beta} \qquad (1)$$

where $q_f = F/Bt$ is the average ice pressure on the pile, Co is the uniaxial compression strength of ice in horizontal direction, for a specimen of width B_o, K is a dimensionless factor, and α and β are exponents, both smaller than 1. For example, the authors' formula for a rectangular pile, can be written in the form

$$q_f/C_o = 3.147\ (B/t)^{-0.1}\ (B/2.5\ cm)^{-0.22} \qquad (2)$$

if it is assumed that Co corresponds to a specimen width of 2.5 cm.

On the other hand, it has been realized that failure of an ice cover in contact with a vertical structure is a complex phenomenon, involving at least two, if not several different modes of failure. Therefore, any empirical formula of the form of Eq. (1), which does not take into account the physical phenomena and does not depend directly on the properties of ice, can have only a limited validity.

A more general approach to the problem may consist in attempting to find a proper theoretical solution for at least two extreme modes of failure of ice, and to bound the experimental curve by these two theoretical limits. How this could be done in principle is illustrated in Fig.1(a), which shows schematically the variation of average pressure of an ice cover of thickness t on a vertical face of a rectangular pile of width B. It will be seen that the curve is bounded by two limiting pressures:

(1) Pressure q_{fI} for an in-plane bearing capacity failure at very small B/t ratios, of the order of 0.1, and

(2) Pressure q_{fII} for an out-of-plane passive resistance failure, when B/t tends to infinity (vertical wall).

Now, if one wants to establish an empirical equation of a smooth curve containing these two bounds, i.e., so that $q_f = q_{fI}$ when $B/t = (B/t)_o$ (≈ 0.1), and $q_f \to q_{fII}$ when $B/t \to \infty$, one can use an expression of the form

$$q_f = q_{fII} + (q_{fI} - q_{fII})[(B/t)_o/(B/t)]^{-a} \qquad (3)$$

where $0 < a < 1$. However, a smooth curve may not be the best approximation, because there are some indications that there may be a jump at about $B/t = 2$, according to recent results by Zabilansky et al. (1975). This proposal is in certain aspects similar to those made earlier by Assur (1971) and Kivisild (1971).

As far as the two limiting pressures are concerned, the value of q_{fII}, involving a passive out-of-plane failure of ice, Fig.1(c), can be put equal to the out-of-plane unconfined compression strength of ice, C_{oop}, obtained in a test where in-plane failure is prevented. Frederking (1972) has shown that such a compressive strength, where failure plane cuts across the ice columns, is about twice as high as the in-plane compressive strength, C_{oip}, where the failure plane follows the contacts between the columns.

For determining the value of the limiting pressure q_{fI}, corresponding to penetration of a thin pile into a thick ice cover the Prandtl's bearing capacity formula has sometimes been used in the past. However, since the observed phenomenon does not resemble the Prandtl type failure but rather that produced by the expansion of a cylindrical cavity in a brittle medium, for which a complete solution exists in the field of rock mechanics (Ladanyi, 1967), the use of the latter type of solu-

tion, describing a type of failure similar to that shown in Fig.1(b), seems preferable.

In addition to describing a failure sequence very similar to that when a thin pile penetrates rapidly into a thick ice sheet with the formation of crushed and radially cracked zones, the latter theory has the advantage over the Prandtl's theory of being able to take into account the parabolic shape of the failure envelope of intact ice, as observed at high strain rates, as well as its elastic properties and the fact that its strength is much lower in crushed state.

From the latter theory (Ladanyi, 1967), the value of pressure q_{fI} can be expressed by

$$q_{fI} = C_{oip} \cdot N + (N - 1)c_r \cdot \cot \phi_r \qquad (4)$$

where C_{oip} is the in-plane uniaxial compression strength of ice, corrected for the size effect, c_r and ϕ_r are the residual Coulomb strength parameters for crushed ice in contact with the pile, while N is a bearing capacity factor given by (for a pile entering an ice sheet):

$$N = 0.6 \frac{(E/C_o)_{ip}^b \, (1 + \tan \phi_r)}{\{2(1+\nu)[1 + (1 - \nu)\ln|C_o/T_o|_{ip}\}^b} \qquad (5)$$

where E_{ip} is the in-plane modulus of elasticity of intact ice, ν its Poisson's ratio, and T_o its tensile strength. The exponent b is defined by

$$b = \frac{\sin \phi_r}{1 + \sin \phi_r} \qquad (6)$$

A sample calculation using Eqs. (4) and (5), and taking for the ice: $(C_o/T_o)_{ip} = 4$, $\nu = 0.4$, $\phi_r = 35^o$, $c_r = 0$, gives $q_{fI} = 3.6\ C_{oip}$, if $(E/C_o)_{ip} = 1000$, and $q_{fI} = 2.8\ C_{oip}$, if $(E/C_o)_{ip} = 500$, which is close to the usually observed values.

References

Assur, A. (1971) - Forces in moving ice fields. Proc. 1st Int. POAC Conf., Trondheim, Norway, Vol. 1, pp. 112-118.

Croasdale, K.R. (1974) - Crushing strength of arctic ice. In "The Coast and Shelf of the Beaufort Sea"(J.C. Reed and J.E. Sater, Eds.), Arctic Inst. of North America, pp. 377-399.

Frederking, R. (1972) - Preliminary results of plane strain compression of columnar-grained ice. Proc. IAHR Symp. on Ice and its Action on Hydraulic Structures, Leningrad 1972, pp. 23-27.

Kivisild, H.R. (1971) - Discussion in Proc. 1st Int. POAC Conf., Trondheim, Norway, Vol. 1, pp. 221-222.

Korzhavin, K.N. (1962) - Action of ice on engineering structures. Transl. from Russian, U.S. Army CRREL Translation TL260, 1971.

Ladanyi, B. (1967) - Expansion of cavities in brittle media, Internat. Journal of Rock Mech. & Mining Sciences, Pergamon Press, Vol. 4, pp. 301-328.

Zabilansky, L.J., Nevel, D.E., and Haynes, F.D. (1975) - Ice forces on model structures. Paper pres. at the 2nd Canadian Hydrotechnical Conf., Burlington, Ont. 1975.

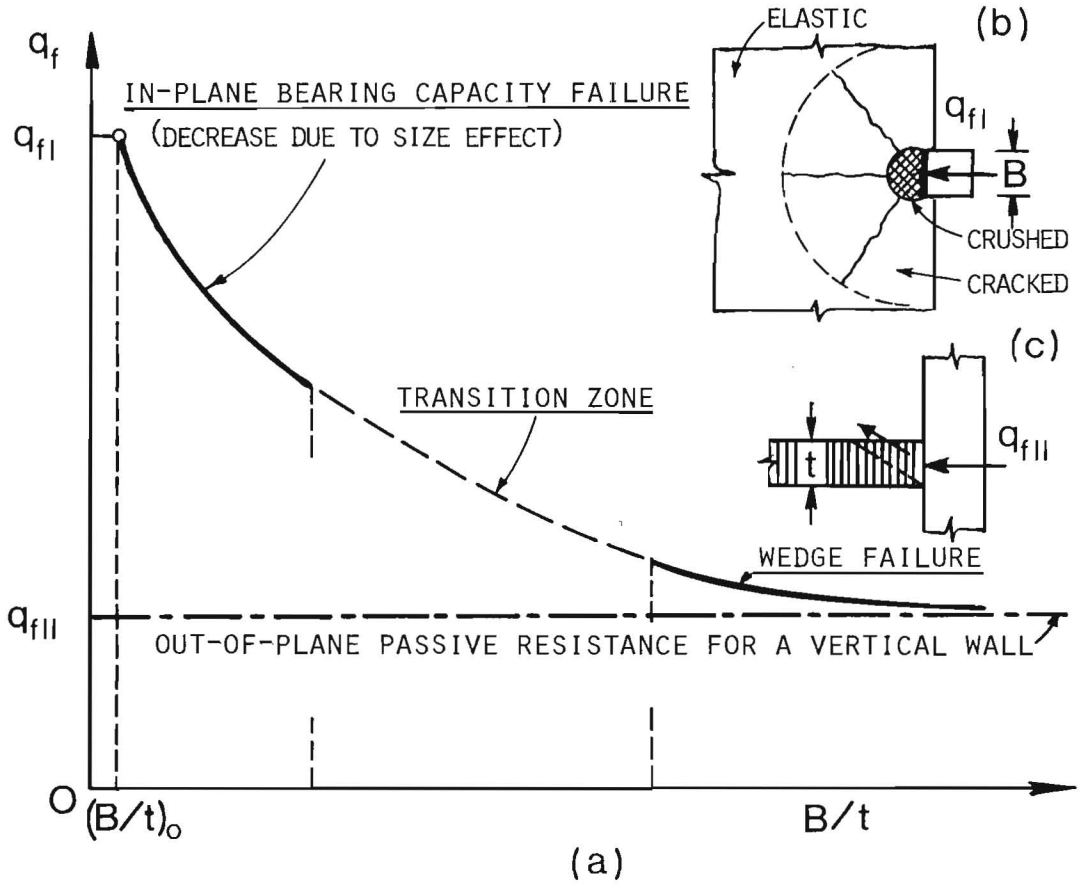

FIG. 1. BOUNDING OF ICE PRESSURES ON A VERTICAL PILE.

THIRD INTERNATIONAL SYMPOSIUM ON
ICE PROBLEMS
Hanover, New Hampshire, USA

PREDICTION OF ICE FORCES ON CONICAL OFFSHORE STRUCTURES

Frank G. Bercha President	F. G. Bercha and Associates Limited	Calgary Canada
Joseph V. Danys Superintendent of Civil Engineering	Ministry of Transport	Ottawa Canada

I. INTRODUCTION

The problem of determining ice forces exerted on static offshore structures, which has received some attention in the past [1, 6, 7, 8]*, is particularly significant today because its solution will facilitate offshore industrial development in the Arctic [2]. A decrease in the force exerted by ice sheets on offshore structures has been effected by constructing structures of conical geometry, so that the impinging ice sheet tends to fail in flexure due to the vertical force generated as the ice sheet slides up the conical surface. Modified versions of the solutions obtained by Nevel [8] or Meyerhof [6] may be used to estimate this vertical force. These flexural solutions, however, do not include the effects of the horizontal force and edge moment generated at the ice-structure interface.

In this paper, an analysis which includes the effects of in plane forces and edge moments, as well as transverse loading, on the forces which ice sheets in a flexural failure mode may exert on conical structures, is developed. The development includes both theoretical and numerical approaches. Using a form of the theory of the flexural failure of a floating ice sheet as a point of departure [8], heuristic corrections accounting for the end force and moment effects are

---

* Numbers in square parentheses refer to publications listed under "References".

obtained. A range of results based on the corrected theory is then corroborated using a finite element simulator having certain refinements over the analytical approach, including a more precise specification of the end actions.

Generally, the analysis is predicated on the predominance of the well known [6, 8] ice sheet flexural failure mechanism. This mechanism is known to result from the formation of radial followed by circumferential cracks in the ice sheet. Some modification of the location of these cracks is predicted due to the end action effects, but the mechanism itself is considered to be the same as the traditional one.

Finally, field observations of a full scale prototype structure are discussed, and comparisons of the theoretical predictions with in situ measured ice forces are referred to.

II. SYSTEM PROPERTIES

Before formal analysis may be attempted, the system parameters must be identified. For the type of system interactions considered herein, the system parameters consist of the geometric and mechanical properties of the structure and the ice, and certain inter-active properties such as interface friction.

The geometry of the structure, of course, is always known, while its mechanical properties are considered to be correspondent to infinite stiffness relative to the ice sheet. Interface friction factors and the ice properties must be determined for the locale in question. Although the determination of these properties is by no means trivial, it is somewhat simplified by the restriction of properties to those associated with upper bound results. That is, the maximum ice strength properties anticipated are used, so that the forces to which the structure is subjected are maximized. For the case numerically studied herein, ice properties for the given location were based on relvant literature [5] as well as on measurements obtained by the Ministry of Transport of Canada. Mechanical properties corresponding to both high (dynamic) and low (static) strain rate generating interactions were considered; however, the analysis is essentially the same for both since accelerations are not large enough to generate appreciable inertial forces.

A summary of the mechanical properties used is given in Table 1. Figure 1 graphically depicts the geometrical idealizations, coordinatization, and some of the notation used herein.

TABLE 1

ICE SYSTEM PROPERTIES

Ice Thickness	3.0 ft	Young's Modulus	0.8×10^6 p.s.i.
Density	58.0 lb/ft^3	Flexural Strength	100.0 p.s.i.
Interface Friction	0.15	Compressive Yield Strength	200.0 p.s.i.

III. PRELIMINARY ANALYSIS

The lowest force required to transform the impinging continuous ice sheet into an assembly of ice fragments having the capability to kinematically travel past the structure, is the highest force which that structure will have to withstand. Accordingly, the failure mode associated with the lowest failure load is the one likely to govern the interaction.

Thus, prior to proceeding with a refined analysis of the interaction, it is essential to ascertain that the correct failure mode is being considered. Failure modes which ought to be considered are: crushing, shear, buckling, and flexure [7, 9]. For conical structures of shallow slopes, it is well known that flexure is the prevalent failure mode. However, as the slope of the cone increases, the total force generated in flexural failure rapidly approaches that associated with a crushing or compression failure.

The amplification in the horizontal force for a given vertical force, due to increases in slope angle can be expressed with a function, ξ, called a "resolution factor". Specifically, the relationship between a vertical force F_z and the horizontal component, F_x, generated when F_z acts on a plane inclined at an angle α to the horizontal, with interface friction coefficient μ is given by:

$$F_x = \xi F_z \tag{1a}$$

where the "resolution factor" ξ is given by:

$$\xi = \frac{\mu\cos + \sin\alpha}{\cos\alpha - \mu\sin\alpha} \tag{1b}$$

A plot of the resolution factor for friction coefficient μ = 0.05, 0.10, 0.15, and 0.20 is shown in Figure 2. A singularity is evident for each case when the denominator vanishes and is marked on the graph. Physically, this singularity may be regarded as the condition at which, regardless of the magnitude of the forces, sliding will not take place.

For the case of a conical obstacle, where the total vertical load F_z is distributed uniformly around the 180° interface, an effective resolution factor ξ' relating the total vertical force and the horizontal force in the x - direction may be obtained by integrating the x - component of the horizontal force over the front perimeter of the cone, giving:

$$\xi' = \frac{2}{\pi}\xi \tag{2}$$

A rough approximation for the forces associated with each of the different failure modes may be obtained using the approximate methods developed by earlier investigators [6, 7, 9], in conjunction with the resolution factor when appropriate. For the specific case considered herein, flexure was found to give the lowest failure load by a significant margin; for the class of cases to which the analysis developed herein is applicable, flexure is assumed to dominate, although compressive or in-plane stress effects are considered.

IV. THEORETICAL ANALYSIS

Consider a wedge whose width, b, varies linearly with the distance x measured along the wedge bisector from the tip, then, $b = b_o x$, where b_o is a constant depending on the wedge angle γ. It was found [8] that the location, x_u, of the circumferential crack depends on the loading or truncation distance, a. The characteristic length l_o is defined as:

$$l_o = \sqrt[4]{\frac{Eh^3}{12k}} \tag{3}$$

where E is Young's modulus, h, the ice thickness, and k, the unit weight of water.

For the case of a wedge truncated at x = a, an approximate equation for the dependence of the ultimate load P_u on a/l_o is given by [8],

$$\frac{6P_u}{b_o \sigma_f h^2} = 1.10 + 2.40 \left(\frac{a}{l_o}\right) - 0.10 \left(\frac{a}{l_o}\right)^3 \tag{4}$$

where σ_f is the flexural strength. The appropriate graphs in Nevel's paper [8] may be used directly to determine the ultimate transverse load for an ice sheet by idealizing it as a fan of wedges having the appropriate properties.

The effects of horizontal thrust on the ultimate failure load depend on the magnitude of the thrust, as well as on the location of its point of application relative to the sheet midsurface. Say, the centroid of the reactive force is located a vertical distance h/3 below the midsurface, and that the horizontal thrust is $P_u'\xi$. Then, taking moments about the intersection of the midsurface and the plane at x_u at which the maximum moment M_u is generated, gives,

$$M_u = P_u' x_u - \xi P_u' \frac{h}{3} - M_B \tag{5a}$$

where M_B is the bouyant force moment. Neglecting M_B and substituting $M_u = P_u x_u$ gives,

$$\frac{P_u'}{P_u} = \frac{x_u}{x_u - \xi \frac{h}{3}} \tag{5b}$$

An approximate expression for the compressive stress generated in the failure zone by the in-plane force component is given by,

$$\sigma = \frac{\xi P_u}{x_u b_o h} \tag{6a}$$

This stress will reduce the flexural tensile stress in the failure zone. It can be shown that a correction factor analogous to the moment correction factor corresponding to the in-plane force effect is given by,

$$\frac{P_u''}{P_u} = (1 + \frac{\xi h K}{6 x_u}) \tag{6b}$$

where K is the right hand side of equation (4), and P_u'' is the corrected load.

And, finally, the combined correction factor corresponding to equations (5b) and (6b) may be expressed as,

$$\frac{P_u \text{ corrected}}{P_u} = 1 + \xi h \left[\frac{3K - \xi \frac{h}{x_u} K + 6}{6(3x_u - \xi h)} \right] \tag{7}$$

The most obvious approach to predicting the ultimate load of a composite of wedges, such as that formed when a semi-infinite ice sheet is edge loaded, is to take the arithmetic sum of the component wedge ultimate loads. One would anticipate some inaccuracy resulting from the asymmetry due to edge conditions of the composite, but if the load is evenly distributed among the wedges, and the radial cracks, as is usually the case, go beyond the peak stress zone, summation of individual wedge loads should give a relatively accurate estimate of the upper bound fan load. As is shown in Section V, the estimate is indeed very accurate.

The graphs in Figures 3 and 4, give predictions of the total vertical and horizontal forces which would have to be resisted by a conical structure of effective water line radius and slope ranging from 0.0 to 30.0 feet and 0.0 to 80 degrees, respectively. The calculation was based on ice having the applicable properties in Table 1. The resolution factor ξ, rather than ξ', was used to ascertain upper bound results for the horizontal force values.

It is noteworthy that the slope of the vertical force curves (Figure 3) is attributable solely to the moment-force correction factor. On the other hand, the horizontal force curves (Figure 4) slope due to a combination of the effects of the resolution factor and the correction factor, although the major slope magnification effect is due to resolution.

V. NUMERICAL ANALYSIS

Each of the two phases of the theoretical analysis -- the single ice wedge and the fan -- were corroborated using a finite element model. Accordingly, the following two problems were considered:

(a) Determination of the state of stress associated with a full or truncated floating ice wedge loaded by end transverse forces, in-plane forces, moments, and combinations of these loads .

(b) Determination of the state of stress in a cracked and uncracked floating ice sheet due to the effect of in-plane and transverse forces of various distributions.

Superimposed thin flat shell elements and thin plate on an elastic foundation elements were used to model the floating ice sheet. The shell elements were used to carry both bending and in-plane stresses in the sheet, while the plate elements were used to simulate only the Winkler-type elastic foundation effect due to the water bouyancy. Boundaries were chosen a distance of approximately ten times the characteristic length away from the wedge apex, to simulate a semi-infinite wedge. The idealizations used for a single wedge, and a wedge composite or fan, are shown in Figure 5.

It was assumed that the onset of yield at a point, in accordance with the Rankine yield criterion, was equivalent to crack formation at that point. Due to the predominance of radial bending stresses in the failure zone, similar results would have been obtained using the Tresca criterion.

Figure 6 shows a stress influence line for a single wedge loaded by a combination of transverse and in-plane loads and end moments. Calculations were carried out for both high and low strain rate properties (Static and Dynamic E), with only insignificant differences. Curves "3" and "5" graphically illustrate the effect of the end moment and in-plane force actions: approximately 30 per cent differences between failure loads due to the exclusion of these effects.

Analytical results based on the methods outlined in Section IV show excellent agreement with the numerical results. Both the transverse and combined loading peak stress values agree to within 5 per cent.

And, finally, a comparison of the results of the programs modelling the composite action of the wedges with those corresponding to an arithmetic sum of individual wedge loads, given in Table 2, also shows good agreement. However, divergence is evident as the indenter diameter increases, suggesting that summation of individual wedge loads for large indenters would give overly conservative results.

TABLE 2

COMPARISON OF DISCRETE AND COMPOSITE RESULTS
TRANSVERSELY LOADED HALF-PLATE

	Obtained using set of discrete wedges		Obtained using entire system simulation	
	ultimate load F_z (KIPS)	location of failure Crack (ft)	ultimate load F_z (KIPS)	location of failure Crack (ft)
Full plate	70.2	-	70.8	-
10 ft cutout	108.5	41.5	110.0	45.0
20 ft cutout	140.0	57.5	133.0	65.0

VI. FIELD OBSERVATIONS AND MEASUREMENTS

Comparison of the forces calculated with those measured in situ on the instrumented light pier during the winter of 1974-75 gave adequate agreement. The average difference between total calculated and measured forces was approximately 16 per cent, while the maximum difference was 20 per cent. Calculated forces were generally the higher values. The calculations were based as much as possible on ice properties measured near the structure; however, measurements for a number of significant properties such as the coefficient of friction at the ice-structure interface were not available, but were obtained from the literature, with a consequent decrease in the significance of the corroboration. A more comprehensive program of ice property and force monitoring is planned for future winters. Details of the measuring installation and associated program are given else where [3].

In addition, it was observed in the field, that pier slopes in excess of 70° from the horizontal tend to give rise to ice sheet failure behaviour characterized by a mode which is transitional between the flexural one, dominant for small slopes, and the crushing one, prevalent when the obstacle is vertical. The instrumented pier has a slope of 74.5°. Crack patterns in the fracturing ice upstream of the pier were often not characterstic of the anticipated flexural failure crack pattern. Also, the analysis of interface actions for high slope angles revealed a great sensitivity of the force to small changes in these angles. Yet the assumption of a pure crushing mode was not justifiable, suggesting scope for further research.

VII. CONCLUSIONS

Analytical expressions for forces exerted by ice sheets impinging on conical structures, including the effects of in-plane forces and edge moments were developed. To the best of the authors' knowledge, these expressions have not appeared before in the literature. These analytical expressions were rigorously corroborated by means of finite element programs, and found to be accurate within the framework of theoretical elasticity. In addition, some indication of their adequacy in a more general sense was given by the favourable but inconclusive comparisons made between analytical results and in situ full scale prototype measurements.

At the present phase of the investigation, the comparison with in situ measurements must necessarily be considered inconclusive because of the lack of confidence attributable to the ice and interface property data currently available. A more precision-oriented ice property measurement program is necessary before a significant corroboration may be made between analytical predictions and in situ force measurements. Such a program is currently under way.

The work to date has served to focus attention on several specific areas requiring further investigation. These are:

(a) Ice-structure contact problem
(b) Flexure-crushing transition for steep cone angles
(c) Dynamic ice-structure interactions

The importance of the properties of the ice-structure interface on the total load exerted on the structure was shown through the analysis of the effects of interface actions. However, the exact magnitude of these actions, which depends on the nature of the ice sheet fracture pattern at the interface, was by no means unequivocally determined. Only a heuristic first approximation approach was used to deal with this interface. In addition, it was assumed that the horizontal semi-circular contact distribution is uniform, whereas it can clearly range somewhere between sequential failure of the wedges to the simultaneous failure assumed here -- with drastic effects on the total forces.

Both the field observations and the analytical studies indicate a tendency toward a crushing failure with the amplification of in-plane stresses in the sheet as the cone angle increases. Although these in-plane stresses were analytically dealt with herein, it is the authors' opinion that the nature of the transition between flexure and crushing for steep slope angles warrants further investigation.

And, finally, the dynamic aspects of the ice-structure interaction, particularly as they relate to interface properties, have not to-date been seriously investigated. It was tacitly assumed that the ice break-up condition, which would result in moving ice floes impinging against the structure, would result in only insignificant difference in ice forces when compared to the static condition. This assumption should

be corroborated with an investigation of the dynamic effects of floe impact on the contact problem, as well as with empirical evaluation of dynamic coefficients of friction and resolution factors.

ACKNOWLEDGEMENTS

The permission to present this paper, granted by Mr. G. L. Smith, Chief of the Marine Aids Division of the Ministry of Transport, which funded the work, is gratefully acknowledged. The work was carried out under the first author's direction while he was at Acres Consulting Services Limited in Calgary, Alberta.

REFERENCES

1. Bercha, F.G. "Mathematical Simulation of Ice-Structure Interactions." *Proceedings of the Fifth Canadian Congress of Applied Mechanics*, Fredericton, May 1975.

2. Bercha, F.G. "New Solid Mechanics Applications in the Arctic" *Proceedings - Second Symposium on Applications of Solid Mechanics*, McMaster University, 1974.

3. Danys J.V. and Bercha, F.G. "Determination of Ice Forces on Conical Offshore Structures." *Proceedings of the Third International Conference on Port and Ocean Engineering Under Arctic Conditions*, University of Alaska, August 1975.

4. Danys, J.V. "Offshore Installations to Measure Ice Forces on Lightpiers in Lac St. Pierre." *Proceedings - IXth International Conference on Lighthouses and Other Aids*, Ottawa, 1974.

5. Gold, L.W. and Krausz, A.S. "Investigation of the Mechanical Properties of St. Lawrence River Ice." *Canadian Geotechnical Journal*, Volume 8, No. 2, May 1971.

6. Meyerhof, G.B. "Bearing Capacity of Floating Ice Sheets." *Transactions*, ASCE, Volume 127, Part 1, 1962.

7. Michel, B. "Ice Pressure on Engineering Structures." *Report No. AD709625*, U.S. Department of Commerce, National Bureau of Standards.

8. Nevel, D.E. "The Ultimate Failure of a Floating Ice Sheet." *Proceedings - Ice Symposium*, Leningrad, 1972.

9. Zubov, N.N. *Arctic Ice*, U.S. Department of Commerce, National Bureau of Standards, Translation AD426972, 1943.

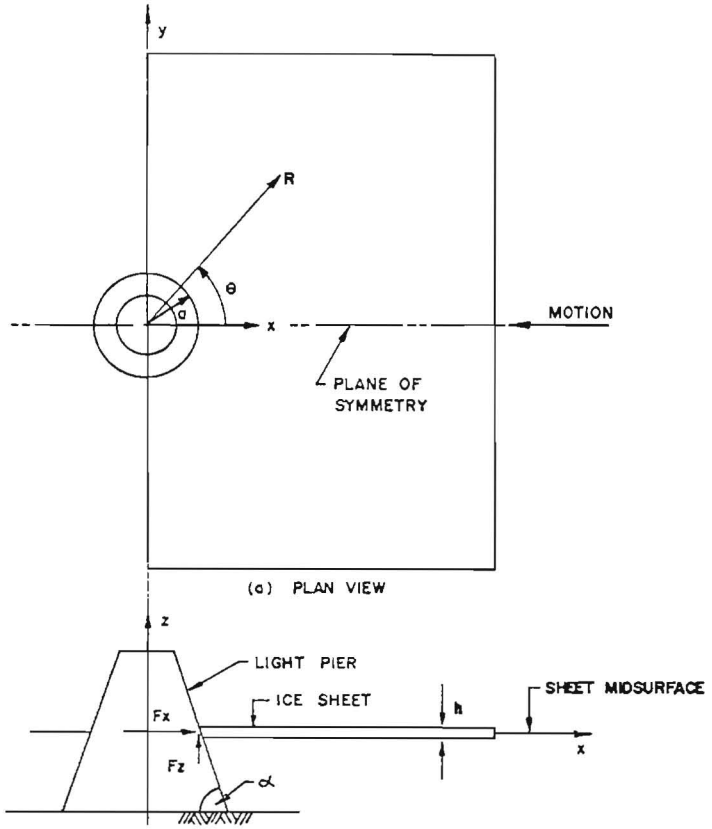

FIGURE 1 SCHEMATIC OF PROTOTYPE SYSTEM

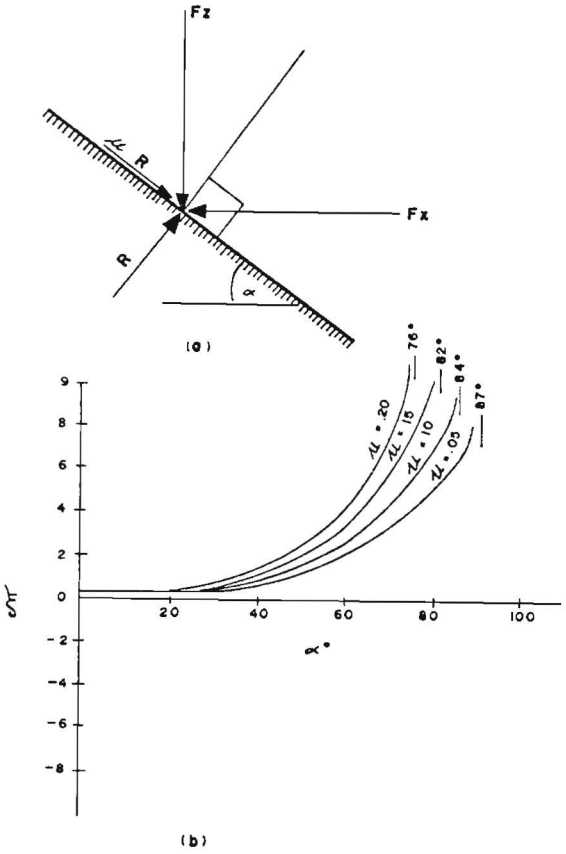

FIGURE 2 RESOLUTION FACTOR

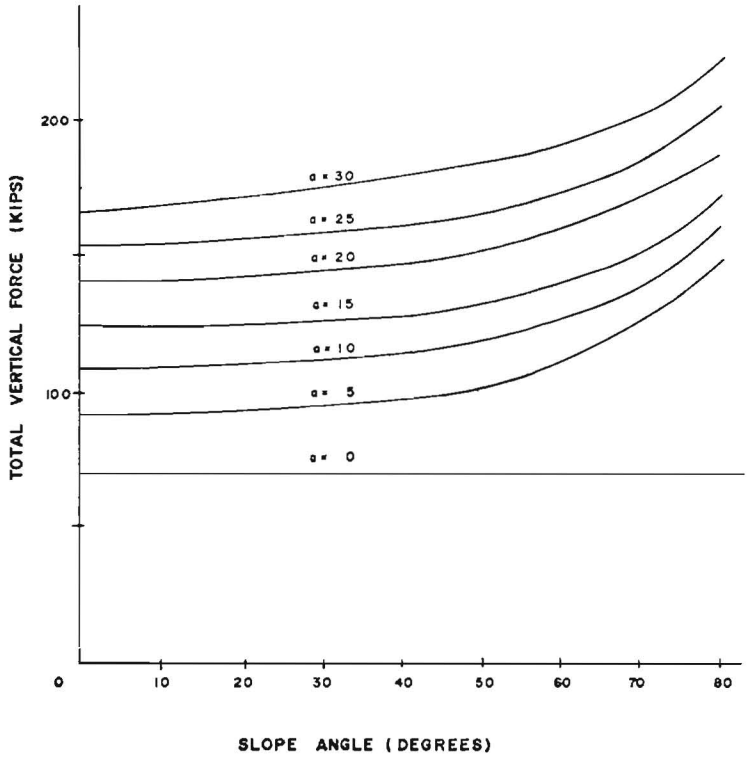

FIGURE 3 VERTICAL FORCE VARIATION WITH PIER SLOPE AND RADIUS

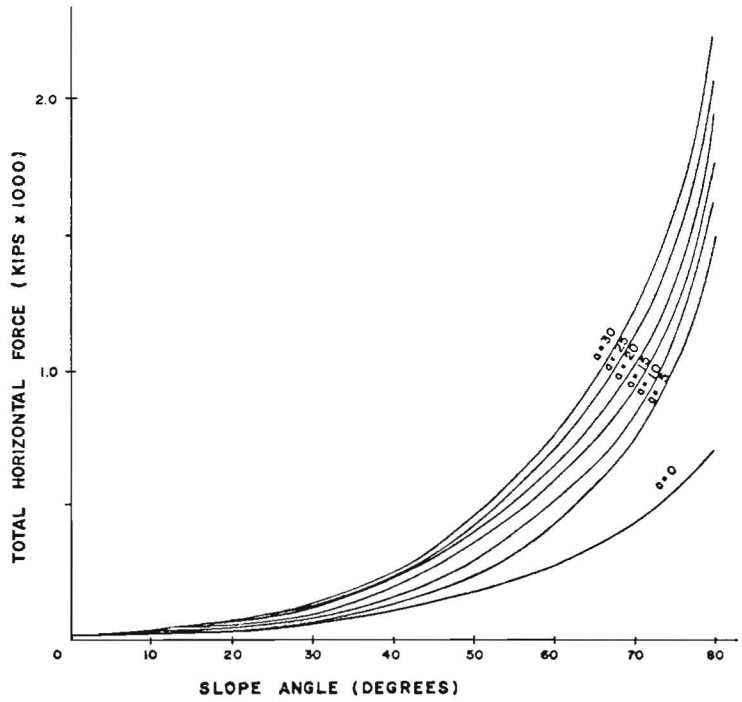

FIGURE 4 HORIZONTAL FORCE VARIATION WITH PIER SLOPE AND RADIUS

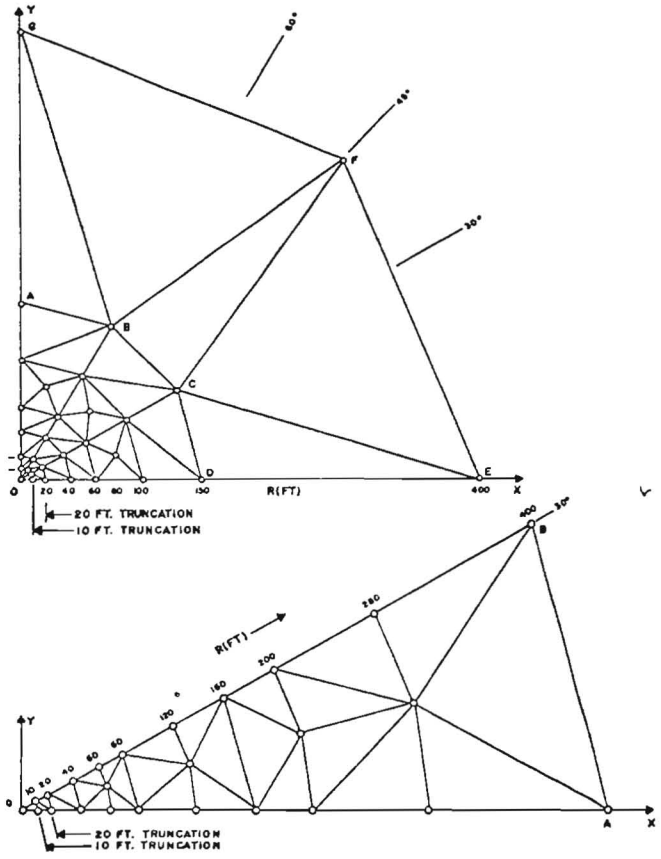

FIGURE 5 FINITE ELEMENT MESH

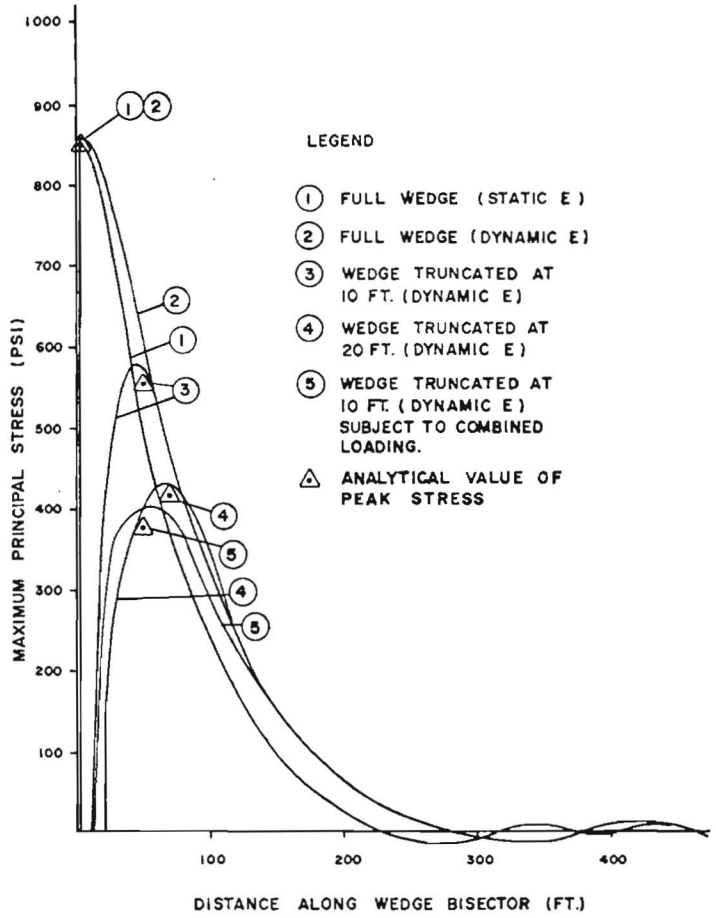

FIGURE 6 STRESS DISTRIBUTIONS FOR 30° WEDGE TRANSVERSELY LOADED BY 100 KIP LOAD AT END AND BY COMBINATION LOADING

THIRD INTERNATIONAL SYMPOSIUM ON
ICE PROBLEMS
Hanover, New Hampshire, USA

ON RECORDING STRESSES IN ICE

M. Metge
A. Strilchuk
P. Trofimenkoff

Imperial Oil Limited

Calgary, Alberta
CANADA

SYNOPSIS

The difficulties associated with recording stresses in ice over long periods of time are discussed, particularly those related to the influence of temperature variations and creep on the stress records.

The effects of the geometry and the rigidity of the stress sensors on their operation are shown. This indicates that there are some advantages in using a wide, thin and soft sensor. Such a sensor can be designed using elastomeric (rubber) materials as the deformable part of the sensor.

RESUME

On discute les difficultés associées avec l'enregistrement des contraintes dans la glace pendant de longues périodes de temps, particulièrement celles relatives à l'influence des variations de température et du fluage sur l'enregistrement des contraintes.

On montre l' effet de la géometrie et de la rigidité des indicateurs de contrainte sur leur operation.

Cela montre que l'utilisation d'un indicateur large, fin et mou présente des avantages. On peut construire un indicateur de cette sorte en utilisant un materiau élastomérique (caoutchouc) pour fabriquer la partie déformable de l'indicateur.

INTRODUCTION

Stress measurements in ice are of interest to many branches of ice engineering. They are needed to study the deformation of ice bodies such as glaciers and ice packs, to understand the formation of ice ridges and the interaction between ice floes. Also, there is an ever more pressing need for dependable and accurate measurements of the forces exerted by ice on man-made structures. Often, in this case, the ice forces can be derived from the deformation of the structure itself or of sensing panels placed at the ice-structure interface (BLENKARN 197 1970, DANYS 1975). However, sometimes the ice-structure interface is badly defined or inaccessible, or the structure is too large for these techniques to be practical. Sometimes also, it would be too expensive to install sensing panels on a finished structure. In those cases it becomes easier to measure the stress in the surrounding ice and derive from it the total force on the structure. This of course, is only feasible in cases where the ice movement is small otherwise the sensors would only be in the vicinity of the structure for a short time.

The ice stress method could apply to the study of ice forces on dams, piers, docks and lighthouses in lakes, but it is particularly well suited to studying the forces exerted by landfast ice on artificial islands used for drilling in the Beaufort Sea. Those islands are too large to be instrumented completely, the ice-island boundary is not well defined and sometimes inaccessible because of ice rubble.

Basically, the problem of measuring stresses in the ice is similar to measuring stresses in other visco-elastic materials such as soils, rocks, concrete, or solid rocket fuel which have received more attention. It is somewhat different however, in that ice is exposed to large temperature changes and is usually present in the form of a sheet of uniform thickness.

Stress in a medium cannot be measured directly; it must be derived from the corresponding deformation (strain) either of the medium itself or of a sensor incorporated in it (inclusion). The application of these techniques to measurements in ice will now be discussed.

STRAIN MEASUREMENTS

At first sight the easiest solution seems to be to measure the strain in the ice. This is a relatively easy task (using commercial resistive strain gauges for instance), but difficulties arise when trying to interpret the strain in terms of stress.

In the case of short term stresses, as long as the ice behaves elastically, there is no difficulty in relating stress to strain if the elastic properties of the ice, Young's Modulus, and Poisson's Ratio are known. However, in ice, these properties, particularly the Young's Modulus, are highly variable with temperature, salinity, grain size, and crystal orientation. Thus, the problem of measuring the stress becomes one of determining the elastic properties of the ice.

In the case of long term loads, the relationship between stress and strain is complicated because the ice creeps and does so at various rates according to temperature, salinity, stress level, stress history, etc. The problem of separating the elastic strain from the creep strain which may be orders of magnitude larger is intractable. The problem of relating the creep strain rate to the stress would require a better knowledge of the creep properties than we have at this time. Thus, ice strain measurements are of little use for recording stresses over long periods of time. However, they have been used to determine localized stresses at some particular time by relieving the stress at a point and measuring the associated elastic strain recovery. In this case, they have to be combined with measurements of elastic properties.

It therefore appears that to record stresses in ice over long periods of time, a different approach must be used -- that of embedded sensors.

STRESS SENSORS

In simple terms a stress sensor is a block of material which has a known stress-strain relationship and of which the deformation can be measured accurately. An infinity of such sensors, using different materials, geometries, and techniques for measuring the strain, can be built. However, any sensor installed in a stressed ice sheet will in general, change the local stress field in the sheet. If the sensor is stiffer than the ice (higher elastic modulus), it will support some of the load that would otherwise be supported by the ice around it and it will "concentrate" the stress. If it is softer than the ice, it will deflect easily requiring the surrounding ice to support more of the load.

Precise knowledge of the strain in the sensor, the stress-strain relationship of the sensor material and the "stress concentration factor" yields the value of the stress in the ice. The main problem is to determine the stress concentration factor and to design the sensor in such a way that it remains as constant as possible even if the ice properties change.

STRESSES NEAR INCLUSIONS

The problem of determining the stress "felt by" an inclusion (sensor) in a stressed medium is not new. The same problem has been encountered in measuring stresses in soils. An elastic solution has been given by A. Coutinho (1969) for a cylindrical inclusion, as well as by M. Rocha (1955) and Peattie and Sparrow (1953). Although there are differences in the expressions given in these references the basic form of the expression is the same and can be written as:

$$\frac{\sigma}{\sigma_1} = \frac{E_1/E + H/D}{E_1/E(1+H/D)} \qquad \ldots(1)$$

where σ is the stress in the medium (the ice)
σ_1 is the stress felt by the sensor (the inclusion)
E is the elastic modulus of the medium
E_1 is the "elastic modulus" of the sensor

H is the thickness of the sensor in the stress direction
D is the width or diameter of the sensor in a direction perpendicular to the stress

Poisson's ratios, of the sensor and of the medium should be included in an exact solution, but the above expression is sufficient to illustrate the effect of different stiffnesses and different geometries. The family of curves described by this equation is plotted in Figure 1. The most interesting features are as follows:

1. If $E_1=E$ then $\sigma=\sigma_1$ for all values of H/D. That is, an "invisible" sensor, where the sensor material is identical to ice, or has the same elastic properties, "feels" the same stress as the ice around it. However, if the sensor is not extremely flat (say if H/D> than 0.01), the stress concentration factor (σ_1/σ) will change sharply with any changes in the elastic modulus of the ice which, in nature, does vary with temperature, load rate, etc.

2. If $E_1/E > 10$, σ/σ_1 becomes asymptotic to a certain value which, while it does depend on the geometry of the inclusion (H/D) is independent from the exact value of E_1/E. In other words, if a very stiff sensor was used, the stress concentration factor would be independent of the elastic properties of the ice. This type of sensor is available commercially, and so far, it has been the most commonly and successfully used. However, it will be shown later that such sensors are sensitive to temperature changes and may be affected by ice creep.

3. If $H/D << 1$, then $\sigma_1/\sigma = 1$ for a large range of values of E/E_1 even for $E_1/E < 1$. In other words with a very thin and very wide sensor, not only does the stress concentration factor not change, even with large variations in elastic modulus at the medium but also its value is unity and does not depend on small changes in sensor geometry. A practical advantage of this type of geometry, is that theoretically, there is no need to calibrate the sensor in the ice to know the stress concentration factor: it is always unity. A two dimensional finite element analysis of a thin, wide sensor embedded in a large sheet of ice was also undertaken in order to further check the behaviour expected on the basis of Equation (1). It was sufficient to work in one quadrant and apply appropriate boundary conditions at the two symmetry planes. The ice sheet containing the sensor was taken to be 40m x 110m. A total of 190 elements and 218 nodes were used in the analysis. The ratio of applied stress to integrated stress in the sensor was determined for a fixed H/D ≃ .002 and two elastic modulii ratios. The results are indicated by the points in Figure 1. As can be seen, good agreement has been obtained between the finite element analysis and the behaviour predicted by Equation (1).

In summary it appears that the best possible sensor would be one that is wide, thin and stiff. Further investigation however, indicates that it may be difficult to instrument. Additionally, as will now be discussed, the effects of temperature variations are more important in the case of a stiff sensor than for a soft one.

EFFECTS OF TEMPERATURE

Under field conditions, the temperature of the ice and of the sensor may change significantly.

The first aspect of temperature changes is that they affect the operation of the strain measuring system. This can usually be eliminated by using corrective devices such as dummy gauges in the case of resistive strain gauge systems.

The second and more important aspect is that, because ice and sensor do not usually have the same thermal expansion coefficients, any temperature change will cause an expansion that is different for the sensor and for the cavity which it occupies. The expansion coefficient of ice is usually higher than for any metal so that if the temperature decreases, the cavity will contract more than the sensor, and this will create a local stress unrelated to the stress in the ice sheet as a whole.

As an example let us take a steel sensor:

$E_{sensor} = 20.10^{10}\ Nm^{-2}$ $\qquad \alpha_{sensor} = 12x10^{-6}\ °C^{-1}$

$E_{ice} = 0.5x10^{10}\ Nm^{-2}$ $\qquad \alpha_{ice} = 50x10^{-6}\ °C^{-1}$

Assuming a temperature change of 10°C the differential strain will be $(50-12)x10^{-6}x10 = 38x10^{-5}$.

Assuming, crudely, that all the corresponding deformation occurs in the ice over a distance equal to the length of the sensor, ie. the strain in the ice is equal to the differential thermal strain, the stress felt by the sensor would then be

$$38x10^{-5} \times 0.5x10^{10} = 19x10^{5}\ Nm^{-2}$$

$$(= 276\ psi)$$

In the case of a soft sensor, however, most of the deformation would occur in the sensor itself and because it is soft would not give rise to high stresses. Take rubber for instance, as the sensor material ($\alpha \simeq 25x10^{-5}\ C^{-1}$) and assume an elastic modulus of $0.5x10^{8}\ Nm^{-2}$, the stress felt by the sensor due to a temperature change of 10 degrees C would be:

$$10 \times (250-50)x10^{-6}x0.5x10^{8} = 10^{5}\ Nm^{-2}$$

$$= (14.5\ PSI)$$

Of course, this spurious thermal effect could be completely eliminated by matching exactly the average expansion coefficient of the sensor to the expansion coefficient of ice, but this is not usually feasible. In other cases, a soft sensor will, in general, be less sensitive to thermal effects than a stiff one.

EFFECTS OF CREEP

When one is concerned with recording ice stress over long periods of time, creep effects must be considered. When a uniform compressive stress

is applied to an ice-sensor system, the stress distribution in the ice directly in front of the sensor is not uniform: if the sensor is stiff it supports more of the load, if it is soft, the ice supports more of the load. In both cases, high stresses are set up in the ice at the edges of the sensor. It seems reasonable to expect that creep would tend to relieve these high stresses. If the stress concentration factor for the sensor as a whole is close to unity as in the case of a very wide and thin sensor, creep has little effect on the sensor response. In fact, in this case, creep can only bring the stress concentration factor even closer to unity.

If the stress concentration factor for the sensor as a whole is considerably different from unity, creep could cause a significant change in the integrated stress on the sensor. This would result in a changing sensor output although the stress in the ice sheet possibly remains constant.

For example, take a stiff sensor ($E_1/E = 100$) with a narrow geometry ($H/D = 3.5$); the average stress on the sensor is approximately three times the applied uniform stress. With time, creep will occur faster in front of the sensor than in the rest of the ice. Assuming (R.O. Ramsier 1971) that the strain rate $\dot{\varepsilon}$ is proportional to the cube of the stress ($\dot{\varepsilon} \alpha \sigma^3$), the creep rate would be 27 times faster in front of the sensor. Intuitively, one would expect this to change the stress distribution and thus to change the stress concentration factor, to some unknown value. However, in contrast with this argument, stiff sensors have been used in viscoelastic media with apparent success. D. Skilton (1971) for instance, mentions that a rigid meter in viscoelastic rock "maintained its calibration values....to within 5% even though the rock material underwent appreciable creep deformation." However, he does mention that his experiments were not wholly conclusive. Thus, until further corroborative evidence establishes that creep does not modify a stiff sensor behaviour, uncertainty still exists as to the effect of creep. In light of these difficulties it therefore appears desirable to design sensors for which creep has little effect in spite of possible relief of stress concentrations.

OTHER ADVANTAGES OF WIDE THIN AND SOFT SENSORS

Bending Stresses

Under field conditions an ice sheet may be subjected to bending. If one is interested in the average compressive stress in the ice, as in the case of artificial islands, this creates a difficulty: if a small sensor is not situated exactly halfway in the ice thickness (and this changes as the ice grows) it will respond to bending stresses. Separating the bending stresses from the overall compressive stresses would require several of these small sensors at various depths in the ice spaced so that the influence of any sensor on its neighbors is negligible. On the other hand, a large sensor that covers the whole ice thickness would average the tensile and compressive stress for any ice thickness.

Size

It is almost by necessity that stiff sensors be small since otherwise they would require a multitude of strain gauges (a commonly used device in a stiff sensor) or a novel technique for measuring the sensor deformation. On the other hand, a soft sensor can be made large while at the same time lending itself to simple instrumentation, for example capacitive readout. Also there is always uncertainty in whether the stress measured by small sensors is representative of the stress in the whole ice sheet since only a localized measurement is taken. There is less uncertainty with a large, wide sensor.

DESIGN OF A THIN, WIDE AND SOFT SENSOR

Since there appeared to be a definite advantage for the use of a thin wide sensor, design and construction of such a sensor was undertaken for measurements of ice pressures around the artificial drilling islands built by Imperial Oil Ltd. Equation (1) was used to determine the required parameters of the sensors so that the stress ratio was near unity. A sketch of the sensor configuration is shown in Figure 2.

The sensor essentially consists of a double sandwich of aluminum plates and elastomeric material which deforms under applied stress. The amount of deformation is determined by measuring the change in capacitance between the metal plates.

The stress-capacitance characteristic of the sensor was subsequently determined by various calibration tests. The results obtained with these sensors are yet confidential. However, it is hoped that the information released here will show the interesting possibilities of a soft stress sensor. The design shown in Figure 1 may not be the best. It may be possible to use other materials or different configurations. The important point is that the concept of a thin wide and soft sensor appears to be sound.

CONCLUSION

The problems associated with measuring stresses in ice have been discussed and the relative merit of sensors with different properties outlined. It is concluded that a thin wide and soft sensor has merit and one possible design of such a sensor has been presented.

ACKNOWLEDGEMENT

The authors wish to thank Imperial Oil Limited for permission to publish this paper. They also wish to thank their colleagues from Imperial and from the University of Alaska, who were instrumental in developing the concept.

BIBLIOGRAPHY

J.W. DANYS, 1975 "Offshore Installations to Measure Ice Forces on the Lightpiers in Lac St. Pierre", IXth International Conference on Lighthouses and Other Aids, OTTAWA 1975.

BLENKARN, 1970 "Measurements and Analysis of Ice Forces on Cook Inlet Structures", IInd Offshore Technology Conference, HOUSTON 1970.

A. COUTINHO, 1949 "Theory of an Experimental Method of Determining Stresses not Requiring an Accurate Knowledge of the Modulus of Elasticity", International Assoc. for Bridge and Structural Engineering, Ninth Volume, 1949, Published by the General Secretariat of Zurich.

M. ROCHA, 1965 "Stress Analysis", O.C. Zienkiewicz and G.S. Holister, P455.

K.R. PEATTIE
R.N. SPARROWS, 1954 "The Fundamental Action of Earth Pressure Cells" Journal of Mechanics and Physics of Solids, pp2, 141-145, April 1954.

D SKILTON, 1971 "Behaviour of Rigid Inclusion Stressmeters in Viscoelastic Rock", In. J. Rock Mech. Min. Sci., Vol. 8, pp 283-289.

R.O. RAMSIER, 1971 "Mechanical Properties of Ice", Proceed. POAC Conference in Trondheim, P206.

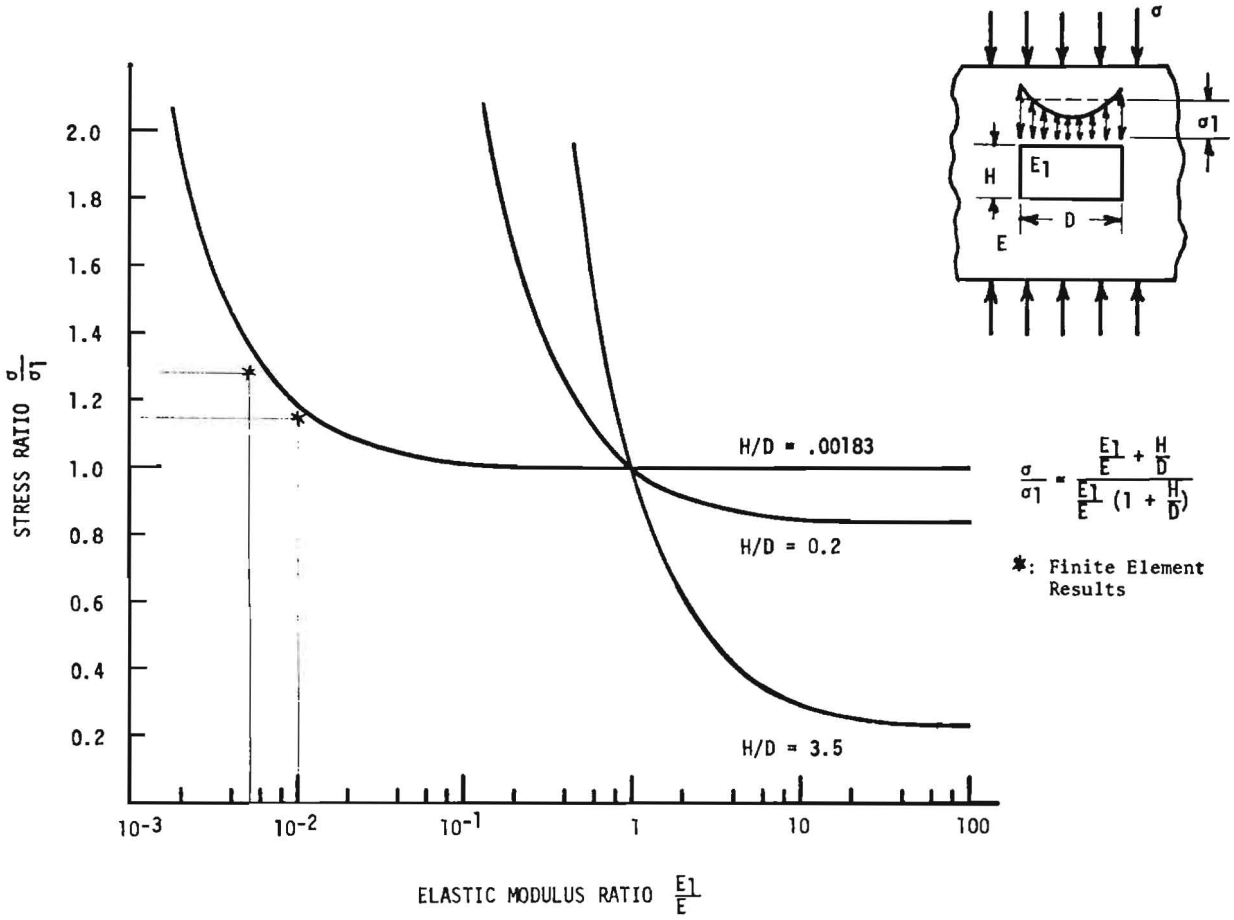
σ
σ1
H
E1
D
E
STRESS RATIO σ/σ1
2.0
1.8
1.6
1.4
1.2
1.0
0.8
0.6
0.4
0.2
H/D = .00183
H/D = 0.2
H/D = 3.5
10-3
10-2
10-1
1
10
100
ELASTIC MODULUS RATIO E1/E
σ/σ1 = (E1/E + H/D) / (E1/E (1 + H/D))
*: Finite Element Results

Figure 1

IOL SENSOR DESIGN

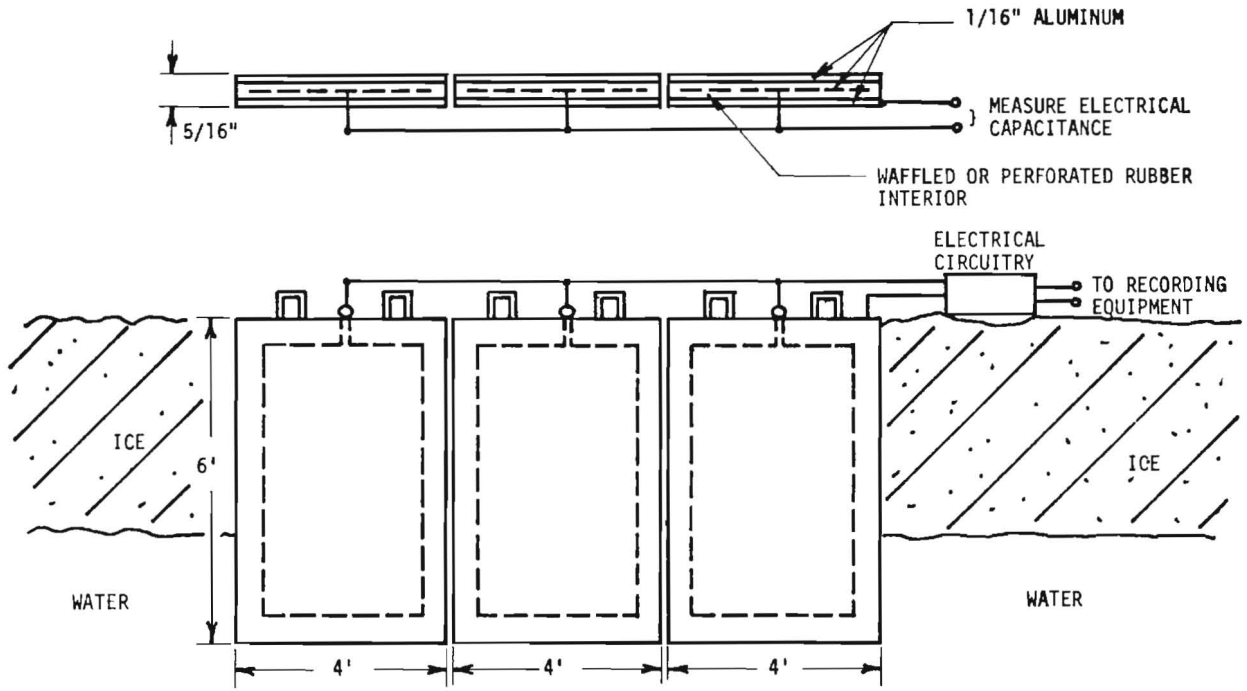

ADVANTAGES

- STRESS MONITORED OVER A LARGE AREA.
- TEMPERATURE EFFECTS RELATIVELY INIMPORTANT.
- SMALL EFFECT OF ICE CREEP ON SENSOR OPERATION.

Figure 2

THIRD INTERNATIONAL SYMPOSIUM ON
ICE PROBLEMS
Hanover, New Hampshire, USA

EFFECT OF HUMMOCKED ICE ON THE PIERS OF MARINE HYDRAULIC STRUCTURES

Yu.V. DOLGOPOLOV, M.Sc.(Eng.)	The B.E. Vedeneev VNIIG	Leningrad, U.S.S.R.
V.P. AFANASIEV, M.Sc.(Eng.)	The Institute of Railway Transport Engineers	Leningrad, U.S.S.R.
V.A. KOREN'KOV, M.Sc.(Eng.)	The B.E. Vedeneev VNIIG the Siberian Branch	Krasnoyarsk, U.S.S.R.
D.F. PANFILOV, M.Sc.(Eng.)	The Institute of Civil Engineering	Gorki, U.S.S.R.

SYNOPSIS

The interaction of ridged ice with vertical and cone-shaped piers of marine hydraulic structures is described. The ice load on a vertical pier should be examined as a summation of forces imposed by solid and disintegrated ice. In the case of a cone-shaped pier the ice load due to solid and disintegrated ice is to be considered consecutively. Design relationships are proposed.

The application of substantiated methods for estimating ice loads is one of the major means of ensuring reliability of structures affected by ice. Such methods are particularly important for the design of isolated structures located at a considerable distance from the shore, since in those cases ice loads are generally greatest as against other loads. Some failures of structures of this type, due to drift ice, indicate that the actual forces are to be adequately considered.

Presented herein are methods for calculating ice loads on isolated piers of marine hydraulic structures, with rafting of primary ice forms and pressure ridges included. The methods are based on field, experimental and analytical data.

Field observations revealed a great variety of sea ice. A uniform solid ice sheet is rarely to be found in the open sea; ice fields incorporating pressure ridges having different thickness, plan dimensions and drift velocity are much more common.

When estimating ice pressures against structures located in relatively small reservoirs, the thickness of a solid ice sheet is usually adopted as design ice thickness. The ice sheet occurring at a con-

siderable distance from the shore is composed of rafted and ridged ice, which should be allowed for in calculations.

Until recently, the effect of ridged ice on structures has been completely neglected in design practice. At present the action of pressure ridges on marine hydraulic structures is taken into account through a magnification factor introduced into design formulae for evaluating pressures from a smooth ice sheet. Based on the field data, a factor of 2.2 is assumed for some coastal regions of the U.S.A. and Canada /1/. In the U.S.S.R. a factor of 1.3-1.5 is taken for temperate seas. The use of such averaged factors for structures of all kind, irrespective of their geometrical dimensions, may be attributed to insufficient knowledge of the problem, which is associated with difficulties experienced in conducting field investigations. In our opinion, the field data now available permit making some refinements in design recommendations. The paper describes calculation procedures considering the effect of pressure ridges on the magnitude of ice load against the structure as a function of the size and state of ridges, and the structure geometry /2/.

Pressure ridges constitute generally accumulations of ice blocks formed due to dynamic processes in the ice sheet. For new ridges less than one winter old (temperate latitudes), the design ratio of the height of the underwater part of the ridge to its draft may be taken equal to 1/4-1/5. An individual ridge may have a trapezoidal cross-section.

The magnitude of ridge pressure against the structure is primarily governed by the dimensions and structural integrity of the ridge, viz. by the degree of bonding between ice blocks. According to I.S. Peschansky /3/, extended periods of time, adequate subfreezing temperatures of water and ice, and sufficient pressures at the contact points between ice blocks are required to attain complete freezing of ice flocs in sea water. Such conditions are rarely encountered in temperate seas. The underwater portion of the ridge represents normally pile-up of unfrozen or partly frozen ice blocks falling spontaneously or under small loads, and rising upwards when the surface ice is damaged.

Interaction between Ice and Vertical Pier

The computational scheme for assessing ridged ice pressure against the pier incorporates both the pressure imposed by the upper part, i.e. a solid sheet including rafting, and that from the lower underwater part of the ridge composed of a mass of separated ice blocks (Fig. 1). The overall ice force, P_0, exerted on the pier is the summation of the forces due to those two parts

$$P_0 = P_f + P_r \,. \qquad (1)$$

The force from the upper part on an isolated vertical pier is found by the formula

$$P_f = mR\beta h_s \,, \qquad (2)$$

where m is the coefficient allowing for the pier shape in plan /4/, β and h_s are the pier width and ice thickness, with rafting incorporated, respectively; $R = \kappa R_c$, R_c is the strength of ice in uniaxial compression depending on its temperature and salinity, κ is

the coefficient taking into account three-dimensional stresses in the sheet.

The coefficient, κ, is determined by the ratio, $\frac{\beta}{h}$ /5/. The effect of the ratio on the magnitude of unit pressure was confirmed in the experiments in which solid ice-vertical pier interaction was simulated, with the values of $\frac{\beta}{h}$ ranging from 1.0 and over

$$\kappa = \sqrt{1+5\frac{h}{\beta}} \qquad (3)$$

The following formula is recommended to define κ for $\frac{\beta}{h} > 10$

$$\kappa = \frac{1}{2\sin\rho}\left[(1+\sin\rho)\exp\lambda\pi - 1 + \sin\rho\right], \qquad (4)$$

where $R = tg\rho$, and ρ is the slope angle of the Mohr envelope for ice equal to 15-25° in a first approximation. The coefficient, κ, is assumed by interpolation for intermediate values of $\frac{\beta}{h}$.

It should be noted that the regularity $\kappa = f\left(\frac{\beta}{h}\right)$ have been corroborated by American investigators both qualitatively and quantitatively /7/.

Proceeding from the recommendations of N.N. Zubov, a relationship is suggested for approximate determination of the values of the rafted ice thickness in the open sea

$$h^2 + 50h = 8\left(\Sigma\theta_1 + \Sigma\theta_2\right), \qquad (5)$$

where h is the thickness of rafted ice, cm; $\Sigma\theta_1$ is the number of degree °C-days of cold for the period after rafting, $\Sigma\theta_2$ is 1000-1300 degree °C-days of cold.

Experimental studies on a model ridge representing a discrete medium as individual plates were undertaken for revealing the physical pattern of the interaction between the pier and the underwater portion of the ridge, and for deriving design formulae. The experiments showed that as the model pier penetrates into the ridge, there forms in front of it a core of orderly oriented strengthened plates which are then displaced on the shear plane at the angle, θ.

The physical pattern of the phenomenon is similar to the deformation of loose medium, which permitted utilization of appropriate theoretical relationships for deducing a design equation of the form

$$P_z = \mu H_z\left(0{,}5 H_z \mu\gamma + 2c\right) j b_z, \qquad (6)$$

where $\mu = tg\left(45 + \frac{\varphi}{2}\right)$, φ is the angle of internal friction in a mass of ice blocks, H_z is the design thickness of the underwater portion of the ridge, γ is ice buoyancy, $j = 1 + \frac{2H}{3\beta}$ is the coefficient considering spatial behaviour of the ice medium, b_z is the design pier width within the boundaries of the underwater portion of the ridge.

Account must be taken of an increase in the thickness of the underwater part of the ridge during interaction with the structure. The design height of the additional ice of triangular cross-section cannot exceed approximately half the pier width. Therefore, the ridge thickness in Eq (6) is adopted with regard to the condition

$$H \geq H_z \leq H'_z + \frac{\beta}{2}, \qquad (7)$$

where H_z' is the initial thickness of the underwater part of the ridge taken from observational data.

The load increase produced by a ridged ice sheet as compared to the load from a uniform sheet may be calculated as

$$\eta = 1 + \frac{\mu H (0{,}5 H_z \mu\gamma + 2c) B_z j}{B h R_c K} \qquad (8)$$

The shape factor of the pier is eliminated from Eq (8), since it is expected that the plan configuration of the front portion exerts a similar effect on the magnitude of both of the total pressure components.

It follows from Eq (8) that the total load increase is a variable governed by the ridge thickness, pier width, solid sheet thickness and ice strength which is a function of salinity and temperature. In Figs 2 to 5 the curves η are plotted for different values of one of the above parameters. As seen from Fig. 2, the effect of ridges on the magnitude of the total ice load decreases with increasing the pier width, other parameters entering into Eq (8) being constant.

Curves 5 and 6 in Fig. 3 show variation of η with monolithic ice sheet thickness alone. Here again, a curve is plotted for the quantity, $\bar{\gamma}_h$, equal to the ratio of the difference, $\eta_h - 1$, to the corresponding difference at $h_1 = 1.0$ m

$$\bar{\gamma}_h = \frac{\eta_h - 1}{\eta_{h_1} - 1}$$

Curves 8 and 9 in Fig. 4 depict variation of η with ice temperature alone. Curve 10 is plotted for the quantity, $\bar{\gamma}_t$, equal to the ratio of the difference, $\eta_t - 1$, to the corresponding difference at $t_1 = 0^{\circ}C$

$$\bar{\gamma}_t = \frac{\eta_t - 1}{\eta_{t_1} - 1}$$

Curves 11 and 12 in Fig. 5 show variation of η with ice salinity alone. Curve 12 is plotted for the quantity, $\bar{\gamma}_s$, equal to the ratio of the difference, $\eta_s - 1$, to the corresponding difference at $S_1 = 0\%$

$$\bar{\gamma}_s = \frac{\eta_s - 1}{\eta_{s_1} - 1}$$

The magnification factor may be calculated by the formula

$$\eta = 1 + \bar{\gamma}_B \bar{\gamma}_h \bar{\gamma}_t \bar{\gamma}_s , \qquad (9)$$

where the values of $\bar{\gamma}_B$, $\bar{\gamma}_h$, $\bar{\gamma}_t$ and $\bar{\gamma}_s$ are assumed from the curves in Figs 2 to 5.

To verify the factor obtained experiments in an ice basin were carried out /2/, alternate interaction of isolated vertical and cone-shaped piers with stretches of a solid and ridged ice sheet being reproduced (Fig. 1). The results obtained are as follows: the magnification factor for the vertical pier made up 1.54 with loose ice blocks in the underwater part of the ridge whereas it amounted to 2.5-2.7 with the ice blocks frozen together. The magnification factor for a cone-shaped pier was 1.45 if ice blocks in the lower part were not bonded together.

Interaction between Ice and Cone-Shaped Pier

To solve the problem on the probability of combined action of a smooth ice sheet and the underwater portion of the ridge on the cone-shaped pier, let us consider the role of the horizontal reaction produced by the sheet. The experiments indicated /6/ that prior to ultimate failure of ice by a cone-shaped pier a number of radial cracks appear forming separate ice strips in a certain sector in front of the pier. Simultaneously a circular crack, due to longitudinal and lateral bending, occurs at some distance from the pier. The solution to the equation /8/

$$D y^{IV} + H y'' + \kappa y = 0 \qquad (10)$$

yields the magnitude of the maximum bending moment as

$$M_{max} = \frac{V}{\lambda} \varphi , \qquad (11)$$

where $\varphi = F(f)$ (Fig. 6), $\lambda = \sqrt[4]{\frac{\kappa}{EJ}}$, $f = \frac{H}{H_{cr}} = \frac{H}{\sqrt{\kappa E J}}$

V and H are vertical and horizontal reactions, respectively.

Formulae for the maximum values of the horizontal reaction at $\kappa = 1 t/m^3$, $J = h^3/12$, and $W = h^2/6$ may be written as

$$H_{max} = \frac{R_\beta}{\frac{6\varphi}{tg\beta} \cdot \frac{\sqrt[4]{4EJ}}{h^2} - \frac{1}{h}} ; \qquad (12)$$

$$H_{max} = \frac{R_c}{\frac{6\varphi}{tg\beta} \cdot \frac{\sqrt[4]{4EJ}}{h^2} + \frac{1}{h}} ; \qquad (13)$$

$$H_{max} = R \cdot h ; \qquad (14)$$

$$H_{max} = \sqrt{EJ} . \qquad (15)$$

Fig. 7 presents H_{max} versus β curves. Calculations are carried out for the values of E varying from $4 \cdot 10^4$ to $4 \cdot 10^5$ t/m^2, $R_\beta = 40$ t/m^2, $R_c = 100$ t/m^2 and ice thicknesses of 0.8, 1.2 and 1.6 m. Fig. 7 shows only the curves for $h = 0.8$ m and $E = 4 \cdot 10^5$ t/m^2. With other values of initial parameters the curves have a similar pattern. The intercept of curves 1 and 2 in Fig. 7 refers to the case when failure may be induced either by tension in bending or by compression in bending. According to calculations, this phenomenon takes place generally at $\beta = 85$–87°. With higher values of β the design values of H_{max} corresponding to failure by bending increase sharply, therefore other modes of failure, due to loss of longitudinal stability and crushing, are quite feasible. Since tension in bending is the most probable cause of ice strip failure, the corresponding values

of H_{max} may be computed from formula (12) by successive approximations. However it is inconvenient from practical viewpoint.

Means to considerably simplify calculations is found. Two more curves 3 and 4 are plotted in Fig. 7. Curve 3 illustrates H_{max} versus β relationship, with compression and bending imposed by the horizontal reaction of the pier ignored. In this case the quantity, φ, conforms to lateral bending of a semi-infinite strip and equals 0.322. Curve 4 illustrates the case when the longitudinal bending from the force, H, is disregarded, and the compression considered. The values of H_{max} are estimated by formula (13) at $\varphi = 0.322$.

The horizontal reaction of the pier has a double effect on the ice strip, viz. on the one hand, it increases bending thus diminishing ice load on the structure, and on the other, it produces compressive stresses increasing ice load on the pier. The coincidence of curves 1 and 3, especially at $\beta = 70\text{-}75^{\circ}$, indicates that the above effects are mutually counterbalanced. The failure of ridged ice being cut through by a cone-shaped pier (Fig. 1), as distinct from a vertical pier, should be examined consecutively: the first stage relates to lifting and separation of a solid sheet from the underwater portion of the ridge, and the second stage to dislocation and dislodging of ridged ice blocks.

A method for evaluating the pressure exerted by a solid ice sheet against cone-shaped piers was developed on the basis of the physical pattern of the sheet failure observed during the laboratory tests conducted by the authors. The ice sheet was reproduced as a series of semi-infinite plates, with radial cracks, on Winkler's elastic foundation, the horizontal and vertical reactions of the pier being applied to the free end of the plates (Fig. 8).

The length of the contour around which forces from the pier are transmitted to the ice equals $S = r\theta$, where θ is the angle determining the relative position of extreme radial cracks. The angle θ varied between 90 to 110° in the tests.

The length of the contour around which a circular crack forms after bending is assessed by $S_1 = (r + \ell)\theta$

A horizontal load may develop at the contact between ice and the pier. It is determined by the formula $H' = H\frac{r+\ell}{r}$, where H is the load originating across the circular crack. Assume that H' is distributed uniformly over the ice-pier contact, then the magnitude of the horizontal reaction of the maximum ice pressure against the pier may be found from

$$P = 2\int_0^{\theta/2} \frac{H'}{\cos\alpha}\, r\,d\alpha = H'r \cdot 2\ln tg\left(\frac{\theta}{4} + \frac{\pi}{4}\right).$$

Assuming $\theta = 110^{\circ}$ and $\ell = \frac{\pi}{4\lambda}$, where $\lambda = \frac{1}{h}\sqrt[4]{\frac{3h}{E}}$ and $a = 0{,}6\sqrt[4]{\frac{3h}{E}}$ and designating the pier diameter through B we obtain

$$P = Rh^2 tg\beta\left[1 + a\left(\frac{B}{h}\right)\right]. \qquad (16)$$

REFERENCES

1. Dinkla E., Sluymer T.J., Ice pressure against isolated structures. - IAHR Ice Symposium, Reykjavik, 1970.

2. Afanasiev V.P., Dolgopolov Yu.V., Effect of ridged ice on isolated piers. - Trudy Koordinatsionnykh Soveshchanii po Gidrotekhnike, 1970, vyp. 56.

3. Peschansky I.S., Glaciology and ice engineering. - "Morskoi Transport", 1963.

4. Korzhavin K.N., Action of ice on engineering structures. - Siberian Department of the Academy of Sciences, Novosibirsk, 1962.

5. Afanasiev V.P., Estimation of ice strength in the design of hydraulic structures. - Gidrotekhnicheskoye Stroitel'stvo, 1968, N 5.

6. Afanasiev V.P., Dolgopolov Yu.V., Schweistein Z.I., Ice pressure against isolated marine piers. - Trudy AANII, 1971, vol. 300.

7. Assur A., Structures in ice infested waters. - IAHR Ice Symposium, Leningrad, 1972.

8. Dolgopolov Yu.V., Compound bending of a floating ice plate interacting with inclined surfaces. - Trudy Koordinatsionnykh Soveshchanii po Gidrotekhnike, 1973, vyp. 81.

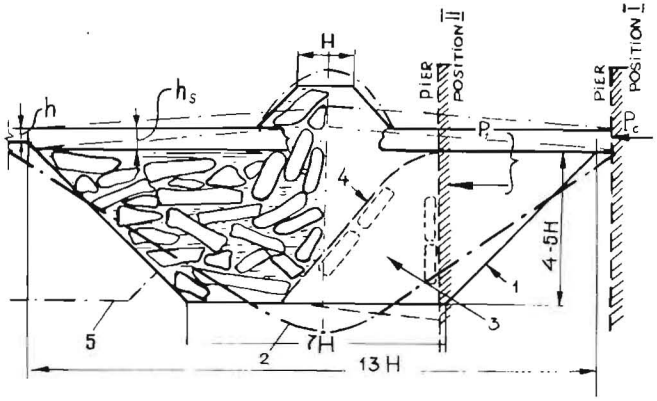

Fig. 1

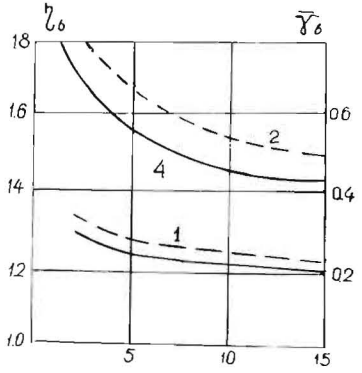

Fig. 2

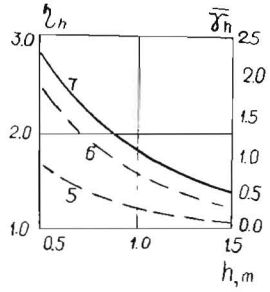

Fig. 3

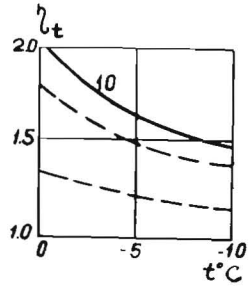

Fig. 4

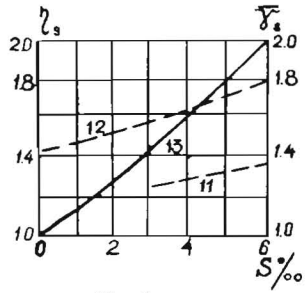

Fig. 5

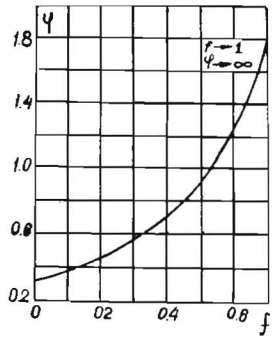

Fig. 6

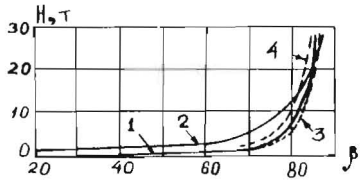

Fig. 7

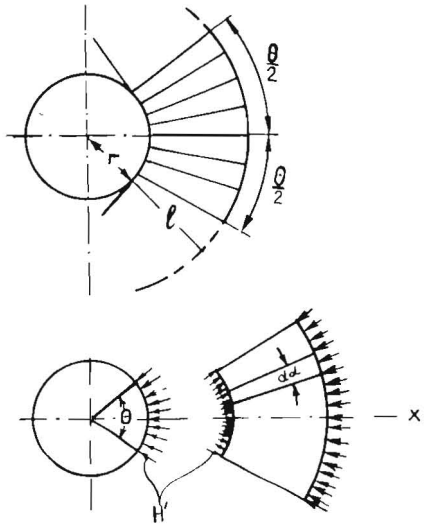

Fig. 8

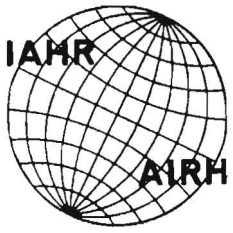

THIRD INTERNATIONAL SYMPOSIUM ON
ICE PROBLEMS
Hanover, New Hampshire, USA

THE STRAIN RATE AND TEMPERATURE DEPENDENCE OF YOUNG'S MODULUS OF ICE

A. Traetteberg,* River and Harbour Research Laboratory, Technical University of Norway, Trondheim, Norway.
L.W. Gold, Assistant Director, Division of Building Research, National Research Council of Canada, Ottawa, Canada.
R. Frederking, Research Officer, Division of Building Research, National Research Council of Canada, Ottawa, Canada.

Measurements were made of Young's modulus of polycrystalline ice over the strain rate range of 10^{-8} to 5×10^{-3} s^{-1} at temperatures of -10, -19.3, -29 and -39.5 °C on two types of ice: naturally formed granular ice and laboratory grown columnar-grained ice. Load was applied at constant rate of cross-head movement until the stress was about 5 kg/cm^2, and then removed immediately at the same rate. Young's moduli were determined from the linear portion of the stress-strain curve during loading. The modulus for both types of ice increased with increasing strain rate over the full range of strain rate covered in the investigation.

* * * * *

The strain rate dependence of the strength of ice is important because of its role in determining the forces that ice can exert on structures. Observations by Gold (1958) of a significant temperature dependence for Young's modulus of columnar-grained ice when subject to a strain rate of about 10^{-5} s^{-1} in the temperature range of 0 to -40 °C, indicate that the modulus should also depend on the strain rate. Hawkes and Mellor (1972) presented evidence of this dependence for granular ice subject to a tensile stress. The work now reported was undertaken to further explore this dependence over the temperature range of -10 °C to -39.5 °C and strain rate range of 10^{-8} to 5×10^{-3} s^{-1}.

---

* Visiting scientist with the Division of Building Research, National Research Council of Canada, 1972-73.

Preparation of Test Specimens

The behaviour of two types of ice was investigated: naturally formed granular ice of grain size of about 1.4 mm and laboratory grown columnar-grained ice with grain area of about 20 mm^2 in the plane perpendicular to the long direction of the grains. The columnar-grained ice had a bias in crystallographic orientation such that the axis of hexagonal symmetry tended to lie in the plane perpendicular to the long direction of the grains.

Rectangular specimens 5 x 10 x 25 cm^3 were used for the measurements. They were cut from blocks using a band saw, and machined to their final shape with a milling machine. The columnar-grained specimens were cut so that the long direction of the grains was perpendicular to the 10 x 25 cm^2 face.

Method of Measurement

Young's modulus was determined by applying a compressive load to the 5 x 10 cm^2 faces of the specimens (i.e., perpendicular to the long direction of the grains for the columnar-grained ice) in a 10,000 kg capacity Instron testing machine. The testing machine applied the load under the condition of a nominally constant rate of cross-head movement until the stress was about 5 kg/cm^2, and then immediately removed it at the same rate of cross-head movement.

The load was measured with a 900 kg capacity load cell which was placed beneath the specimen. The strain was measured with an extensometer which was clamped directly to the specimen. The extensometer, which had a gauge length of 15 cm, contained two linear differential transformers that were located on either side of the specimen. Their outputs were added and, with the output of the load cell, recorded on a two channel, galvanometer type recorder with a full scale response time of less than 0.02 sec.

The specimens were prepared and the measurements determined in a cold room whose temperature could be controlled to within ±0.1 Celsius degrees. After machining, the specimens were stored in kerosene until the time of testing. Young's modulus was determined at the temperature of -10, -19.3, -29.0 and -39.5 °C. Specimens were maintained at the test temperature at least 24 hours prior to mounting in the testing machine. Precautions were taken to prevent sublimation when the time required for a measurement was sufficiently long for it to occur.

Results

A typical stress-strain curve determined from the load and strain record is shown in Fig. 1. In most cases, the stress-strain curve during loading was essentially linear; the curve representing unloading was parallel to it for part of its length. The Young's moduli presented in this paper were determined from the linear portion of the stress-strain curve during loading.

Young's moduli measured at -10 °C for both columnar and granular ice, are plotted against strain rate in Fig. 2. The strain rate was determined from the linear part of the strain-time record associated with each modulus. The results show that there is a decrease in modulus with decreasing strain rate for both the columnar-grained and granular ice over the full range of strain rate covered in the investigation. It was not possible to apply sufficiently high strain rates to clearly establish the maximum value of the modulus for the two types of ice. Measurements made by dynamic methods, however, show that the maximum value is about 10^{10} N m^{-2} (about 10^5 kg cm^{-2}).

When the strain rate was less than about 10^{-5} s^{-1}, permanent deformation occurred during a load cycle. A correction was made for this by assuming that the strain rate associated with it was proportioned to σ^2, where σ is the applied compressive stress. The strain correction as a function of time was calculated using the load-time curves with the condition that the strain correction equal the permanent strain remaining after relaxation at the end of a test. The assumed time dependent permanent strain contribution was subtracted from the measured strain before calculating Young's modulus.

Each curve in Fig. 2 is for one set of measurements. More than one set of measurements were usually made on a specimen. The first numeral in the identification number for each curve identifies the specimen and the second indicates the order in which the sets of measurements were made. For each set, the tests were conducted in order of increasing rate of cross-head movement, beginning with the lowest rate. Evidence which was obtained from one of the columnar-grained specimens that had not been subjected to prior loading, indicates that the moduli obtained from the first set of measurements on this ice type can be larger at a given strain rate than those obtained from subsequent sets of measurements (e.g., 5 -1, -2, -3, -4, Fig. 2).

The strain dependence of Young's modulus at temperatures of -19.3, -29 and -39.5 °C for one specimen of columnar-grained and one of granular ice, is shown in Figs. 3 and 4, respectively. These figures illustrate the general increase in Young's modulus with decreasing temperature that was observed for each specimen.

Discussion

The observations clearly show that Young's modulus of ice undergoes a relaxation in the strain rate range of 10^{-3} to 10^{-8} s^{-1}, the same range associated with the ductile to brittle transition in behaviour. Present understanding of the factors controlling crack initiation and propagation indicates that the relaxation processes involved probably play a significant role in the ductile to brittle transition.

The results are being analyzed assuming that ice behaves as a linear anelastic solid (Zener 1948, Gold and Traetteberg 1974). An investigation of the relaxation that occurred for each specimen at -10 °C after the load was removed suggests that the non-elastic

behaviour is not determined by only one process with a constant relaxation time, but rather by two or more processes, one of these with a relaxation time of about 1 sec, and a second with a relaxation time that increases with time. Analyses to date indicate that the observed strain rate dependence of Young's modulus is determined primarily by the latter process. The time dependence of the relaxation of Young's modulus for a columnar-grained and granular specimen at -10 °C is given in Fig. 5. The theoretical analysis shows that, with the conditions under which the measurements were determined, Young's modulus is not essentially a function of strain rate but rather of time.

Young's modulus of ice should depend on the density. The values obtained from the first set of measurements on the granular specimens at -10 °C and strain rate of 10^{-5} s^{-1} are plotted against density in Fig. 6. There appears to be a well defined dependence, which, if valid, would account for much of the difference that was found between the Young's moduli of the various granular specimens.

Conclusions

Young's modulus of granular and columnar-grained ice, with the axis of hexagonal symmetry of each grain tending to be perpendicular to the long direction of the grains, undergoes a relaxation in the range of strain rate of 10^{-3} to 10^{-8} s^{-1}. This relaxation is both time and temperature dependent and probably plays a significant role in the ductile transition that occurs in the same range of strain rate.

* * * * *

This paper is a contribution from the Division of Building Research, National Research Council of Canada, and is published with the approval of the Director of the Division.

References

Gold, L.W., 1958. Some Observations on the Dependence of Strain on Stress for Ice. Can. J. Phys., Vol.36, pp. 1265-1275.

Gold, L.W. and A. Traetteberg, 1974. Young's Modulus of Ice and Ice Engineering Problems. Proc., Second Symposium on Applications of Solid Mechanics, Dept. Mech. Eng., McMaster Univ., Hamilton.

Hawkes, I. and M. Mellor, 1972. Deformation and Fracture of Ice under Uniaxial Stress. J. Glaciol., Vol. 11, pp. 103-132.

Zener, C.M., 1948. Elasticity and Anelasticity of Metals. University of Chicago Press, Chicago.

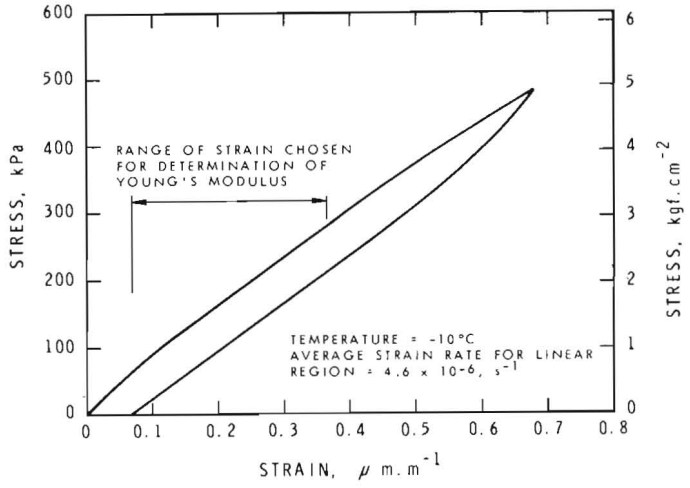

FIGURE 1
STRESS - STRAIN CURVE FOR COLUMNAR - GRAINED ICE

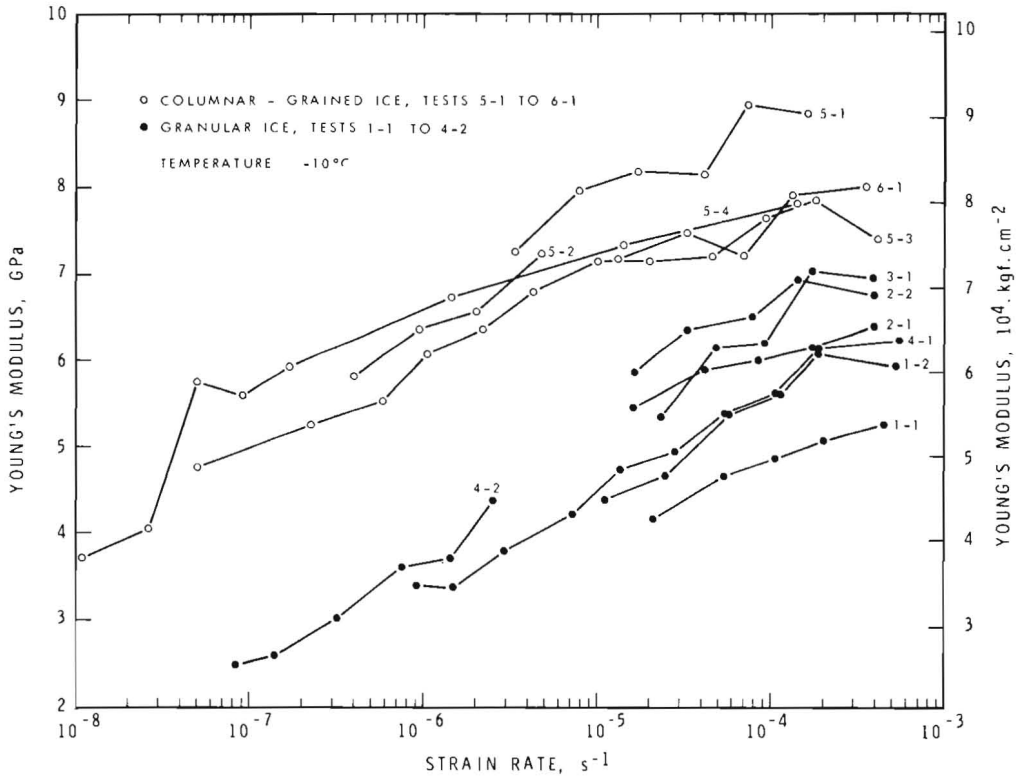

FIGURE 2
STRAIN RATE DEPENDENCE OF YOUNG'S MODULUS

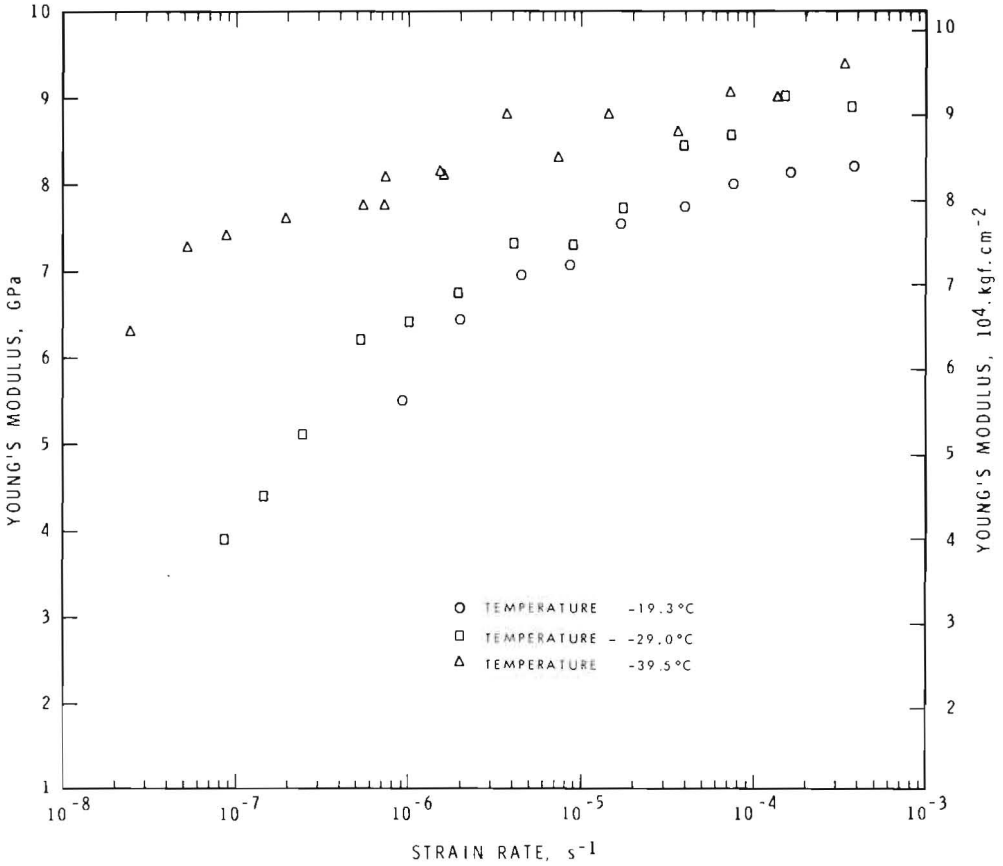

FIGURE 3

TEMPERATURE AND STRAIN RATE DEPENDENCE OF YOUNG'S MODULUS OF COLUMNAR-GRAINED ICE

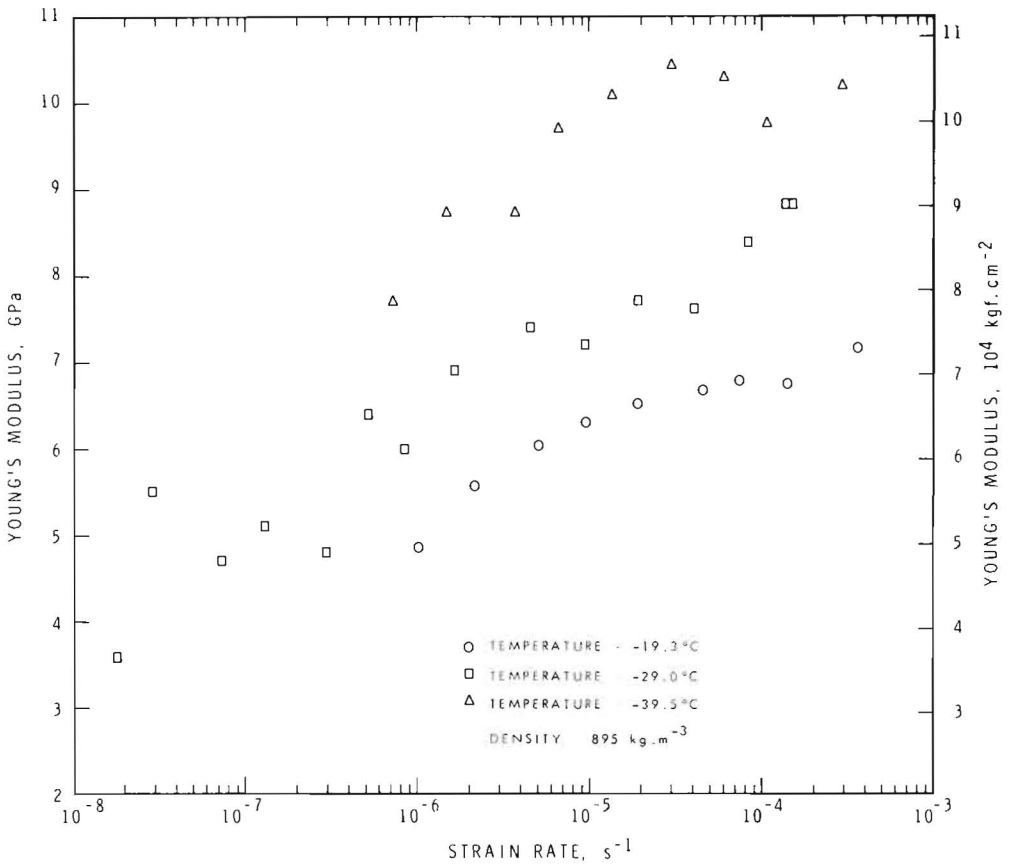

FIGURE 4
TEMPERATURE AND STRAIN RATE DEPENDENCE OF YOUNG'S MODULUS OF GRANULAR ICE

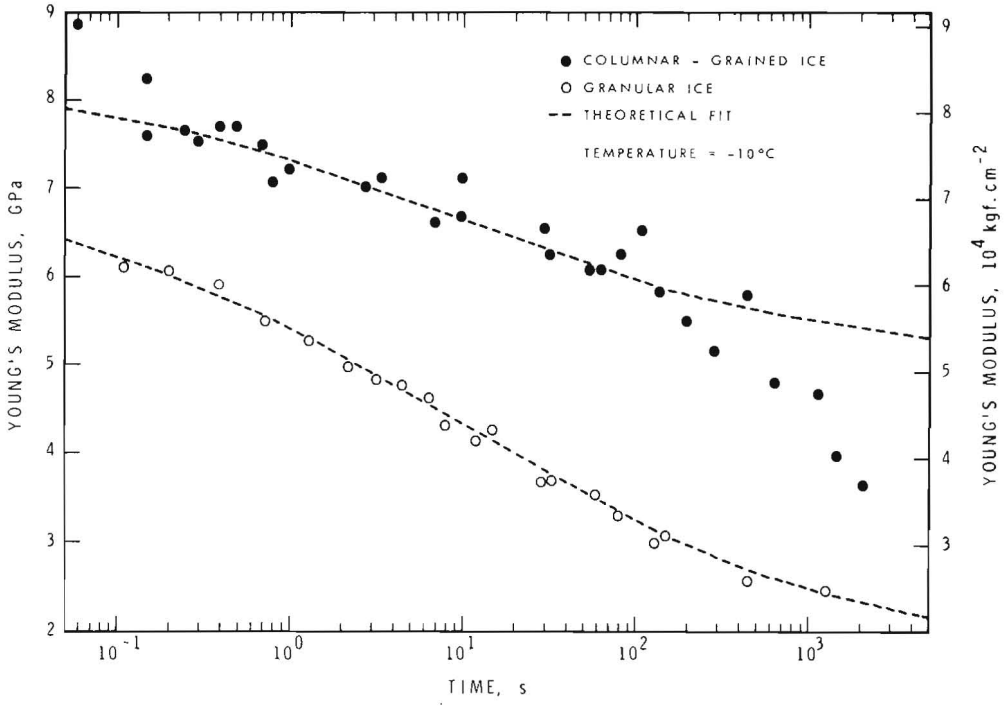

FIGURE 5
TIME DEPENDENCE OF YOUNG'S MODULUS

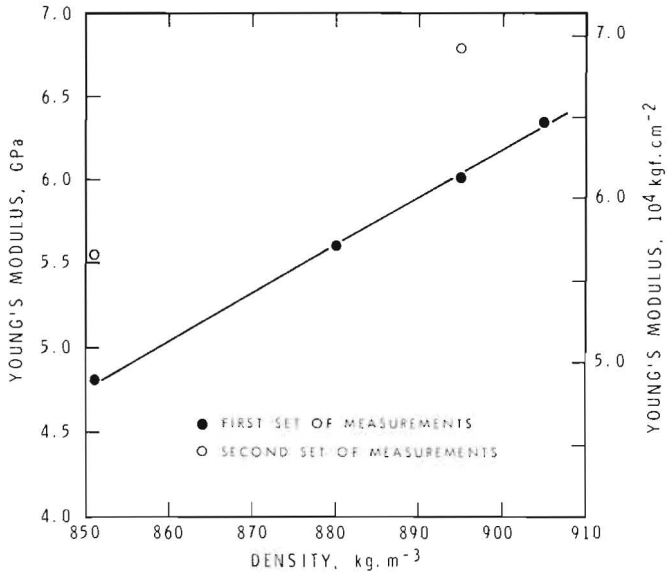

FIGURE 6
DENSITY DEPENDENCE OF YOUNG'S MODULUS OF SNOW ICE

THIRD INTERNATIONAL SYMPOSIUM ON
ICE PROBLEMS
Hanover, New Hampshire, USA

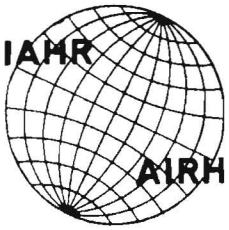

CONTROL OF THE THICKNESS AND STRENGTH OF THE ICE COVER

A.I. PEKHOVICH, M.Sc.(Eng.)
V.M. ZHIDKIKH, M.Sc.(Eng.)
I.N. SHATALINA, M.Sc.(Eng.)
S.M. ALEINIKOV, Head of Research Group

The B.E. Vedeneev All-Union Research Institute of Hydraulic Engineering (VNIIG)

Leningrad, U.S.S.R.

SYNOPSIS

Considered herein is the effect of individual factors on the rate of ice growth and strength, with major emphasis on the development of methods of thermal calculations for prediction of the rate of ice growth under different conditions, as well as on engineering measures for control of the thickness and strength of the ice cover.

I. Formulation of the problem

The thickness and strength of the ice cover in rivers and reservoirs, in channels and river stretches downstream from hydraulic structures are the factors which largely govern the navigation period, ice loads on hydraulic structures, and harmful ice effects. An intended variation of these factors makes it feasible to control complex ice phenoma.

A great variety of practical tasks of control may be set. A most common case is the necessity of limiting the thickness of ice and its strength (e.g., for extending the navigation period). But sometimes the task is to maintain the thickness and strength of ice to certain prescribed values (for providing ice roads, crossings, etc.). It is necessary to distinguish between short- and long-term regulation tasks. Accordingly, in the first case, it may be sufficient to weaken the ice only during the passage of the ship, whereas in the second, it is essential that the ice cover thickness do not exceed a certain value during the whole winter.

The physical basis of control of the ice thickness lies in the

variation of the conditions of heat exchange with the environment (water and air), while the ice strength control may be based on the variation of the following physical parameters: the temperature and chemical composition of ice, its structure and mechanical bonds between crystals, the amount of air entrapped in the ice, as well as ice reinforcement.

Considered herein is the effect of individual factors on the rate of ice growth and strength, with major emphasis on the development of methods of thermal calculations for prediction of the rate of ice growth under different conditions, as well as on engineering measures for control of the thickness and strength of the ice cover.

II. Calculation procedure

One way of solving problems with motion of the phase interface during solidification and melting is to assume a quasi-stationary temperature regime both in the solid and the liquid regions. This assumption is very helpful, since there is no need to calculate temperatures and it remains only to determine the position of the solidification boundary. The motion of the solidification boundary can be determined using the heat balance equation

$$\lambda_1 \left.\frac{\partial t_1}{\partial x}\right|_{x=x_c-0} - \lambda_2 \left.\frac{\partial t_2}{\partial x}\right|_{x=x_c+0} = L_v \frac{\partial x_c}{\partial \tau} \qquad (1)$$

or

$$S_1 - S_2 = L_v \frac{\partial x_c}{\partial \tau}$$

with the temperatures at the phase interface

$$t_1\Big|_{x=x_c-0} = t_2\Big|_{x=x_c+0} = t_c, \qquad (2)$$

where $L_v = mc\rho$ – is the volume heat of phase transition;
S_1 – is the heat flux from the phase interface across the solid region;
S_2 – is the heat flux towards the phase interface from the liquid region; and
t_c – is the temperature of crystallization.

Though the temperature does change both in the solid and the liquid zones, however its distribution at each given moment may be considered to correspond to that of steady state. In this case transition from one steady state to another is possible, provided that the coefficient of the thermal diffusivity of ice is infinitely large. Actually this value is finite, and with the progress of the freezing boundary, the enthalpy of the solid zone varies. The heat flux due to variations in the enthalpy of the solid mass can be taken into account if the latent heat of ice formation L_v will be always replaced by

$$L^* = L_v + \frac{c_1\rho_1(t_c - t_a)}{2} \qquad (3)$$

The values of the heat balance components, Eq(1), for different cases can be readily obtained. Thus, if the ice cover has already formed, then a heat flux from the ice mass towards the solidification boundary will be

$$S_1\Big|_{x=x_c} = S_1\Big|_{x=0} = \frac{\lambda_1 (t_c - t_s)}{x_c}. \qquad (4)$$

If the ice cover has not yet formed, then S_1 is characterized by the heat balance components at the air-water interface.

The determination of a heat flux from the water towards the under surface of ice depends on the specific conditions of the process. If the temperature of water is close to that of crystallization, then we may take $S_2 \approx 0$. The quantity S_2 may be assumed constant with a linear distribution of temperatures across the water depth and constant heat transfer coefficient and mean temperature.

For example, with

$$t_{\tau=0} = t_c + \beta x, \qquad (5)$$
$$S_2 = \lambda_2 \beta = const$$

and

$$S_2 = \alpha (t_2 - t_c). \qquad (6)$$

For a still liquid with a uniform initial temperature we have

$$S_2 = \frac{S_0}{\sqrt{\tau}}, \qquad (7)$$

where

$$S_0 = (t_0 - t_c) \sqrt{\frac{\lambda_2 c_2 \rho_2}{\pi}}.$$

Let us illustrate the fundamental principles of the above procedure by the solution of some specific problems. Relevant calculation formulae and curves permit the determination of the ice growth rate, the limit ice thickness, the effect of heat insulation, air temperature, etc.

Problem 1. Let us determine the position of the solidification boundary (x_{crust}) and the time of water freezing (τ) if the surface temperature of a semiconfined body or an unconfined plate is constant, $t_c < t_s$; the initial temperature is equal to that of freezing, $t_0 = t_c$; and, consequently, $S_2 = 0$.

With a constant temperature at the surface of the body, a heat flux from the solidified region towards the freezing boundary is defined by Eq(4), and the balance equation (1) assumes the form

$$\lambda_1 \frac{t_c - t_s}{x_c} = L_v \frac{dx_c}{d\tau} \qquad (8)$$

If for $\tilde{\tau} = 0$ we have $x_{czyst} = 0$, then the solution to Eq(8) will be as follows

$$\tilde{\tau} = \frac{x_c^2}{2\lambda_1(t_c - t_s)/L_v} \tag{9}$$

and

$$x_c = \sqrt{\frac{2\lambda_1(t_c - t_s)}{L_v}\tilde{\tau}} \tag{10}$$

If on the surface of the body there is a heat insulating layer, h_{ins}, then

$$S_1 = \lambda_1 \frac{t_c - t_s}{x_c - h_t}$$

where

$$h_t = h_{ins}\frac{\lambda_1}{\lambda_{ins}}$$

Hence, the solution will be obtained as

$$\tilde{\tau} = \frac{X_c^2}{2\lambda_1(t_c - t_s)/L_v} + \frac{h_t}{\lambda_1(t_c - t_s)/L_v}x_c \tag{11}$$

and

$$x_c = -h_t + \sqrt{h_t^2 + \frac{2\lambda_1(t_c - t_s)}{L_v}\tilde{\tau}} \tag{12}$$

If the water surface has already been covered with an ice layer, $x_{czyst,0} > 0$, then the solution of the problem of determining the time of freezing will be as follows

$$\tilde{\tau} = \frac{x_c^2}{2\lambda_1(t_c - t_s)/L_v} - \frac{x_{c,0}^2}{2\lambda_1(t_c - t_s)/L_v}. \tag{13}$$

The position of the freezing boundary will be written as

$$x_c = \sqrt{x_{c,0}^2 + \frac{2\lambda_1 (t_c - t_s)}{L_v}\tau} . \qquad (14)$$

If there is an insulating layer and an initial layer of ice simultaneously, $x_{czyst,0}$ (with the origin of coordinates located on the ice surface under the insulation), then

$$\tau = \frac{x_c^2 - x_{czyst,0}^2}{2\lambda_1 (t_c - t_s)/L_v} + \frac{h_t}{\lambda_1 (t_c - t_s)/L_v}(x_c - x_{c,0}) \qquad (15)$$

and

$$x_c = -h_t + \sqrt{(h_t + x_{c,0})^2 + \frac{2\lambda_1 (t_c - t_s)}{L_v}\tau} .$$

If the surface temperature of a semiconfined body varies linearly, $t_{x=0} = t_0 + \beta\tau$, and there is an insulating layer, then

$$\tau = \frac{t_c - t_0}{\beta} + \sqrt{\frac{(t_c - t_0)^2}{\beta^2} - \frac{L_v}{\lambda_1 \beta}\left[x_c^2 - x_{c,0} - 2(x_c - x_{c,0})\right]} \qquad (16)$$

and

$$x_c = -h_t + \sqrt{(h_t + x_{c,0})^2 + \frac{2\lambda_1 (t_c - t_0 - \beta\tau/2)}{L_v}\tau} .$$

With a harmonic variation of the surface temperature

$$x_c = -h_t + \sqrt{\left(\frac{h_t}{2} + x_{c,0}\right)^2 + \frac{\lambda_1 (t_c - t_{mean})}{L_v}\tau - \frac{\lambda_1 T_s \tau_0}{2\pi L_v}\sin\frac{2\pi\tau}{\tau_0}} \qquad (17)$$

Problem 2. Let us determine the position of the solidification boundary (t_{czyst}) and the time of water freezing (τ) if the surface temperature of a semiconfined body or an unconfined plate, $t_{czyst} < t_{surf}$, is constant; the heat flux from the liquid towards the solidification boundary, $S_2 > 0$, is also constant.

The balance equation at the solidification boundary for the case considered will be

$$\lambda_1 \frac{t_c - t_s}{x_c} - S_2 = L_v \frac{dx_c}{d\tau}. \qquad (18)$$

Integration of Eq (18) will give

$$\eta_c - \ln(1-\eta_c) + \Pi = 0, \qquad (19)$$

where

$$\Pi \equiv \frac{S_2^2 \tau}{\lambda_1 L_v (t_c - t_s)}; \quad \eta_c \equiv \frac{x_c S_2}{\lambda_1 (t_c - t_s)} \equiv \frac{x_c}{x_{lim}}.$$

The calculation formula for the solidification boundary will be

$$x_c = \eta_c \frac{\lambda_1 (t_c - t_s)}{S_2}.$$

For heat insulation $h_t \neq 0$ Eq (19) is replaced by

$$\eta_K + \Pi_s \ln \frac{\Pi_s - 1 - \eta_c}{\Pi_s - 1} + \Pi_K = 0, \qquad (20)$$

where

$$\Pi_K \equiv \frac{S_2 \tau}{L_v h_t}; \quad \Pi_s \equiv \frac{\lambda_1 (t_c - t_s)}{S_2 h_t}; \quad \eta_c \equiv \frac{x_c}{h_t}$$

Using Eqs (19) and (20), calculation curves (Fig. 1) were obtained which permit to determine the position of the solidification boundary

$$x_c = \eta_c h_t$$

as well as its limit position

$$x_{lim} = h_t (\Pi_s - 1).$$

Some more problems may be considered in which the heat fluxes on the surface and at the solidification boundary are constant, but differ in magnitude and sign, or vary by a certain law. For all these cases corresponding solutions are available which can be used as a basis for developing engineering measures of control of the ice thickness and strength, but these findings will be reported later.

For calculation of the magnitude of the heat flux at the ice surface and at the freezing boundary in accordance with Newton's law $S_2 = \alpha (t_c - t_s)$ or $S_1 = \alpha (t_s - \vartheta)$, it is essential to eva-

luate the heat transfer coefficient α . The experimental data commonly used for determining α were obtained for plates and surfaces of finite dimensions and therefore cannot be used directly in calculation of the growth of the ice cover in water bodies which are practically of infinlte extent. To evaluate the heat transfer coefficient for surfaces of any length, a procedure is suggested which allows to calculate α for long surfaces using the data obtained earlier for plates of finite dimensions. The method is based on the concepts of the physical structure of a flow along the heat transfer surface and the corresponding heat and mass transfer models suggested by R. Higbie and E. Ruckenstein. It was experimentally found that particles carried from the main flow into the wall layer move for a while directly along the wall and then in the tranverse direction.

E. Ruckenstein /1/ proposed a boundary layer model consisting of individual sections of the length x_0 . Within this length turbulent fluctuations set the flow elements into contact with the wall surface and then carry them into the main flow. The motion is continuously repeated within sections of the length x_0 . It is assumed that for these sections boundary layer equations are valid.

R. Higbie /2/ put forward the hypothesis that the mechanism of mass transfer is governed by the movement of turbulent eddies from the flow core towards the interface, accompanied by periods of nonsteady diffusion from the interface into the liquid. The intensity of mass transfer depends on the time of residence of eddy near the surface $\tilde{\tau}_{res}$.

According to Higbie's method, first it is necessary to relate the time of residence of eddy near the surface to a heat transfer coefficient. Finally this relationship is written as

$$\alpha_{mean} = 2c\rho\sqrt{\frac{a}{\pi\tilde{\tau}_{res}}}. \qquad (21)$$

In terms of the adopted model, transition from the experimentally obtained heat transfer coefficients to the sought values of α for long surfaces is possible only in the case when the length of the experimental plate is equal to that of eddy interaction with the surface.

Usually plates of an arbitrary length are used in the experiments. With prescribed wind and flow velocities, an arbitrary number of sections of the length x_0 can be laid off along the length of the plate. One can reasonably suggest that with one of the flow velocities $v = v_0$, the length of the plate will just be equal to that of the eddy path $l = x_0$, along which the eddy motion will occur during the time $\tilde{\tau}_{res}$. Under these conditions the experimental values of will satisfy Eq (21).

Now, if we use the experimental data obtained by W. Jurges and A. Frank for heat transfer from a solid surface to the atmosphere

$$Nu = 0{,}032\,Re^{0{,}8} \qquad (22)$$

or those by M.A. Mikheev for heat transfer from a solid surface to water

$$Nu = 0{,}0356\,Re^{0{,}8}Pr^{0{,}4} \qquad (23)$$

and solve Eqs (22) and (23) in combination with Eq (21), we shall obtain α as

$$\alpha = B v_0. \tag{24}$$

For heat transfer from a solid surface to air the coefficient α in Eq (24) will be

$$B = \frac{c\rho K_1}{P_2} \sqrt[3]{\frac{\bar{f} K_1^2}{4 P_2}}, \tag{25}$$

For heat transfer from a solid surface to water it will be

$$B = c\rho K_2 \sqrt[3]{\frac{\bar{f} K_2^2}{4 P_2^2}} \tag{26}$$

where $K_1 = 0.032$ and $K_2 = 0.0356$.

By way of example, let us evaluate the coefficient of heat transfer from a solid surface to air, with the wind velocity along the surface of 3 m/sec and the air temperature of 20°C.

By Eq (24)

$$\alpha = B v_0.$$

At a temperature of 20°C the value of in Eq (25) is equal to 1.66×10^{-3} W hr/m^3 °C. Hence the value of the heat transfer coefficient for the prescribed conditions will be 17.9 W/m^2 °C.

In a more general form, the value of the heat transfer coefficient for surfaces of any roughness may be written as

$$B = \frac{c\rho \varkappa^2}{\ln \frac{z}{z_0}}, \tag{27}$$

where $\varkappa = 0.4$ is the universal constant of a turbulent flow; z_0 is surface roughness; and z is the thickness of the boundary heat layer.

III. Engineering measures for control of the ice cover thickness and strength

The engineering measures intended for the ice thickness and strength control may be as follows:

a) changing of the heat exchange conditions at the upper surface of the ice cover (by applying an insulating layer);
b) changing of the heat exchange conditions at the under surface of the ice cover (by raising warm water from the bottom, releasing water downstream from the hydro power plant, etc.);
c) changing of the structure and chemical composition of ice (by reinforcing it and using chemical and dark materials).

The heat exchange conditions on the top of the ice cover can be altered by applying an insulating layer. The insulation contributes both to slowing down of the rate of ice growth and to an increase of the mean temperature of the ice, which affects its strength (Figs 2 and 3). By using the calculation formulae (11-17) it is possible to determine the required rate of ice growth and the corresponding thickness of the insulating layer depending on specific conditions.

The variation in the mean ice temperature with a linear temperature distribution across the ice depth may be expressed as

$$t_{mean} = \frac{\vartheta h_i}{2 h_t}, \qquad (28)$$

where

$$h_t = h_i + h_{ins} \frac{\lambda_i}{\lambda_{ins}}.$$

Depending on the season when insulating material is applied to the ice cover, the objectives may be not only to slow down the rate of ice growth and to reduce the ice strength, but quite opposite, i.e. to preserve ice and to improve its strength properties. In autumn and winter the primary task is to weaken the ice cover, whereas in spring, when the ice thickness reaches its maximum, the insulation applied should protect the ice from penetrating radiation.

As heat insulating materials may be used those described in Table 1. Considering easy handling, preference should be given to the quick-hardening foam (БТП) and foam ice. By their heat insulating properties these materials are not only by no means worser than the other, but outperform them in many respects.

The БТП foam is manufactured by mixing aqueous solution of urea - formaldehyde resin with foam-producing agent and hydrochloric acid as a hardener. Foam ice is a frozen foam obtained from aqueous solution of foam-producing agent; it freezes at temperatures below zero directly on the surface to which it is applied.

There are different methods of control of the ice thickness by varying the heat exchange conditions at the under surface of the ice cover. For instance, this can be done by raising warm water from the bottom up to the under surface of ice with air bubbles. In lakes and reservoirs, possessing some heat accumulated near the bottom, this method may be efficiently used to control the ice thickness by circulating a water and air flow under the ice cover, increasing the coefficients of heat transfer at the water-ice interface and the amount of heat spent on ice melting.

Another example of the ice thickness control is releasing water downstream from the hydro power plants to keep the required ice regime. In this case an increase or decrease in the water discharge results in the corresponding changes of the heat transfer coefficients at the under surface of the ice. The ice thickness can be controlled using the relationships (24-27) for evaluating α and the curves plotted for Problem 2 (Fig. 1).

Table 1

Material	Volume weight, kg/m^3	Specific heat capacity, kcal/kg	Thermal conductivity coefficient, kcal/m hr °C	Thermal diffusivity, 10^3 m^2/hr	Cost of 1 m^3, roubles
Mineral wool	100	0.17	0.04	2.2	13.6
Sawdust	300	0.55	0.11	0.7	-
Peat briquettes	460	0.43	0.34	1.7	23.3
Mineral felt	250	0.18	0.07	1.5	14.2
Mipora	20	0.34	0.03	5.1	9.8
Cork crumbs	85	0.42	0.04	1.2	17.0
Quick-hardening foam (БТП)	20-50	0.34	0.03-0.06	4.0	5.7
Foam ice	25-100	0.50	0.1	4.0	1.0

In a search for controlled variation of the structure and chemical composition of ice various methods have been developed, such as ice reinforcement and the application of chemical and dark materials for weakening the ice strength.

The effect of chemicals is based on the ability of ice to yield in combination with some salts low-melting eutectics, i.e. mixtures of chemicals with ice, having a lower melting temperature than their components. When chemical material is applied to the ice surface, pits filled with a mixture of solution and ice crystals are formed in the ice. A concentrated application (in the shape of strips) of chemicals from the airplane permits to cut the ice cover.

The effect of dark materials on the ice strength is based on the variation of the reflecting capacity of the ice surface and increase in the flux of solar radiation penetrating into the ice.

REFERENCES

1. Ruckenstein E., Equation for the mass- or heat transfer coefficient in turbulent motion. - Internat. J. of Heat and Mass Transfer, 1966, vol. 9, N 5, p. 441-451.

2. Higbie R., The rate of absorption of a pure gas into a still liquid during short periods of exposure. - Trans. Am. Inst. Chem. Engrs, 1935, vol. 51, N 1, p. 365-390.

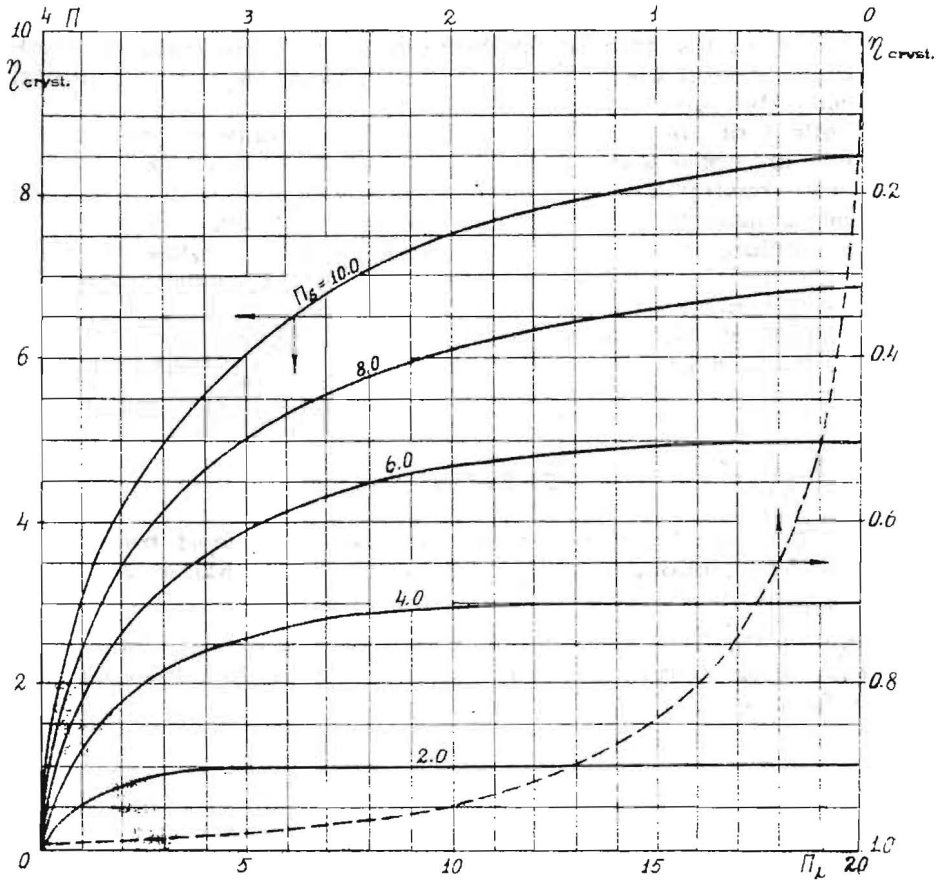

Fig. 1

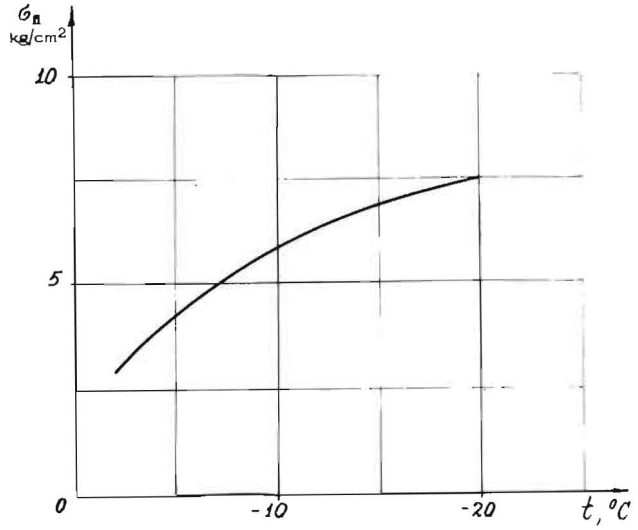

Fig. 2

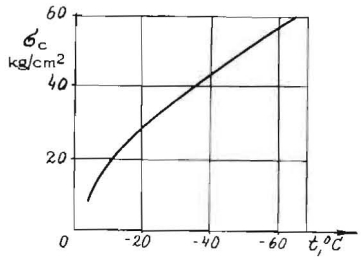

Fig. 3

THIRD INTERNATIONAL SYMPOSIUM ON
ICE PROBLEMS
Hanover, New Hampshire, USA

STOCHASTIC RESPONSE OF A THREE-DIMENSIONAL OFFSHORE TOWER TO ICE FORCES

D.V. Reddy[+]
P.S. Cheema*
A.S.J. Swamidas[++]
A.K. Haldar[+++]

+, ++ & +++ Faculty of Engineering and Applied Science, Memorial University of Newfoundland, St. John's, Newfoundland.

* Academic Department, College of Trades and Technology, St. John's, Newfoundland, Canada.

INTRODUCTION

Ice-force measurements at Cook Inlet, Alaska made by Blenkarn [1] and at several bridge piers in Alberta by Neill [2,3] and Neill, Saunders and Schulz [4] are highly random indicating a strong need for stochastic analysis. The probabilistic dynamic analysis of a fixed three-dimensional offshore tower presented in this paper forms part of a continuing research project on "Stochastic Analysis of Ice-Structure Interaction" which is relevant to the extensive programme in Cold Regions-Oriented Ocean Engineering at Memorial University of Newfoundland. The work is an extension of earlier investigations of a single-degree-of-freedom system by Sundararajan and Reddy [5] and multi-degree-of-freedom systems, based on cantilever beam and two-dimensional frame models with lumped masses, by Reddy and Cheema [6] and Reddy, Cheema and Swamidas [7]

REVIEW OF LITERATURE

Korzhavin's [8] comprehensive studies on ice strengths under dynamic loading, and failure of ice-floes by impact on vertical and inclined piers are well known and have been summarized by Michel [9]. Based on measurements of ice properties and laboratory and field investigations of ice-structure interaction at Cook Inlet, Alaska, Peyton [10-14] made many useful recommendations for design. Refs. 2 & 3 describe measurements of ice forces on several bridge piers in Alberta including the synchronization of force recording and movie photography at one site to compare force fluctuations with the nature of the ice failure. The use of model basins to simulate and predict full-scale ice-

structure interaction has been described by Voelker and Levine [15], Coon [16], Nevel, Perham and Hogue [17] and Hirayama, Schwarz and Wu [18]. Danys [19, 20, 21, 22] studied ice forces on lighthouses with reference to the interaction on cone-shaped structures, ice damage to isolated structures in the St. Lawrence River, an instrumented conical lighthouse in Lac St. Pierre and the effect of ice and wave forces on the design of offshore lighthouses, which includes a study of the influence of substructure shape on the reduction of dynamic forces. Reinius, Haggard and Ernstons [23] have discussed ice pressures on offshore lighthouses in the Baltic with some reference to two structural failures. The ice pressures based on these modes of failure were estimated by Bergdahl [24]. Kivisild [25] described the structural design of a year-round oil terminal in ice-covered waters in the St. Lawrence River. Ross, Hanagud and Sidhu [26] considered interaction between ice sheets and a rigid offshore pile in which the dynamic plane stress problem is solved by a computer code to obtain complete stress fields in the ice sheet and the forces experienced by the pile. Assur [27, 28] studied forces of moving ice fields on structures, the relationship of loading to strength, elasticity and internal friction and problems of buckling in model testing. Afanas'ev [29] developed an empirical equation for loading on vertical surfaces based on experimental and theoretical studies. Frederking and Gold [30] described a mathematical model for calculating ice forces against an isolated pile that takes into account the influence of ice type, strain rate, pile geometry and temperature. Bercha [31] has described the mathematical simulation of ice-structure interaction with particular reference to his work on the adjustment of analytical models (obtained from classical theories) using three-dimensional finite element simulators. The Russian code of practice [32] presents formulae for the dynamic and static ice loads on river structures. The American Petroleum Institute [33] has indicated pressures of 200-500 psi for crushing strengths of ice for calculating ice forces. Haugsoen [34] indicated the urgent need for further model testing of offshore towers in ice conditions. Edwards [35] reviewed current developments in dimensional analysis, mathematical and physical modelling, full scale ice testing and the world's ice model basins. Croasdale [36, 37] described a nutcracker ice strength tester in the Beaufort Sea (Tuktoyaktuk Harbour near the Mackenzie Delta) and the measurements of ice crushing strengths (4×10^6 to 6×10^6 Nm^{-2}). Ref. 17 has described a similar test in which a pile was pushed into the ice sheet against a concrete bearing wall by a hydraulic cylinder. Drouin, Simard and Michel [38] described a technique used for ice floe velocity measurement from bridges in the St. Lawrence River. Schwarz [39] established a relationship between strength in laboratory tests and the pressures in floating ice fields, taking into consideration, temperature, deformation, velocity, and pressure direction.

Assuming the primary structural response to ice floe excitation to be in its fundamental mode of vibration, Matlock, Dawkins and Panak [40] analysed a cantilever pier, idealized as a damped single-degree-of-freedom system and subjected to a postulated saw-tooth type of deterministic loading. As the loading was expressed as a function of

space and time, the differential equation was solved numerically and the results checked with Peyton's [14] field measurements. Ref. 5 studied the random responses of the Matlock et al [40] model to ice floe loading, given by an actual field record of Ref. 1 and assumed to be stationary and ergodic. The work was extended to multi-degree-of-freedom systems in Ref. 6. The ice force records were those determined from two instrumented structural devices [1]: i) a strain-gauged test pile driven into the ocean bottom adjacent to an existing temporary offshore drilling platform. ii) a field test beam hinged at both ends to the platform leg with a load cell measuring the reaction at the upper hinge.

Neill[41] has recently reviewed selected aspects of ice forces on piers and piles. An ice force "response spectrum" modal analysis of offshore towers has been described in Ref. 7 to obtain the maximum numerical values of the responses. The method takes advantages of the similarity between ice-force and earthquake records and, as far as the authors' knowledge goes, this is the first time response spectra have been developed for ice forces.

THE PROBLEM

PROCEDURE

The structure analysed is a fixed offshore tower shown in Fig. 1, which is roughly similar to that analysed by Corotis and Martin [42]. The members are assumed to be rigidly connected and the added water mass is assumed equal to the mass of the water displaced. This assumption for the added water mass has been found to be reasonable for the first few modes although there has been considerable discussion regarding possible frequency dependence and modified values for flexible members. The masses per unit length of the members in the plane of the frame are computed by summing up the structural mass, the mass of the water contained in the tube and the mass of the water displaced. By identifying the degrees of freedom in the x-direction at the nodal plane levels, the flexibility matrix of the 3-D frame is obtained and inverted to obtain the stiffness matrix. The eigenvalues and eigen-vectors are determined with the mass and stiffness matrices of the cantilever the same as those of the 3-D frame. After obtaining the stiffness matrix, the structure is idealized as a cantilever with nodes at the same level as the 3-D frame. This approach implies the concept of the three-dimensional simulator in modelling (Fig. 2). The interval of digitization for the ice force records [1] is based on the Nyquist frequency. The Kolmogorov-Smirnov test is used to verify that the ice-force records are drawn from identical continuous distributions. The power spectral densities of the typical ice force records are obtained and plotted by using the Time Series Analysis BMD 02T computer programme developed by the Health Sciences Computing Facility, University of California, Los Angeles. The power spectral densities of the deflections are evaluated and plotted for the averaged values of the power spectral densities of the force records. The mean square response is then determined. The deterministic time-history responses

of the structure to the different ice-force records are obtained and averaged. The mean square values will enable the calculation of probabilities that the responses at the various levels of the structure will not exceed specified values. This can be used to establish confidence limits.

Theory

The equations of motion for a n-degree-of-freedom system are

$$[m]\{\ddot{x}\}+[c]\{\dot{x}\}+[k]\{x\} = \{Q(t,y)\} \qquad (1)$$

where $\{x\}$, $\{Q\}$ = random displacement and force vectors respectively,

$[m]$, $[c]$ and $[k]$ = mass (sum of the structural and added water masses), damping (viscous equivalent of the structural and hydrodynamic damping) and stiffness matrices respectively.

and $[c] = \alpha[m]$ in which α is constant.

The rth decoupled equation of Eqs. (1) obtained by the Normal Mode Method [43] is

$$\ddot{\eta}_r + 2\zeta_r\omega_r\dot{\eta}_r + \eta_r^2 = \frac{\{\phi_r\}^T\{q(y)\}F(t)}{M_r} \qquad (2)$$

where η_r = normal coordinate (r=1, ...n),

$$\zeta_r = \frac{\{\phi_r\}^T [c] \{\phi_r\}}{2\omega_r M_r}, \text{ a fraction of critical damping}$$

in which $\{\phi_r\}$ is the modal vector,

ω_r = circular frequency of the rth mode,

$M_r = \{\phi_r\}^T [m] \{\phi_r\}$ = generalized mass

$q(y)$ = force distribution function

$F(t) = Q_1 f(t)$

$f(t)$ = time dependence

Q_1 = maximum value of the forcing function.

The modal participation factors are defined by

$$\Gamma_r = \{\bar{\phi}_r\}\{q(y)\}$$

where $\{\bar{\phi}_r\}$= normalized eigenvector.

The spectral density $S_{xx}(\Omega)$ of the displacement x_r

is given by Bolotin[44] as

$$S_{xx}(\Omega) = \frac{S_{ff}(\Omega)}{(\omega_r^2 - \Omega^2)^2 + (2\alpha\Omega\omega_r)^2} \qquad (4)$$

where $S_{ff}(\Omega)$ = spectral density of Q(t)

and Ω = excitation frequency.

Neglecting the contribution of cross product terms and the phase relationship, the approximate solution for the mean square response is determined as [43],

$$x_i^2 = \sum_{r=1}^{n} \frac{\bar{\phi}_{ri}^2 \Gamma_r^2 S_{ff}(\omega_r)}{8\alpha\omega_r^2} \qquad (5)$$

SOLUTION

Stiffness Matrix

(Kips/ft.)

4411.20	-3239.90	1309.10	-437.35	129.30	-34.69	4.10	-3.80	1.57	3.36	-4.46
	31751.00	-3409.70	-13964.00	-646.00	662.36	27.30	1520.90	48.62	-1269.70	1243.70
		5611.50	-5017.30	2299.90	-634.80	72.29	34.10	-35.63	28.54	-16.79
			42240.00	-7412.60	-15846.00	-3657.20	5723.60	-1483.20	-185.49	642.72
				11979.00	-8698.10	2776.50	-299.58	-499.91	653.34	-430.31
	Symmetric				48754.00	-3722.70	-21727.00	2121.20	-3337.30	2805.50
						19368.00	-20496.00	670910.00	260.53	-1307.30
							51601.00	-22314.00	8982.40	-2134.10
								32100.00	-20886.00	4246.30
									58474.00	-43566.00
										39332.00

Mass Matrix

(Kip.sec^2/ft)

22.995									
	22.236								
		18.431							
			17.562						
				12.934					
					11.522				
						10.414			
							9.432		
								0.374	
									6.096
									14.153

Damping

6% of the critical value

For the first three modes, the natural frequencies, mode shapes, generalized mass matrix and participation factors are

Natural Frequencies
(Hertz)

$$\{f\} = \begin{Bmatrix} 1.0226 \\ 1.7488 \\ 1.9883 \end{Bmatrix}$$

Mode Shapes

$$\begin{bmatrix} 0.0349 & -0.2142 & -19.6117 \\ 0.0757 & -0.5610 & -1.5748 \\ 0.1422 & -1.3522 & 8.4540 \\ 0.1801 & -0.8803 & -0.7423 \\ 0.2574 & -0.8488 & -3.1520 \\ 0.2762 & -0.9134 & -1.2063 \\ 0.2753 & -1.1074 & -0.9176 \\ 0.3806 & -0.7892 & -0.9102 \\ 0.6866 & 0.1210 & -0.0329 \\ 0.9498 & 0.8684 & 0.8172 \\ 1.0000 & 1.0000 & 1.0000 \end{bmatrix}$$

Generalized Mass Matrix

(Kip-sec^2/ft.)

$$[M] = \begin{bmatrix} 24.743 & & \\ & 111.745 & \\ & & 10406.467 \end{bmatrix}$$

Force Distribution Vector

$$\{p(y)\} = \begin{Bmatrix} 0 \\ 0 \\ 0 \\ 0 \\ 0 \\ 0 \\ 0 \\ 1 \\ 0 \\ 0 \\ 0 \end{Bmatrix}$$

Participation Factors

$\Gamma_1 = 0.0765$, $\Gamma_2 = -0.0747$, $\Gamma_3 = -0.0089$

Results

Six ice-force records shown in Fig. 3 were selected out of the eleven segments of the ice-force records of Ref. 1 based on the Kolmogorov-Smirnov test. The force magnitudes were not modified because the tower leg diameter at the loading level is nearly the same as that of the test pile considered by Ref. 1. The power spectral densities of these excitations were determined, averaged and plotted in Fig. 4. The power spectral densities of the deflections corresponding to the first three natural frequencies were obtained from Eqn. 4 and plotted in Fig. 4. The individual time histories for the six records were determined by using STRUDL-II and averaged. The results are summarised in Table I.

TABLE I

Q (t)	Fig. 3		
Mean deflection obtained from time-history response at mass point 8 (ft.)	0.0194		
$S_{ff}(t)$ (kip^2/Hz)	Fig. 3		
f_i (Hz)	1.0226	1.7488	1.9883
$S_{xx}(w)$ $(ft.^2\ sec/rad)$	Fig. 4	Fig. 4	Fig. 4
$\overline{x_8^2}$ $(ft.^2)$	0.00006		

DISCUSSION

The problem of identifying the x-directional flexural modes for a three-dimensional frame was resolved by using the frame stiffness matrix (obtained for x displacements only) for the lumped mass cantilever model. This approach implies the concept of the three-dimensional frame simulator in modelling. The considerable amount of computer time required for the eigen-analysis of the three-dimensional frame necessitated the modelling to a lumped mass cantilever. The assumption of the added water mass being equal to the mass of the water displaced is a reasonable one - Liaw and Reimer [45] - although there has been considerable discussion regarding possible frequency dependence and modified values for flexible members.

The power spectral density displacement plots indicate significant "peaking" of the system at resonance ($\Omega=\omega_n$) with response to excitation for $\Omega<\omega_n$ and filtering out for $\Omega>\omega_n$. The results indicate that the assumptions of stationarity, ergodicity, and Gaussian distribution are reasonable.

The work can be extended to include foundation flexibility by adding two extra members to each support to provide lateral and axial spring action as shown in Ref. 42 for linear analysis. The study should be extended to nonlinear soil-water-structure interaction effects. Sanden and Neill [46] and Ref. 4, indicate the urgent need for more field measurements of ice forces and dynamic displacements in order to reduce the design ice pressure. The design ice pressure values of approximately 200 psi indicated in Ref. 22 agree with the suggested values (150-200 psi) of Ref. 4. Guidelines for ice pressures should account explicitly for the velocity effects of the ice floes as in the U.S.S.R. Code [32].

ACKNOWLEDGEMENT

The authors are grateful to Dr. R.T. Dempster, Dean of Engineering and Applied Science, and Dr. A.A. Bruneau, Vice-President of Professional Schools and Community Services, Memorial University of Newfoundland; Mr. O.S. Toope, Academic Head and Mr. K.F. Duggan, President, College of Trades and Technology, St. John's for their keen interest and encouragement. Appreciation is expressed to Professor D. Dunsiger, Faculty of Engineering and Applied Science, Memorial University of Newfoundland, for valuable discussions on the sampling of data. The support of the investigation by Imperial Oil Co. Grant No. 04-2026 and D.R.B. Grant No. 9767-08 is gratefully acknowledged.

REFERENCES

1) Blenkarn, K.A., "Measurement and Analysis of Ice Forces on Cook Inlet Structures," Preprint, Offshore Technology Conference (OTC), Vol. II, 365-378 (1969).

2) Neill, C.R., "Ice Pressure on Bridge Piers in Alberta," Proc. IAHR Symposium on Ice and its Action on Hydraulic Structures, Reykjavik, Iceland, 1970.

3) Neill, C.R., "Force Fluctuations during Ice-Floe Impact on Piers," Proc. Ice Symposium on Ice and its Action on Hydraulic Structures, Leningrad, U.S.S.R., 1972.

4) Neill, C.R., Saunders, H.D., and Schultz, H., "Measurements of Ice Forces on Bridge Piers," 1970 and 1971, Research Council of Alberta, Edmonton, Alberta, 1972.

5) Sundararajan, C. and Reddy, D.V., "Stochastic Analysis of Ice-Structure Interaction," Proc. Second Int. Conf. on Port and Ocean Engineering under Arctic Conditions (POAC), Reykjavik, Iceland, 345-353 (1973).

6) Reddy, D.V. and Cheema, P.S., "Response of an Offshore Structure to Random Ice Forces," Proc. IEEE, Int. Conf. on Eng. in the Ocean Environment, Halifax, Vol. I, 84-88 (August 1974).

7) Reddy, D.V., Cheema, P.S., and Swamidas, A.S.J., "Ice Force Response Spectrum Modal Analysis of Offshore Towers," Proc. Third POAC Conf., University of Alaska, Fairbanks, Alaska, August 1975.

8) Korzhavin, K.N., "Action of Ice on Engineering Structures," Novosibirsk, Akad, Nauk., U.S.S.R., 1962, English Translation, Cold Regions Research and Engineering Laboratory, Hanover, New Hampshire, U.S.A., 1971.

9) Michel, B., Ice Pressure on Engineering Structures, U.S. Army Cold Regions Research and Engineering Laboratory, Monograph III - Bib., 1970.

10) Peyton, H.R., "Sea Ice Strength," Final Report to Office of Naval Research, Geophysical Institute, University of Alaska, College, Alaska, 1966.

11) Peyton, H.R., "Sea Ice Forces," Proc. Conf. on Ice Pressures Against Structures, Laval University, Quebec, Nov. 1966, National Research Council of Canada, Ottawa, N.R.C. No. 9851 (March 1968).

12) Peyton, H.R., "Ice and Marine Structures, Part I - The Magnitude of Ice Forces Involved in Design," Ocean Industry, Vol. 3, No. 3, 40-44 (1968).

13) Peyton, H.R., "Ice and Marine Structures, Part II - Sea Ice Properties," Ocean Industry, Vol. 3, 59-65 (1968).

14) Peyton, H.R., "Ice and Marine Structures, Part III - The Importance of Design Alternatives," Ocean Industry, Vol. 3, No. 12, 51-58 (1968).

15) Voelker, R.P. and Levine, G.H., "Use of Ice Model Basins to Simulate and Predict Full Scale Ice-Structure Interactions," Preprint, OTC, Vol. II, 583-592 (1972).

16) Coon, M.D., "Mechanical Behaviour of Compacted Arctic Ice Floes," Preprint, OTC, Vol. II, 603-608 (1972).

17) Nevel, D.E., Perham, R.E. and Hogue, G.B., "Ice Forces on Vertical Piles," Conference Preprint, U.S. Army Cold Regions Research and Engineering Laboratory, Hanover, New Hampshire, 1972.

18) Hirayama, K., Schwarz, J. and Wu, H.C., "Model Technique for the Investigation of the Forces on Structures," Proc. Second POAC Conf., Reykjavik, Iceland, 332-344 (1973).

19) Danys, J.V., "Effect of Cone-shaped Structures on Impact Forces of Ice Floes," Proc. First POAC Conf., Trondheim, Norway, 609-620 (1971).

20) Danys, J.V., "Offshore Installations to Measure Ice Forces on the Lightpiers in Lac St. Pierre," Preprint IXth Int. Conf. on Lighthouses and other Aids, Ottawa, 1975.

21) Danys, J.V., "Effect of Ice and Wave Forces on the Design of Canadian Offshore Lighthouses," Canadian J. Civil Engg., Vol. 2, No. 2, 138-153 (1975).

22) Danys, J.V., "Effect of Ice Forces on some Isolated Structures in the St. Lawrence River," Proc. IAHR Sym. Ice and its Action on Hydraulic Structures, Leningrad, U.S.S.R., 229-231 (1972).

23) Reinius, E., Haggard, S. and Ernstons, E., "Experiences of Offshore Lighthouses in Sweden," Proc. POAC, First Conf., Vol. I, Trondheim, Norway, 657-673 (1971).

24) Bergdahl, L., "Two Lighthouses Damaged by Ice," Proc. IAHR Sym. Ice and its Action on Hydraulic Structures, Leningrad, U.S.S.R., 234-238 (1972).

25) Kivisild, H.R., "Year-round Oil Terminal in Ice Covered Waters," Proc. First POAC Conf., Vol. I, Trondheim, Norway, 621-631 (1971).

26) Ross, B., Hanagud, S. and Sidhu, G.S., "Ice Floe - Offshore Platform Interaction," Proc. First POAC Conf., Vol. I, Trondheim, Norway, 674-682 (1971).

27) Assur, A., "Structures in Ice Infested Waters," Proc IAHR Sym. Ice and its Action on Hydraulic Structures, Leningrad, U.S.S.R., 93-97 (1972).

28) Assur, A., "Forces in Moving Ice Fields," Proc. First POAC Conf., Vol. I, Trondheim, Norway, 112-118 (1971).

29) Afanas'ev, V.P., "Ice Pressure on Vertical Structures," Translated from Russian, N.R.C. TT-1708, 1973.

30) Frederking, R. and Gold, L.W., "Ice Forces on an Isolated Circular Pile," Proc. First POAC Conf., Vol. I, Trondheim, Norway, 73-92 (1971).

31) Bercha, F.G., "Mathematical Simulation of Ice-Structure Interaction," Proc. Fifth Canadian Cong. App. Mech., Frédericton, New Brunswick, 203-204 (1975).

32) "Instructions for Determining Ice Loads on River Structures," State Committee of the Council of Ministers (USSR) for Construction (GOSSTROI, USSR), NRC TT-1663, 1973.

33) API Recommended Practice for "Planning, Designing, and Construction-Fixed Offshore Platforms," American Petroleum Institute, New York, January 1971.

34) Haugsoen, P., "Model Testing in Ice Conditions - An Urgent Necessity," Northern Offshore, Oslo, Norway, Vol. 4(1), 26-27 (1975).

35) Edwards, R.Y., "Cold Region Marine Technology: Current Contributions and Future Challenges," Naval Engineering Journal, 35-52 (August 1973).

36) Croasdale, K.R., "Crushing Strength of Arctic Ice," Arctic Institute of North America, pp. 377-399.

37) Croasdale, K.R., "The Nutcracker Ice Strength Tester and its Operation in the Beaufort Sea," Proc. IAHR Ice Sym., Reykjavik, Iceland, 1970.

38) Drouin, M., Simard, L., and Michel, B., "Ice Floe Velocities in the St. Lawrence River," Proc. IAHR Ice Sym. and its Action on Hydraulic Structures, Léningrad, U.S.S.R., 109-116 (1972).

39) Schwarz, I.J., "The Pressure of Floating Ice-Fields on Piles," Proc. IAHR Ice Sym., Reykjavik, Iceland, 1970.

40) Matlock, H., Dawkins, W.P. and Panak, J.J., "Analytical Model for Ice-Structure Interaction," Proc. ASCE, EMD, Vol. 97, 1083-1092 (1971).

41) Neill, C.R., "Selected Aspects of Ice Forces on Piers and Piles," Proc. Canadian Soc. Civ. Engg. Atlantic Regional Hydrotechnical Conf., Fredericton, New Brunswick, 1974.

42) Corotis, R.B. and Martin, C.H., "Approximate Dynamic Modelling of an Offshore Tower," Preprint 2439, ASCE National Struct. Engg. Convention, New Orleans, April 1975.

43) Hurty, W.C. and Rubinstein, M.R., Dynamics of Structures, Prentice-Hall Inc., New Jersey, 1964.

44) Bolotin, V.V., Statistical Methods in Structural Mechanics, Holden-Day Inc., San Francisco, 115-117 (1969).

45) Liaw, C.Y. and Reimer, R.B., "Hydrodynamic Interaction Effect on the Cylindrical Legs of Deepwater Platforms," Proc. OTC, Vol. II, 777-786 (1975).

46) Sanden, E.J. and Neill, C.R., "Determination of Actual Forces on Bridge Piers Due to Moving Ice," Proc. Canadian Good Roads Association, Convention, 1968.

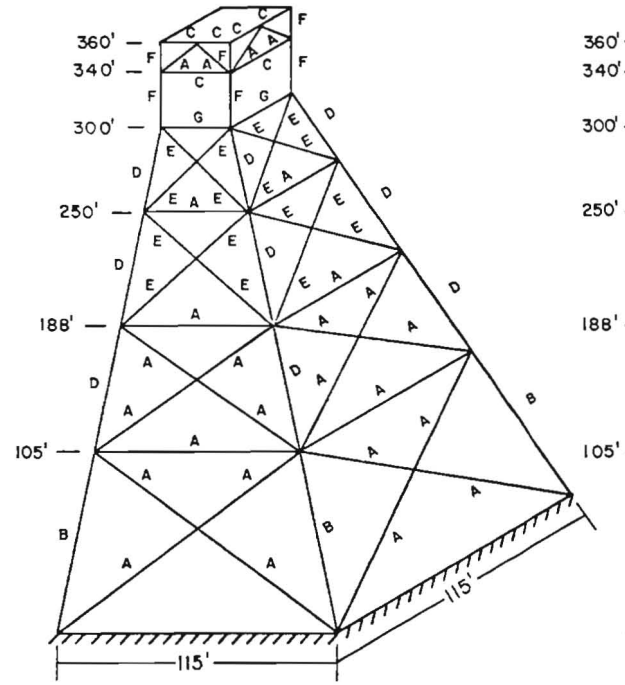

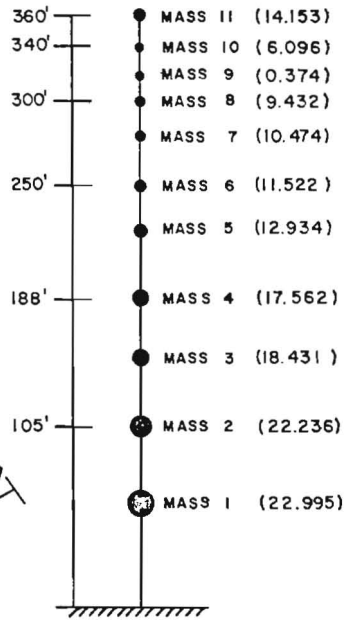

MEMBER	CROSS-SECTIONAL AREA (FT^2)	MOMENT OF INERTIA (FT^4)
A	0.224	0.818
B	1.658	2.0726
C	0.501	1.0853
D	1.297	0.9814
E	0.202	0.0602
F	0.807	0.9598
G	0.180	0.0424

FIG. 1 THREE-DIMENSIONAL OFFSHORE TOWER AND LUMPED MASS MODEL

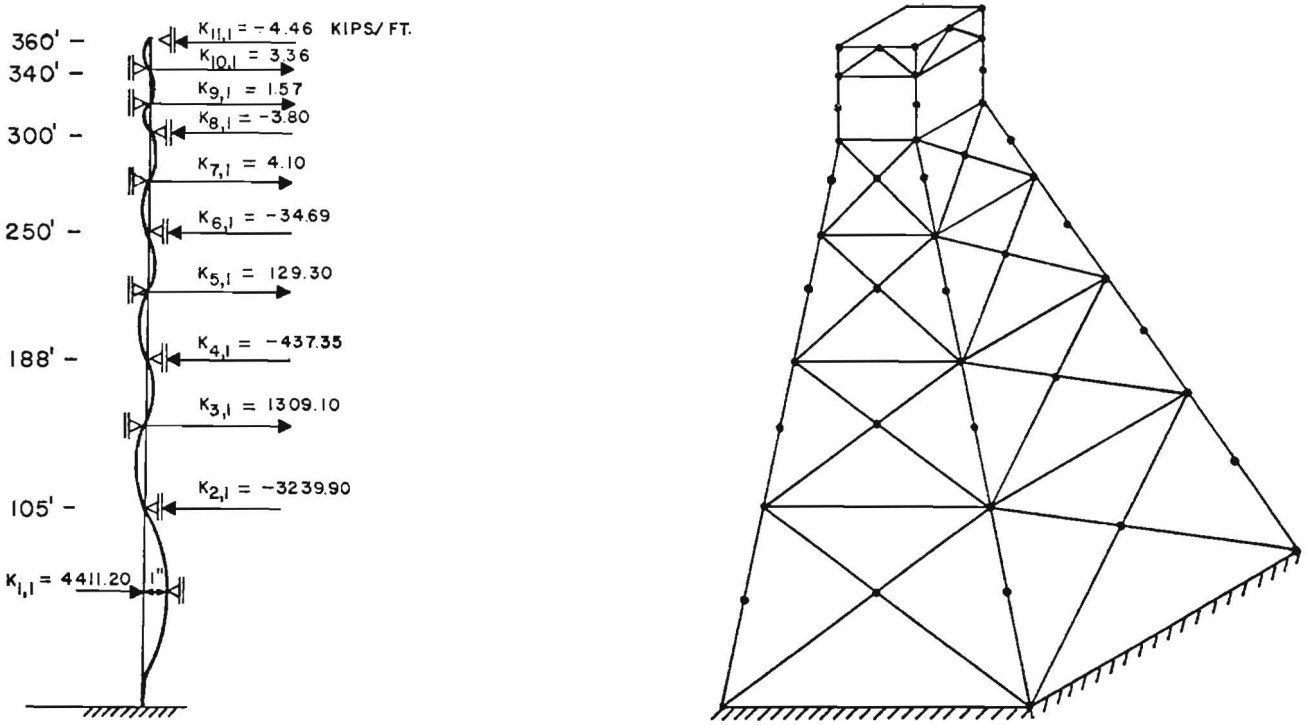

FIG. 2 TYPICAL STIFFNESS EQUIVALENCE FOR CANTILEVER

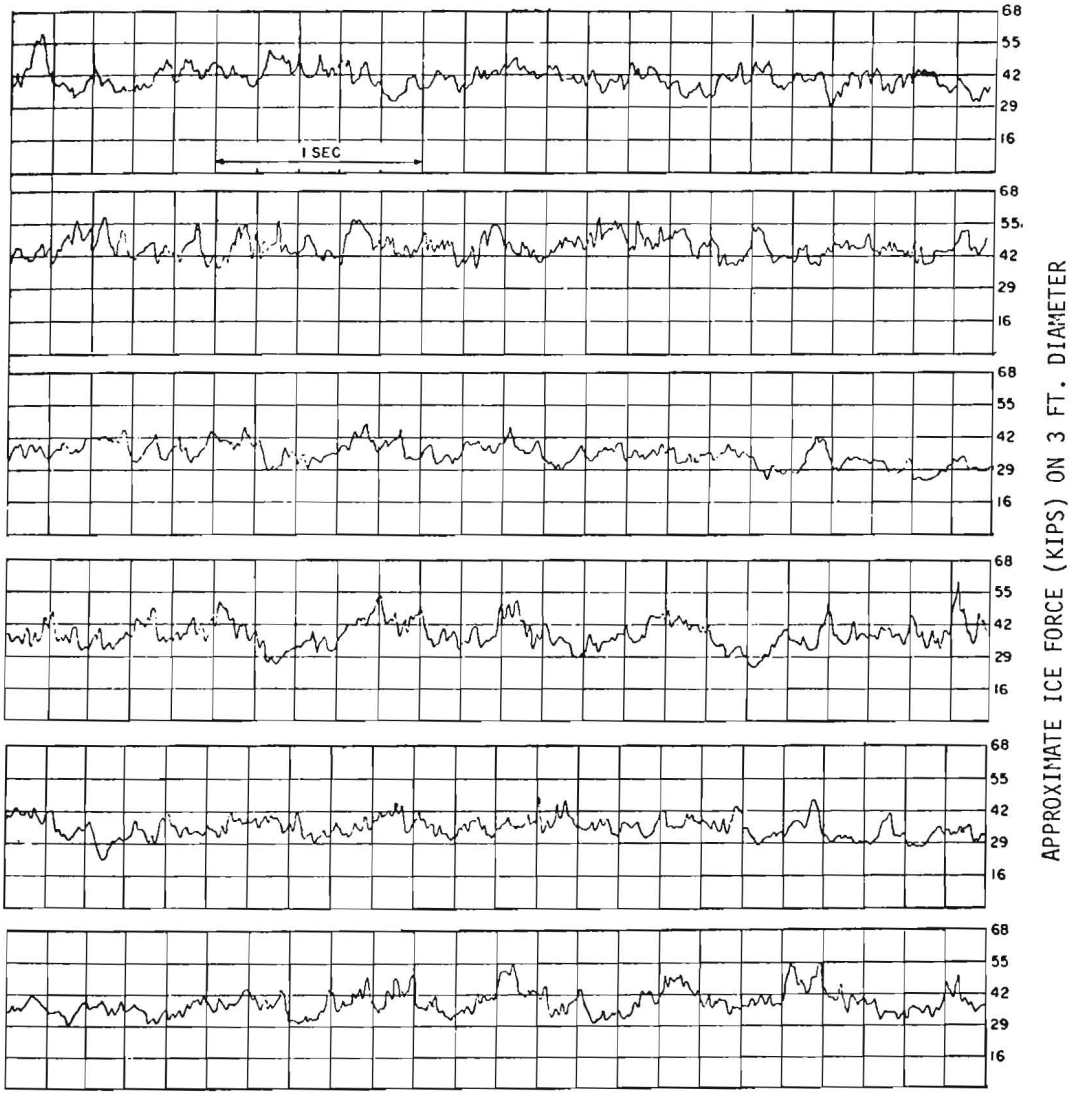

FIG. 3 BLENKARN'S ICE FORCE RECORD

(APPROXIMATE VELOCITY OF ICE FLOE=3 FT./SEC)

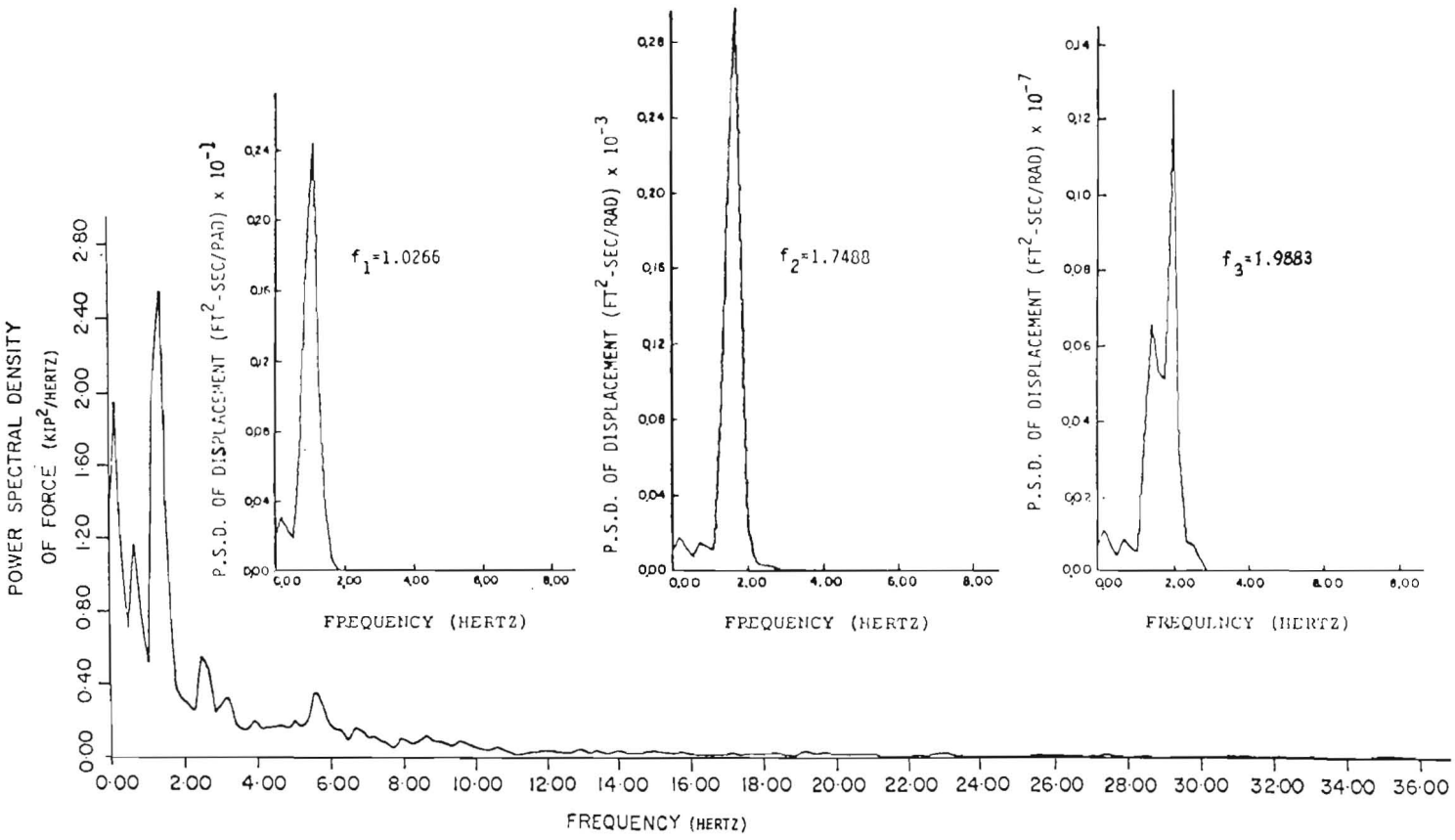

FIG. 4 POWER SPECTRAL DENSITIES

THIRD INTERNATIONAL SYMPOSIUM ON
ICE PROBLEMS
Hanover, New Hampshire, USA

VISCOELASTIC FINITE ELEMENT ANALYSIS OF SEA ICE SHEETS

Kennon D. Vaudrey
Rsch Civil Engineer

Michael G. Katona
Rsch Struct. Engineer

Civil Engineering
Laboratory
Naval Construction
Battalion Center

Port Hueneme,
CA 93043

INTRODUCTION

In recent years operational use of ice-covered waters in polar regions has greatly increased to coincide with the advent of a world-wide energy crisis. No longer can remote polar locations be considered too inhospitable or uneconomical to search for or harvest energy resources. In particular, Naval operations continue to depend on sea-ice airfields and roads to provide heavy cargo and logistics support for United States activities. Therefore, a better understanding of the behavior of sea-ice sheets under aircraft and vehicular loading is required to ensure continued safe operations. To this end the Civil Engineering Laboratory (CEL) was initially engaged in performing experiments and developing analyses, assuming sea-ice sheets behave elastically. The culmination of this elastic-properties research on sea ice was the development of an elastic finite element computer code, having the capability of modeling temperature-dependent properties as a function of ice sheet thickness(1).

However, it is known that sea ice behaves elastically only for small to moderate load magnitudes applied over short time durations. Consequently, parked aircraft, cargo storage, over-ice platforms or stations, and even snow overburden cannot be correctly analyzed by elastic-behavior solutions to determine their actual effect on ice sheets. To expand the range of load magnitudes and time durations, the theory of linear viscoelasticity has been coupled with the finite element technique to provide more realistic characterization of sea-ice behavior. Certainly, linear viscoelasticity is not new to the discussion of floating ice sheets(2)(3)(4), but its application to the finite element method provides solutions to rather complicated boundary value problems previously considered intractable.

ANALYTICAL FORMULATION

The following discussion presents a brief description of the finite element formulation implementing linear viscoelasticity and its associated assumption and limitations. A more thorough presentation is made by Katona(5). Viscoelastic materials are often called "memory" materials because the current state of stress in the material is determined not only by the current deformation, but also by all past deformation states. Moreover, the "memory" exhibits a fading phenomenon, since past deformations have less influence on the current stress state than do more recent deformation states.

Viscoelastic Representation

The above characteristics can be modeled either by differential or integral equations(6). The differential equation approach interprets the viscoelastic model in terms of a mechanical analogy composed of springs and dashpots. However, integral equations are more readily adaptable to laboratory testing results, and, thus, easily applied to the solution of boundary value problems. An expression for stress as an integral function of any arbitrary strain input, $\varepsilon(t)$, can be written as:

$$\sigma(t) = Y(t)\varepsilon_o + \int_0^t Y(t-\tau) \frac{\partial \varepsilon(\tau)}{\partial \tau} d\tau \qquad (1)$$

where ε_o is the initial elastic strain, while $Y(t)$ is termed the relaxation function and is an inherent characteristic of the material model.

It is desirable here to elaborate on the merits of the integral form of Equation (1). First, standard laboratory procedures for testing viscoelastic materials involve only direct measurement of the relaxation function (or its inverse, the creep function). A test specimen is subjected to a constant state of unit deformation, and the resulting stress is measured as a function of time. Clearly, it is not necessary to deduce an equivalent mechanical analog, since the laboratory data can be used directly in Equation (1).

For isotropic materials, it can be shown that there are only two independent relaxation functions required to describe the constitutive relation. It is convenient in solving boundary value problems to choose the relaxation functions as the responses to bulk and shear deformation. The bulk relaxation function, $K(t)$, is defined as the hydrostatic stress history due to a prescribed unit Heaviside volume deformation. Likewise, the shear relaxation function, $G(t)$, is defined as the shear stress history due to a prescribed unit Heaviside shear strain. Both $K(t)$ and $G(t)$ are positive, monotonically decreasing, independent relaxation functions. They can be written in the form of a prony series:

$$K(t) = K_o + \sum_{i=1}^{m_K} K_i e^{-t/\lambda_i}; \quad G(t) = G_o + \sum_{i=1}^{m_G} G_i e^{-t/\beta_i} \qquad (2)$$

Here both relaxation functions are represented as a constant and summation of exponential terms; where K_0, K_1,...,K_{m_K}, G_0, G_1, ..., G_{m_G} are positive moduli constants with units of stress, and λ_1, ..., λ_{m_K}, β_1, ..., β_{m_G} are positive constants referred to as "relaxation times."

In the prony series form, the relaxation functions are capable of representing a large class of linear viscoelastic materials. In essence, any linear viscoelastic material which exhibits an instantaneous elastic deformation followed by a creep phase can be modeled by Equation (2) with a sufficient number of exponential terms. In practice it is seldom justified to use more than four exponential terms, and usually two terms are sufficient. It can be noted that neither K(t) nor G(t) is the most convenient response for laboratory measurement, but converting normal laboratory results will be discussed later for specific viscoelastic saline-ice tests.

Displacement Method

In this derivation a brief outline of the finite element technique is presented, wherein quasi-static loading, small deformations, axisymmetric/plane strain geometry, and the absence of thermal effects are assumed. First, the viscoelastic constitutive relation of Equation (1) can be presented as a matrix of Stieltjes integrals:

$$\{\sigma(t)\} = \left[D(t)\right] \{\varepsilon(o)\} + \int_0^t \left[D(t-\tau)\right] \frac{\partial}{\partial\tau} \{\varepsilon(\tau)\} d\tau \qquad (3)$$

where $\{\sigma(t)\}$ is the stress vector at the current time, t; $\{\varepsilon(\tau)\}$ is the strain history vector for $0 \leq \tau \leq t$; and $\left[D(t-\tau)\right]$ is the constitutive matrix, composed of the two independent relaxation functions, K(t) and G(t), in the form of Equation (2).

When this constitutive model is used in a displacement finite element formulation based on virtual work, the resulting equilibrium equations have the form:

$$\int_0^t \left[K(t-\tau)\right] \frac{\partial}{\partial\tau} \{u(\tau)\} d\tau = \{R(t)\} \qquad (4)$$

where $\{u(\tau)\}$ is the nodal point displacement history vector, $\{R(t)\}$ is the current load vector, and $\left[K(t-\tau)\right]$ is the viscoelastic stiffness-history matrix. For the sake of clarity, inertial terms are not included in Equation (4) because they can be treated independently of the viscoelastic terms.

In order to solve Equation (4) for the nodal displacements at the current time, $t = t_n$, a step-by-step numerical integration procedure must be employed. To this end, the time integral is subdivided into n time increments and the time increment, Δt, is chosen sufficiently small to assume that the nodal displacements vary linearly within each time step. With this approximation the nodal velocities $\partial/\partial\tau\{u(\tau)\}$ can be replaced by displacement increments for each time step, Δt_k, by $(1/\Delta t_k)\ \{\Delta u_k\}$. Next, by shifting all time-interval integrations to the

right-hand side, except the current time interval, Δt_n, Equation (4) can be expressed as

$$\left[K(\Delta t_n)\right] \{\Delta u_n\} = \{R(t_n)\} - \{H(t_n)\} \tag{5}$$

where $\left[K(\Delta t_n)\right]$ is the current viscoelastic stiffness matrix which is dependent only on the current time-step size, and $\{H(t_n)\}$ is the viscoelastic force-history vector dependent upon all past time steps,

$$\{H(t_n)\} = \sum_{k=1}^{n-1} \left[K(t_n - t_k)\right] \{\Delta u_k\} \tag{6}$$

Using Equation (5), it is possible to solve for $\{\Delta u_n\}$ in a step-by-step fashion beginning with elastic solution, n = 0, and increasing n successively through the time of interest while accumulating the incremental displacements. Since the current viscoelastic stiffness matrix is dependent only on the time-step size, the matrix need only be reformed and triangularized again when the size of time step is changed.

Although this procedure is tractable, the calculation of the force history vector in its defined form is computationally unpractical since it requires the storage of all past incremental displacements and the formation of new viscoelastic stiffness matrices at each time step. To circumvent this difficulty, a technique introduced by Taylor (7) can be exploited. Taylor's technique requires that the relaxation functions in Equation (3) be in the form of a prony series, such as Equation (2). When the relaxation functions are of the form given in Equation (2), it is possible to restructure the force history vector as a summation of only $m_K + m_G + 1$ vectors rather than a summation of all history vectors. Moreover, the exponential form of the relaxation functions permits a simple recursion relationship for updating the force history vector at each time step.

Fluid Foundation

In the previous section, the viscoelastic boundary value problem was generated to include any arbitrary, axisymmetric or plane-strain, geometrical application. Now the geometry is specialized to plate-type structures, supported by a Winkler-type fluid foundation. By definition, a Winkler foundation produces a vertical resistance force proportional to the vertical displacement of the nodes at the plate-fluid interface. Consequently, these additional vertical nodal forces at the interface can be expressed as $\left[K_w\right] \{u_n\}$, where $\left[K_w\right]$ is a sparse global Winkler stiffness matrix with non-zero entries associated only with vertical displacements at the plate-fluid interface.

Considering Equation (5) as a force equilibrium equation, the influence of the fluid foundation can be added directly to give:

$$\left[K(\Delta t_n)\right]\{\Delta u_n\} + \left[K_w\right] \{u_n\} = \{R(t_n)\} - \{H(t_n)\} \tag{7}$$

To complete the inclusion of the fluid foundation, the components of the Winkler stiffness matrix, $[K_w]$, need to be derived, consistent with the concept of virtual work (5).

Superposition of Loads

For this concept the geometry is assumed to be an axisymmetric, half-space system such that material properties vary only in the vertical direction, and the radial boundary extends to infinity. Loading is represented by uniform circular surface pressure discs, and their location is completely arbitrary. Specified load histories are assumed proportional to one another; in other words, the pressure of each disc, $p_i g(t)$, contains a pressure magnitude, p_i, and a loading history, $g(t)$, which is common to all discs. With the above assumptions, the state of stress under any pressure disc can be determined by solving for the stresses produced by that single disc, and using stress transformations and superposition to calculate the stress contributions from all other discs (5).

OBTAINING RELAXATION FUNCTIONS FROM CREEP DATA

During the past year a laboratory viscoelastic testing program was begun to supply quantitative information for determining constitutive relations. All tests are performed on saline ice specimens, right circular cylinders with a L/D ratio of 2:1. Ice growth has been controlled to maintain a constant salinity range, density, and crystal size representative of natural sea ice. The output from each individual test is the strain history, depending on a set of four test parameter combinations: (1) ice temperature; (2) loading condition; (3) stress level; and (4) crystal orientation.

Four different ice temperatures are chosen to bracket the two major precipitation points of sea ice salts: -4, -10, -20, and -27°C. Both compression and tension tests are conducted as uniaxial loading conditions. Three stress levels have been selected as 10, 25, and 50% of the average uniaxial compressive and tensile strength, determined from previous tests conducted at CEL. Saline ice specimens are extracted so that the direction of load application is either perpendicular or parallel to the preferred direction of crystal growth.

As stated previously, the output from all of these 48 parametric combinations is the strain history resulting from the sudden application of a constant stress. Thus, the creep data being measured must be converted into relaxation functions in order to be input for the viscoelastic finite element computer code. Initially, all creep data should be discretized into M data points for specified time steps. Then, the objective is to fit a creep function, J(t), in the form of a prony series, similar to Equation (2), but with an additional linear term for continuous creep, if desired. J(t) is defined as the strain history response to a prescribed unit Heaviside stress input. This curve-fitting technique can be accomplished by a linear least square error analysis based on m unknown creep moduli, $J_0, J_1, \ldots, J_m$, with preselected times, λ_i, which can be optimized by trial and error. Once J(t) is determined, using Laplace transformation the inverse of J(t), the relaxation function, Y(t),

can be found. However, while Y(t) is of the form of Equation (2), it does not represent either the bulk, K(t), or shear, G(t), relaxation functions, but rather Y(t) = E(t), the Young's modulus relaxation function. Assuming Poisson's ratio, ν, to be constant, then the relaxation functions, K(t) and G(t), required for computer input become:

$$K(t) = \frac{E(t)}{3(1 - 2\nu)} \; ; \; G(t) = \frac{E(t)}{2(1 + \nu)} \tag{8}$$

In Figure 1, typical creep curves are shown for three stress levels (10, 25, and 50%) on laboratory-grown saline-ice specimens at -27°C. The ice specimens were subjected to a uniaxial compressive load perpendicular to the crystal growth. By comparing the σ_o and $2.5\sigma_o$ stress-level curves one can observe that the strains differ by a ratio of 2.5:1 for all time. Therefore, the superposition principle is valid, and the ice behaves as a linear viscoelastic material between these stress levels. If both the σ_o and $2.5\sigma_o$ curves were normalized with respect to their applied stress levels, this resulting creep data can be transformed into a single relaxation function representing the time-dependent Young's modulus (stress history) for all stress levels up to $2.5\sigma_o$. If one exponential term of Equation (2) is deemed sufficient (equivalent to a standard linear solid model), then an expression for the relaxation function, E(t), can be written as:

$$E(t) = E_0 + E_1 e^{-t/\lambda_1} \tag{9}$$

where $E_0 = 1.06(10^5)$ kN/m^2, $E_1 = 3.67(10^6)$ kN/m^2, and $\lambda_1 = 16.8$ minutes.

However, no such constant ratio exists between $2.5\sigma_o$ and $5.0\sigma_o$ stress-level strain-history curves, indicating nonlinearity occurring somewhere between these two stress levels. This demonstrates, when working with functions based on linear viscoelasticity, the domain of validity should be defined in terms of load magnitudes and durations.

VISCOELASTIC SEA ICE EXAMPLES

To demonstrate the capability of the viscoelastic finite element computer code, the structural response of an infinite sea-ice plate on a fluid foundation is investigated for different loading conditions and using material properties found from laboratory data. In both examples, the time-dependent surface deflections of an Arctic sea-ice sheet, measured during Project Iceway (8) are compared with those calculated by the finite element method. The first experimental loading consisted of 7-meter-diameter, 1.1-meter-high ice discs, formed on top of a 1.32-meter-thick ice sheet. Initially, the weight was 422.6 kiloNewtons, then at t = 50 hours, the weight was increased to 633.9 kiloNewtons. The finite element idealization of the boundary value problem is illustrated in Figure 2.

Relaxation functions for the sea ice were not determined during the experimental program. Since the average ice sheet temperature at

the time of the experiment was near $-10^{o}C$, a relaxation function for Young's modulus is obtained for that ice temperature from CEL laboratory creep data. These data are found for a 10% stress level (σ_o = 226.6 kN/m^2) and compression loading perpendicular to the crystal growth. The relaxation function E(t) can be written in the form of Equation (9), where $E_0 = 1.33(10^5)$, $E_1 = 2.26(10^5)$, and $E_2 = 8.57(10^5)$ kN/m^2; λ_1 = 400 and λ_2 = 4.2 min. Of course, relaxation functions for bulk and shear moduli can be found from Equation (8), assuming $\nu = 0.3$, and both K(t) and G(t) are given in the insert to Figure 3. This figure shows predicted ice sheet displacement profiles for four different times and the corresponding experimental data points from Project Iceway.

The second exponential term in E(t) decays rapidly, thereby influencing only the initial viscoelastic behavior. Eventually, this relaxation function will reach an asymptotic modulus of E_0. For this experiment, which lasted for hours, the first term is indeed lost, and a limiting deflection is reached prior to 100 hours. However, from the experimental field data this asymptotic behavior either does not occur or would occur much later than t = 100 hours. It is difficult to determine which is the case because of continued step loading. While the analytical and experimental deflection profiles in Figure 3 do not quite coincide, the incremental deflections caused by step loading at t = 50 hours are equal.

The second Project Iceway experiment under consideration consisted of parking a KC-135 aircraft (weighing 698.3 kiloNewtons) on a 1.32-meter-thick ice sheet for 40 minutes, then removing the load. The computer code can handle both step loads (as in the first problem) and rebound effects after load removal. The finite element idealization of the aircraft problem is shown in Figure 4. The loading depicted here represents only one of the eight main wheels of the aircraft; the contributions of the other seven are calculated by superposition.

The relaxation function given above for Young's modulus is still applicable; consequently, both K(t) and G(t) given in Figure 3 are used in the computer code. The analytical results are plotted over a 50-minute time frame in Figure 5 along with ice deflections found near the main landing gear. The last ten minutes show the rebound of the ice sheet after the aircraft has been removed. Analytical and experimental field results of both Figures 3 and 5 are generally in good agreement--somewhat surprising, considering the ice disc experiment was of long duration, while the aircraft test lasted less than one hour. It is emphasized that the intention here was not to provide a curve-fitting technique to field experiments, but rather to demonstrate the applicability of the viscoelastic finite element computer program for analyzing time-dependent ice sheet behavior, using any appropriate model determined from controlled laboratory testing.

CONCLUSIONS

The viscoelastic finite element analysis technique and resulting computer program developed in this investigation have proved to be an accurate, versatile, and powerful tool for solving ice sheets subjected to arbitrary surface loading. Its versatility is best displayed by the

ability to include: (1) separate material-layer characterization, (2) arbitrary load-history functions; and (3) superposition of any number of loads. While the viscoelastic model includes independent bulk and shear relaxation functions, not easily found by material properties testing, it becomes a straightforward three-step transformation of: (1) creep data into creep functions, (2) creep functions into relaxation functions, $E(t)$ and $\nu(t)$; and (3) $E(t)$ and $\nu(t)$ into relaxation functions, $K(t)$ and $G(t)$. Of course, the effectiveness of the computer program, or of any other analytical formulation, is dependent on obtaining proper moduli and relaxation parameters for sea ice material characterization. The extensive experimental program on saline ice specimens now underway should continue to provide more accurate and reliable values for material properties.

To increase the scope of the analysis to include dynamic response, minimal effort would be required to include inertial terms through a consistent mass matrix. It is recognized that linear viscoelasticity definitely has limits on its application; however, its domain does include a significantly improved step above elastic limits. For that next step into the viscoplastic range, it is possible, computationally, to base a viscoplastic formulation on the algorithms developed in this study.

REFERENCES

1. Katona, M. G. and Vaudrey, K. D., Ice Engineering: Summary of Elastic Properties Research and Introduction to Viscoelastic and Nonlinear Analysis of Saline Ice, Naval Civil Engineering Laboratory Technical Report R-797, Port Hueneme, CA, Aug 1973.
2. Jellinek, H. H. G., and Brill, R., "Viscoelastic Properties of Ice," Journal of Applied Physics, Vol. 27, No. 10, 1956, pp. 1198-1209.
3. Tabata, T., "Studies on Viscoelastic Properties of Sea Ice," from Arctic Sea Ice, National Academy of Sciences - National Research Council Publication 598, Washington, DC, December 1958.
4. Nevel, D. E., Time Dependent Deflection of a Floating Ice Sheeet, U.S. Army Cold Regions Research and Evaluation Laboratory Research Report 196, Hanover, NH, July 1966.
5. Katona, M. G., Ice Engineering: Viscoelastic Finite Element Formulation, Naval Civil Engineering Laboratory Technical Report R-803, Port Hueneme, CA, Jan 1974.
6. Flugge, W., Viscoelasticity, Blaisdell Publishing Co., Waltham, MA, 1967.
7. Taylor, R. L., "An Approximate Method for Thermoviscoelastic Stress Analysis," Nuclear Engineering and Design, Vol. 4, 1966, p. 21.
8. Kingery, W. D., et al., Sea-ice Engineering: Summary Report - Project Ice Way, Naval Civil Engineering Laboratory Technical Report R-189, Port Hueneme, CA, Sept 1962.

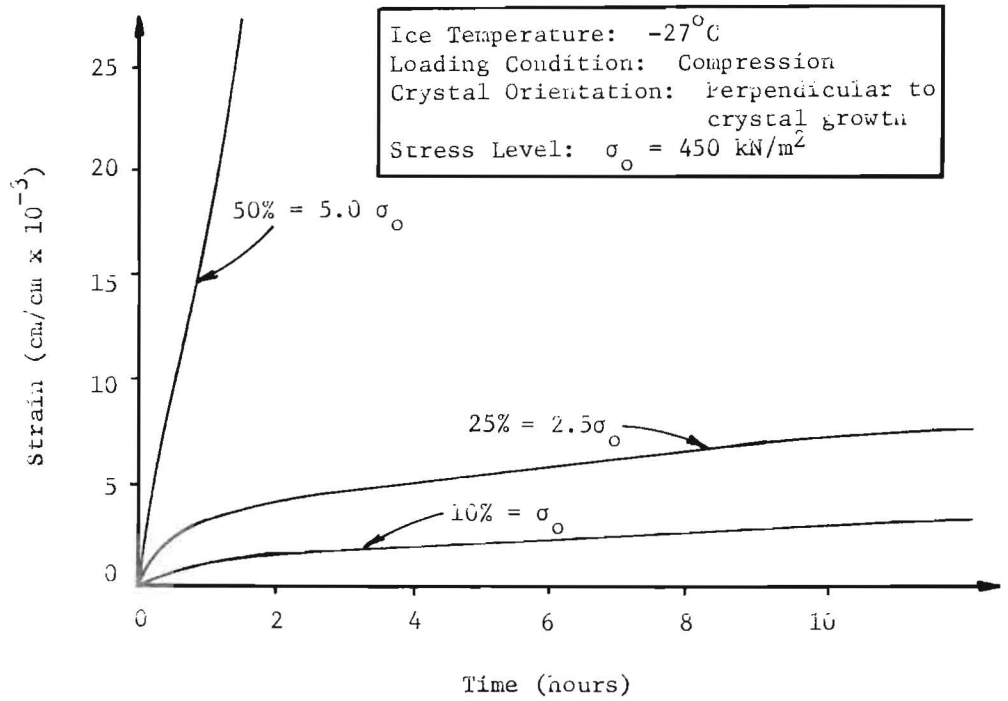

Figure 1. Typical creep curves for saline-ice specimens at -27°C.

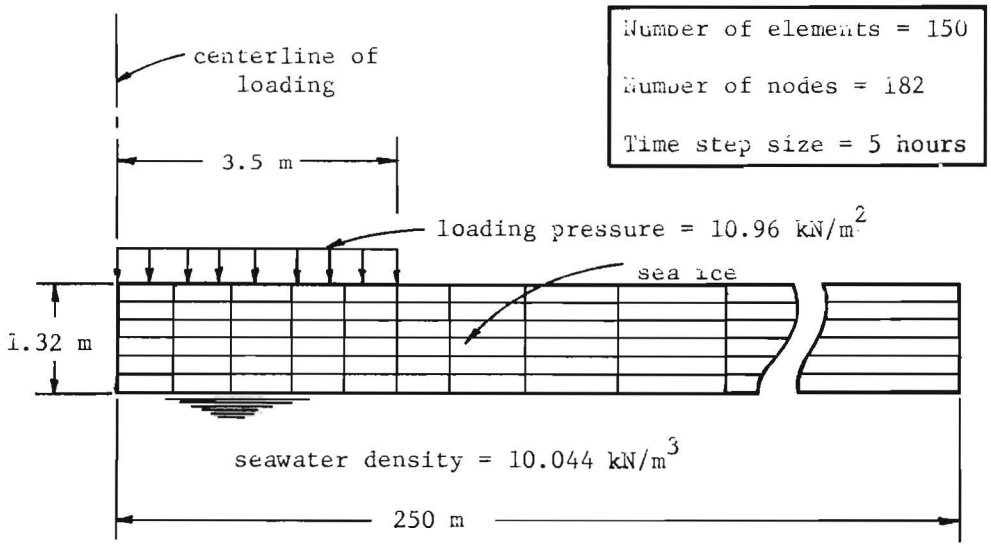

Figure 2. Finite element idealization of ice sheet for ice disc experiment.

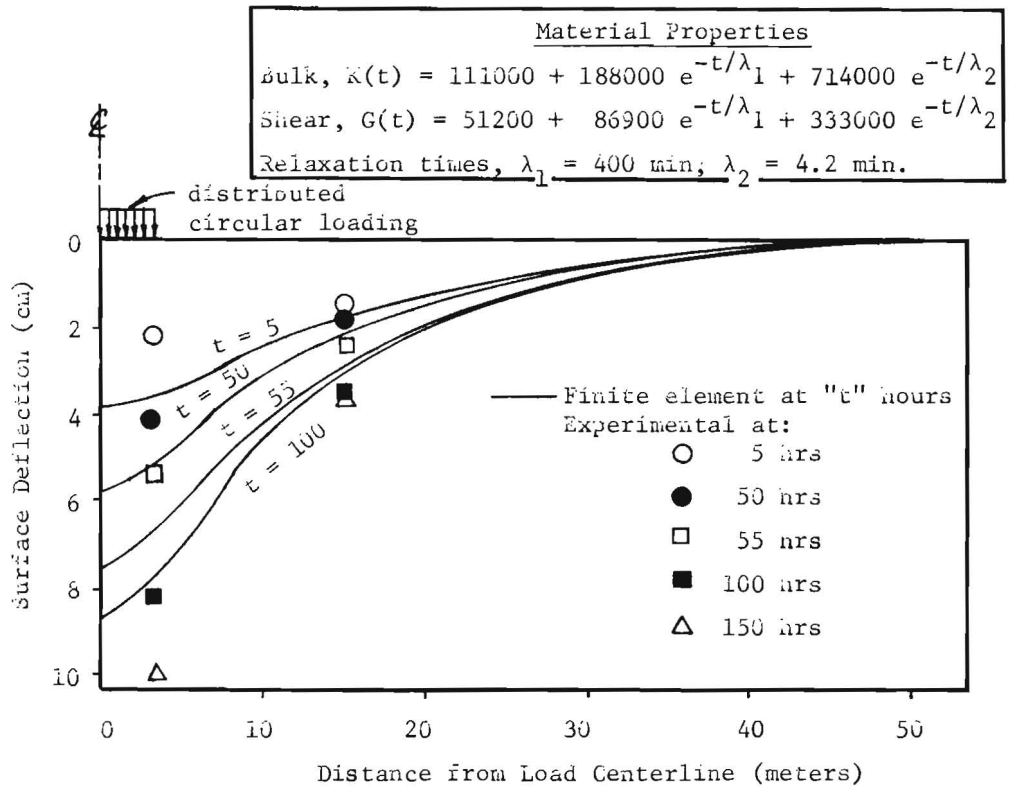

Figure 3. Deflection profile for ice disc experiment.

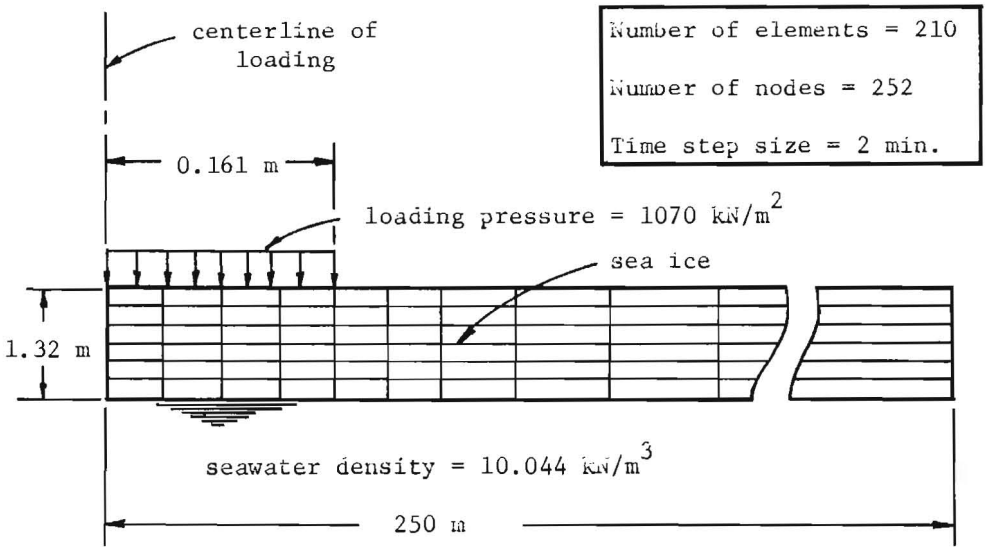

Figure 4. Finite element idealization of ice sheet for aircraft experiment.

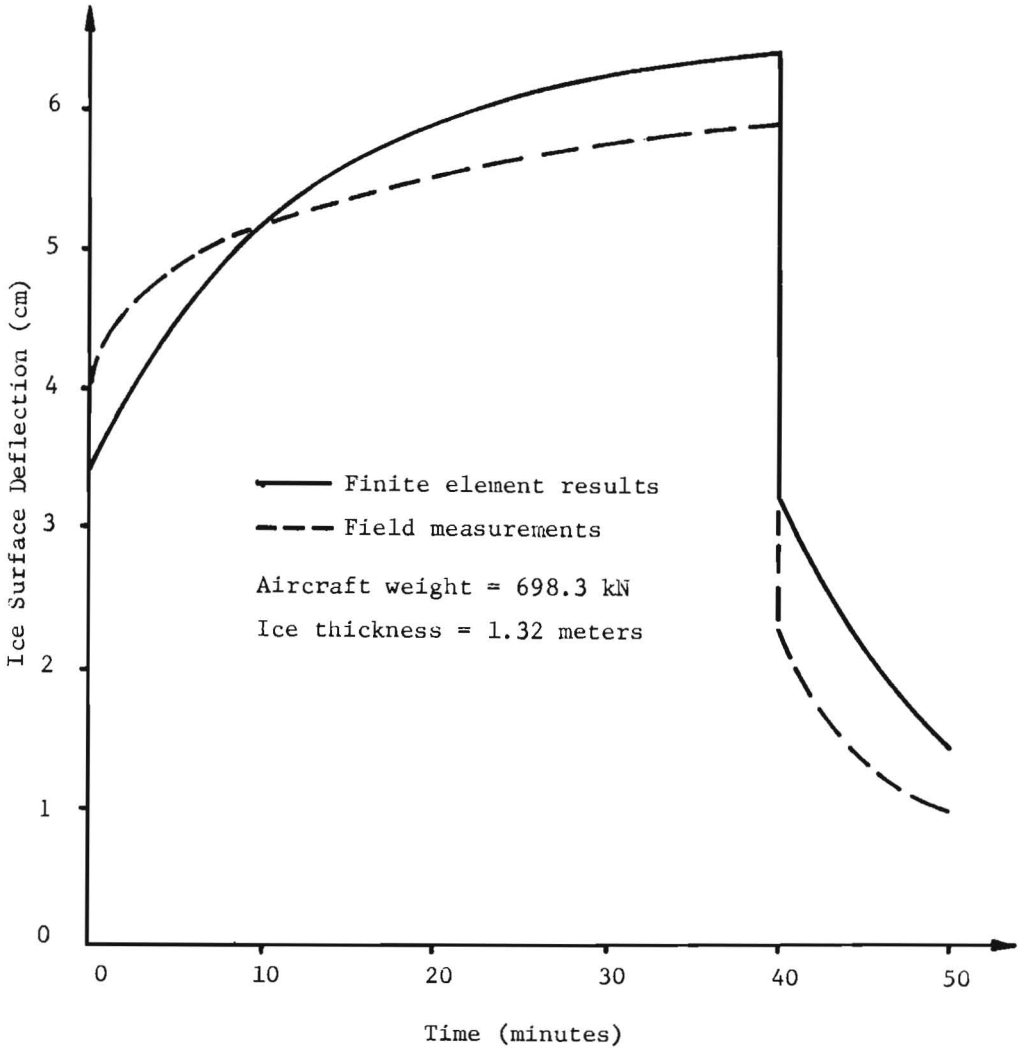

Figure 5. Ice deflection near or at main landing gear for KC-135 aircraft.

THIRD INTERNATIONAL SYMPOSIUM ON
ICE PROBLEMS
Hanover, New Hampshire, USA

STRESS FIELDS IN PACK ICE

R. J. Evans, Associate Professor	Dept. of Civil Engineering University of Washington	Seattle, Washington
D. A. Rothrock, Principal Scientist	AIDJEX University of Washington	Seattle, Washington

ABSTRACT

A pack ice model is described which treats the mass, ice velocity, and ice stress as averages over a region large enough to contain many ice floes. Some relations are then developed between this large-scale stress and the local stresses of importance in engineering problems.

INTRODUCTION

Stress in pack ice can be considered on two distinct scales. On a scale large enough to include many floes and many events of ridging or opening, stress is a continuous variable which affects the motion of the ice. This stress is transmitted through the pack, however, by local stresses at floe boundaries which can be significantly different from the large-scale or continuum ice stress. The two types of stress are completely analogous to the macrostress and microstress of heterogeneous media [Volkov, 1962]. For most heterogeneous materials, the macrostresses rather than the microstresses are of interest; for pack ice both are of interest--the continuum stress for the large-scale momentum balance, the local stress for design purposes and for understanding the mechanics of deformation.

This paper describes a predictive model, one of whose primary variables is the continuum ice stress. The model, developed for the Arctic Ice Dynamics Joint Experiment (AIDJEX), solves the constitutive law and the equations of mass and momentum balance, by treating the pack as a continuum. Because pack ice is an aggregate of floes ranging up to kilometers in size, it can be modeled as a continuum only on a scale of about 100 km. In the AIDJEX model, the variables are, then,

comparable to observed quantities averaged over this 100 km scale. A continuum element of this size not only contains many floes but, as it deforms, activates the controlling mechanisms of floe interaction at many locations. These mechanisms are pressure ridge formation, shearing at flow boundaries, and opening of cracks between floes to form leads.

The constitutive law of this element is postulated to be elastic-plastic. The plastic floe embodies the significant deformation and is associated with ridging and opening. In contrast to viscous constitutive laws [Rothrock, 1975a] which prescribe the stress to be proportional to the strain rate, the plastic law allows significant strain rates in shear or divergence to occur where stresses are low, and also permits compressive stresses with little straining.

The model allows the calculation of time-dependent fields of mass per unit area m, velocity $\underset{\sim}{v}$, stress[1] $\underset{\sim}{\sigma}$ and strength p^* for initial- and boundary-value problems. For instance, the extent, movement and stresses in the Arctic Ocean or for the entire Antarctic ice pack can be treated. Here, we show a solution to the simplified one-dimensional case of an onshore wind pushing the ice against the shore.

Although the stress $\underset{\sim}{\sigma}$ affects the motion of the ice, it does not determine the local stresses generated by the forces of action and reaction between individual floes. To apply the model output to operational uses, we must know the extent to which local stresses can be related to $\underset{\sim}{\sigma}$. In the latter part of the paper, we derive upper bounds on local stresses and distributions of local stress in terms of the continuum stress. The local stress treated here is the mean pressure within a floe which we take to be a measure of interfloe forces.

THE AIDJEX MODEL

Because of the continual occurrence of ridging and opening and the rapid growth of ice in leads during most of the year, each element of the continuum has a distribution $G(h)$ of ice of various thicknesses h; $G(h)$ is defined as the fraction of area of ice no thicker than h. The thickness distribution determines the mass m (= ice density $\times$ $\int_0^1 h(G)dG$) and the strength p^*, and is governed by the equation [Thorndike et al., 1975]

$$\frac{dG}{dt} = -f\frac{\partial G}{\partial h} + \Psi - G \operatorname{div} \underset{\sim}{v} \qquad (1)$$

where d/dt is the material derivative, and $f(h)$ is the thermodynamic growth rate and is specified.

The quantity Ψ, called the redistribution function, models opening and ridging and is a known function of h, strain rate, and the instantaneous thickness distribution. It has two terms, each multiplied by a coefficient which depends on the rates of shearing and divergence or convergence. One of these terms is a unit step function at $h = 0$ and represents a source of open water. Its coefficient is largest in

---

[1] Quantities are all integrated through the ice thickness. Thus what we call continuum stress is formally a stress resultant with dimensions of force per length.

pure divergence, moderate in shear, and zero in pure convergence. The other term is a function $W_r(h,G)$ which is negative for small h and positive for larger h representing a transfer by ridging of thin ice into thick ice. The precise function $W_r(h)$, though, depends on the instantaneous thickness distribution G in a known way. The coefficient of the ridging term is zero in pure divergence, moderate in shear, and largest in pure convergence.

The major terms in the momentum balance are the air stress $\underset{\sim}{\tau}^a$ applied to the upper surface by the wind, the water stress $\underset{\sim}{\tau}^w$ which acts on the lower surface whenever there is relative movement between the ice and the ocean, the Coriolis force and the divergence of the ice stress $\underset{\sim}{\nabla}\cdot\underset{\sim}{\sigma}$. We have too little experience with the model and with reality to be certain, but it appears that $\underset{\sim}{\nabla}\cdot\underset{\sim}{\sigma}$ plays a modest role in the central Arctic Ocean but a major role within several hundred kilometers of shore. Several other terms in the momentum balance are of secondary importance. These are the inertial term $m\, d\underset{\sim}{v}/dt$, the component of gravitational acceleration down the sloping sea surface, and the force due to the horizontal gradient of the surface atmospheric pressure. In the example below, we will disregard Coriolis force, approximate the water stress by $\underset{\sim}{\tau}^w = -A\underset{\sim}{v}$, with $A = 0.06$ dyn sec cm^{-3}, and, so, consider the momentum equation

$$m\frac{d\underset{\sim}{v}}{dt} = \underset{\sim}{\tau}^a - A\underset{\sim}{v} + \underset{\sim}{\nabla}\cdot\underset{\sim}{\sigma} \qquad (2)$$

The elastic-plastic constitutive law has several parts. The first is the yield criterion $F(\underset{\sim}{\sigma}) = 0$ which determines what stresses are sufficient to cause plastic flow. We work with two convenient invariants, σ_I and σ_{II}, which are respectively half of the sum and half of the difference of the principal stresses (σ_1 and σ_2). Thus, σ_I is half the negative pressure and σ_{II} is the maximum shear stress. Because we assume that cracks run through the ice cover in all directions, we choose a yield curve that prohibits all tensile stresses, as shown in Figure 1. The determination of the compressive strength p^* will be described below.

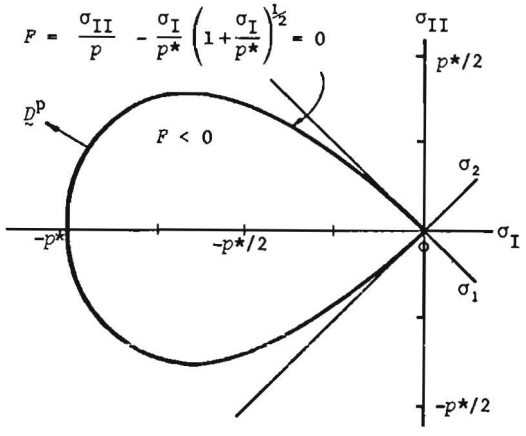

Fig. 1. The yield curve $F = 0$ in stress space. With a stress state lying inside the curve ($F < 0$), the ice is elastic and deforms very little. When the stress is on the yield curve, plastic flow occurs. The ice cannot support stresses outside the curve.

The second element of the constitutive law is a linear elastic law relating stress and elastic strain $\underset{\sim}{e}$. The elastic modulus and strength p^* are such that failure occurs after an elastic strain of about 0.1%. The plastic strain rate $\underset{\sim}{D}^P$ obeys the flow rule

$$\underset{\sim}{D}^P = \begin{cases} 0 , & F < 0 \\ \lambda \dfrac{\partial F}{\partial \underset{\sim}{\sigma}} , & F = 0 \end{cases} \tag{3}$$

which states that $\underset{\sim}{D}^P$ is normal to the yield curve in the $\underset{\sim}{\sigma}$-plane. (More precisely, we can express $\underset{\sim}{D}^P$ as a vector with components $\underset{\sim}{D}^P_I$ and $\underset{\sim}{D}^P_{II}$ equal to the sum and difference of the principal values of $\underset{\sim}{D}^P$. Then equation (3) requires that the principal axes of $\underset{\sim}{D}^P$ and $\underset{\sim}{\sigma}$ are aligned and that the vector (D^P_I, D^P_{II}) is perpendicular to $F(\sigma_I, \sigma_{II}) = 0$ as in Figure 1.) What this means is that for a given $\underset{\sim}{\sigma}$ on the yield curve ($F = 0$), the ratio of shear to divergence D^P_{II}/D^P_I is fixed, but the magnitude of the strain rate $|\underset{\sim}{D}^P|$ can take any value.

Finally, the strain rate decomposition equates the total strain rate $\underset{\sim}{D} = 1/2\ (\partial v_i/\partial x_j + \partial v_j/\partial x_i)$ to the sum of several terms: the elastic strain rate $d\underset{\sim}{e}/dt$, the plastic strain rate $\underset{\sim}{D}^P$, and two terms which allow for spin to rotate the elastic strain tensor, $\underset{\sim}{e}\underset{\sim}{W} - \underset{\sim}{W}\underset{\sim}{e}$, where $\underset{\sim}{W}$ is the spin $1/2\ (\partial v_i/\partial x_j - \partial v_j/\partial x_i)$ [Pritchard, 1975]. Once plastic straining starts, $\underset{\sim}{D}$ tends to $\underset{\sim}{D}^P$. All significant straining is plastic, and in a typical problem, we follow the material through very large plastic deformations.

An additional assumption, required to determine p^*, is that the plastic work equals the rate at which energy is consumed by ridge building. As a ridge is built, some ice must be raised to form the pile above the original top surface of the ice and much more ice must be pushed down to form an inverted pile under the ice. The potential energy thus supplied to the ice cover is not recoverable since ridges usually do not collapse once they have congealed. This process also dissipates some energy in friction as the blocks rub against each other. The rate of energy dissipation by these two mechanisms during pure convergence can be written in the form

$$- K \int_0^\infty h^2 \frac{dW_r(h)}{dh}\, dh \ \text{div}\ \underset{\sim}{v} \tag{4}$$

where K involves the densities of ice and water, the acceleration of gravity, the coefficient of friction between ice blocks, and the slope of the side of a ridge [Rothrock, 1975].

Equating (4) to the plastic work in convergence, $-p^*$ div $\underset{\sim}{v}$, we obtain the expression

$$p^* = K \int_0^\infty h^2 \frac{dW_r(G,h)}{dh}\, dh \tag{5}$$

which determines p^* in terms of the thickness distribution. When we consider this same energy relation for a general strain rate, we find, in addition to a definition for p^*, an expression for the coefficients of the step function and of W_r (in Ψ) in terms of the shape of the yield curve which has been assumed.

THE RESPONSE OF THE MODEL

For given boundary conditions on velocity or stress, we can choose initial conditions for $G(h)$, ς, ϱ and integrate the equations forward in time. Equation (2) updates velocities; equation (1) updates the thickness distribution from which values of mass and strength p^* are calculated; and the solution of the nonlinear constitutive relations provides updated stresses and elastic strains.

To illustrate the response of the model, we consider an idealized one-dimensional case, with no y-derivatives, and boundaries at $x = 0$ and $x = L = 300$ km as in Figure 2. This ice is initially at rest, unstressed and with a uniform typical thickness distribution as in Table 1. We ignore Coriolis force and push the ice against the left-hand boundary ($x = 0$) with a uniform and constant wind stress $\tau_x^a = -0.5$ dyn cm^{-2}.

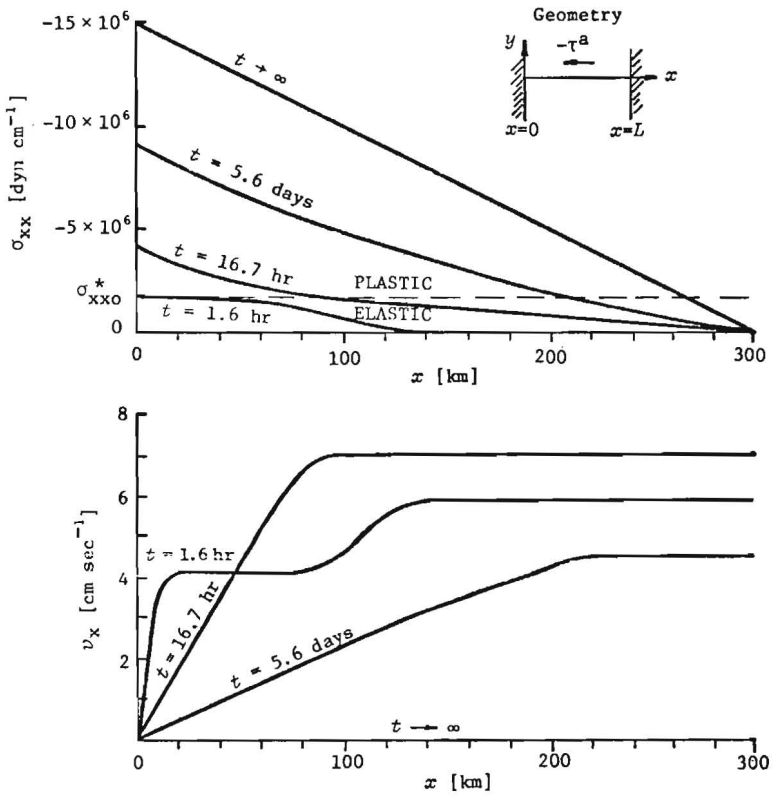

Fig. 2. The response of the AIDJEX model in an idealized case of uniaxial motion.

The solution is shown in Figure 2. As the ice accelerates uniformly toward the wind-driven velocity $\tau_x^a/A = -8.33$ cm sec^{-1}, the stress builds up at the left-hand boundary and propagates out into the pack. Within 1.6 hours, the stress has penetrated about 100 km. The ice to the left of this point moves more slowly than the wind-driven

velocity because of the small opposing stress gradient. The ice tends for a day or so towards the uniform velocity $1/A(\tau_a^x - \sigma^*_{xxo}/L) = -7.3$ cm sec^{-1}, where σ^*_{xxo} is the value of σ_{xx} at failure (*) for the initial thickness distribution (o).

The intense and continued convergence at the left-hand boundary closes up open water and thus strengthens the ice. As this effect accumulates, ice further to the right of the boundary begins in turn to fail and harden. During this phase of the response, the stress can be said to diffuse out into the ice cover with a time scale of about ten days. The plastic region moves to the right with the stress. Asymptotically, the ice comes to rest with the stress distribution $\sigma_{xx} = \tau_a^x (L - x)$.

LOCAL ICE STRESS

With continuum ice models such as the AIDJEX model, time-dependent stress fields can be predicted from an adequate knowledge of the forcing winds and currents. The promise of such prediction for operations in ice-covered seas is great. The relation, however, between continuum stress $\underline{\sigma}$ and local stresses experienced on smaller spatial scales is not well understood. It is the latter quantity which is of interest to the engineer who must design structures to withstand ice stress or ice-breakers to overcome ice pressure. The question addressed in the remainder of this paper is: To what extent can we determine local stress if the continuum stress is known?

While the determination of continuum stress from local stress is a straightforward procedure, the converse problem is quite complex and requires a knowledge of the mechanical constitutive law for each floe and for each floe boundary. Since these would be different for every 100 km element, it seems more reasonable either to seek bounds on the local stress or to investigate its distribution in the probabilistic sense; both approaches will be considered here.

We do not consider conditions in which a structure itself will significantly alter local ice stress. For example, the presence of any intrusion having properties different from those of a typical ice floe will alter the local stress just as the presence of an inclusion in an elastic body causes stress concentrations. The change of local stress will be greater, however, when an external force may be transmitted to the ice; such will be the case for an ice-breaking ship under power or, more importantly, for a structure which is fixed to the ocean floor.

BOUNDS ON LOCAL STRESS BY ENERGY THEOREMS

The problem here and the problem for which energy theorems have been useful is that of estimating the work required to deform a body by known loads and surface displacements without performing a laborious calculation of the full stress field or displacement field within the body. The theorem of Minimum Potential Energy, for example, states that for a linear elastic solid the potential energy calculated for any guessed displacement field is greater than (or equal to) the potential energy for the true displacement field. Similarly, the complementary energy calculated from any assumed stress field is greater than (or equal to) the complementary

energy for the true stress field. More formally: Let an elastic body of volume V and surface S be in equilibrium under body forces F per unit volume, under surface tractions t[2] specified on surface S_t, and under surface displacements $\hat{u}$ specified on surface S_d.

Minimum Potential Energy

Let the actual but unknown displacement field be u, and let u^* be any assumed displacement field compatible with $\hat{u}$ and having strains $e^*_{ij} = \frac{1}{2}(u^*_{i,j} + u^*_{j,i})$. The potential energy U^* $(= U(u^*))$ is defined by

$$U^* = \frac{1}{2}\int_V e^{*T} K e^* dV - \int_{S_t} t^T u^* dS - \int_V F^T u^* dV \tag{6}$$

where K is the stiffness matrix. Then,

$$U^* \geq U \tag{7}$$

where U denotes $U(u)$.

Minimum Complementary Energy

Let the actual but unknown stress field be τ and let τ^* be any assumed stress field consistent with F and t. The complementary energy C^* $(= C(\tau^*))$ is defined by

$$C^* = \frac{1}{2}\int_V \tau^{*T} K^{-1} \tau^* dV - \int_{S_d} t^{*T} \hat{u}\, dS \tag{8}$$

and

$$C^* \geq C \tag{9}$$

If we assume sea ice to be a linear elastic material, we can use these theorems to provide bounds on local stresses. (The upper bound of the crushing strength and the lower bound of zero are self-evident.) To do this, we treat the ice as a heterogeneous material made up of individual constituents--in our case, floes.

A similar procedure has been used previously to obtain bounds on the moduli of heterogeneous material [Paul, 1960], and we begin by reviewing this development. U^* provides a lower bound while C^* gives an upper bound. Suppose we have a heterogeneous elastic body of volume V and surface S made up of N separate constituents, the Ith having a bulk modulus k_I and occupying a fraction of the volume n_I.

For a pressure p and a volume change ΔV, equating internal and external work gives

$$\sum_{I=1}^{N} \int_V \tau_I^T e_I dV = p\Delta V \equiv k\frac{\Delta V^2}{V} \equiv \frac{p^2}{k} V \tag{10}$$

where the bulk modulus k of the body is defined by

$$p = k\frac{\Delta V}{V} \tag{11}$$

---

(2) Indicial notation is used for subscripted expressions while the same quantities without subscript are column vectors. The superscript T denotes the transposed matrix.

Thus, the potential and complementary energy for the composite body can be written

$$U = \frac{1}{2} k \frac{\Delta V^2}{V} - p \int_S \hat{u}\, dS \tag{12}$$

and

$$C = \frac{1}{2} \frac{p^2}{k} V \tag{13}$$

where, here, $\hat{u}$ is associated with ΔV. If, in estimating the potential energy in all of the constituents, we assume a linear displacement field (i.e., a uniform strain field), we find

$$U^* = \frac{1}{2} \sum_{I=1}^{N} k_I n_I \frac{\Delta V^2}{V} - p \int_S \hat{u}\, dS \tag{14}$$

Substituting (12) and (14) into the inequality (7) gives the upper bound

$$k \leq \sum_{I=1}^{N} n_I k_I \tag{15}$$

for the bulk modulus. To estimate the complementary energy, we can assume constant stress, obtaining

$$C^* = \frac{1}{2} \sum_{I=1}^{N} \frac{n_I}{k_I} p^2 V \tag{16}$$

Substitution into the inequality (9) provides a lower bound on the bulk modulus

$$\frac{1}{k} \leq \sum_{I=1}^{N} \frac{n_I}{k_I} \tag{17}$$

In our problem, it is the stress in a floe rather than the bulk modulus which is unknown, and we can use these same theorems to provide bounds on the local stress. Suppose that the local stress is adequately represented by the average pressure p_I in the Ith floe, and that this floe experiences a volumetric strain $e_I = p_I/k_I$. The stress in the composite is represented by its average pressure p which we assume to be given by the continuum stress $\underset{\sim}{\sigma}$. For a two-dimensional material such as pack ice, both p_I and p have dimensions of force/length, and n_I is the fraction of the 100 km area occupied by the Ith floe. The inequalities from these two theorems are now manipulated to find expressions which bound p_I in terms of p.

Applying the theorem of minimum potential energy, we can assume that $e_I^* = \Delta V/V$ for all I. Then U^* is given by (14) while U is just

$$\frac{1}{2} \sum_{I=1}^{N} k_I n_I e_I^2 V - p \int_S \hat{u}\, dS \tag{18}$$

The inequality (7) then provides that

$$\frac{1}{2} \sum_{I=1}^{N} k_I n_I e_I^2 V \leq \frac{1}{2} \sum_{I=1}^{N} k_I n_I \frac{\Delta V^2}{V^2} V \tag{19}$$

which, in terms of stress, becomes

$$\sum_{I=1}^{N} \frac{p_I^2 n_I}{k_I} \leq \frac{p^2}{k^2} \sum_{I=1}^{N} k_I n_I \tag{20}$$

The theorem of minimum complementary energy, with the assumption that $p_I^* = p$ for all I, leads to (16) for C^* while

$$C = \frac{1}{2} \sum_{I=1}^{N} \frac{n_I}{k_I} p_I V \tag{21}$$

The inequality (9) gives

$$\sum_{I=1}^{N} \frac{p_I^2 n_I}{k_I} \leq p^2 \sum_{I=1}^{N} \frac{n_I}{k_I} \tag{22}$$

Both (20) and (22) provide upper bounds on the stresses p_I. If all the k_I equal k, then the two inequalities are identical.

Other upper bounds, or inequalities on p_I, could, in principle, be obtained by assuming different displacement and stress fields; bounds on individual stresses, however, are rather wide. Because every quantity in each term of (20) or (22) is positive, a bound on a particular p_I is obtained by simply removing the summation sign on the left-hand side of either inequality. Thus from (22)

$$p_I^2 \leq \frac{k_I}{n_I} \sum_{J=1}^{N} \frac{n_J}{k_J} p^2 \tag{23}$$

As must be expected intuitively, local stress can be orders of magnitude greater than the continuum stress without violating (23) and is bounded by the crushing strength of ice. In fact, because a typical 100 km square is composed of many continguous floes together with open water, a great variation of stress must be expected and it is unlikely that one can find bounds closer than those given by (23).

It should also be noted that the mean floe stresses which have been bounded may be of less interest than interfloe forces. In fact, the energy formulations can be modified to include interfloe forces which do work through the discontinuities in displacement at floe boundaries. It is a straightforward procedure to rederive the energy theorems to include discontinuous displacement fields at floe boundaries. Thus, for a linear relationship between interfloe forces F_I and interfloe displacement discontinuities, Δu_I, (6) becomes

$$U^* = \frac{1}{2} \int_V e^{*T} K e^* dV + \frac{1}{2} \sum F_I^T \Delta u_I^* dS_I - \int_{S_T} t^T u^* dS - \int_V F^T u^* dV \tag{24}$$

and (7) follows. In the above, the summation in the second term is over all internal floe boundaries. It is known that essentially all of the strain in pack ice originates from interfloe slip or ridging and that the strain in the floes themselves is zero. Accordingly in applying, say, (24) only the second term on the right-hand side would contribute to the internal strain energy. Bounds on the interfloe forces would then follow in a manner similar to that used above for p_I.

PROBABILITY DISTRIBUTION FOR LOCAL STRESS

The lower and upper limits of ice stress are given, respectively, by zero and by the crushing strength of ice (the latter quantity will be assumed here to be a known deterministic quantity), from which, for a given ice thickness, the upper bound on local ice stress is known. As in the preceding section, we will consider only the bulk stress here, but the argument applies to any stress component for which an upper bound and lower bound are available.

The mean of the local stress is, as discussed previously, the continuum stress. In the absence of other available information we wish to obtain the minimally prejudiced probability distribution $f(\tilde{p})$ for the local pressure $\tilde{p}$, that is, the distribution for which the entropy

$$S = -\int_0^{\tilde{p}_u} f(\tilde{p}) \log \tilde{p} \, d\tilde{p} \tag{25}$$

is maximum [Tribus, 1969]. In (25), $\tilde{p}_u$ is the local pressure which, for the thickness of ice under consideration, corresponds to crushing.

The distribution which maximizes (25) subject to the constraints

$$\int_0^{\tilde{p}_u} f(\tilde{p}) d\tilde{p} = 1 \tag{26}$$

$$\int_0^{\tilde{p}_u} f(\tilde{p}) \, \tilde{p} \, d\tilde{p} = p \tag{27}$$

where p is the continuum ice pressure (Backman, personal communication), is

$$f(\tilde{p}) = \frac{\lambda e^{-\lambda \tilde{p}}}{1 - e^{-\lambda \tilde{p}_u}} \tag{28}$$

where λ is obtained from the equation

$$\lambda = \frac{1 - (1 + \lambda \tilde{p}_u) e^{-\lambda \tilde{p}_u}}{p(1 - e^{-\lambda \tilde{p}_u})} \tag{29}$$

Typical distributions are shown in Figure 3. For the case $p = \frac{1}{2} \tilde{p}_u$, $\lambda = 0$, and the distribution is uniform.

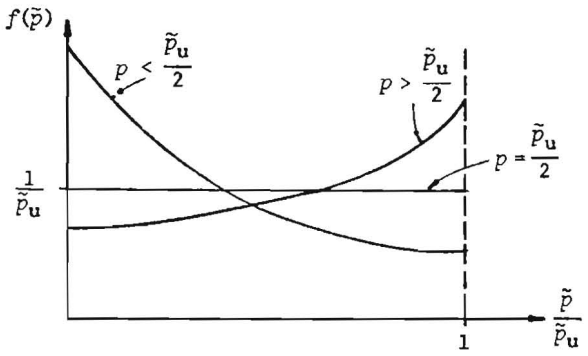

Fig. 3. Distributions of local stress $\tilde{p}$.

For the Arctic pack ice, typical values of p from the AIDJEX model are on the order of 10^7 dyn/cm. For 1 m ice, the crushing strength in compression is more than 10^9 dyn/cm. Thus, even for thin ice, $\tilde{p}_u$ is large compared with p. For such cases, $\lambda \simeq 1/p$, and a close approximation to $f(\tilde{p})$ is the exponential distribution

$$f(\tilde{p}) = \frac{1}{p} e^{-\tilde{p}/p} \tag{30}$$

appropriate for 10 cm ice. For this case, $f(\tilde{p}_u) = 4.5 \times 10^{-12}$ cm/dyn, so that even 10 cm ice will rarely be crushed. For example, the probability that $\tilde{p}$ will be greater than half the crushing strength [i.e. $\int_{.5\,\tilde{p}_u}^{\infty} f(\tilde{p})d\tilde{p}$ with $f(\tilde{p})$ as in equation (30)] is 0.0067.

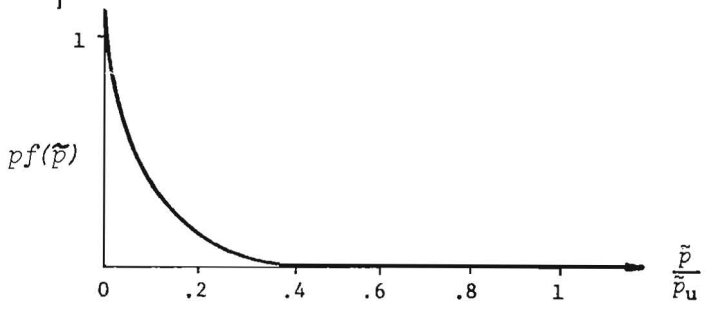

Fig. 4. The distribution $f(\tilde{p})$ for $\tilde{p}_u = 10^8$ dyn/cm and $p = 10^7$ dyn/cm.

CONCLUDING REMARKS

Although the AIDJEX continuum stress is the mean of the local ice stress, large variations in the latter quantity may be expected. There is a small but non-zero probability that crushing may occur at some locations. With regard to the design of structures to withstand ice pressure it would seem that there are cases where the potential cost of failure would justify designing to the crushing strength of ice. There may, on the other hand, be cases where such design is not necessary. An example is the design of an ice-breaking ship. For commercial purposes, a hull designed to withstand the crushing strength of ice might be uneconomically heavy, in which case (30) would provide the basis for a rational probabilistic design procedure.

Similarly, route selection for trans-Arctic shipping could be made on the basis of $\tilde{p}$ and, through (30), on p. This would mean that the stress calculated by the continuum stress would have direct application to operations in ice-covered seas and that the AIDJEX model would become an important aid to ice forecasting.

At the risk of pointing out the obvious, it should be noted that p is basically limited by forces associated with ridging [Parmerter and Coon, 1973] and that the pack is far stronger in compression than it is in flexure. In most cases an economical design of an ice structure results from selecting a geometrical configuration such that ice pressures are withstood by force systems which give rise to flexure in the ice. Flexural cracking then occurs at force levels well below those associated with crushing of the ice.

The AIDJEX model represents a tool which we hope will become increasingly valuable in the many specific problems of design and operations in ice-covered seas. The present consideration of the relation between large-scale stress and local stresses is only an initial step toward applying large-scale ice models to practical engineering problems.

TABLE 1

INITIAL THICKNESS DISTRIBUTION

h (cm)	G
0	.000
25	.004
50	.017
100	.079
150	.149
200	.262
250	.396
300	.522
350	.602
500	.736
1500	.970
2560	1.000

ACKNOWLEDGMENT

The authors would like to thank B. Backman for pointing out the distribution given by equations (28) and (29). This work was supported under National Science Foundation grant OPP71-04031 to the University of Washington.

REFERENCES

Parmerter, R. R., and M. D. Coon. 1973. Mechanical models of ridging in the arctic sea ice cover. *AIDJEX Bulletin*, 19, pp. 59-112. National Technical Information Service No. PB 221 039.

Paul, B. Prediction of elastic constants in multiphase materials. *Transactions of the Metallurgical Society of AIME*, *218*, 36-41.

Pritchard, R. S. 1975. An elastic-plastic constitutive law for sea ice. *Journal of Applied Mechanics*, *42*, E, no. 2, 379-384.

Rothrock, D. A. 1975a. The mechanical behavior of pack ice. *Annual Review of Earth and Planetary Sciences*, *3*, 317-342.

Rothrock, D. A. 1975b. The energetics of the plastic deformation of pack ice by ridging. *Journal of Geophysical Research* (in press).

Thorndike, A. S., D. A. Rothrock, G. A. Maykut, and R. Colony. 1975. The thickness distribution of sea ice. *Journal of Geophysical Research* (in press).

Tribus, M. 1969. *Rational Descriptions Decisions and Designs.* New York: Pergamon Press.

Volkov, S. D. 1962. *Statistical Strength Theory.* (Translated from Russian.) New York: Gordon and Breach.

THIRD INTERNATIONAL SYMPOSIUM ON
ICE PROBLEMS
Hanover, New Hampshire, USA

MEASUREMENT OF SEA ICE DRIFT FAR FROM SHORE USING LANDSAT AND AERIAL PHOTOGRAPHIC IMAGERY

W.D. Hibler III
Research Physicist
W.B. Tucker
Research Geologist
W.F. Weeks
Research Geologist

USA Cold Regions
Research & Engrg.
Laboratory

Hanover
New Hampshire
USA

ABSTRACT

This paper discusses recent work on the development of analysis procedures for obtaining drift and deformation measured from sequential visual imagery of sea ice that is located far from land. In particular for LANDSAT images far from land a semi automatic procedure for transferring the location coordinates of a common set of ice features from the Earth coordinate system of one image to another is discussed. Necessary inputs for the transfer are the location coordinates (latitude and longitude) of the center of each image and the location of two arbitrary points on a known line of longitude; all this information is available from LANDSAT, although with some error. Errors in the transferral technique are examined using imagery over land and are found to be dominated by deviations (as large as 8 km) in the actual position of the center of the image from its stated position. The errors on the average are, however, less than typical one day ice drift distances. The LANDSAT image location errors also introduce uncertainties in the orientation of the coordinate systems after transfer. These errors will produce spurious apparent strains if velocities are estimated by simply taking position differences. This subtle effect may also occur if the coordinate system of a given floe is used as the common coordinate system. A least-squares strain program utilizing polar coordinates, which eliminates such spurious effects, is discussed.

With regard to measuring strain from sea ice aerial imagery without ground control, errors in such measurements are examined using uncorrected photographs obtained during April 1975 by NASA using a

RC-8 camera over the main AIDJEX camp. During the time of the photographic flights a ~7 kilometer "calibration" line was monitored on the ground. The errors in using such uncorrected imagery and using common undeformed ice floes to establish a common scale are found to be of the order of 1% whereas typical maximum differential motions are as large as 5%.

INTRODUCTION

One use of the satellite and aerial imagery of considerable importance for modelling studies is the estimation of sea ice drift and deformation by using sequential overlapping images. Such a use of LANDSAT imagery near land has been discussed by a number of authors (eg. Crowder et. al., (1974); Shapiro and Burns, 1975). In these papers the basic procedure has been to identify common features on sequential images so that relative distance changes can then be measured. If some points on the image of interest are on land then drift rates in addition to deformation rates may be estimated since the land points do not move.

However, when LANDSAT images far from shore are used for analysis, the problem of obtaining both drift and strain rates becomes considerably more difficult. The principal difficulty with drift rate estimation is that no immovable land points are available for "calibration" and consequently one has to use the coordinates of the centers of the images as well as available longitude marks to fix the image locations. In principal the problem of drift then becomes one of first projecting common ice features (on sequential images) onto the spheroid and then back onto a common tangent plane. A somewhat more useful procedure, which we will discuss in this paper, is to transfer the coordinates of both images (considered to be tangent planes) onto a common intermediately located, tangent plane. In practice, such a procedure simply consists of appropriately translating and rotating the polar coordinates of all points in sequential images to the coordinate system of the first image.

The estimation of the strain rate, on the other hand, is dependent in a more subtle way on the transfer of coordinates from one image to another. The key problem here is caused by spurious rotations of the coordinate system that can be induced by errors in longitude lines. Such spurious rotations can also be induced by using a common rotating floe to establish a common coordinate system. The basic problem is that if velocities are estimated by merely subtracting location coordinates in a rectangular coordinate system then such spurious rotations will induce concomitant errors in the diagonal components of the strain rate tensor. Such undesirable effects can be avoided by using an appropriate least-squares strain program in polar coordinates, an example of which will be discussed later.

In the following we will discuss procedures used to estimate the drift and deformation of sea ice from LANDSAT images of areas located far from land. We then briefly examine some results obtained from uncorrected aerial imagery photographed from 9144 m (30,000 ft) altitude.

DRIFT AND DEFORMATION FROM LANDSAT IMAGERY

Drift Rate Estimation

In principle, if the center locations of two sequential overlapping LANDSAT images are known, then drift rates may be estimated by identification of ice features common to both images. One way to do this is to transfer the coordinates from the image planes onto the spheroid, and then onto a common plane. Such a procedure is, however, relatively complex. A simpler procedure, adequate for LANDSAT imagery is to assume that both images are effectively co-planar so that the transfer of coordinates becomes a simple translation and rotation in a given plane.

In particular it is convenient to assume that both images are in the plane whose perpendicular is given by the cross product of the two north vectors tangent to the earth at latitude θ, and parallel to the longitude lines ϕ and ϕ'. The angle between these two vectors defines the angle between the x-axes of the two image coordinate systems for image centers on the same latitude line. For simplicity we also take this angle to be the same if the second image is on both a different longitude line and a different latitude than the first, an assumption inducing errors of order d^3/R^2. By taking an inner product, the angle between these two vectors γ, is given by

$$\gamma = \cos^{-1} \left\{ \cos^2 \theta + \sin^2 \theta \cos [\phi' - \phi] \right\}$$

For small values of $(\phi' - \phi)$ this expression reduces to

$$\gamma \simeq \cos^{-1} \left\{ 1 - \frac{[\phi' - \phi]^2}{2} \sin^2 \theta \right\}$$

$$\simeq \cos^{-1} \left\{ \cos [(\phi' - \phi) \sin \phi] \right\} = [\phi' - \phi] \sin \phi$$

With the above assumptions the geometry for the coordinate transfer is given in Figure 1, where points 1 and 2 are the centers of images 1 and 2 respectively. The angle of rotation between the coordinate systems is given by γ and the translation distance is defined by the chord distances D_1 and D_2 along the latitude and longitude lines. The values of D_1 and D_2 can be calculated from the expressions:

$$D_1 = \frac{2 \sin \left[\frac{\phi' - \phi}{2} \right]}{[\phi' - \phi]} \; D_{LAT}$$

$$D_2 = \frac{2 \sin \left[\frac{\theta' - \theta}{2} \right]}{[\theta' - \theta]} \; D_{LONG}$$

where D_{LAT} is the distance on the International Spheroid between longitude ϕ' and ϕ measured along latitude line θ, and D_{LONG} is the international Spheroid distance between latitudes θ' and θ measured along longitude line ϕ'. Approximate expressions for these distances are given on page 1187 of Bowditch (1958).

In order to give an idea of the errors induced by the approximations in the coordinate transfer procedure, we have compared the distance and angles between a number of points obtained using our LANDSAT projection procedure for both a sphere (referred to as the LANDSAT SPHERE) and the International Spheroid (referred to as the LANDSAT SPHEROID) with the results obtained by using a planar projection onto a fixed plane tangent to point 1. For the spherical cases, we considered point 1 to be at lat 80°, long 0° and have also considered 9 other points, 3 located along lat 80° at increasing distances toward the west, 3 located along long 0° at increasing distances toward the north and 3 located at increasing distances toward the northwest. The results are summarized in Table I with positive angles being measured in a clockwise direction from the x (north) axis. Point 1 is taken to be the origin. In the spherical calculations a radius equal to the average radius of the International Spheroid was used. The great circle distance was computed using the spherical surface. In general, Table I shows that there is very little difference between the various projections with the maximum difference being about 1 km at 600 km. In actual practice the maximum transfer distances are rarely greater than 250 km so that differences in the various projections are hardly significant.

In order to test the transferral technique in actual practice we utilized a number of overlapping LANDSAT images of Alaska. From pairs of such images common land features were identified and their coordinates were transferred from the second image to the coordinate system of the first image. Because the points were "immovable", apparent motions could be identified as errors.

After examination of a number of such image pairs it became apparent that the dominant source of error in the coordinate transfer was caused by deviations between the actual location of the center of the image and its stated location. On the average these positional inadequacies induced errors of the order of one kilometer.

The actual errors obtained from a series of 6 photo pairs are given in Table II. In this table rms errors before and after correcting the location of the center position are given. The center positions were corrected by overlaying the images on accurate survey maps with a zoom transfer scope. As can be seen from Table II, using the actual center position improves the translation errors by about half a kilometer on the average. The actual errors, however, between the true and stated center location can be as large as 8 km. This is illustrated in Table III, which summarizes the center position errors of 17 photographs. The maximum deviation observed was 8.12 km (in the

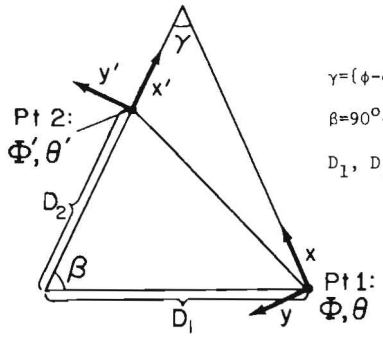

$\gamma=\{\phi-\phi\}\sin\theta$

$\beta=90^{o}-\gamma/2$

D_1, D_2= Chord distances along latitude and longitude lines

Figure 1. GEOMETRY FOR "LANDSAT" PLANAR TRANSFERRAL

TABLE I. COMPARISON OF PLANAR AND LANDSAT PROJECTIONS.

Location of initial pt. 80°N, 0°W.
Radius of Reference Sphere was 6371.299 km

Location of Final Pt		Great Circle Distance	LANDSAT SPHERE Projection		Planar Projection using Sphere		LANDSAT SPHEROID Projection using International Spheroid*	
Long	Lat	Distance	Angle	Distance	Angle	Distance	Angle	Distance
0°W	81.2°N	133.439 km	0°	133.436 km	0°	133.429 km	0°	133.572 km
0°W	82.6°N	289.117	0°	289.092	0°	289.018	0°	289.414
0°W	85 °N	555.995	0°	555.819	0°	555.290	0°	556.415
6°W	80 °N	115.806	-87.046	115.804	-87.045	115.799	-87.044	115.932
14°W	80 °N	269.681	-83.106	269.661	-83.105	269.600	-83.105	269.959
25°W	80 °N	479.030	-77.690	478.917	-77.684	478.579	-77.688	479.446
6°W	81.2°N	172.110	-36.308	172.113	-36.302	172.089	-36.310	172.294
14°W	82.6°N	370.874	-32.413	370.915	-32.390	370.693	-32.411	371.323
25°W	85 °N	651.477	-21.262	651.759	-21.152	650.342	-21.261	652.459

*The parametric latitude values of the points used for the spherical calculations were converted to geographical latitude values for use with the Spheroid program.

TABLE II. RMS TRANSLATION ERRORS.

Photo Pair	Before Center Position Correction ΔX(North)	ΔY(East)	After Center Position Correction ΔX(North)	ΔY(East)
1	1.66 km	1.14 km	.37 km	.11 km
2	2.14	.49	1.22	.49
3	1.63	.49	.72	.15
4	2.43	.24	.53	.13
5	.55	.11	.55	.58
6	.17	.25	.20	.24
Average	1.43 ± .89	.45 ± .37	.60 ± .35	.28 ± .20

TABLE III. SUMMARY OF CENTER POSITION ERRORS FOR 17 IMAGES OVER ALASKA.

	X(North)	Y(East)
Max. Deviation	1.73 km	8.12 km
Min. Deviation	0.20	0.19
RMS Deviation	0.84	3.50

east-west direction). These numbers are in general agreement with the study by Colvocoresses (1974) who has found 1 to 8 km errors in the latitude and longitude center indicators on LANDSAT photos.

The reason that such center errors do not induce greater errors in the transfer appears to be due to the consistency of the offset errors; that is, pairs of photos will have similar errors in both the magnitude and the direction of their center positions. However, there is no assurance that the updating of orbital parameters will not be made in the middle of a sequence.

Deformation Rate Estimation

A convenient way of estimating least-squares strain rates and vorticity has been to note that the x and y ice velocities at position i, (u_{x_i}, u_{y_i}) are related to the strain rate and vorticity by (assuming a linear velocity field)

$$\begin{aligned} u_{x_i} &= x_i \dot{\varepsilon}_{11} + y_i [\dot{\varepsilon}_{12} - w] + A_1 \\ u_{y_i} &= x_i [\dot{\varepsilon}_{12} + w] + y_i \dot{\varepsilon}_{22} + A_2 \end{aligned} \qquad (1)$$

where $\dot{\varepsilon}_{ij}$ is the strain rate defined by

$$\dot{\varepsilon}_{ij} \equiv \frac{1}{2}\left[\frac{\partial u_i}{\partial x_j} + \frac{\partial u_j}{\partial x_i}\right]$$

and w is the vorticity defined by

$$w \equiv \frac{1}{2}\left[\frac{\partial u_2}{\partial x_1} - \frac{\partial u_1}{\partial x_2}\right]$$

A complete discussion of the application of least-squares equations of this type to sea ice deformation is given in Hibler et al. (1974). This approach has the advantage that the velocity points further apart automatically affect the strain-rate estimates more than do velocities of points close together. Also the vorticity is computed in a normal least-squares way.

A drawback to this approach is that if velocities are estimated by merely subtracting location coordinates in a rectangular coordinate system errors will be induced in the strain rate by spurious rotations of the coordinate system. The basic problem can be easily visualized by examining Figure 2. In it we consider three points, which are stationary relative to one another and consequently undergo zero strain. Using the three relative distances between these points we would in fact find a strain rate of zero for all components of the strain rate rensor. However, using rectangular coordinates and equations (1) we would obtain, for a clockwise rotation of θ radians per unit time, the strain rates and vorticity:

$$\dot{\varepsilon}_{12} = 0$$

$$\dot{\varepsilon}_{11} = \dot{\varepsilon}_{22} = \cos\theta - 1$$

$$w = \sin\theta$$

or for a 3° rotation $\dot{\varepsilon}_{11}=\dot{\varepsilon}_{22}= -1.37.10^{-3}$ per unit time. A consistent way around this problem is to calculate the coordinates and velocities of the points in polar coordinates using as the direction of the unit $\hat{r}$ and $\hat{\theta}$ vectors the initial polar coordinates of the points. In particular, if the initial and final positions of a point are given by the polar coordinates (r,θ) and (r',θ') with θ measured clockwise from the y axis, then the x and y velocities are given by

$$u_x = (r'-r)\sin\theta + r[\theta'-\theta]\cos\theta$$

$$u_y = (r'-r)\cos\theta - r[\theta'-\theta]\sin\theta$$

Using these velocity estimates in equation 1, we would obtain (using Figure 2) for a clockwise rotation of θ per unit time

$$\varepsilon_{11} = \varepsilon_{22} = \varepsilon_{12} = 0$$

$$w = [\theta'-\theta]$$

For the general case of many points utilizing least-squares equations based on Equations 1, it can be shown (Hibler et al., 1974) that adding a constant rotation to all angles only changes the vorticity.

Besides the special example considered here, this rotation effect can be illustrated by actual data. Such an illustration is given in Figure 3, where various rotational errors in the coordinate transfer of five common ice features between two LANDSAT images was purposely added. As can be seen, in agreement with the simple example of Figure 2, rotations of 3° can cause significant undesirable effects.

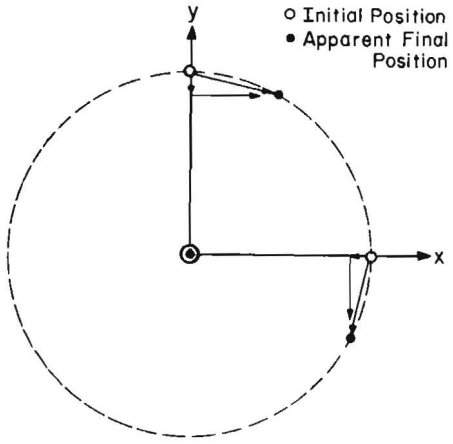

Figure 2. EFFECT OF SPURIOUS ROTATIONS ON ESTIMATED VELOCITIES

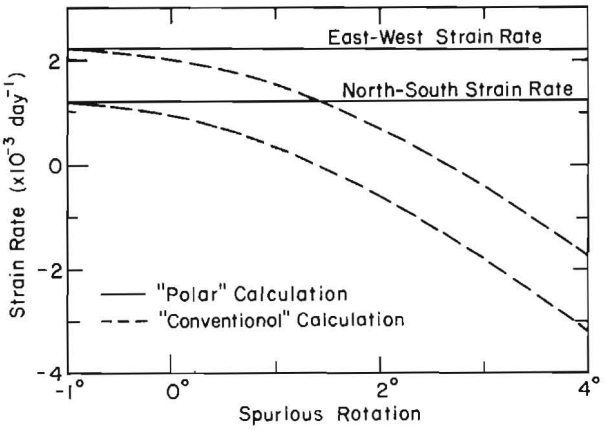

Figure 3. EFFECT OF SPURIOUS ROTATIONS ON ESTIMATED STRAINS

TABLE IV. APPARENT STRAINS ON LAND MASSES.

Units: Percent per day

Photo Pair	$\dot{\epsilon}_{xx}$	$\dot{\epsilon}_{yy}$	Shear	Vorticity
1	-0.069 ± 0.106	-0.276 ± 0.087	0.044 ± 0.069	0.063 ± 0.069
2	-0.178 ± 0.041	-0.033 ± 0.108	0.247 ± 0.058	-0.386 ± 0.058
3	0.024 ± 0.049	0.098 ± 0.053	-0.246 ± 0.036	0.143 ± 0.036
4	-0.241 ± 0.104	0.118 ± 0.098	0.108 ± 0.072	-0.051 ± 0.072
5	-0.142 ± 0.046	0.159 ± 0.053	0.109 ± 0.035	0.294 ± 0.035
6	-0.020 ± 0.157	0.402 ± 0.089	-0.078 ± 0.090	0.125 ± 0.090
RMS	0.139	0.219	0.159	0.215

In using this "polar" technique it should be noted that as long as one chooses one of the points as the origin, where the center of rotation is located has no effect on the results. This is because all lines connecting points will rotate by the same amount regardless of where the center of rotation is located. This will not, however, be true if one chooses for the origin some arbitrary point which may not actually represent a point on the ice.

Although the above procedure allows strain estimates to be independent of coordinate transfer errors, there will nevertheless still be some strain errors because of the registration error in marking common features and the non-linearities in the images. Besides being dependent on such factors, vorticity estimates additionally depend on errors in the orientation estimates of the coordinate systems on the two images.

To make a direct estimate of these errors we calculated least-squares strain and vorticity for the photo pairs used in the above transferral study. The results are shown in Table IV where we list the average strain rates and vorticities (which should be zero since there has been no motion) together with the inhomogeneity errors. As can be seen, on the average the strains are of the order of 0.1 to 0.2% per day which would represent a 0.2 km variation over 100 km, the approximate size of the arrays we were using.

However, not all the error can be attributed to random errors such as the registration errors. If this were the case then the average strain rates in Table IV would cluster around zero with the error being somewhat larger than the average strain. A more consistent way to interpret the results in Table IV would be to say that in addition to registration errors there are certain distortions in the photos. Assuming such distortions are approximately linear, the estimated strain would be equal to the average distortion with the residual error indicative of the registration error. For the six photos analyzed the average residual error is 86 m which is almost exactly the stated resolution (80 m) of the LANDSAT multispectral scanning system. The rest of the strain can be accounted for by saying that distortions induce about 100 m errors per 100 km. Consequently as a practical manner for estimating experimental errors in strain we can assign equal errors of about 100 m to the registration of points (which is in agreement with Colvocoresses (1974) estimates of geometric fidelity) and to image nonlinearities over distances of 100 km.

With regard to vorticity errors the rms vorticity in Table IV was only a little larger than the rms strain rate indicating that rotation effects were relatively minor. However, comparisons of the angles of the line of longitude passing through the center of a LANDSAT image, as obtained from different lines longitude marked on the image, indicate that the estimated andles often differ by 0.01 radian. This effect is somewhat ameliorated by taking the average estimated angle from two

longitude lines located as near to the image center as the image tic marks allow. Still, because of such errors, it would seem safer to assume the experimental vorticity error to be of the order of 0.5% per day.

To illustrate the application of these techniques to actual sea ice drift and deformation measurements, we examined three sequences of images from March 1973 in the region 78°N', 170°W. The starting position and day for each sequence is shown in Figure 4. Seq. 11 consisted of 7 images; Seq. 12, 6 images; and Seq. 13, 4 images. Four to six common ice features were digitized on each sequential image pair and the average drift and deformation calculated. The drift rates are shown in Figure 5. The westward drift rates generally decrease as one moves to the north, a fact which is in general agreement with the clockwise motion of the Pacific Gyre. Also the drift rates are on the average several kilometers a day which is larger than the observed transferral error of about 1 km per day. In general, these drift rates also agree with average drift rates of ice islands which are found to typically drift about 3.6 km/day in this region (Dunbar and Wittmann, 1962).

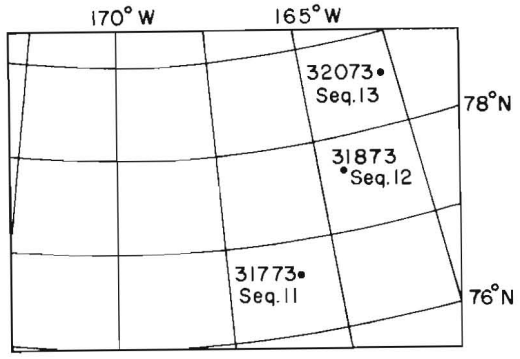

Figure 4. LOCATION OF INITIAL IMAGES IN SEA ICE IMAGE SEQUENCES

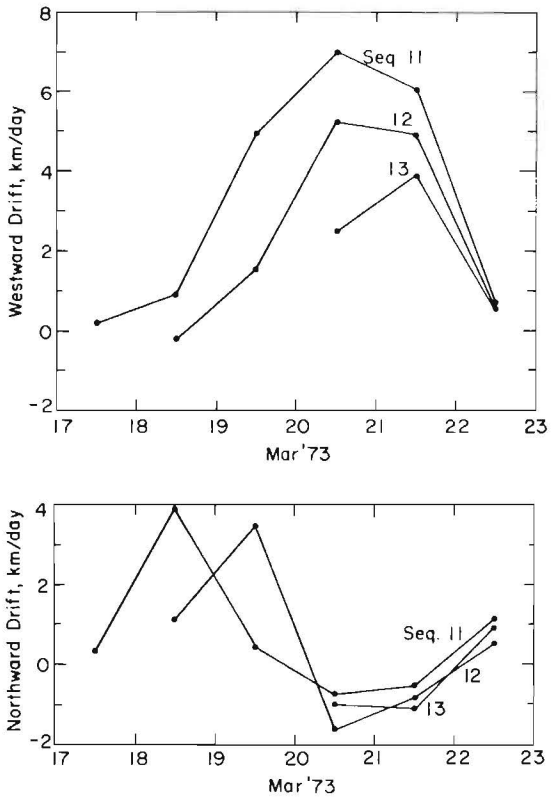

Figure 5. DRIFT RATES FROM SEA ICE IMAGE SEQUENCES

DEFORMATION RATE ESTIMATES FROM AERIAL IMAGERY

Because of its regular orbit, LANDSAT produces imagery which has a consistent orientation and linearity that makes it quite useful for estimating deformation rates. Aerial imagery unless corrected by photogrammetric techniques will have orientation differences due to changes in both the altitude and orientation of the aircraft during the reconnaissance run. To obtain some estimates of how well such uncorrected imagery can be used to measure distance changes bewteen ice features, and hence strain, we have utilized a series of aerial photos take at 9144 m (30,000 ft) by the NASA Convair 990 in April 1975 over the AIDJEX main base camp. On the ice two 40' by 40' black cloth targets were constructed and placed approximately 7 km apart. The changes in the distance between these two targets were measured to an accuracy of $\pm$ 2 meters using two theodolites separated on a baseline of $\simeq$1.5 km in length.

Using six sequential images over the camp relative distance changes between the targets were estimated by comparing the target

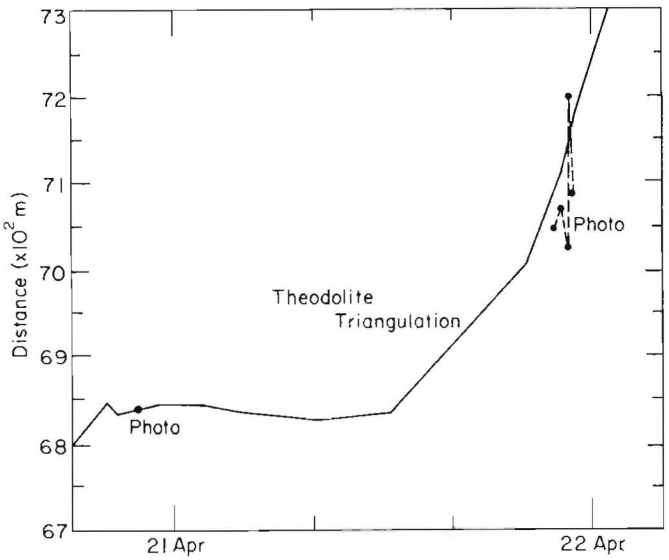

Figure 6. COMPARISON OF PHOTOGRAPHICALLY ESTIMATED DISTANCES TO ACTUAL DISTANCES

distances to distances between fixed "immovable" points on undeformed areas of a multiyear ice floe. In particular, 3 non parallel lines several kilometers in length were identified on a given floe. The average ratio of the lengths of these lines as determined from one photo in the sequence to their lengths as determined in an earlier photo was determined and used as a correction factor to be applied to the distance between the visual targets. The comparison of actual and photo estimated distances are given in Figure 6, where we have assumed the target distance on the first photo to be equal to the actual distance. As can be seen, the photo distances show a spread of about 100 m or 1.5% at 7 km. Although this is a significant error it is still small relative to the actual distance change between the targets which was several hundred meters ($\simeq$ 5%). Another estimate of this type of error was made by examining the variation from photo to photo of the ratios of the three fixed calibration lines among themselves. If there were no errors, these ratios would not change, whereas in practice the standard deviation over 6 photographs varied from 1.7% to 2.2%.

Consequently, these limited results suggest that 2% is a reasonable estimate for the error in measuring distance from high quality aerial imagery without photogrammetric corrections. Because actual sea ice distance changes are often 10% when measured on the small scale, such error can occasionally be neglected. An example of such a case would be a study where only the widths of the leads are important.

CONCLUSIONS

We believe that this study has shown that, when analyzed with appropriate techniques, LANDSAT imagery is adequate for estimating sea ice drift rates at locations far from land. The transferral geometry described in this paper gives a simple and rapid way to transfer coordinates from one image to another with the errors in the transferral equations being negligible over the transferral distances used. In general, the errors in the transferral process are dominated by the deviation of the actual image centers from their stated centers. The effect of such uncertainties, however, is not enough to mask effects caused by typical sea ice drift.

As regards deformation rates, typical results show that it is important to use a least squares procedure that is independent of rotation effects. Also, the magnitude of errors in strain rates, due to experimental errors and non-linearities in the ice velocity field, suggest that two day averages of strain rates should be used when estimating deformation rates from LANDSAT images. When estimating deformation rates from uncorrected aerial imagery of sea ice, typical errors appear to be of the order of 2% which although large are again less than observed differential distance changes as measured on a small scale (several kilometers).

ACKNOWLEDGEMENTS

The authors would like to acknowledge the support of the Arctic Program, Office of Naval Research and of the Office of Polar Programs, National Science Foundation.

REFERENCES

Bowditch, N. (1958) American Practical Navigator. U.S. Navy Hydrographic Office Publication No. 9, U.S. Government Printing Office, 1524 pp.

Colvocoresses, A.P. (1974) Evaluation of the first Earth Resources Technology Satellite (ERTS-1) for cartographic application. Symposium of Commission I (Primary Data Acquisition) of the International Society for Photogrammetry (28 August 1974) Stockholm.

Crowder, W.K., McKim, H.L., Ackley, S.F., Hibler, W.D. and Anderson, D.M. (1974). Mesoscale deformation of sea ice from satellite imager. In "Advanced Concepts and Techniques in the Study of Snow and Ice Resources" (H.S. Santeford and J.L. Smith, eds), p. 563-573, Washington, D.C., National Academy of Sciences.

Dunbar, M. and Wittmann, W. (1963). Some features of ice movement in the Arctic Basin. In "Proceedings Arctic Basin Symposium" (Hershey, Pennsylvania, October 1962), p. 90-104, Arctic Institute of North America.

Hibler, W.D., Weeks, W.F., Kovacs, A. and Ackley, S.F. (1974). Differential sea ice drift I: Spatial and temporal variations in sea ice deformation. Journal of Glaciology 13 (69), 437-455.

Shapiro, L.H. and Burns, J.J. (1975). Satellite observations of sea ice movement in the Bering Strait region. In "Climate of the Arctic" (G. Weller and S.A. Bowling, eds.), p. 379-386, Fairbanks, University of Alaska Press.

THIRD INTERNATIONAL SYMPOSIUM ON
ICE PROBLEMS
Hanover, New Hampshire, USA

SOME MEASUREMENTS OF LATERALLY-LOADED ICE SHEETS

G. D. Rose, Branch Manager
D. M. Masterson, Manager, Arctic Projects
C. E. Friesen, Engineer
Foundation of Canada Engineering Corporation Limited (FENCO)
Edmonton, Alberta, Canada
Calgary, Alberta, Canada

During the spring of 1973 a test load was placed on the ice offshore in the Kristoffer Bay area of Ellef Ringnes Island to study deflection behaviour of the ice sheet. The test load was constructed by filling with water a circular reservoir 50 ft. (15.2 m) in diameter with walls consisting of a snow dyke. At the same time three stratigraphic holes were drilled offshore in the Kristoffer Bay area of Ellef Ringnes Island using the natural ice as a support for the drilling rig. The holes were drilled with a truck-mounted service rig (Kenting Big Indian Rig 3) weighing approximately 135,000 lbs. (62,000 kg). Panarctic Oils Ltd. of Calgary retained FENCO to provide specifications for safe ice loading procedures for the strat holes and to conduct onsite monitoring during drilling, both at the rig sites and at the load test site.

Vertical deflections of the ice were measured at each load site continuously. During drilling a close watch was kept on the time-deflection curves so that accelerating deflection rates and the onset of failure could be detected and the safety of personnel and equipment assured. As well, ice strengths, temperatures and thicknesses were measured regularly.

Procedure

Load Test Pond Construction

To build the Load Test Pond, snow dykes were constructed to a height of 5 ft. (1.5 m) above the existing ice surface

forming an almost circular pond of 50 ft. (15.2 m) diameter. The natural ice thickness was between 6 and 8 ft. (1.8 and 2.4 m) at the test site. The pond was flooded to a total water depth of 4 ft. (1.2 m) above the original ice surface in intervals of 6 to 15 in. (15 to 38 cm). Mean ice temperature varied but measurements show that this difference did not affect the ice sheet deflections under constant load conditions. During flooding, deflections were monitored through the already-installed measuring system. By April 7, 1973, the sea water in the pond was at its final level and the total weight of the experimental load was computed to be 550 tons (500 metric tons). The total volume of the pond was computed by taking 8 thickness profiles on radial lines across the centre of the pond. The exact value of the weight was not calculated from depth alone for two reasons. Some of the sea water leaked through the snow dykes and the ice surface shape was not constant because of the successive deflections beneath the pond itself.

On the upper part of Figure 3 one can see the successive loads of the test pond computed from measurements of the flood depth. A simple depth gauge consisted of a 2" x 4" (5 cm x 10 cm) stake graduated in inches and frozen in the original ice sheet at the edge of the pond for rough control of the built-up ice thickness.

Load Test Pond Deflection Measurements

A system of deflection measurement pillars was set up at the beginning of the loading and the initial measurements were taken simultaneously with the first sea water pumping. The pillars consisted of stakes 2" x 4" x 8' (5 cm x10 cm x2.4 m) frozen in the perpendicular position in the original ice sheet at a depth of about 2 ft. (.6 m). Six-inch and twelve-inch steel rulers were fixed on the two-by-four stakes in a pre-levelled horizontal line.

Deflections were measured on a daily basis by precise levelling using the rulers fixed on the two-by-four stakes. A Wild N_3 level equipped with a micrometer was used for the measurement. Due to a malfunction of the Wild N_3 level, an available Wild T_2 theodolite, corrected for vertical index error, was used later.

Figure 1 "Load Test Pond and Measuring System" shows the arrangement of the measuring pillars aligned in two perpendicular directions, approximately orientated to the North-South and East-West lines and called "E-Line" and "N-Line" respectively.

Results of Test Pond Deflection Measurements

Figure 3 shows a plot of deflection measurements for the first stake of both line "E" and "N" vs. days from start of test.

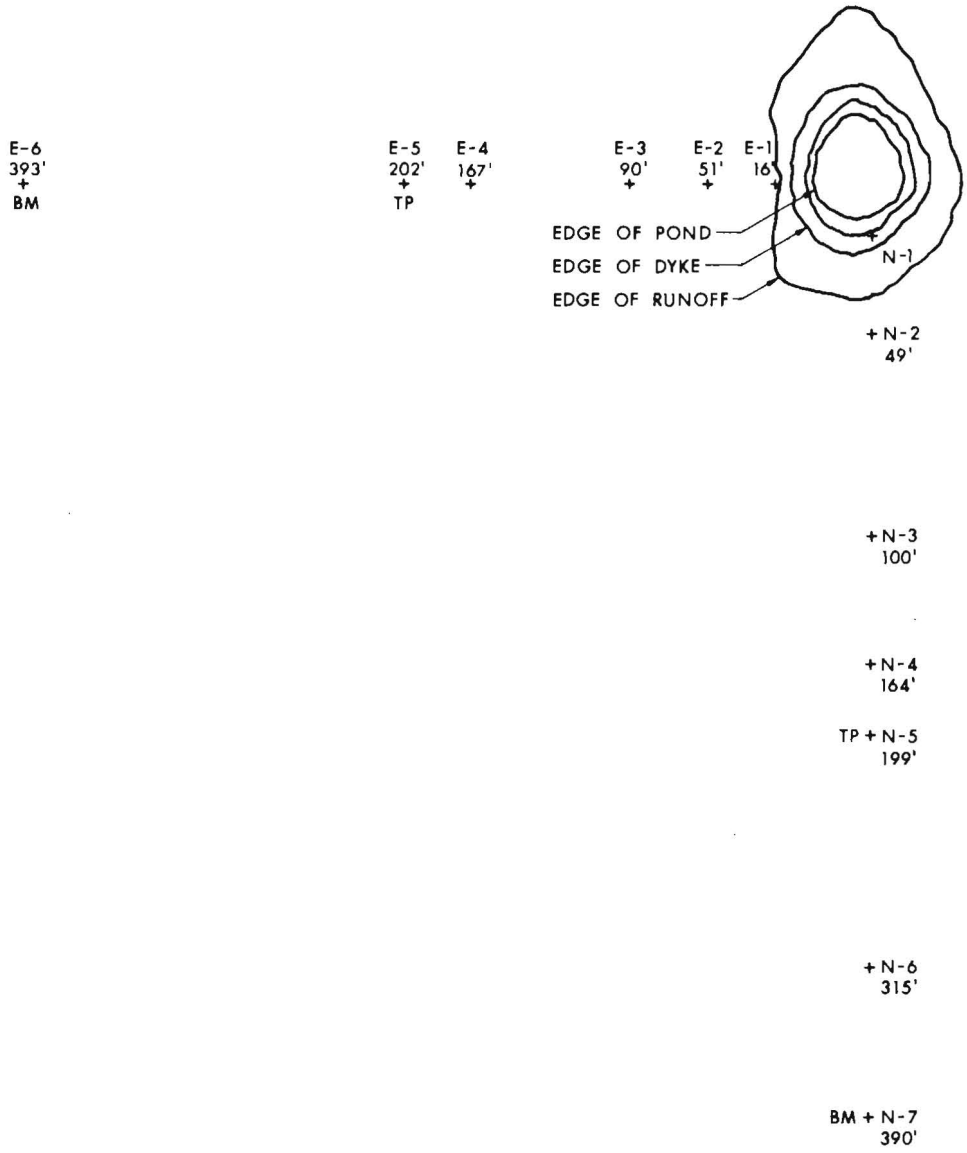

LOAD TEST POND AND MEASURING SYSTEM

FIGURE NO. 1

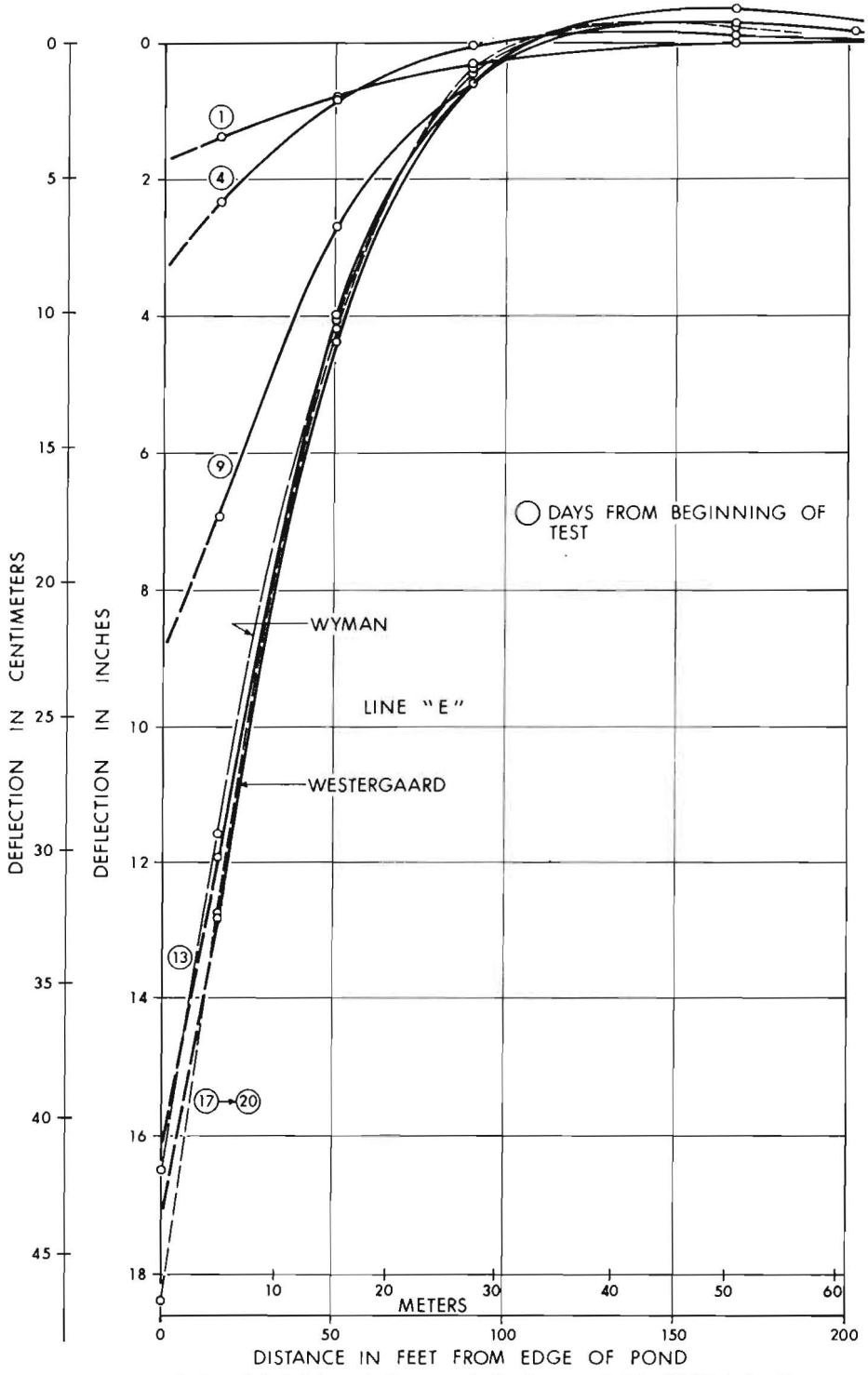

PLOT OF DRAW DOWN CURVE AT LOAD TEST POND

FIGURE NO. 2

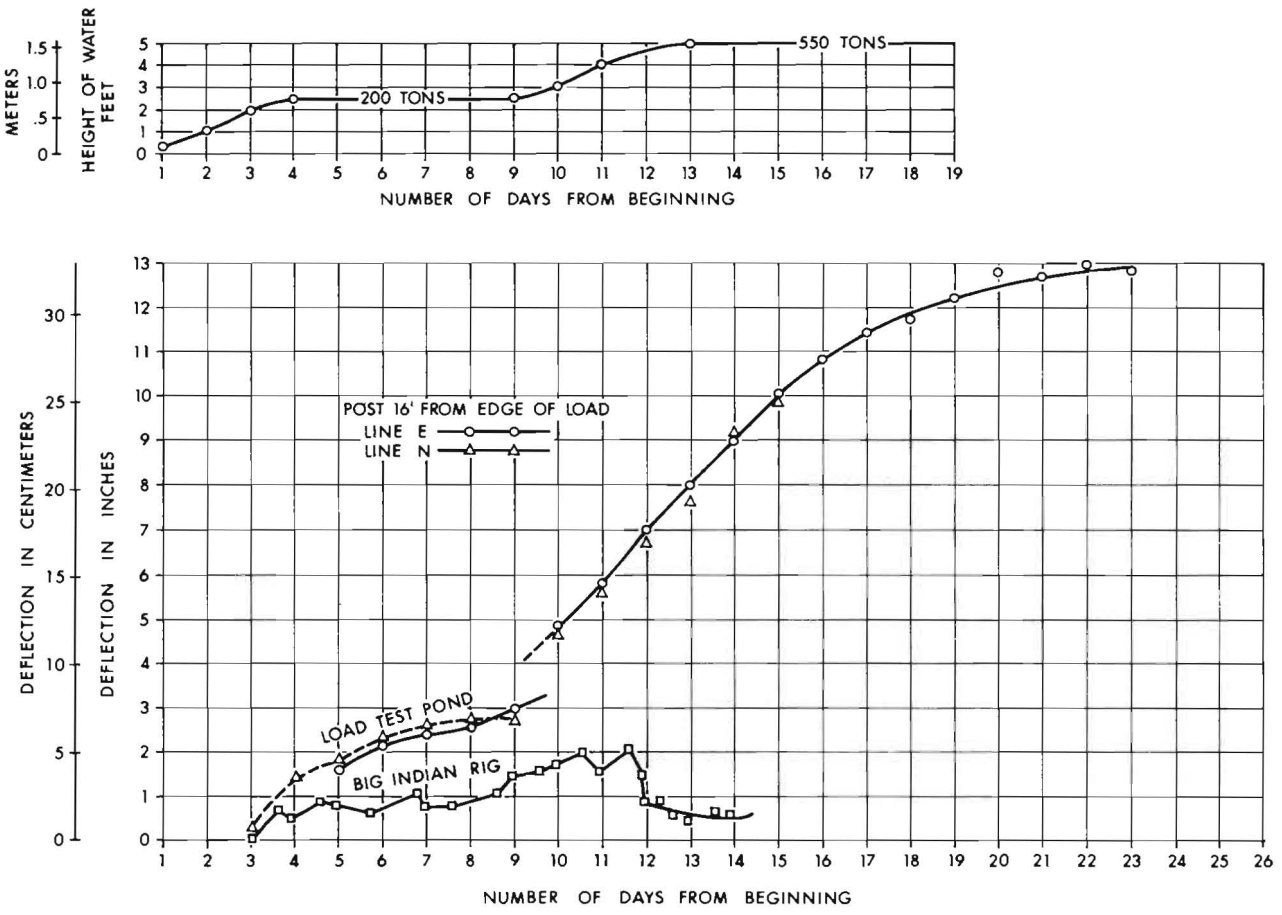

PLOT OF DEFLECTION AT LOAD TEST POND

FIGURE NO. 3

The curve slope is continually decreasing with time as opposed to a failure condition where the slope would tend to increase with time. The curve shows considerably more deflection than the theory for infinite plates on elastic foundations predicts, assuming an elastic material with modulus of elasticity equal to that of ice.

Figure 2 shows the deflections for the first few stations at various times during the loading sequence.

These deflection curves confirm that the ice is behaving in a plastic manner since elastic theory would predict the point of zero deflection to occur at 330 ft (100.0 m) from the edge of the pond when in fact it occurs at 110 (33.5 m) to 115 (35.0 m) feet.

Big Indian Rig #3 Deflection Measurements

A deflection measurement system similar to that used for the Test Pond was installed at the site of Big Indian Rig operations (see Fig. 4).

Figure 3 shows the deflection of the Big Indian Rig at its center as well as the Load Test Pond deflection.

Figure 5 shows the radial deflection profile of the rig load at various times during the L-45 stratigraphic test hole. The initial deflection which occurs when the load is first applied is not included in this curve.

Figure 6 records the deflection of the surrounding ice sheet after the rig was removed. The residual deformations of the ice show clearly that some deflection was due to plastic deformation. Deflections were monitored every 8 hours for a period of 48 hours after the rig was removed.

During the second half of May, 1973 deflection measurements were performed at two other stratigraphic hole locations. The main purpose for these measurements was to monitor deflection to ensure the safety of the rig. The results of these measurements were inconclusive and have not been shown .

Theoretical Analysis of Measured Deflections

The mathematical analysis of the measured deflections was based on elastic theory. Sea ice behaves elastically during short-term loading and plastically if the load remains for a prolonged period. Plastic analysis is very complex and hence it is advantageous to treat the problem as an elastic one if possible. Since the ultimate plastic deflection is what is

BIG INDIAN RIG No. 3 LAYOUT

STRATIGRAPHIC HOLE L - 45

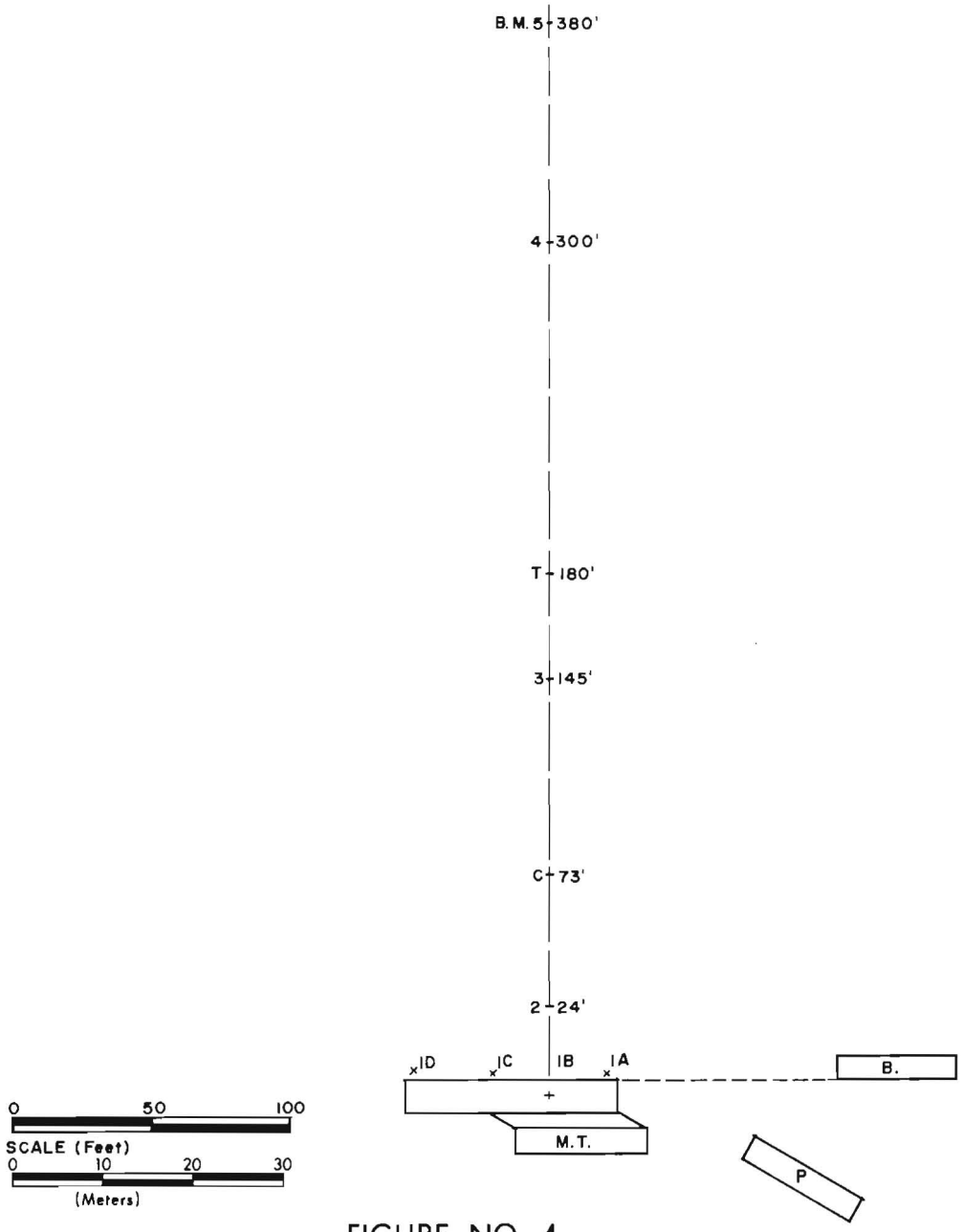

FIGURE NO. 4

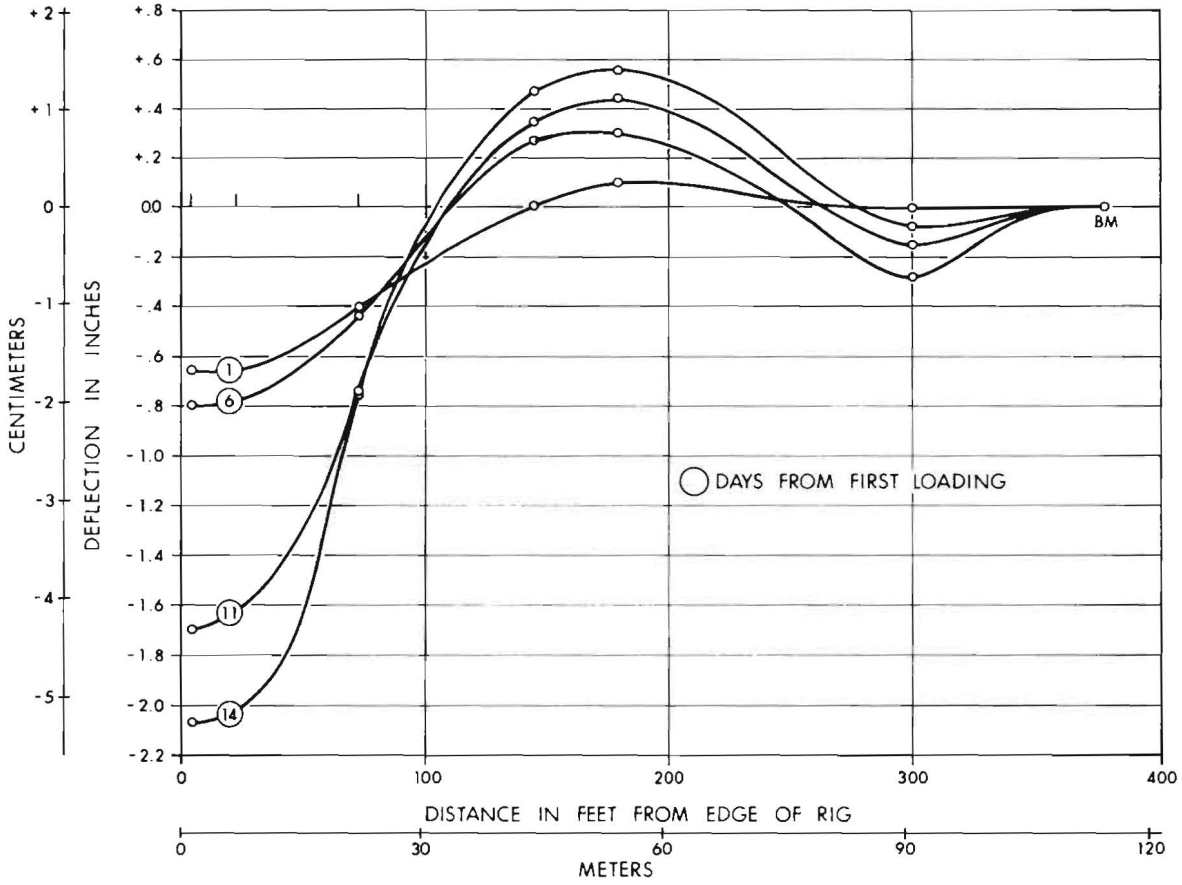

RADIAL DEFLECTION CURVE OF ICE SHEET AT BIG INDIAN 3 RIG – STRAT HOLE L-45

FIGURE NO. 5

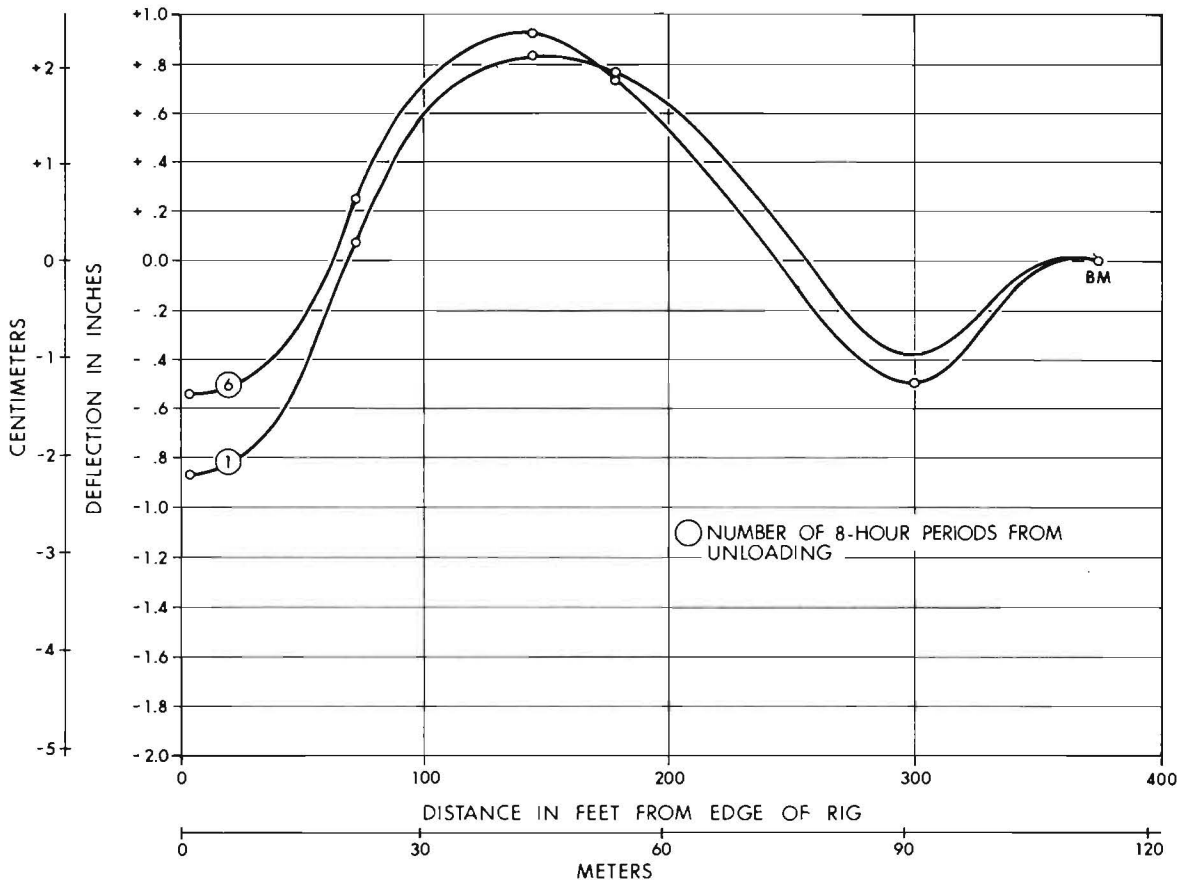

REBOUND OF RADIAL DEFLECTION CURVE OF ICE SHEET AT BIG INDIAN 3 RIG STRAT HOLE L-45

FIGURE NO. 6

required, an attempt was made to fit the elastic theory to the equilibrium deflection measured in the field.

The factor varied to make elastic theory fit was E, the elastic modulus. Cold, low salinity sea ice has an elastic modulus under short-term loading of about 6.0×10^5 psi (4.2×10^4 kg/cm^2).

Westergaard's (1926) theory for plates on elastic foundation was used initially.

This theory gives deflection of a plate equal to:

$$\delta = \frac{P}{KL^2} \times R$$

where:

$$L = \left(\frac{Eh^3}{12(1-\mu^2)K} \right)^{\frac{1}{4}}$$

P = total load on plate

K = modulus of subgrade reaction

L = radius of relative stiffness

R is a factor accounting for distance from load which Westergaard presents in a graph. Its value is 1/8 at the center.

h = plate thickness

μ = poissons ratio for the plate

E = elastic modulus

From the diagram in the Westergaard paper we see that R and deflection are zero at a distance of about four times the radius of relative stiffness. Using the expression for L above and the diagrams of measured deflection we can find a value for E.

$$E = \frac{L^4 \times 12(1-\mu^2)K}{h^3}$$

for this case:

$\mu = .3$

$K = .037$ lb/in^3 (1.0×10^{-3} kg/cm^3)

$h = 84$ in (213 cm)

The zero point for the load test pond from Figure 2 is at 135' (41.1 m). Therefore L is about 45' (10.4 m) and E is 2.0×10^4 psi (1.4×10^3 kg/cm^2). Using Westergaard's function for deflection a value of E of 1.5×10^4 psi (1.0×10^3 kg/cm^2) gives a close approximation to the measured final deflection line (see Fig. 2).

Another relation was also used to approximate the deflection line. Westergaard theory assumes a point load; however, theory put forth by Wyman (1950) includes the variable of load radius as follows:

$$\delta_r = \frac{P}{\pi a L} \times \frac{1}{K} \left[ber'\,(a/L)\ ker\,(r/L) - bei'\,(a/L)\ kei\,(r/L) \right]$$

a = load radius

r = deflection radius

ber', bei', ker, kei = Bessel functions (McLachlan, 1934)

A value of E of 1.5×10^4 psi again gives a good approximation as seen in Fig. 2.

E of 1.5×10^4 (1.0×10^3 kg/cm^2) seems to be a safe value then. This is 1/40 the short term E of 6×10^5 (4.2×10^4 kg/cm^2).

Using 1.5×10^4 psi (1.0×10^3 kg/cm^2) as E to predict the deflection under the Big Indian Rig we get deflection of 3.1 in (7.9 cm). The Fig. 5 indicates plastic deflection of 2.1 in (5.3 cm) and Fig. 6 shows elastic rebound of 1.2 in (3.0 cm) [2.1 in (5.3 cm) - .9 in (2.3 cm)]. This gives a total deflection of 3.3 in (8.4 cm). The extra .2 in (.5 cm) deflection can be explained by the considerable and variable live load of a drill rig which probably caused extra plastic deflections.

Conclusions

The above analysis of the field measurements indicates that elastic plate theory loads can be used to predict the ultimate deflection of an ice sheet under longer term vertical loading. Both elastic and time dependent deformations can be estimated by reducing the value of the modulus of elasticity. Short term, elastic deflections can be approximated by simply using the elastic modulus for ice commonly found from short time small scale or sonic tests.

In the two cases of loading, theoretical deflections closely approximating the measured ones were computed using a modulus of about 1/40 the initial value after corrections had been made for initial deflections and variable load effects.

This good agreement between an empirical theoretical analysis and experimental measurements verifies the earlier stress calculations performed before the rigs were placed on the ice. Future estimations of ice stresses and deflections can be calculated with some confidence using similar methods.

Since this work was done in 1973, similar methods have been used to successfully design ice pads to support a much larger rig weighing about a million pounds. Two offshore deliniation wells have been drilled by Panarctic in the Canadian Arctic Islands using these pads.

References:

1. McLachland, N.W. Bessel Functions for engineers. Oxford University Press, London, New York, Toronto. 1934.

2. Westergaard, H.M., "Stresses in Concrete Pavements Computed by Theoretical Analysis", Public Roads, Vol. 7, 1926.

3. Wyman, M., "Deflections of an Infinite Plate" Canadian Journal of Research, Vol. A28, 1950.

THIRD INTERNATIONAL SYMPOSIUM ON
ICE PROBLEMS
Hanover, New Hampshire, USA

ALASKAN ARCTIC COAST ICE AND SNOW DYNAMICS AS VIEWED BY THE NOAA SATELLITES

Douglas L. Kane, Research Hydrologist — Institute of Water Resources, Fairbanks, Alaska
Robert F. Carlson, Director
Richard D. Seifert, Research Hydrologist — University of Alaska — 99701

ABSTRACT

Coastal processes associated with ice dynamics along the northern coast of Alaska are not well understood. Transportation planning and future construction require that additional environmental data be obtained for this region. Discussed in this paper are various ice-related applications made with the imagery from NOAA series satellites for this coastal region.

INTRODUCTION

The rapidly developing energy exigency and the imminent development of transportation schemes have given rise to data needs related to ice conditions along the northern coast of Alaska. This is an area of very sparse hydrological and climatological data. Near-coastal information on ice conditions is of present interest to summer barge traffic, winter overland traffic, and general scheduling of construction and exploration activities. It is also necessary to have an understanding of the ice/water dynamics for assessing the environmental changes caused by pollutants in the course of this development.

It is evident that future exploration will proceed both along the coast as well as offshore in the Beaufort Sea, resulting in additional barge traffic and permanent engineering structures spanning the major river systems of this area. The utilization of remote

sensing techniques is a logical choice for observing the ice dynamics of this region. Discussed in this paper are the specifications and ice-related applications of the NOAA series VHRR (Very High Resolution Radiometer) satellites, with special emphasis on near-coastal studies.

Studies related to ice dynamics in the Arctic Basin have been augmented by the application of remote sensing with satellites. Several papers discuss the earlier work using TIROS, ESSA, NIMBUS, Air Force DAPP, and ERTS imagery (Wendler, 1973; Barnes *et al.*, 1972; Shapiro and Burns, 1975; and DeRycke, 1973). While the resolution of the earlier weather satellites was too coarse for detailed studies, ERTS imagery provided excellent resolution. The main disadvantage of ERTS imagery was the 18-day time period between overpasses. McClain (1974, 1975) discusses the capabilities of the NOAA (VHRR) satellites and gives special attention to sea ice analysis.

NOAA SATELLITE CAPABILITIES AND PRODUCT DEVELOPMENT

The NOAA series satellites are in polar, sun-synchronous orbits. Satellite imagery is transmitted to a data acquisition station at Gilmore Creek, near Fairbanks, Alaska, three to four times each day, and coverage is possible over northwestern Canada and Alaska (a span of 1700 km x 6000 km). Other ground stations exist and limited storage of data is possible within the satellite. On board the satellite are many sensors - among them, the VHRR used to acquire the imagery in this study. The VHRR is designed to provide operational coverage in two bands, the visible (0.6-0.7 μm) and the thermal infrared (10.5-12.5 μm). Resolution is 900 meters at nadir. Both the infrared (IR) and visible imagery are produced very nearly simultaneously (one scan line out of phase), and are quite easy to compare. They have the added advantage of being synoptic.

Most of the present work with NOAA-VHRR imagery has been done using the visible band imagery. However, recently it has become possible to calibrate the IR imagery and measure the surface temperatures with an accuracy of 1°C. When there is a substantial temperature difference of the radiating surface, the infrared imagery is capable of illustrating this clearly. Several alternatives are available for enhancing the product. First, the images can be enlarged; the sharpness of the image can be partially retained in enlargements by presenting each scan line twice (Figure 1). Additionally, more than one gray scale can be used when printing the image. The capability exists to define the temperature range to be represented by each gray scale. A particular temperature range or temperature may be further enhanced by choosing a black on white display. Using more than two gray scales on one image, however, makes it very hard to interpret the results.

NEAR-SHORE ICE AND SNOW DYNAMICS

Satellite imagery is a valuable tool for studying the large-scale ice movements in the Arctic Ocean and adjacent seas. However, at this time, information is greatly needed on the river-coastal ice interaction; this is the zone of present activity, both in shipping and exploration.

Breakup in the Alaskan Arctic is initiated in the mid-elevations of the Brooks Range. This runoff reaches the coast while snow cover is still present on the ground and there is no deterioration of sea ice. Runoff from the river flows out over the sea ice, flooding a very large area, while the snowmelt continues both toward the coast and toward higher elevations. Sediment carried by the streams is deposited on top of the ice and eventually the water that carried the sediment drains through holes (strudels) in the sea ice which have developed in seal vents or along cracks. Prior to surface flooding, the ice may be in contact with the sea bottom, particularly in areas less than 2 m deep. In deeper water, the flooding water acts as a surcharge, deforming the sea ice. Once the water drains through the strudels, the ice is lifted vertically. This movement, as well as the sediment that was deposited on the surface, helps to deteriorate the nearshore ice.

A number of specialized studies have been carried out along the northern Alaskan coast. Walker (1972), by observation and salinity measurements, determined that surface flooding extended 12 to 18 km from the Colville River delta while a wedge of fresh water developed over the more dense salt water beneath the sea ice. This wedge extended 35 to 40 km northward from the delta. He reports that this water moved northward beneath the sea ice at a rate of 4 to 5 cm/sec. Reimnitz *et al.* (1974) and Barnes and Reimnitz (1973) studied the phenomena of strudel development. They found that most strudels develop within 30 km of river mouths, forming depressions in the sea floor more than 4 m deep and 20 m or more in diameter. They carried out their work principally in the bays off the Colville, Kuparuk, and Sagavanirktok Rivers. Reimnitz and Bruder (1972) made reconnaissance observations of river discharge and related sediment dispersal into the Beaufort Sea. Similar work was carried out by Short and Wiseman (1975). Data on arctic hydrology of these rivers is found in a report by Kane and Carlson (1973) and in various U.S. Geological Survey data reports for Alaska.

ICE AND SNOW RELATED APPLICATIONS OF SATELLITE IMAGERY

The NOAA-VHRR imagery became operationally available in February, 1974. Since that time we have had the opportunity to study two spring breakup sequences over a span of 1-1/2 years. This series of satellites has been used to study a number of dynamic ice-linked processes. Because of the area of coverage of this satellite, it is an obvious choice for studying macro-scale dynamics in the Arctic Ocean (Figure 2).

Only infrared imagery is obtained during periods of low sun angle. Although near-coastal activity is minimal in March, large quasi-elliptically shaped leads develop in the Arctic Ocean from Barrow to the southwest coast of Banks Island of the Canadian Archipelago. Due to the wide variation in surface temperatures, these leads are very detailed on the infrared imagery. Gradual refreezing of the leads is apparent by changes in the gray tones. The development and disappearance of leads can be followed throughout the winter months. These leads are very close to the coastline at Barrow, but farther east they gradually diverge from the coast, the zone of shorefast ice increasing in width. The extent of shorefast ice varies with the time of year and during late spring new leads develop much closer to the coastline.

Coastal activity starts in late May following the sequence of snowmelt runoff from the Brooks Range. Snowmelt first is apparent in upper valleys in the Brooks Range in late April and early May. The first river discharging flow into the ocean is the Sagavanirktok River, around May 20. Other rivers in this vicinity, Kuparuk, Canning, Colville, and Putuligayuk, follow within ten days and the rivers and streams draining the arctic coastal plain near Barrow are still later. Snow-free areas are best mapped from enhanced IR imagery. The techniques that we found most useful was to indicate the 0-1°C isotherm as a white stippled area on the image while temperatures above this range were represented as black. An ascending gray scale was utilized for the temperatures below 0°C. Areas with no snow would be indicated as black when adjacent to a white stippled contour on the image (Figure 3).

The NOAA satellites have been very useful for mapping the area flooded at the mouths of various rivers (Table 1). Both water and the silt load carried by the water accelerate the rate of ablation

Table 1: Area (km^2) of Sea Ice Flooded by Freshwater

Date	Kuparuk River	Sagavanirktok River	Colville River
21 May 74	-	61	15
26 May 74	10	151	50
4 June 74	30	185	61
6 June 74	30	40	120
4 June 75	101	208	219
9 June 75	69	179	276

of the ice. For the most part, open water areas that develop along the coast are confined to the region between the coast and offshore barrier islands. In late July the ice begins to retreat northward from the coast. At this time there is very little difference in the temperature of open water and surface ice; therefore, the visible imagery is far better for discerning this boundary. Also, the presence of low stratus clouds and light fog often obscure the coast

in summer, making IR observation impossible, but still allowing visible band observations. By late October, when new sea ice forms, complete ice cover is achieved, and only the new leads give any indication of activity in this region.

It has been stated that the NOAA imagery is excellent for determining areal extent of snow cover; this data is useful for monitoring coastal runoff processes. Once the snowpack has ablated substantial temperature differences exist between the rivers and surrounding ground during the summer months. The ground temperatures are much higher than the river water or aufeis. Melting aufeis and snowmelt water from higher elevations are sources of runoff water throughout the summer. Large aufeis fields exist in the Sagavanirktok drainage and have been located and mapped using this imagery. It should be noted that the spring snowmelt runoff event is by far the most dynamic and impressive hydrologic event in the Arctic. It is this event that has the greatest impact on coastal ice processes.

CONCLUSIONS

Various remote sensing applications of the NOAA series satellites for studying coastal dynamics on the Alaska arctic coast have been discussed. With satellite imagery, it has been possible to monitor the growth and disappearance of leads, to determine the location and rate of snowpack ablation, to measure the extent of flooding over the sea ice by fresh water, to follow the retreat and return of the solid ice along the northern coast, and to map the extent of aufeis in the Sagavanirktok Basin. At the present time, almost all activity is confined to a narrow ribbon along the coast. The need for additional hydraulic and hydrologic data is documented, and the NOAA satellite imagery is one very productive method of acquiring some of this information.

ACKNOWLEDGEMENT

This project was supported by a grant from the National Oceanic and Atmospheric Administration (NOAA), National Environmental Satellite Service (NESS).

REFERENCES

Barnes, J. C.; Chang, D. T.; and Willand, J. H. (1972). Image Enhancement Techniques for Improving Sea-Ice Depiction in Satellite Infrared Data, *Journal of Geophysical Research, 77*, 3, pp. 453-462.

Barnes, P. W. and Reimnitz, E. (1973). New Insights into the Influence of Ice on the Coastal Marine Environment of the

Beaufort Sea, Alaska. *Proceedings Symposium on Significant Results Obtained from the Earth Resources Technology Satellite -1*, NASA, pp. 1307-1314.

DeRycke, R. J. (1973). Some Seasonal Variations of the Ice Cover in Beaufort Sea: Evidence of Macroscale Ice Dynamics Phenomena. AIDJEX Bulletin 18, pp. 46-50

Kane, D. L. and Carlson, R. F. (1973). Hydrology of the Central Arctic River Basins of Alaska. Institute of Water Resources, University of Alaska, Report No. IWR-41.

McClain, E. P. (1974). Some New Satellite Measurements and Their Application to Sea Ice Analysis in the Arctic and Antarctic. *Proceedings Symposium Advanced Concepts and Techniques in the Study of Snow and Ice Resources*, National Academy of Sciences, pp. 457-466.

McClain, E. P. (1975). Environmental Research and Applications Using the Very High Resolution Radiometer (VHRR) on the NOAA-2 Satellite - A Pilot Project in Alaska, *Climate of the Arctic*, Twenty-fourth Alaska Science Conference, University of Alaska, pp. 415-429.

Reimnitz, E. and Bruder, K. F. (1972). River Discharge into an Ice-Covered Ocean and Related Sediment Dispersal, Beaufort Sea, Coast of Alaska. *Geological Society of America Bulletin, 3*, pp. 861-866.

Reimnitz, E.; Roderick, C. A., and Wolf, S. C. (1974). Strudel Scour: A Unique Arctic Marine Geologic Phenomena, *Journal of Sedimentary Petrology, 44*, 2, pp. 409-420.

Shapiro, L. H. and Burns, J. J. (1975). Satellite Observations of Sea Ice Movement in the Bering Strait Region. *Climate of the Arctic*, Twenty-Fourth Alaska Science Conference, University of Alaska, pp. 379-386.

Short, A. D. and Weisman, W. J., Jr. (1975). Coastal Breakup in the Alaskan Arctic, *Geological Society of America Bulletin, 86*, pp. 199-202.

Walker, H. J. (1973). Spring Discharge of an Arctic River Determined from Salinity Measurements Beneath Sea Ice. *Water Resources Research, 9*, 2, pp. 474-480.

Walker, H. J. (1973). Salinity changes in the Colville River Delta, Alaska During Breakup. Symposium - *The Role of Snow and Ice in Hydrology*, IAHS-UNESCO-WMO, pp. 514-527.

Wendler, G. (1973). Sea Ice Observations by Means of Satellite, *Journal of Geophysical Research, 78*, 9, pp. 1427-1448.

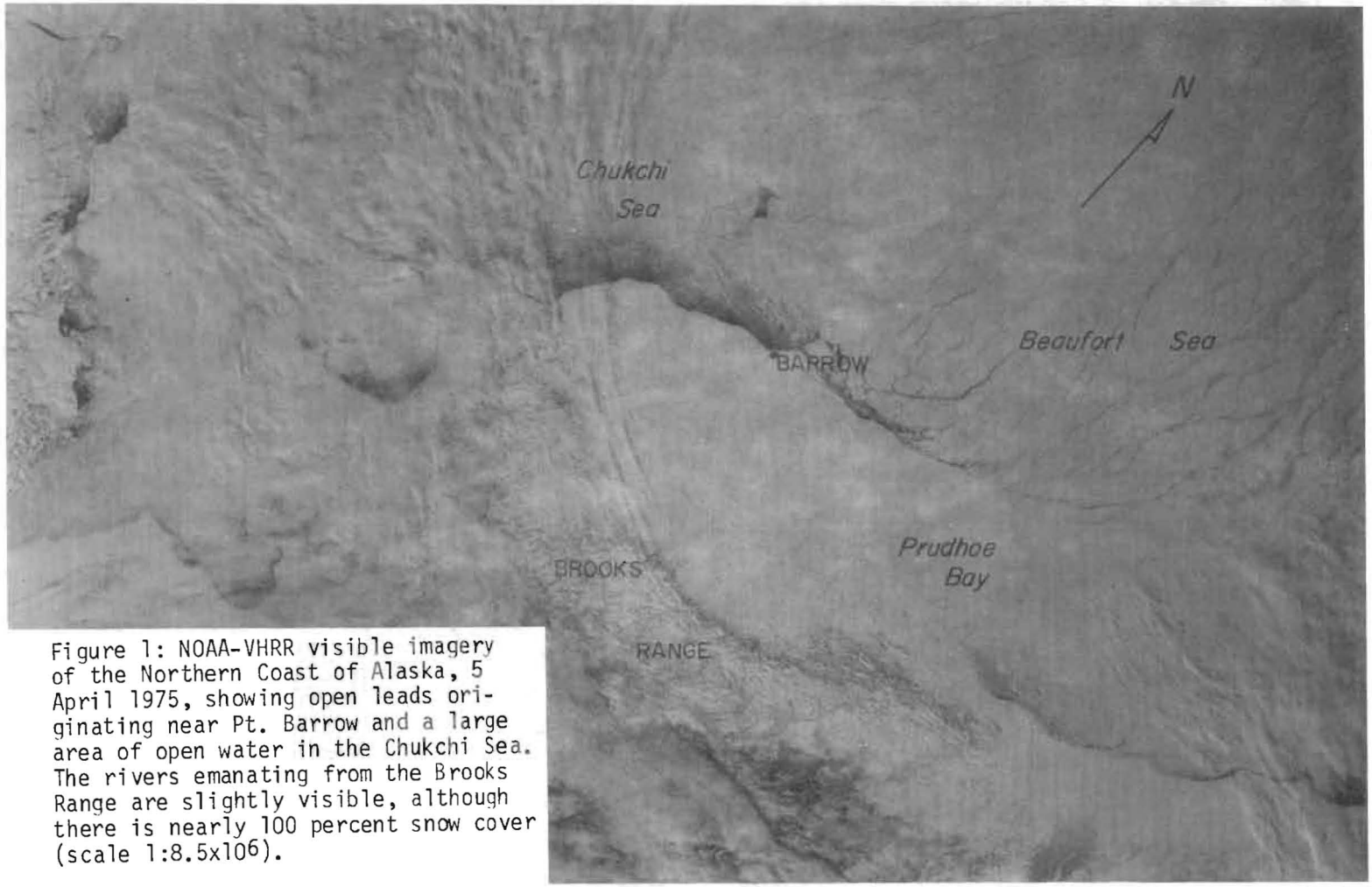

Figure 1: NOAA-VHRR visible imagery of the Northern Coast of Alaska, 5 April 1975, showing open leads originating near Pt. Barrow and a large area of open water in the Chukchi Sea. The rivers emanating from the Brooks Range are slightly visible, although there is nearly 100 percent snow cover (scale 1:8.5x10^6).

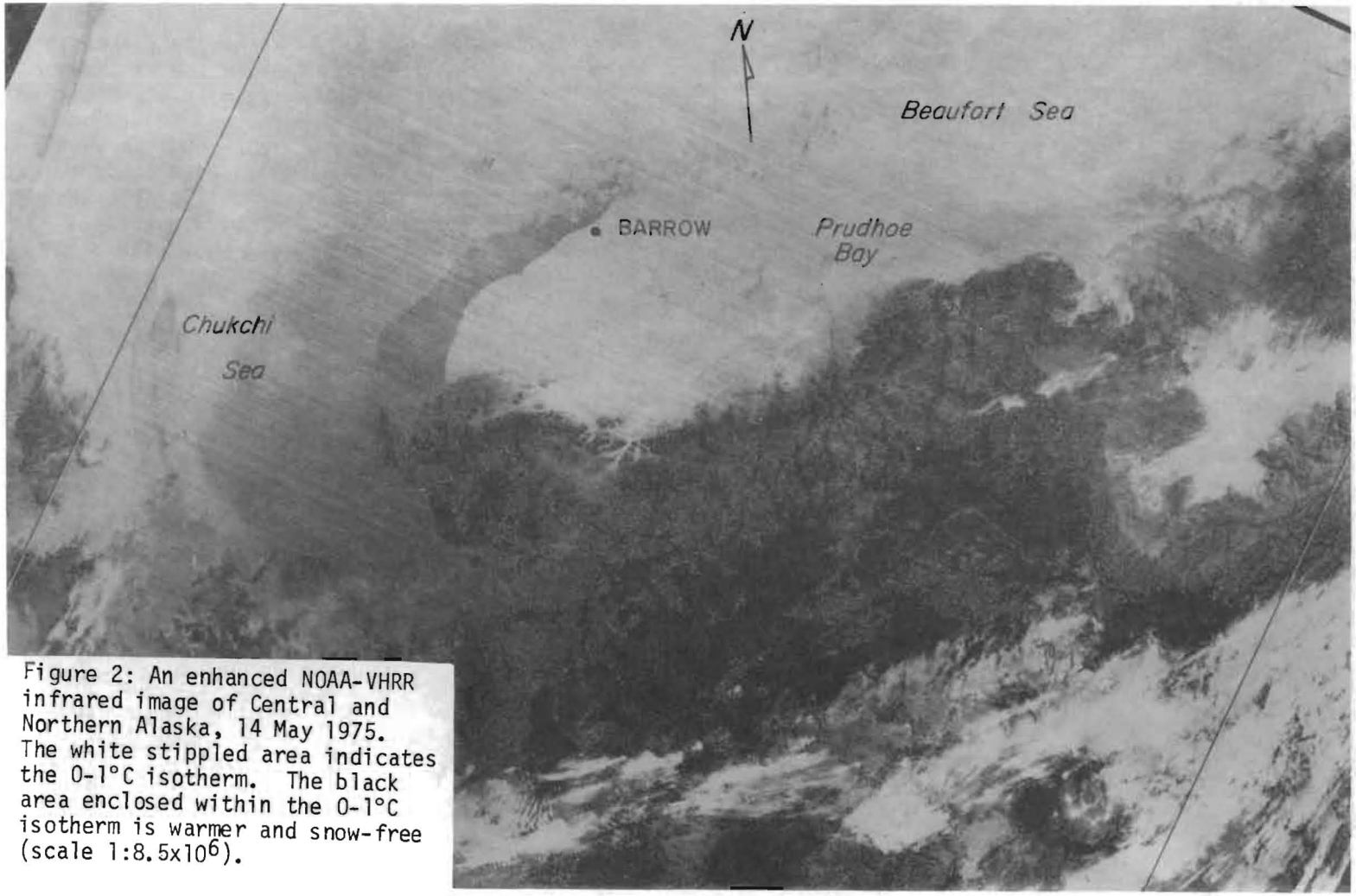

Figure 2: An enhanced NOAA-VHRR infrared image of Central and Northern Alaska, 14 May 1975. The white stippled area indicates the 0-1°C isotherm. The black area enclosed within the 0-1°C isotherm is warmer and snow-free (scale 1:8.5x10^6).

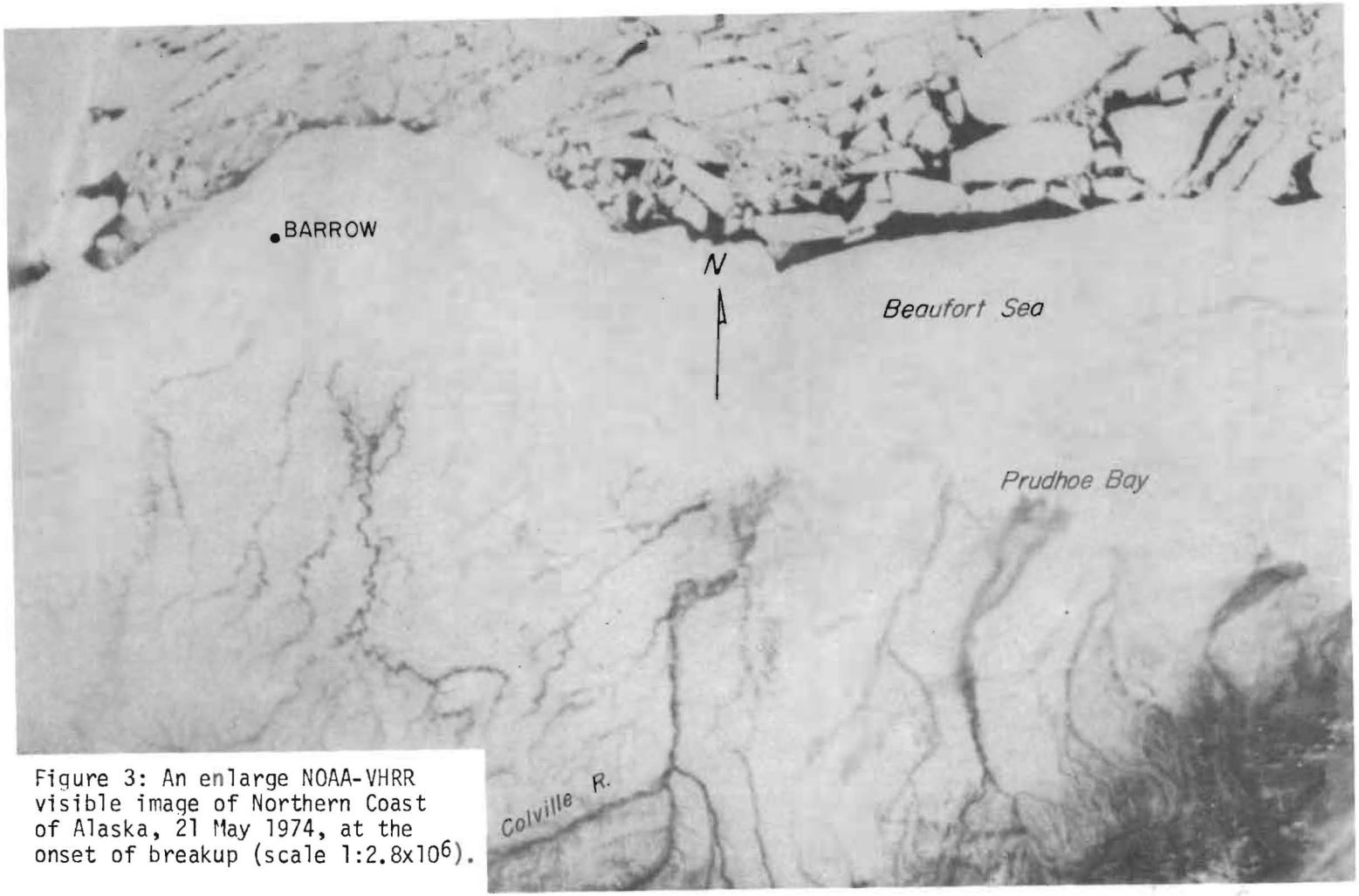

Figure 3: An enlarge NOAA-VHRR visible image of Northern Coast of Alaska, 21 May 1974, at the onset of breakup (scale $1:2.8 \times 10^6$).

International Association of Hydraulic Research (IAHR)
Committee on Ice Problems
International Symposium on Ice Problems
18-21 August 1975
Hanover, New Hampshire

COMMENTS

Paper Title: Alaskan Arctic Coast Ice Dynamics as Viewed by the NOAA Satellites

Author: R. F. Carlson, D. L. Kane, R. D. Seifert

Your name: Kartha, V. C. Tel. (204) 474-3542

Address: Head, Hydrologic Studies Section, System Planning Division, Manitoba Hydro, 820 Taylor Avenue, Winnipeg R3C 2P4, Canada

Comment:

1. When the proposed infrared imagery analysis could be completed would you be able to obtain the temperature of the land-mass, sea-ice surface and open water-surface? If so, what input data would be required for this purpose and what would be the precision of the temperature data obtained?

2. What is the scale of the NOAA photographs (standard)? If one measures the length of ice-cover in, say, Yukon River at several dates since freeze-up what is the maximum error possible?

3. In Canada ERTS pictures are used to estimate the extent of ice-cover during winter months. Does NOAA picture have any specific advantage over ERTS?

Author's Reply:

1. The ability to display surface temperatures using the thermal IR on NOAA-VHRR imagery is accomplished by calibration of the satellite detector. The satellite carries on-board standard radiation sources and the detector transmits the responses to the standard sources along with the imagery for each orbital pass. Consequently the calibration can be accomplished for each pass with these references points since we know the respone equations of the VHRR. The response equations are programmed on an HP-65 calculator on site at the satellite tracking stations and calibration of the IR output can be achieved in about 20 minutes. By knowing the analog voltage corresponding to certain temperatures, one can then manipulate the normal gray scale display to enhance temperatures of interest. For instance, if one were interested in distinguishing sea ice from open water the logical choice for enhancement would be a temperature of -1.5°C. Through experience and experimentation, one could adapt the enhanced display technique for land surfaces; and it has already been used for sea surface temperature measurements. The temperature measurements have been shown to be accurate, with qualifications, to $\pm$1°C. Interpretation of surface temperature measurements are strongly affected by surface winds, and their use should be tempered in the context of synoptic weather patterns.

2. The scale of the standard NOAA image is $\approx$1:8.5x 10^6, varying at different areas of the image due to panoramic distortion. No attempt was made to monitor river ice conditions; and we would only suggest its use for large rivers since the resolution of the NOAA imagery at nadir (0.9 km) is limiting. Thermal IR might again be useful here in detection temperature differences between frozen and unfrozen portions of the river.

Also, please be aware that photographic enlargements of NOAA imagery are common practice; 1:3x10^6 is a common enlargement size, and very useful enlargements of 1:10^6 scale have been produced. This is the same scale as the 9"x9" LANDSAT images.

3. In estimating ice cover, NOAA's major advantages over ERTS (LANDSAT) are its synoptic quality and daily availability. Sea ice monitoring is generally agreed to be the best and most productive application of NOAA imagery. Again the only drawback of NOAA imagery is the lesser resolution.

THIRD INTERNATIONAL SYMPOSIUM ON
ICE PROBLEMS
Hanover, New Hampshire, USA

FIELD STUDIES OF ICE ACTION ON STRUCTURES

V.M. Siniavskaya,
M.Sc. (Eng.), Chief
Volgograd Branch
P.G. Dick,
Division Chief

The "Hydroproject"
Institute Research
Center

Volgograd,
USSR

SYNOPSIS

Results of field studies of ice statical pressure on gates (vertical-lift and taintor types) of three dams, under various service, climatic and hydrologic condition are described. Stresses in main bearing members from the ice load and thermal stresses are given both for conditions of gates frozen in ice without arrangement of artificial lanes and heating and with lanes being maintained.

During a number of seasons and under various conditions studies of statical action of ice on gates of three dams were conducted. The structure and strength parameters of ice, deformations of ice fields in storage reservoirs in front of water outlet structures and the state of stress in steel gates of dams under the ice action were investigated.

Climatic and hydrological features of projects under investigation, for the years of studies, are given in Tables 1 and 2.

Table 1

Air Temperatures, °C

Accumulated negative temperature	Minimum temperature	Maximum daily temperature rise	Single-valued periodic rise of average daily temperature	
			Number of cases during the winter	Maximum temperature rise
1	2	3	4	5
		Dam I. Lower Volga		
306 to 1,501	-30.8	21.1	7 to 15	28.0
		Dam II. Middle course of Volga		
1,000 to 2,300	-31.9	22.9	3 to 10	24.6
		Dam III. Mamakan river in the North		
3,380 to 4,630	-51.0	26.0	8 to 15	33.5

Table 2

Hydrological Conditions of Studied Projects

Project	Duration of complete water freezing, days	Maximum thickness of ice, cm	Maximum thickness of snow cover cm	Daily water level fluctuations, cm	Maximum winter draw-down of reservoir, m	Flow velocity at the dam during freeze-up, m/sec
1	2	3	4	5	6	7
Dam I	up to 143	40 to 80	0 to 12	5 to 50	2.0	0.5

1	2	3	4	5	6	7
Dam II	up to 155	60 to 100	6 to 30	10 to 100	6.0	0.2
Dam III	up to 217	72 to 105	23 to 60	1 to 15	15.0	0.02

The ice cover at dams I and II is laminated, in upper layers snow ice and frazil ice are occuring; the lower layers feature columnar grain structure. The ice bending strength at zero temperature equals to 1.1 to 3.0 kg per sq. cm., according to data of field tests. A rather distinct system of cracks of ice was observed (Fig. 1).

At the dam III pure water ice was formed, with large amount of air bubbles in upper layers. The bending strength of ice attains 15 kg per sq. cm, this resulting in combination with inconsiderable length of reservoir, in the rigidity of the ice field. The ice cracks appeared only along the structure periphery and the banks being formed at the drawdown of the reservoir.

Dams I and II are equipped with welded vertical-lift gates, 11 and 12 m high respectively. The span width is 20 m. The spillway dam piers are extending upstream of the gate skin plate for 12 m (dam I) and 25 m (dam II). The width of the piers of both dams is 5.2 m; two half-piers are 6.8 m wide together. During the period of freeze-up the gates of dams I and II were not heated and ice holes were not made around them.

Dam III is equipped with taintor gates 6.65 m high, the span width being equal to 12 m. The gate body and arms are welded. The arms are connected with the gate body and support hinges with the help of bolts. The spillway dam piers are extending upstream for 3.5 m from the gate skin plate. The piers are 3 m wide, the shape of piers ends being semi-cylindrical like that of dams I and II. Ice holes were arranged in front of six gates of the total number of eight gates at the dam III. All gates were not heated. Investigations on the dam III were carcied out both with gates frozen in ice and with ice holes around the gates.

The ice temperatures at different levels were measured with the help of resistance thermometer, with accuracy of $\pm 0.1^{\circ}C$. The readings were recorded with the help of electronic potentiometers. String surface tensometers, of TH-150 model, were used to measure the stresses in bearing structural members of gates. The stresses in the

ice field were measured with the help of string sensors and small-sized pressure pickups with hydraulic convertor; these instruments were connected to the electronic potentiometer. The readings of the string instruments were recorded with the help of ЦС -5 freqency meter. The entire set of observations and measurements at each dam was carried out from the beginning till the end of the freezing period. The readings of string instruments were taken daily in moments of the morning air temperature minimum and the daily air temperature maximum.

The temperature of the ice surface at the dams I and II is often enough close to the air temperature and follows the latter due to irregularity of the snow cover. The heat wave is damped at about a half of the ice thickness. Due to the considerable snow cover thickness the ice temperature did drop below 8,8°C below zero (the air temperature being 48°C below zero), the heat wave is damped within the limits of one third of the ice thickness.

The studies have shown that the gates being fully prepared for the winter storage (without heating and lanes) are directly subjected to the ice cover action when the ice is thermally expanded during the first period of freeze-up. Then, as the negative temperatures are accumulated, the gates are jammed by ice (the second period of freeze-up) and behave with the ice together as a whole until the spring when a part of contacts may be broken (the third period of freeze-up) and the action of the ice cover resulting from its thermal expansion becomes again a substantial factor.

The nature of ice formation at vertical-lift gates can be seen in Figs. 1, 3 and 4. The thickness of the bottom ice forming layers on the gate skin plate attains 80 cm at the dam I, 100 cm at the dam III and 150 cm at the dam III (in the case an ice hole is provided at the dam III, the ice thickness is 30 cm). The thickness of the ice field between the piers (at the gate) attains 80 cm and 135 cm at the dam I, 100 and 180 cm at the dam II and 105 and up to 250 cm at the dam III (the first figure shows the ice thickness in the middle of the spillway bay, the second one - at the piers). Cracks in ice are often filled with water and regelated. Such massive ice formations and their strong contacts with the gate lead to considerable stresses in the gate members due to thermal strains in the gates.

Which of the abovementioned periods of freeze-up is to be adopted as the design one for various types of gates is determined proceeding not only from the temperature variations but too from the nature of the reservoir level fluctuations.

Fig. 2 shows that the fluctuations of the reservoir level being not single-valued within the range of 1 m, the upper girder was subjected to the maximum ice load during the second period when the component of the stress ordinate from the ice action reached the value of 630 kg per sq. cm (52 per cent of the total stress). The corresponding stress component in the middle girder was in this period 460 kg per sq. cm (35 per cent of the total stress). The stresses in the upper and middle girder varied in prportion to the air temperature variations, i.e. were governed mainly by thermal expansion of ice. This phenomenon is not observed in the nature of stresses of the lower girder because the latter is more efficiently relieved by the lever action of the ice sheet on the gate skin plate and is subjected mainly to thermal stresses which attain the value of about 370 kg per sq. cm in the third period due to jamming in thick ice formations on the spillway crest. The maximum recorded total stresses in the girderd were not in excess of 1,420 kg per sq. cm during the last decade of records.

At the dam II a case of an intensive reservoir drawdown occured in the winter. The lower girder was subjected to the greatest load in this case (Fig. 3). The component of the stress ordinate from ice and temperature action attained in this girder in the second period of freeze-up the value of 820 kg per sq. cm (68 per cent of the total stress). The maximum stress in the lower girder was recorded in the first period of freeze-up at high water level and thermal expansion of ice and amounted to 1,400 kg per sq. km. The upper girder was loaded less (the ice component being only 250 kg per sq. cm). The middle girder was loaded appreciably higher - the ice component of stress attained in the second period 600 kg per sq.cm (70 per cent of the total stress); still the total stress was high enough in the first period of freeze-up too (1,080 kg per sq. cm). Fig. 3 shows a rather distinct correlation between the ice temperature and the stresses in the upper and middle girders. During two years of records the maximum measured total stresses were not in excess of 1,400 kg per sq. cm in winter.

The dam III provides an example of a heavy-duty service conditions of gates in the North, the reservoir drawdown being large. In the first period of freeze-up when the ice was free from snow and the reservoir water level was high compressive stresses in the upper chord of the taintor gate arm were recorded, these stresses attaining up to 1,700 kg per sq. cm (1975). As Fig. 4 shows, in the second period variations of thermal stresses in arms chords were recorded, these variation being synchronous with air temperatures variations mainly. The stress value attained 1,400 kg per sq. cm. In the third period - when the gate emerged from the water and experienced no hydro-

static water pressure - increase of thermal stresses occured during the spring thaw. These stresses attained 1,480 kg per sq. cm in the lower chord of the gate arm the ice hole being provided around the gate and 1,200 kg per sq. cm the ice hole being not provided. Such high stresses with the ice hole being provided may be attributed to the limit compressive stress in the arm at extremely low temperatures in the moment of formation of the ice sheet on the gate skin plate. Maximum measured stresses in bearing members of taintor gates of the dam III (operating under conditions of full winter storing) were not in excess of 1,700 kg per sq. cm during three years of records.

CONCLUSION

1. Maximum measured total stresses in main bearing members of gates operated under conditions of complete winter storing did not exceed 1,400 to 1,700 kg per sq. cm and amounted to about 75 to 80 per cent of the total design stress induced by the hydrostatic pressure and wave-action loads. This shows the possibility of leaving the gates frozen into the ice in the winter without heating and ice holes around them. It is advisable to perform check calculations for the ice load in this case while designing new gates. In these calculations allowances should be made for the operation conditions of structures and for the ice conditions near the dam.

2. Field studies showed the necessity of a more differentiated approach to account for the natural factors of the ice conditions development at each particular hydroproject when designing the gates and prescribing operation duties for them.

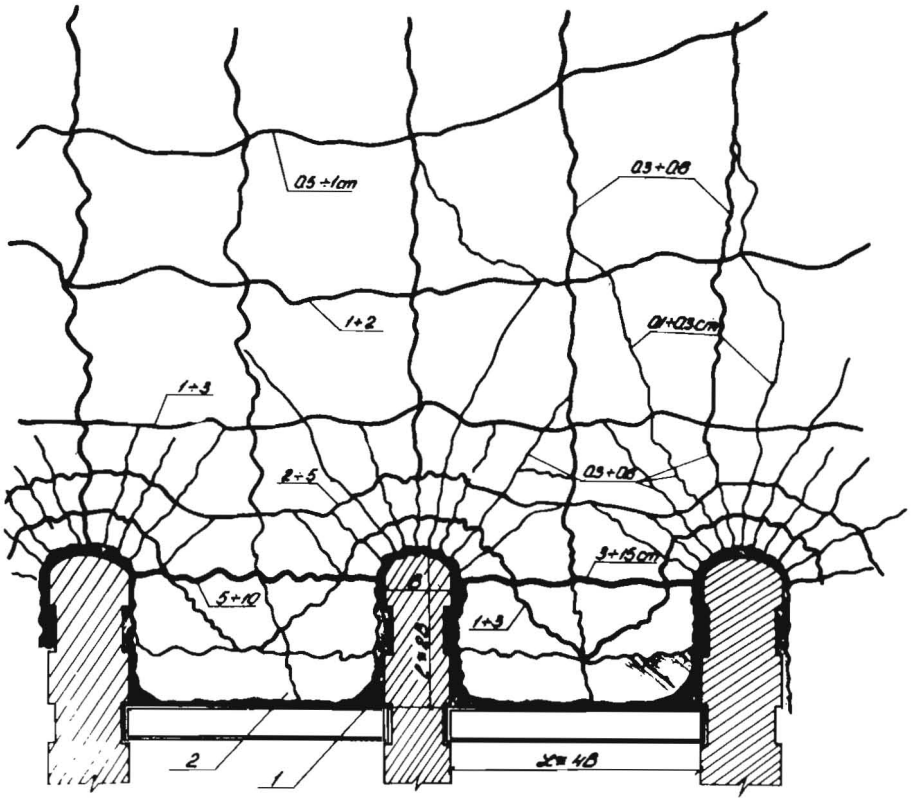

Fig. 1 Typical system of cracks in the ice cover at the dam I.

1 - contour of strong contact;
2 - zones of variable contacts.

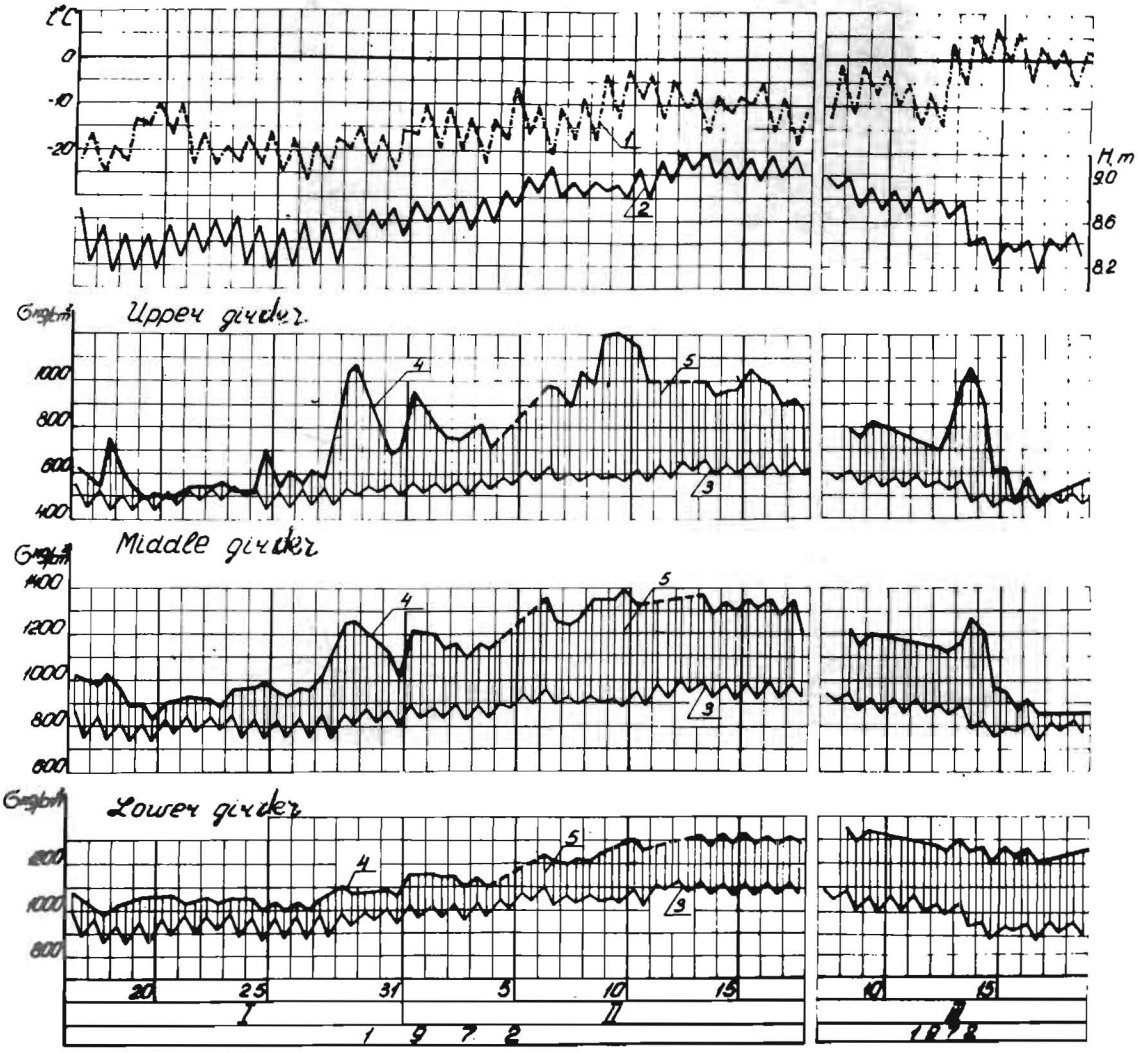

Fig. 2 Stresses in gate girders (dam I):

1 - air temperatures;
2 - water levels;
3 - stresses from hydrostatic load;
4 - total measured stresses in middle section;
5 - ice action and thermal strains components of stress.

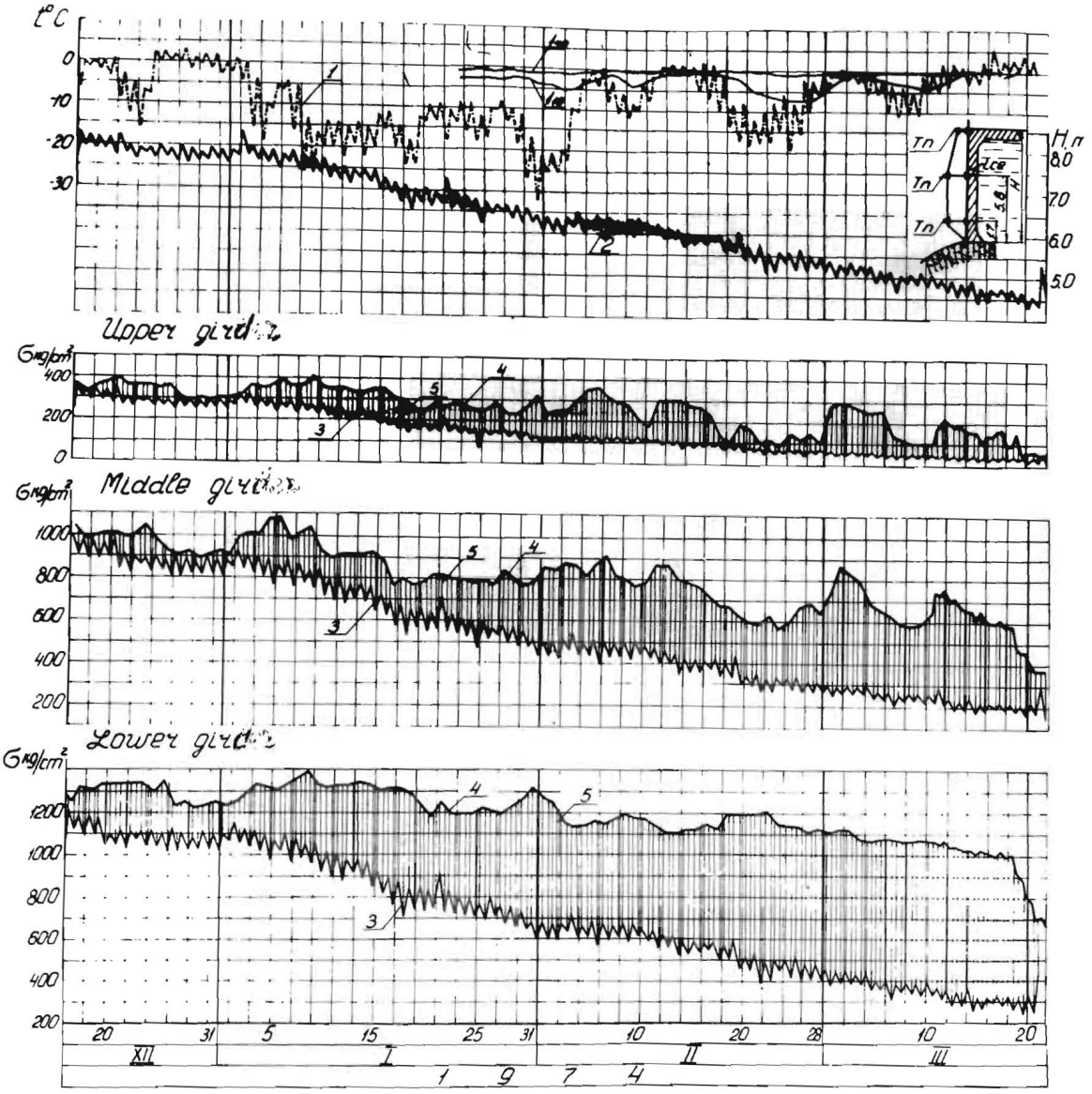

Fig. 3 Stresses in gate giders (dam II)

1 - air temperatures;
I_{10} - ice temperature at the 10 cm depth;
I_{50} - ice temperature at the 50 cm depth;
2 - water levels;
3 - stresses from hydrostatic load;
4 - total measured stresses in middle section;
5 - ice action and thermal strains component in stress.

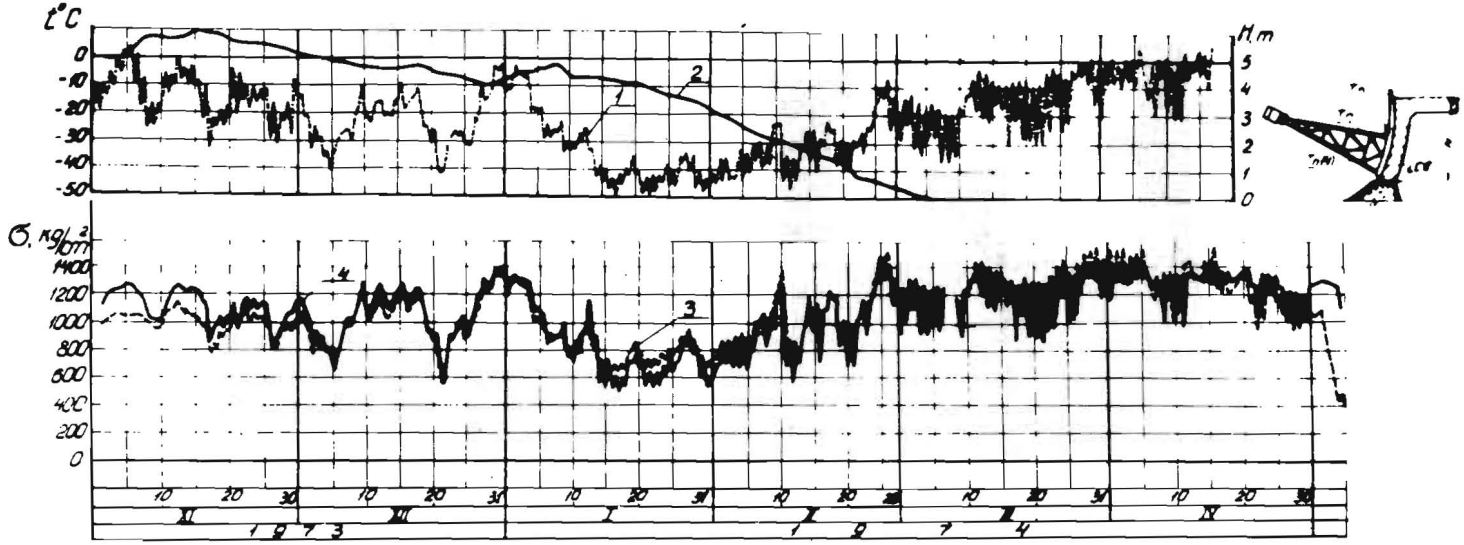

Fig. 4 Stresses in the lower chord of taintor gate arms (Dam III)

1 - air temperature;
2 - water levels;
3 - total measured stresses (ice holes being provided);
4 - ditto (ice holes being not provided).

THIRD INTERNATIONAL SYMPOSIUM ON
ICE PROBLEMS
Hanover, New Hampshire, USA

A SIMPLE FIELD MEASURE OF ICE STRENGTH

Robert Gerard, Research Officer
Highway and River Engineering Division, Alberta Research Council
Edmonton Alberta, Canada

Synopsis

A simple penetration test is proposed to provide an index of ice strength. The penetration involved is that of a fastener fired into the ice sheet using a commercially available power tool.

The correlation between fastener penetration and ice strength has been established from compression tests carried out in the field over the past three winters. In the paper these tests are described, the correlation presented and analysed and the application of the test discussed.

The penetration is most sensitive to strength for weak ice and the test is carried out in-situ. These features make it attractive for the study of breakup or melt phenomena, when the ice is weak and in-situ tests are almost mandatory.

In addition the test has proved to be simple, rapid, inexpensive and reasonably accurate, and the equipment rugged and portable. It may therefore also prove useful for an easy and objective assessment of the strength of even 'strong' ice in otherwise difficult circumstances.

Introduction

Ice strength is probably the most important *material* property governing ice forces on a structure and field investigations of ice phenomena have been hampered by lack of an easy measure of this parameter. The application of the results of these investigations ideally requires a knowledge of the statistical variation of ice strength in both space and time. This can only come from an extensive field data collection programme. Such a programme would be much more viable if a simple strength test existed.

Reliance for strength measurements has been placed on either small-scale compression tests and cantilever beam tests, both of which are quite laborious, or on relating ice strength to some other more easily measured parameter such as temperature, ice type or, in sea ice, brine content - parameters which themselves are not particularly easy to measure and which have dubious worth for ice well into the melt.

In this paper a simply-procured index of ice strength is proposed. It is based on a correlation between ice strength and penetration of a power tool fastener. The measurement simply requires firing the fastener into the ice sheet using a power tool and measuring the fastener's penetration. The method has proved to be simple, inexpensive and reasonably accurate. The correlation between fastener penetration and ice strength has been established from tests carried out in various locations over the past three winters. Details of the power tool equipment, compression tests, and field programme, and an evaluation of the effect on the correlation of ice type, charge (cartridge) strength and fastener type are presented in the remainder of the paper.

Description of proposed test and equipment

The equipment required for the proposed test is shown in Figure 1. For tests of subsurface ice an auger is also required. Details of the power tool are sketched in Figure 2. It operates as a gun, using a .22 calibre cartridge to fire the fastener into the ice. For safety reasons a 5 lb force is required on the barrel before the trigger will activate the cartridge. The fasteners are made of austempered steel and their dimensions are shown in Figure 5.

Cartridges used were all .22 calibre. Larger .38 calibre cartridges were tried but these are more expensive, are harder on the operator, require a special heavy-duty tool and give a penetration that seems little more sensitive to ice strength.

The power tool equipment is readily available commercially, its usual application being in the building industry for rapid fastening into steel or concrete. A photograph of the tool in operation is shown in Figure 3.

Description of test programme

One special test series was carried out on lake ice to evaluate the effect of fastener type and cartridge charge strength on penetration. Another series was carried out in the laboratory using

artificial ice blocks to verify that penetration would indeed respond to an increase in ice strength. Except for these preliminary tests all results described below were obtained in conjunction with small-scale compression strength measurements carried out in the field over the past three winters. The ice tested has varied from clear dense lake ice in early winter to melting rotten snow ice and candling clear ice on rivers in late spring.

Compression test

The specimens tested were 100 x 100 x 200 mm blocks cut from the ice sheet with their long axis in the horizontal plane. Large blocks (> 0.3 m cube) were first rough-cut from the ice sheet with a chain saw and then transported as quickly as possible to a 4-wheel drive 'pick-up' truck carrying the ice testing equipment. The latter is shown in Figure 4. The block was cut to size with a band saw and the ends made plane by placing each briefly on a slightly warm machined plate.

The compression strength of the block was determined by loading it in a small, gear-driven compression machine. For a 200 mm long block the approximately constant rate of crosshead movement corresponds to a strain rate of 0.0042/sec, which is in the region of the 'plateau' usually found in ice strength - strain rate relationships. The load was sensed with a strain gauge transducer beneath the lower platten and recorded on an oscillographic chart recorder. The upper platten was attached to a spherical head.

Some analysis

The major variables in the penetration test are considered to be: the nominal cartridge energy E (taken from Canadian Standards Association Standard #Z166-1966); a measure, ζ, of the losses in the conversion of this energy to that of the fastener just before it enters the ice; fastener diameter d; a measure, ξ, of the fastener shape; fastener penetration p; ice strength σ; and a measure, η, of the other effects of ice type. That is

$$f(p, \sigma, E, d, \xi, \eta, \zeta) = 0 \qquad (1)$$

To determine an appropriate dimensionless combination of these variables it is useful to consider some simple mechanics. The energy associated with the fastener just prior to impact is released by the fastener in doing work against the ice during penetration, and in the strain energy stored within the ice after the fastener stops.

For the 'standard' fastener (see below) the resistance to penetration should be dominated by 'form drag' on the head rather than 'skin friction' on the head and shank. It should therefore vary much as the product of ice strength and the square of the fastener head diameter. The associated work done is therefore given by

$$E_p \propto \sigma p d^2 \qquad (2)$$

The zone of ice remaining strained after penetration has ceased is also a function of the fastener head diameter and the ice strength.

The strain energy stored per unit volume within this zone is presumably a function of the elastic moduli of the ice which can, at least crudely, also be related to ice strength. Hence the strain energy should be given by

$$E_s \propto \sigma d^3 \tag{3}$$

That is, very approximately

$$E \sim a\sigma d^3 + b\sigma p d^2 \tag{4}$$

In 'weak' ice the stored strain energy should be small and the second term in Equation 4 will dominate. For this extreme the penetration should therefore be inversely proportional to ice strength. In 'strong' ice the strain energy and the resistance of the shank will dominate (indeed in the limit it may be so great as to prevent penetration altogether) and penetration will be small and insensitive to strength.

Equation 4 can be rewritten in dimensionless terms as

$$\frac{p}{d} \sim a \frac{E}{\sigma d^3} + b \tag{5}$$

Hence it would seem that a convenient dimensionless form of Equation 1, which is free of spurious correlation, is

$$\frac{p}{d} = f\left(\frac{\sigma d^3}{E}, \xi, \eta, \zeta\right) \tag{6}$$

This relationship is considered in the following discussion of penetration variation with ice strength, ice type, fastener type and charge strength.

Results

Effect on penetration of charge strength and fastener type. This was determined from a test series carried out in the field on 0.70 m thick lake ice (0.18 m snow ice over 0.52 m clear ice). The tests were carried out within a few hours in random order in the same general area. Ice type and strength was therefore constant. The fasteners, charge strengths and results are shown in Figure 5. There is a trend in the variation of penetration with both fastener type and charge strength.

An ice section showing the shatter pattern generated by these fasteners during penetration is shown in Figure 6.

Compared to the 'studs' the centre of resistance of the 'pins' is more localised; the variation of their penetration with charge strength more consistent and they are considerably cheaper. For these reasons pins seemed preferable despite their smaller penetration. Of those tested the #3336 drive pin was chosen as standard as the larger head provided a more localised resistance and was easier to locate in the hole. The above results and those of some additional tests indicated that the #4 and #6 charge strengths provided the best compromise between sensitivity to ice strength, economy, ease and insensitivity to ice heterogeneities.

Effect of ice strength. To determine if penetration does indeed vary with ice strength a series of penetration tests was carried out in

the laboratory using the selected #3336 fastener and nos. 4 and 6 charges. These tests were made in 1.22 x 0.61 x 0.30 m ice blocks obtained from a commercial ice manufacturing plant. Ice type was therefore constant. The ice strength was varied by varying the ice temperature. Prior to each test the blocks were stored for two days in a cold room set at a pre-selected temperature. This was sufficient time to ensure the block temperature was homogeneous and equal to that of the cold room.

The penetration tests were carried out in the cold room. One penetration test was made in the centre of the large face of each block, and 4 to 7 tests made for each charge strength/temperature combination. To check consistency the tests were repeated for three temperatures. An example of a tested block is shown in Figure 7 and the penetration results are shown in Figure 8.

The first point to note is that penetration does indeed vary with ice temperature - or ice strength. The second point is the consistency of the results - both in the trend of penetration with temperature and in the repeatability of the results shown by the tests rerun at -1, -3 and -10°C.

Effect of ice strength and type in the field. In accordance with Equation 5 the results of the penetration and strength tests carried out in the field were plotted as p/d against $E/\sigma d^3$ in linear coordinates. The result was not inconsistent with the predicted straight line trend. However there was one physical inconsistency. The straight line fitted to the data, when extrapolated, gave a non-zero value for p/d when $E/\sigma d^3$ was zero. This is physically meaningless. Presumably then, for very high strengths, the relationship between p/d and $E/\sigma d^3$ must change so that $E/\sigma d^3$ is positive for p/d = 0. However as there was no strong indication that this change occurs within the range of strengths tested to date the linear relation was accepted as a sufficient approximation.

The value of b in Equation 5 was fairly sharply defined by the available data and was found to be a function of both ice type and charge strength. The values found for each combination tested are shown on Figures 9 and 10. The data, plotted as (p/d + b) against $\sigma d^3/E$ in logarithmic coordinates, is shown in Figures 9 and 10. It can be seen that the assumed linear relation between p and $1/\sigma$ does indeed fit the data reasonably well, and that there seems little reason to change the position of the line because of either charge strength or ice type. Hence the parameter a in Equation 5 was taken as constant and equal to 6×10^{-3}.

The linear relation between penetration and charge strength for the standard fastener shown in Figure 5 (which is for fixed ice strength and type) infers that, given the constraints of the form of Equation 5, parameter b should also be a linear function of charge strength. The three available values of b for snow ice agree with such a relationship, requiring changes of less than 5% to make them colinear.

The large scatter evident in Figures 9 and 10 is somewhat disconcerting. However, in terms of the large coefficient of variation of the ice strengths (0.15 to 0.30) and the few tests feasible in each case (rarely more than four) it is perhaps understandable. In contrast the

penetration measurements had a considerably smaller coefficient of variation (0.05 to 0.15) and, because of their ease, more were generally carried out. Nevertheless the existence of the scatter requires that more strength/penetration tests be carried out to better define the relationships.

Special field problems

This penetration test is not confined to surface ice. Ice at various depths has been tested by drilling a hole to the required depth with an auger and making the penetration test at the bottom of the augered hole. However the safety device built into the power tool, which requires pressure against the barrel before it will fire the cartridge, prevents its operation on the conical section left at the bottom of the auger hole. This must therefore be reamed flat using a flat-ended auger bit.

This same safety device also prevents the tool operating on very weak ice. When encountered in the field this problem has been overcome by firing the fastener through a piece of stiff cardboard placed on the ice. This has a negligible influence on the penetration.

More than an inch or so of water on top of, or included in, the ice sheet make the results of doubtful value because of the energy dissipated by the fastener when passing through the water. This is not an uncommon situation in the spring, particularly with a heavy snow cover on the ice. The only resort in this situation is to carry out the penetration tests on blocks cut from the ice sheet.

Conclusion

There is a significant correlation between the penetration of a power tool fastener and ice strength. The penetration is particularly sensitive to ice strength for weak ice and the test is simple and performed in-situ. These features make the test most useful as an index of ice strength during the spring melt period when in-situ tests are nearly mandatory.

Charge strength, fastener type and ice type all have an effect on the relation between the chosen dimensionless parameters for penetration and ice strength. These must therefore either be standardised or a different relation developed for each. In the tests described above a 'drive pin #3336' fastener was chosen as standard and relations between penetration and ice strength, for both snow ice and clear ice, developed for two charge strengths - #4 and #6.

Acknowledgements

Thanks are due to the technologists of the Highway and River Engineering Division - in particular H. Schultz, G. Putz and G. Childs - for the many hours of hard work involved in collecting the above data. Discussion with Dr. S. Beltaos was also appreciated. The work was carried out as part of a continuing programme of research in ice engineering under the auspices of the Alberta Cooperative Research Programme in Highway and River Engineering. The moral and financial support of Bridge Branch, Alberta Transportation, is gratefully acknowledged.

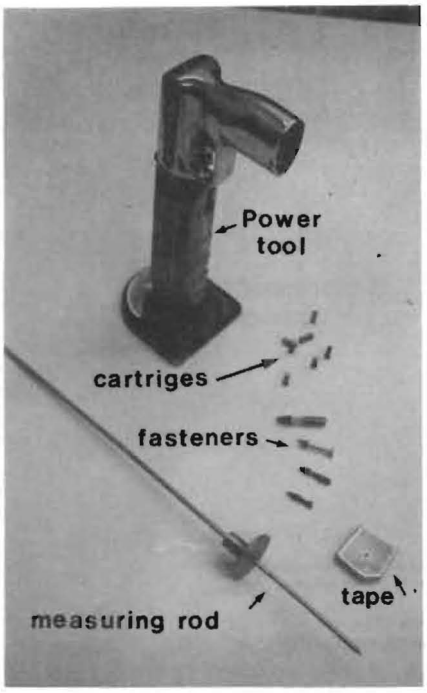

Figure 1. Penetration test equipment

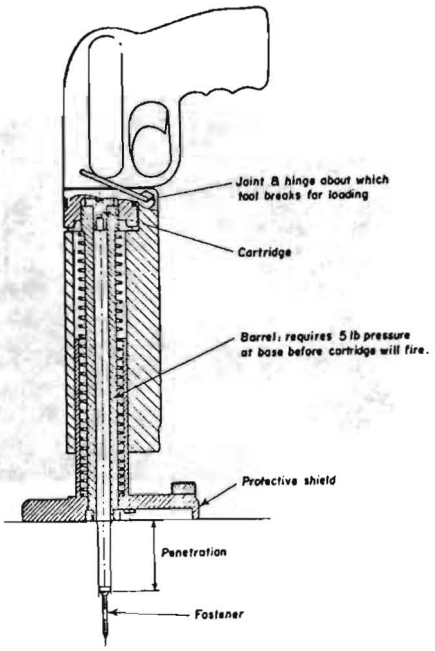

Figure 2. Sketch of power tool

Figure 3. Penetration test on river ice

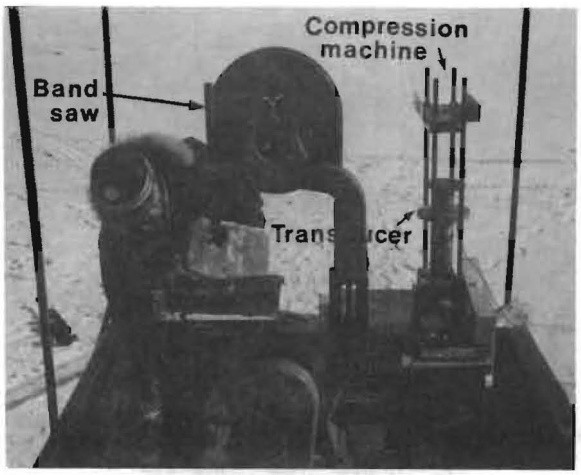

Figure 4

Compression test equipment

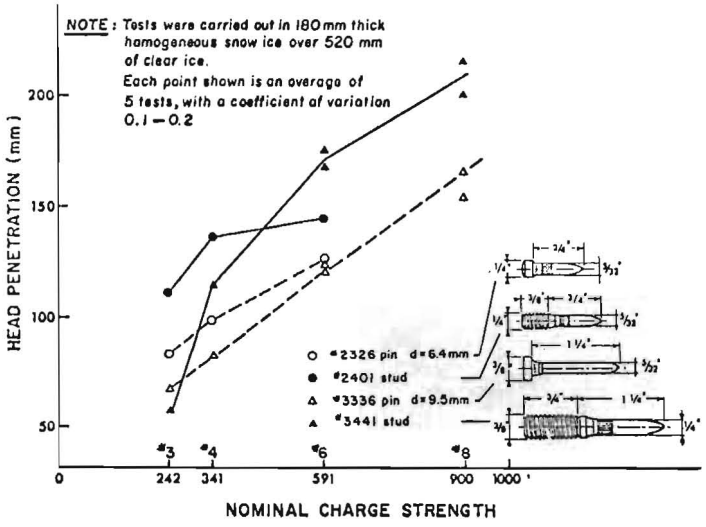

Figure 5

Variation of penetration with charge strength and fastener type

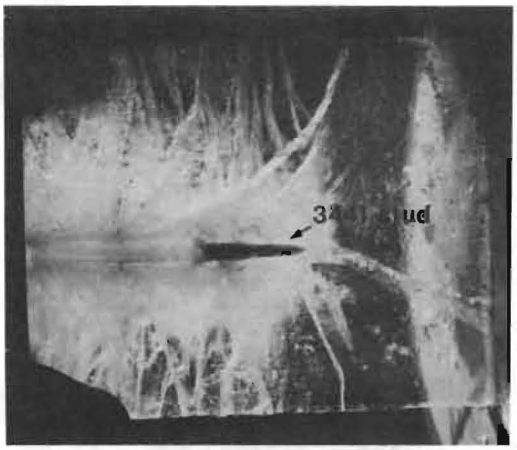

Figure 6

Shatter pattern caused by fastener penetration

Figure 7

Penetration test in artificial ice block

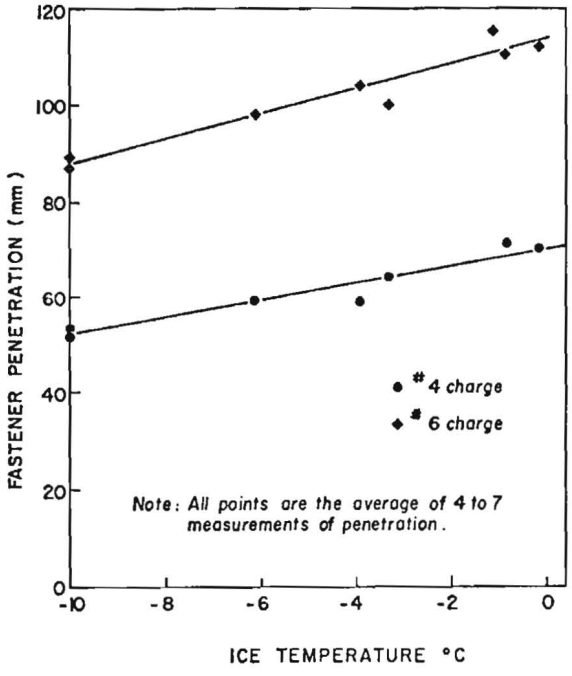

Figure 8

Variation of penetration with ice temperature

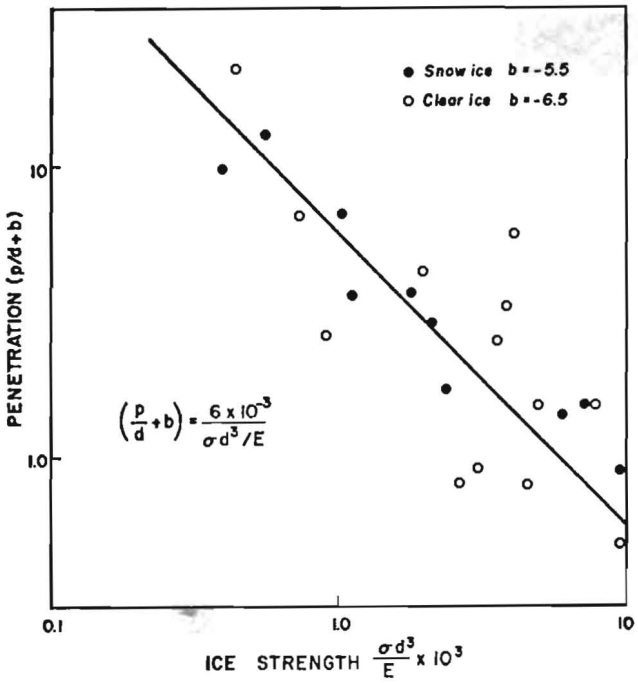

Figure 9
Fastener penetration
for #4 cartridge

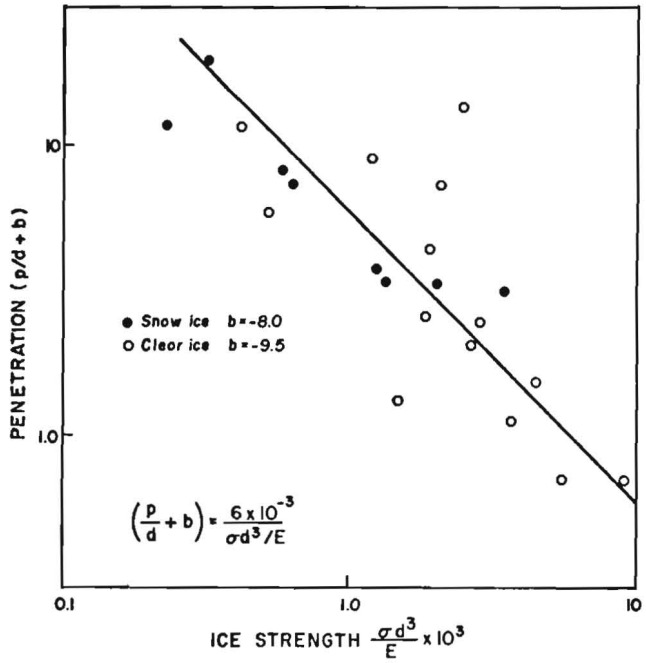

Figure 10
Fastener penetration
for #6 cartridge

Addendum to paper 'A Simple Field Measure of Ice Strength'
by Robert Gerard

One point that should be added to the paper concerns the field compression tests. As discussed at the Symposium there may be a considerable difference between results obtained from compression tests in the field using steel platens and melting the ends of the specimen, and carefully controlled laboratory tests using machined ends. This is demonstrated in Figure 3 of the Draft Report of Task Committee on Standardising Testing Methods for Ice which was circulated at the Symposium. From the figure it seems the ratio of steel platen/melted ends strengths to 'standard' strengths is about 0.60 for good ice. The difference might be less for weak ice.

The use in the field of the 'Flexane' platens proposed by CRREL should largely overcome this problem and further field tests are planned to determine the effect of this type of platen on the field strength measurements.

Two points raised during discussion of this paper at the Symposium deserve further comment:

1. It was pointed out that the penetration versus temperature plot shown in Figure 8 does not reflect the more rapid decrease in ice strength generally found from compression tests for temperatures higher than about -5°C.

A possible explanation for this is that at temperatures near the melting point creep has an almost unavoidable and probably considerable effect on 'normal' compression tests and may be responsible for the rapid decrease in strengths found at the higher temperatures. The penetration test, on the other hand, is essentially instantaneous and should be free of any creep effects.

2. One discusser felt rather strongly that the large scatter evident in Figures 9 and 10 rendered the measure of little value as an index of ice strength.

While there is no intent to try and 'sell' the test, it is thought that such a conclusion does not do justice to the results as reported and certainly seems to ignore the realities of field work in ice mechanics, particularly during the melt period of river and lake ice. Hence the author would like the reader to keep in mind the following points when evaluating the worth of the test:

(a). As pointed out in the paper the scatter is probably due in large measure to the scatter in the compression test results. The investigation of the correlation was not intended to be definitive - merely demonstrative. A more elaborate and refined series of tests could probably refine the definition of the relation between penetration and strength.

(b). Notwithstanding the scatter, these two figures exhibit an obvious correlation between penetration and ice strength, particularly for weak ice. The measured penetrations have varied from a few millimetres in 'good' ice to several hundred millimetres in severely candled ice.

(c). In many instances (if not most) the availability of such a simple strength test for field use will mean the difference between having some objective measure of the ice strength and none at all.

(d). The simplicity of the penetration test permits the easy procurement of many 'strength' tests for a given field situation. On the other hand the difficulty of the usual compression test, if it can be carried out at all, severely limits the number of samples that can be tested. This better sampling of the nonhomogeneity of the ice sheet with the penetration test (or a similar easily executed test) may more than compensate for the scatter in the strength-penetration correlation.

(e). In practice many ice problems (again if not most) seem to depend only slightly on ice strength. For such situations a rough measure of ice strength (if indeed the penetration measurement turns out to be such), if it is objective, would suffice.

(f). The rapidity of the penetration test ensures that it is independent of the creep characteristics of the ice. This is probably particularly important for ice near or at the melting point.

(g). The test is carried out in-situ - another important feature for ice at or near the melting point.

APPENDIX A

ATTENDEES IAHR Symposium on Ice Problems
18-20 August 1975 at Hanover, NH

H. Aamot, CRREL

John B. Adams, III
SLSDC, Seaway Circle
Massena, N.Y. 13662

N.D. AbdEl-Had
Civil Engineering Dept.
University of New Brunswick
Fredericton, N.B., Canada

R.S. Arden
Ontario Hydro
620 University Avenue
Toronto, Ont. M5G 1X6, Canada

Carl Argiroff
U.S. Army Eng. Dist. Detroit
P.O. Box 1027
Detroit, Mich. 48231

G. Ashton, CRREL

A. Assur, CRREL

Gordon Ayre
Dufresne-Henry
Precision Park
North Springfield, Vt. 05150

M.A. Ball
Marine Safety Branch
Ministry of Transport
Ottawa, Ont. K14-0N7, Canada

W.M. Baxley
c/o Commander (ecr)
Ninth Coast Guard District
1240 East 9th St.
Cleveland, Ohio 44199

Lars Bengtsson
University of Lulea
S-951-87-Lulea, Sweden

F.G. Bercha
1001-10th Avenue S.W.
Calgary, Alta. T2R 0B7, Canada

D. Berenger
Arctec Canada
1440 St. Catherine St. West
Montreal, P.Q. H3G 1R8, Canada

M. Bilello, CRREL

F. Boulanger
Lasalle Hydraulic Laboratory
6250 St. Patrick St.
Lasalle, P.Q., Canada

Theodore Bratanow
Dept. Of Eng. Mechanics
University of Wisconsin
Milwaukee, Wis. 53201

D.I. Bray
Dept. of Civil Engineering
University of New Brunswick
Fredericton, N.B., Canada

R. Brisebois
Hydro Quebec
75 Dorchester W
Montreal, P.Q., Canada

Jerry Brown, CRREL

David Bruce
Lower Churchill Consultants
P.O. Box 908, Station B
Montreal, P.Q., Canada

Philip H. Burgi
Bureau of Reclamation
Room 25-F, Bldg 56
Denver Federal Center
Denver, Colo. 80255

D. Calkins, CRREL

T. Carstens
Technical University of Norway
Trondheim, Norway

Donald Carter
1281 Bishop
Quebec G1W 3E4, Canada

F.M. Chang
Hydraulics Engineer
F.H.W.A. Office of Engineering HNG-31
Washington, D.C. 20590

P.S. Cheema
College of Trades of Technology
St. John's, Nfld., Canada

Kenneth R. Croasdale
Imperial Oil Ltd.
339 50th Ave. S.E.
Calgary, Alta. T2G 2B3, Canada

Col. R. Crosby, CRREL

J.V. Danys
Ministry of Transport
Marine Services
Place de Ville
Tower "C", Ottawa, Ont., Canada

Arnold Dean, CRREL

V.V. Degtyarev
Novosibirsk Institute of Water
Transport Engineers
33 Stetinkin St.
Novosibirsk, U.S.S.R.

M. Dembinski
C.D. Howe Co. Ltd.
4333 St. Catherine W.
Montreal 215, P.Q., Canada

S.L. DenHartog, CRREL

Marc Drouin
James Bay Energy Corp.
Edifice Dupuis (16)
800 East Boul. de Maisonneuve
Montreal, P.Q., Canada

E. Dumalo
SLSA
5250 Ferrier
Montreal, P.Q. H4P 1L4, Canada

M. Edo
Mitsui Shipbuilding & Eng. Co.
One World Trade Center, Suite 2029
New York, N.Y. 10048

R.Y. Edwards Jr.
1440 St. Catherine St. West
Montreal, P.Q., H3G 1R8, Canada

Elias Eliasson
National Power Company
Sudurlandsbraut 14
Reykjavik, Iceland

W.P. Erdle
U.S. Army Eng. Dist., Buffalo
1776 Niagara St.
Buffalo, N.Y. 14207

Andrew Fountain, CRREL

G. Frankenstein, CRREL
R. Frederking
Division of Building Research
National Research Council
Ottawa 7, Ont. K1A 0R6, Canada

Sigmundur Freysteinsson
Verkfraeoistofa Sig. Thoroddsen s.f.
Armuli 4
Reykjavik, Iceland

Donald Garfield, CRREL

R. Gerard
Alberta Research
303 Civil-Electrical Bldg.
University of Alberta
Edmonton, Alta. T6G 2G7, Canada

Lorne W. Gold
Geotechnical Section
Division of Building Research
National Research Council
Ottawa 7, Ont. K1A 0R6, Canada

A. Gow, CRREL

N.J. Gruber
Dames & Moore
2996 Belgium Rd.
Baldwinsville, NY 13027

B. Hanamoto, CRREL

T.O. Hanley
Wheeling College
Wheeling, W. Va. 26003

M. Hare
Ontario Hydro
620 University Ave., Room M333
Toronto, Ont., Canada

Ivor Hawkes, CRREL

Donald Haynes - CRREL

Mr. M. Henriksson
Swedish State Power Board
The Hydraulic Laboratory
S-81070, Alvkarleby, Sweden

Matti Herva
Pohjolan Voima Oy
Kemi, Finland

Ken-ichi Hirayama
Civil Engineering Dept.
University of Iwate
Ueda 3-5-4, Morioka
Iwate, Japan

W. Hibler, CRREL

J.H. Ho
620 University Ave.
Toronto, Ont., Canada

R.J. Hodek
Civil Engineering Dept.
Michigan Technological University
Houghton, Mich. 49931

A. Hollmer
PASNY
P.O. Box 277
Niagara Falls, NY 14302

Y. Horten
Cleveland-Cliffs Iron Company
Marine Department
1460 Union Commerce Building
Cleveland, Ohio 44115

Philip R. Johnson
USACRREL
Fort Wainwright, Alaska 99701

Edvigs V. Kanavin
Iskontoret, NVE
Boks 5091, Maj.
Oslo 3, Norway

Douglas Kane
Institute of Water Resources
University of Alaska
Fairbanks, Alaska 99701

Viswanathan C. Kartha
Manitoba Hydro
Box 815, Winnipeg
Manitoba R3T 2G6, Canada

I.B. Kelly
7322 Baylor
College Park, Md. 20740

John F. Kennedy
Iowa of Hydraulic Research
University of Iowa
Iowa City, Iowa 52240

Arnold Kerr
Dept. of Civil and Geol. Eng.
Princeton University
Princeton, N.J. 08540

Austin Kovacs, CRREL

M. Kumai, CRREL

B. Ladanyi
CINEP
Ecole Polytechnique
C.P. 6079, St. A,
Montreal H3C 3A7, P.Q., Canada

A.P. Larsen
Lund Institute of Technology
S 22007, Lund, Sweden

S. Lavender
Acres Ltd.
5259 Dorchester Road
Niagara Falls, Ont., Canada

G. Lemieux, CRREL

Dinh Levan
Hydro-Quebec
Place DuPuis, 16th Floor
855 E. St. Catherine St.
Montreal, P.Q., Canada

J.W. Lewis
ARCTEC, Inc.
9104 Red Branch Rd.
Columbia, Md. 21045

D.S.H. Louie
Harza Engineering Co.
150 South Wacker Drive
Chicago, Ill. 60606

Mauri Maattanen
University of Oulu
90100 Oulu 10
Finland

M. Mellor, CRREL

Michel Metge
c/o Imperial Oil Ltd.
339-50th Ave. S.E.
Calgary, Alta., Canada

M. Michailidis
N.R. C. Montreal Road
Bldg. M-22
Ottawa, Ont. K1A 0R6, Canada

Bernard Michel
Laval University
Quebec 10, Canada

L.D. Minsk, CRREL

R.M. Morey
Geophysical Survey Systems Inc.
217 Middlesex Turnpike
Burlington, Mass. 01803

Ch. R. Neill
Northwest Hydraulic Consultants Ltd.
4823-99 St.
Edmonton, Alta. T6E 271, Canada

D.E. Nevel, CRREL

K.G. Nolte
Amoco Production Company
4502 E. 41st Street
P.O. Box 591
Tulsa, Okla. 74102

T. Osterkamp
Geophysical Institute
University of Alaska
Fairbanks, Alaska 99701

E. Palosuo
Dept. of Geophysics
University of Helsinki
Vironkatu 7B
00170 Helsinki 17, Finland

V. Parameswaran, CRREL

P. Pay
M.O.T. 20 G, Tower "C"
Place de Ville
Ottawa, Ont. K1A ON7, Canada

R. Perham, CRREL

J. Peter
ARCTEC In.
9104 Red Branch Rd.
Columbia, Md. 21045

B.D. Pratte
Hydraulics Laboratory
N.R.C. Montreal Road
Ottawa, Ont. K1A 0R6, Canada

L. Racicot
Hydro-Quebec
620 Dorchester Blvd. West
Montreal, P.Q., Canada

G.H. Reusswig
The Offshore Co.
P.O. Box 2765
Houston, Tex. 77001

David C.N. Robb
St. Lawrence Seaway Development Corp.
800 Independence Ave. S.W.
Washington, D.C. 20591

Morris Root
Dufresne-Henry
Precision Park
North Springfield, Vt. 05150

D.A. Rothrock
Aidjex
4059 Roosevelt Way NE
Seattle, Wash. 98105

R.R. Rumer, Jr.
Center for Inland Water Resources
State University of N.Y.
Buffalo, N.Y. 14214

C.L. Sabourin
Marine Services, M.O.T.
Cite du Havre
Montreal, P.Q. H3C 3R5, Canada

G.W. Samide
Technical Services Division
Alberta Environment
10040-104 St.
Edmonton, Alta., T53 076, Canada

F. Sampson
B.C. Hydro & Power
700 W. Pender
Vancouver, B.C. V67 2S5, Canada

John J. Scheuren, Jr.
25 Cushing Avenue
Hingham, Mass. 02043

Joachim Schwarz
Hamburgische Shiffbau-Versuchsanstalt
2000 Hamburg 33
Bramfelder Str. 164, W. Germany

O.W. Scott
U.S. Army Eng. Div., North Central
536 South Clark Street
Chicago, Ill. 60605

Peter Sector, CRREL

P.V. Sellmann, CRREL

J.L. Simms
Office of Lock Operations
St. Lawrence Seaway Development Corp.
Massena, N.Y. 13662

N. Sinha
NRC, Montreal Road
Ottawa 7, Ont. K1A OR6, Canada

I.N. Sokolov
B.E. Vedeneev All-Union Res. Inst.
of Hydraulic Engineering
Leningrad, U.S.S.R.

D.S. Sodhi
Faculty of Eng. and Applied Science
Memorial University of Newfoundland
St. John's, Nfld., Canada
Presently: CRREL

A.G. Spillette
Exxon Production Research Co.
P.O. Box 2189
Houston, Tex. 77001

O. Starosolsky
Dept. for Water Resources
National Water Authority
Budapest I.
Fo ut., 48-50, Hungary

T. Tabata
Inst. of Low Temperature Sciences
Hokkaido University
Sapporo, Japan

H. Tabuchi
Mitsui Shipbuilding & Engr. Co.
One World Trade Center, Suite 2029
New York, N.Y. 10048

S. Takagi, CRREL

J.C. Tatinclaux
Institute of Hydraulic Research
University of Iowa
Iowa City, Iowa 52242

E. Tesaker
River and Harbour Laboratory
Klaebovn 153
Trondheim, Norway

J.E. Tilley
Canatom Ltd.
Nuclear Consultants
1134 St. Catherine St. W.
Montreal, P.Q., Canada

Gee Tsang
Canada Centre for Inland Waters
Burlington, Ont., Canada

Per Tryde
Institute of Hydrodynamics
and Hydraulic Engineering
Technical University of Denmark
Building 115
DK-2800 Lyngby, Denmark

Gerry Turgeon
Hydro-Quebec
620 Dorchester West
Montreal 115, P.Q. Canada

D.B. Tutt
B.C. Hydro & Power
700 W. Pender
Vancouver, B.C. V6C 2S5, Canada

M.S. Uzuner
Arctec, Inc.
9104 Red Branch Rd.
Columbia, Md. 21045

K.D. Vaudrey
Polar Division, NCEL
Port Hueneme, Calif. 93043

R. Wahanik
Gilbert Associates
Reading, Pa.

R.A. Walker
Ontario Hydro
620 University Ave.
Toronto, Ont. M5G 1X6, Canada

Walter E. Webb
General Engineering Division
Engineering Branch
St. Lawrence Seaway Authority
P.O. Box 200
St. Laurent, Montreal 379
P.Q., Canada

W. Weeks, CRREL

G. Westerstrom
University of Lulea
S951-87 Lulea, Sweden

Richard Worsfold
Center for Cold Oceans Resources
and Engineering
Memorial University of Nfld.
St. John's, Nfld., Canada

A.F. Wuori, CRREL

Y-C. Yen, CRREL

Leonard Zabilansky, CRREL

International Association of Hydraulic Research (IAHR)
Committee on Ice Problems
International Symposium on Ice Problems
18-21 August 1975
Hanover, New Hampshire

APPENDIX B

Report of Task-Committee on Standardizing Testing Methods for Ice

I. Introduction

The Committee on Ice Problems of the International Association of Hydraulic Research decided in January 1974 to form a subcommittee on establishing standards for testing the mechanical properties of ice. The reason for this decision was that research on Ice Engineering has been strongly hampered because almost every ice research group has used different methods of testing, which has led to widely scattered, or even contradictory, results of apparently similar tests.

Meanwhile, the subcommittee consisting of representatives from Canada, Japan, Scandinavia, Federal Republic of Germany, USA, and USSR has prepared first recommendations on testing ice in uniaxial compression and tension. The recommendations are considered to be guidelines in order to improve the quality, comparability, and usefulness of ice strength data. The adoption of the guidelines is purely voluntary.

This first edition of recommendations has been discussed in a special session at the IAHR Ice Symposium in Hanover, N.H. on August 19, 1975.

Further suggestions are welcomed. The recommendations on testing ice properties are not final and complete; they remain open for corrections and additions as the development of methods for testing ice continues.

The recommendations will be discussed with other ice research oriented organizations, such as the International Glaciological Society and the International Commission on Snow and Ice.

The development of uniform methods for testing the mechanical properties of ice has to distinguish between laboratory and field tests. In laboratory tests, first class equipment can be used in order to obtain a high degree of accuracy, while in field investigations a compromise is usually necessary between theoretically possible and practically and economically reasonable equipment and performance. However, the difficulty of obtaining ice properties in the field should be stressed. Since a complete test program for the investigation of ice strength in relation to strain rate, temperature and grain size is too laborious in the field, it is suggested that reference curves might be established by laboratory tests which provide the relationship between the various parameters. As soon as these reference curves are available, only a few field tests are necessary to describe the material properties.

II. Recommended procedures and requirements for testing ice in uniaxial compression and tension

1) General remarks

Ice occurs in nature in various forms according to its origin, its grain size, crystal structure and orientation, and also in respect to impurities, salinities, and density. All these parameters affect the mechanical properties. An identification of the type of ice is therefore a basic objective in connection with the investigation of mechanical properties. The most general classification is that of the following division:

1. Lake or River Ice (freshwater ice)
2. Sea Ice (saltwater ice)
3. Glacier Ice
4. Ground Ice

A more detailed classification for lake and river ice has been proposed by Michel and Ramseier (1969) and by Cherepanov (1974). Both schemes describe the material with respect to its origin, grain structure, and crystallographic orientation, and either can be adopted and applied when the mechanical properties are being investigated.

A classification of sea ice is in preparation; it will be based on similar items as the one for lake ice, but should additionally include the degree of liquid or solid impurities, the depth from which the ice sample has been taken, and the history of the ice.

2) Collection and storage of ice samples

Test material is collected in the field in the form of rough or dressed blocks, of small slabs, or of cores. The material should be marked to indicate the original position and orientation in regard to the horizontal ice surface. Between collecting the ice from the field and the time of testing, the ice samples should be transported and stored in such a way that they are minimally affected crystallographically, physically, or mechanically. In this regard it is very important not to expose the ice to solar radiation, since this radiation may cause considerable weakening of the bonds between the ice crystals, with subsequent reduction of its strength. The thermal history, especially the rate of temperature change should be recorded.

Special attention has to be given to preserving the brine content within sea ice. More explicit recommendations on this problem will follow in the next edition.

Crystallographic changes can be minimized by storing the ice at temperatures no warmer than -15°C (about). Ice samples should be stored in plastic bags in order to avoid vaporization. Ice must be handled very carefully, like a fragile material; crack initiation due to rough handling may lead to spurious results.

3) Crystallographic investigation

The investigation of the crystallographic structure (texture) of ice normally requires the preparation of thin sections. These sections can be obtained by different methods, but in all cases the fundamental operations are melting and/or shaving. One common method involves freezing the ice specimen on a glass plate and cutting off layers of ice until the remaining thin section is about 0.5 mm thick. The shaving tool should preferably be a microtome. This approach is adequate for determination of grain size crystal orientation and general structural classification (granular, columnar, etc.). For field tests a sharp hand planing tool such as a spokeshave or the warm plate technique can be used. If the warm plate technique is in use, the crystallographic investigation must follow immediately.

For more detailed crystallographic examination of grain boundary effects thin section techniques involving melting should not be used. As an alternative to melting, the following procedure is suggested. An ice section 3-5 mm thick is cut with a band saw. This thick section is "welded" to a glass plate by freezing droplets of water at intervals around its perimeter. The ice surface is then shaved on a microtome until a smooth and plane surface is obtained. Next the ice section is separated from the glass plate, turned over and again attached to the glass plate. The second surface of the ice section is shaved on the microtome until it is smooth and the required thickness.

Thin sections should be prepared from several horizontal layers of the ice sheet and one section from a vertical plane. The location of each horizontal section should be carefully recorded. Each thin section should be at least 75 mm in width. Sublimation and recrystallization of the ice specimen can both be prevented by keeping the glass plate with the thin section attached inside a tightly sealed plastic envelope refrigerated at temperatures no warmer than about -15°C.

The crystallographic investigation usually consists of measurements on crystal orientation and grain size and of observations of any included material (impurities, air bubbles, etc.). The orientation of the ice crystals, i.e., the direction of the c-axis relative to the horizontal plane of the ice cover, and the grain size can be determined with a polarizing microscope fitted with a universal stage, or the Rigsby stage which was designed specially to deal with the large size of crystals normally encountered in natural ice covers.

An etch pit technique described by Higuchi (1958) may be useful to distinguish between S1- and S2-ice. Any crystallographic investigation should be completed by taking photographs of thin sections using polarized light. If the crystals are very small, pictures should be taken through a microscope.

4) Preparation of ice specimen for testing in uniaxial compression

a) Conventional method of testing ice in uniaxial compression

After the ice has been collected from the field or grown under laboratory conditions rough cutting of prismatic ice blocks or of cylindrical cores is advisable in order to obtain manageable sample size. Three different shapes are in use: (i) cylindrical cores, (ii) prismatic, and (iii) cubic samples. Since there is a widespread opinion that tests on cubic specimens may introduce significant errors, it is suggested that the use of such specimens be discontinued. In recognition of the fact that a large amount of data exists for cubic specimens, appropriate conversion formulae, similar to those developed in the field of rock mechanics and concrete technology, should be developed for ice.

Cylindrical specimens are usually prepared by a coring drill. Specimen diameter should be within a range of 7.0 to 10 cm. Specimen ends must be plane and parallel within close tolerances; this can be achieved by a rotary cut-off machine,by a milling machine, or by a lathe. The specimen length should be approximately 2.5 times the diameter.

Prismatic specimens can be prepared by a precise cut-off machine (stiff cut-off blade rotating in one plane).

Ice specimens for laboratory tests should be prepared by the use of a milling machine or lathe, while for field tests the cut-off machine and the lapping and melting method can be used, the latter one with caution (see table on page 10).

The compressive strength, and probably also the tensile strength, of ice depends on the ratio of sample size to crystal size. In order to be independent of this ratio, it is desirable to have the sample width d some 15 to 20 times the crystal diameter d_{cr}. Since this requirement would lead sometimes to very large specimens, it may be advisable to use a standard cylindrical or prismatic specimen of 7.5 cm to 10 cm diameter (width), correcting the result from reference curves to be established by a separate systematic investigation.

b) New method for testing ice in uniaxial compression

In the conventional uniaxial compression test, axial force is applied to the ends of a right circular cylinder through steel platens that make direct contact with the test specimen. Friction between platen and specimen produces radial restraint, so that there is a triaxial state of stress near

the end planes; the triaxial field is significant over an axial distance from the end planes of about one specimen radius. Interposition of highly compliant sheet (elastic or plastic) between platen and specimen often changes the sign of radial end forces, but does not eliminate the triaxial stress state. On a different scale, irregularities in the specimen end planes also create localized stress perturbations, and in brittle material these commonly initiate microcracks that lead to premature failure of the specimen. Further stress gradients can be produced by eccentric loading and by lack of parallelism between specimen end planes or between end planes and loading platens.

In tests that lead to brittle fracture, these are serious problems, and they are not easily solved. Since most attempts at solution have proved unsuccessful or impractical, the usual procedure is to accept positive frictional restraint at the specimen end planes and to use a specimen that is long enough to provide a mid-section that is reasonably free from end-effect stress perturbations (length/diameter ratio of 2 to 3). Extreme care is exercised in specimen preparation to produce end planes that are normal to the axis of symmetry and flat within very strict tolerances. A very thin sheet of compressible material (e.g. paper) may be interposed between specimen and platen to compensate for very small surface irregularities, and a "locking" spherical seat of suitable design may be used to compensate for small departures from parallelism. Flexure and racking of the specimen are avoided by strict alignment procedures and by provision of high rigidity in the loading device to avoid rotation or lateral translation of the platens.

This type of procedure has proved acceptable for high quality tests on materials such as rocks, ceramics, concrete, etc. However, these materials are quite stable in typical test environments, in contrast to ice, which is usually tested at very high homologous temperatures.

When ice is tested at temperatures above $-15^{o}C$ or so, it seems to be extremely difficult to obtain valid results with the conventional uniaxial compression test, even when great care is exercised. Hawkes and Mellor (1972) took exaggerated care in preparing and testing right circular cylinders, but at high loading rates they were unable to achieve strength values that approached those measured on specially designed dumbbell specimens.

In cold regions field work, test quality is often below the standards that are attainable in a research laboratory, so that it may be unrealistic to seek a solution in very rigorous quality control. The potential laboratory alternative of using precisely formed dumbbell specimens may also be impractical for field operations, especially when tests have to be made on broken material obtained by inexpert core drilling. An attempt has therefore been made to develop a new technique that is capable of giving accurate results with simple equipment.

The ideal way to load a uniaxial compression specimen would be to apply hydrostatic pressure to the ends, using a fluid that is incapable of transmitting shear stress. This does not appear to be practicable, but there are possibilities for use of compliant solids. The objective is to apply axial normal force through a deformable material that conforms to the shape of the specimen end plane, while at the same time avoiding any significant radial stresses.

Theoretically, the required result could be obtained by pressing the specimen between platens that have a lower modulus than the specimen, but which undergo radial strain that is exactly equal to that of the specimen. The condition for equality of radial strain is that Young's modulus divided by Poisson's ratio should have the same value for both specimen and platen materials. Thus, if the platen is to have a modulus significantly lower than the specimen, it will also need to have a Poisson's ratio that is proportionately low, and this does not seem to be a practical proposition.

A more reasonable alternative is to use a low modulus solid that is laterally confined to prevent gross radial deformation. This approach was pioneered by Kartashov et al. (1970), who made a compliant platen for rock testing by inserting a low modulus plug into an open-ended steel cylinder and pre-loading it be means of a screw-in steel plug. Using this kind of platen, it was found that apparent strength did not vary with the length/diameter ratio of the specimen over a range of approximately 0.5 to 3 (Fig. 1).

In adapting this technique to ice-testing, a low modulus plug was cast inside an aluminum cylinder (Fig. 2). To prevent extrusion of the insert, the inside diameter of the confining cylinder was slightly greater (of the order of 0.1 mm) than the diameter of the test specimen at failure (allowing for radial strain). The insert itself was a cast urethane (Flexane 94) that is similar in mechanical properties to hard rubber. The surface of the insert was faced-off in a lathe with a sharp tool to ensure that it was plane and normal to the axis of the confining cylinder.

This first version of the cast platen had some shortcomings, chiefly air bubbles in the urethane and a tendency for the urethane to pull away from the aluminum due to differential thermal strain at low temperatures. Nevertheless, it was put through a series of evaluation tests by D. Haynes of USACRREL.

The first trial was a length/diameter (L/D) experiment, in which 2.7 in. (70 mm) diameter cylinders of bubbly polycrystalline ice were tested at a temperature of +15°F (-9.5°C) with a displacement rate of 100 in./min (42 mm/sec). A total of 21 specimens were tested at L/D ratios from 0.74 to 2.5, and there was no detectable dependence of strength on L/D within this range.

For the second trial, 2.7 in. (70 mm) diameter specimens of bubbly polycrystalline ice with L/D = 2.35 were tested at a temperature of +15°F (-9.5°C) and at a displacement rate of 10 in./min (4.2 mm/sec). Half of the specimens were tested by the conventional method, using steel platens, while the other half were tested by the new method, using compliant platens. Within each of these groups there was further subdivision, half of the specimens having their ends prepared by careful lapping, and the other half having their ends left rough after sawing. All specimens tested by the new method gave consistent and plausible values for strength, while the specimens tested between steel platens gave erratic and dubious results, showing clearly the trend of error introduced by poor end preparation (Fig. 3).

Compliant platens for the testing of both cylindrical and prismatic specimens were then made by R. M. W. Frederking and his associates at the

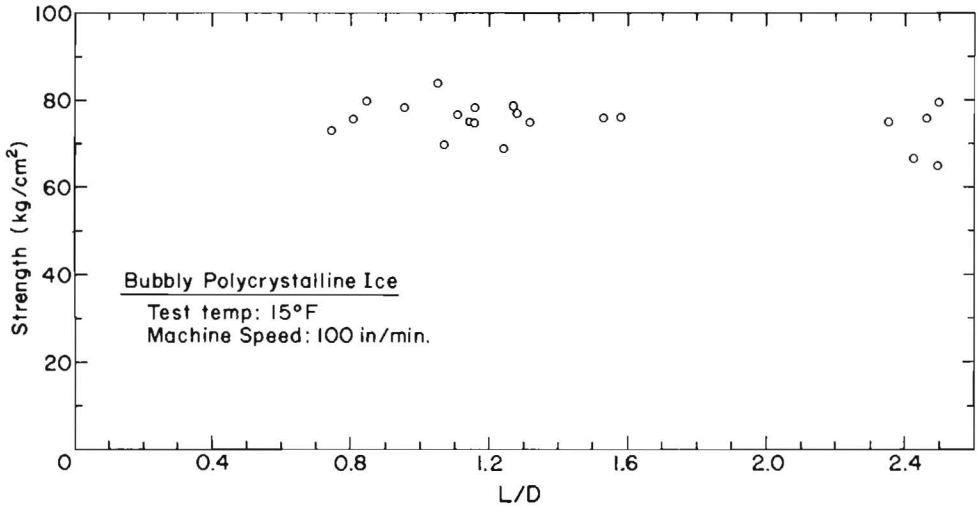

FIGURE 1

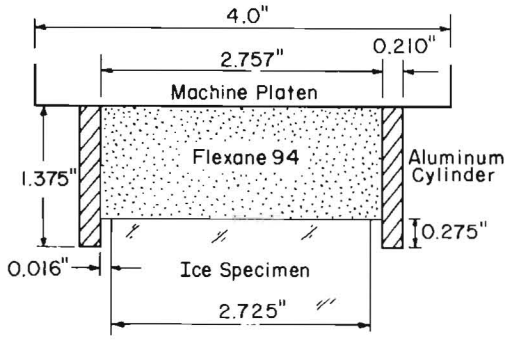

FIGURE 2

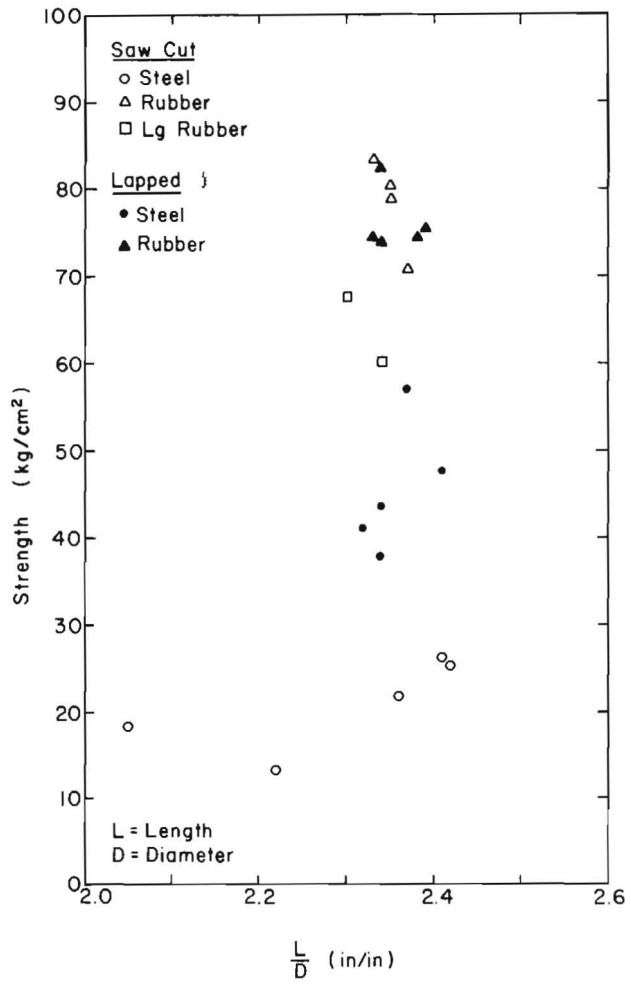
Saw Cut
o Steel
Δ Rubber
□ Lg Rubber
Lapped
• Steel
▲ Rubber
L = Length
D = Diameter
Strength (kg/cm²)
L/D (in/in)
100
90
80
70
60
50
40
30
20
10
0
2.0
2.2
2.4
2.6

FIGURE 3

National Research Council of Canda. Improved techniques for casting the urethane were developed, but the Canadian group also experienced the problem of separation between the urethane and the confining frame due to differential thermal strain at low temperature. So far, evaluation tests at Ottawa have been made at rather low strain rates (7×10^{-5} sec^{-1}) because of machine limitations, and this has introduced certain complications (strength is significantly dependent upon strain rate in this range, and platen compliance will have to be taken into account). However, first indications are that the compliant platens perform effectively.

It appears that compliant platens offer a means of making reliable strength measurements where high-quality end preparation is not feasible, and they permit the use of short specimens, thus allowing more effective and economical use of hard-won core samples.

Further evaluation tests are needed, and the method of making compliant platens has to be refined. In particular, bubble-free insert material has to be produced, and the confining frame has to pre-strain the insert so as to prevent separation at low temperatures. Provision for a properly designed spherical seat should also be made on the upper platen. If strains or strain-rates are to be measured or controlled, a displacement transducer should be fitted directly to the test specimen in order to obviate problems arising from deformations within the platens.

Various Methods for Preparation of Ice Samples for Testing in Compression

Method of preparation of the specimen	Testing method: Conventional (with frictional end effects)	Testing method: New (with constrained rubber end caps)
1. Facing off by a lathe	additional finishing usually necessary	fully satisfactory
2. End milling	satisfactory	satisfactory but not even necessary
3. Mitre sawing	further finishing always necessary (lapping, milling, etc.)	further finishing might be necessary
4. Cut-off wheel	further finishing usually necessary(lapping,milling)	probably adequate
5. Lapping	recommended after rough cutting by 3) and 4), especially for field tests; preferable against melting method	recommended after preparation by 3) and 4)
6. Melting	after preparation by 3) and 4), possible method under field conditions; not recommended for lab tests. Difficulties have been experienced in obtaining satisfactory results with this method.	after preparation by 3) and 4), possible method under field conditions, not recommended for lab tests

5) Preparation of specimen for tension tests

Uniaxial tensile strength can only be determined unambiguously by direct tension tests. Any substitute indirect tests like ring tensile, brazil or beam tests induce complicated stress states within the sample and stress-strain relationships have to be assumed in calculating the test results.

Perhaps the most promising method used so far has involved dumbbell specimens frozen into metal end caps, with close tolerances on alignment and concentricity. The diameter of the testing section should be half the diameter of the core. For more information on tensile strength tests with dumbbell specimens, see Dykins (1970) and Hawkes and Mellor (1970, 1972).

This method can produce excellent results in the laboratory but under field conditions it is necessary to develop equipment for forming the dumbbell specimen.

6) Testing Facility

a) Laboratory test facility.

Since the mechanical properties of ice, especially the compressive strength, are highly temperature and strain rate dependent, laboratory tests should be performed under controlled temperature conditions and the testing machine should provide a strain rate control system in which an extensiometer attached to the specimen regulates the plate velocity in such a way that the strain rate is constant (closed loop testing machine). The laboratory testing machine should allow strength measurements over a range of strain rates from $\dot{\varepsilon} = 10^{-5}$ to 10^{-1} sec^{-1}. The applied load should be measured by a load cell of adequate capacity in order to provide sufficient resolution of the result.

b) Field test equipment.

Main parts of the field test equipment should be:

1. Portable testing machine including constrained rubber heads (compliant platens).

2. Temperature controlled freezer for storage.

3. Sample preparation tools (see table on page 10).

4. Instruments for crystallographic investigation (see Section II.2,3).

5. Equipment for measuring density and salinity.

Since it would be too laborious and time-consuming to run compression tests over a wide range of temperatures, strain rates, and sample sizes, these parameters have to be examined in special laboratory tests in order to provide the field experimenter with reference curves.

In this case only a few tests are necessary to characterize the mechanical properties of ice at test sites in the field. This also allows simplification of the field testing machine, and permits lightweight construction (weight low enough for transportation by man). The required capacity, the range of speed and the accuracy will be determined as the special laboratory tests for developing the design curves proceed. Contacts with various manufacturers of testing machines have already been made.

7) Test conditions

During the period of the test there shall be no spatial or temporal variation in the temperature of the specimen. The specimen's temperature shall be measured and recorded. Required precision of temperature measurement may vary with the temperature range, e.g. $\pm$ 0.5°C below -10°C, and possibly within 0.1°C at temperatures close to the melting point.

The testing performance in respect to strain rate, sample shape and size should be uniform. The load direction versus crystal orientation or direction of growth must be recorded. Recommendations on specific standards will be elaborated as the reference curves for the strength-strain rate relationship and the convertibility between different shapes proceed.

8) Future work

The development of uniform testing methods in ice is just at the beginning. This first proposal will be revised and extended as future work on this matter continues.

While the development of reference curves for the effect of strain-rate, temperatures, d/d_{cr} ratio, and the shape for compression and tension tests are in progress, the Task Group will continue its work on recommendations for measurements of modulus data, friction parameters, and of strength and deformation in biaxial and triaxial stress fields. The development of uniform procedures in the use of new methods of measuring mechanical properties with the help of seismoacoustic methods are further goals.

Dykins, USA
Frederking, Canada
Gavrilo, USSR
Hirayama, Japan
Mellor, USA
Petrov, USSR
Schwarz, Federa Republic of Germany, Chairman
Tryde, Denmark

References

(1) Dykins, J. E. (1970)
"Ice Engineering-Tensile Properties of Sea Ice Grown in a Confined System"
Naval Civil Engineering Lab., Port Hueneme, Calif.
R 689

(2) Cherepanov, N. V. (1974)
"Classification of Ice of Natural Water Bodies"
Proceedings of IEEE Ocean-74 Conference
Bedford, Nova Scotia

(3) Hawkes, I. and Mellor, M. (1972)
"Deformation and Fracture of Ice under Uniaxial Stress"
J. of Glaciology, Vol. 2, No. 61

(4) Hawkes, I. and Mellor, M.(1970)
"Uniaxial Testing in Rock Mechanics Laboratories"
Engineering Geology, Vol. 4, No. 3, pp. 177-285

(5) Higuchi, Keiji (1958)
"The Etching of Ice Crystals"
Acta Metallurgica, Vol. 6, pp. 636-642

(6) Kartashov, Yu. M., Mazur-Dzurilovskii, Yu. D., Grokhol'skii, A.A. (1970)
"Determination of the Uniaxial Compressive Strengths of Rocks"
Fiziko-Tekhnicheskie Problemy Razrabotki Poleznykh, no. 3, pp. 108-110,
May-June (English translation in Soviet Mining Science, May-June 1970,
no. 3, pp. 339-341)

(7) Michel, B. and Ramseier, R. O. (1969)
"Classification of River and Lake Ice Based on its Genesis, Structure and Texture"
Department of Civil Engineering, University of Laval
Quebec, Que. Report S-15

International Association of Hydraulic Research (IAHR)
Committee on Ice Problems
International Symposium on Ice Problems
18-21 August 1975
Hanover, New Hampshire

APPENDIX C

General Meeting

O. Starosolszky

Distinguished Participants!

In the life of our Committee it is customary that the chairman of the Committee inform the Participants at the end of Symposia about the discussions held and decisions taken at the Committee Meetings.

During this general meeting the members of the Association compose the Section of the Ice and can express their views concerning the past activities and the future plans of the Committee.

Because not everybody among the participants is informed about our Association, may I call to your attention that the International Association for Hydraulic Research, established in 1935, is a non-governmental technical-scientific organization having corporate members (institutes) and individual members. (The number of the individual members is roughly 2500.) The yearly individual membership fee is about 20 dollars, which covers the subscription of the Hydraulic Research Journal, as well. The Association works mainly through the Committees, one of them is ours, devoted to ice problems. The Association is governed by a Council.

We would welcome all the specialists interested in our Association and simultaneously in our Committee. Kindly contact in this matter Dr. Ashton or Mr. Frankenstein, or in Canada, Dr. Frederking.

The Committee has decided to distribute the Minutes of our meetings for your better information. I do not intend to repeat these, but I wish to pick out some topics.

The most important is the formation of the Task Force Groups.

Besides the continuation of the Task Force Group on Physical and Mechanical Properties of Ice, two additional Task Force Groups have been formed:

One, headed by Mr. Frankenstein, for clarifying ice jamming phenomena,

Another, headed by Dr. Carstens, for studying the effects of ice on structures.

We wish to prepare state-of-art reports on selected topics and we are awaiting volunteers who will prepare draft reports. I would be pleased to get offers from the audience concerning participation in a survey on thermal aspects of ice formation and decay.

The other item is the next symposium; we have already accepted the invitation from Sweden for 1978.

The subjects to be dealt with are included in the Minutes, and cover several problems of ice engineering.

Before closing the work of our symposium, I have to say many thanks on one hand to the Organizing Committee, headed by Mr. Frankenstein, his collaborators and especially to his family assisting him in his tedious job, to Colonel Crosby for hosting; on the other hand to the session chairmen, to the invited lecturers, to the authors of the papers presented, and to the participants.

I think we can be satisfied, our Symposium was successful. The vivid discussions and the flexible organizations of the session made it possible to exchange a vast amount of information.

On behalf of the Ice Committee, let me wish all of you a pleasant journey both for the study-tour and in your trip home.

Obtaining so-so many impulses, we never shall forget the wonderful town of Hanover, the marvelous land of New Hampshire and the hospitality of our hosts!

See-you-again in Sweden! Good by!

International Association of Hydraulic Research (IAHR)
Committee on Ice Problems
International Symposium on Ice Problems
18-21 August 1975
Hanover, New Hampshire

APPENDIX D

Report of Organizing Committee

G. E. Frankenstein, Chairman

The committee on ice problems of the IAHR had two business meetings during the symposium. The president has summarized the results of these meetings in his opening and closing addresses.

The organizing committee consisted of many individuals of the CRREL laboratory, especially Mr. S. DenHartog. Mr. R. MacMillen of Dartmouth College provided invaluable assistance in preparation and conducting the symposium. Many thanks to them all, but in particular the latter two.

The organizing committee would also like to thank the four invited speakers. Their lectures were well received and covered the symposium themes very well. No conference could have had better guest lecturers.

I appreciate the contributions from the authors. The papers were generally very good. Any formal discussions follow the papers in these proceedings.

Last, but not least, I would like to thank all of the participants. Without you there could not have been a conference.

In closing, I would like to offer my assistance to the Swedish Organizing Committee and lots of good luck!

APPENDIX E

RIVER AND LAKE ICE TERMINOLOGY (in English) prepared by H. Kivisild	TERMINOLOGIE DE LA GLACE DE LAC ET DE RIVIERE (en français) préparé par M. Drouin, D.Sc. B. Michel, Dr.-Ing.	ТЕРМИНОЛОГИЯ ОЗЕРНОГО И РЕЧНОГО ЛЬДА (на русском) подготовлена В. Баланиным, к.т.н. А. Пеховичем, к.т.н. Р. Донченко, к.т.н. И. Соколовым, к.т.н.
English	Français	Русский
agglomerate (ice)	glace agglomérée	смерзшиеся ледяные образования
anchor ice	glace de fond	донный лед
anchor ice dam	seuil de glace	скопления донного льда
bare ice	glace vive	бесснежный лед
beginning of break-up	début de la débâcle	начало вскрытия
beginning of freeze-up	début de la prise des glaces	начало ледостава
border ice (shore ice)	glace de rive	забереги
black ice	glace noire	прозрачный лед
brackish ice	glace saumâtre	солоноватый лед
brash ice	brash	ледяная каша (битый лед)
break-up	débâcle	вскрытие
break-up date	date de la débâcle	дата вскрытия
break-up period	période de la débâcle	период вскрытия
candle ice	glace en chandelles	ослабленный игольчатый лед
channel lead	chenal	промока
columnar ice	glace columnaire	столбчатый лед
compacted ice	glace compactée	сплоченный лед
concentration	concentration	балльность льда
concentration boundary	frontière de concentration	границы льда различной балльности
consolidated ice cover	couverture de glace soudée	ледяной покров из смерзшихся льдин

English	Français	Русский
corn snow ice	glace de neige pourrie	ослабленный снежный лед
crack	fissure	трещина
deformed ice	glace déformée	деформированный лед
dendrites	dendrites	дендриты
diffuse ice edge	front diffus des glaces	кромка разреженного льда
drifting ice	glace à la dérive	дрейфующий лед
dry crack	fissure sèche	сухая трещина
duration of ice cover	durée de la couverture de glace	длительность ледостава
dynamic ice pressure	poussée dynamique des glaces	динамическое давление льда
fast ice	banquise côtière	заберег
floating ice	glace flottante	плавучнй лед
floe	glaçon	льдина
flooded ice	glace inondée	затопленный лед
fracture	fracture	разводье, разрыв, трещина
fracture zone	zone de fracture	зона разводий (трещин)
fracturing	par rupture	вэлом льда
frazil	frasil	шуга
freshwater ice	glace d'eau douce	пресноводный лед
floc	flocon	хлопья шуги
frazil shush	slush de frasil	скопление шуги под ледяным покровом
freeze-up period	période de la prise des glaces	период ледостава
frost smoke	brume d'évaporation	мороэный туман
frozen frazil slush	glace de frasil	шуговой лед
granular ice	glace granulaire	гранчлированный лед
grounded ice	glace échouée	лед на мели
glare ice	glace réfléchissante	эеркальный лед
hanging (ice) dam	barrage suspendu	эажор

English	Français	Русский
hinge crack	fissure en charnière	трещина, обусловленная изменением уровня воды
hummocked ice	glace hummockée	торосистый лед
hummock	hummock	торос
hummocking	hummockage	торошение
ice boom	estacade à glace	запань для удержания льда
ice bridge	pont de glace	ледяная перемычка
ice clearing	dégagement des glaces	разводье, полынья, очищение ото льда
ice cover	couverture de glace	ледяной покров
ice cover progression	progression de la couverture de glace	продвижение ледяной кромки
ice crossing	traverse de glace	ледяная переправа
ice edge	front de glace	кромка льда
ice field	champ de glace	ледяное поле
ice foot	banquette côtière	подошва припая
ice-free	libre de glace	свободный ото льда
ice grain	grain de glace	зерно льда
ice gorge	gorge de glace	проран в заторе
ice jam	embâcle	затор
ice jamming	blocage des glaces	заторообразование
ice ledge	bordure de glace	остаточные забереги
ice needle	aiguille de glace	игла льда
ice piling	empilement de glace	навал льда
ice pot hole	marmite de glace	местная промоина
ice push	poussée des glaces	подвижка льда
ice rind	glace en feuille	пластинка льда
ice run	descente des glaces	ледоход
ice sheet	nappe de glace	сплошной ледяной покров
ice shove	glissement de glace	надиг льда на берег
ice twitch	détachement saccadé de glace	подвижки льда

English	Français	Русский
ice wrinkle	ride de glace	невысокая ледовая гряда
icing (aufeis, surface ice, naled)	glaciation (naleyd)	наледь
insitu break-up	débâcle locale	местное вскрытие
lake ice	glace de lac	озерный лед
lead	chenal	протока
new ice	glace nouvelle	молодой лед
freeze-up date	date de la prise des glaces	ледостав
pancake ice	glace en crêpes glace en assiettes	блинчатый лед
polynya	polynya	полынья
puddle	mare	лужа
rafted ice	glace empilée	наслоенный лед
rafting	empilement	наслоение льда
ridge	crête	гряда торосов
ridged ice	glace en crête	торосистый лед
ridging	encrêtement	грядообразование
river ice	glace de rivière	речной лед
rotten ice	glace pourrie	"гнилой" лед
rough ice	glace rugueuse	неровный лед
sea ice	glace de mer	морской лед
shale ice	glace en schiste	слоистый лед
shear crack	fissure de cisaillement	трещина сдвига
shearing	cisaillement	сдвит льда
shore lead	chenal de rive	закраина
shore depression	dépression riveraine	понижение ледяного покрова у берега
sludge (shuga)	glace en bouillie	шуга
skim ice	glace primaire	сало
slush ball	boule de slush	ком шуга
slush ice run	descente de slush	шугоход
snow ice	glace de neige	снежный лед

English	Français	Русский
snow slush	slush de neige	снежура
stationary ice	glace stationnaire	неподвижный лед
stranded ice	glace d'estran	лед на берегу
static ice pressure	poussée statique des glaces	статическое давление льда
surface crack	fissure superficielle	поверхностная трещина
tabular ice	glace tabulaire	пластинчатый лед
thaw hole	trous de fonte	проталина
thermal crack	fissure thermique	термическая трещина
through crack	fissure complète à travers	сквоэная трещина
tide crack	crevasse de marée	приливная трещина
unconsolidated ice cover	couverture de glace non-soudée	плавающие ледяные поля